REPORT DOCUMENTATION PAGE

Form Approved OMB NO. 0704-0188

1. REPORT DATE (DD-MM-YYYY)	2. REPORT TYPE	3. DATES COVERED (From - To)
06-08-2012	Final Report	25-May-2009 - 24-May-2012

4. TITLE AND SUBTITLE
Support from the Army Research Office to be used towards student travel fellowships for the National Radio Science Meetings in January 2010, 2011, and 2012

5a. CONTRACT NUMBER
W911NF-09-1-0264

5b. GRANT NUMBER

5c. PROGRAM ELEMENT NUMBER
611102

6. AUTHORS
Katherine Bailey-Mathae

5d. PROJECT NUMBER

5e. TASK NUMBER

5f. WORK UNIT NUMBER

7. PERFORMING ORGANIZATION NAMES AND ADDRESSES
National Academy of Sciences
The National Academies
2101 Constitution Ave, NW
Washington, DC 20418 -

8. PERFORMING ORGANIZATION REPORT NUMBER

9. SPONSORING/MONITORING AGENCY NAME(S) AND ADDRESS(ES)
U.S. Army Research Office
P.O. Box 12211
Research Triangle Park, NC 27709-2211

10. SPONSOR/MONITOR'S ACRONYM(S)
ARO

11. SPONSOR/MONITOR'S REPORT NUMBER(S)
56120-EL.1

12. DISTRIBUTION AVAILIBILITY STATEMENT
Approved for Public Release; Distribution Unlimited

13. SUPPLEMENTARY NOTES
The views, opinions and/or findings contained in this report are those of the author(s) and should not contrued as an official Department of the Army position, policy or decision, unless so designated by other documentation.

14. ABSTRACT
The 2012 USNC-URSI National Radio Science Meeting was held in Boulder, Colorado, 04-07 January 2012. This open science meeting is sponsored by the U.S. National Committee (USNC) of the International Union of Radio Science (URSI), and held in cooperation with the IEEE Antennas and Propogation Society, Circuits and Sensing Society, Communications Society, Electromagnetic Compatiblity Society, Geoscience and Remote Sensing Society, Information Theory Society, Instrumentation and Measurement Society, Microwave Theory and

15. SUBJECT TERMS
electromagnetic metrology, fields and waves, signals and systems, electronics and photonics, electromagnetic environment and interference, wave propagation and remote sensing, ionospheric radio and propagation, waves in plasmas, radio astronomy,

16. SECURITY CLASSIFICATION OF:			17. LIMITATION OF ABSTRACT	15. NUMBER OF PAGES	19a. NAME OF RESPONSIBLE PERSON
a. REPORT	b. ABSTRACT	c. THIS PAGE			Kathie Bailey-Mathae
UU	UU	UU	UU		19b. TELEPHONE NUMBER: 202-334-2606

Standard Form 298 (Rev 8/98)
Prescribed by ANSI Std. Z39.18

Report Title

Support from the Army Research Office to be used towards student travel fellowships for the National Radio Science Meetings in January 2010, 2011, and 2012

ABSTRACT

The 2012 USNC-URSI National Radio Science Meeting was held in Boulder, Colorado, 04-07 January 2012. This open science meeting is sponsored by the U.S. National Committee (USNC) of the International Union of Radio Science (URSI), and held in cooperation with the IEEE Antennas and Propogation Society, Circuits and Sensing Society, Communications Society, Electromagnetic Compatiblity Society, Geoscience and Remote Sensing Society, Information Theory Society, Instrumentation and Measurement Society, Microwave Theory and Techniques Society, and Nuclear Science Society. Papers were presented in the interest areas of the URSI Scientific Commissions (c.f. www.ursi.org): Electromagnetic Metrology, Fields and Waves, Signals and Systems, Electronics and Photonics, Electromagnetic Environment and Interference, Wave Propagation and Remote Sensing, Ionospheric Radio and Propagation, Waves in Plasmas, Radio Astronomy, and Electromagnetics in Biology and Medicine.

Enter List of papers submitted or published that acknowledge ARO support from the start of the project to the date of this printing. List the papers, including journal references, in the following categories:

(a) Papers published in peer-reviewed journals (N/A for none)

Received Paper

TOTAL:

Number of Papers published in peer-reviewed journals:

(b) Papers published in non-peer-reviewed journals (N/A for none)

Received Paper

TOTAL:

Number of Papers published in non peer-reviewed journals:

(c) Presentations

Number of Presentations: 0.00

Non Peer-Reviewed Conference Proceeding publications (other than abstracts):

Received Paper

TOTAL:

Number of Non Peer-Reviewed Conference Proceeding publications (other than abstracts):

Peer-Reviewed Conference Proceeding publications (other than abstracts):

Received Paper

TOTAL:

Number of Peer-Reviewed Conference Proceeding publications (other than abstracts):

(d) Manuscripts

Received Paper

TOTAL:

Number of Manuscripts:

Books

Received Paper

TOTAL:

Patents Submitted

Patents Awarded

Awards

Graduate Students

NAME	PERCENT_SUPPORTED

FTE Equivalent:
Total Number:

Names of Post Doctorates

NAME	PERCENT_SUPPORTED

FTE Equivalent:
Total Number:

Names of Faculty Supported

NAME	PERCENT_SUPPORTED

FTE Equivalent:
Total Number:

Names of Under Graduate students supported

NAME	PERCENT SUPPORTED

FTE Equivalent:

Total Number:

Student Metrics

This section only applies to graduating undergraduates supported by this agreement in this reporting period

The number of undergraduates funded by this agreement who graduated during this period:	0.00
The number of undergraduates funded by this agreement who graduated during this period with a degree in science, mathematics, engineering, or technology fields:.....	0.00
The number of undergraduates funded by your agreement who graduated during this period and will continue to pursue a graduate or Ph.D. degree in science, mathematics, engineering, or technology fields:.....	0.00
Number of graduating undergraduates who achieved a 3.5 GPA to 4.0 (4.0 max scale):	0.00
Number of graduating undergraduates funded by a DoD funded Center of Excellence grant for Education, Research and Engineering:	0.00
The number of undergraduates funded by your agreement who graduated during this period and intend to work for the Department of Defense	0.00
The number of undergraduates funded by your agreement who graduated during this period and will receive scholarships or fellowships for further studies in science, mathematics, engineering or technology fields:	0.00

Names of Personnel receiving masters degrees

NAME

Total Number:

Names of personnel receiving PHDs

NAME

Total Number:

Names of other research staff

NAME	PERCENT SUPPORTED

FTE Equivalent:

Total Number:

Sub Contractors (DD882)

Inventions (DD882)

Scientific Progress

The purpose of this grant was to provide travel support to allow graduate students to participate in the National Radio Science Meeting (NRSM), fostering their career development as future radio scientists. For the 2012 NRSM, $5,350 was spent for this purpose.

A total of 110 students were supported at the 2012 NRSM, including 11 through this grant, and 99 through the private funds of the U.S. National Committee for URSI. The 11 graduate students who received travel fellowships to the 2012 NRSM through this award were:

- Divya Agrawal

Paper: Approximating D-Region Electron densities Using ELF/VLF Wave Generation Experiments at HAARP (GH1-4)
University: University of Florida, Gainesville, FL
Co-author: Robert C. Moore

- Mustafa Aksoy

Paper: Radio Frequency Interference Analysis of L-band Microwave Radiometry Missions (F6-6)
University: The Ohio State University, Columbus, OH
Co-author: Joel T. Johnson

- Darrin Albers

Paper: Development and Demonstration of 92, 130, and 166 GHz Radiometers for Improved Coastal Wet-Tropospheric Correction in SWOT (F2-8)
University: Colorado State University, Fort Collins, CO
Co-authors: Alexander Lee, Steven Reising, Shannon Brown, Pekka Kangaslahti, Douglas Dawson, Todd Gaier, Oliver Montes, Daniel Hoppe, and Behrouz Khayatian

- Shubhendu Bhardwaj

Paper #1: Understanding the Cross-Pol Generation in Patch Antennas: A Near-Field Approach (B6-9)
Paper #2: C-Shaped, E-Shaped, and U-Slotted Patch Antennas: A Comprehensive Comparative Study (B8-3)
University: University of California, Los Angeles, CA
Co-author: Yahya Rahmat-Samii

- Timothy Brockett

Paper: A New Paradigm in Solar Energy Harvesting: Characterization of High Absorption Nanopillar Array Photovoltaics (B10-1)
University: University of California, Los Angeles, CA
Co-authors: Harish Rajagopalan, Yahya Rahmat-Samii

- Petar Bukovcic

Paper: A Winter Storm Transition Revealed with Polarimetric Radar and 2DVD Observations (F3-4)
University: University of Oklahoma, Norman, OK
Co-authors: Dusan Zrnic, Guifu Zhang

- Salva Campione

Paper: Complex Modes and Artificial Magnetism in Composite Materials Made of Spherical Particles Accounting for Coupled Electric and Magnetic Dipoles (B7-8)
University: University of California, Irvine, CA
Co-author: Filippo Capolino

- Vicki Hsu

Paper: First Detection of Meteoric Smoke Using the Poker Flat Incoherent Scatter Radar (HG3-2)
University: University of Illinois at Urbana-Champaign, IL
Co-authors: J.T. Fentzke, and C.M.G. Brum

- Ryan Jacobs

Paper #1: Microwave-Induced Thermoacoustic Imaging Hybrid FDTD Modeling and Experimental Study (KB1-1)
Paper #2 (second author): Frequency Response and Polarization of ELF/VLF Signals Generated at the HAARP Facility (GH1-1)
University: University of Colorado, Denver, CO
Co-authors: Yiming Deng and Mark Golkowski (#1), Jason Carpenter and Mark Golkowski (#2)

- Swaroop Sahoo

Paper: Remote Sensing of Tropospheric Humidity using a Ground-Based Network of Scanning Compact Microwave Radiometers (F1-7)
University: Colorado State University, Fort Collins, CO
Co-authors: Xavier Bosch-Lluis, Steven Reising, J. Viviekanandan

- Miao Tian

Paper: Improved Jacobian Formulation for a Scattering-Based Discrete Ordinate Radiative Transfer Model (F1-5)
University: University of Colorado, Boulder, CO
Co-author: Albin Gasiewski

Most NRSM travel awardees received $600; those from Colorado received $350.

The U.S. National Committee for URSI, which organizes the NRSM, is organized around ten Commissions.
A - Electromagnetic Metrology
B - Fields and Waves, Electromagnetic Theory and Applications
C - Radio Communication Systems and Signal Processing
D - Electronics and Photonics
E - Electromagnetic Environment and Interference
F - Wave Propagation and Remote Sensing
G - Ionospheric Radio and Propagation
H - Waves in Plasmas
J - Radio Astronomy
K -Electromagnetics in Biology and Medicine

Students were selected across this spectrum. In order to receive a travel fellowship to the NRSM, students had to be the first author and presenter of a paper, and enrolled full-time in a graduate degree program at a U.S. university. The recipients were all expected to present their research, participate in sessions, and attend special events where students and young scientists were recognized. A special lunch for student travel awardees, student paper competition finalists, U.S. commission chairs, and USNC-URSI officers was held immediately following the meeting plenary session. This lunch provided an additional opportunity for students to meet each other and to speak with more senior researchers in the field.

The student program at the NRSM helps build future academic and research infrastructure. Through their participation in these events, the students are exposed to leaders in radio science, have opportunities to present and discuss their work and interact with their peers from multiple research institutions. These interactions are important elements of the education process as they help to maintain interest among U.S. students for pursuing scientific careers and foster engagement in the radio science community.

Support of students at the NRSM has been a priority of the U.S. National Committee for several years. The Board on International Scientific Unions (BISO) at the National Academies regularly surveys recipients of all travel award programs to obtain feedback on the program and data on participation.

The USNC/URSI operates largely as a professional society, but also includes and has close ties to several other societies including the American astronomical Society, the American Geophysical Union, the American Meteorological Society, IEEE Antennas and Propagation Society, IEEE Geoscience and Remote Sensing Society, and the IEEE Microwave Theory and Techniques. Information about the travel awards was sent to all of the above and included on USNC/URSI webpages (http://www.usnc-ursi.org/ and http://sites.nationalacademies.org/PGA/biso/URSI/index.htm).

Technology Transfer

Table of Contents

International Union of Radio Science/Union Radio Scientifique Internationale

Founded in 1919, the International Union of Radio Science (URSI) coordinates studies, research, applications, scientific exchange, and communication in all fields of radio science from telecommunications and radio astronomy to medicine (www.ursi.org).

Both the Union and the U.S. National Committee are organized into ten commissions:

Electromagnetic Metrology (Commission A)
Fields and Waves (Commission B)
Radiocommunication Systems and Signal Processing (Commission C)
Electronics and Photonics (Commission D)
Electromagnetic Environment and Interference (Commission E)
Wave Propagation and Remote Sensing (Commission F)
Ionospheric Radio Propagation (Commission G)
Waves in Plasmas (Commission H)
Radio Astronomy (Commission J)
Electromagnetics in Biology and Medicine (Commission K)

About the USNC-URSI

The U.S. National Committee of URSI (USNC-URSI) is appointed by the National Research Council of the National Academies and represents U.S. radio scientists in URSI. It encourages studies in radio science, provides a forum for the dissemination of research findings, and provides an organizational infrastructure for the radio science community in the United States.

The USNC-URSI hosts the National Radio Science Meeting each January in Boulder, Colorado. The IEEE International Symposium on Antennas and Propagation and USNC-URSI National Radio Science Meeting, co-sponsored by the USNC-URSI and the Antennas and Propagation Society of the Institute of Electrical and Electronics Engineers (IEEE/AP-S), is held each summer. Every five to seven years, a North American Radio Science Meeting (NARSM) is organized, co-sponsored by the U.S. and Canadian National Committees to URSI. Ottawa, Canada hosted the most recent NARSM meeting in July 2007.

The international URSI General Assembly and Scientific Symposium is held every three years in locations around the world. The 30th URSI General Assembly and Scientific Symposium was held in Istanbul, Turkey on August 13-20, 2011. Over 1,000 U.S. and international scientists, including 264 students and Young Scientists, participated in sessions covering all ten commissions. The USNC-URSI is also proud to have hosted the 29th General Assembly in Chicago, Illinois August 7-16, 2008. The USNC-URSI helped to support meeting expenses for approximately 200 U.S. and international students and Young Scientists to attend that meeting. The 31st URSI General Assembly and Scientific Symposium will be held in Beijing, China, in 2014. For further information on USNC-URSI, please visit www.usnc-ursi.org.

U.S. National Committee Leadership and Commission Chairs (2012-2014)

(In addition to the individuals below, the USNC-URSI includes Members at Large, Society Representatives, and scientists serving in executive roles in international URSI.)

Steven C. Reising
USNC Chair
Professor of Electrical and Computer Engineering
Colorado State University
Email: steven.reising@colostate.edu

Yahya Rahmat-Samii
USNC Past Chair
Northrop Grumman Professor of Electrical Engineering
University of California at Los Angeles
Email: rahmat@ee.ucla.edu

David R. Jackson
USNC Secretary and Chair-Elect
Professor of Electrical and Computer Engineering
University of Houston
Email: djackson@uh.edu

Gary S. Brown
USNC Accounts Manager
Bradley Distinguished Professor of Electromagnetics
Virginia Polytechnic Institute and State University
Email: randem@vt.edu

Kathie Bailey-Mathae
Director, Board on International Scientific Organizations
The National Academies
Email: kbmathae@nas.edu

Christopher L. Holloway
Chair, USNC Comm. A
Electromagnetics Division
National Institute of Standards and Technology (NIST)
Email: holloway@boulder.nist. gov

Sembiam Rengarajan
Chair, USNC Comm. B
Professor of Electrical and Computer Engineering
California State University, Northridge
Email: srengarajan@csun.edu

Amir I. Zaghloul
Chair, USNC Comm. C
Professor
Bradley Department of Electrical and Computer Engineering
Virginia Tech
Email: amirz@vt.edu

Jennifer T. Bernhard
Chair, USNC Comm. D
Professor
Department of Electrical and Computer Engineering
University of Illinois at Urbana-Champaign
Email: jbernhar@illinois.edu

Everett G. Farr
Chair, USNC Comm. E
Farr Fields, LC
Email: efarr@farr-research.com

V. Chandrasekar
Chair, USNC Comm. F
Professor of Electrical and Computer Engineering and Biomedical Engineering
Colorado State University
Email: chandra@engr.colostate.edu

Frank Lind
Chair, USNC Comm. G
Research Engineer, Atmospheric Sciences Group
MIT Haystack Observatory
Email: flind@haystack.mit.edu

Victor Pasko
Chair, USNC Comm. H
Professor of Electrical Engineering
The Pennsylvania State University
Email: vpasko@psu.edu

Richard F. Bradley
Chair, USNC Comm. J
Scientist/Senior Research Engineer
National Radio Astronomy Observatory
Email: rbradley@nrao.edu

Erdem Topsakal
Chair, USNC Comm. K
Associate Professor
Department of Electrical and Computer Engineering
Mississippi State University
Email: topsakal@ece.msstate.edu

UNITED STATES NATIONAL COMMITTEE
INTERNATIONAL UNION OF RADIO SCIENCE

TECHNICAL PROGRAM

National Radio Science Meeting
4-7 January 2012
University of Colorado at Boulder
Sponsored by USNC-URSI

Tuesday Evening **3 January 2011**

19:00 – 23:00 USNC-URSI Committee, Millennium Hotel

Wednesday Morning **4 January 2012**

Session A1: Electromagnetic Metrology and Applications
Room 105

Co-Chairs: William Coburn, *US Army Research Laboratory*
William Young, *NIST*

08:20 A1-1 INTEGRATED MICRO-FLUIDIC CHANNEL ON RF CIRCUIT TOWARD LAB-ON-A-CHIP APPLICATION

Pouya Talebbeydokhti*[1], Mingguang Tuo[1], Qi Tang[1], Pak Wong[2], Hao Xin[1]
[1]*Electrical and Computer Engineering, University of Arizona, Tucson, AZ*
[2]*Aerospace and Mechanical Engineering, University of Arizona, Tucson, AZ*

08:40 A1-2 COMPLEX PERMITTIVITY PHANTOM TISSUE MEASUREMENTS USING A TRL CALIBRATION FIXTURE

Xavier Palomer Ripoll*[1], Ved Topkar[2], Zoya Popovic[1]
[1]*University of Colorado, Boulder, CO*
[2]*Fairview High School, Boulder, CO*

09:00 A1-3 ELECTROMAGNETIC METROLOGY ON CONSTRUCTION MATERIAL AND CORROSION: CONCRETE AND IRON OXIDES

Sung Kim*[1], Jack Surek[1], James Baker-Jarvis[1], Dat Duthinh[2], Paul Stutzman[2], Shuangzhen Wang[2], Edward Garboczi[2]
[1]*NIST, Boulder, CO*
[2]*NIST, Gaithersburg, MD*

09:20 A1-4 A 50-W 71%-EFFICIENT CW GAN AMPLIFIER FOR TISSUE ABLATION

Jennifer Imperial*, Michael Roberg, Zoya Popovic
Covidien and the University of Colorado at Boulder, Boulder, CO

09:40 A1-5 ANALYTICAL MODEL OF A HELMET-MOUNTED CONFORMAL PATCH ANTENNAS FOR AN ASSORTMENT OF CANONICAL SHAPES

Boliong Amang*
Morgan State University, Baltimore Maryland

10:00 Break

10:20 A1-6 AUTOMATED AIRBORNE COMMUNICATION TEST SYSTEM

Michael Breckenridge*, Henry Suoto, Brian Higa
Antenna & Spectrum Analysis Div., US Army CERDEC S&TCD, Aberdeen Proving Ground, MD

10:40 A1-7 RF PROPAGATION MEASUREMENTS IN MOUNTAINOUS TERRAIN

William O. Coburn*, Mark D. Berry, Neal Tesny, Brian R. Gollsneider
RDRL-SER-M, US Army Research Laboratory, Adelphi MD

11:00 A1-8 ACOUSTICAL MODULATION SENSOR MEASUREMENTS

William A. Davis*[1], Taeyoung Yang[1], John Coggin[2], Russell May[2]
[1]*Elec. & Comp. Engr, Virginia Tech, Blacksburg, VA*
[2]*Prime Photonics, Blacksburg, VA*

11:20 A1-9 SMAP RADIOMETER FRONT END INTEGRATED MICROWAVE ASSEMBLY

Negar Ehsan*[1], Joseph Knuble[1], Kevin Horgan[1], Fred Sacks[2], Dale Bankus[3], Jeffrey Piepmeier[1]
[1]*NASA Goddard Space Flight Center, Greenbelt, MD*
[2]*Base2 Engineering, LLC, Annapolis, MD*
[3]*Orbital Sciences Corporation, Greenbelt, MD*

Session B1: Antenna Arrays
Room 155

Co-Chairs: John Volakis, *The Ohio State University*
Gregory Huff, *Texas A&M University*

08:20 B1-1 SUPERSTRATE-ENHANCED ULTRAWIDEBAND TIGHTLY COUPLED ARRAY WITH RESISTIVE FSS

William F. Moulder*, Kubilay Sertel, John L. Volakis
The Ohio State University, Columbus, OH

08:40 B1-2 EFFICIENT EVALUATION OF RADIATION PATTERN FOR PERIODIC STRUCTURE USING RECIPROCITY IN PERIODIC FDTD METHOD

Minshen Wang*, Ji Chen, David R. Jackson, Donald R. Wilton
ECE, University of Houston, Houston TX

09:00 B1-3 UNIT CELL AUTONOMY VIA WIRELESS CONTROL OF A SPACE-FED PHASED ARRAY ANTENNA

Matthew Stoneback*, Yasuo Kuga
Electrical Engineering, University of Washington, Seattle, WA

09:20 B1-4 RADIATION CHARACTERISTICS OF TRIANGULARLY-BOUND RANDOM ARRAYS

Kris R. Buchanan*, Gregory H. Huff
Electrical Engineering, Texas A&M University, College Station, Texas

09:40 B1-5 SMART PHONE ENABLED COGNITIVE CONTROL OF A PHASED ARRAY

Jeffrey S. Jensen*, Jean-Francois Chamberland, Gregory Huff
Texas A & M University, College Station, TX

10:00 Break

10:20 B1-6 COMPENSATING FOR ANTENNA ARRAY TRACKING MEASUREMENT ERRORS

Randy L. Haupt*, Aaron Lyons, Brian Thrall, Martin Huisjen
Ball Aerospace, Westminster, CO

10:40 B1-7 AN UWB 7X7 SINGLE-POLARIZED TIGHTLY COUPLED DIPOLE ARRAY WITH INTEGRATED FEED AND TERMINATIONS

Ioannis Tzanidis*, Kubilay Sertel, John L. Volakis
The Ohio State University, Columbus Ohio

11:00 B1-8 MICROWAVE LENS MODELING FOR MM-WAVE COMMUNICATIONS

John H. Brady*, Nader Behdad, Akbar Sayeed
Electrical and Computer Engineering, University of Wisconsin - Madison, Madison, WI

11:20 B1-9 DESIGN DIRECTIONS FOR WIDE-ANGLE ARRAY SCANNING

Nicholas Host*
The ElectroScience Laboratory, Ohio State University, Columbus, OH

Session B2: Metamaterials I
Room 1B40

Co-Chairs: Piergiorgio Uslenghi, *University of Illinois at Chicago*
Christopher Holloway, *NIST*

08:20 B2-1 CYLINDRICAL RESONATOR SECTORALLY FILLED WITH DNG METAMATERIAL AND EXCITED BY A LINE SOURCE

Piergiorgio L. E. Uslenghi*[1], Vito G. Daniele[2], Roberto D. Graglia[2], Guido Lombardi[2]
[1]*Dept. of ECE, University of Illinois at Chicago, Chicago, Illinois*
[2]*Dip. di Elettronica, Politecnico di Torino, Torino, Italy*

08:40 B2-2 EXISTENCE OF SURFACE WAVES AND COMPLEX MODES ON METASURFACES

Christopher L. Holloway*[1], Derik C. Love[1,2], Edward F. Kuester[3], Josh A. Gordon[1], David A. Hill[1]
[1]*NIST, Boulder, CO*
[2]*USFA, Dayton, OH*
[3]*Univeristy of Colorado, Boulder, co*

09:00 B2-3 A PHASE-RECONFIGURABLE REFLECTARRAY ELEMENT USING FLUIDIC NETWORKS

Stephen A. Long*, Gregory H. Huff
Texas A&M University, College Station, TX

09:20 B2-4 ABSORBING BOUNDARY CONDITIONS AND THE HOMOGENIZATION MODEL FOR MULTILAYERED WIRE MEDIA

Yashwanth Reddy Padooru*[1], Alexander B. Yakovlev[1], Chandra S. R. Kaipa[1], George W. Hanson[2], Francisco Medina[3], Francisco Mesa[4], Allen W. Glisson[1]
[1]*Electrical Engineering, University of Mississippi, University, MS*
[2]*Electrical Engineering and Computer Science, University of Wisconsin-Milwaukee, Milwaukee, WI*
[3]*Electronics and Electromagnetism, University of Seville, Seville, Spain*
[4]*Applied Physics I, ETS de Ingeniera Informtica, University of Seville, Seville, Spain*

09:40 B2-5 ALL-ANGLE NEGATIVE REFRACTION BY AN INDUCTIVELY LOADED UNIAXIAL WIRE MEDIUM TERMINATED WITH PATCH ARRAYS

Chandra S. R. Kaipa*[1], Alexander B. Yakovlev[1], Mario G. Silveirinha[2], Stanislav I. Maslovski[2]
[1]*Department of Electrical Engineering, University of Mississippi, University, MS*
[2]*Departamento de Engenharia Electrotcnica, Universidade de Coimbra, Polo, Coimbra, Portugal*

10:00 Break

10:20 B2-6 ISOIMPEDANCE ANISOTROPIC SUBSTRATES FOR PLANAR ANTENNA PROFILE REDUCTION

Hayrettin Odabasi*, Fernando L. Teixeira
Electrical and Computer Engineering, The Ohio State University, Columbus/Ohio

10:40 B2-7 FABRICATION SENSITIVITY OF DOUBLE-SIDED SPLIT-RING RESONATOR ARRAYS

Frank Trang*, Edward F. Kuester, Horst Rogalla, Zoya Popovic
Dept. of Electrical, Computer, and Energy Engineering, University of Colorado, Boulder, Bouder, Colorado

11:00 B2-8 WIDEBAND, OPTICALLY TRANSPARENT, BAND-SELECTIVE GROUND PLANES FOR ANTENNA APPLICATIONS

Mani Kashanianfard*, Kamal Sarabandi
EECS, University of Michigan, Ann Arbor

11:20 B2-9 OMNIDIRECTIONAL SMALL ANTENNAS BASED ON ε-NEAR-ZERO METAMATERIAL CHANNELS

Jason C. Soric*, Andrea Alu
Electrical and Computer Engineering, The University of Texas at Austin, Austin, Texas

11:40 B2-10 ULTRA-BROADBAND MANTLE CLOAK USING NON-FOSTER NEGATIVE-IMPEDANCE METASURFACES

Pai-Yen Chen*, Andrea Alu
Electrical and Computer Engineering, University of Texas at Austin, Austin

Session F1: Passive Remote Sensing of the Earth's Environment: Radiometer Calibration and Radiative Transfer
Room 150

Co-Chairs: Steven Reising, *Colorado State University*
Albin Gasiewski, *University of Colorado at Boulder*

08:20 F1-1 CHARACTERIZATION OF AUTOEMISSION REFLECTION FOR PRECISE RADIOMETER CALIBRATION

Albin J. Gasiewski*, David Kraft, Vladimir Leuski
Center for Environmental Technology, University of Colorado at Boulder, Boulder, CO

08:40 F1-2 BEAM-EFFICIENCY EXTRACTION METHOD FOR BRIGHTNESS-TEMPERATURE MEASUREMENT

Dazhen Gu*, Derek Houtz, James Randa, David K. Walker
Electromagnetic, National Institute of Standards and Technology, Boulder, CO

09:00 F1-3 WIDEBAND ELECTROMAGNETIC ANALYSIS OF PYRAMIDAL RADIOMETER CALIBRATION TARGETS USING FDTD

Srikumar Sandeep*, Albin J. Gasiewski
University of Colorado at Boulder, Boulder, CO

09:20 F1-4 OPTIMAL CALIBRATION OF PASSIVE MICROWAVE RADIOMETERS FOR THE 2008 ARCTIC MECHANISIMS OF INTERACTIONS BETWEEN THE SURFACE AND ATMOSPHERE (AMISA) MISSION

Michael Zucker*, Albin J. Gasiewski
University of Colorado at Boulder, Boulder, CO

10:00 Break

10:20 F1-5 IMPROVED JACOBIAN FORMULATION FOR A SCATTERING-BASED DISCRETE ORDINATE RADIATIVE TRANSFER MODEL

Miao Tian*, Albin J. Gasiewski
ECEE, University of Colorado, Boulder, Boulder, Colorado

10:40 F1-6 AN OVERLAND WET PATH DELAY RETRIEVAL ALGORITHM FOR NADIR-VIEWING MICROWAVE RADIOMETERS

Kyle L. Gilliam*[1], Xavier Bosch-Lluis[1], Steven C. Reising[1], Alan B. Tanner[2]
[1]*Microwave Systems Laboratory, Colorado State University, Fort Collins CO*
[2]*Jet Propulsion Laboratory, California Institute of Technology, Pasadena CA*

11:00 F1-7 REMOTE SENSING OF TROPOSPHERIC HUMIDITY USING A GROUND-BASED NETWORK OF SCANNING COMPACT MICROWAVE RADIOMETERS

Swaroop Sahoo*[1], Xavier Bosch-Lluis[1], Steven C. Reising[1], Jothiram Vivekanandan[2]
[1]*Electrical and Computer Engineering, Colorado State University, Fort Collins, CO*
[2]*Earth Observing Laboratory, National Center for Atmospheric Research, Boulder, CO*

11:20 F1-8 AN ANISOTROPIC OCEAN SURFACE EMISSIVITY MODEL BASED ON WINDSAT POLARIMETRIC BRIGHTNESS OBSERVATIONS

Dean F. Smith*[1], Albin J. Gasiewski[1], Srikumar Sandeep[1], Bob L. Weber[2]
[1]*ECEE, University of Colorado at Boulder, Boulder, CO*
[2]*DeTect, Inc., Longmont, CO*

Session H1: Waves in Space and Laboratory Plasmas I
Room 245

Co-Chairs: Anatoly Streltsov, *Embry-Riddle Aeronautical University*
Stephen Vincena, *University of California at Los Angeles*

10:20 H1-1 OUTSTANDING ISSUES IN UNDERSTANDING THE ROLE OF VLF WAVES IN THE INNER MAGNETOSPHERE

Michael J. Starks*[1], Jonah J. Colman[1], Jay M. Albert[1], Richard S. Selesnick[1], Christopher E. Sillence[1], Richard A. Quinn[2]
[1]*Space Vehicles Directorate, Air Force Research Laboratory, Kirtland AFB, NM*
[2]*AER, Inc., Lexington, MA*

10:40 H1-2 SAID/SAPS-RELATED VLF WAVES AND THE OUTER RADIATION BELT BOUNDARY

Evgeny Mishin*[1], Jay Albert[1], Ondrej Santolik[2]
[1]*RVBX, Air Force Research Laboratory, Albuquerque, New Mexico*
[2]*Department of Space Physics, Institute of Atmospheric Physics, Praha, Czech Republic*

11:00 H1-3 HIGH-POWER RADIO WAVE HEATING OF THE D-REGION IONOSPHERE ABOVE HAARP

Robert C. Moore*
Department of Electrical and Computer Engineering, University of Florida, Gainesville, FL

11:20 H1-4 ALFVEN WAVES, CURRENT SHEETS AND THE EVOLUTION OF AURORAL FORMS

Christopher C. Chaston*
Space Sciences Laboratory, University of California Berkeley, Berkeley, CA

11:40 H1-5 ULF WAVES GENERATED BY THE IONOSPHERIC FEEDBACK INSTABILITY NEAR DISCRETE AURORA

Anatoly V. Streltsov*[1], Nan Jia[2], Eric D. Donovan[3], Harald U. Frey[4], Todd R. Pedersen[5]
[1]*Department of Physical Sciences, Embry-Riddle Aeronautical University, Daytona Beach, FL*
[2]*Thayer School of Engineering, Dartmouth Colege, Hanover, NH*
[3]*Physics Department, University of Calgary, Calgary, Canada*
[4]*Space Science Laboratory, University of California, Berkeley*
[5]*Space Vehicles Directorate, AFRL, Albuquerque*

Session HG1: Lightning and its Interaction with the Ionosphere I
Room 200

Co-Chairs: Ningyu Liu, *Florida Institute of Technology*
Morris Cohen, *Stanford University*

08:20 HG1-1 PHOCAL 2011: FIRST RESULTS

Walter A. Lyons*[1], Steven A. Cummer[2], Steven A. Rutledge[3], Timothy J. Lang[3], Tiffany Meyer[3], Tom A. Warner[4]
[1]*Yucca Ridge Field Station, FMA Research, Inc., Fort Collins, CO*
[2]*Electrical & Computer Engineering, Duke University, Durham, NC*
[3]*Dept. of Atmospheric Sciences, Colorado State University, Fort Collins, CO*
[4]*Inst.of Atmospheric Sciences, SD School of Mines & Technology, Rapid City, SD*

08:40 HG1-2 THEORETICAL ANALYSIS OF ELVES GENERATED BY ROCKET-TRIGGERED LIGHTNING

Christopher J. Biagi*, Robert C. Moore
Department of Electrical and Computer Engineering, University of Florida, Gainesville, FL

09:00 HG1-3 UNDERSTANDING SPRITE MORPHOLOGY

Jianqi Qin*, Sebastien Celestin, Victor P. Pasko
Electrical Engineering, The Pennsylvania State University, University Park

09:20 HG1-4 INVESTIGATION OF LUMINOSITY AND PROPAGATION CHARACTERISTICS OF SPRITE STREAMERS INITIATED FROM SMALL IONOSPHERIC DISTURBANCES IN LIGHTNING ELECTRIC FIELD BELOW BREAKDOWN THRESHOLD FIELD

Burcu Kosar*, Ningyu Y. Liu, Hamid K. Rassoul
Department of Physics and Space Sciences, Florida Institute of Technology, Melbourne,FL

09:40 HG1-5 LIGHTNING INDUCED SFERICS CORRELATED WITH WHISTLER PROPAGATION

Andrew J. Compston*[1], Ryan Said[1], Ivan Linscott[1], Morris Cohen[1], Umran Inan[1,2], Nikolai Lehtinen[1], Michel Parrot[3]
[1]*Electrical Engineering, Stanford University, Stanford, CA*
[2]*Koc University, Istanbul, Turkey*
[3]*LPC2E, CNRS, Orleans, France*

10:00 Break

10:20 HG1-6 IONOSPHERIC EFFECTS OF WHISTLER WAVES LAUNCHED BY ROCKET-TRIGGERED LIGHTNING

Christopher J. Biagi*[1], Robert C. Moore[1], Mark Golkowski[2]
[1]*Department of Electrical and Computer Engineering, University of Florida, Gainesville, FL*
[2]*Department of Electrical Engineering, University of Colorado Denver, Denver, CO*

10:40 HG1-7 THE METHOD OF STUDY IN THE IONOSPHERE OF THE PHYSICAL PROCESSES OCCURRING IN HIGH-ALTITUDE ATMOSPHERIC THUNDERSTORMS

Stanislav I. Klimov*[1], Gali K. Garipov[2], Vladimir M. Gotlib[1], Alexander V. Gurevich[3], Jean-Louis Pincon[4], Sergei I. Svertilov[2], Lev M. Zelenyi[1]
[1]*Space Plasma Physics Department, Space Research Institute of the Russian Academy of Sciences, Moscow, Russian Federation*
[2]*Cosmic Rays Department, Institute of Nuclear Physics of the MSU, Moscow, Russian Federation*

[3]*Department of Theory, P.N.Lebedev Physical Institute (FIAN) of RAS, Moscow, Russian Federation*
[4]*Plasma Physics Department, Centre dEtude Spatiale des Rayonnements, Toulouse, France*

11:00 HG1-8 LIGHTNING MORPHOLOGY AND IMPULSE CHARGE MOMENT CHANGE OF HIGH PEAK CURRENT NEGATIVE STROKES

Gaopeng Lu*[1], Steven A. Cummer[1], Richard J. Blakeslee[2], William H. Beasley[3], Stephanie A. Weiss[3]
[1]*Electrical and Computer Engineering Department, Duke University, Durham, North Carolina*
[2]*Earth Science Office, NASA Marshall Space Flight Center, Huntsville, Alabama*
[3]*School of Meteorology, University of Oklahoma, Norman, Oklahoma, Earth Science Office*

11:20 HG1-9 NUMERICAL MODELING OF INITIATION OF LIGHTNING LEADERS FROM TALL STRUCTURES BY SPRITE-PRODUCING LIGHTNING DISCHARGES

Victor P. Pasko*
Communications and Space Sciences Laboratory, Penn State University, University Park, Pennsylvania

11:40 HG1-10 A WAVEGUIDE MODEL OF THE RETURN STROKE CHANNEL WITH A METAMATERIAL CORONA

Nikolai G. Lehtinen*
Stanford University, Stanford, CA

Session J1: Radio Astronomy Teaching Labs and Educational Instruments
Room 265

Co-Chairs: Steven Ellingson, *Virginia Polytechnic Institute & State University*
Geoffrey Bower, *UC Berkeley*

08:20 J1-1 THE UC BERKELEY UNDERGRADUATE RADIO ASTRONOMY LABORATORY

Geoffrey C. Bower*, Carl Heiles, Aaron Parsons, Andrew Siemion
Astronomy Department & Radio Astronomy Laboratory, UC Berkeley, Berkeley, CA

08:40 J1-2 AN INEXPENSIVE, TABLE-TOP INTERFEROMETER AND UNDERGRADUATE LABS TO TEACH THE BASICS OF APERTURE SYNTHESIS

Jonathan M. Marr*[1], Alan E. E. Rogers[2], Vincent L. Fish[2], Arndt B. Martina[3]
[1]*Dept. of Physics and Astronomy, Union College, Schenectady, NY*
[2]*MIT Haystack Observatory, Westford, MA*
[3]*Bridgewater State College, Bridgewater, MA*

09:00 J1-3 MEASURING CMB TEMPERATURE WITH AN INEXPENSIVE, STUDENT-BUILT LAB EXPERIMENT

Meredith A. MacGregor*[1], John M. Kovac[1], Robert Wilson[2], Robert Kimberk[2], Students of Harvard Astro. 191[1]
[1]*Astronomy, Harvard University, Cambridge, MA*
[2]*Smithsonian Astrophysical Observatory, Cambridge, MA*

09:20 J1-4 THE ARECIBO REMOTE COMMAND CENTER: HIGH SCHOOL AND UNDERGRADUATE STUDENTS SEARCH THE GALAXY FOR RADIO PULSARS

Fredrick A. Jenet*
University of Texas at Brownsville, Brownsville, TX

09:40 J1-5 GASE INTERFEROMETRY AND COSMOLOGY ON THE ROOF

Miguel F. Morales*
University of Washington, Seattle, Seattle

10:00 Break

10:20 J1-6 THE LONG WAVELENGTH ARRAY: A DYNAMIC OBSERVATORY FOR RADIO ASTRONOMY EDUCATION

Jacob M. Hartman*[1], Gregory B. Taylor[2], Steven W. Ellingson[3]
[1]JPL, Pasadena, CA
[2]UNM, Albuquerque, NM
[3]VT, Blacksburg, VA

10:40 J1-7 SETI OPEN SOURCE DATA AND ANALYSIS TOOLS

Jon Richards*
The SETI Institute, Mountain View, CA

11:00 J1-8 SOFTWARE DEFINED RADIO: A LOW COST INTRODUCTION TO RADIO ASTRONOMY FOR MEXICAN UNIVERSITIES AND HIGH SCHOOLS

Stan E. Kurtz*[1], David E. Fields[2], Marcus D. Leech[3]
[1]Centro de Radioastronomia y Astrofisica, UNAM, Morelia, Michoacan, Mexico
[2]Tamke-Allan Observatory, Harriman, Tenn
[3]Shirleys Bay Radio Astronomy Consortium, Ottawa, Ontario, Canada

Session KB1: Emerging Diagnostic and Therapeutic Applications of Electromagnetics
Room 151

Co-Chairs: Mahta Moghaddam, *University of Michigan*
Susan Hagness, *University of Wisconsin-Madison*

08:20 KB1-1 MICROWAVE-INDUCED THERMOACOUSTIC IMAGING HYBRID FDTD MODELING AND EXPERIMENTAL STUDY

Ryan T. Jacobs*, Yiming Deng, Mark Golkowski
electrical engineering, University of Colorado Denver, Englewood, CO

08:40 KB1-2 THERMAL ACOUSTIC SIGNALS WITH DIFFERENT MICROWAVE PULSES AND DETECTION TARGETS

Xiong Wang*[1], Daniel Bauer[2], Russell Witte[2], Hao Xin[1]
[1]Electrical and Computer Engineering, the University of Arizona, Tucson, AZ
[2]Radiology, the University of Arizona, Tucson, AZ

09:00 KB1-3 SNR-ENHANCED INVERSE SCATTERING FOR MICROWAVE BREAST IMAGING

Matthew J. Burfeindt*, Susan C. Hagness, Barry D. Van Veen
Department of Electrical and Computer Engineering, University of Wisconsin-Madison, Madison, Wisconsin

09:20 KB1-4 EVALUATION OF A FULL-CAVITY NUMERICAL CHARACTERIZATION APPROACH FOR AN EXPERIMENTAL MICROWAVE BREAST IMAGING SYSTEM

Mark Haynes*, John Stang, Mahta Moghaddam
University of Michigan, Ann Arbor, Michigan

09:40 KB1-5 VIRTUAL ELECTRODES: INCREASING SPATIAL RESOLUTION OF NEURAL INTERFACES BEYOND THE ACTUAL ELECTRODE COUNT

Carlos J. Cela*, Kyle Loizos, Gianluca Lazzi
Electrical and Computer Engineering, University of Utah, Salt Lake City, UT

10:00 Break

10:20 KB1-6 A TRANSCUTANEOUS MICROWAVE THERMAL THERAPY SYSTEM PROTOTYPE FOR BREAST CANCER TREATMENT USING IMAGE BASED TIME-REVERSAL FOCUSING

John Stang*, Mark Haynes, Mahta Moghaddam
University of Michigan, Ann Arbor, MI

10:40 KB1-7 OPTIMIZATION APPROACH FOR MICROSTRIP SPIRAL ANTENNAS USED IN DEEP TISSUE RADIOMETRY

Sara Salahi*[1], Paolo Maccarini[2], Alina Boico[2], Paul Stauffer[2]
[1]*Biomedical Engineering, Duke University, Durham, NC*
[2]*Radiation Oncology, Duke University, Durham, NC*

11:00 KB1-8 MICROWAVE RADIOMETRY FOR NON-INVASIVE DETECTION OF VESICOURETERAL REFLUX (VUR)

Paul R. Stauffer*[1], Paolo F. Maccarini[1], Sara Salahi[1], Kavitha Arunachalam[2], Brent W. Snow[3]
[1]*Radiation Oncology, Duke University, Durham NC*
[2]*Engineering Design, Indian Institute of Technology, Madras, Chennai, India*
[3]*3Primary Childrens Medical Center, University of Utah, Salt Lake City, Utah*

11:20 KB1-9 MICROWAVE PROBE ARRAY FOR DIELECTRIC SURGICAL MARGIN TESTING

Paul M. Meaney*[1], Tian Zhou[2], Neil Epstein[1], Keith D. Paulsen[1]
[1]*Thayer School of Engineering, Dartmouth College, Hanover, NH*
[2]*Kuang-Chi Institute of Advanced Technology, Guangdong, China*

11:40 KB1-10 SENSOR DEVELOPMENT FOR IN VIVO DIELECTRIC PROPERTY MEASUREMENT

Camerin C. Hahn*, Sima Noghanian
University of North Dakota, North Dakota

Session AB1: Measurement and Numerical Uncertainties
Room 200

Co-Chairs: Amir Zaghloul, *Virginia Tech*
Roger Lang, *George Washington Uniiversity*

15:20 AB1-1 A METROLOGY INFRASTRUCTURE FOR SCIENTIFIC COMPUTING

Andrew M. Dienstfrey*
Information Tedchnology Laboratory, National Institute of Standards and Technology, Boulder, CO

15:40 AB1-2 METHODS OF ESTIMATING MEASUREMENT UNCERTAINTIES

Michael H. Francis*
Electromagnetics, National Institute of Standards and Technology, Boulder, Colorado

16:00 AB1-3 CHARACTERIZATION OF PARALLEL PLATE WAVEGUIDES FOR MATERIAL MEASUREMENTS

Youn M. Lee*[1], Amir I. Zaghloul[1,2]
[1]*SEDD, US Army Research Laboratory, Adelphi, MD*
[2]*Electrical and Computer Engineering, Virginia Tech, Falls Church, Virginia*

16:20 AB1-4 INCREASED ACCURACY IN THE MEASUREMENT OF THE DIELECTRIC CONSTANT OF SEAWATER AT 1.413 GHZ

Yiwen Zhou*, Roger Lang
Electrical and Computer Engineering, The George Washington University, Washington, DC

16:40 AB1-5 UNCERTAINTIES ASSOCIATED WITH POINT SOURCE MODELING IN FDTD

Gregory M. Noetscher*, Sergey N. Makarov
Electrical and Computer Engineering, Worcester Polytechnic Institute, Worcester, MA

Session B3: Guided Waves and Waveguiding Structures
Room 155

Co-Chairs: Leo Kempel, *Michigan State University*
Aly Fathy, *U. Tennessee*

13:20 B3-1 2.5D MICROMACHINED 240 GHZ CAVITY-BACKED COPLANAR WAVEGUIDE TO RECTANGULAR WAVEGUIDE TRANSITION

Mehrnoosh Vahidpour*, Kamal Sarabandi
University of Michigan, Ann Arbor, MI

13:40 B3-2 SMOOTHED SIGMOID AND STEPPED CIRCULARLY POLARIZED SEPTUM DESIGNS USING PARTICLE SWARM OPTIMIZATION

Ilkyu Kim*, Joshua Kovitz, Yahya Rahmat-Samii
Electrical Engineering Department, UCLA, Los Angeles and California

14:00 B3-3 ANALYSIS OF LAYERED ISOTROPIC AND GYROMAGNETIC MATERIALS IN A RECTANGULAR WAVEGUIDE

Benjamin R. Crowgey*, Ozgur Tuncer, Edward J. Rothwell, Leo C. Kempel, B Shanker
Electrical and Computer Engineering, Michigan State University, East Lansing, Michigan

14:20 B3-4 SURFACE WAVE PROPAGATION ALONG A ONE-DIMENSIONAL METAL CUT-WIRE ARRAY

Yang Li*[1], Hao Ling[2]
[1]*Electrical and Computer Engineering, Baylor University, Waco, Tx*
[2]*Electrical and Computer Engineering, The University of Texas at Austin, Austin, TX*

Session B4: Reflectarray antennas
Room 155

Co-Chairs: Sembiam Rengarajan, *California State University*
Kamal Sarabandi, *The University of Michigan*

15:20 B4-1 A NOVEL REFLECTARRAY ANTENNA BASED ON GROUNDED LOOP-WIRE MINIATURIZED ELEMENT

Arezou Edalati*, Kamal Sarabandi
EECS department, University of Michigan, Ann Arbor, MI

15:40 B4-2 ELECTRONICALLY-SCANNED REFLECTARRAY IMPACT ON MILLIMETER-WAVE IMAGING SYSTEM PERFORMANCE

Charles R. Dietlein*, Abigail S. Hedden, David A. Wikner
US Army Research Laboratory, Adelphi, MD

16:00 B4-3 EXPERIMENTAL VALIDATION OF SUB-REFLECTARRAY DISTORTION COMPENSATION TECHNIQUE FOR REFLECTOR ANTENNAS

Yahya Rahmat-Samii*, Harish Rajagopalan
Electrical Engineering, University of California Los Angeles (UCLA), Los Angeles, CA

16:20 B4-4 A STUDY OF PIECEWISE-PLANAR PARABOLIC REFLECTARRAYS

Sembiam R. Rengarajan*
Department of Electrical and Computer Engineering, California State University, Northridge, CA

16:40 B4-5 RADIATION ANALYSIS OF REFLECTARRAY ANTENNAS: NUMERICAL APPROACHES VERSUS FULL-WAVE SIMULATIONS

Payam Nayeri*, Fan Yang, Atef Z. Elsherbeni
Electrical Engineering, The University of Mississippi, University, MS

Session B5: Cognitive Radio and Radar
Room 1B40

Co-Chairs: Christos Christodoulou, *University of New Mexico*
Joel Johnson, *The Ohio State University*

13:20 B5-1 COGNITION AND RADAR SENSING

Chris J. Baker*, Graeme E. Smith
ECE, Ohio State University, Columbus, Ohio

13:40 B5-2 SOFTWARE DEFINED RADAR FOR COGNITIVE APPLICATIONS

Kyle B. Stewart*, Mark T. Frankford, Ninoslav Majurec, Joel T. Johnson
ElectroScience Lab, The Ohio State University, Columbus, OH

14:00 B5-3 A GREEDY APPROACH FOR SENSOR SELECTION AND POWER ALLOCATION IN A COGNITIVE RADAR NETWORK

Phani Chavali*, Arye Nehorai
Preston M Green Department of Electrical and Systems Engineering, Washington University in St Louis, St Louis, Missouri

14:20 B5-4 THE USE OF RECONFIGURABLE ANTENNAS IN A COGNITIVE RADIO ENVIRONMENT

Youssef Tawk[1], Joseph Costantine[2], Christos Christodoulou*[1]
[1]*Electrical and Computer Engineering Department, University of New Mexico, Albuquerque NM*
[2]*Electrical Engineering, California State University Fullerton, Fullerton CA*

14:40 B5-5 A FREQUENCY-TUNABLE PATTERN DIVERSITY ANTENNA FOR COGNITIVE RADIO APPLICATIONS

Ali Ramadan[1], Mohammed Al-Husseini[1], Youssef Tawk[2], Joseph Costantine[3], Christos Christodoulou*[2], Karim Kabalan[1], Ali El-Hajj[1]
[1]*Electrical and Computer Engineering Department, American University of Beirut, Beirut, Lebanon*
[2]*Electrical and Computer Engineering Department, University of New Mexico, Albuquerque, NM*
[3]*Electrical Engineering Department, California State University Fullerton, Fullerton, USA*

15:00 Break

15:20 B5-6 COUPLING ANALYSIS OF A NULL RECONFIGURABLE ELEMENT FOR SMALL ADAPTIVE PHASED ARRAYS

Matthew W. Young*, Jennifer T. Bernhard
Department of Electrical and Computer Engineering, University of Illinois at Urbana-Champaign, Urbana, IL

15:40 B5-7 A FREQUENCY RECONFIGURABLE SLOT ANTENNA USING MICROVASCULAR DELIVERY OF CONDUCTIVE LIQUID

Aaron J. King*[1], Jason F. Patrick[2], Nancy R. Sottos[3], Scott R. White[4], Gregory H. Huff[5], Jennifer T. Bernhard[1]
[1]*Department of Electrical and Computer Engineering, University of Illinois at Urbana-Champaign, Urbana, IL*
[2]*Department of Civil and Environmental Engineering, University of Illinois at Urbana-Champaign, Urbana, IL*
[3]*Department of Materials Science and Engineering, University of Illinois at Urbana-Champaign, Urbana, IL*
[4]*Department of Aerospace Engineering, University of Illinois at Urbana-Champaign, Urbana, IL*
[5]*Department of Electrical and Computer Engineering, Texas A&M University, College Station, TX*

16:00 B5-8 A COGNITIVE RADIO PLANAR ANTENNA SYSTEM WITH A RECONFIGURABLE SUBSTRATE HEIGHT

Joseph Costantine[1], Youssef Tawk[2], Joe Himmelheber[1], Mostafa Shiva[1], Christos G. Christodoulou*[2]
[1]*Electrical Engineering, California State University Fullerton, Fullerton, CA*
[2]*Electrical and Computer Engineering, University of New Mexico, Albuquerque,NM*

16:20 B5-9 A RECONFIGURABLE FILTER FOR COGNITIVE RADIO APPLICATIONS

Youssef Y. Tawk[1], Joseph Costantine[2], Christos Christodoulou*[1]
[1]*Electrical and Computer Engineering Department, University of New Mexico, Albuquerque NM*
[2]*Electrical Engineering, California State University Fullerton, Fullerton CA*

Session E1: High-Power Electromagnetics
Room 1B51

Co-Chairs: Everett Farr, *Farr Fields, LC*
Dave Giri, *Pro-Tech*

13:20 E1-1 A STANDARD FOR CHARACTERIZING ANTENNAS IN THE TIME DOMAIN

Everett G. Farr*
Farr Fields, LC, Albuquerque, NM

13:40 E1-2 THE EFFECT OF A LOCAL GROUNDPLANE ON THE RADIATION CHARACTERISTICS OF THE IMPULSE RADIATING ANTENNA (IRA)

D V. Giri*[1], F M. Tesche[2]
[1]*Pro-Tech, Alamo, CA*
[2]*EMConsultant, Saluda,NC*

14:00 E1-3 PHOTOIONIZATION PROCESSES IN LIGHTNING RETURN STROKE INITIATION CONDITIONS

Robert L. Gardner*
Consultant, Alexandria, VA

14:20 E1-4 X-RAYS PRODUCED BY FIRST AND SUBSEQUENT STROKES IN NATURAL LIGHTNING

Shreeharsh Mallick*[1], Vladimir A. Rakov[1], Joseph R. Dwyer[2], John A. Cramer[3]
[1]*Department of Electrical and Computer Engineering, University of Florida, Gainesville, Florida*
[2]*Department of Physics and Space Sciences, Florida Institute of Technology, Melbourne, Florida*
[3]*Vaisala Inc., Tucson, Arizona*

15:00 Break

15:20 E1-5 TIME DOMAIN FRACTAL LIGHTNING MODELING STUDY OF FIELD CHANGE ARRAY DATA

Can Liang*[1], Brant E. Carlson[1,2], Phillip M. Bitzer[3], Hugh J. Christian[3], Nikolai G. Lehtinen[1], Umran S. Inan[1,4]
[1]*electrical engineering, stanford university, stanford CA*
[2]*University of Bergen, Bergen, Norway*
[3]*University of Alabama, Huntsville,AL*
[4]*Electrical Engineering, Ko University, Rumelifeneri Yolu, Turkey*

15:40 E1-6 AUTOMATED AND ADAPTIVE RF EFFECTS TESTING

Everett G. Farr*[1], Leland H. Bowen[1], W. Scott Bigelow[1], Robert L. Gardner[2], Peter Finlay[3]
[1]*Farr Fields, LC, Albuquerque, NM*
[2]*Consultant, Alexandria, VA*
[3]*RDHA, Air Force Research Laboratory, Kirtland AFB, NM*

16:00 E1-7 RANDOM NON-DIRECTED AND DIRECTED GRAPH MODELS FOR MOBILE RESILIENT SENSOR AND INFORMATION SYSTEMS

Ira Kohlberg*
Kohlberg Assoicates, Inc., Reston, VA

Session F2: Passive Remote Sensing of the Earth's Environment: Sensors and Missions
Room 150

Co-Chairs: Albin Gasiewski, *University of Colorado at Boulder*
Steven Reising, *Colorado State University*

13:20 F2-1 NANOSATELLITES FOR EARTH ENVIRONMENTAL MONITORING: THE MICROMAS PROJECT

William J. Blackwell*[1], Gregory Allen[1], Mark Bury[1], Ronald Efromson[1], Christopher Galbraith[1], Timothy Hancock[1], R V. Leslie[1], Idahosa Osaretin[1], Larry Retherford[1], Michael Scarito[1], Michael Shields[1], David Toher[1], Kurt Wight[1], David W. Miller[2]
[1]*MIT Lincoln Laboratory, Lexington, MA*
[2]*MIT Space Systems Laboratory, Cambridge, MA*

13:40 F2-2 APPLICATION OF WIDEBAND SINGLE SIDEBAND THZ RECEIVERS TO SPACEBORNE MEASUREMENT OF CLOUD ICE

Albin J. Gasiewski*[1], William Deal[2], Michael McGrath[3], Frank Evans[4], Aaron Swanson[2], David Walker[5], Stefan Buehler[6], Ginger Drake[3], Neil White[3]
[1]*ECEE, University of Colorado at Boulder, Boulder, CO*
[2]*Northrop Grumman Corporation, Redondo Beach, CA*
[3]*Laboratory for Space Physics, University of Colorado at Boulder, Boulder, CO*
[4]*ATOC, University of Colorado at Boulder, Boulder, CO*
[5]*National Instutute of Standards and Technology, Boulder, CO*
[6]*Lulea Institute of Technology, Kiruna, Sweden*

14:00 F2-3 THE GEOSTAR ASIC DIGITAL CORRELATOR

Christopher Ruf*[1], Bruce Block[1], Michael Flynn[2], Phil Knag[2], Aaron Rocca[2], Zhangya Zhang[2], Todd Gaier[3], Bjorn Lambrigtsen[3], Alan Tanner[3]
[1]*Space Physics Research Laboratory, University of Michigan, Ann Arbor, MI*
[2]*Electrical Engineering and Computer Science, University of Michigan, Ann Arbor, MI*
[3]*Jet Propulsion Laboratory, California Institute of Technology, Pasadena, CA*

14:20 F2-4 DESIGN AND ANALYSIS OF A HYPERSPECTRAL MICROWAVE RECEIVER SUBSYSTEM

William J. Blackwell*[1], Christopher Galbraith[1], Timothy Hancock[1], R. V. Leslie[1], Idahosa Osaretin[1], Michael Shields[1], Paul E. Racette[2], Lawrence M. Hilliard[2]
[1]*MIT Lincoln Laboratory, Lexington, MA*
[2]*NASA Godddard Space Flight Center, Greenbelt MA*

14:40 F2-5 RFI-MITIGATING MULTICHANNEL DUAL POLARIZATION AIRBORNE L-BAND RADIOMETER

Fredrick S. Solheim*
Radiometrics Corporation, Boulder, CO

15:00 Break

15:20 F2-6 SIMULTANEOUS RETRIEVAL OF OCEAN SURFACE SALINITY AND WIND USING AQUARIUS COMBINED ACTIVE-PASSIVE L-BAND DATA

Simon Yueh*, Wenqing Tang, Alexander Fore
Jet Propulsion Laboratory, California Institute of Technology, Pasadena, CA

15:40 F2-7 THE GLOBAL PRECIPITATION MEASUREMENT (GPM) MISSION AND FALLING SNOW ALGORITHM DEVELOPMENT

Gail Skofronick-Jackson*, Arthur Y. Hou
Code 613.1, NASA Goddard Space Flight Center, Greenbelt, MD

16:00 F2-8 DEVELOPMENT AND DEMONSTRATION OF 92, 130, AND 166 GHZ RADIOMETERS FOR IMPROVED COASTAL WET-TROPOSPHERIC CORRECTION ON SWOT

Darrin Albers*[1], Alexander Lee[1], Steven C. Reising[1], Shannon T. Brown[2], Pekka Kangashlahti[2], Douglas E. Dawason[2], Todd C. Gaier[2], Oliver Montes[2], Daniel J. Hoppe[2], Behrouz Khayatian[2]
[1]*Microwave Systems Laboratory, Colorado State University, Fort Collins, CO*
[2]*Jet Propulsion Laboratory, California Institute of Technology, Pasadena, CA, Uniteds States*

16:20 F2-9 STABILITY OF MILLIMETER-WAVE RADIOMETERS USING INTERNAL CALIBRATION SOURCES

Chaitali R. Parashare*[1], Pekka P. Kangaslahti[1], Shannon T. Brown[1], Douglas E. Dawson[1], Todd C. Gaier[1], Sharmila Padmanabhan[1], Steven C. Reising[2], Oliver Montes[1], James S. Shell[1], Dennis Harding[1], Daniel Higley[1], Stephen Pomes[1]
[1]*Jet Propulsion Laboratory, California Institute of Technology, Pasadena, CA*
[2]*Electrical and Computer Engineering, Colorado State University, Fort Collins, CO*

16:40 F2-10 AIRBORNE AND FUTURE GEOSTATIONARY ATMOSPHERIC HUMIDITY MEASUREMENTS APPLYING THE LATEST LNA MMIC TECHNOLOGY

Pekka Kangaslahti*[1], Boon Lim[1], Todd C. Gaier[1], Alan Tanner[1], Mikko Varonen[1], Lorene Samoska[1], Shannon Brown[1], Bjorn Lambrigtsen[1], Steven C. Reising[2], Jordan Tanabe[1], Oliver Montes[1], Douglas E. Dawson[1], Chaitali Parashare[1]
[1]*Jet Propulsion Laboratory, California Institute of Technology, Pasadena, CA*
[2]*Microwave Systems Laboratory, Colorado State University, Fort Collins, CO*

Session G1: Radar and Radio Techniques
Room 105

Co-Chairs: Thomas Gaussiran, *Applied Research Laboratories, The University of Texas at Austin*
Terence Bullett, *CIRES, University of Colroado Boulder*

13:20 G1-1 LOW EARTH ORBIT SPECTRUM ANALYZER FOR IONOSPHERIC DISTURBANCES

Mario I. Ortega*, Anthony J. Bentley, Nicholas R. Clegg, Brian M. Hare, Michael J. Thomas, Rosemary R. Williams, Scott C. Wilson
Electrical and Computer Engineering, University of New Mexico, Albuquerque, New Mexico

13:40 G1-2 THE VARY-CHAP TOPSIDE ELECTRON DENSITY PROFILE FOR IRI AND GIRO

Bodo Reinisch*[1,2], Patrick Nsumei[1], Xueqin Huang[1], Dieter Bilitza[3]
[1]*University of Massachusetts Lowell, Lowell, MA*
[2]*Lowell Digisonde International, Lowell, MA*
[3]*George Mason University, Fairfax, VA*

14:00 G1-3 ASSIMILATION OF GIRO DATA IN THE REAL-TIME IRI

Ivan A. Galkin*[1], Bodo W. Reinisch[1,2], Xueqin Huang[1], Dieter Bilitza[3]
[1]*University of Massachusetts Lowell, Center for Atmospheric Research, Lowell, MA*
[2]*Lowell Digisonde International, LLC, Lowell, MA*
[3]*Space Weather Laboratory, George Mason University, Fairfax, VI*

14:20 G1-4 INITIAL ASSESSMENT OF THE NEW-GENERATION METEOR RADARS TO MEASURE GRAVITY WAVES MOMENTUM FLUXES

Diego Janches*[1], David C. Fritts[2], Wayne Hocking[3]
[1]*GSFC/Space Weather Lab, NASA, Greenbelt, MD*
[2]*CoRA Div, NorthWest Research Asociates, Boulder, CO*
[3]*Dept. of Physics, University of Western Ontario, London, ON, Canada*

14:40 G1-5 ELECTRIC FIELD AND CONDUCTIVITY VARIATIONS NEAR SUBSTORM ONSET TIMES

Krishna Prasad Gudivada*[1,2], Brenton.J Watkins[1]
[1]*Geophysical Institute, University of Alaska,Fairbanks, Fairbanks,Alaska*
[2]*Electrical Engineering, University of Alaska,Fairbanks, Fairbanks,Alaska*

15:00 Break

15:20 G1-6 INCOHERENT SCATTER RADAR ANALYSIS IN A FLEXIBLE SOFTWARE RADAR FRAMEWORK

Philip J. Erickson*, William C. Rideout, Frank D. Lind
Atmospheric Sciences Group, MIT Haystack Observatory, Westford, MA

15:40 G1-7 DIGITAL ARRAY RADAR FOR A GLOBAL GEOSPACE ARRAY

Frank D. Lind*, Philip J. Erickson, James R. Marchese
MIT Haystack Observatory, Westford, MA

16:00 G1-8 SEARCH FOR IONOSPHERIC EFFECTS AT 150 MHZ WITH PAPER

Nicole Gugliucci*[1], Richard Bradley[2]
[1]Astronomy, University of Virginia, Charlottesville, VA
[2]National Radio Astronomy Observatory, Charlottesville, VA

Session H2: Waves in Space and Laboratory Plasmas II
Room 245

Co-Chairs: Stephen Vincena, *University of California at Los Angeles*
Anatoly Streltsov, *Embry-Riddle Aeronautical University*

13:20 H2-1 EFFECT OF HALL CONDUCTIVITY ON FEEDBACK-UNSTABLE ULF WAVES AT HIGH LATITUDES

Nan Jia*, Anatoly Streltsov
Thayer School of Engineering, Hanover,NH

13:40 H2-2 OBSERVATION OF WHISTLER WAVE RESONANCES IN LABORATORY PLASMA

Bill Amatucci*[1], Dave Blackwell[1], Erik Tejero[1], Chris Cothran[2], Leonid Rudakov[3], Guru Ganguli[1], Dave Walker[2]
[1]Plasma Physics Division, Naval Research Laboratory, Washington, DC
[2]Global Strategies North America, Inc, Crofton, MD
[3]Icarus Research, Bethesda, MD

14:00 H2-3 LABORATORY STUDIES OF ELECTROMAGNETIC VELOCITY SHEAR-DRIVEN INSTABILITIES

Erik M. Tejero*[1], William E. Amatucci[1], Christopher Crabtree[1], Gurudas Ganguli[1], Christopher D. Cothran[2]
[1]Plasma Physics Divsion, Naval Research Laboratory, Washington, DC
[2]Sotera Defense Solutions, Crofton, MD

14:20 H2-4 USING LASER-PRODUCED ENERGETIC ELECTRONS TO MODEL IONOSPHERIC PHENOMENA IN THE LABORATORY

Stephen Vincena*
Department of Physics and Astronomy, University of California at Los Angeles, Los Angeles, CA

14:40 H2-5 SCATTERING OF LOWER HYBRID WAVES INTO WHISTLERS THROUGH DENSITY PERTURBATIONS

David D. Blackwell*[1], William E. Amatucci[1], Erik M. Tejero[1], Christoper D. Cothran[2]
[1]US Naval Research Laboratory, Washington DC
[2]Global Strategies Group North America Inc., Crofton, MD

15:00 Break

15:20 H2-6 THE EFFECTS OF KINETIC ALFVEN AND WHISTLER WAVE TURBULENCE AND THE EVOLUTION OF ELECTRON DISTRIBUTION IN SOLAR WIND PLASMA

Manish Mithaiwala*[1], Leonid Rudakov[2], Gurudas Ganguli[1], Chris Crabtree[1]
[1]Naval Research Laboratory, Washington DC
[2]Icarus Research Inc., Bethesda MD, US

15:40 H2-7 METHODOLOGY FOR INVESTIGATION OF IONOSPHERE PLASMA-WAVE PROCESSES IN THE NEAR SURFACE REGION OF SUPER-LARGE SPACE OBJECTS.

Stanislav I. Klimov*, Valery A. Grushin, Denis I. Novikov
Space Research Institute of the RAS, Moscow, Russian Federation

16:00 H2-8 ARBITRARY AMPLITUDE ION-ACOUSTIC SOLITONS IN DUSTY PLASMAS

Tatiana V. Losseva*, Sergey I. Popel, Anatoly P. Golub'
Russian Academy of Sciences, Institute of Geospheres Dynamics, Moscow,MO, Russian Federation

16:20 H2-9 DESIGN AND MULTIPACTING SIMULATION OF DOUBLE-GAP BUNCHER CAVITY

Ki R. Shin*[1], Yoon W. Kang[2], Aly E. Fathy[1]
[1]University of Tennessee, Knoxville, TN
[2]ORNL, Oak Ridge, TN

16:40 H2-10 SPACECRAFT CHARGING IN A DUST-RICH ENVIRONMENT

Hsiang-Wen Hsu*[1], Mihaly Horanyi[1], Sascha Kempf[1], Eberhard Gruen[1,2]
[1]LASP, University of Colorado at Boulder, Boulder, CO
[2]MPI fuer Kernphysik, Heidelberg, Germany

Session HG2: Lightning and its Interaction with the Ionosphere II
Room 200

Co-Chairs: Morris Cohen, *Stanford University*
Ningyu Liu, *Florida Institute of Technology*

13:20 HG2-1 REMOTE SENSING OF ELECTRIC FIELDS ABOVE THUNDERSTORMS VIA THE KERR EFFECT: INSTRUMENT STATUS

David Lauben*[1], Morris Cohen[1], Brant Carlson[2], Robert Marshall[1], Umran Inan[3]
[1]Stanford University, Stanford
[2]University of Bergen, Bergen, Norway
[3]Koc University, Instanbul, Turkey

13:40 HG2-2 HIGH ENERGY OBSERVATIONS OF TERRESTRIAL GAMMA-RAY FLASHES BY AGILE

Marco Tavani*[1], Martino Marisaldi[2], Fabio Fuschino[2], Claudio Labanti[2], Andrea Argan[3]
[1]INAF-IASF Roma, Rome, Italy
[2]INAF-IASF Bologna, Bologna, Italy
[3]INAF Headquarters, Rome, Italy

14:00 HG2-3 SPECTRAL AND TEMPORAL CHARACTERISTICS OF TERRESTRIAL GAMMA-RAY FLASHES PRODUCED BY ENERGETIC ELECTRONS DURING THE STEPPING OF LIGHTNING LEADERS

Sebastien J. Celestin*, Victor P. Pasko
Pennsylvania State University, University Park, Pennsylvania

Session J2: New Telescopes, Techniques, and Observations I
Room 265

Co-Chairs: Richard Prestage, *NRAO - Green Bank*
Richard Bradley, *National Radio Astronomy Observatory*

13:20 J2-1 THE ATACAMA LARGE MILLIMETER/SUBMILLIMETER ARRAY: AN UPDATE

Jeff Mangum*
National Radio Astronomy Observatory, Charlottesville, VA

13:40 J2-2 ALMA SYSTEM VERIFICATION

Richard A. Sramek*
National Radio Astronomy Observatory, Longmont, CO

14:00 J2-3 COMMISSIONING, OPERATIONS, AND EARLY RESULTS FOR THE LONG WAVELENGTH ARRAY

Joe Craig*
Physics and Astronomy, University of New Mexico, Albuquerque, Nm

14:20 J2-4 RESULTS FROM LWA1 COMMISSIONING: SENSITIVITY, BEAM CHARACTERISTICS, AND CALIBRATION

Steve Ellingson*
Virginia Tech, Blacksburg VA

14:40 J2-5 CURRENT OPTICS DESIGN FOR THE U.S. SKA TECHNOLOGY DEVELOPMENT PROJECT

William A. Imbriale*[1], Lynn Baker[2], German Cortes-Medellin[2]
[1]Jet Propulsion Laboratory, California Institute of Technology, Pasadena, CA
[2]Cornell University, Ithaca, NY

15:00 Break

15:20 J2-6 WIDEBAND 3-MM RECEIVER DEVELOPMENT FOR CARMA

James W. Lamb*
Radio Astronomy, California Institute of Technology, Big Pine, CA

15:40 J2-7 W-BAND HETERODYNE MODULE DEVELOPMENT FOR LARGE ARRAYS

Rohit S. Gawande*[1], Kieran Cleary[1], Anthony C. S. Readhead[1], Rodrigo Reeves[1], Todd C. Gaier[2], Pekka Kangaslahti[2], Lorene Samoska[2], Sarah Church[3], Matt Sieth[3], Patricia Voll[3], Andrew Harris[4]
[1]Astronomy, California Institute of Technology, Pasadena, CA
[2]Jet Propulsion Laboratory, Pasadena, CA
[3]Physics, Stanford University, Stanford, CA
[4]Astronomy, University of Maryland, College Park, MD

16:00 J2-8 A CRYOGENIC PROBE STATION FOR W-BAND MMIC LOW NOISE AMPLIFIERS

Rodrigo A. Reeves*[1], Kieran Cleary[1], Rohit Gawande[1], Anthony Readhead[1], Damon Russell[2], Sander Weinreb[2], Todd Gaier[3], Pekka Kangaslahti[3], Lorene Samoska[3], Mikko Varonen[3]
[1]Astronomy dept., Caltech, Pasadena, CA
[2]Electrical Engineering dept., Caltech, Pasadena,CA
[3]Jet Propulsion Lab, Pasadena, CA

16:20 J2-9 EFFICIENT SNAPSHOT CALIBRATION FOR POLARIMETRIC PHASED ARRAY RADIOMETERS

Taylor D. Webb*, Karl F. Warnick
Electrical and Computer Engineering, Brigham Young University, Provo, Utah

16:40 J2-10 THE IMPROVED C-BAND SYSTEM ON THE VLBA

Steven J. Durand*, Robert H. Hayward
National Radio Astronomy Observatory, Socorro, New mexico,

Session K1: Telemetry for Monitoring and Biosensing
Room 151

Co-Chairs: Erdem Topsakal, *Mississippi State University*
William Chappell, *Purdue University*

13:20 K1-1 PORCINE MODELS IN TELEMETRY: HYDRATION EFFECTS AND TISSUE STORAGE PROTOCOL

Robbin Bertucci*[1], Jun Liao[1], Erdem Topsakal[2]
[1]*Agricultural and Biological Engineering, Mississippi State University, Starkville, MS*
[2]*Electrical and Computer Engineering, Mississippi State University, Starkville, MS*

13:40 K1-2 SPECIFIC ABSORPTION RATIO (SAR) REDUCTION IN WIRELESS POWER TRANSFER SYSTEM USING MULTI-COIL APPROACH

Anil K. RamRakhyani*, Gianluca Lazzi
ECE, University of Utah, Salt lake City, Utah

14:00 K1-3 MINIATURIZED, PARYLENE-BASED, WIRELESS INTRAOCULAR PRESSURE SENSOR SYSTEM USING HARMONIC DETECTION TECHNIQUE

Tse-Yu Lin*[1], Byungguk Kim[1], Dohyuk Ha[1], Wilhelmine N. de Vries[2], Robin W. Irazoqui[3], Simon W. M. John[2], Pedro P. Irazoqui[1], William J. Chappell[1]
[1]*Purdue University, West Lafayette, IN*
[2]*The Jackson Laboratory, Bar Harbor, ME*
[3]*Universitat de Girona, Girona, Catalua, Spain*

14:20 K1-4 DETERMINING THE RELATIVE PERMITTIVITY OF HUMAN BODY MASSES

Safa Salman*, Dimitris Psychoudakis, John L. Volakis
The Electrosience Laboratory, The Ohio State University - The Electroscience Laboratory, COLUMBUS, Ohio

14:40 K1-5 A MINIATURIZED IMPLANTABLE ANTENNA FOR CONTINUOUS GLUCOSE MONITORING

Kristin Sharp*, Erdem Topsakal
Electrical and Computer Engineering, Mississippi State University, Mississippi State, MS

15:00 Break

15:20 K1-6 INTEGRATION OF CELL PHONE IMAGING WITH MICROCHIP ELISA TO DETECT OVARIAN CANCER HE4 BIOMARKER IN URINE AT THE POINT-OF-CARE

ShuQi Wang[1], Xiaohu Zhao[1], Imran Khimji[1], Ragip Akbas[2], Weiliang Qiu[3], Dale Edwards[4], Daniel W. Cramer[4], Bin Ye[4], Utkan Demirci*[1,5]
[1]*Demirci Bio-Acoustic-MEMS in Medicine (BAMM) Laboratory, Harvard Medical School, Brigham and Women's Hospital,, Cambridge*
[2]*Autodesk, Inc., Manchester*
[3]*Channing Laboratory, Harvard Medical School, Brigham and Women's Hospital,, Boston*
[4]*Department of Obstetrics and Gynecology and Reproductive Biology, Harvard Medical School, Brigham and Women's Hospital,, Boston*
[5]*Harvard Medical School, Harvard-MIT Health Sciences & Technology, Cambridge*

15:40 K1-7 ROBUST AND EFFICIENT RECONFIGURABLE RF FRONT END FOR IMPLANTABLE BIOMEDICAL DEVICES

Anatoly A. Yakovlev*, Ada S. Y. Poon
Electrical Engineering, Stanford University, Stanford, CA

16:00 K1-8 A NON-INVASIVE TECHNIQUE FOR BLOOD GLUCOSE MONITORING

Erdem Topsakal, Mina Tahai*
Electrical and Computer Engineering, Mississippi State University, Mississippi State, MS

16:20 K1-9 COMPACT NESTED DIPOLE PROBE FOR NEAR-FIELD RADIOMETRIC TEMPERATURE MEASUREMENT OF THE BODY

Rob Scheeler*, Xavier Palomer, Zoya Popovic
Dept. Electrical, Computer, and Energy Engineering, University of Colorado at Boulder, Boulder, Colorado

Business Meetings

17:00	Commission E	Room 1B51
17:00	Commission F	Room 150
17:00	Commission H	Room 245
18:00	Commission D	Room 155
18:00	Commission K	Room 151

Reception

Engineering Center Lobby 18:30-21:00
(Beer and Wine provided)

Plenary Session: Ernest K. Smith USNC-URSI Student Paper Competition
Mathematics Auditorium

Chair: Danilo Erricolo, University of Illinois at Chicago

8:20 Announcements

8:30 Rules and Guidelines of the Competition

8:40 Student Paper Presentations

9:40 Break

Session P2: Meeting Highlight: Global Navigation Satellite Systems and Radio Science
Mathematics Auditorium

Co-Chairs: Frank Lind, USNC Commission G Chair (2009-2011), *MIT Haystack Observatory*
Bill Amatucci, USNC Commission H Chair (2009-2011), *Naval Research Laboratory*

10:20 P2-1 OBSERVING GEOSPACE WITH GPS

Anthea J. Coster*
MIT Haystack Observatory, Westford, MA

10:40 P2-2 EVOLUTION OF THE GLOBAL NAVIGATION SATELLITE SYSTEM (GNSS)

Christopher J. Hegarty*
The MITRE Corporation, Bedford, MA

11:40 Awards Ceremony for Student Paper Competition

12:00 Lunch for Student Travel Awardees, USNC Officers and Commission Chairs (Leeds Business School Atrium)

Session B6: Antenna Theory, Design and Measurement
Room 155

Co-Chairs: Donald Wilton, *University of Houston*
Edward Rothwell, *Michigan State University*

13:20 B6-1 ESTIMATES OF Q FOR PATCH ANTENNAS HAVING MAGNETODIELECTRIC SUBSTRATES

Steven Weiss*
SEDD, US Army Research Lab, Adelphi, MD

13:40 B6-2 BANDWIDTH LIMITS FOR LOW PROFILE SCANNING ARRAYS

Jonathan P. Doane*, Kubilay Sertel, John Volakis
ElectroScience Laboratory, Ohio State University, Columbus, OH

14:00 B6-3 SURFACE TOLERANT EBG-DIPOLE AND FAT-FOLDED-DIPOLE RFID TAG ANTENNAS: A COMPARATIVE STUDY

Harish Rajagopalan*, Yahya Rahmat-Samii
Electrical Engineering, UCLA, Los Angeles

14:20 B6-4 METHODS TO ACHIEVE CIRCULAR POLARIZATION AND BANDWIDTH ENHANCEMENT FOR MESHED PATCH ANTENNAS

Tursunjan Yasin*, Reyhan Baktur
ECE, Utah State University, Logan, Utah

14:40 B6-5 BROADBAND PROBE-FED AND APERTURE-COUPLED CYLINDRICAL DIELECTRIC RESONATOR ANTENNAS

Adam P. Huynh*, David R. Jackson, Stuart A. Long, Donald R. Wilton
Electrical and Computer Engineering, University of Houston, Houston TX

15:00 Break

15:20 B6-6 AN OPTICAL ALIGNMENT TOOL FOR SIMULTANEOUS IMAGING AND PRECISION ALIGNMENT OF TWO MM-WAVE ANTENNAS

Joshua A. Gordon*, David R. Novotny
PML, NIST, Boulder, CO

15:40 B6-7 MULTIPLE-BEAM CONTROL AND SWITCHING USING A LUNEBURG LENS ANTENNA

Rafael A. Sabory-Garcia*, Min Liang, Wei-Ren Ng, Michael E. Gehm, Hao Xin
Electrical and computer Engineering, University of Arizona, Tucson, Arizona

16:00 B6-8 ANALYSIS AND DESIGN PROCESS OF A STRIPLINE ARCHIMEDEAN SPIRAL ANTENNA

Teng-Kai Chen*, Gregory H. Huff
Department of Electrical and Computer Engineering, Texas A&M University, College Station, TX

16:20 B6-9 UNDERSTANDING THE CROSS-POL GENERATION IN PATCH ANTENNAS: A NEAR-FIELD APPROACH

Shubhendu Bhardwaj*, Yahya Rahmat-Samii
University of California, Los Angeles, CA

Session B7: Metamaterials II
Room 1B40

Co-Chairs: Arthur Yaghjian, *Research Consultant*
Filippo Capolino, *University of California Irvine*

13:20 B7-1 ELECTROMAGNETIC WAVE TUNNELING THROUGH MULTIPLE EPSILON-NEGATIVE METAMATERIAL LAYERS: A MICROWAVE FILTER THEORY APPROACH

Chien-Hao Liu*, Nader Behdad
Electrical and Computer Engineering, University of Wisconsin-Madison, Madison

13:40 B7-2 WAVEGUIDE POWER DIVIDER BASED ON ENZ MATERIAL

Santosh Seran*, John P. Donohoe
Department of Electrical and Computer Engineering, Mississippi State University, Starkville,MS

14:00 B7-3 SUPERCOUPLING OF ELECTROMAGNETIC ENERGY FROM A WAVEGUIDE TO FREE SPACE USING ENZ MATERIALS

Santosh Seran*, John P. Donohoe
Department of Electrical and Computer Engineering, Mississippi State University, Starkville,MS

14:20 B7-4 EFFECT OF SCATTERER SIZE VARIATIONS ON THE REFLECTION AND TRANSMISSION PROPERTIES OF A METAFILM

Kendra Kumley*, Edward F. Kuester
Electrical, Computer and Energy Engineering, University of Colorado Boulder, Boulder, Colorado

14:40 B7-5 GENERALIZED RETRIEVAL PROCEDURE TO DETERMINE LOCAL EFFECTIVE PARAMETERS OF METAMATERIALS BASED ON FIRST-PRINCIPLE HOMOGENIZATION THEORY

Xing-Xiang Liu*, Andrea Alu
Electrical and Computer Engineering, The university of Texas at Austin, AUSTIN

15:00 Break

15:20 B7-6 EXACT REPRESENTATION OF 3D PERIODIC METAMATERIAL ARRAYS BY GENERALIZED ELECTRIC AND MAGNETIC POLARIZATION DENSITIES

Arthur D. Yaghjian*
Research Consultant, Concord, MA

15:40 B7-7 TRAVELING WAVES ON THREE-DIMENSIONAL SIMPLE-TETRAGONAL PERIODIC ARRAYS OF TWO DIFFERENT MAGNETODIELECTRIC SPHERES

Nicola Bowler*[1], Yang Li[2]
[1]*Materials Science and Engineering, Iowa State University, Ames, IA*
[2]*Electrical and Computer Engineering, Iowa State University, Ames, IA*

16:00 B7-8 COMPLEX MODES AND ARTIFICIAL MAGNETISM IN COMPOSITE MATERIALS MADE OF SPHERICAL PARTICLES ACCOUNTING FOR COUPLED ELECTRIC AND MAGNETIC DIPOLES

Salvatore Campione*, Filippo Capolino
University of California, Irvine, Irvine, CA

16:20 B7-9 MULTI-LAYER TENSOR IMPEDANCE SURFACE ANALYSIS

Amit M. Patel*, Anthony Grbic
Electrical Engineering and Computer Science, University of Michigan, Ann Arbor, MI

16:40 B7-10 SMALL ANTI-JAM GPS ARRAYS LOADED WITH METAMATERIAL ISOLATORS FOR REDUCED MUTUAL COUPLING

Ahmad A. Gheethan*, Gokhan Mumcu
University of South Florida, Tampa, FL

Session C1: Radar Signal Processing, Target Detection, Localization, and Tracking
Room 1B51

Co-Chairs: Fernando Teixeira, *Ohio State University*
Eric Mokole, *Naval Research Laboratory*

15:20 C1-1 A PASSIVE BISTATIC RADAR FOR DETECTION OF AIRCRAFT USING NON-COOPERATING SPACEBORNE TRANSMITTERS

William C. Barott*, Brian Butka
Electrical, Computer, Software, and Systems Engineering Department, Embry-Riddle Aeronautical University, Daytona Beach, FL

15:40 C1-2 TIME-REVERSAL BASED CHANGE DETECTION ALGORITHM FOR GROUND PENETRATING RADAR APPLICATIONS

Mehmet E. Yavuz[1], Ahmed E. Fouda*[2], Fernando L. Teixeira[2]
[1]*Intel Corporation, Hillsboro, OR*
[2]*ElectroScience Lab., Dept. of Electrical and Computer Engineering, The Ohio State University, Columbus, OH*

16:00 C1-3 INTEGRATION OF SI/SIGE TRANSMITTER TOWARDS SUB-MILLIMETER ACCURACY FOR UWB SYSTEM

Essam A. Elkhouly*[1], Dayang Lin[2], Quanhua Liu[1], Aly Fathy[1], Hermann Schumacher[2], Mohamed Mahfouz[3]
[1]*EECS, University of Tennessee, Knoxville, TN*
[2]*Institut fr Elektronische Bauelemente und Schaltungen, Ulm University, Ulm, Germany*
[3]*MABE, University of Tennessee, Knoxville, TN*

16:20 C1-4 A SUB-WAVELENGTH RF SOURCE TRACKING DEVICE FOR GPS-DENIED ENVIRONMENTS

Fikadu T. Dagefu*, Kamal Sarabandi
Electrical Engineering and Computer Science, University of Michigan, Ann Arbor

16:40 C1-5 PARAMETRIC AND EXPERIMENTAL STUDY ON THE STATISTICAL STABILITY OF ULTRAWIDEBAND TIME-REVERSAL IMAGING IN RANDOM MEDIA

Ahmed E. Fouda*, Victor Lopez-Castellanos, Fernando L. Teixeira
ElectroScience Lab., Dept. of Electrical and Computer Engineering, The Ohio State University, Columbus, OH

Session D1: THz Devices and their Characterization I
Room 105

Co-Chairs: Zoya Popovic, *University of Colorado*
Erich Grossman, *NIST*

13:20 D1-1 DEVICE AND SYSTEM CHALLENGES FOR VIDEO-RATE THZ RADAR IMAGING

Ken B. Cooper*
Jet Propulsion Laboratory, Pasadena, CA

13:40 D1-2 MODULATED MULTIMODE MIXING ILLUMINATION FOR THE ELIMINATION OF SPECKLE AND TARGET ORIENTATION REQUIREMENTS IN ACTIVE IMAGING

Frank C. De Lucia[1], Mark A. Patrick*[1], Colin D. Joye[2]
[1]*Physics, Ohio State University, Columbus, OH*
[2]*U. S. Naval Research Laboratory, Washington, DC*

14:00 D1-3 APPLICATION OF PHOTONIC PROCESSING TO INTERFEROMETRIC PASSIVE MILLIMETER-WAVE IMAGING

Christopher A. Schuetz*[1], Richard D. Martin[1], Thomas E. Dillon[1], Julien Macario[2], Peng Yao[2], Dennis W. Prather[2]
[1]*Phase Sensitive Innovations, Inc., Newark, DE*
[2]*Electrical and Computer Engineering, University of Delaware, Newark, DE*

14:20 D1-4 TERAHERTZ CHARACTERIZATION OF BIOLOGICAL TISSUES

Woon-Gi Yeo*, Niru K. Nahar, Robert Lee, John L. Volakis, Charles L. Hitchcock
Ohio State University, Columbus

14:40 D1-5 IN VIVO THZ MEDICAL IMAGING

Zachary Taylor*[1], Jun Sung[1], Rahul Singh[1], Martin Culjat[1], Jean Pierre Hubschman[2], Neha Bajwa[1], Priyamvada Tewari[1], Elliott Brown[3], Warren Grundfest[1]
[1]*Bioengineering, UCLA, Los Angeles*
[2]*Jules Stein Eye Institute, UCLA, Los Angeles*
[3]*Physics, Wright State University, Dayton*

15:00 Break

15:20 D1-6 HETEROSTRUCTURE BACKWARD DIODE DETECTORS FOR MILLIMETER-WAVE THROUGH THZ DETECTION AND IMAGING

Patrick Fay*, Ze Zhang, Yi Xie, Md. Itrat Shams
Dept. of Electrical Engineering, Univ. of Notre Dame, Notre Dame, IN

15:40 D1-7 MEMS-BASED UNCOOLED THZ DETECTORS FOR STARING IMAGERS

J. A. Cox*, R. Higashi, F. Nusseibeh, C. Zins
Honeywell Sensors & Wireless Laboratory, Plymouth, MN

16:00 D1-8 CHARACTERIZATION OF THZ POWER DETECTORS AT 119UM AND 394UM WAVELENGTHS

Nina P. Basta*, John Lehman, Erich Grossman, Marla Dowell
National Institute of Standards and Technology, Boulder, CO

16:20 D1-9 WAVEGUIDE FLANGE MISALIGNMENT AND CALIBRATION AT SUBMILLIMETER WAVELENGTHS

Robert M. Weikle*[1], Huilin Li[1], Alexander I. Arsenovic[1], Jeffrey L. Hesler[2], Anthony R. Kerr[3]
[1]*Electrical Engineering, University of Virginia, Charlottesville, Virginia*
[2]*Virginia Diodes, Inc., Charlottesville, VA*
[3]*National Radio Astronomy Observatory, Charlottesville, VA*

16:40 D1-10 DEVELOPMENT OF A CALIBRATED FREQUENCY-DOMAIN SCATTEROMETER IN THE MMWAVE TO SUB-TERAHERTZ RANGE

David R. Novotny*, Joshua Gordon, Edwin Heilweil, Shu-Zee Lo, Erich Grossman, Brian Stillwell, Jeffrey Guerrieri
Physical Measurements Laboratory, National Institute of Standards and Technology, Boulder, CO

Session F3: Radar Remote Sensing of Precipitation
Room 150

Co-Chairs: Guifu Zhang, *University of Oklahoma*
Chandrasekar V Chandra, *Colorado State University*

13:20 F3-1 A BAYES ALGORITHM TO SEPARATE PRECIPITATION FROM GROUND CLUTTER USING SCAN-TO-SCAN CORRELATION TECHNIQUE

Yinguang Li*[1,2], Guifu Zhang[2,3], Richard Doviak[4], Darcy Saxion[5]
[1]*School of Electrical and Computer Engineering, The University of Oklahoma, Norman, OK*
[2]*Atmospheric Radar Research Center, The University of Oklahoma, Norman, OK*
[3]*School of Meteorology, The University of Oklahoma, Norman, OK*
[4]*National Severe Storms Laboratory, NOAA, Norman, OK*
[5]*Radar Operation Center, NOAA, Norman, OK*

13:40 F3-2 TWO-YEAR EVALUATION OF THE QUANTITATIVE PRECIPITATION ESTIMATION IN THE CASA IP5 WEATHER RADAR NETWORK TEST BED

V. Chandrasekar*, Haonan Chen
Department of Electrical and Computer Engineering, Colorado State University, Fort Collins, Colorado

14:00 F3-3 DROP SIZE DISTRIBUTION RETRIEVAL USING DUAL FREQUENCY AND DUAL POLARIZATION GROUND RADAR

Minda Le*[1], V. Chandrasekar[2]
[1]*Electrical and computer engineering, Colorado State University, fort collins,CO*
[2]*Colorado State University, fort collins,CO*

14:20 F3-4 A WINTER STORM TRANSITION REVEALED WITH POLARIMETRIC RADAR AND 2DVD OBSERVATIONS

Petar Bukovcic*[1,2,3,4], Dusan Zrnic[2], Guifu Zhang[3,4]
[1]*Cooperative Institute for Mesoscale Meteorological Studies, University of Oklahoma, Norman, Okalhoma*
[2]*National Severe storms Laboratory, NOAA, Norman, Okalhoma*
[3]*School of Meteorology, University of Oklahoma, Norman, Okalhoma*
[4]*Atmospheric Radar Research Center, University of Oklahoma, Norman, Okalhoma*

15:00 Break

15:20 F3-5 VERTICAL PROFILES STATISTICS OF POLARIMETRIC RADAR MEASUREMENTS IN THE MEDITERRANEAN REGION

Renzo Bechini[1], V. Chandrasekar*[2], Luca Baldini[3]
[1]*Arpa Piemonte, Torino, Italy*
[2]*Colorado State University, Fort Collins, CO*
[3]*ISAC-CNR, Roma, Italy*

15:40 F3-6 A NEW 449 MHZ WIND PROFILER RADAR WITH LOW COST 3 KW TRANSMITTER

Brad Lindseth*[1,2], William O. J. Brown[1], Jim Jordan[3], Daniel Law[3], Terry Hock[1], Stephen A. Cohn[1], Zoya Popovic[2]
[1]*Earth Observing Laboratory, National Center for Atmospheric Research, Boulder, CO*
[2]*Electrical and Computer Engineering, University of Colorado, Boulder, CO*
[3]*National Oceanic and Atmospheric Administration, Boulder, CO*

16:00 F3-7 CROSS-POLARIZATION REDUCTION OF THE PHASED ARRAY RADAR FOR PRECIPITATION MEASUREMENTS

Shaya Karimkashi*, Guifu Zhang
ARRC, University of Oklahoma, Norman, OK

Session G2: Ionospheric Space Weather Events and Models
Room 200

Co-Chairs: Anthea Coster, *MIT Haystack Observatory*
Attila Komjathy, *NASA JPL/Caltech*

13:20 G2-1 TOTAL ELECTRON CONTENT ANOMALY OVER MID-NORTH AMERICA

Alexander P. Davidson*[1], Anthea J. Coster[2], Shunrong Zhang[2], Evan Thomas[3]
[1]*Phillips Academy Andover, Andover, MA*
[2]*MIT Haystack Observatory, Westford, MA*
[3]*Bradley Department of Electrical and Computer Engineering, Virginia Tech, Blacksburg, VA*

13:40 G2-2 MODELING MSTID PROPAGATION WITH THE SAMI3 FRAMEWORK

Timothy Duly*[1], Jonathan J. Makela[1], Joe Huba[2], Jonathan Krall[2]
[1]*University of Illinois at Urbana-Champaign, Urbana, IL*
[2]*Naval Research Laboratory, Washington D.C.*

14:00 G2-3 GLOBAL OBSERVATIONS OF SUB-AURORAL POLARIZATION STREAM (SAPS) EVENTS FROM MID-LATITUDE SUPERDARN RADARS

Joseph B. H. Baker*[1], Lasse B. N. Clausen[2], Bharat S. R. Kunduri[1], J. Michael Ruohoniemi[1], Evan G. Thomas[1]
[1]*Center for Space Science and Engineering Research, Virginia Tech, Blacksburg, VA*
[2]*Institute for Geophysics and Extraterrestrial Physics, University of Braunschweig, Braunschweig, Germany*

14:20 G2-4 COMPARISONS OF THE NRL SAMI3 PHYSICS-BASED IONOSPHERIC MODEL WITH GLOBAL IONOSONDE, GPS, AND COSMIC ELECTRON DENSITY MEASUREMENTS

Carl L. Siefring*[1], Paul A. Bernhardt[1], Anish Tondwalkar[2], Joseph D. Huba[1], Jonathan F. Krall[1], Sarah E. McDonald[3], John T. Emmert[3], Douglas P. Drob[3], Judith L. Lean[3], Glenn Joyce[4]
[1]Plasma Physics Division, Naval Research Laboratory, Washington, DC
[2]ASEE Science and Engineering Appretice Program, Naval Research Laboratory, Washington, DC
[3]Space Sciences Division, Naval Research Laboratory, Washington, DC
[4]Icarus Research, Inc, Bethesda, MD

14:40 G2-5 SIMULTANEOUS OBSERVATIONS OF MID-LATITUDE IONOSPHERIC DENSITY STRUCTURES BY SUPERDARN RADARS AND THE GLOBAL GPS RECEIVER NETWORK

Evan G. Thomas*[1], Joseph B. H. Baker[1], J Michael Ruohoniemi[1], Lasse B. N. Clausen[2], Anthea J. Coster[3]
[1]Bradley Dept. of Electrical and Computer Engineering, Virginia Tech, Blacksburg, VA
[2]Institute for Geophysics and Extraterrestrial Physics, TU Braunschweig, Braunschweig, Lower Saxony, Germany
[3]Atmospheric Sciences Group, MIT Haystack Observatory, Westford, MA

15:00 Break

15:20 G2-6 THE EFFECTS OF 3D ERROR COVARIANCE AND BACKGROUND MODEL BIAS FOR AN IONOSPHERIC DATA ASSIMILATION MODEL

Chi-Yen Lin*[1,2,3], Tomoko Matsuo[1,2], Eduardo A. Araujo-Pradere[1,2], Jann-Yenq Liu[3]
[1]Cooperative Institute for Research in Environmental Sciences, University of Colorado, Boulder, CO.
[2]Space Weather Prediction Center, National Oceanic and Atmospheric Administration, Boulder, CO.
[3]Institute of space science, National Central University, Jhongli, TAIWAN, TAIWAN

15:40 G2-7 DATA ASSIMILATION OF FORMOSAT-3/COSMIC ELECTRON DENSITIES USING THE NCAR TIE-GCM

I-Te Lee*[1,2], Tomoko Matsuo[3], Arthur Richmond[2], Jann-Yenq Liu[2], Wenbin Wang[1], Ming-Quey Chen[2], Charles Lin[4]
[1]National Center for Atmospheric Research, High Altitude Observatory, Boulder,CO
[2]National Central University, Institute of Space Science, Taoyuan, Taiwan
[3]University of Colorado at Boulder, Boulder,CO
[4]National Cheng Kung University, Department of Earth Science, Tainan, Taiwan

16:00 G2-8 THE TAIWAN IONOSPHERIC MODEL (TWIM) AND ITS APPLICATIONS ON HF PROPAGATION AND GPS IONOSPHERIC CORRECTION

Lung-Chih Tsai*[1,2], Ernest P. Macalalad[2], G. H. Chen[3], M. H. Tian[4]
[1]Center for Space and Remote Sensing Research, National Central University, Professor, Chung-Li, Taiwan
[2]Institute of Space Science, National Central University, Chung-Li, Taiwan
[3]Multimedia and Game Science Department, Taipei College of Maritime Technology, Taipei, Taiwan
[4]Department of Marine Leisure and Tourism, Taipei College of Maritime Technology, Taipei, Taiwan

16:20 G2-9 TRIPL-DA- BACKGROUND ENSEMBLE MODELS AND DATA ERRORS

Thomas L. Gaussiran*, Roy S. Calfas, David Rainwater
Applied Research Laboratories, The University of Texas at Austin, Austin, TX

16:40 G2-10 A ROUTINE VALIDATION OF NEAR-REAL TIME GAIM ASSIMILATION OF GROUND AND SPACE-BORNE GPS TEC DATA USING INDEPENDENT DATA SOURCES

Attila Komjathy*, Philip Stephens, Mark Butala, Brian Wilson, Olga Verkhoglyadova, Anthony Mannucci
NASA JPL/Caltech, Pasadena, California

Session H3: Physics of the Radiation Belts
Room 245

Co-Chairs: Mark Golkowski, *University of Colorado Denver*
Chris Crabtree, *NRL*

13:20 H3-1 SIMULATIONS OF RADIATION BELT ELECTRON DYNAMICS IN HIGH-SPEED-STREAM STORMS

Anthony A. Chan*[1], Yen-fei Chen[1], Scot R. Elkington[2]
[1]*Physics and Astronomy, Rice University, Houston, Texas*
[2]*LASP, University of Colorado, Boulder, Colorado*

13:40 H3-2 WHISTLER MODE SIGNALS AT L=1.9 CONJUGATE TO A RUSSIAN ALPHA TRANSMITTER: STATISTICS AND MODELING

Morris B. Cohen*[1], Mark A. Golkowski[2], Nikolai G. Lehtinen[1], Umran S. Inan[1,3], Michel Parrot[4]
[1]*Electrical Engineering, Stanford University, Stanford, CA*
[2]*Electrical Engineering, University of Colorado at Denver, Denver, CO*
[3]*Electrical Engineering, Koc University, Sariyer Istanbul, Turkey*
[4]*LPC2E, CNRS, Orleans, France*

14:00 H3-3 NEW PROXY FOR THE ANALYSIS OF NON-LINEAR WAVE GROWTH IN CHORUS WAVES AND TRIGGERED EMISSIONS

Mark Golkowski*[1], Andrew Gibby[2]
[1]*Electrical Engineering, University of Colorado Denver, Denver, CO*
[2]*Arion Systems Inc., Chantilly, VA*

14:20 H3-4 KEY PARAMETERS CONTROLLING THE NONLINEAR CYCLOTRON INSTABILITY FOR WHISTLER MODE WAVES IN THE MAGNETOSPHERE

Vijay Harid*[1], Mark Golkowski[2], Morris Cohen[1], Timothy F. Bell[1], Umran S. Inan[1]
[1]*Electrical Engineering, Stanford University, Stanford, CA*
[2]*Electrical Engineering, University of Colorado, Denver, Denver, CO*

14:40 H3-5 OFF EQUATORIAL CHORUS WAVES OBSERVED BY THE POLAR PLASMA WAVE INSTRUMENT AND IMPLICATIONS FOR THE RADIATION BELTS

Nicholas L. Bunch*[1], Maria Spasojevic[1], Yuri Y. Shprits[1], Daniel I. Golden[2,3]
[1]*STAR Lab, Dept. of Electrical Engineering, Stanford University, Stanford*
[2]*Institute of Geophysics and Planetary Physics, University of California at Los Angeles, Los Angeles*
[3]*Department of Atmospheric Sciences, University of California at Los Angeles, Los Angeles*

15:00 Break

15:20 H3-6 WEAK TURBULENCE IN THE MAGNETOSPHERE: FORMATION OF WHISTLER WAVE CAVITY BY NONLINEAR SCATTERING

Chris E. Crabtree*[1], Leonid Rudakov[2], Gurudas Ganguli[1], Manish Mithaiwala[1], Vitaly Galinsky[3], Valentin Shevchenko[3]
[1]*Division of Plasma Physics, NRL, Washington*
[2]*Icarus Research Inc., Bethesda, MD*
[3]*University of California, San Diego, CA*

15:40 H3-7 MODELING QUASI-LINEAR AND NONLINEAR WAVE-PARTICLE INTERACTIONS IN THE RADIATION BELTS

Jay M. Albert*
Air Force Research Lab, Albuquerque, NM

16:00 H3-8 ENHANCED SCATTERING AT SELECTED ELECTRON ENERGIES BY DISPERSING LIGHTNING WHISTLERS

David S. Lauben*[1], Timothy F. Bell[1], Nikolai G. Lehtinen[1], Umran S. Inan[2]
[1]*Stanford University, Stanford*
[2]*Koc University, Istanbul, Turkey*

Session J3: Timely Technical Tutorials
Room 265

Co-Chairs: Richard Bradley, *National Radio Astronomy Observatory*
Tommy Thompson, *NASA*

13:20 J3-1 DELAY/DELAY-RATE FILTERS FOR LOW-FREQUENCY INTERFEROMETERS

Aaron R. Parsons*
University of California, Berkeley, Berkeley, CA

14:00 J3-2 MOFF CORRELATOR

Miguel F. Morales*
University of Washington, Seattle, Seattle

14:40 J3-3 THE MMIC FRONTIER FOR RADIO ASTRONOMY

Matthew A. Morgan*
National Radio Astronomy Observatory, Charlottesville, VA

15:00 Break

15:40 J3-4 GPUS IN RADIO ASTRONOMY

Paul Demorest*
National Radio Astronomy Observatory, Charlottesville, VA

16:20 J3-5 THE 36-FT MILLIMETER-WAVE RADIO TELESCOPE: HISTORICAL PERSPECTIVE

Mark A. Gordon*
National Radio Astronomy Observatory, Tucson, AZ

Session KB2: Computational Biophotonics and Nanophotonics
Room 151

Co-Chairs: Jamesina Simpson, *University of New Mexico*
Ilker Capoglu, *Northwestern University*

13:20 KB2-1 ANGORA: AN OPEN-SOURCE FINITE-DIFFERENCE TIME-DOMAIN SOFTWARE PACKAGE

Ilker R. Capoglu*[1], Allen Taflove[2], Vadim Backman[1]
[1]*Biomedical Engineering Department, Northwestern University, Evanston, IL*
[2]*Electrical Engineering and Computer Science Department, Northwestern University, Evanston, IL*

13:40 KB2-2 OPTIMIZATION OF SILICON PHOTONIC BIOSENSORS

Michael Gould*[1], Elijah Christensen[2], Daniel M. Ratner[2], Michael Hochberg[1]
[1]*Department of Electrical Engineering, University of Washington, Seattle, WA*
[2]*Department of Bioengineering, University of Washington, Seattle, WA*

14:00 KB2-3 NEAR-INFRARED NARROW-BAND IMAGING OF TUMORS USING PLASMONIC GOLD NANOPARTICLES

Priyaveena Puvanakrishnan*[1], Parmeshwaran Diagaradjane[2], Jon Schwartz[3], Sunil Krishnan[2], James Tunnell[1]
[1]*Biomedical Engineering, The University of Texas at Austin, Austin*
[2]*Radiation Oncology, UT MD Anderson Cancer Center, Houston, Unted States*
[3]*Nanospectra Biosciences, Houston*

14:20 KB2-4 SPATIAL LIGHT INTERFERENCE MICROSCOPY (SLIM)

Gabriel Popescu*
University of Illinois at Urbana-Champaign, Urbana, IL

14:40 KB2-5 MULTI-CHANNEL DIFFUSE OPTICAL SPECTROSCOPIC IMAGING

Hosain Haghany*
University of california, Irvine- Beckman Laser Institute, Irvine, CA

15:00 Break

15:20 KB2-6 JONES MATRIX MONTE CARLO SIMULATION OF COHERENT BACKSCATTERING IN BIOLOGICAL MEDIA

Andrew J. Radosevich*, Jeremy D. Rogers, Allen Taflove, Vadim Backman
biomedical engineering, Northwestern University, Northwestern, Il

15:40 KB2-7 NUMERICAL AND IN VITRO PHANTOMS FOR HYPERTHERMIC MONITORING OF BREAST CANCER

Erin Colebeck*[1], Erdem Topsakal[1], Lynn Dyess[2], Toi Spates[1]
[1]*Electrical and Computer Engineering, Mississippi State University, Starkville MS*
[2]*Department of Surgery, University of South Alabama, Mobile, AL*

16:00 KB2-8 POSSIBLE APPLICATION OF PHOTONIC NANOJETS TO ULTRA EARLY-STAGE CANCER DETECTION

Hamide Seidfaraji*, Cesar Mendez-Ruiz, Jamesina J. Simpson
Electrical Engineering Faculty, University of New Mexico, Albuquerque, NM

Business Meetings

17:00	Commission B	Room 1B40
17:00	Commission G	Room 200
17:00	Commission J	Room 265
18:00	Commission A	Room 155
18:00	Commission C	Room 1B51

Session B8: Microstrip and Printed Antennas; Flexible Electronics
Room 155

Co-Chairs: Yahya Rahmat-Samii, *University of California Los Angeles (UCLA)*
David Jackson, *University of Houston*

08:20 B8-1 A WIDE BAND CONFORMAL ANTENNA INSIDE COMPOSITE MATERIAL

Yun Seo Koo*[1], Richard Fink[2], Ahmad Hoorfar[3], Aly E. Fathy[1]
[1]*EECS, University of Tennessee, Knoxville, TN*
[2]*Applied Nanotech, Inc, Austin, TX*
[3]*ECE, Villanova University, Villanova, PA*

08:40 B8-2 SILICON CARBIDE (SIC) ANTENNAS FOR HIGH TEMPERATURE AND HIGH POWER APPLICATIONS

Tutku Karacolak*[1], Rooban Venkatesh K. G. Thirumalai[2], Joseph N. Merrett[3], Yaroslav Koshka[2], Erdem Topsakal[2]
[1]*School of Engineering and Computer Science, Washington State University Vancouver, Vancouver, WA*
[2]*Department of Electrical and Computer Engineering, Mississippi State University, Mississippi State, MS*
[3]*Air Force Research Laboratory, Wright-Patterson Air Force Base, OH*

09:00 B8-3 C-SHAPED, E-SHAPED and U-SLOTTED PATCH ANTENNAS: A COMPREHENSIVE COMPARATIVE STUDY

Shubhendu Bhardwaj*, Yahya Rahmat-Samii
University of California, Los Angeles, CA

09:20 B8-4 NEXT GENERATION MEMS RECONFIGURABLE E-SHAPED PATCH ANTENNA DESIGN USING PARTICLE SWARM OPTIMIZATION

Joshua M. Kovitz*, Harish Rajagopalan, Yahya Rahmat-Samii
Electrical Engineering, University of California Los Angeles, Los Angeles, California

10:00 Break

10:20 B8-5 HIGHLY FLEXIBLE TEXTILE ANTENNAS ON ORGANZA AND POLYMER SUBSTRATES

Zheyu Wang*, Lanlin Zhang, Yakup Bayram, Dimitris Psychoudakis, John L. Volakis
ElectroScience Laboratory, Dept. of Electrical and Computer Engineering, The Ohio State University, Columbus, Ohio

10:40 B8-6 PIXELATED DIELECTRIC COMPOSITE SUBSTRATES FOR MICROWAVE FREQUENCY APPLICATION

Lanlin Zhang*, Dimitris Psychoudakis, John L. Volakis
Electrical and Computer Engineering, The Ohio State University, Columbus, Ohio

11:00 B8-7 INKJET-PRINTED FLEXIBLE SMART-SKIN WIRELESS SENSORS

Vasileios Lakafosis*, Rushi Vyas, Anya Traille, Hoseon Lee, Manos M. Tentzeris
ECE, Georgia Tech, Atlanta, GA

Session B9: Numerical Methods
Room 1B40

Co-Chairs: Gary Brown, *Virginia Tech*
Branislav Notaros, *Colorado State University*

08:20 B9-1 CONSIDERATIONS WITH NUMERIC STABILITY WHEN OPTIMIZING MOMI FOR LONG RANGE PROPAGATION COMPUTATIONS

Daniel E. Davis*, Benjamin A. Westin, Gary S. Brown
Virginia Polytechnic Institute and State University, Blacksburg

08:40 B9-2 DRIFT-DIFFUSION AND TRANSPORT MODELS FOR THE ANALYSIS OF NON-LOCAL PLASMAS AND METAMATERIALS

Ebrahim Forati*[1], George W. Hanson[1], Tao Shen[2], Thomas Wong[2]
[1]*Electrical Engineering and Computer Science, University of Wisconsin-Milwaukee, Milwaukee, Wisconsin*
[2]*Electrical and Computer Engineering, Illinois institute of technology, Chicago, Illinois*

09:00 B9-3 RULES FOR ADOPTION OF EXPANSION AND INTEGRATION ORDERS IN MOMENT-METHOD COMPUTATION OF ELECTROMAGNETIC SCATTERING AND RADIATION

Nada J. Sekeljic*[1], Elene Chobanyan[1], Milan M. Ilic[1,2], Branislav M. Notaros[1]
[1]*Electrical & Computer Engineering Department, Colorado State University, Fort Collins, Colorado*
[2]*School of Electrical Engineering, University of Belgrade, Belgrade, Serbia*

09:20 B9-4 EFFICIENT ELECTROMAGNETIC ANALYSIS USING ELECTRICALLY LARGE CURVED P-REFINED HIERARCHICAL ANISOTROPIC INHOMOGENEOUS FINITE ELEMENTS

Ana B. Manic*[1], Sanja B. Manic[1], Slobodan V. Savic[2], Milan M. Ilic[1,2], Branislav M. Notaros[1]
[1]*Electrical & Computer Engineering Department, Colorado State University, Fort Collins, Colorado*
[2]*School of Electrical Engineering, University of Belgrade, Belgrade, Serbia*

10:00 Break

10:20 B9-5 TIME-DOMAIN RESPONSE OF 3-D WAVEGUIDE AND SCATTERING STRUCTURES CALCULATED BY HIGHER ORDER FREQUENCY-DOMAIN FEM TECHNIQUE AND DFT

Sanja B. Manic*[1], Slobodan V. Savic[2], Milan M. Ilic[1,2], Branislav M. Notaros[1]
[1]*Electrical & Computer Engineering Department, Colorado State University, Fort Collins, Colorado*
[2]*School of Electrical Engineering, University of Belgrade, Belgrade, Serbia*

10:40 B9-6 MULTIPHYSICS MODELING OF OPTOELECTRONIC NANO-STRUCTURES TOWARDS OPTIMIZATION OF DIFFERENT SOLAR CELLS

Ahmadreza Ghahremani*, Aly E. Fathy
Electrical Engineering, University Of Tennessee Knoxville, Knoxville, TN

Session C2: Advances in MIMO and Signal Processing for Advanced Antenna Systems
Room 1B51

Co-Chairs: Amir Zaghloul, *Virginia Tech*
Gregory Huff, *Texas A&M University*

08:20 C2-1 COMPARISON OF MULTISTATIC RADAR AMBIGUITY FUNCTIONS

Tegan Webster*[1], Jerry Kim[1], Ivan Bradaric[2], Margaret Cheney[3]
[1]*Radar Division, Naval Research Laboratory, Washington, DC*
[2]*Capraro Technologies, Utica, NY*
[3]*Department of Mathematical Sciences, Rensselaer Polytechnic Institute, Troy, NY*

08:40 C2-2 TIME-REVERSAL TECHNIQUES FOR MISO AND MIMO WIRELESS COMMUNICATION SYSTEMS

Ahmed E. Fouda*, Fernando L. Teixeira
ElectroScience Laboratory, Department of Electrical and Computer Engineering, The Ohio State University, Columbus, OH

09:00 C2-3 USE OF EVOLUTIONARY ALGORITHMS FOR MULTIUSER MIMO-OFDM SYSTEMS

Mina Labib*[1], Amir I. Zaghloul[1,2]
[1]*Bradley Department of Electrical and Computer Engineering, Virginia Polytechnic Institute and State University, Blacksburg, Virginia*
[2]*US Army Research Laboratory, Adelphi*

09:20 C2-4 RECONFIGURABLE ANTENNAS, PREEMPTIVE SWITCHING AND VIRTUAL CHANNEL MANAGEMENT

Jean-Francois Chamberland*, Gregory H. Huff, Srinivas Shakkottai
Texas A&M University, College Station, Texas

10:00 Break

10:20 C2-5 CRYSTALLOGRAPHIC-BASED ANTENNA CONFIGURATIONS FOR DIRECTION-OF-ARRIVAL ESTIMATION

Zhenchun Xia*[1,2], Gregory H. Huff[1], Jean-Francois Chamberland[1], Henry Pfister[1], Raktim Bhattacharya[2]
[1]*Electrical and Computer Engineering, Texas A&M University, College Station, TX*
[2]*Aerospace Engineering, Texas A&M University, College Station, TX*

10:40 C2-6 IMPROVING EFFICIENCY OF A LINEAR AMPLIFIER BY INJECTION OF SECOND HARMONIC POWER AT THE OUTPUT

Asmita Dani*, Michael Roberg, Zoya Popovic
Electrical Engineering, University of Colorado, Boulder

11:00 C2-7 CHANNEL-BASED WIRELESS ENCRYPTION USING RECONFIGURABLE ANTENNAS

David L. Rolando, Hung D. Ly, Tie Liu, Gregory H. Huff*, James P. Erskine, Joshua B. Yang, Jeremy A. Joachim
Texas A&M University, College Station, TX

Session D2: THz Devices and their Characterization II
Room 105

Co-Chairs: Erich Grossman, *NIST*
Zoya Popovic, *University of Colorado*

08:20 D2-1 POINT AND CHEMICAL SENSORS IN THE MILLIMETER AND SUBMILLIMETER SPECTRAL REGION

Frank C. De Lucia*
Physics, Ohio State University, Columbus, OH

08:40 D2-2 CW THZ PHOTOMIXER BEAM CHARACTERIZATION

Richard A. Chamberlin*[1,2], Erich N. Grossman[2]
[1]*University of Colorado, Boulder, CO*
[2]*National Institute of Standards and Technology, Boulder, CO*

09:00 D2-3 MICRO-FABRICATED W-BAND AND G-BAND FREQUENCY SCANNED ANTENNA ARRAYS

Leonardo M. Ranzani*[1], Evan D. Cullens[1], Kenneth J. Vanhille[2], Zoya Popovic[1]
[1]*ECEE, University of Colorado at Boulder, Boulder, CO*
[2]*Nuvotronics LLC, Blacksburg,VA*

09:20 D2-4 CONTACTLESS THZ PROBES FOR DEVICE CHARACTERIZATION

Georgios Trichopoulos*, Kagan Topalli, Kubilay Sertel
The Ohio State University, Columbus

Session F4: Waves in Random and Complex Media
Room 150

Co-Chairs: Saba Mudaliar, *Air Force Research Laboratory*
Akira Ishimaru, *University of Washington, Seattle*

08:20 F4-1 SHORT PULSE FOCUSED BEAM AND POWER TRANSFER THROUGH TURBULENCE AND DISCRETE SCATTERERS

Akira Ishimaru*, Matthew Stoneback, Yasuo Kuga
Electrical Engineering, University of Washington, Seattle, WA

08:40 F4-2 CONCEPT OF COHERENCE IN ADAPTIVE SYSTEMS AND ITS APPLICATIONS

Valerian I. Tatarskii*[1], Viatcheslav V. Tatarskii[2]
[1]*Radio-Hydro-Physics LLC, Boulder, CO*
[2]*Georgia Institute of Technology, Atlanta, GA*

09:00 F4-3 IMAGING THROUGH OBSCURING MEDIA BY SUPPRESSION OF DIFFUSION IN THE MUTUAL COHERENCE FUNCTION

Elizabeth H. Bleszynski*, Marek K. Bleszynski, Thomas Jaroszewicz
Monopole Research, Thousand Oaks, CA 91360

09:20 F4-4 SOME INSIGHT INTO LARGE AMPLITUDE SMALL PERIOD (LASP) SURFACE SCATTERING

Gary S. Brown*
Bradley Dept. of Electrical & Computer Engineering, Virginia Tech, Blacksburg, VA

09:40 F4-5 BOUNDARY CONDITIONS FOR RADIATIVE TRANSFER EQUATIONS FOR LAYERED RANDOM MEDIA

Saba Mudaliar*
Sensors Directorate, Air Force Research Laboratory, Wright-Patterson AFB, Ohio

10:00 Break

10:20 F4-6 A STUDY OF THE FOURTH ORDER SMALL PERTURBATION METHOD FOR SCATTERING FROM TWO-LAYER ROUGH SURFACES

Metin A. Demir[1], Joel T. Johnson*[2], Thomas J. Zajdel[2]
[1]Aselsan, Inc., Ankara, Turkey
[2]Electrical and Computer Engineering and ElectroScience Laboratory, The Ohio State University, Columbus, OH

10:40 F4-7 BISTATIC SCATTERING EFFECTS OF A FINITE-SUPPORT SURFACE ROUGHNESS SPECTRUM

Benjamin A. Westin*, Daniel E. Davis, Gary S. Brown
Virginia Polytechnic Institute and State University, Blacksburg, VA

11:00 F4-8 3D SCATTERING FROM LAYERED SUBSURFACES WITH BURIED ROOT-LIKE DISCRETE RANDOM MEDIA

Xueyang Duan*, Mahta Moghaddam
University of Michigan, Ann Arbor

11:20 F4-9 FAST COMPUTATION OF THE SECOND-ORDER SUCCESSIVE SCATTERING BY TWO SCATTERERS IN THE FRESNEL REGION OF EACH OTHER

Ronald J. Hooker*, Roger H. Lang
Department of Electrical and Computer Engineering, The George Washington University, Washington, DC

11:40 F4-10 POLARIMETRIC TECHNIQUES FOR THE IDENTIFICATION OF BIOLOGICAL AND CHEMICAL MATERIALS: COMPARISON OF METHODS BASED ON MEASUREMENTS OF MUELLER MATRICES, LATERAL AND SURFACE WAVES.

Ezekiel Bahar*
Electrical Engineering, University of Nebraska-Lincoln, Lincoln, Nebraska

Session F5: Mesoscale Numerical Weather Prediction in Support of Wave Propagation Modeling
Room 151

Co-Chairs: Tracy Haack, *NRL*
Robert Marshall, *Naval Surface Warfare Center, Dahlgren*

08:20 F5-1 A METHODOLOGY TO DERIVE FINE RESOLUTION RAIN ATTENUATION FIELDS STARTING FROM NWP DATA

Lorenzo Luini*, Carlo Capsoni
Dipartimento di Elettronica e Informazione (DEI), Politecnico di Milano, Milano, Italy

08:40 F5-2 WRF-MODEL ASSIMILATION OF ANGLE-OF-ARRIVAL EXCESS MEASUREMENTS FROM AN ANTENNA OF GPS RECEIVERS

Francois C. Vandenberghe*[1], Bonnie Valant-Spaight[2], Martin Hall[2]
[1]Research Applications Laboratory, National Center for Atmospheric Research, Boulder, CO
[2]Propagation Research Associates, Marietta, GA

09:00 F5-3 A COMPARISON OF MEASURED AND MODELED METEOROLOGY FOR A UNIQUE DATA SET

Victor R. Wiss*, Isha M. Renta, Katherine L. Horgan
Naval Surface Warfare Center Dahlgren Division, Dahlgren, VA

09:20 F5-4 HORIZONTAL RESOLUTION COMPARISON IN THE COUPLED OCEAN / ATMOSPHERE MESOSCALE PREDICTION SYSTEM (COAMPS) AND ITS EFFECT ON REFRACTIVITY DURING A SEA BREEZE EVENT

Katherine L. Horgan*[1], Robert E. Marshall[1], Tracy Haack[2]
[1]Naval Surface Warfare Center Dahlgren Division, Dahlgren, VA
[2]Naval Research Laboratory Monterey, Monterey, CA

09:40 F5-5 THE ROLE OF PLANETARY BOUNDARY LAYER PHYSICS IN MESOSCALE NWP MODEL-EM PROPAGATION PREDICTIONS

Tracy Haack*
NRL, Monterey CA

10:00 Break

10:20 F5-6 ANALYSIS OF SOUTHERN CALIFORNIA CLIMATOLOGY FOR MODELING AND SIMULATION APPLICATIONS

Ian C. Will*
Naval Research Lab, Washington, DC

10:40 F5-7 UNCERTAINTY PROJECTION BETWEEN REFRACTIVITY FROM CLUTTER AND NUMERICAL WEATHER PREDICTION

Caglar Yardim*[1], Ali Karimian[1], Peter Gerstoft[1], Ted Rogers[2]
[1]*UCSD, La Jolla, CA, US*
[2]*SSC Pacific, San Diego, CA, US*

11:00 F5-8 NUMERICAL WEATHER PREDICTION SUPPORTING ADVANCED RADAR TECHNOLOGY INTEGRATED SYSTEM TESTBED INTEGRATION AND TRIALS TEST EFFORT

Lonnie E. Carpenter*, Katherine L. Horgan, Isha M. Renta, Victor R. Wiss
Q32, Naval Surface Warfare Center Dahlgren Laboratory, Dahlgren, VA

11:20 F5-9 CHARACTERIZING NEAR-SURFACE REFRACTIVITY CONDITIONS WHEN USING NWP MODEL DATA FOR EM SYSTEM PERFORMANCE PREDICTIONS

Paul A. Frederickson*
Department of Meteorology, Naval Postgraduate School, Monterey, CA

11:40 F5-10 WORLDWIDE DUCTING PROBABILITIES FROM RADIOSONDE DATA: A COMPARISON OF HISTORICAL AND MODERN DATA

Thomas R. Hanley*, Jonathan Z. Gehman
Johns Hopkins University - Applied Physics Laboratory, Laurel, MD

Session GHF1: Global Navigation Satellite Systems and Radio Beacon Remote Sensing I
Room 200

Co-Chairs: Carl Siefring, *Naval Research Laboratory*
Charles Carrano, *Boston College*
Valery Zavorotny, *NOAA/Earth System Research Laboratory*

08:20 GHF1-1 THE USE OF SIMULATIONS FOR INTERPRETING BEACON SATELLITE DATA

Charles L. Rino*[1], Charles S. Carrano[2]
[1]*Rino Consulting, Menlo Park, CA*
[2]*Institute for Scientific Research, Boston College, Chesnut, Hill, MA*

08:40 GHF1-2 TURBULENCE DETECTION USING GNSS OCCULTATIONS

Larry Cornman*
Research Applications Laboratory, National Center for Atmospheric Research, Boulder, CO

09:00 GHF1-3 DEDUCING IONOSPHERIC TURBULENCE PARAMETERS FROM BEACON SATELLITE SCINTILLATION MEASUREMENTS

Charles S. Carrano*[1], Charles L. Rino[2], Ronald G. Caton[3], Keith M. Groves[1]
[1]*Institute for Scientific Reserach, Boston College, Chestnut Hill, MA*
[2]*Rino Consulting, Menlo Park, CA*
[3]*Kirtland AFB, Albuquerque, NM*

09:20 GHF1-4 REMOTE SENSING OF IONOSPHERIC IRREGULARITIES: CITRIS MEASUREMENTS OF TEC AND RADIO SCINTILLATION

Carl L. Siefring*, Paul A. Bernhardt
Plasma Physics Division, Naval Research Laboratory, Washington, DC

09:40 GHF1-5 TANDEM INSTRUMENTED CUBESATS IN LOW EARTH ORBIT FOR CONTINUOUS OCCULTATION OBSERVATIONS OF THE IONOSPHERE

Paul A. Bernhardt*[1], Carl L. Siefring[1], Joe D. Huba[1], John Abrams[2], Nestor Voronka[3]
[1]*Naval Research Laboratory, Washington, DC*
[2]*ARES Corporation, Torrence, CA*
[3]*Tethers Unlimited, Bothell, WA*

10:00 Break

10:20 GHF1-6 THE CONSTRUCTION OF THE GROUND-BASED GPS TEC MAP OVER US USING THE NON-STATIONARY WAVELET-BASED ERROR COVARIANCE

Yang-Yi Sun*[1,2,3], Tomoko Matsuo[1,2], Eduardo A. Araujo-Pradere[1,2], Jann-Yenq Liu[3]
[1]*Cooperative Institute for Research in Environmental Sciences, University of Colorado, Boulder*
[2]*Space Environmental Center, NOAA, Boulder*
[3]*Institute of Space Science, National Central University, Jhongli, Taiwan*

10:40 GHF1-7 RECENT RESULTS FROM GNSS-REFLECTIONS REMOTE SENSING

Stephen T. Lowe*
Jet Propulsion Laboratory, La Canada, CA

11:00 GHF1-8 POLARIMETRIC BISTATIC SCATTERING PATTERNS OF CIRCULARLY POLARIZED WAVES FROM OCEAN-LIKE SURFACES

Jeffrey D. Ouellette*, Joel T. Johnson
Electrical and Computer Engineering, The Ohio State University, Columbus, OH

11:20 GHF1-9 THE CYCLONE GLOBAL NAVIGATION SATELLITE SYSTEM (CYGNSS) MISSION

Christopher Ruf*[1], Scott Gleason[2], Zorana Jelenak[3], Stephen Katzberg[4], Aaron Ridley[1], Randall Rose[5], John Scherrer[5], Valery Zavorotny[6]
[1]*University of Michigan, Ann Arbor, MI*
[2]*Concordia University, Montreal, QC, Canada*
[3]*NESDIS/StAR-UCAR, National Oceanic and Atmospheric Administration, Silver Spring, MD*
[4]*South Carolina State University, Orangeburg, SC*
[5]*Southwest Research Institute, San Antonio, TX*
[6]*Earth System Research Laboratory, National Oceanic and Atmospheric Administration, Boulder, CO*

Session HG3: Meteors, Impacts and Dusty Plasmas I
Room 245

Co-Chairs: Jonathan Fentzke, *NWRA, CoRA Division | Arecibo Observatory, SAS Dept.*
Mihaly Horanyi, *LASP, University of Colorado*

08:20 HG3-1 THE CHAMPS (CHARGE AND MASS OF METEORITIC SMOKE PARTICLES) ROCKET CAMPAIGN

Shannon Dickson*[1], Mihaly Horanyi[1], Scott Knappmiller[1], Devin Konecny[1], Scott Robertson[1], Zoltan Sternovsky[1], Biff Williams[2], Diego Janches[3], Martin Friedrich[4], Michael Gausa[5], Jorg Gumbel[6]
[1]*Univ. of Colorado - Boulder, Boulder, CO*
[2]*Northwest Research Associates, Boulder, CO*
[3]*Goddard Space Flight Center, Greenbelt, MD*
[4]*Graz University of Technology, Graz, Austria*
[5]*Andoya Rocket Range, Andenes, Norway*
[6]*Stockholm University, Stockholm, Sweden*

08:40 HG3-2 FIRST DETECTION OF METEORIC SMOKE USING THE POKER FLAT INCOHERENT SCATTER RADAR (PFISR)

Vicki W. Hsu*[1], Jonathan T. Fentzke[2], Christiano M. G. Brum[3]
[1]*Electrical and Computer Engineering, University of Illinois at Urbana-Champaign, Urbana, IL*
[2]*Applied Physics Laboratory, Johns Hopkins University, Laurel, MD*
[3]*SAS Department, Arecibo Observatory, Arecibo, Puerto Rico*

09:00 HG3-3 ELECTRIC POTENTIAL DISTRIBUTIONS ABOVE A SURFACE IN A MAGNETIC DIPOLE FIELD

Xu Wang*[1,2], Scott Robertson[3,2], Mihaly Horanyi[1,3,2]
[1]*LASP, University of Colorado, Boulder,CO*
[2]*CCLDAS, University of Colorado, Boulder,CO*
[3]*Physics, University of Colorado, Boulder,CO*

09:20 HG3-4 MODELING DUST CLOUDS ON THE MOON

Jamey Szalay*[1,2], Mihaly Horanyi[1,2]
[1]*Physics, University of Colorado at Boulder, Boulder, CO*
[2]*Laboratory for Atmospheric and Space Physics, Boulder, CO*

09:40 HG3-5 THE ELECTROSTATIC LUNAR DUST ANALYZER (ELDA): DATA ANALYSIS

Jianfeng Xie*[1,2], Zoltan Sternovsky[1,3], Eberhard Grn[1], Siegfried Auer[4], Mihaly Horanyi[1,2], Huy Le[1], Keith Drake[1]
[1]*Laboratory for Atmospheric and Space Physics, University of Colorado at Boulder, Boulder,Colorado*
[2]*Department of Physics, University of Colorado at Boulder, Boulder,Colorado*
[3]*Department of Aerospace Engineering Sciences, University of Colorado at Boulder, Boulder,Colorado*
[4]*A&M Associates, Basye, Virginia*

10:00 Break

10:20 HG3-6 UNDERSTANDING SPACECRAFT FAILURES BY CHARACTERIZING HYPERVELOCITY IMPACT PLASMAS

Nicolas Lee*, Sigrid Close
Stanford University, Stanford

10:40 HG3-7 DETECTION OF RADIO FREQUENCY EMISSIONS FROM HYPERVELOCITY IMPACTS

David Strauss*[1], Ivan Linscott[1], Theresa Johnson[2], Nicolas Lee[2], Ashish Goel[2], Sigrid Close[2]
[1]*Electrical Engineering, Stanford University, Stanford, CA*
[2]*Aeronautics and Astronomics, Stanford University, Stanford, CA*

11:00 HG3-8 ELECTRIC FIELD CHARACTERISTICS FROM HYPERVELOCITY PARTICLE IMPACT PLASMA

Theresa L. Johnson*[1], David Strauss[2], Ivan Linscott[2], Sigrid Close[1], Richard Adamo[3]
[1]*Aeronautics and Astronautics, Stanford University, Stanford, CA*
[2]*Electrical Engineering, Stanford University, Stanford, CA*
[3]*Space Technology and Integration Program, SRI International, Menlo Park, CA*

11:20 HG3-9 DISCRIMINATING ESD VS EMP EFFECTS IN HYPERVELOCITY IMPACT EXPERIMENTS

David S. Lauben*, Sigrid Close, Theresa L. Johnson, Nicolas Lee, Ivan R. Linscott, David A. Strauss
Stanford University, Stanford

11:40 HG3-10 MODELING PLASMA FORMATION FROM HYPERVELOCITY METEOROID IMPACTS

Alex Fletcher*, Sigrid Close, Robert W. MacCormack
Aeronautics & Astronautics, Stanford University, Stanford, CA

Session J4: EoR and Dark Ages: Observations and Instrumentation
Room 265

Co-Chairs: Jacqueline Hewitt, *Massachusetts Institute of Technology*
Judd Bowman, *Arizona State University*

08:20 J4-1 RECENT ADVANCES WITH EDGES AND THE STATUS OF GLOBAL 21 CM EXPERIMENTS

Alan E. E. Rogers*[1], Judd D. Bowman[2]
[1]*MIT Haystack Observatory, Westford, MA*
[2]*Arizona State University, Tempe, AZ*

08:40 J4-2 EOR FOREGROUND SUBTRACTION AND THE LATEST MWA RESULTS

Miguel F. Morales*, Bryna Hazelton
Physics, University of Washington, Seattle, Seattle

09:00 J4-3 PAPER-64: MINIMUM- AND MAXIMUM-REDUNDANCY OBSERVATIONS

Aaron R. Parsons*[1], Team Paper[2]
[1]*University of California, Berkeley, Berkeley, CA*
[2]*NRAO, U. Virginia, U. Pennsylvania, SKA South Africa, ..., US/SA*

09:20 J4-4 UPDATES ON THE GMRT-EOR PROJECT

Tzu-Ching Chang*
ASIAA, Taipei, Taiwan

09:40 J4-5 DEEP LOFAR OBSERVATIONS OF POTENTIAL EOR FIELDS

Michiel A. Brentjens*
Radio Observatory, ASTRON, Dwingeloo, Netherlands

10:00 Break

10:20 J4-6 OBSERVING COSMIC DAWN WITH THE LONG WAVELENGTH ARRAY

Jacob M. Hartman*
JPL, Pasadena, CA

10:40 J4-7 DETECTING THE UNIVERSE BEYOND REDSHIFT 20

Lincoln J. Greenhill*
harvard / smithsonian, Cambridge, MA

11:00 J4-8 A CONSTRAINT ON THE 21-CM SIGNAL AT Z=20 FROM VLA OBSERVATIONS

Katie M. Chynoweth*[1], Joseph Lazio[2], Joseph Helmboldt[3]
[1]*Remote Sensing, NRC Fellow at Naval Research Laboratory, Washington, DC*
[2]*JPL, California Institute of Technology, and NLSI, Pasadena, CA*
[3]*Remote Sensing, Naval Research Laboratory, Washington, DC*

11:20 J4-9 A PAPER SOUTHERN SKY CATALOG

Danny Jacobs*
SESE, Arizona State University, Tempe, AZ

11:40 J4-10 THE DARK AGES RADIO EXPLORER (DARE)

Jack O. Burns*
CASA, University of Colorado at Boulder, Boulder, CO

Session K2: Biomedical Applications
Room 105

Co-Chairs: Utkan Demirci, *Harvard Medical School*
Erdem Topsakal, *Mississippi State University*

10:20 K2-1 TOWARDS A MINIMALLY-INVASIVE APPLICATOR FOR CANCER ABLATION

Kyle M. Loizos*, Carlos J. Cela, Erik S. Gamez, Darin Furgeson, Gianluca Lazzi
University of Utah, Salt Lake City, UT

10:40 K2-2 COMPUTATIONAL STUDY OF EXTERNAL FIXATION DEVICES SURFACE HEATING IN 1.5T AND 3T MRI SYSTEMS

Yan Liu*[1], Jianxiang Shen[1], Ji Chen[1], Wolfgang Kainz[2]
[1]*Electrical and Computer Engineering, University of Houston, Houston, TX*
[2]*Center for Devices and Radiological Health, U.S. Food and Drug Administration, Rockville, MD*

11:00 K2-3 MAGNETIC NANOPARTICLE AND MAGNETIC FIELD BASED ASSEMBLY FOR MICROSCALE HYDROGELS

Feng Xu, Dylan Finley, Yuree Sung, Banu Sridharan, Umut A. Gurkan, Utkan Demirci*
Harvard Medical School, Harvard-MIT Health Sciences & Technology, Cambridge

Session A2: Reverberation Chamber Measurements and Techniques
Room 1B40

Co-Chairs: Christopher Holloway, *NIST*
John Ladbury, *National Institute of Standards and Technology*

13:20 A2-1 A FIRST-ORDER ANTENNA MODEL WITH APPLICATIONS TO REVERBERATION CHAMBER MEASUREMENTS

John M. Ladbury*, Jason B. Coder, Ryan Pirkl
National Institute of Standards and Technology, Boulder

13:40 A2-2 PRACTICAL CONSIDERATIONS FOR MEASURING ANTENNA EFFICIENCY IN A REVERBERATION CHAMBER

Jason B. Coder*[1], John M. Ladbury[1], Mark Golkowski[2]
[1]*RF Fields Group, National Institute of Standards and Technology, Boulder, CO*
[2]*Electrical Engineering, University of Colorado Denver, Denver, CO*

14:00 A2-3 A ONE-ANTENNA REVERBERATION-CHAMBER TECHNIQUE FOR ESTIMATING THE TOTAL AND RADIATION EFFICIENCY

Christopher L. Holloway*, Haider A. Shah, Ryan Pirkl, John Ladbury, William F. Young, David A. Hill
NIST, Boulder, CO

14:20 A2-4 MEASURING TOTAL RADIATED POWER OF WIRELESS DEVICES IN A REVERBERATION CHAMBER

Colton Dunlap*, William F. Young, John Ladbury, Erik Engvall, Christopher L. Holloway
Electromagnetics Division, The National Institute of Standards and Technology, Boulder, CO

14:40 A2-5 COMPARISON OF VARIOUS ANTENNA EFFICIENCY DETERMINATION METHODS

Rick Smith*
ITT Corporation, Fredericksburg, VA

15:00 Break

15:20 A2-6 VERIFICATION OF K-FACTOR BASED FORMULA FOR MEASUREMENT UNCERTAINTY IN REVERBERATION CHAMBER

Xiaoming Chen[1], Erik Engvall*[2], Per-Simon Kildal[1]
[1]*Signals and Systems, Chalmers University of Technology, Gothenburg, Sweden*
[2]*National Institute of Standards and Technology, Boulder*

15:40 A2-7 IMPROVING THE ACCURACY OF REVERBERATION CHAMBER MEASUREMENTS: OPTIMAL STIRRING PROCEDURES

Ryan J. Pirkl*[1], Kate A. Remley[1], Christian S. Lotback Patane[2]
[1]*National Institute of Standards and Technology, Boulder, CO*
[2]*Bluetest AB, Gothenburg, Sweden*

16:00 A2-8 UTILIZING REVERBERATION CHAMBERS AS A VERSATILE TEST ENVIRONMENT FOR ASSESSING THE PERFORMANCE OF COMPONENTS AND SYSTEMS

Dennis Lewis*
Metrology, Boeing, Seattle, Washington

16:20 A2-9 RESPONSE OF CAVITIES WITH BOTH REGULAR AND CHAOTIC RAY TRAJECTORIES

Ming-Jer Lee*, Thomas Antonsen Jr, Edward Ott
Institute for Research in Electronics and Applied Physics (IREAP), University of Maryland, College Park, Maryland

16:40 A2-10 RANDOM COUPLING MODEL FOR APERTURE EXCITATION OF WAVE CHAOTIC ENCLOSURES

Gabriele Gradoni*, Thomas Antonsen, Steven Anlage, Edward Ott
Institute for Research in Electronics and Applied Physics, University of Maryland, College Park, Maryland

Session B10: Electromagnetic Interaction and Coupling
Room 155

Co-Chairs: Edward Rothwell, *Michigan State University*
David Jackson, *University of Houston*

13:20 B10-1 A NEW PARADIGM IN SOLAR ENERGY HARVESTING: CHARACTERIZATION OF HIGH ABSORPTION NANOPILLAR ARRAY PHOTOVOLTAICS

Timothy J. Brockett*, Harish Rajagopalan, Yahya Rahmat-Samii
Electrical Engineering, University of California, Los Angeles, Los Angeles, CA

13:40 B10-2 EFFECTS OF BEAM WIDTH AND SURFACE CURVATURE ON THE REFLECTION COEFFICIENT FOR A CONDUCTOR COATED WITH MAGRAM

Edward J. Rothwell*
Electrical and Computer Engineering, Michigan State University, East Lansing, MI

14:00 B10-3 WIRELESS POWER TRANSMISSION FOR GEOPHYSICAL APPLICATIONS

Xiyao Xin*[1], Ji Chen[1], David R. Jackson[1], Paul Tubel[2]
[1]*Dept. of Electrical and Computer Engineering, University of Houston, Houston, TX*
[2]*Tubel Energy, Inc., The Woodlands, TX*

14:20 B10-4 SIMPLIFIED TEST AND MODELING FOR PASSIVE RFID TAG BACKSCATTER LINK ANALYSIS

Daniel G. Kuester*[1,2], David R. Novotny[1], Jeffrey R. Guerrieri[1], Zoya Popovic[2]
[1]*RF Fields Group, NIST, Boulder, CO*
[2]*Electrical, Computer, and Energy Engineering, University of Colorado at Boulder, Boulder, CO*

15:00 Break

15:20 B10-5 GREEN'S FUNCTIONS FOR LAYERED MEDIA HAVING ANISOTROPIC PROPERTIES

Gregory Mitchell*, Steven Weiss
SEDD, US Army Research Lab, Adelphi, MD

15:40 B10-6 PARTICLE BEAM DRIVEN NONLINEAR DIELECTRIC STRUCTURES: SIMULATION AND PROPOSED EXPERIMENTS

Paul Schoessow*[1], Alexei Kanareykin[1], Stanislav Baturin[2]
[1]*Euclid Techlabs, Solon OH*
[2]*LETI, St Petersburg, Russia*

Session F6: Radio Frequency Interference Identification and Mitigation
Room 150

Co-Chairs: David Kunkee, *The Aerospace Corporation*
Jennifer Bernhard, *University of Illinois at Urbana-Champaign*

13:20 F6-1 RADIO SCIENCE AT THE 2012 WORLD RADIOCOMMUNICATION CONFERENCE

Andrew W. Clegg*
National Science Foundation, Arlington, Virginia

13:40 F6-2 REVISING ITU-R RECOMMENDATION P.528 TO SUPPORT SATELLITE FREQUENCY SHARING

Teresa Rusyn*
Institute for Telecommunication Sciences, Boulder, CO

14:00 F6-3 2011 SPECTRUM SURVEY OCCUPANCY MEASUREMENTS IN DENVER, CO

Chriss A. Hammerschmidt*, Heather Ottke, Randy Hoffman
ITS.M, National Telecommunications and Information Administration, Boulder, Colorado

14:20 F6-4 SPECTRUM CHALLENGES IN RADAR DESIGN

Lawrence Cohen*, Eric L. Mokole
Radar Div, Naval Research Laboratory, Washington DC

14:40 F6-5 THIRD-ORDER INTERMODULATION PRODUCTS, WHAT THEY MEAN AND HOW THEY ARE MEASURED

Eric L. Mokole*[1], Lawrence Cohen[1], Tegan Webster[1,2]
[1]*Radar Div, Naval Research Laboratory, Washington DC*
[2]*Dept of Mathematical Sciences, Rensselaer Polytechnic Institute, Troy NY*

15:00 Break

15:20 F6-6 RADIO FREQUENCY INTERFERENCE ANALYSIS OF L-BAND MICROWAVE RADIOMETRY MISSIONS

Mustafa Aksoy*, Joel T. Johnson
Dept. of Electrical and Computer Engineering and ElectroScience Lab, The Ohio State University, Columbus, OH

15:40 F6-7 RFI ANALYSIS AND ALGORITHM DEVELOPMENT USING DIRECT-SAMPLED DATA MEASURED DURING THE CARVE FLIGHT MISSION

Sidharth Misra*, Sharmila Padmanabhan, Ian O'Dwyer, Steven Dinardo, Todd Gaier
Jet Propulsion Laboratory, Pasadena, CA

16:00 F6-8 MITIGATING WIND TURBINE INTERFERENCE TO RADAR BY ADAPTIVE PROCESSING BASED ON TELEMETRY

Fanxing Kong*[1,2], Yan Zhang[1,2], Robert D. Palmer[1,3], Ying Bai[1,2]
[1]*Atmospheric Radar Research Center, University of Oklahoma, Norman, OK*
[2]*School of Electrical and Computer, University of Oklahoma, Norman, OK*
[3]*School of Meteorology, Universit of Oklahoma, Norman, OK*

16:20 F6-9 INTERFERENCE SUPPRESSION STUDIES WITH THE PHASED ARRAY ANTENNA AT THE NATIONAL WEATHER RADAR TESTBED

Mark Yeary*[1], Jerry Crain[1], Chris Curtis[2]
[1]*ECE/ARRC, University of Oklahoma, Norman, OK*
[2]*National Severe Storms Laboratory, Norman, OK*

16:40 F6-10 RADAR POWER AMPLIFIER SPECTRUM OPTIMIZATION FOR CHIRP WAVEFORMS USING ACPR LOAD-PULL MEASUREMENTS

Josh Martin*, Matthew Moldovan, Charles Baylis, Robert Marks
Electrical and Computer Engineering, Baylor University, Waco

Session F7: Active Remote Sensing and Propagation Measurements and Models
Room 151

Co-Chairs: Chandrasekar V Chandra, *Colorado State University*
Valery Zavorotny, *NOAA/Earth System Research Laboratory*

13:20 F7-1 WAVE SHADOWING AND MODULATION OF MICROWAVE BACKSCATTER FROM THE OCEAN

William J. Plant*, Gordon Farquharson
Applied Physics Laboratory, University of Washington, Seattle WA

13:40 F7-2 BACKSCATTERING FROM THE SEA SURFACE UNDER THE SMALL SLOPE APPROXIMATION

Jimmy Alatishe*[1], Wasyl Wasylkiwskyj[2]
[1]*Radar Division, US Naval Research Laboratory, Washington DC*
[2]*Electrical and Computer Engineering, The George Washington University, Washington, DC*

14:00 F7-3 MULTIPLE GRAZING ANGLE SEA CLUTTER MODELING

Ali Karimian*[1], Caglar Yardim[1], Peter Gerstoft[1], William Hodgkiss[1], Amalia Barrios[2]
[1]*University of California, San Diego, San Diego, CA*
[2]*SPAWAR, San Diego*

14:20 F7-4 EXPERIMENTS FOR RF TOMOGRAPHY

Vittorio Picco*[1], Tadahiro Negishi[1], Marcus Stephens[1], Shingo Nishikata[2], Danilo Erricolo[1]
[1]*ECE, University of Illinois at Chicago, Chicago, IL*
[2]*Nagoya Guidance & Propulsion Systems Works, Mitsubishi Heavy Industries, LTD., Komaki, Aichi Prefecture, Japan*

14:40 F7-5 A SEMI-EMPIRICAL MODEL FOR PREDICTING SIGNAL STRENGTH AT VHF AND UHF BAND USING SURFACE REFRACTIVITY MEASUREMENT AT NSUKKA, SOUTH-EASTERN NIGERIA

Benjamin G. Ayantunji*
Centre for Basic Space Science,, Nsukka, Enugu State, Nigeria

15:00 Break

15:20 F7-6 A COUPLED FDTD/SAMI3 MODEL FOR ELECTROMAGNETIC WAVE PROPAGATION IN THE EARTH-IONOSPHERE SYSTEM

Jiajun Niu*, Jamesina J. Simpson
Electrical and Computer Engineering, University of New Mexico, Albuquerque, NM

15:40 F7-7 EVALUATING RAYLEIGH DISTRIBUTION ASSUMPTIONS IN FADING CHANNEL MODELS

Timothy J. Riley*, Christopher J. Behm
NTIA/ITS.E, US Department of Commerce, Boulder, CO

16:00 F7-8 FREE-FIELD MEASUREMENTS OF THE ELECTRICAL PROPERTIES OF SOIL USING THE SURFACE WAVE PROPAGATION BETWEEN TWO MONOPOLE ANTENNAS

Nicholas N. DeMinco*, Robert T. Johnk, Paul M. McKenna, Chriss A. Hammerschmidt, Wayde Allen
Institute for Telecommunication Sciences, Boulder, Colorado

16:20 F7-9 IMPACT OF METEOROLOGICAL PARAMETERS ON THE VLF-LF PROPAGATION AT MIDLATITUDES

Andrey N. Lyakhov*, Andrey A. Egoshin, Vladimir Ermak, Stanislav I. Kozlov, Vladimir P. Kudryavtsev, Yuri V. Poklad, Ekaterina N. Yakimenko, Yuli I. Zetzer
Institute of Geospheres Dynamics, Moscow, Russian Federation

Session GH1: Ionospheric Modification
Room 105

Co-Chairs: Michael Sulzer, *Arecibo observatory*
Stanley Briczinski, *Naval Research Laboratory, Plasma Physics Division*

13:20 GH1-1 FREQUENCY RESPONSE AND POLARIZATION OF ELF/VLF SIGNALS GENERATED AT THE HAARP FACILITY

Jason R. Carpenter*, Ryan T. Jacobs, Mark Golkowski
Electrical Engineering, University of Colorado Denver, Denver, CO

13:40 GH1-2 SATURATION EFFECTS IN THE VLF SCATTERING OFF HF HEATED IONOSPHERE

Nikolai G. Lehtinen*[1], Timothy F. Bell[1], Umran S. Inan[1,2]
[1]*Stanford University, Stanford, CA*
[2]*Koc University, Istanbul, Turkey*

14:00 GH1-3 HIGH FREQUENCY RESOLUTION AND HIGH SPATIAL RESOLUTION TOA ANALYSIS FOR ELF/VLF WAVE GENERATION EXPERIMENTS AT HAARP

Shuji Fujimaru*, Robert C. Moore
Department of Electrical and Computer Engineering, University of Florida, Gainesville, FL

14:20 GH1-4 APPROXIMATING D-REGION ELECTRON DENSITIES USING ELF/VLF WAVE GENERATION EXPERIMENTS AT HAARP

Divya Agrawal*, Robert C. Moore
Department of Electrical and Computer Engineering, University of Florida, Gainesville, FL

14:40 GH1-5 INVESTIGATION OF DUSTY SPACE PLASMAS IN THE NEAR-EARTH SPACE ENVIRONMENT USING THE ACTIVE MODIFICATION OF POLAR MESOSPHERIC SUMMER ECHOES

Alireza Mahmoudian*, Wayne Scales
ECE department, Virginia Tech, Blacksburg,VA

15:00 Break

15:20 GH1-6 TWISTED BEAM SEE OBSERVATIONS OF IONOSPHERIC HEATING FROM HAARP

Stanley J. Briczinski*[1], Paul A. Bernhardt[1], Todd R. Pedersen[2], Serafin P. Rodriguez[3], Geoffrey S. San Antonio[3]
[1]*Plasma Physics Division, Naval Research Laboratory, Washington, DC*
[2]*Air Force Research Laboratory, Kirtland AFB, NM*
[3]*Radar Division, Naval Research Laboratory, Washington, DC*

15:40 GH1-7 WAVE DISTURBANCES IN THE IONOSPHERE ACCOMPANYING THE PLASMA MODIFICATION BY SURA FACILITY RADIATION

Leonid F. Chernogor[1,2], Igor F. Domnin[2], Sergii V. Panasenko*[2], Valery P. Uryadov[3]
[1]*Dept. of Space Radio Physics, Kharkiv V. N. Karazin National University, Kharkiv, Ukraine*
[2]*Institute of Ionosphere, Kharkiv, Ukraine*
[3]*Radiophysical Research Institute, N. Novgorod, Russia*

16:00 GH1-8 INVESTIGATING THE THRESHOLD AND STRENGTH OF EMISSION LINES GENERATED BY MAGNETIZED STIMULATED BRILLOUIN SCATTER (MSBS) USING HAARP FACILITIES

Alireza Mahmoudian*[1], Wayne Scales[1], Paul Bernhardt[2], Stan Briczinski[2]
[1]*ECE department, Virginia Tech, Blacksburg,VA*
[2]*Plasma Physics, Naval Research Labratory, Washington D.C*

16:20 GH1-9 ON DEMAND SPACE PLASMA GENERATION: THE METAL OXIDE SPACE CLOUD EXPERIMENT

Ronald G. Caton*[1], Keith M. Groves[2], Theodore L. Beach[3], Paul A. Bernhardt[4]
[1]*Space Vehicles Directorate, Air Force Research Laboratory, Kirtland AFB, NM*
[2]*Institute for Scientific Research, Boston College, Chestnut Hill, MA*
[3]*Creare Inc, Hanover, NH*
[4]*Plasma Physics Division, Naval Research Laboratory, Washington DC*

16:40 GH1-10 THE FUTURE OF ROCKET EXHAUST INTERACTIONS IN THE IONOSPHERE AFTER THE SPACE SHUTTLE

Paul A. Bernhardt*[1], Wayne A. Scales[2], Haiyang Fu[2], Alireza Mahmoudian[2], Maitrayee Bordikar[2]
[1]*Naval Research Laboratory, Washington, DC*
[2]*Department of EE, Virginia Tech, Blacksburg, VA*

17:00 GH1-11 ANTENNA MEASUREMENT AND OTHER COMMISSIONING TASKS FOR COMPLETION OF THE NEW ARECIBO HF FACILITY

Michael P. Sulzer*
Space and Atmospheric Sciences, Arecibo observatory, Arecibo, PR

Session GHF2: Global Navigation Satellite Systems and Radio Beacon Remote Sensing II
Room 200

Co-Chairs: Valery Zavorotny, *NOAA/Earth System Research Laboratory*
Carl Siefring, *Naval Research Laboratory*
Charles Carrano, *Boston College*

13:20 GHF2-1 GNSS AND RADIO BEACONS REFLECTED WAVEFORMS MODELED WITH SMALL SLOPE APPROXIMATION

Alexander G. Voronovich*, Valery U. Zavorotny
Physical Sciences Division, NOAA/Earth System Research Laboratory, Boulder CO, Boulder CO

13:40 GHF2-2 OCEAN SURFACE WIND SPEED MEASUREMENTS FROM HIGH-ALTITUDE AIRCRAFT USING GPS DELAY-DOPPLER MAPS

Valery U. Zavorotny*[1], Nereida Rodriguez-Alvarez[1,2], Dennis M. Akos[3]
[1]*Physical Sciences Division, NOAA/Earth System Research Laboratory, Boulder CO*
[2]*Remote Sensing Laboratory, Universitat Politcnica de Catalunya and IEEC CRAE/UPC, Barcelona, Spain*
[3]*Department of Aerospace Engineering Sciences, University of Colorado at Boulder, Boulder CO*

14:00 GHF2-3 SNOW MONITORING AT NIWOT RIDGE USING GPS INTERFEROMETRIC REFLECTOMETRY

Felipe G. Nievinski*, Kristine M. Larson
University of Colorado at Boulder, Boulder, CO

14:20 GHF2-4 GNSS-R ADVANCES AT THE REMOTE SENSING LAB UPC

Adriano Camps[1], Nereida Rodriguez-Alvarez[1], Enric Valencia[1], Hyuk Park[1], Juan Fernando Marchan-Hernandez[2], Albert Aguasca[1], Merce Vall-llosera[1], Isaac Ramos-Perez[1], Giuseppe Forte[1], Xavier Bosch-Lluis*[3]
[1]*TSC, RSLab, Universtitat Politecnia de Catalunya, Barcelona, Spain*
[2]*Institut Cartogrfic de Catalunya, Barcelona, Spain*
[3]*ECE, MSL, Colorado State University, Fort Collins, Colorado*

Session HG4: Meteors, Impacts and Dusty Plasmas II
Room 245

Co-Chairs: Mihaly Horanyi, *LASP, University of Colorado*
Jonathan Fentzke, *NWRA, CoRA Division | Arecibo Observatory, SAS Dept.*

13:20 HG4-1 COLORADO SOFTWARE DEFINED RADAR: HARDWARE, RESULTS, RECONFIGURABITY AND DEPLOYMENT

Cody Vaudrin*, Scott Palo
University of Colorado, Boulder, CO

13:40 HG4-2 PRELIMINARY RADAR OBSERVATIONS FROM THE PENN STATE METEOR RADAR

Julio V. Urbina*[1], Lars P. Dyrud[2], Jonathan Fentzke[2], Ryan Seal[1], Robert Sorbello[1]
[1]*The Pennsylvania State University, University Park, PA*
[2]*Applied Physics Laboratory, John Hopkins University, Columbia, MD*

14:00 HG4-3 WAVEFORM EFFECTS ON HPLA RADAR METEOR MEASUREMENTS

Ryan Volz*, Sigrid Close
Aeronautics and Astronautics, Stanford University, Stanford, CA

14:20 HG4-4 TRANSMITTER POWER INFLUENCE ON METEOR RADAR HEAD ECHO RETURNS

Stanley J. Briczinski*[1], John D. Mathews[2], Philip J. Erickson[3]
[1]*Plasma Physics Division, Naval Research Laboratory, Washington, DC*
[2]*Electrical Engineering, Penn State, State College, PA*
[3]*MIT Haystack Observatory, Westford, MA*

14:40 HG4-5 ON THE EFFECT OF TURBULENCE ON SPECULAR METEOR ECHOES

Freddy Galindo[1], Julio Urbina*[1], Lars Dyrud[2], Jonathan Fentzke[2]
[1]*Pennsylvania State University, University Park, Pennsylvania*
[2]*Applied Physics Laboratory, John Hopkins University, Columbia, Maryland*

15:00 Break

15:20 HG4-6 NON-SPECULAR MODELING WITH DISCRETE POWER INTERVALS

Heather Jiles*[1], Lars Dyrud[1], Jonathan Fentzke[1], Freddie Galindo[2], Julio Urbina[2]
[1]*Johns Hopkins Applied Physics Laboratory, Washington DC*
[2]*Department of Electrical Engineering, Pennsylvania State University, University Park, PA*

15:40 HG4-7 RESULTS FROM ARECIBO METEOR OBSERVATIONS SHOWING MULTI-PIECE METEOR DETECTION

Emily Logan[1], Michael Sulzer*[2]
[1]*University of Colorado at Boulder, Boulder, CO*
[2]*Arecibo Observatory, Arecibo, PR, US*

16:00 HG4-8 INFLUENCE OF IONOSPHERIC ELECTROJETS ON METEOR TRAIL EVOLUTION

Lars P. Dyrud*[1], Jonathan T. Fentzke1[1], Julio Urbina[2]
[1]*Johns Hopkins Applied Physics Laboratory, Laurel, MD*
[2]*Penn State Univeristy, State College, UNited States*

16:20 HG4-9 A PROBABILISTIC APPROACH TO ESTIMATING METEOROID PRESENCE IN EARTH ORBIT FROM GROUND-BASED RADAR OBSERVATIONS

Steven Pifko*[1], Diego Janches[2], Sigrid Close[1]
[1]*Aeronautics & Astronautics, Stanford University, Stanford, CA*
[2]*Space Weather Lab, NASA Goddard Space Flight Center, Greenbelt, MD*

16:40 HG4-10 CHARACTERIZING METEOROID BULK DENSITIES

Sigrid Close*[1], Alex Macdonell[2], Steven Pifko[1], Ryan Volz[1], Meers Oppenheim[2]
[1]*Stanford University, CA*
[2]*Boston University, Boston, MA*

Session J5: New Telescopes, Techniques, and Observations II
Room 265

Co-Chairs: Richard Prestage, *NRAO - Green Bank*
Richard Bradley, *National Radio Astronomy Observatory*

13:20 J5-1 A NEW TECHNIQUE FOR PRIMARY BEAM CALIBRATION OF DRIFT-SCANNING, WIDE-FIELD ANTENNA ELEMENTS

Jonathan C. Pober*, Aaron R. Parsons
UC Berkeley, Berkeley, CA

13:40 J5-2 NEXT GENERATION POLARIMETER MODULES FOR THE QUIET EXPERIMENT

Kieran Cleary*[1], Rodrigo Reeves[1], Rohit Gawande[1], Anthony C. S. Readhead[1], Todd Gaier[2], Pekka Kangaslahti[2], Lorene Samoska[2], Mikko Varonen[2], Hogan Nguyen[3], Fritz DeJong[3], Donna Kubik[3], Osamu Tajima[4], Masaya Hasegawa[4], Makoto Nagai[4], Koji Ishidoshiro[4], Sarah Church[5], Patricia Voll[5], Mark McCulloch[6], Lucio Piccirillo[6]
[1]*California Institute of Technology, Pasadena, CA*
[2]*Jet Propulsion Laboratory, Pasadena, CA*
[3]*Fermi National Accelerator Laboratory, Batavia, IL*
[4]*High Energy Accelerator Research Organization (KEK), Tsukuba, Ibaraki, Japan*
[5]*Stanford University and Kavli Institute for Particle Astrophysics, Stanford, CA*
[6]*University of Manchester, Manchester, Cheshire, UK*

14:00 J5-3 ULTRA-WIDEBAND SAMPLER (10 TO 20GSPS) ANALYSIS AND TEST RESULTS

David W. Hawkins*[1], David P. Woody[1], Kevin P. Rauch[2]
[1]*PMA-OVRO, California Institute of Technology, Big Pine, CA*
[2]*Astronomy, University of Maryland, College Park, MD*

14:20 J5-4 GPU ACCELERATED PROCESSING FOR VLBI DIGITAL BACKENDS

Mark D. McCurry*[1], Christopher Beaudoin[2], Geoffrey B. Crew[2]
[1]*ECE Department, Clarkson University, Potsdam, NY*
[2]*MIT Haystack, Westford, MA*

14:40 J5-5 INSTRUMENTATION FOR REAL-TIME CYCLIC SPECTROSCOPY OF PULSAR SIGNALS

Glenn Jones*[1], Paul B. Demorest[2]
[1]*Caltech, Pasadena, CA*
[2]*NRAO, Charlottesville, VA*

15:00 Break

15:20 J5-6 FAST RADIO TRANSIENT DETECTION AS A BIG DATA CHALLENGE

Dayton L. Jones*, Kiri L. Wagstaff, David R. Thompson, Larry R. D'Addario, Robert Navarro, Chris A. Mattmann, Walid A. Majid, Joseph Lazio, Robert A. Preston, Umaa D. Rebbapragada
Jet Propulsion Laboratory, California Institute of Technology, Pasadena, CA

15:40 J5-7 SIGNAL EXTRACTION FOR SKY-AVERAGED 21-CM EXPERIMENTS

Geraint J. Harker*[1], Jonathan R. Pritchard[2], Jack O. Burns[1], Judd D. Bowman[3]
[1]*Center for Astrophysics and Space Astronomy, University of Colorado, Boulder, CO*
[2]*Physics Department, Imperial College London, London, United Kingdom*
[3]*School of Earth and Space Exploration, Arizona State University, Tempe, AZ*

16:00 J5-8 A RADIO SEARCH FOR EXTRATERRESTRIAL INTELLIGENCE IN THE KEPLER FIELD

Andrew P. V. Siemion*[1], Paul Demorest[2], Abhimat Gautam[1], Eric Korpela[1], Ron Maddalena[2], Dan Werthimer[1], Jeff Cobb[1], John Ford[2], Andrew Howard[1], Glen Langston[2], Matt Lebofsky[1], Geoff Marcy[1], Jill Tarter[3]
[1]*University of California, Berkeley, Berkeley, California*
[2]*National Radio Astronomy Observatory, Green Bank, West Virginia*
[3]*SETI Institute, Mountain View, California*

16:20 J5-9 MEASURING THE SMALL-SCALE CMB POLARIZATION WITH ACTPOL

Michael D. Niemack*
NIST, Boulder, CO

16:40 J5-10 MODELING OF RADAR SCATTER FROM ICY AND YOUNG ROUGH LUNAR CRATERS

Thomas W. Thompson*[1], Eugene A. Ustinov[1], Paul D. Spudis[2], Brian W. Fessler[2]
[1]*Caltech / Jet Propulsion Laboratory, Pasadena, CA*
[2]*Lunar and Planetary Institute, Houston, TX*

17:00 J5-11 KA-BAND SOLAR FLUX STUDY FOR G/T MEASUREMENTS

Arthur C. Densmore*[1,2], Gerry Seck[1], Yahya Rahmat-Samii[2]
[1]*Datron Advanced Technologies, L-3 Communications, Simi Valley, CA*
[2]*EE, UCLA, Los Angeles, CA*

Author Index

A B C D E F G H I J K L M N O P Q R S T U V W X Y Z

A

B

C

D

E

F

G

H

I

J

K

L

M

N

O

P

Q

R

S

T

U

V

W

X

Y

Z

Integrated Micro-Fluidic Channel on RF Circuit toward Lab-on-a-Chip Application

Pouya Talebbeydokhti, Mingguang Tuo, Qi Tang, Pak Wong, and Hao Xin
University of Arizona, Department of Electrical and Computer Engineering, Tucson AZ
University of Arizona, Department of Aerospace and Mechanical Engineering, Tucson AZ

This work presents the research done on design, simulation, fabrication, and measurement of an integrated micro-fluidic channel on a coplanar waveguide (CPW) over the continuous frequency range from 1 GHz to 10 GHz towards lab-on-a-chip application. Lab-on-a-chip is a rapidly emerging field in which micro volumes of fluidics are manipulated for further characterization. The high field associated with these electrically small structures may be exploited for means of detecting the presence of a foreign body or substance. In order to be able to do this, channels with appropriate dimensions are needed.

Polydimethylsiloxane (PDMS) was used for fabrication of the micro-fluidic channel. PDMS is an important material for lab-on-a-chip, an emerging technology to automate biological and chemical operations in micro-fluidic devices. The CPW structure was fabricated from gold on a quartz substrate using electron beam evaporation. The channel with a width and height of 1 mm and 0.5 mm inside the PDMS is fabricated using a laser cut machine and bonded to the quartz substrate with the oxygen plasma treatment.

For measurement we applied on-wafer calibration technique to accurately determine the scattering parameters of the integrated device. Figure 1 shows on-wafer measurement setup. Various types of liquids including distilled water, alcohol, E Coli solution, solutions containing gold nano-particles and carbon nanotubes (CNT) have been measured using the fabricated micro-fluidic channel and CPW structure. Finite-element modeling using High Frequency Structure Simulator (HFSS) has also been performed to evaluate the accuracy of characterizing liquid dielectric properties using this integrated micro-fluidic channel and CPW structure.

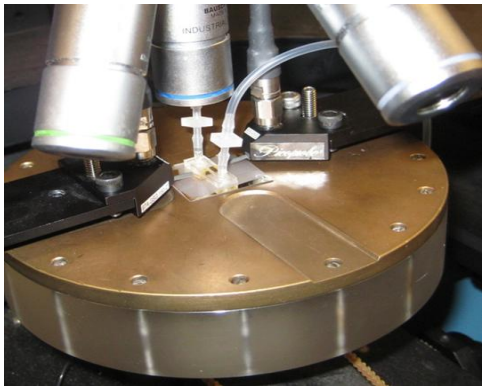

Figure 1. Experiment set-up of the wafer probed CPW transmission line integrated with a PDMS micro-fluidic channel.

Complex Permittivity Phantom Tissue Measurements using a TRL Calibration Fixture

Xavier Palomer*[(1)], Ved Topkar[(2)], and Zoya Popovic[(1)]
(1) University of Colorado, Boulder, USA
(2) Fairview High School, Boulder, USA

When designing body-worn or implanted antennas, it is important to know the electrical properties of the human tissues in the neighborhood of the antenna. In addition, testing of such antennas is often not practical with live models, and phantom tissue models can be used as an approach to design and validation (Topsakal et al, IEEE T-MTT, vo. 56, pp. 1001-1008, Apr.2008). A common method for measuring tissue parameters is an open-ended coaxial probe, which however requires full-wave modeling of the fringing fields, implying difficult calibration (Stuchly et al, IEEE T-MTT, vo 30, pp 82-86, Jan 1982). Tissue properties range from $\varepsilon r=40$ and $\sigma=1 Sm^{-1}$ (skin) to $\varepsilon r=5.2$ and $\sigma=0.05\ Sm^{-1}$ (for fat) and are difficult to exactly and repeatably reproduce. Tissue phantoms are typically made by mixing water, oil, salt, household detergent, agarose and p-toluic acid resulting in a gel-like consistency, making it difficult to fabricate in standard shapes used for microwave material measurements.

Here we present an alternative method for tissue phantom measurements using thru-reflect-line (TRL) calibration with custom-designed low-cost fixtures shown in the figure below. Since the TRL calibration error network has fewer unknowns than the number of measurements, additional information, such as complex propagation constant or reflection coefficient of the reflect standard can be extracted from the measurement. Here we use this property of TRL to extract complex propagation constant of a superstrate covered microstrip line, from which the superstrate properties can be found. Several superstrates with properties mimicking skin, fat and muscle are fabricated and will be presented. The frequencies of interest for implanted and body-worn antennas are investigated (approximately 1-10GHz).

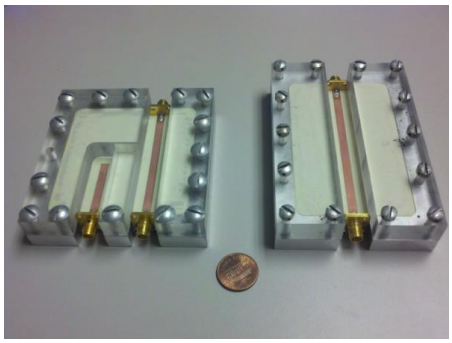

Figure: Photograph of fixture for TRL-calibrated measurements of complex permittivity of phantom tissues.

Electromagnetic Metrology on Construction Material and Corrosion: Concrete and Iron Oxides

Sung Kim* [(1)], Jack Surek[(1)], James Baker-Jarvis[(1)], Dat Duthinh[(2)],
Paul Stutzman[(2)], Shuangzhen Wang[(2)], and Edward Garboczi[(2)]
(1) National Institute of Standards and Technology, Boulder, Colorado USA
(2) National Institute of Standards and Technology, Gaithersburg, Maryland USA

Over the last several decades, many of electromagnetic measurement approaches such as ground penetrating radar (GPR), induction, thermography, and direct-current (DC) electrochemical impedance have been developed to qualitatively and quantitatively investigate concretes and embedded reinforcing bars. Most of these methods, however, are not very effective in monitoring and assessment of corrosion on steel reinforcements. This paper reports on dielectric and magnetic measurements and characterizations for concrete and corrosion samples. Our main goal is to find unique spectra of corrosion to quantify its extent.

This paper discusses the dielectric characterization of concrete and the investigation of the frequency response of iron oxides involved in corrosion. To quantify concrete and corrosion, we extracted material parameters from measured S-parameters. Concrete samples collected from a bridge along US Highway 34 near Estes Park, CO, were machined to fit into a 77-mm coaxial transmission line, WR-284 (S-band), and WR-90 (X-band) rectangular waveguides, which cover the frequency band from 45 MHz to 12 GHz, although there are some frequency gaps. In the case of the 77-mm coaxial measurement, we examined the temperature variation from -60 to +80 ^{o}C to obtain the permittivity (ε_r') and loss tangent ($\tan\delta$). Interestingly, it is seen that both of permittivity and loss tangent increase, as temperature is increased. In addition, the skin depth (σ_s) and attenuation constant (α) of the concrete sample were computed using the data from the coaxial transmission line and waveguide measurements, which give some useful information to the GPR approach—we plot propagation loss in dB/cm and show its variation 1.2 and 2.4 dB/cm, respectively, for concrete and mortar at 10 GHz. In order to study the material properties of the corrosion, iron oxide components that are in the form of pigment powders (hematite (α-Fe_2O_3), magnetite ($FeO.Fe_2O_3$), goethite (α-FeOOH), and maghemite (γ-Fe_2O_3)) were tested. Also, powder ground from corrosion sample harvested as flakes from a bridge girder from US Highway 34 was measured and compared. The dielectric and magnetic material parameters, ε_r and μ_r, of the iron oxides in powder form were calculated from the S-parameters measured at 0 to 6 GHz using a 7-mm coaxial fixture. Finally, we performed a 2.4-mm coaxial open probe measurement on these powders to mimic the *in-situ* measurement. These corrosion measurements indicate that magnetite is the most lossy of the pigment powders.

A 50-W 71%-Efficient CW GaN Amplifier for Tissue Ablation

Jennifer Imperial*, Michael Roberg and Zoya Popovic
Department of Electrical, Computer, and Energy Engineering
University of Colorado, Boulder, CO 80309

This paper presents design and measurements of a narrowband, high efficiency, and high power GaN amplifier at 2.45 GHz intended for medical tissue ablation and cauterization applications. High-efficiency operation for several Triquint TGF2023 device sizes is achieved by driving the devices into heavy compression and shaping the waveforms with harmonic terminations at the output. To present the terminations at the virtual drain reference plane of the device, the parasitic associated with the device and package are estimated from the datasheet and bond-wire and package models created using full-wave (HFSS) and circuit (AWR MO) simulations. The amplifiers are designed on 30-mil Rogers 4350B substrate and the terminations are created using open-stub resonators.

Class F^{-1} amplifiers using 2.5-mm and 5-mm devices yield power added efficiencies (PAE) of 77% and 82% at output powers of 3.8W and 12.6W, respectively and with a 30-V drain supply. Class F^{-1} is the chosen for the class of operation to exploit the high-voltage handling capabilities of GaN devices. Desired harmonic terminations for the large devices are difficult to achieve due to the high 5.9-pF output capacitance, so a Class-C design was implemented. PAE of 71% with 50W of output power at the drain of the device is reported at a drain voltage of 34V.

Physical efficiency limiting factors are output capacitance, possible odd mode excitation of the device and unit cell power combining topology. To reduce sensitivity to fabrication tolerance and to address possible odd mode excitation, the microstrip taper can be made much wider than the device and the harmonic resonators at the output will be placed farther from device in the next 20mm device design. Challenges related to tissue ablation which results in load variations are also addressed.

Figure: Measured CW power amplifier performance at 2.45 GHz.

Analytical Model of a Helmet-Mounted Conformal Patch Antennas for an Assortment of Canonical Shapes

Boliong Amang*[(1)], Gregory M. Wilkins [(1)], and Steven Weiss [(2)]
(1) Morgan State University, Baltimore, MD 21251
(2) Army Research Laboratory, Adelphi, MD 20783

The analytical analysis of a conformal patch antenna situated on the helmet of a soldier is presented. This analysis uses the classical cavity model of the patch antenna and is primarily directed to determine resonant modes for a variety of canonical shapes. As a helmet is approximately spherical in shape, patch antennas having curvatures described with spherical coordinates are presumed.

The shapes analyzed in this presentation are presented in Figure 1. Because of span limitations in the "theta" and "phi" directions, non-integer orders of associated Legendre functions emerge in the analytical formulation of the resonant (eigenvalue) modes. Application of these functions must be carefully applied and such details will be presented. In addition to the non-integer order(s) of the associated Legendre functions, the effects of the radius of curvature are quantified. The resonant modes found to approximate the Schumann resonance formulations normally applied to the analysis of global electromagnetic resonances. These analytical results are compared to solutions of the transcendental equations that emerge when solving for the electric fields underneath the patch in the r-direction. Perturbations of this equation demonstrate that the height of the patch above the ground plane is not a first order effect on the resonance as long as this height is much less than the radius to the center of the spherical coordinate system. The calculated resonances are then compared to measured data for validation of the theory.

Additionally, each of the shapes is modeled on HFSS to compare the analytic and measured results to simulated data. The simulations provide an additional check on the models and lend insight into the placement of the probe feeding the antenna.

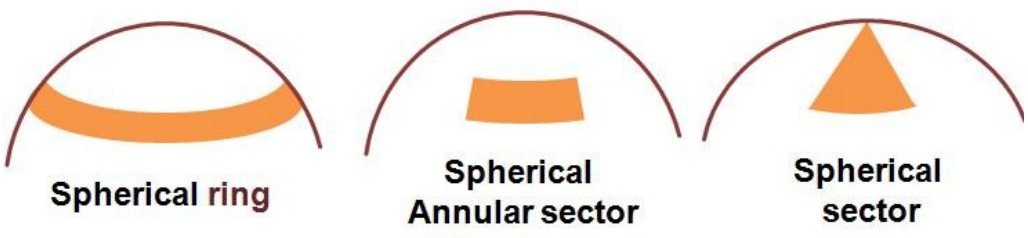

Figure 1 – Canonical shapes

Automated Airborne Communication Test System

The U.S. Army's Communications-Electronics Research, Development, and Engineering Center (CERDEC) Space and Terrestrial Communications Directorate (S&TCD) is the Army's primary investigator for testing and evaluation of antennas for Army aviation platforms. To aide in this work, CERDEC S&TCD is developing the Automated Airborne Communications Test System (AACTS) to provide an automated system for in-field aviation antenna testing with wireless control of airborne-mounted test equipment with the goal of reducing flight time and provide repeatable, quantitative results for digital and analog signals. The final product is a single system capable of conducting tests for performance patterns, communication range, and bit error rate (BER) and signal-to-noise-and-distortion (SINAD) tests automatically with minimal operator intervention.

The AACTS system will replace current measurement techniques involving an engineer located on the airborne platform to manually configure equipment during testing. Airborne equipment will be consolidated into a single rack-mounted unit that will be configured by engineers at a ground station. Test capabilities will be expanded to allow for simultaneously measurement of antenna performance patterns on four frequencies. Two antennas will be able to be tested during a single flight without the need to land for reconfiguring with the incorporation of RF switching. These functions will provide a reduction in flight time and operator cost.

Range testing of antenna effects on analog systems is currently performed by a subjective voice quality metric. The AACTS will enable the support of wide and narrow-band analog and digital system testing and eliminate subjectivity will the incorporation of automated SINAD for analog systems and BER testing for digital waveforms. The quantitative results will provide a more robust characterization of the antennas performance and affects on the waveform.

RF Propagation Measurements in Mountainous Terrain

William O'Keefe Coburn*, Mark Berry, Neal Tesney and Brian Gollsneider
U.S. Army Research Laboratory, Adelphi, MD 20783, USA

The U.S. Army Research Laboratory (ARL) conducted experiments using amplifiers and an array of antennas to characterize the propagation of radio frequency (RF) signals at White Sands Missile Range (WSMR), NM. The motivation for this work is that current communication systems still experience dead zones and shadowed areas. Further understanding of propagation effects, especially comparisons between experimental and modeling results, should lead to improved coverage. The amplifier/antenna systems were put together by Raytheon in Tucson, AZ. The five systems are comprised of FM radio transmitters and six-element array antennas mounted on a portable tower system, as shown in Figure 1. Propagation studies were conducted at 86 MHz both experimentally and by modeling using two different software packages. The terrain map for the area was obtained from the internet with the transmitter/receiver layout defined using the known GPS coordinates. Comparisons will be made between the experimental and selected modeling results. The path loss exponent is estimated by curve fitting the measured and calculated field strength as a function of range. An average of the measurements indicates $1/R^{3.4}$ dependence for received power with distance in mountainous terrain at WSMR. The Longley-Rice model for far-field propagation produced $1/R^3$ range dependence. At distances greater than 1 km, the Longley-Rice results track the data within a few dB for most of the transmitter sites.

(a) (b)

Figure 1. Transmitter system in (a) nested position and (b) erected.

Acoustical Modulation Sensor Measurements

W. A. Davis[1]*, T. Yang[1], J. Coggin[2], and R. May[2]
1. Virginia Tech Antenna Group, Blacksburg, VA 24061-0111
2. Prime Photonics, 1116 South Main Street, Suite 200, Blacksburg, VA 24060
http://antenna.ece.vt.edu/; http:// www.primephotonics.com

Typical RFID tags send a modulated signal back to the reader in order to avoid detection issues. However, RFID tags use low power integrated chips to create the modulated signal. Commercial RFID chips would not survive in a high temperature and vibration environments of interest. Instead a mechanical vibration is used to modulate the RF signal as a sensor for either vibration or temperature. The mechanical vibration may be created by vibrations in the system or by an acoustical signal used to modulate a temperature dependent vibration of an electromagnetic structure, hence a RFID type of sensor.

The proposed sensor system is depicted below. A high-frequency RF power source excites the sensor. At the same time, a low-frequency acoustic power source may be used to excite the beam on the temperature sensor in order to modulate the impedance of the sensor. For a vibration sensor, the acoustic source is not needed. As a result, the reflected signal from the sensor has a modulated form. The sensor consists of a resonant structure that is modified by the modulation process. At the reader, the modulated reflected signal is mixed with the original high-frequency RF signal. A simple diode detector and low-pass filter are sufficient to detect the beam vibration frequency (ω_m). The beam vibration frequency (ω_m) changes as temperature changes or with vibration in the system. Thus, we can estimate the temperature or vibration by monitoring the detected vibration frequency. Due to the low-frequency aspect, acoustic energy couples to the beam very efficiently, compared to the RF coupling case. The proposed system is a hybrid approach using both acoustic and RF excitations.

Basically, the RF excitation and detection approach in the figure is a Doppler radar system, which is widely used in detecting and monitoring object movement. Due to the popularity, Doppler radar systems would be relatively cheap.

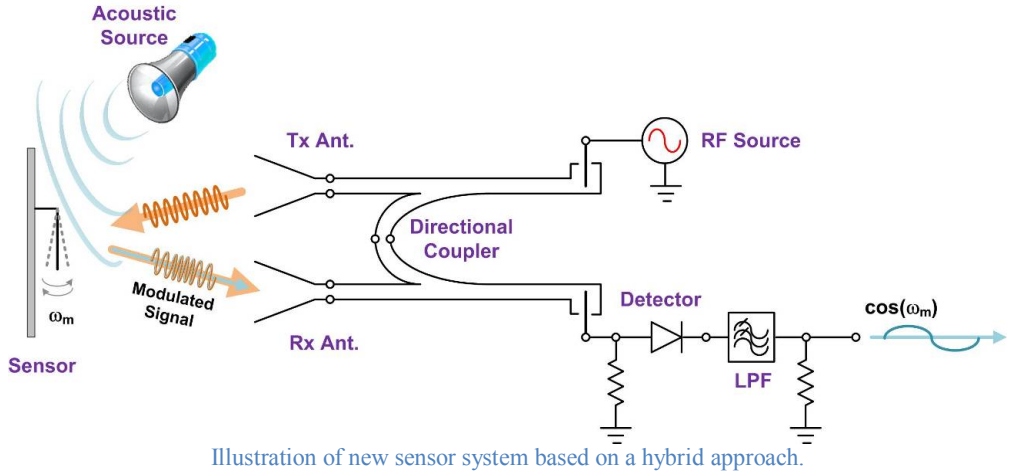

Illustration of new sensor system based on a hybrid approach.

SMAP Radiometer Front End Integrated Microwave Assembly

Negar Ehsan*[(1)], Joseph J. Knuble[(1)], Kevin Horgan[(1)], Fred E. Sacks[(2)], Dale F. Bankus[(3)], and Jeffrey R. Piepmeier[(1)]

(1) NASA Goddard Space Flight Center, Greenbelt, MD, 20771
(2) Base2 Engineering, LLC, Annapolis, MD, 21401
(3) Orbital Sciences Corporation, Greenbelt, MD, 20770

This paper presents the design, fabrication, and characterization of the Soil Moisture Active/Passive (SMAP) radiometer's Integrated Microwave Assembly (IMA). The IMA supports four primary functions for the radiometer, (1) sets the subsystem noise figure, (2) provides a stable, correlated brightness temperature calibration source, (3) provides isolation from the on-board radar, and (4) provides a temperature stable reference load for additional calibration purposes. The operational frequency of the radiometer is 1.4135 GHz with 24 MHz of bandwidth. Shown below is a block diagram of the entire radiometer; the inset shows a scaled drawing of the IMA enclosure and components. This radiometer analyzes horizontal and vertical polarized ground emissions simultaneously. The IMA comprises both custom planar (microstrip and stripline) microwave component designs and custom packaged components. The noise source, couplers and divider are planar configurations, while the switches, isolators and LNAs are separately packaged components. We will discuss the design, fabrication, and test of the components as well as the integration of the entire assembly and measurement results. The IMA is characterized for S-parameter performance, linearity, gain variation, and survival.

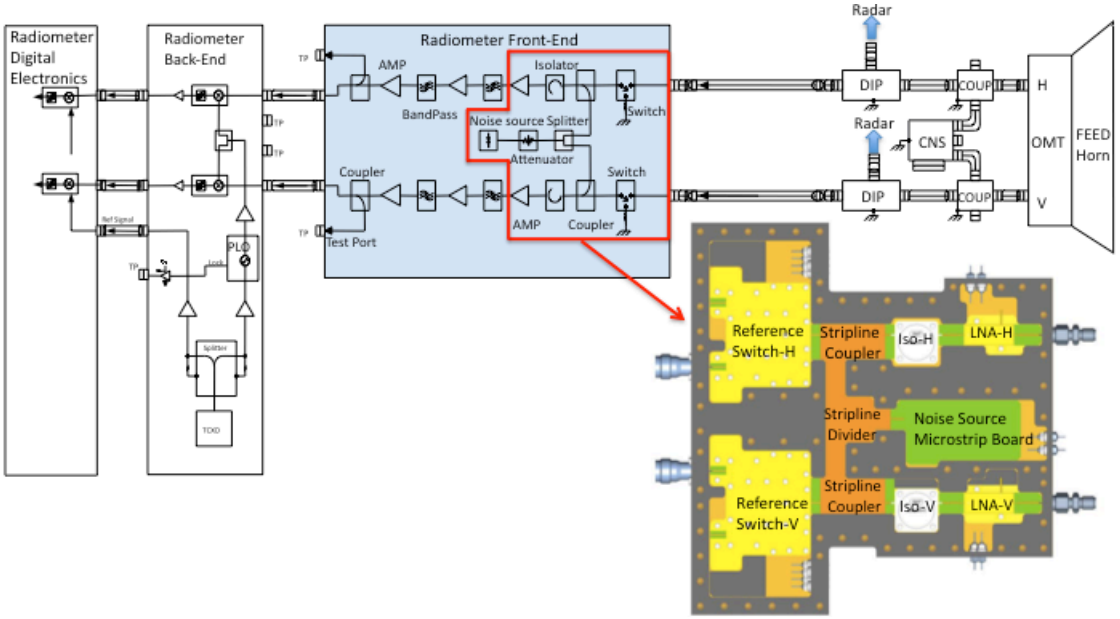

Figure 1. Radiometer block diagram. Radiometer consists of an antenna (shared between radar and radiometer), couplers, correlated noise source, diplexers (to isolate the radar and the radiometer), front-end, back-end, and digital electronics. The red box outlines the IMA inside the radiometer front-end, and the inset on the bottom right shows a scaled drawing of the IMA enclosure and components.

A First-Order Antenna Model with Applications to Reverberation Chamber Measurements

John M. Ladbury, Jason B. Coder, Ryan Pirkl

National Institute of Standards and Technology (NIST), Electromagnetics Division,
325 Broadway, Boulder, CO 80305 USA,
ladbury@boulder.nist.gov, 303-497-5372

In any measurement involving antennas, the characteristics of the antennas will be present in results. Mismatches and losses in the antennas will translate into decreased coupling between antennas, and it is difficult to separate out the antenna effects from the environmental effects. Various methods have been developed for dealing with these problems when the antennas are in low-reflection environments (anechoic chambers or free space, with the antennas sufficiently separated such that multiple reflections between antennas are minimized), but high-reflection environments (such as typical urban, office, and laboratory spaces) become significantly more complicated. A simple, practical, approach in such environments can be useful, even if it may not be perfectly applicable for all antennas.

In this presentation, we develop a simple first-order model for antennas that is consistent with, but more general than, most free-space models available in the literature. This model consists of a simple two-port network that accounts for all of the imperfections of the antenna (mismatch and loss), connected to an ideal (perfectly matched and lossless) antenna. We then determine the behavior of this model when the antennas are placed in an ideal reverberation chamber and show that predicted results are consistent with observed measured results. Finally, we examine the behavior of the models assuming a few special combinations of antenna loss, antenna mismatch, and chamber loss, and suggest a few practical approaches for determining the model parameters. In some special cases we can uniquely determine the model parameters with a few simple measurements, but in others the best we can do is determine possible ranges for the parameters.

RANDOM COUPLING MODEL FOR APERTURE EXCITATION OF WAVE CHAOTIC ENCLOSURES

Gabriele Gradoni, Thomas Antonsen Jr, Steven Anlage, and Edward Ott

Institute for Research in Electronics and Applied Physics (IREAP)
University of Maryland,
College Park, Maryland 20742, USA
(September 21, 2011)

Abstract

The random coupling model (RCM) is a statistical model that generates impedance and scattering matrices describing complicated electromagnetic systems. The RCM assumes that the trajectories of rays inside the system are chaotic and the system is coupled with external world through single or multiple ports. In the original model [Zhang *et al*. Electromagnetics, 26:3–35, 2006] the ports were assumed to be small compared with a wavelength. Recently, we proposed a generalization of RCM to include the case of large three-dimensional enclosures excited by extended sources and apertures [Antonsen *et al*. Proceedings of IEEE EMC 2011, p. 220].

In this contribution, we continue this analysis, first discussing the rigorous calculation of the (deterministic) *radiation admittance* for electrically wide rectangular apertures. In particular, we derive an integral dyadic expression for both the free-space conductance and susceptance. It is found that the radiation susceptance can be obtained by direct *Hilbert transform* of the radiation conductance. We obtained approximate closed-form expressions for the radiation admittance in the case of electrically wide and thin apertures.

The radiation conductance of the aperture is a key ingredient for the RCM for cavities with apertures. We present a numerical computation of the (statistical) cavity admittance distribution based on the calculated radiation conductance. In so doing, the universal fluctuation matrix of the chaotic scattering is used to transform the system dependent part modeled by the radiation admittance matrix. Finally, we compare the theory with numerical full-wave (FDTD) simulations. Achieved results are of interest in the analysis of mode-stirred reverberation chambers.

Work supported by AFOSR and ONR.

Practical Considerations for Measuring Antenna Efficiency in a Reverberation Chamber

Jason B. Coder[(1)], John M. Ladbury [(1)], and Mark Golkowski[(2)]
(1) National Institute of Standards and Technology, Boulder, CO USA
(2) University of Colorado Denver, Dept. of Electrical Engineering, Denver, CO USA

The ability to measure the efficiency of an antenna in a quick and accurate manner has long been desired. Current methods of measuring antenna efficiency are generally long, cumbersome, and can have high uncertainties (i.e. radiation pattern integration, Wheeler cap, etc.). In previous publications, it has been shown that modeling an antenna as an unknown two-port network could yield a quick way of determining the efficiency of an antenna inside a reverberation chamber. The downside of this method is that it only provides a lower bound of the antenna's efficiency. In addition to only providing a lower bound, one must be careful as to how this measurement is conducted and what data are acquired. Acquiring an insufficient amount of data could result in a poor lower bound (antenna efficiency <10%). Other measurement factors, such as antenna placement, other objects in the reverberation chamber during the measurement, and the stirring method used can have a significant influence on the quality of the lower bound estimate.

This presentation will show the two-port antenna model, and its specific application to antenna efficiency. After covering the equations relevant to finding antenna efficiency, we will show how different reverberation chamber configurations can affect the final result. This comparison will be made by measuring the same antenna in different chamber configurations and comparing the resulting lower bound of efficiency. Of particular interest is how different stirring configurations will impact the result. We will explore the differences of platform stirring, continuous stirring, frequency stirring, and stepped stirring in hopes of identifying the advantages and disadvantages of each. Part of this optimal configuration will also be to show examples of measurements where there are too few or too many data points.

A One-Antenna Reverberation-Chamber Technique for Estimating the Total and Radiation Efficiency

Christopher L. Holloway, Haider A. Shah, Ryan Pirkl,
John Ladbury, William F. Young, David A. Hill

National Institute of Standards and Technology (NIST), Electromagnetics Division,
325 Broadway, Boulder, CO 80305 USA,
holloway@boulder.nist.gov, 303-497-6184

In this presentation, we present a new one-antenna reverberation chamber method that allows for the determination of the total and radiation efficiencies of an antenna. A reverberation chamber is basically a shielded room (metallic walls) with an arbitrarily shaped metallic rotating paddle (stirrer or tuner). The paddle is designed to be non-symmetric and is used to create continuously changing boundary conditions of the electromagnetic fields in the chamber. Rotating the paddle creates a statistical environment in a reverberation chamber and this statistical environment offers a unique test facility. Electromagnetic reverberation chambers are becoming popular as an alternative test facility for both electromagnetic and electromagnetic compatibility measurements. Initially, reverberation chambers were used as high field amplitude test facilities for electromagnetic interference and compatibility, and are currently used for a wide range of other measurement applications. While reverberation chambers have been used in the past for estimating the antenna efficiency of an antenna, the previous approaches either: (1) requires knowledge of the efficiency of a reference antenna, or (2) assumes two identical antennas are used. The approach discussed in this paper allows one to estimate the efficiency of one antenna, and does not require one to know the efficiency of a reference antenna. The technique combines both time-domain and frequency-domain processed data collected in reverberation chamber experiments. Combining data in these two domains allows for the determining of the efficiency of an unknown antenna. In this paper we present the technique and present experimental data in order to illustrate the validity of the one-antenna technique. This technique assumes ideal chamber behavior, and any deviation in this assumed behavior can dominate uncertainties in this one-antenna approach (this point will be discussed in the paper).

Measuring Total Radiated Power of Wireless Devices in a Reverberation Chamber

Colton Dunlap*, William F. Young, John Ladbury, Erik Engvall,
Christopher L. Holloway
The National Institute of Standards and Technology (NIST), Electromagnetics Division, 325 Broadway, Boulder, CO 80305 USA,
colton.dunlap@nist.gov, 303-497-7358; wfy@boulder.nist.gov, 303-497-3471

Electromagnetic reverberation chambers have been used for a variety of measurements in the past, such as radiated immunity of components and large systems, radiated emissions, biological and biomedical effects. More recently, these chambers are serving as testing environments for estimating antenna efficiency and simulating wireless multipath. Here we discuss using the reverberation chamber for measuring the total radiated power (TRP) of a portable wireless device. Knowing the differences in TRP are important when analyzing radio frequency propagation results where these radios are used as the radiating source.

In testing wireless systems, it is often difficult to separate the antenna from the actual wireless device because the antenna is closely integrated with the device. The antenna may be part of the device case or embedded within the circuitry, and thus the antenna radiation pattern and impedance mismatch are impacted by the presence of the device. Even if the antenna is detachable, in many cases the TRP is best measured using the combination of the antenna and wireless device because that mimics the operational configuration more closely. Here we use the reverberation chamber to measure the TRP of several radios used in narrowband radio frequency propagation studies. We discuss the reverberation chamber TRP measurement procedure and provide results for portable radios operating at 430, 750, 900, 1800, 2400, and 4900 MHz. The measurement process includes quantifying the chamber losses at the specific frequencies of interest. One insight obtained by these measurements includes the ability to quantify the variation in TRP results caused by the overall inefficiency associated with the complete device and antenna setup. Finally, we discuss some measurement challenges unique to reverberation chambers when measuring the TRP.

Comparison of Various Antenna Efficiency Determination Methods

Rick Smith[(1)]
(1) ITT Corporation, Fredericksburg, VA 22406

ITT has been using both its own ETS-Lindgren SMART200 mode-stirred chamber (MSC) and a commercial Satimo STARGATE-64 3-D anechoic-chamber range for antenna efficiency measurements for some time. Prior to the appearance of the self-contained MSC measurement method recently presented by Holloway [*Holloway, Shah, Pirkl, Ladbury,. Young, and Remley,* "Determining the Antenna Efficiency in a Reverberation Chamber Using a Three-Antenna Method," APS-URSI Conference, July 2011.], MSC efficiency measurements made at ITT were confined to the well-known method involving comparison with an antenna of known efficiency [*Piette*, "Antenna radiation efficiency measurements in a reverberation chamber**,"** Radio Science Conference, 2004. Proceedings. 2004 Asia-Pacific, 24-27 Aug. 2004, pp. 19 – 22]. Recently ITT has implemented the new method. Comparisons between efficiency measurements of several antennas made in the ITT MSC and in the Satimo range, along with measurements of some of the same antennas performed in the MSC at NIST in Boulder, CO will be presented. For some of the antennas tested, efficiencies predicted by computer simulations, including HFSS, will also be presented for comparison. For the ITT MSC measurements, the effects of frequency and position/polarization stirring on the accuracy will be shown for specific cases. Antennas tested will include AEL H-1479 and ETS-Lindgren 3117 horns and an ETS-Lindgren 3148B log-periodic, along with other antennas. Accuracies of the MSC method vs. that of the 3-D anechoic chamber method will be discussed. Peak gain measurements obtained at the Satimo range will be compared with manufacturer specifications for the commercial antennas, as a separate check of accuracy. Factors potentially affecting the accuracy of the efficiencies predicted by the computer simulations will also be discussed. Issues specific to the SMART200 chamber and other equipment used in the measurements at ITT, including two different vector network analyzers, will be discussed, as well.

Verification of K-factor Based Formula for Measurement Uncertainty in Reverberation Chamber

Xiaoming Chen [(1)], Erik Engvall *[(2)], and Per-Simon Kildal [(1)]
(1) Chalmers University of Technology, Gothenburg, Sweden
(2) National Institute of Standards and Technology, Boulder, USA

To achieve good measurement accuracy in reverberation chamber (RC) it is of importance to have as large number of independent measurement samples as possible. In RC, independent samples are usually introduced by moving, or rotating, mode stirrers. The RC used in this paper is Bluetest HP reverberation chamber (see Fig. 1 (left)), which makes use of plate, platform and wall antenna stirring to generate independent samples. Previously, the theoretical measurement uncertainty STD was found to be inversely proportional to the square root of the number of independent samples N_{ind}, and that this N_{ind} increases with the square of the frequency, but experimental STDs do not follow this behavior. Instead there is a residual error that in practice cannot be overcome. It has also been shown previously that the field amplitude distribution becomes Rician when the chamber is loaded with absorbing objects. We have found that the Rician K-factor determines the residual uncertainty of measured efficiency-related results in the reverberation chamber, and that this can be reduced inversely proportional to the number of platform positions (platform stirring) and chamber antennas used (polarization stirring). The findings have resulted in the following uncertainty formula for the STD:

$$\sigma = \sqrt{1/N_{ind} + K_{av}^2/N_{UMP}} \,/\, \sqrt{1+K_{av}^2} \tag{4}$$

where N_{ind} is the number of independent samples when the average K-factor K_{av} is zero, and N_{UMP} is the number of fixed chamber antennas (antennas normally mounted on the walls of the RC) times that of independent platform positions. We will present results from measuring STD in two different Bluetest reverberation chambers for verification of the correctness of the theory. One example of results is shown below.

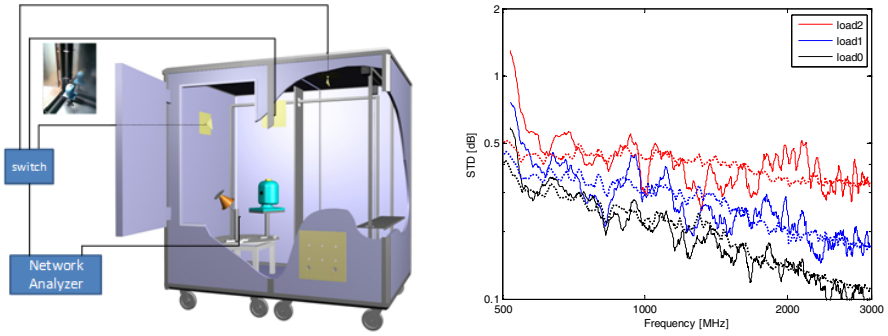

Figure 1: Drawing of Bluetest HP reverberation (left); measured STDs v.s. theoretical models for different loadings (right).

Improving the Accuracy of Reverberation Chamber Measurements: Optimal Stirring Procedures

Ryan J. Pirkl*[1], Kate A. Remley[1], and Christian S. Lötbäck Patané[2]

[1] National Institute of Standards and Technology, Boulder, CO, USA
[2] Bluetest AB, Gothenburg, Sweden

Reverberation chambers are statistics-based measurement tools, whereby their utility depends on their ability to generate a set of nominally independent measurements. As with any statistical quantity, correlation among reverberation chamber measurements will degrade the accuracy of the desired measurement statistic (e.g., average power). Although measurement correlation may be compensated by simply taking more measurements, this brute force solution results in an inefficient measurement procedure that is complicated by the fact that correlation increases as more measurements are taken. A more efficient solution is to minimize measurement correlation by optimizing experiment design.

This presentation examines how correlation between reverberation chamber measurements is impacted by one's stirring procedure (i.e., the process or algorithm used to choose a set of stirrer positions/angles for the measurements). Using autocovariances, correlation matrices, and an entropy-based correlation metric quantifying the effective number of uncorrelated measurements in a given measurement dataset, we evaluate the performance of various synchronous, asynchronous, and interleaved stirring procedures. Analysis of the correlation metrics reveals that measurement pairs tend to be highly correlated when (1) one stirrer's position/angle is identical for both measurements or (2) the relative change in all stirrers' positions/angles is small. In the former, one of the stirrers is not being used to decorrelate the measurements; in the latter, none of the stirrers are displaced/rotated by a distance/angle that exceeds their coherence distance/angle. These observations suggest that an optimal stirring procedure should (1) use unique stirrer positions/angles for all measurements and (2) uniformly distribute the measurement points in the stirrers' position/angle space. Experimental results for a stirring procedure meeting these criteria confirm their importance in minimizing measurement correlation.

"Utilizing Reverberation Chambers as a Versatile Test Environment for Assessing the Performance of Components and Systems"

Abstract: Electromagnetic reverberation chambers have been used for many years by the Electromagnetic Compatibility (EMC) community to measure the susceptibility and emissions for various electronic components and systems. This presentation describes how statistical processes were used to reduce the uncertainty of these chambers to a level necessary for precision metrology applications. These processes were applied to the calibration of electromagnetic field probes and the assessment of antenna efficiencies. A brief comparison of traditional calibration methods employing transverse electromagnetic (TEM) cells and anechoic chambers to the new statistical reverberant environment will be shown.

The presentation also shows how these techniques were later applied to a wide variety of aircraft measurements. A technique which utilizes two side by side reverberation chambers sharing a common wall with an arbitrary shaped aperture, useful for the assessment of component shielding, will be discussed. Utilizing this same approach, it is also possible to assess the shielding of large structures such as commercial aircraft. These aircraft shielding measurements are necessary for High Intensity Radiated Field Susceptibility (HIRF) certifications.

With the proliferation of wireless devices, it is important to understand how they behave in complex electromagnetic environments and how they interact with other devices and systems with which they are collocated. Aircraft environments have been shown to behave similarly to reverberation chambers and therefore these techniques can be employed to study propagation environments and system interactions. This presentation will provide examples of how these techniques were employed to measure bulk absorption used to simulate passenger loading of aircraft, field mapping which is useful for the evaluation of signal coverage and channel interference, as well as signal propagation characteristics.

By the conclusion of the presentation, attendees will understand the basic test methodology of reverberation chambers and how they may be used for cost effective and efficient testing of a wide variety of devices as well as for diverse applications.

Response of cavities with both regular and chaotic ray trajectories

Ming-Jer Lee*, Thomas Antonsen Jr, and Edward Ott
Institute for Research in Electronics and Applied Physics (IREAP)
University of Maryland, College Park, Maryland 20742, USA

The premise of the random plane wave hypothesis used to characterize fields in enclosures is that the underlying classical ray trajectories are ergodic. That is, rays visit all available space with all possible directions uniformly. For some shapes of enclosures this is not the case. In so called mixed systems, some rays are chaotic and visit subregions of space ergodically, while some rays are regular returning to the same place and traveling in the same direction. We study the statistical properties of the impedance matrix for a cavity in which both regular and chaotic ray trajectories coexist. For pure chaotic systems, the impedance can be described by Lorentzian random variables with a predicatable mean and width which are based on Random Matrix Theory. We generalize the theory to mixed systems by separating the impedance formula into regular and chaotic parts, treating each as a random variable and calculating the statistical properties individually. The contributions to impedance depend on properties of eigen modes which we characterize as being either regular or chaotic The chaotic eigenfunction amplitude at a given port can be described by a restricted random plane wave model and the regular eigenfunctions can be described by a random variable that is determined by the port position and the geometry. We show that chaotic and regular parts are both Lorentzian random variables for both one-port and two-ports cases, so the total normalized impedance is also Lorentzian distributed. We test the theory by solving the Helmholtz equation in a mushroom shaped cavity where there is a clear separation between regular and chaotic phase space. We solve the first 15000 eigenmodes, classify all of them into either chaotic or regular modes and calculate the corresponding impedance at different frequencies as different realizations. We compare the theoretical result with the numerical calculation for one-port and two-ports cases at different port positions.

A Metrology Infrastructure for Scientific Computing

Andrew Dienstfrey

Information Technology Lab, NIST, Boulder, CO

Computing has become an indispensable component of modern science and engineering research. As has been repeatedly observed and documented, processing speed measured in floating point operations per second has experienced exponential growth for several decades. These hardware efficiencies have been accompanied by innovations in mathematical algorithms, numerical software, and programming tools. The result is that, by any measure, the modern computer is many orders of magnitude more powerful than its early predecessors, capable of simulating physical problems of unprecedented complexity.

Given the success of scientific computation as a research tool, it is natural that scientists, engineers, and policy makers strive to harness this immense potential by using computational models for critical decision-making. Increasingly, computers are being used to supplement experiments, to prototype engineering systems, or to predict the safety and reliability of high-consequence systems. Such use inevitably leads one to question "How good are these simulations?" or, more succinctly, "Would you bet your life on them?" Unfortunately, most computational scientists today are ill equipped to address such important questions with the same scientific rigor that is routine in experimental science.

This talk will present an overview of the Virtual Measurement Systems Program under development in the Information Technology Laboratory of NIST. The purpose of this program is to advance a metrology infrastructure to support scientific computing. To understand this goal, the components of the metrology infrastructure to support physical measurement will be reviewed and the extensions necessary to bridge these concepts to scientific computing will be presented. Topics will include: verification, validation, and uncertainty propagation. Preliminary results from two diverse application areas – fire modeling for nuclear power plant safety and calibration of high-speed microwave oscilloscopes – will be presented as representative case studies.

Methods of Estimating Measurement Uncertainties

Michael H. Francis [(1)]
(1) National Institute of Standards and Technology, Boulder, CO 80305,
email: francis@boulder.nist.gov

The talk will cover various aspects of uncertainties. The difference between error and uncertainty will be indicated. What distinguishes type A from type B uncertainties, and the International Standards Organization (ISO) method of combining uncertainties (including the use of a coverage factor) and the limitations of this method will be discussed. The conditions for the validity of the Central Limit Theorem (n large is not sufficient) will be presented. We will also discuss general methods of estimating uncertainties such as theoretical and computational modeling, and changing the measurement set-up. We will present an approach to accounting for systematic errors. Some examples of determining uncertainties that are pertinent to antenna measurements will be given.

According to the ISO Guide to the Expression of Uncertainty in Measurement type A uncertainties are those determined by statistical methods, while type B methods are determined using any other method. Uncertainties are type B, when there is an insufficient amount of data to have reliable statistics. In this case, one must use non-statistical methods (such as theoretical models, or numerical simulations or making a limited number of changes to the measurement system). Some examples of these methods will be presented.

For systematic errors, one makes a correction using the best available knowledge. This knowledge is imperfect and there is a residual uncertainty associated with it that contributes to the overall measurement uncertainty.

It is often asserted that because there are a large number of uncertainty terms that the Central Limit Theorem applies. However, other conditions are necessary - especially that there not be a dominating uncertainty term.

This abstract is submitted for the Special Session on Numerical and Measurement Uncertainties.

CHARACTERIZATION OF PARALLEL-PLATE WAVEGUIDES FOR MATERIAL MEASUREMENTS

Youn Lee*[(1)], Amir I. Zaghloul[(1,2)]
e-mail: youn.m.lee2.civ@mail.mil
[(1)]US Army Research Laboratory, Adelphi, MD 20783
[(2)] Bradley Department of Electrical and Computer Engineering
Virginia Tech, VA 24061

The permittivity ε and permeability μ of a material can be deduced through measuring the transmission and reflection characteristics in a controlled medium that contains the material in question. Ray tracing and scattering matrix parameters are two methods used to calculate the refractive index n, and the associated ε_r and μ_r of the material. One of the controlled media that can be used in this process is the parallel plate waveguide, which supports dispersion-less TEM mode. The electric field is vertically polarized between the two horizontal conducting parallel plates. The transmitter and receiver are chosen to match the polarization in the parallel plate structure. A vertical probe, an open-ended waveguide, and an H-plane sectoral horn are among the feeds that satisfy this condition. This configuration was used to measure the parameters of metamaterials at the U.S. Army Research Laboratory (ARL) using sectoral horns as transmitting and receiving antennas. The parallel plate structure produced significant levels of noise, which in turn produced high levels of uncertainties in the measured data. Reflections off the edges of the parallel plate waveguide and considerable mismatches at the horns contributed to these uncertainties. Similar issues on scattering measurements in parallel plate waveguides have also been addressed recently (Larson, et al., URSI GASS, Istanbul, 2011). In this paper, resistive strips are used at the edges of the parallel plate waveguide, and they are optimized in values and locations to minimize the reflections into the region where the material under test is situated. This is illustrated in Figure1, where the transmitting and receiving antennas are connected to a network analyzer to measure the S parameters and receiving patterns for different locations of the transmitting antenna around the periphery of the circularly-shaped parallel plate waveguide. Varying the location of the transmitting antenna helps in measuring the isotropic versus non-isotropic nature of the material under test.

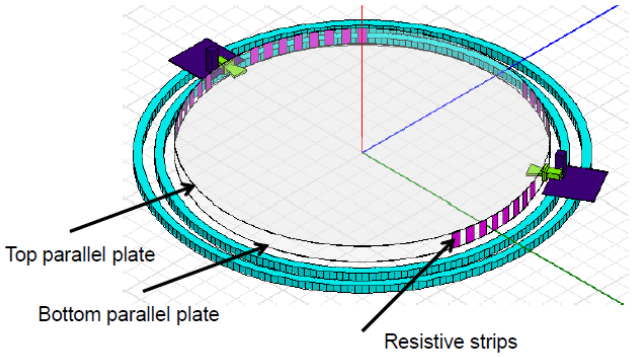

Figure 1. Parallel-Plate Waveguide Set Up

Increased Accuracy in the Measurement of the Dielectric Constant of Seawater at 1.413 GHz

By

Y. Zhou[1], R. Lang[1], C.Utku[2] and D. Le Vine[2]

1. The George Washington University, Dept. of Electrical & Computer Engineering, Washington, DC, 20052 USA
2. Ocean Sciences Branch / Code 614.2 NASA Goddard Space Flight Center, Greenbelt, MD 20771 USA

This paper describes the latest results for the measurements of the dielectric constant at 1.413 GHz by using a resonant cavity technique. The purpose of these measurements is to develop an accurate relationship between salinity/temperature and the dielectric constant of seawater for use by the Aquarius inversion algorithm. Aquarius is a NASA/CONAE satellite mission launched in June of 2011 with the primary mission of measuring global sea surface salinity to an accuracy of 0.2 psu. Aquarius measures salinity with a 1.413 GHz radiometer and uses a scatterometer to compensate for the effects of surface roughness.

The core part of the seawater dielectric constant measurement system is a brass microwave cavity that is resonant at 1.413 GHz. The seawater is introduced into the cavity through a capillary glass tube having an inner diameter of 0.1 mm. The change of resonance frequency and the cavity Q value are used to determine the real and imaginary parts of the dielectric constant of seawater introduced into the thin tube. Measurements are automated with the help of software developed at the George Washington University.

In this talk, new results from measurements made since September 2010 will be presented for salinities of 30, 35 and 38 psu with a temperature range of 0^{o}C to 35^{o} C in intervals of 5^{o}C. These measurements are more accurate than earlier measurements made in 2008 because of a new method for measuring the calibration constant using methanol. In addition, the variance of repeated seawater measurements has been reduced by letting the system stabilize overnight between temperature changes. The new results are compared to the Kline Swift and Meissner Wentz model functions.

Uncertainties Associated with Point Source Modeling in FDTD

Gregory M. Noetscher*[(1,2)], and Sergey N. Makarov[(1)]
(1) ECE Department, Worcester Polytechnic Institute, 100 Institute Rd., Worcester, MA 01609
(2) U.S. Army Natick Soldier Research, Development and Engineering Center, Natick, MA 01760

Point Sources modeled in the Finite Difference Time Domain (FDTD) Method include infinitely small electric and magnetic dipoles. Their modeling is important for path loss simulation, in particular when inhomogeneous dielectric and magnetic materials are considered. Potential sources of error include:

a) the effective size of "point" sources (cell vs. sub-cell models);
b) electric and magnetic static charging of point sources;
c) point sources located on a boundary separating two distinct media;
d) multiple point sources in close proximity to each other;
e) point sources as receiving elements (Faraday's coil).

In this study, we review the error sources listed above and provide methods of mitigating each. Special attention is given to a novel model of a magnetic current loop simulating an infinitely small electric dipole. A few illustrative examples related to Wireless Body Area Network (WBAN) applications are considered.

A New Paradigm in Solar Energy Harvesting: Characterization of High Absorption Nanopillar Array Photovoltaics

Timothy Brockett, Harish Rajagopalan, and Yahya Rahmat-Samii
University of California, Los Angeles, Los Angeles, CA 90095
brockett@ee.ucla.edu, harish@ee.ucla.edu, rahmat@ee.ucla.edu

Widespread utilization of solar energy has been limited due to practical issues such as low conversion efficiency and high cost. Although much research has been done in improving these issues, the technology has not progressed far enough to make solar energy a popular alternative for energy production. With solar energy being readily available and abundant, the ever-increasing demands for renewable energy have made new concepts in solar energy collection a paramount task for researchers.

Nanostructured photovoltaic solar cells have recently been introduced as improved alternatives to conventional bulk photovoltaics in increasing efficiency of solar energy collection. Such nanostructures feature inherent advantages that make them excellent candidates for maximizing solar energy absorption, conversion, and extraction. It has been suggested that these devices have the potential to exceed efficiencies of current solar cell technologies. In addition, they have the potential for favorable broadband and angle-independent performance that may eliminate the need for antireflection coatings or mechanical tracking used in many commercial solar cell installations.

This paper will present some of the first comprehensive investigations into the electromagnetic performance of these nanostructure solar cells and their implications in the overall improvement of solar cell technology. It will focus primarily on nanopillar arrays, which are large patterned arrays of nanosized columns that are one of the basic nanostructures currently processed. It will demonstrate the following: (a) Nanopillar array versus bulk (flat) solar cell absorption properties. (b) Material considerations including the dependence of the constitutive parameters on optical wavelength. (c) Examination of electric field magnitude inside and in the vicinity of the nanopillars. (d) Parametric investigations of nanopillar dimensions and configurations for absorption properties. (e) The application of traditional electromagnetic theory and concepts for nanopillar arrays. (f) Future concepts in nanostructure design for maximizing optical absorption. These detailed investigations can potentially lead directly to improved understanding and performance of nanostructured solar cells that will spearhead a new direction in efficient photovoltaic technology.

Effects of Beam Width and Surface Curvature on the Reflection Coefficient for a Conductor Coated with MagRAM

Edward J. Rothwell
Department of Electrical and Computer Engineering, Michigan State University,
East Lansing, MI, 48824, http://www.egr.msu.edu/~rothwell

Air vehicles are often coated with magnetic radar absorbing materials (MagRAM) to control radar cross section. Since the performance of these materials may degrade with time, it is essential to accurately measure the electromagnetic properties of such coatings *in situ*. In one technique a focused beam is used to illuminate the conductor-backed coating, and the measured reflected field is used to define a reflection coefficient. By comparing the measured reflection coefficient to one determined from theory, the properties of the coating may be found as the solution to the inverse problem.

It is essential that the material characterization process be accomplished in real time, and thus the theoretical reflection coefficient should be based on a simple model of the incident field and the coated surface. In practice, coated surfaces are of varying curvature with varying coating thickness, and the focused beam has a non-planar wavefront with a non-uniform phase distribution. Even so, to promote computational efficiency a simple scattering model based on an infinite planar structure illuminated by a plane wave is often assumed.

To assess the accuracy and usability of the simple model, the reflection coefficient for a two-dimensional Gaussian focused beam incident on a conducting cylinder with a MagRAM coating of constant thickness is computed. The incident field is represented as an angular spectrum of plane waves, and the coupling into each of the Fourier-Bessel coefficients of the coated cylinder scattered field is computed numerically. By varying the focused beam width and the radius of the cylinder, the relationship between the width of the beam and the curvature of the surface to produce a certain error compared to the simple planar model may be determined. To produce a realistic comparison, the theoretical scattered field is calibrated using a flat conducting surface (a metal plate) as is done in practice.

Wireless Power Transmission for Geophysical Applications

Xiyao Xin[(1)], Ji Chen[(1)], David R. Jackson[(1)], and Paul Tubel[(2)]

(1) Department of ECE, University of Houston, Houston, TX 77204-4005

(2) Tubel Energy, Inc., 800 Research Forest Drive, The Woodlands, TX 77381-4142

Wireless power transmission is useful whenever it is difficult or undesirable to physically connect a power source directly to a load or receiving device. Such a situation arises in various applications, one of which is in the geophysical area, where it is desirable to wirelessly power sensors situated along a pipe inside of an oil-producing well that is drilled horizontally. The pipe may have a break in it, as for example when connecting between a vertical well and a lateral well, and it is desirable to transmit wirelessly across the break. This investigation will focus on optimizing the achievable range and power transfer efficiency when transmitting wirelessly between two coils that are wrapped around a pipe in the presence of a lossy environment. Many of the conclusions apply to other applications, however, including wireless transmission between coils in free space or in other environments.

A CAD model for the transmit and receive coils is used in which each coil is modeled as an inductor in series with a resistor, along with a shunt capacitance placed across the circuit to model the stray capacitance of the coil and a shunt resistor placed across the inductor to model the eddy current losses in the lossy environment. This frequency-dependent resistor accounts for eddy current inside the pipe as well as in the external environment, which may include a lossy earth and/or water having various amount of salinity. The coil interaction is accounted for by a mutual inductance between the two coils.

Based on the simple CAD model, the power transfer efficiency is calculated, which is defined as the power that can be delivered to a match load on the receive coil to the power supplied by an ideal source connected to the transmit coil. Simple approximate formulas are also derived (in the weak-coupling limit) that directly show in a simple way the effects of the various coil parameters on the power transfer efficiency. The formulas show that in the weak-coupling limit the theoretical maximum power transfer efficiency is 50%, but the actual values achieved are usually much lower than this and depend on the level of coupling (which in turn depends on the coil separation), the frequency, the coil parameters, and the losses in the model. The effects of adding a ferrite layer between the coils and the pipe is also explored in an effort to improve the power transfer efficiency.

Simplified Test and Modeling for Passive RFID Tag Backscatter Link Analysis

Daniel G. Kuester[2], David R. Novotny[1], Jeffrey R. Guerrieri[1], and Zoya Popović[2]

[1] NIST, Boulder, CO, USA, 80305
[2] University of Colorado, Boulder, CO, USA, 80309

A passive radio frequency identification (RFID) tag backscatter measurement and analysis approach that does not use differential radar cross-section (RCS) (σ_Δ) is introduced. It is based instead on a new figure of merit that relates tag circuit parameters (efficiencies and chip sensitivity) to link power levels at a reader in any linear environment. The characterization depends on forward-link losses, which allow fading effects to be analyzed in terms of better-understood transmission effects.

A test method based on a new backscatter calibration device enables measurements to determine a tag's figure of merit. The device reflects pre-characterized modulation to calibrate measurements from ultra-high frequency (UHF) device under test (DUT) with ± 0.5 dB estimated uncertainty. Like σ_Δ, this error contributes proportionally to uncertainty of link estimates. Tests can be performed in realistic propagation scenarios, including path loss, and apply to link analysis under detuning similar to the test conditions. Experimental validation of the model comparing measured link parameters against circuit parameters on the tag agree to within the testbed uncertainty, both in free space and under detuning conditions.

For link analysis, the model gives a lower bound for backscatter into any monostatic reader from tag test data in a tag detuning state independent of fading. This lower bound is dependent on the tag impedance tuning state, but can be determined from tests in realistic environments. For return link power estimation of either bistatic or monostatic systems, backscatter fading into a reader can be decomposed into separate transmission losses of each of the incident and scattered paths, which are better understood channels than the backscatter link taken as a whole.

Green's Functions for Layered Media Having Anisotropic Properties

Gregory A. Mitchell[(1)] and Dr. Steven J. Weiss[(1)]
(1) The U.S. Army Research Laboratory, Adelphi, MD, 20783

The advent of metamaterials with tailored values of permittivity and permeability has considerably expanded the design space for applications to devices such as antennas. Inherently, such metamaterials are anisotropic. To gain insight into the effects such materials have on device performance, it is important to have properly formulated Green's functions. This paper will investigate such materials as configured in a stratified media. In the past, such work has been done for materials having naturally occurring anisotropic permittivities, but little information is available for the anisotropic permeability case. As metamaterials now offer new options to the engineering community, it becomes important to quantitatively analyze the Green's functions for metamaterials with anisotropic permeability for use in antenna applications. Two important considerations are the bi-axial and the uni-axial cases.

The Green's function for metamaterials that exhibit anisotropic permeability will be derived from a Hertzian dipole source for arbitrary values of the anisotropic permeability and permittivity tensors. General solutions to an anisotropic wave equation will be used to determine the final form of the Green's function. Once appropriate relationships for the Green's function have been derived, the stationary phase method will be utilized to determine the far-field radiation approximation for a dipole suspended above a quarter wavelength cavity. The cavity will be filled with a metamaterial exhibiting an anisotropic permeability and permittivity. The rigorous calculation of the Green's function for this type of metamaterial will provide an in depth view of what tradeoffs to expect in optimizing antenna performance for anisotropic values of permeability and permittivity.

Recent advances in nonlinear ferroelectric ceramics have resulted in new possibilities for advanced nonlinear devices for particle accelerator and rf applications. Beam diagnostics based on nonlinear waveguides are one possibility, since the frequency spectrum is a function of both beam intensity and pulse shape. Nonlinear structures may also find applications in rf sources for frequencies (such as sub-mm waves) not accessible by conventional technologies. Electromagnetic shock formation can be used to produce intense short broadband rf bursts. Finally, application of wave steepening/pulse compression effects in nonlinear waveguides to enhance the performance (gradient and efficiency) of wakefield accelerators is an exciting possibility.

A ferroelectric ceramic possesses an electric-field-dependent dielectric permittivity that can be rapidly varied by an applied bias voltage pulse. Ferroelectrics have unique intrinsic properties that make them extremely interesting for a number of high-energy accelerator and microwave applications. Response times of $\sim 10^{-11}$ sec for the crystalline form and $\sim 10^{-10}$ sec for ceramic compounds have been measured. Unlike semiconductors and plasma devices, ferroelectrics allow control of their dielectric properties in two directions using a single external control pulse, offering unique capabilities for high-power switching and tuning devices intended for accelerator and other rf applications.

The high dielectric constant of ferroelectrics (~500) is not desirable for many applications. For example, the use of high permittivity materials leads to enhanced wall losses in cylindrical geometries. Lowering the permittivity (and the loss tangent) through the use of ferroelectric-low loss tangent dielectric composites is the approach that is followed. Recent theoretical work has shown that ferroelectric composites can be designed that also preserve or even enhance the tunability of the material, and DC permittivities ~100 in nonlinear ferroelectric ceramics are feasible.

The new FACET (Facility for Advanced Accelerator Experimental Tests) at SLAC provides an opportunity to use the GV/m fields from its intense short pulse electron beams to perform experiments using the nonlinear properties of ferroelectrics. Simulations of Cherenkov radiation in the THz planar and cylindrical nonlinear structures to be used in FACET experiments will be presented. Signatures of nonlinearity are clearly present: superlinear scaling of field strength with beam intensity, frequency upshift, and development of higher frequency spectral components.

Superstrate-Enhanced Ultrawideband Tightly Coupled Array with Resistive FSS

William F. Moulder, Kubilay Sertel and John L. Volakis
ElectroScience Laboratory
The Ohio State University
Columbus, OH, 43212

Low-profile ultrawideband antenna arrays are critical in a number of military and commercial communications systems. Existing wideband arrays such as tapered slot (or Vivaldi) arrays are too thick ($0.5\lambda_{low}$) for some low frequency applications. Arrays of wideband planar elements (e.g. bowties, spirals) are subject to bandwidth deterioration when placed near a ground plane. EBG structures have been used to effectively alleviate ground effects in such planar arrays, but only operate over a narrow bandwidth. Ferrite ground planes can improve profile and bandwidth, but their weight and broadband losses are problematic. Tightly Coupled Arrays (TCAs), which exploit inter-element capacitance to counteract ground plane inductance, have been shown to provide bandwidths in excess of a (10:1) in conformal implementations. However, the bandwidth of these arrays is still limited by the presence of the ground plane. Specifically, the aperture height must be less than $\lambda/2$ above the ground plane at the highest frequency.

This paper presents a TCA configuration where a resistive FSS and superstrate are employed for enhanced bandwidth. The resistive FSS suppresses ground plane interference at frequencies where the ground plane spacing is roughly $\lambda/2$. Adding a superstrate greatly alleviates the efficiency degradation caused by the FSS. In effect, the superstrate draws power away from the FSS. The FSS and superstrate are synergistically designed to maximize bandwidth and efficiency.

As an example, a tightly coupled bowtie array with a bandwidth of 21:1 and efficiency greater than 74% across the band is presented. The configuration is validated with measurements of a prototype 4x4 coupled bowtie array with a resistive FSS and superstrate.

Efficient Evaluation of Radiation Patterns for Arbitrarily-Excited Antenna Arrays using Reciprocity in the Periodic FDTD Method

Minshen Wang*, Ji Chen, D. R. Jackson, and D. R. Wilton
Department of Electrical and Computer Engineering
University of Houston, Houston, TX, 77204-4005, USA

The array scanning method (ASM) provides the possibility of obtaining the radiation pattern for arbitrarily excited antenna arrays using a single-element modeling technique (*R. Qiang et al., IEEE Microwave and Wireless Components Letters, 2007*). However, in the ASM technique, a near-field to far-field transformation is still required. For highly directive leaky-wave antenna structures (*T. Zhao and D. R. Jackson, IEEE Trans. on Antennas and Propagation, 2005*), it may require significant CPU time in order to evaluate the near field accurately. In addition, truncation error can be introduced in the near-to-far field transformation.

In this paper, an efficient far-field radiation pattern evaluation method for periodic structures is presented. The method is based on reciprocity together with a periodic finite-difference time-domain (FDTD) method. Rather than integrating over the entire spectral axis, this approach evaluates the fields only within the visible spectral region. Using this technique, the far field radiation patterns of arbitrarily-excited arrays can be evaluated very efficiently. For comparison, radiation patterns calculated by the reciprocity approach, the array scanning method (ASM) approach, and the conventional FDTD method are obtained to demonstrate the efficiency and accuracy of the proposed method.

In addition, the far field radiation pattern of a complex 2-D periodic leaky-wave antenna with a high directivity is also calculated using our proposed method and is compared to the pattern obtained using the periodic spectral-domain method of moments (MoM). The results agree very well with the solution obtained by the MoM, even when the angle of the main beam is close to grazing (i.e., close to the horizon).

Unit Cell autonomy via Wireless Control of a Space-Fed Phased Array Antenna

Matthew Stoneback* and Yasuo Kuga
Department of Electrical Engineering
University of Washington, Box 352500, Seattle, WA 98195

In an effort to realize a phased array antenna which has reduced weight and complexity we have developed a unique wireless control scheme to realize unit cell autonomy. A prototype space-fed phased array antenna is presented to illustrate the key features of the wireless control mechanism and demonstrate its effectiveness. The antenna is a double-sided printed patch array functioning as a space-fed phased array. One side of the array faces the wirelessly propagated RF source and one side of the array faces outward towards the target-side or space-side of the system. This prototype builds on a previously demonstrated passive space-fed phased array by introducing a phase shifter between space-side and feed-side radiating elements. This allows for path length compensation such that the feed-side radiating elements are properly focused upon the wirelessly propagated RF source and also allows for rapid reconfiguration of the scan angle of the collimated beam on the space-side of the wireless phased array antenna. To control the array the each phase shifter is commanded with a modulated signal that is propagated wirelessly to each unit cell on a channel independent of the primary space-fed RF signal. This wireless control signal is processed by a small demodulator and interpreted by a processor at each unit cell. From this wireless control signal, the digital control signals required to command the RF phase shifter are uniquely generated at each unit cell. Additionally, a portion of the incident command signal is rectified and provided as DC power to the processor and phase shifter. In this manner the phased array unit cell is made to be autonomous. By eliminating the interconnects between unit cells in the phased array we propose that it can be reproduced and arrayed in a quantity and arrangement that is independent of any underlying RF or control signal distribution networks.

Radiation Characteristics of Triangularly-Bound Random Arrays

Kristopher R. Buchanan and Gregory H. Huff
Electromagnetics and Microwave Laboratory
Department of Electrical and Computer Engineering
Texas A&M University, College Station, TX 77843-3128 USA

Antenna arrays with periodic half-wavelength spacing and resonant elements are frequently used with narrow-band elements. Acceptable beam patterns are produced in this familiar periodic environment and it is well-known that grating lobes develop when the electrical separation increases beyond this ideal element spacing. This spacing becomes impractical for electrically large antennas that are not designed to incorporate mutual coupling and other systems with antennas on inter-linked mobile platforms that cannot physical provide this spacing. In either case the overall functionality of the array becomes impaired and the full utilization of the instantaneous bandwidth may be unachievable. Thus, in the context of wireless communication and network centric topologies for portable communication networks it remains important to investigate new distributed beamforming techniques.

Removing the periodicity and positioning the elements aperiodically (randomly) into a larger aperture remains a historically-relevant solution to this problem. It allows for greater bandwidth in beamforming operations, removes restrictions on mutual coupling, and enables more sophisticated techniques such as collaborative beamforming. In a general context it utilizes a randomly distributed antenna array with fitting phase coefficient for the elements and a wide variety of topologies and distributions can be used to geometrically confine these mobile random elements for analysis. A Gaussian and Uniform element population occupying a triangular region are considered in this work and used to statistically derive closed-form expressions for the average beampattern, sidelobe behavior, beamwidth, and directivity. Numerical simulations and analytically-derived quantities for this topology will be compared to other planar and volumetric encapsulating topologies for random arrays.

SMART PHONE ENABLED COGNITIVE CONTROL OF A PHASED ARRAY

Jeffrey S. Jensen, Jean-Francois Chamberland, and Gregory H. Huff
Electromagnetics and Microwave Laboratory
Department of Electrical and Computer Engineering
Texas A&M University, College Station, TX 77843-3128 USA

A cognitive radio network relies on computer software and computational resources to change or reconfigure transmit/receive parameters to achieve better quality of service or efficiency. The recent emergence of smart phones has made these computing resources more accessible and mobile, thereby lowering the barrier for incorporating their sensing and geolocation capabilities into more complex network structures for adaptive control and tracking. This work therefor examines the smart phone as an essential tool for adaptive wireless control within a cognitive radio network by pairing a phased array control system into the local network of control devices and servers on the remotely located phone via a Bluetooth connection. In this context, the phone serves as a wireless communications bridge between a phased array and a network server for bi-directional communication of health monitoring data, state information, and control signals. It also uses phone's internal sensors to feed geolocation and motion-dynamic information to configure the algorithms that control the beam direction of a phased array.

This work begins by considering conventional beam steering methods for phased arrays and evaluating the smart phone's capability to operate as a controller within the confines of these methods. Analysis indicates that reliable information from the phone's tilt sensors (gyroscope, magnetometers, and accelerometer) can be utilized to determine the required element phasing in the array to maintain tracking during motion. A Bluetooth channel exists between the phone and a microcontroller to pass sensor data to control circuitry and networked microcontrollers control individual antenna elements by adjusting the phase shift on individual phase shifters. Additional analysis and algorithms are presented to show the phased array's ability to track an object in space utilizing GPS and tilt sensors in the smart phone.

Compensating for Antenna Array Tracking Measurement Errors

Randy Haupt, Aaron Lyons, Brian Thrall, Martin Huisjen
Ball Aerospace & Technologies Corp.
Westminster, CO 80021

Testing a phased array antenna in an anechoic range often requires more than just measuring antenna patterns. The range hardware was designed to move the antenna while transmitting and/or receiving signals from the antenna under test. Phased arrays, however, often perform complex beam manipulations, such as tracking, searching, scanning, adaptive nulling, beam shaping, etc. We tested the tracking capability of a large phased array panel in the Ball Aerospace 35ft by 35ft by 65ft compact range with an 8ft quiet zone. We simulated antenna and/or source motion by controlling the antenna position. Tracking algorithms followed the source by steering the beams toward the source as the phased array turned.

The S band planar 820kg, 4.1m^2 hexagonal phased array has 777 elements grouped into 21 subarrays of 37 elements each. The hexagonal panel was mounted to a roll positioner atop a high load tower. The high load tower was then mounted to an azimuth turntable. We used a level and beam scanning to determine the amount of vertical tilt induced by the antenna weight. Mounting this large of an antenna on a positioner causes some tilt that must be taken into account when performing the measurements and analyzing the results.

In order to isolate the tracking induced error for analysis we needed to determine the systematic or test setup bias and compensate for it. The test setup bias was primarily due to the antenna sag from the panel weight and encoder offset caused by mounting errors. These errors result in a constant elevation offset that can be characterized using linear regression. We will describe the mounting of this large array and associated mechanical errors that impact the tracking data. Then, we will describe how we removed these errors in order to evaluate the tracking performance.

An UWB 7x7 Single-Polarized Tightly Coupled Dipole Array with Integrated Feed and Terminations

Ioannis Tzanidis*, Kubilay Sertel, John L. Volakis
{tzanidis.1, sertel.1, volakis.1}@osu.edu
The Ohio State University, ElectroScience Laboratory
1330 Kinnear Rd, Columbus, Ohio, 43212

High data rates for wireless communication systems and high resolution imaging sensors require antennas of large bandwidth, high gain, polarization diversity and beam steering capabilities. Unlike traditional phased arrays, tightly coupled arrays (TCAs) have been shown to possess these features. Typically, TCAs are comprised of very small elements, $\lambda/10$ in size, which are packed tightly and placed at close distance above a ground plane ($\lambda/10$ height). As a result, mutual coupling dominates their impedance and is utilized to cancel the ground plane's inductance leading to ultrawideband (UWB) performance (bandwidth 5:1). In addition, due to their small thickness TCAs can be inconspicuously installed on vehicular, airborne and naval platforms. However, designing such arrays presents us with many challenges. Among them: (1) an UWB balanced feed is needed to feed the elements and suppress possible common mode radiation, and (2) for better gain-bandwidth compromise, strategic termination of the array edge elements needs be considered.

In this paper, we propose an UWB single-pol. 7x7 tightly coupled dipole array (TCDA) with integrated feed. The single pol. array is comprised of 21 active and 28 terminated elements. The active elements are excited uniformly through a network of equal split power dividers. The terminated elements are strategically loaded to achieve a favorable tradeoff between efficiency and bandwidth. Most importantly, we present an UWB, planar, balun/impedance transformer for feeding the array. The feed is comprised of a printed transmission line section and a lumped balun/impedance transformer. It exhibits more than 3:1 bandwidth with impedance transformation from 50Ω-200Ω. In the conference we will present simulated and measured data for the 7x7 array.

Microwave Lens Modeling for mm-wave MIMO Communications

John H. Brady, Nader Behdad, and Akbar Sayeed
Department of Electrical and Computer Engineering, University of Wisconsin - Madison, Madison, WI, 53706

In recent years the capacity requirements of wireless communications have been expanding rapidly with the proliferation of consumer wireless devices such as smart phones, tablet PCs, handheld gaming devices, and laptops. Millimeter wave (mm-wave) communications systems have several characteristics that make them uniquely suited to such high data-rate communications applications, namely small wavelengths and large bandwidths. However the current state-of-the-art mm-wave systems are unable to take full advantage of these characteristics. Continuous aperture dish systems are able to take advantage of large power gains, yet can only support a single data stream. Conversely, conventional multiple-input multiple-output (MIMO) systems are able to support multiple data streams, but possess lower power gains than dish systems. Phased array systems can in principle achieve both multiplexing and power gains through digital beamforming, but are prohibitively expensive and difficult to implement due to the high complexity of the spatial digital-to-analog (D/A) beamformer. A recently proposed, new transceiver architecture, Continuous Aperture Phased MIMO (CAP-MIMO), is able to take advantage of the power gains of dish systems, and the multiplexing gains of conventional MIMO, whilst avoiding the high D/A complexity of digital beamforming through the use of a Miniaturized Element Frequency Selective Surface (MEFSS) Discrete Lens Array (DLA) that enables analog beamforming. This paper will discuss the construction and modeling of the DLA in the context of the CAP-MIMO system. In particular, it will present how a relatively simple and computationally efficient model of the lens has proven to be a powerful tool in analysis of the CAP-MIMO system.

Design Directions for Wide-Angle Array Scanning

Nicholas Host*, Chi-Chih Chen, John Volakis
The ElectroScience Laboratory, Columbus, OH, 43212,
http://electroscience.osu.edu/

Phased array antennas are used to steer the beam in the direction of satellites. However, steering far away from boresight and towards the horizon (in the case of conformal arrays) has been a challenge. Specifically, when scanning away from boresight, its active impedance changes, the pattern distorts, and the array beam widens. For the latter, this is due to projected effective aperture when steering. In addition, the element pattern, particularly in the E-plane for dipoles, forces the field to zero at grazing angles.

Mutual coupling is typically the cause of pattern distortion and active impedance variations. Such mutual coupling is due to scattered fields among nearby array elements and the feed structure. In essence, S_{11} changes as a result of the field coupled to and scattered by adjacent elements leading to impedance variations. To mitigate distortions due to mutual coupling (which is much stronger at low scanning angles), the traditional approach has been to suppress it by placing the elements further apart and by introducing isolation barriers between them.

In this paper we consider suitable superstrates to bend the array elements to higher angles (closer to boresight) and avoid strong mutual coupling when the array scans towards grazing. This presentation will discuss how to achieve wide angle scanning by avoiding mutual coupling when scanning at low angles, and by properly designing the dipole element. We will discuss the effects of superstrate permittivity and thickness and provide guidance on avoiding surface waves. Multilayed superstrates will be considered along with desirable layer to layer dielectric constants.

CYLINDRICAL RESONATOR SECTORALLY FILLED WITH DNG METAMATERIAL AND EXCITED BY A LINE SOURCE

Vito G. Daniele[(1)], Roberto D. Graglia[(1)], Guido Lombardi[(1)], Piergiorgio L. E. Uslenghi[(2) (*)]
[(1)]Dipartimento di Elettronica, Politecnico di Torino, Italy
vito.daniele@polito.it, roberto.graglia@polito.it, guido.lombardi@delen.polito.it
[(2)]Department of ECE, University of Illinois at Chicago, USA
uslenghi@uic.edu

A circular cylindrical resonator with metallic (PEC) walls sectorally filled in part with double-positive (DPS) material and in part with double-negative (DNG) metamaterial is considered. The boundaries separating the DPS and DNG regions are the faces of a wedge of arbitrary aperture angle, whose edge coincides with the axis of the resonator. The DPS region is filled with a linear, uniform and isotropic material characterized by a real positive electric permittivity ε and a real positive magnetic permeability μ, or alternatively by a real positive wavenumber $k = \omega\sqrt{(\varepsilon\mu)}$ and a real positive intrinsic impedance $Z = \sqrt{(\mu/\varepsilon)}$, where ω is the angular frequency. The DNG region is filled with a linear, uniform and isotropic material characterized by a real negative permittivity $-\varepsilon$ and a real negative permeability $-\mu$, or alternatively by a real negative wavenumber $-k$ and a real positive intrinsic impedance Z. Thus, the DPS and DNG regions of the resonator are filled with materials having real refractive indexes of opposite sign and the same real intrinsic impedance. The analysis is conducted in phasor domain with time-dependence factor $\exp(+j\omega t)$. The results obtained are valid at those frequencies where the DNG metamaterial behaves as postulated. Because of the dispersive properties of passive DNG materials, broadbanding may be achievable only by the use of active (non-Foster) metamaterials.

A preliminary analysis by the same authors of the structure considered herein was presented at the URSI Meeting in Spokane, WA (July 2011), but was limited to the study of possible field distributions inside the resonator when the electric field is parallel to the resonator axis, without considering possible types of excitation of the cavity. In the present work, excitation by an electric line source parallel to the resonator axis and located anywhere inside the resonator is studied. Orthonormal modes are found via the Gram-Schmidt process. Several particular cases corresponding to different wedge angles are analyzed in detail. Particular attention is paid to the case of a wedge of π radians, in which case the resonator becomes size-independent and therefore can be miniaturized. Numerical results and plots of field distributions are presented and discussed.

Ultra-Broadband Mantle Cloak Using Non-Foster Negative-Impedance Metasurfaces

Pai-Yen Chen* and Andrea Alù
University of Texas at Austin, Department of Electrical and Computer Engineering, Austin, TX, 78712, U.S.A.

We propose here the concept and practical design of an ultra-broadband, ultra-thin mantle cloak at microwaves, for which a "non-Foster" inductive surface, necessary for achieving ultra-broadband cloaking, is synthesized by the passive frequency-selective-surface (FSS) loaded with the negative capacitance converter (NCC). We use an array of sub-wavelength metal square-patches loaded at their gaps by NCC. The analysis of equivalent surface impedance for such active mantle cloak is based on (1) the analytical formula for square-patch FSS and (2) the small-signal equivalent model, considering parasitic and shunted elements. The optimal physical parameters of mantle cloak (including active and passive constituent components) are automatically extracted by the genetic algorithm optimization, which gives the optimum cloaking performance and best possible bandwidth. Our numerical results show that this active cloaking device, practically loaded with NCC circuits, may enable low visibility over a very wide range of frequencies, remarkably broader than any conventional passive cloak, further beating the Foster's reactance theorem and bandwidth constrains. We also investigate in time-domain by launching a short-pulse signal to impinge the cloaked object and observe that with this active, broadband mantle cloak, the signal distortion is almost neglected, which in turn verifies its broadband nature in the frequency domain. For an ideal passive cloak, although a certain segment in the middle-part of the short-pulse is well preserved, pertaining to the narrow cloaking bandwidth around the frequency of interest, dramatic pulse distortions and stretched-out time responses are, however, obtained, as the no cloaking case. This active mantle cloak, with intriguing features of very broad bandwidth, very low-profile, realization with simple analog components, may have tremendous impacts on applications not only in invisibility and camouflaging, but also in non-invasive probing, cloaked sensing and detection, and low-noise communication.

Existence of Surface Waves and Complex Modes on Metasurfaces

Christopher L. Holloway[1], Derik C Love[1,2], Edward F. Kuester[3],
Joshua A. Gordon[1], and David A. Hill[1]

[1]*National Institute of Standards and Technology (NIST), Electromagnetics Division, 325 Broadway, Boulder, CO 80305 USA,* holloway@boulder.nist.gov*, 303-497-6184*
[2]*was with NIST, now at US Air Force, Dayton, OH*
[3]*Department of Electrical, Computer and Energy Engineering University of Colorado, Boulder, Co 80309*

A metasurface (also referred to as a metafilm) is the two-dimensional equivalent of a metamaterial, and is essentially a surface distribution of electrically small scatterers characterized by electric and magnetic surface susceptibilities. Much like classical slab media, metasurfaces can support guided waves. However, unlike a conventional dielectric slab, forward and backward surface waves as well as complex modes can be excited simultaneously on the metasurface, a direct consequence of engineering the properties of the constituent scatterers. In this paper we show how sheet transition conditions (GSTCs) can be used to examine the existence of guided waves (both surface waves and complex modes) on the metasurface. In this work, excitation of a metasurface by both electric and magnetic line currents is investigated. The characteristics of the guided waves for both these polarizations are expressed in terms of the surface susceptibilities, which are directly related to the electric and magnetic polarizabilities of the scatterers composing the surface. We present conditions for the surface susceptibilities that must be met in order for the metasurface to support either surface waves or complex modes. In order to validate the predictions presented here, we present numerical results for a magnetic line source placed above a metasurface composed of spherical dielectric particles. Figure 1 illustrates these results. Figure 1(a) illustrates a tightly confirmed surface wave, and Figure 1(b) illustrates the case when complex modes are present. The complex modes come in pairs, and cannot carry time-average power along the surface.

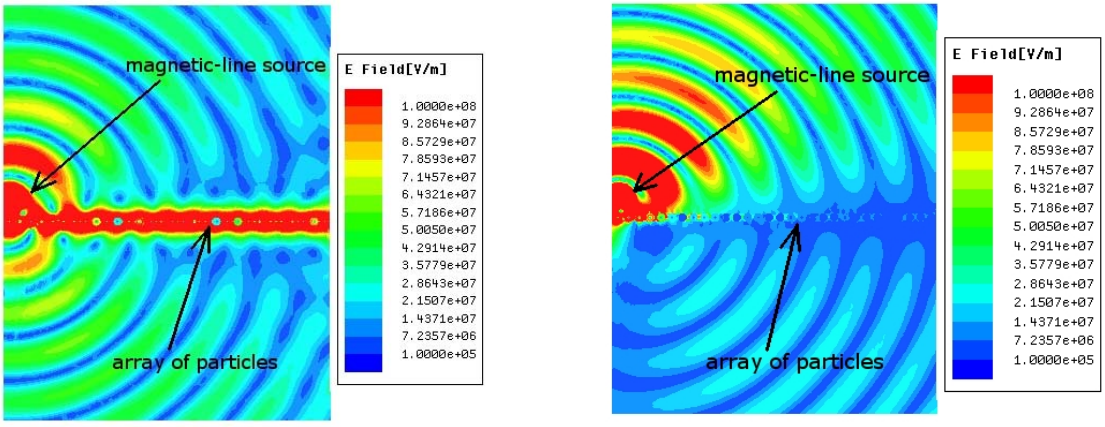

(a) Surface wave: f=1.42 GHz (b) Complex mode: f=1.5 GHz

Figure 1: Magnitude of the E-field for a line source placed above an array of spherical particles.

A PHASE-RECONFIGURABLE REFLECTARRAY ELEMENT USING FLUIDIC NETWORKS

Stephen A. Long* and Gregory H. Huff
Electromagnetics and Microwave Laboratory
Department of Electrical and Computer Engineering
Texas A&M University, College Station, TX 77843-3128 USA

Reflectarray (RA) antennas offer both the feeding efficiency of conventional shaped reflector antennas along with the planar form and beam-pointing capabilities of microstrip phased arrays. Recent phase-shifting technologies for the latter have been adapted in RA elements to provide dynamic beam-steering. The resulting topologies are typically switch-based or material-based and rely on bias lines or other control circuitry integrated onto or within the antenna. In some cases this can lead to design challenges, fabrication difficulties, and potentially significant losses in the reflected signal. Recent works have highlighted the use of microfluidics to perform localized material perturbation in order to reconfigure antennas, filters, and other RF devices. This work proposes a microfluidic reactive impedance loading mechanism to achieve low-loss and continuous phase control over the signal reflected from a RA microstrip patch element. Conceptually, this mechanism blends the conventional microstrip stub technique with the permittivity manipulation performed via a liquid crystal (LC) loaded RA element. However, this mechanism removes the need for bias and control lines in the vicinity of the RA element.

This work begins by introducing the theory and design principles behind the RA element and loading mechanism. In all, three iterations of a prototype are presented. A first proof-of-concept design without a dynamic fluid delivery system illustrates the impact of particle geometry and other design parameters. Measured results for the dispersions used and the fabricated prototype are then provided. A second prototype and test fixture featuring a closed-loop fluidic system are then presented along with results (measured and simulated) that provide insight into the materials used. Finally, a third prototype redesigns the fluidic network for easier fabrication and modifies the design dimensions of the element for more stable operation.

Absorbing Boundary Conditions and the Homogenization Model for Multilayered Wire Media

Yashwanth R. Padooru*(1), Alexander B. Yakovlev (1), Chandra S. R. Kaipa (1), George W. Hanson (2), Francisco Medina (3), Francisco Mesa (4), and Allen W. Glisson (1)

(1) Dept. of Electrical Engineering, University of Mississippi, University, MS 38677, USA, E-mail: ypadooru@olemiss.edu

(2) Dept. of Electrical Engineering and Computer Science, University of Wisconsin-Milwaukee, Milwaukee, WI 53211, USA, E-mail: george@uwm.edu

(3) Dept. of Electronics and Electromagnetism, Faculty of Physics, University of Seville, 41012 – Seville, Spain, E-mail: medina@us.es

(4) Dept. of Applied Physics I, ETS de Ingeniería Informática, University of Seville, 41012 – Seville, Spain, E-mail: mesa@us.es

In recent years, homogenization models are shown to be very effective in modeling a variety of complex electromagnetic structures in comparison to the tedious and extensive computations demanded by the numerical methods. In particular, characterization of the metamaterial structures, which constitute wire media, has attracted special attention due to their ability in enabling anomalous phenomena such as negative refraction. It has been shown in (P. A. Belov, et. al., *Phys. Rev. B*, vol. 67, 2003, 113103(1-4)) that wire media exhibits strong spatial dispersion at microwave frequencies, and that the constitutive relations between the macroscopic fields and the electric dipole moment are non-local. In (M. G. Silveirinha, et. al., *IEEE Trans. Antennas Propag*., vol. 56, no. 2, pp. 405-415, Feb. 2008 and A. B. Yakovlev, et. al., *IEEE Trans. Microw. Theory Tech*., vol. 57, no. 11, pp. 2700-2714, Nov. 2009) the role of spatial dispersion has been discussed and it was demonstrated that nonlocal homogenized models with additional boundary conditions (ABCs) become essential in solving electromagnetic problems associated with wire media.

In this work we obtain a generalized nonlocal homogenization model for the analysis of the reflection properties of a multilayered mushroom structure with thin (resistive) patches, as an extension of the model presented for a single-layered mushroom structure (A. B. Yakovlev, et. al., *IEEE Trans. Microw. Theory Tech*., vol. 59, no. 3, pp. 527-532, Mar. 2011). Based on charge conservation two-sided ABCs are derived at the interface of two uniaxial wire mediums with thin imperfect conductors at the junction. The scattering problem is solved by imposing the classical boundary conditions along with the newly derived ABCs obtained at the wire-patch junctions. To illustrate the validity of the homogenization model, we characterize the reflection properties of the multilayer structure, demonstrating that such a configuration with proper choice of the geometrical parameters acts as an absorber. Interestingly, it is noticed that the presence of vias results in the enhancement of the absorption bandwidth and an improvement in the absorptivity performance for increasing angles of the obliquely incident TM-polarized plane wave.

All-Angle Negative Refraction by an Inductively Loaded Uniaxial Wire Medium Terminated with Patch Arrays

Chandra. S. R. Kaipa* (1), Alexander. B. Yakovlev (1), Stanislav. I. Maslovski (2), and Mário G. Silveirinha (2)

(1) Department of Electrical Engineering, University of Mississippi, University, MS 38677, USA, ckaipa@olemiss.edu

(2) Instituto de Telecomunicacões - Universidade de Coimbra, Departamento de Engenharia Electrotécnica, Pólo II, 3030 Coimbra, Portugal

Artificial media formed by arrays of metallic wires are typically characterized by strong spatial dispersion (SD) effects, and may behave very differently from a material with indefinite properties at microwaves and low THz frequencies. However, it was recently shown that the SD effects in the wire medium can be significantly reduced by either coating the wires with a magnetic material or by attaching large conducting plates to the wires (A. Demetriadou and J. B. Pendry, *J. Phys.*: *Condens. Matter*, 20, 29, 295222, 2008). More recently, it was shown that by periodically attaching metallic patches to an array of metallic wires the SD effects can be significantly weakened (residual SD effects may however be still observed at wide incident angles), and that it is possible to observe a strong negative refraction in the microwave regime, analogous to what is observed at optics but without using the patches (M. G. Silveirinha and A. B. Yakovlev, *Phys. Rev. B*, 81, 23, 233105, 2010).

In this work, we show that at microwaves and low THz frequencies the SD effects can be nearly suppressed, even for wide incident angles, by loading the WM slab with lumped inductive loads. It is observed that with an increase in the value of the inductive load, there is a decrease in the plasma frequency, and this enables the design of an ultra-thin structure with the electrical length of the unit cell being less than $\lambda_0/15$ at the frequency of operation. The proposed structure exhibits an indefinite dielectric response, high transmission, and all-angle negative refraction below the plasma frequency. The analysis is carried out using different homogenization models developed for the uniaxial WM loaded with conducting plates and (or) impedance insertions based on the quasistatic approach (which can model both a uniform and a discrete loading), and take into account the SD effects in the wires (S. I. Maslovski et al., *New. J. Phys.*, 12, 113047, 2010). The homogenizations results of the transmission properties are in a very good agreement with the full-wave numerical results. The proposed concept of negative refraction is further numerically confirmed by the excitation of the structure with a Gaussian beam.

Isoimpedance Anisotropic Substrates for Planar Antenna Profile Reduction

Hayrettin Odabasi*, and Fernando L. Teixeira
ElectroScience Lab. and Dept. of Electrical and Computer Engineering,
The Ohio State University, Columbus, OH 43212.

The use of metamaterials for antenna applications is of great interest for miniaturization and performance enhancement [K. B. Alici and E. Ozbay, *Appl. Phys. Lett*., no. 101, pp. 083104, 2007], [P. Jin and R. W. Ziolkowski, *IEEE Trans. Ant. Propag*., no. 5, pp. 1446-1459 2011], [N. Engheta and R. W. Ziolkowski, *Metamaterials: Physics and Engineering Explorations*, Wiley-IEEE Press, 2006]. Transformation optics (TO) provides a systematic, if idealized, methodology to design metamaterial blueprints with desired functionalities. TO explores the fact that a change on the metric of space can be mimicked by properly chosen constitutive tensors [F. L. Teixeira and W. C. Chew, *J. Electromagn. Waves Appl*., no. 13, pp. 665-686, 1999], [J. B. Pendry, *Science*, no. 312, pp. 1780-1782, 2006]. The resulting constitutive tensors correspond to a doubly anisotropic medium with $[\varepsilon]=\varepsilon_0[\Lambda]$, $[\mu]=\mu_0[\Lambda]$, where $[\Lambda]$ is associated with the Jacobian of the metric transformation. Recently, we have explored TO to design metamaterial substrates for backing up planar radiators on top of ground planes, allowing for a much reduced overall antenna height [H. Odabasi and F. L. Teixeira, *Int. Symp. on Personal Indoor Mobile Radio Comm*., pp. 1107-1110, 2010]. The resulting metamaterial substrate is isoimpedance to free-space and effectively mimics a thicker (air-filled) gap between antenna and ground plane. In this sense, this approach is quite different from other approaches commonly used for antenna profile reduction.

Because of their doubly anisotropic nature, fabrication of such metamaterial substrates remains a challenge. However, depending on the application, only a few of the permittivity and permeability tensors components may be need (for example, those associated with either TE or TM polarization). This has the potential to make fabrication considerably easier. In this study, we numerically analyze the performance of dipole antenna on top of such anisotropic substrates, designed via TO. We investigate the antenna performance versus changes on the constitutive parameters. We show that simplified metamaterial substrates with only two modified tensor components can approximate the original performance of ideal substrates very well. To isolate the effect of such tensor approximations, we assume ideal material (lossless, non-dispersive) response for $[\varepsilon]$ and $[\mu]$. The effect of frequency dispersion will be considered separately, using appropriate dispersion models that depend on the specific periodic elements employed for the metamaterial substrate.

Fabrication Sensitivity of Double-Sided Split-Ring Resonator Arrays

Frank Trang*, Edward F. Kuester, Horst Rogalla, and Zoya Popović
Department of Electrical, Computer, and Energy Engineering
University of Colorado, Boulder, CO, 80309

Split-ring resonators, introduced in 1999 (Pendry, et al., IEEE MTT, 47, 11, 2075-2084, 1999), have been studied as building blocks for negative index materials (Shelby, et al., Science, 292, 77-79, 2001) and for use in EM cloaks (Schurig, et al., Science, 314, 977-980, 2006). Since these structures are resonant, imperfections in the fabrication will likely affect the performance, which to the best of our knowledge, has not been investigated in literature. In this talk, we present experimental and simulated results for the frequency response sensitivity of double-sided split-ring resonator arrays to various fabrication tolerances. The arrays are designed for operation at X-band and are measured in a waveguide environment. Several imperfections were investigated: ring misalignment, air-gaps in the waveguide, variation in metal dimensions, and thickness variation of the substrate.

Double-sided split-ring resonators were chosen for this investigation because of the multiple coupled resonances. In the nominal design, the printed ring size is 4mm by 4mm and the aligned rings are printed on both sides of a 0.762mm thick Rogers 4350B substrate with a relative permittivity of 3.66. The printed lines are 0.5mm wide copper. Five 2x4 array, with periodicity of 5.08mm, of nominally identical test structures were fabricated and measured to quantify the fabrication tolerances. The arrays are placed in a WR-90 waveguide as shown in Figure 1 and their scattering parameters are measured with a network analyzer. A calibration using two offset shorts, a load, and a through section was performed to set the reference planes at the end of our waveguide adapters. The results show an average 8.6% shift in resonance relative to the nominal simulated results using HFSS.

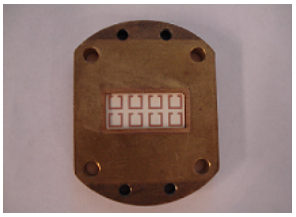

Figure 1: A double-sided SRR array inside a WR-90 waveguide section

Wideband, Optically Transparent, Band-Selective Ground Planes for Antenna Applications

M. Kashanianfard* and K. Sarabandi
University of Michigan, Ann Arbor, MI, 48105,
http://www.eecs.umich.edu/

To mitigate some of the adverse effects of the communication channel, such as multi-path fading, attenuation, non-line-of-sight, etc., wireless operation at lower frequencies (VHF and UHF) is usually preferred for ad hoc communication systems. One drawback of operation, for mobile platforms, at these frequencies is the size of the antenna. Also considering the issues related to near-earth wave propagation, vertical polarization is the preferred choice to achieve minimum path-loss. Placement of such large vertical dipole or monopoles on vehicles create air drag, is anaesthetic, and for situations where different channels or space diversity are needed the close proximity of many such antennas results in co-site interference and other undesired issues.

To avoid such problems, the focus has shifted towards finding methods for embedding radar and communication antennas within or around the body of the platforms. Advantages of embedded antenna systems includes reducing the visual signature of the vehicle, potential for reducing the cost, improving reliability and reducing maintenance, preserving the mechanical and aerodynamic properties of the platform and reducing the issues related to co-site interference. Among all positions on ground vehicles that cover a relatively large surface area and are well above the ground (the higher the antenna, the lower the path loss) are the vehicle's windshield and other windows. For a window embedded antenna, optical transparency becomes another important constraint. In addition, radiation inside the vehicle must be minimized to isolate the effect of the cabin interior and the passengers on the antenna input impedance and the radiation pattern. More importantly in the transmit mode for high power applications the passengers need be protected from exposure to high RF power. Hence a transparent band-selective ground plane will be needed behind the radiating element to reduce the radiation inside the vehicle and at the same time increase the directivity of the antenna. Transparent band selective ground plane(BSGP)systems can also be used for other applications such as electromagnetic shielding and interference mitigation.

This paper presents a technique for design of wideband optically transparent BSGP using the concept of miniaturized element frequency selective surfaces (MEFSS). The proposed multi-layer approach can provide very large bandwidth and high out of band rejection while keeping the thickness of the ground plane very low. Essentially the thickness of the ground plane made to be almost independent of the bandwidth in order to reduce its weight and sensitivity to the angle of incidence and the shape of the wavefront of the incoming radiation. As a starting point, a single pole MEFSS is studied and its performance in terms of transparency and bandwidth is compared to the traditional wire grid and transparent conductive coatings. Next, the proposed multi-pole BSGP design method is introduced and its performance is evaluated numerically and experimentally.

Omnidirectional Small Antennas Based on ε-Near-Zero Metamaterial Channels

Jason C. Soric*, Andrea Alù
The University of Texas at Austin, Electrical and Computer Engineering
1 University Station
Austin, TX 78712, http://www.ece.utexas.edu, USA

We present a simple analytical model and practical designs to realize cylindrically-symmetric antennas based on the anomalous transmission properties of ε-near-zero (ENZ) ultranarrow radial channels. The flexibility offered by ENZ metamaterials are used here to tune and match cylindrically-symmetric small antennas, without the need of complex external matching networks, envisioning exciting antenna designs in terms of electrical size, tunability, and efficiency. We first model the problem by loading an ultranarrow channel in a cylindrical post with an ideal zero-permittivity metamaterial, in order to show its unique radiation properties when inserted in a much thicker parallel-plate waveguide. Using this model, we show that it is possible to describe the electromagnetic behavior of the ENZ-loaded channel in terms of transmission-line theory, and easily predict its exotic radiation properties inside the waveguide. Our work demonstrates a unique matching mechanism, based on these anomalous properties, with several appealing features, such as uniformly enhanced electric field inside the channel, which translates into perfect matching at the ENZ frequency, invariant with the position of an input coaxial probe inside the channel. We then replace the ideal ENZ material with a realistic metamaterial shell, obtained with radial metallic implants in a high-dielectric substrate. We show that the proposed geometry may accurately reproduce the ENZ matching properties and we derive design rules to optimize its performance in order to realize an ENZ-loaded small antenna. Finally, we apply our design to practical single- and multi-band cylindrical antennas with a wide range of tunability. The designed antennas operate in the ultra-high frequency (UHF) band, with tunability spanning over 64% frequency bandwidth. We envision applications in frequency-hopping multi-band omnidirectional antennas with ultralow-profile.

2.5D Micromachined 240 GHz Cavity-backed Coplanar Waveguide to Rectangular Waveguide Transition

Mehrnoosh Vahidpour, *Student Member, IEEE*, and Kamal Sarabandi*, Fellow, IEEE*

A novel in-plane cavity-backed coplanar waveguide (CBCPW) to rectangular waveguide transition having a 2.5D geometry compatible with micromachining fabrication technique is presented. In this approach, the need for fabricating suspended resonant probe which is used in traditional transitions is eliminated and for the ease of fabrication at high millimeter-wave frequencies, a short-circuited pin is used in conjunction with resonant sections of CPW line over the broad wall of a reduced height waveguide segment to facilitate impedance matching. Although the bandwidth of this transition is smaller than the standard suspended probe transitions, the structure is very simple with all its features aligned with the Cartesian coordinate planes in order to make it compatible with microfabrication processes. The transition is modeled by an equivalent circuit to help with the initial design which is then optimized using a full-wave analysis. A back-to-back structure at 240 GHz for standard WR-3 rectangular waveguides is microfabricated on two silicon wafers with multi-step DRIE silicon etching which are later gold-coated and bonded together using gold-gold thermocompression bonding technique (a hermetic bond) to ensure excellent metallic contact needed for formation of the waveguide. The validity of the transition design is demonstrated by measuring the S-parameters of a back-to-back transition prototype at 240 GHz using a vector network analyzer with WR-3 frequency extenders connected to GSG probes. It is shown that the measured S-parameters of the back-to-back transition are in good agreement with the simulation results by providing less than 1 dB of insertion loss over more that 17% fractional bandwidth.

Smoothed Sigmoid and Stepped Circularly Polarized Septum Designs Using Particle Swarm Optimization

Ilkyu Kim*, Joshua Kovitz and Yahya Rahmat-Samii
Department of Electrical Engineering, University of California, Los Angeles
Los Angeles, CA 90095, USA
E-mail: ilkyukim@ucla.edu, jmkovitz@ucla.edu, rahmat@ee.ucla.edu

A septum is an effective polarizer to generate circular polarization from a linear excitation in a waveguide. Comprehensive studies have been conducted on the theoretical analysis of the septum polarizer. However, the field propagation and mode analysis inside the septum has rarely been investigated to visualize the operation of the septum. Moreover, previous septum designs were restricted to simple stepped or slanted designs, and optimized using *trial-and-error* techniques, which may not have led to the best design.

In this paper, the fundamental operation of the septum polarizer will be revisited using full-wave simulations. A graphical illustration of the mode analysis will be presented. The generation of the circularly polarized electric field is demonstrated as it propagates through the septum polarizer. Next, Particle Swarm Optimization (PSO), a global nature-inspired optimization technique, will be used to optimize several different septum designs. In order to optimize the electromagnetic structure, one must link the physical design realization to the optimizer through the use of numerical electromagnetic solvers, allowing the extraction of parameters of interest such as return loss and axial ratio. A specified fitness function relates these parameters to the optimizer. The optimizer improves the impedance matching and axial ratio versus a wide frequency range. In this work a smooth contour septum design using the Sigmoid function is also investigated. This Sigmoid function enables smooth transitions for stepped profiles and slanted profiles.

Using the PSO technique, conventional stepped septum designs with a different number of steps are optimized. Compared with an amenable design, similar performance is achieved using a smaller number of steps, which accommodates a simpler design of the septum. Next, the Sigmoid septum is optimized through the use of PSO, and this represents a challenging constrained optimization problem, which can be extremely difficult to solve. Simulated results show less than -20 dB impedance matching and less than 0.5 dB axial ratio over 25% bandwidth. The simulated results of both septum designs loaded with a practical horn antenna will be provided to demonstrate its practical use.

Analysis of Layered Isotropic and Gyromagnetic Materials in a Rectangular Waveguide

Benjamin R. Crowgey*, Ozgur Tuncer, Edward J. Rothwell, Leo C. Kempel, and B. Shanker
Department of Electrical and Computer Engineering, Michigan State University, East Lansing, MI, 48824, http://www.egr.msu.edu/~rothwell

Recent interest in manufactured materials, where different dielectric and magnetic materials are used to form composites, has generated a need to accurately characterize the effective properties for use in the material design process. This paper concentrates on the extraction of the effective permittivity and permeability of alternating layers of isotropic and gyromagnetic materials. It is customary for optimizers to be used to determine the constitutive parameters of materials in rectangular waveguides. In these methods, the reflection and transmission coefficients from a material placed in the cross-sectional plane of a waveguide are measured and compared to theoretical scattering parameters. It is therefore essential to have accurate formulations of the theoretical scattering parameters for valid characterization of materials.

Modal analysis is used to determine the reflection and transmission coefficients of the dominant mode from a single layer of gyromagnetic material filling the cross section of a rectangular guide. A method that combines such analysis with the wave matrix method is used for the formulation of multiple layers of isotropic and gyromagnetic materials. The wave matrix method is a common and useful tool for the analysis of layer media, since the propagation though each layer can be taken into account with wave transmission chain matrices. This simple method allows for reasonable computation times when determining the reflection from and transmission through a composite consisting of many layers. This becomes important when effective material parameters are extracted by solving the inverse problem using an optimizer.

Details on the methodology for obtaining the reflection and transmission coefficients are presented along with a comparison to a finite element full wave solver. The effects of the number of individual constituent layers and the properties of those layers on the S-parameters are described.

Surface Wave Propagation Along a One-Dimensional Metal Cut-Wire Array

Yang Li* [(1)] and Hao Ling [(2)]
[(1)]Department of Electrical and Computer Engineering, Baylor University, Waco, TX 76798
[(2)]Department of Electrical and Computer Engineering, The University of Texas, Austin, TX 78712
Email: Yang_Li1@baylor.edu

A metal cut-wire array, also known as wire-medium slab, is a two-dimensional (2-D) periodic array of finite-length metal wires. The structure has received considerable attention in the literature for its unique electromagnetic properties. It is known that that a surface wave can be supported in this structure at frequencies below the cut-wire resonance. Simulation and measurement of the surface wave mechanism were reported by us recently (Li *et al.*, *IEEE Antennas Wireless Propagat. Lett*., 9, 179-182, 2010). The surface wave propagates along the interface between the array and free space and experiences negligible propagation loss, implying this mechanism can efficiently carry electromagnetic energy on a 2-D metal cut-wire array over a long distance.

In this paper, we focus on the case of a single column of cut-wires, i.e., a 1-D cut-wire array. It is found that electromagnetic energy can be well guided even along a single column of closely-spaced wires. This phenomenon was reported earlier by Maier *et al.*, *Apl. Phys. Lett.*, 78, 16-18, 2001. Through measurement and simulation, they observed that the energy propagation loss is small in the microwave regime on such a structure. To provide more physical insights into the wave propagation and energy transport along the 1-D cut-wire array, we simulate and examine the field distribution inside the structure. It is found that the dominant propagation mechanism in the 1-D array is similar to the 2-D case, a surface wave. The propagation constant, attenuation constant, and field distribution of the surface wave are extracted. The results show good agreement with the reported measurement data. Moreover, numerical simulations are carried out to study the effect of array geometrical parameters (wire height, radius and spacing) on the surface wave propagation. Finally, we compare the surface wave propagation characteristics between the 1-D and 2-D cut-wire arrays.

A Novel Reflectarray Antenna Based on Grounded Loop-Wire Miniaturized Element

Arezou Edalati*(1), and Kamal Sarabandi(1)
(1) University of Michigan, EECS Department, 1301 Beal Avenue
Ann Arbor, MI 48109-2122

Microstrip reflectarray antennas have become attractive alternative to both conventional parabolic reflector antennas and phase array antennas due to several advantages such as high gain, flatness, low loss, low cost, low volume and less manufacturing complexity. These structures are usually composed of a small feed and a planar surface consisting of small resonant radiating elements. By changing the geometry of the elements (detuning the elements) or terminating the elements by proper reactive loads, a reflected phase is introduced to compensate for the path delay differential of the incident ray from the feed to the reflectarray elements. Traditional Frequency Selective Surfaces (FSSs) have been used as reflectarray elements as well. However, the dimension of these elements should be about λ/2 which makes them sensitive to the angle of incident wave. In addition, to have the expected response, multiple of FSS unit cells are needed. Hence, computational extensive optimization algorithms are required to achieve the proper operation (M. R. Chaharmir et al, IEEE Trans. Antennas and Propagat., 57, 3363-3366, 2009).

Recently, Miniaturized FSS (MFSS) with sub-wavelength elements have been introduced with unique characteristics such as low sensitivity to the angle of incidence, and localized frequency-selective behavior with minimal dependency to the neighboring elements. They are operating in the TEM mode and they are harmonic free (K. Sarabandi, et al., IEEE Trans. Antennas and Propagat., 55, 1239-1245, 2007). Considering the aforementioned properties of MFSS structures, MFSS is ideal for designing reflectarray antennas. MFSS allows for reflectarrays with smaller unit cell and less sensitivity to the angle of incident. In this paper, a single sided loop-wire structure with high order frequency selectivity and a large phase variation across its band is chosen for designing a reflectarray antenna. The building block of these MFSSs is formed by wire grid and metallic loop inside of it, backed by a metallic surface, as shown in Figure 1(a). By changing the dimension of metallic loops, the phase of the reflection coefficient at the operating frequency is modified (Figure 1(a)). By arranging each element in a proper position, the required phase distribution across the reflectarray surface is achieved. The proposed reflectarray antenna operates at 10.7 GHz. With total dimensions of 10λ*10λ, 27dBi gain is achieved as presented in Figure 1(b). The measurement results will be presented in the conference.

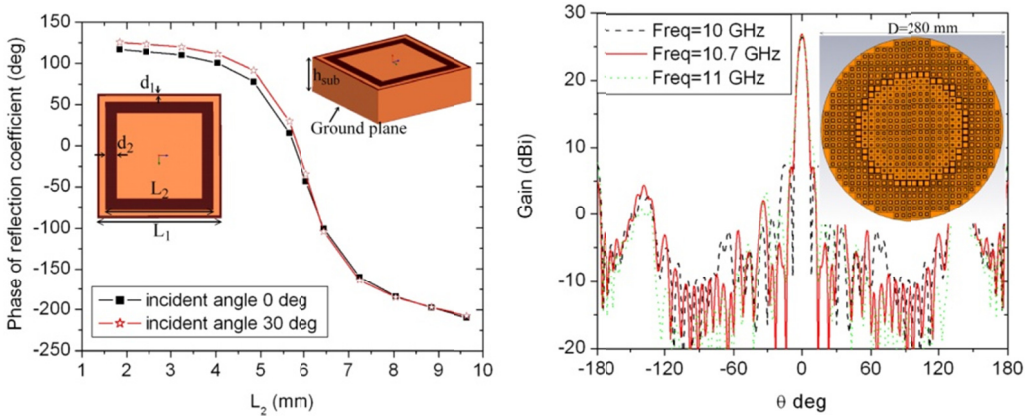

(a) (b)

Figure 1: (a) Phase of reflection coefficient at 10.7 GHz, (b) Reflectarray gain at different frequencies excited with horn antenna (D/F=1). d_1=0.08 mm, d_2=0.9 mm, periodicity=L_1=10 mm, h_{sub}=3.175 mm, ε_r=2.2,

Electronically-scanned reflectarray impact on millimeter-wave imaging system performance

Charles R. Dietlein*, Abigail S. Hedden, and David A. Wikner
U.S. Army Research Laboratory, Adelphi, MD, 20783

This paper presents an analysis of the multi-faceted impact of utilizing a digital electronically-scanned reflectarray as the beam-steering element in a millimeter-wave imaging system. The imaging system we consider is a confocal Gregorian design, configured for surveilling terrestrial scenes at standoff distances encountered in urban areas. Traditionally, a spinning polygonal disc serves as the mechanical steering element in this optical configuration: each facet of the disc is a mirror with a different elevation deflection. Although they are successfully employed by existing systems, mechanical steering elements feature intrinsic disadvantages such as size, weight, power consumption, and inflexibility in the order of sequential beam positions.

Future systems will utilize all-electronic beam scanning, likely implemented with a reflectarray. Electronic phase control of each unit cell can be implemented with analog or digital methods; we consider the digital case due to realistic implementation constraints. We examine the effects introduced by digital electronically-scanned reflectarrays of various wafer sizes and phase quantization levels (bits of phase resolution), which ultimately fall into two classes: scan angle pointing error, and undesirable quantization lobes. The effect of the former is simply to reduce the imager's spatial resolution below the nominal diffraction-limited case. The latter can cause non-deterministic image artifacts due to the presence of an additional (but weaker) beam propagating through the camera's optics, and the naturally high dynamic range found in terrestrial millimeter-wave/terahertz scenes. The effect of nonideal phase states will also be discussed. Our analysis provides quantifiable results that assist in defining the volumetric footprint of future systems, the requirements for future wafer-scale electronically-scanned reflectarrays, and understanding nonideal imaging performance due to realistic reflectarray manufacturing constraints.

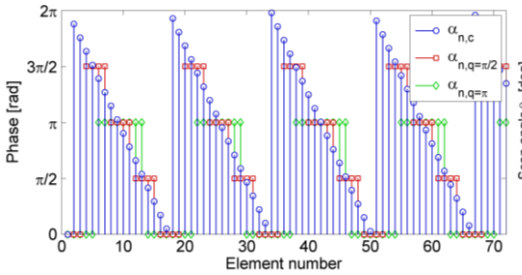

Figure 1
Phase distribution across a 50 mm linear array at 220 GHz, for element spacing of $\lambda/2$. The ideal phase and the quantized phases shown steer a normally incident beam in the $\theta_0 = 7°$ direction.

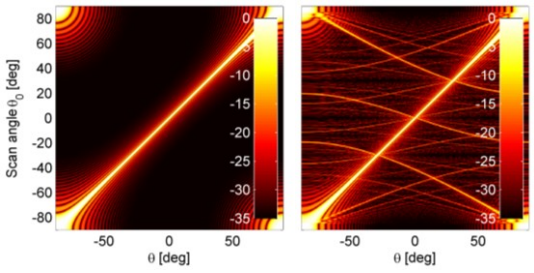

Figure 2
Ideal (left) and quantized-phase (right) array factors (x-axis) as a function of scan angle (y-axis). Quantization lobes are visible in the digitially-controlled case.

Experimental Validation of Sub-reflectarray Distortion Compensation Technique for Reflector Antennas

Harish Rajagopalan and Yahya Rahmat-Samii
Department of Electrical Engineering, University of California, Los Angeles
420 Westwood Plaza, Los Angeles, CA 90095-1594, USA
harish@ee.ucla.edu, rahmat@ee.ucla.edu

With the continuing advances in the development of large reflector antennas, reflector surface distortion compensation has been attracting significant attention. It is known that, a few millimeters deviation of the reflector antenna surface especially at high operating frequencies can cause directivity loss and considerably affect the radiation performance of the overall antenna system. In the past, the array feed and shaped subreflector are some of the techniques that have been proposed for reflector surface distortion compensation. For the array feed approach to work accurately, the design and implementation of a beam forming network to provide the complex excitations forms the integral part of the system. At higher frequencies this BFN can become increasingly lossy. The subreflector shaping approach has its limitations for compensation of due to its curved profile.

Recently, the *sub-reflectarray distortion compensation technique* has been proposed where a reflectarray acts as a subreflector. Assuming that the surface distortions on a main reflector are known either through the subreflector probing method or analytically described by a mathematical expression, then a reflectarray can be used as a subreflector. By properly adjusting the phase shifts of individual reflectarray elements, the re-radiated wavefront is optimized so that the aperture phase errors (caused by distortions) are corrected and the radiation performances of the antenna system are restored. By implementing active elements (MEMS) in the sub-reflectarray, an active optimized scattered wavefront can be generated thus allowing for real time distortion compensation.

In this paper, the sub-reflectarray compensation technique is validated through extensive simulations and measurements on a symmetric dual reflector system. Two types of distortions are created on this antenna system. Firstly, the feed is displaced from the focus of this dual reflector system causing axial defocusing distortion (spherical aberration). Secondly, an annular ring-type distortion is added to the main reflector surface representing thermal distortions. These two distortions significantly deteriorate the antenna performance causing aperture phase errors and main beam degradation. Bipolar planar near-field measurements are performed and these distortions are successfully detected using back projection holographic diagnostics. Conjugate field matching method is used to determine the phase requirements at the sub-reflectarray element locations. A sub-reflectarray is then designed, analyzed and tested to correct for both these distortions. It is effectively demonstrated by measurements that the designed sub-reflectarray restores the antenna performance, thus validating the sub-reflectarray compensation technique for the first time through experimental demonstration.

A Study of Piecewise-Planar Parabolic Reflectarrays

Sembiam R. Rengarajan
Department of Electrical and Computer Engineering
California State University, Northridge, CA 91330 USA
E-mail: srengarajan@csun.edu

Microstrip reflectarray antennas are widely used in many radar and remote sensing applications. Piecewise-planar parabolic (PPP) reflectarrays exhibit a small value of the angle of incidence at any patch for a wave incident from the feed. This minimizes the reflection phase difference between two orthogonal linear polarizations for certain geometries. Large planar reflectarrays suffer from bandwidth limitation because large path length variations compensated by modulo 2π values of the reflection phase of the patch, introduce substantial phase errors away from the design frequency. PPP reflectarrays obviate this limitation. PPP reflectarray was first patented (Roederer, U. S. Patent no. US 2001/0020914 A1, Sep. 13, 2001) and subsequently studied for scan performance. Scan performance of a symmetric PPP reflectarray was found to be good whereas that of a tilted PPP was found to be poor (Hodges and Zawadzki, IEEE Aerospace Conference, Big Sky, MT, pp. 1131-1139, 2005).

We have investigated the scanning properties of a PPP reflectarray for interferometric radar applications. Results of this study will be presented at the symposium. Because of the scan limitation of dual polarized dual beam tilted PPP reflectarray, we propose such a reflectarray with rectangular patches that can be designed simultaneously for two offset dual polarized dual beam feeds. The receive mode design technique (S. R. Rengarajan, IEEE Antennas and Wireless Propagation Letters, 8, 1206-1209, 2009) is used with input reflection phase data computed for each of the panels for dual polarization dual beams. The design technique and computed results for the patterns and gains will be presented.

Radiation Analysis of Reflectarray Antennas: Numerical Approaches versus Full-Wave Simulations

Payam Nayeri, Fan Yang, and Atef Z. Elsherbeni

The University of Mississippi, Department of Electrical Engineering, University, MS 38677-1848, USA
Emails: pnayeri@olemiss.edu, fyang@olemiss.edu, atef@olemiss.edu

Reflectarray antennas imitate the conventional parabolic reflectors, with the added advantage of having a flat surface instead of the curved reflecting surface. The flat surface of the reflectarray antenna consists of phase changing elements, which create the collimated beam. As such, the reflectarray antenna can be viewed as a phased array antenna with a spatial feed network which is simple, and low-loss. With the rapid advancement of printed circuit technology, reflectarray antennas can offer a low profile, low mass, and low cost solution for high-gain antennas in deep space communication systems.

Various numerical approaches have been developed over the years to calculate the radiation characteristics of the reflectarray antenna. The goal of this study is to review the numerical methods for reflectarray antenna analysis, and provide a comparative study on the accuracy, limitations, and challenges in program development for these approaches. We review two basic numerical methods for analysis of the reflectarray antenna radiation performance. In the first approach, the radiation pattern of the reflectarray antenna is calculated using the conventional array summation with proper element excitation. In the second approach, the radiation pattern of the antenna is calculated using the tangential fields on the reflectarray aperture. Numerical results are presented for various reflectarray configurations using both approaches. It is shown that the computed radiation patterns and antenna directivity obtained by both numerical methods are in close agreement.

In the next stage, the radiation patterns computed with these numerical approaches are compared to full-wave simulations which can provide a good measure in terms of the accuracy of these approaches, since the full-wave simulations will take into account all approximations in reflectarray element design and mutual coupling in addition to diffraction effects. Comparison with full-wave simulations obtained using the commercial software FEKO (FEKO v 6.1, EM Software & Systems Inc., 2011), showed that these numerical approaches accurately calculate the general pattern shape, main beam direction, beam-width, and sidelobe and cross-polarization level in the main beam area, which makes them time-efficient analysis tools for antenna engineers to evaluate the performance of their own reflectarray designs.

Cognition and Radar Sensing

G.E. Smith and C.J. Baker

Historically the development of hardware to support new radar concepts always outstripped the understanding of electro-magnetic scattering. Modern radar hardware has already reached a point where basic operating parameters such as transmission frequency, power, pulse length, waveform etc. can be varied on a pulse-by-pulse basis. With such sophisticated functionality available, the associated improvements in radar system capabilities have reaching a point of diminishing return. That is to say, while a system can be made more sensitive, have higher resolution, operate using multiple polarizations etc. the overall performance is only marginally improved. These two drivers provide a strong motivation for future radar systems that are able to autonomously modify their own sensing parameters, perhaps at the rate of thousands of times per second, in order to extract the information required to successfully complete a chosen function. Consequently, the radar sensor itself will need to have a sufficient perception of its surroundings so that it might navigate and interact with that environment much as we do as humans. This implies a cycle of sensing, processing, decision-making and action closely paralleling that of cognition. If successful, this will pave the way for autonomous behaviors far in advance of anything possible today and open up a plethora of new applications. In this paper we outline the case for cognition in advanced radar systems that takes many of its cues from observations of the echo locating bat. This provides a basis for a highly simplified cognitive-like processing architecture that is used to illustrate the potential power of such an approach.

Software Defined Radar for Cognitive Applications

Kyle B. Stewart*, Mark T. Frankford, Ninoslav Majurec, and Joel T. Johnson
The Ohio State University, Columbus, Ohio

The potential benefits of "software defined radar" for cognitive applications are being investigated at The ElectroScience laboratory of The Ohio State University via the use of a multi-purpose software defined radar platform. This system combines dual-channel ADC and DAC modules with four Xilinx FPGAs, eight Texas Instruments digital signal processors, high-speed interconnects, and a frequency-agile RF frontend in order to implement a radar system capable of tuning 500 MHz of bandwidth on a center frequency anywhere from 2 to 18 GHz. The "software defined" aspects of this system enable it to react to its surroundings by adjusting radar operating parameters, such the pulse repetition frequency and the transmitted waveform. Two simple waveform adaptations have been implemented and tested at present, and will be described in this presentation.

In the first, the radar is configured with an adaptive Pulse Repetition Frequency (PRF) that is used to improve velocity measurements for a moving target. The PRF sets the time between radar pulses and is directly proportional to the unambiguous Doppler frequency of a moving target. An adaptive software implementation enables the radar to increase its PRF in order to prevent a high-velocity moving target from aliasing in Doppler-space or to decrease the PRF in order to improve the separation of low-velocity targets from stationary clutter. PRF adaptation can also be useful when the unambiguous range that is necessary varies with the scene observed so that the maximum number of pulses can be integrated in any situation.

The second demonstration focuses on the imaging of a stationary scene with a pseudo-noise waveform. Waveforms of this type are relevant for Multiple-Input Multiple-Output (MIMO) radar systems where the goal is to simultaneously operate with multiple transmit waveforms. When these waveforms share a common bandwidth they cannot be perfectly orthogonal, and their non-zero mutual correlations introduce errors in MIMO measurements. These errors can be reduced, but only at the cost of unambiguous range or imaging speed. Thus, given an acceptable level of mutual correlation and a maximum physical range, a software controlled system can optimize the length of its transmitted pulse for the observed environment.

In both of these applications, the radar system alters its operational parameters to attain better results from a particular environment, thus acting in a cognitive manner. These demonstrations serve as a subset of the potential that cognitive radar holds for creating a new generation of multipurpose, adaptive sensors.

A Greedy Approach for Sensor Selection and Power Allocation in a Cognitive Radar Network

Phani Chavali and Arye Nehorai
Department of Electrical and Systems Engineering,
Washington University in St. Louis.

We propose a greedy algorithm for sensor selection and power allocation in a cognitive radar network (CRN) for the task of tracking multiple targets. CRN incorporates several radar sensors working together to achieve the task of enhanced remote sensing capability, and is characterized by feedback from the receiver to the transmitter. The feedback facilitates intelligent control and adaptive processing at the transmitter. In this paper, we consider a CRN that employs sequential Bayesian filtering at the receiver to estimate the state vector. At each time, the CRN selects only a few radar sensors for acquiring measurements. The intuition for selecting a subset of sensors is the observation that the measurements from all the antennas are not equally useful. Sometimes the cost incurred by a sensor for measurement acquisition and communication to the fusion center is higher than the information that the measurement provides. In such scenarios, it is better to redistribute the available power among the other sensors. Hence, the optimal sensor selection and power allocation can be considered as intelligent control performed by the cognitive transmitter to the environment perceived by the receiver.

We use the posterior Cramer-Rao bound (PCRB) as an optimization criterion for sensor selection and power allocation. The PCRB is a lower bound on the mean square error (MSE) of the Bayesian estimates of the state vector and hence we seek to find the optimal sensor set and the corresponding power to be transmitted by these sensors by minimizing the PCRB under suitable constraints. The constraints represent the bounds on the power and communication cost. This joint optimization problem is NP hard to solve.

We propose a two pass greedy algorithm to find a suboptimal solution to this problem. We separate the problem into two parts: the problem of finding the sensors to be employed and the problem of finding the power to be allocated to these sensors. In the first pass, we consider that all the sensors transmit equal power. We then compute the PCRB of state vector due to each sensor, and weigh the PCRB with the distance of the sensor from the fusion center. We then select the sensors sequentially in the decreasing order of weighted PCRB until there are no more sensors left or a sensor does not satisfy the communication cost constraint. At this point, we recompute the PCRB due to all the sensors selected, labeled as first set, and compare it with the PCRB due to the sensor that violated the communication cost, labeled as the second set. We select the set that offers lower PCRB. Once the sensor set is selected, in the second pass, we distribute the power on these antennas, again using a greedy approach. We demonstrate the advantage of the sensor selection and power allocation methods using numerical examples. Preliminary results show that the performance (measured by the mean squared error in the estimates of the target state) using sensor selection and power allocation is better compared to the performance obtained using the all the sensors with equal power allocation.

The Use of Reconfigurable Antennas in a Cognitive Radio Environment

Y. Tawk[(1)], J. Costantine[(2)], and C. G. Christodoulou[*(1)]
(1) University of New Mexico, Albuquerque NM, USA
(2) California State University Fullerton, Fullerton CA, USA

A cognitive radio is an intelligent communication system that is able to *learn* from the environment and *adapt* to the variations in its surrounding by deciding to change its transmitter and receiver parameters. The challenging point in such a system is to monitor the wireless spectrum to determine the parts of the spectrum that are idle. The RF front-end for a cognitive radio environment must be able to change its operating frequencies in response to changes in the RF environmental conditions or system requirements. To achieve these functionalities, two sets of antennas are needed: One dedicated to sense the spectrum (*Sensing Antenna*) and the other dedicated to communicate (*Reconfigurable Communicating Antenna*). The sensing antenna is an ultra-wideband antenna (UWB) that spans a wide band of frequencies (for example 3 GHz-11 GHz). The reconfigurable communicating antenna should be able to tune its operating frequency to achieve communication at a certain band. To obtain the required reconfigurability in the antenna operating frequency, some kind of electrical switching components such as PIN diodes and varactors or optical switching components such as Silicon (Si) switches should be employed to redirect the antenna surface currents. Another approach is to alter the antenna structure via a physical movement of the antenna radiating parts.

The reconfigurable communicating antenna can also be achieved by integrating a reconfigurable filter within the antenna feeding line. The antenna should be a wideband antenna and the embedded filter a reconfigurable narrow band-pass one. The reconfigurability in the filter response is achieved also by incorporating some kind of switching components (electrical or optical) within the filter structure. The combination of the antenna and the filter provide tuning in the communicating antenna resonant frequency. Similar to the first approach, a UWB antenna is dedicated for sensing. The importance of such configuration is that no switching elements are present in the radiating plane of the antenna; therefore the antenna radiation pattern will be less affected by the frequency tuning of the filter.

In this work, we will focus in detailing the need and the importance of using reconfigurable antenna structures to achieve communication between the different users of a cognitive radio system. Various reconfigurable antenna structures will be also presented based on the different types of switching techniques. A comparison between the two RF front-ends for a cognitive radio environment is also detailed. The decision on which RF front-end is more suitable for such a system should be based on several key parameters:

1) The coupling (cross-talk) between the sensing and the reconfigurable communicating antenna
2) The gain/radiation pattern shape of the communicating antenna
3) The switching speed of the communicating antenna between different operating bands.

A Frequency-Tunable Pattern Diversity Antenna for Cognitive Radio Applications

A. Ramadan[(1)], M. Al-Husseini[(1)], Y. Tawk[(2)], J. Costantine[(3)], C. G. Christodoulou[*(2)], K. Y. Kabalan[(1)], and A. El-Hajj[(1)]
(1) The American University of Beirut, Beirut Lebanon
(2) University of New Mexico, Albuquerque NM, USA
(3) California State University Fullerton, Fullerton CA, USA

The inherent gain-bandwidth product limitations of wideband antennas, whose output can be heavily corrupted by wideband noise, and thus resulting in a low SNR, bring in narrowband-tunable antennas as good candidates for use in spectrum sensing. Moreover, narrowband-tunable antennas don't require high-speed analog-to-digital converters, which have higher quantization errors, and may not be practical for use in cognitive radio applications. In this paper, we propose a narrowband-tunable pattern diversity antenna, which combats multi-path fading, while sensing channels. The presented antenna, as shown in Fig. 1, is driven by an open loop resonator (OLR)-based filter to achieve narrowband frequency tunability. The simulated S-parameters of the antenna are given in Fig. 2. A better than -18 dB ports isolation was achieved over the operable frequency bands. The gain pattern of the antenna, at 3.5 GHz, with a peak gain of 4.7 dB is depicted in Fig. 3. The computed envelope correlation coefficient (ρ_e) and mean effective gain (*MEG*) at the operating frequencies, as shown in Table 1, reveal a high diversity gain, and as a result, the proposed antenna can provide pattern diversity to mitigate multi-path fading in wireless channels.

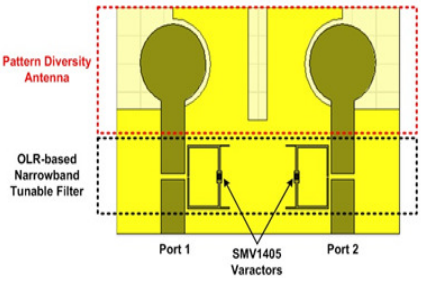

Fig. 1 The antenna structure

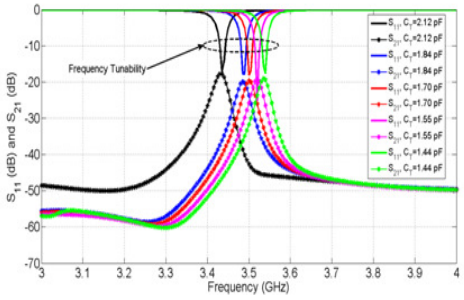

Fig. 2 The S-parameters of the antenna

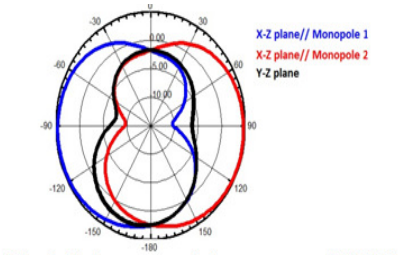

Fig. 3 The gain pattern @ 3.5 GHz

Table 1 The computed diversity parameters of the antenna

f (GHz)	3.435	3.485	3.5	3.52	3.54
$\rho_e < 0.5$	31.18e-5	7.873e-5	11.39e-5	1.536e-5	17.84e-4
MEG_1	21.1861	22.8473	22.8577	22.4888	22.1971
MEG_2	23.840	23.1236	23.3972	22.8055	22.8411
Ratio of MEGs ≈ 1	0.8897	0.9881	0.9769	0.9861	0.9718

Coupling Analysis of a Null Reconfigurable Element for Small Adaptive Phased Arrays

M. W. Young* and J. T. Bernhard
Department of Electrical and Computer Engineering
University of Illinois at Urbana-Champaign
Urbana, IL 61801
mwyoung3@illinois.edu and jbernhar@illinois.edu
http://antennas.ece.illinois.edu

Significant work has been done to study adaptive arrays with identical fixed pattern elements. In these arrays, adaptive processing algorithms have control over the magnitude and phase of each array element. If the fixed pattern elements are replaced by pattern reconfigurable elements, an additional form of array pattern control is introduced. By modeling an adaptive array with null reconfigurable element patterns, recent work has shown that the optimum signal-to-interference-plus-noise ratio (SINR) is most often achieved by steering the null of each reconfigurable element toward an interfering signal instead of steering each pattern maximum toward the desired (T. L. Roach, Ph.D. dissertation, Univ. of Illinois Urbana-Champaign, 2010). This study, however, assumed an environment free of element coupling. Strong mutual coupling between array elements, often a result of their close proximity, can significantly distort each element pattern and substantially affect the predicted adaptive array performance.

The effects of mutual coupling in a two element array configuration have been studied. The study uses a previously designed null reconfigurable element (S. Yong and J. T. Bernhard, in *Proc. of the 2010 IEEE Int. Symp. on Phased Array Systems and Tech. (ARRAY)*). The analysis will aid the design of null reconfigurable adaptive arrays that contain close element spacing and small element numbers. The null reconfigurable element was studied for two possible states: a null at broadside or a null at 30 degrees from broadside. The coupling between elements was analyzed through simulation and measurement as a function of element spacing. As expected, it was found that the coupling between elements for all state configurations consistently decreased as the element spacing increased. However, it is shown that although the coupling decreases with increased element spacing for all state configurations, its effect on the null magnitude and location in each active element pattern varies significantly between state configurations. At times, the coupling even results in the formation of an additional unexpected null. The implications of the mutual coupling results are discussed as it pertains to the implementation of a small adaptive array.

A Frequency Reconfigurable Slot Antenna Using Microvascular Delivery of Conductive Liquid

A. J. King* [(1)], J. F. Patrick [(2,3)], N. R. Sottos [(2,4)], S. R. White [(2,5)],
G. H. Huff [(6)], J. T. Bernhard [(1)]
(1) Department of Electrical and Computer Engineering
(2) Beckman Institute for Advanced Science and Technology.
(3) Department of Civil and Environmental Engineering
(4) Department of Materials Science and Engineering
(5) Department of Aerospace Engineering
University of Illinois at Urbana-Champaign, Urbana, IL 61801
(6) Department of Electrical and Computer Engineering,
Texas A&M University, College Station, TX 77843
ajking2@illinois.edu and jbernhar@illinois.edu
http://antennas.ece.illinois.edu/

As the number of wireless devices continues to increase throughout the world, spectrum-conserving wireless implementations such as cognitive radio will become necessary in order to efficiently use the electromagnetic spectrum. Reconfigurable antennas will be key components of these adaptable systems due to their abilities to reject unwanted signals by changing operating frequency, pattern, or polarization. This reconfigurability has previously been achieved using PIN diodes, varactors, or RF MEMS switches. However, the first two switching methods rely on nonlinear devices which generate harmonics that may radiate, further cluttering the spectrum. More problematic is that each of these methods requires a DC bias network, which can be difficult to implement for a slot antenna due to the DC continuity of the ground plane. In order to overcome this issue, the ground plane is typically segmented to allow for a DC bias while coupling capacitors are used to create an RF short between segments, restricting the RF current to narrow paths (e.g., M. Fries, M. Gräni, R. Vahldieck, *IEEE Microwave and Wireless Components Letters*, **13(11)**, 490-492).

Recent advances in composite fabrication have introduced the possibility of embedding microvascular channels in a substrate in order to use conductive liquid as a switching mechanism (A. Esser-Kahn, P. Thakre, H. Dong, J. Patrick, V. Vlasko-Vlasov, N. Sottos, J. Moore, S. White, *Advanced Materials*, **32(23)**, 3654-3658). By introducing channels running along the width of a slot antenna the length of the radiating section of the slot can be adjusted by filling the channels with conductor and shorting across the slot. The passive nature of this switching mechanism produces linear behavior, while the use of embedded channels does not require the ground plane to be segmented, allowing radiating currents to flow normally. This paper will explore the frequency reconfiguring capabilities of such a design. Simulation and measured results will be presented along with a transmission line model of the antenna and filled channel switches.

A Cognitive Radio Planar Antenna System with a Reconfigurable Substrate Height

J. Costantine[(1)], Y. Tawk [(2)], J. Himmelheber[(1)], M. Shiva[(1)], and C. G. Christodoulou[(2)]
(1) California State University Fullerton, Fullerton, CA 92834,USA
(2) University of New Mexico, Albuquerque, NM87131, USA

Recent investigations into cognitive radio antenna systems propose the use of two antennas. The first antenna which is an ultra-wide band antenna senses the channel for idle frequencies and the second is the communicating antenna that is dynamically tuned to transmit over emerging unused frequencies. The channel spectrum usage optimization imposes a constant monitoring and swift tuning of the communicating antenna. Designers usually resort to switching components such as p-i-n diodes or RF MEMS to achieve reconfiguration; however these techniques suffer from interference and destructive effects caused by their biasing networks. In this work we propose a new planar antenna system for a cognitive radio environment. The antenna system is composed of a typical ultra wide band antenna and a reconfigurable antenna with variable substrate height. The height of the substrate is changed by introducing an air gap of different height below the transmitting antenna. As a result frequency tuning is achieved.

The antenna system is printed on Rogers Duroid 5880 Substrate with 7cm * 7 cm dimensions. Substrate height is composed of two 0.16 cm layers. The transmitting antenna has a partial ground plane of dimensions 7 cm *0.6 cm, while the partial ground plane of the sensing antenna is of 3.4cm *0.7 cm. A slit of 0.5 cm *0.2 cm is introduced into the sensing antenna partial ground plane for tuning purposes. The patches dimensions are shown with the antenna structure in Fig.1. The frequency tuning of the communicating antenna is shown in Fig.2a for different substrate heights. The ultra-wideband behavior of the sensing antenna is shown in Fig.2.b. The change in height is achieved physically by integrating a piezoelectric transducer or a stepper motor into the antenna system structure.

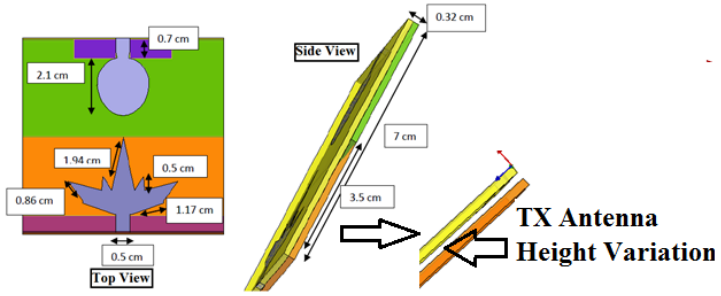

Fig. 1 The Antenna Structure with reconfiguration technique

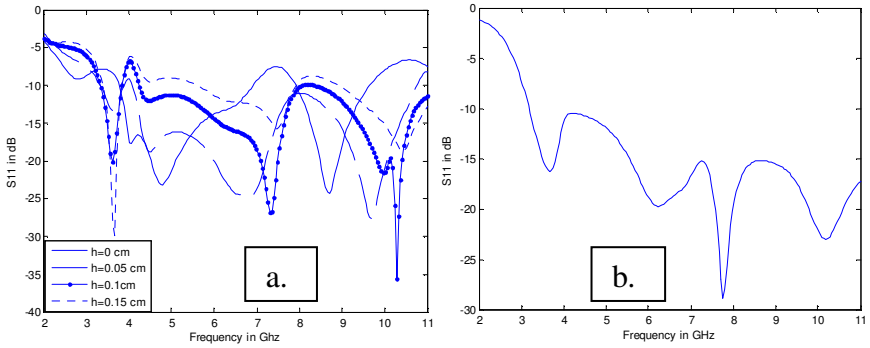

Fig.2 a.Transmitting antenna reflection coefficient for different substrate heights. b. Sensing antenna reflection coefficient

A Reconfigurable Filter for Cognitive Radio Applications

Y. Tawk[(1)], J. Costantine[(2)], and C. G. Christodoulou[*(1)]
(1) University of New Mexico, Albuquerque NM, USA
(2) California State University Fullerton, Fullerton CA, USA

An antenna system for cognitive radio applications should consist of two sets of antennas: A sensing antenna to search for unused frequency bands and a reconfigurable antenna to tune its operating frequency in order to achieve communication based on the channel users' activity. The reconfigurable antenna can be implemented by using the traditional technique which is based on incorporating some switching elements to connect the different parts of the antenna structure. In this work, we propose to implement a reconfigurable antenna for cognitive radio by incorporating a reconfigurable band-pass filter within the antenna feeding line. The antenna tunes its operating frequency based on the mode of operation of the filter. The importance of such configuration is that the antenna radiation pattern will be less perturbed since all the switching elements and their biasing networks are not going to reside in the antenna radiating plane.
In this paper, we present a reconfigurable filter that can be integrated within the feeding line of a wideband antenna. The filter structure and its dimensions are shown in Fig. 1(a). It is printed on Rogers Duroid 5880 substrate of dimension 30 mm X 30 mm. The filter consists of a full ground in the bottom layer and a stripline of width 5 mm in the top layer. A varactor is placed in the middle of the structure to allow the filter to tune its band-pass frequency. The varactor changes its capacitance from 2.67 pF to 0.63pF by varying its junction voltage from 0V to 30V. Two small gaps of width G_W=0.2 mm are etched to isolate the dc bias current from the two ports of the filter. These gaps act as bypass capacitors and are responsible to produce a band-pass response. Two bias lines of width B_W=0.4 mm and length B_L= 11.87 mm are incorporated to provide the dc voltage to the varactor. Two 1.2 nH inductors are included between the filter structure and the bias lines to isolate the RF current from leaking to the power supply. The tuning in the filter measured band-pass frequency for different voltage levels is shown in Fig. 1(b).

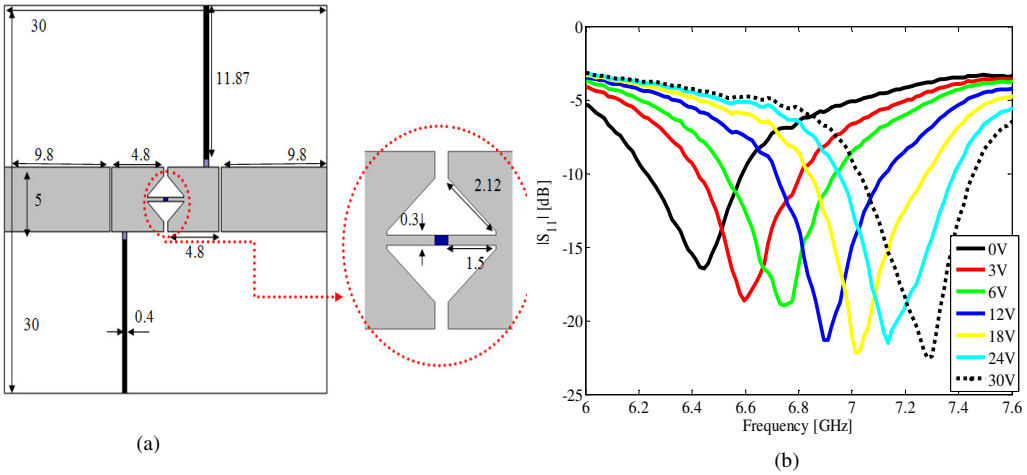

(a) (b)

Fig. 1 (a) The filter structure (b) the measured |S11| of the filter

Estimates of Q for Patch Antennas having Magnetodielectric Substrates

Steven J. Weiss
The U.S. Army Research Laboratory, Adelphi, MD, 20783

Antenna structures based on stratified media consisting of magnetodielectric material are of interest to antenna design engineers as they hold the promise of increasing the bandwidth the device. This work describes the efficiency of such antennas through calculation of values of Q. As a case study, these values are derived for a rectangular patch antenna finding of the power radiated as well as the power launched into surface waves, the power dissipated in the material (loss tangent), and the power lost due to the finite conductivity of the metallic ground plane and patch. The inspiration for this work was presented more than two decades ago for a patch antenna over a dielectric substrate (Y. T. Lo and S. W. Lee, Antenna Handbook, Van Nostrand, New York, 1988, PP 10-50.) Such design curves are invaluable for contributing insight into the optimal design ultimately achieved through computer simulations.

The procedure adopted will be to model the patch using the classic cavity model to estimate filamentary magnetic currents about the perimeter of the patch. Using these estimates and the appropriate Green's functions, one can find the power radiated as well as power launched into surface waves. Internal losses (conducting and dielectric) can be estimated from the cavity model as can the energy stored between the patch and the ground plane. From these calculations, it is then possible to estimate of the optimal thickness of the magnetodielectric that will maximize the radiated power. Once accomplished, families of plots are developed to indicate trends given different values of permittivity and permeability.

Bandwidth Limits for Low Profile Scanning Arrays

Jonathan Doane*, Kubilay Sertel, and John Volakis
ElectroScience Laboratory
Dept. of Electrical and Computer Engineering
The Ohio State University, Columbus, OH
doane.15@osu.edu, sertel.1@osu.edu, volakis.1@osu.edu

Wide band antennas and arrays are essential for high-resolution radar and tracking systems, high data rate communication links, and multi-waveform, multi-function frontends. Although conventional planar "frequency independent" structures such as spirals and self complementary antennas/arrays can provide significant bandwidth, their wideband performance suffers greatly when they are placed over a conducting surface, which is often required for practical platform integration.

We recently developed a simple closed form expression for the fundamental bandwidth limit of PEC-backed planar arrays. Based on Fano's matching theory, we have shown that planar 2D periodic arrays are limited to 8.3:1 impedance bandwidth when no material treatments are used, and 12.1:1 bandwidth when a dielectric superstrate layer is placed above the aperture ($VSWR \leq 2$). However, the impedance bandwidth progressively suffers as the array becomes electrically thinner or as the array is scanned further from broadside. Consequently, the overall usable bandwidth of phased arrays is limited to that of the maximum scan angle. Unfortunately, inherent assumptions that were used in applying the Fano matching theory do not allow a straight forward extension of the method to account for arbitrary array thickness and scan angle.

Here, we develop a new approach based on the H^∞ method that extends the previous results to scanning arrays of arbitrary thickness. Substrate and superstrate material loading is also considered and we show that the maximum realizable bandwidth is proportional to the cosine of the scan angle times the total height of the array. We will present several design curves for optimal material loading of ultra-wideband planar arrays.

Surface Tolerant EBG-Dipole and Fat-Folded-Dipole RFID Tag Antennas: A Comparative Study

H. Rajagopalan and Y. Rahmat-Samii

Department of Electrical Engineering, University of California, Los Angeles
420 Westwood Plaza, Los Angeles, CA 90095-1594, USA
harish@ee.ucla.edu and rahmat@ee.ucla.edu

Radiofrequency Identification (RFID) technology is a rapidly evolving technology that uses RF signals for detection/identification of objects. Currently RFID systems find applications in various areas like asset management, inventory control, vehicle security, animal tracking, and patient identification in hospitals. RFID systems typically consist of a host computer which controls the reader antenna (circularly polarized) and RFID tags (antenna + microchip) which are tagged to the object. Due to the varied nature of the applications, it is desired that the tag antenna performance remains robust on different surfaces. Dipole-type tags are very commonly used in inventory control and other applications as they are simple to design and extremely cheap to manufacture. But when these dipole tags are placed close to metallic surfaces and or humans, their performance deteriorates significantly.

Electromagnetic band gap (EBG) structures have been proposed for low profile dipole antennas over ground plane for wireless applications. The EBG structure essentially shields the dipole from the ground plane while maintaining its impedance and radiation characteristics. These EBG structures can be embedded below the dipole tags thus forming platform tolerant robust tags. Patch-type tags have also been suggested for robust performance on different surfaces. Due to the presence of magnetic currents on the radiating edges these tags work well on ground plane and other surfaces.

In this paper, the performance of a dipole tag with EBG substrate will be compared to a fat-folded dipole type tag at the US-UHF RFID band (902-928MHz). For the dipole tag with EBG, the EBG structure will be characterized based on its reflection phase characteristics and band gap features. The dipole tag will be designed to complex conjugate match to the microchip for maximum power transfer. For the fat-folded dipole type tag, investigations will be performed into the working mechanisms of the tag. Both the RFID tags will be placed on different surfaces (particularly human arm/torso model) and their performance will be evaluated based on dimensions, impedance match, and radiation characteristics. Conformal versions of these tags will also be investigated with the potential for integrating them with textile materials thus forming wearable RFID tag designs.

Methods to Achieve Circular Polarization and Bandwidth Enhancement for Meshed Patch Antennas

Tursunjan Yasin* and Reyhan Baktur
Department of Electrical and Computer Engineering,
Utah State University, Logan UT 84322, USA

Meshed patch antennas have been shown to be effective transparent antennas that can be integrated with solar cells for satellite applications. Previous studies have focused on the mesh geometry and the trade-offs between the transparency and antenna efficiency. Important antenna parameters such as circular polarization (CP) and bandwidth enhancement have not yet studied. This paper is aimed to present our on-going study in achieving CP and improving the bandwidth of meshed antennas.

Similar to a solid patch antenna, a normal meshed patch antenna has a narrow bandwidth. While designed in array configuration, it is found that one may study the coupling between feed-lines and antennas to determine appropriate array geometry to improve the bandwidth. In this study, multiple meshed patch elements, slightly different in size, were placed on the same plane and fed by a microstrip line. Due to the multiple resonances, it is shown that the bandwidth can be significantly improved.

CP is another important antenna property that is desirable in space application. Compared to the solid patch antennas, it is harder to design a CP meshed antenna by using a single feed. The reason is clear — mesh lines have limiting effect on current path on the antenna surface and thus not all the methods for solid patches can be applied for meshed ones. Our method to achieve CP is to utilize the 90-degree difference in both phase and space between two meshed antennas fed by a common microstrip line.

In both methods, the antenna structure is coplanar and has the advantage of the ease to be integrated with solar panels. The feed line can be conveniently placed between solar cells without blocking them.

Broadband Probe-Fed and Aperture-Coupled Cylindrical Dielectric Resonator Antennas

Adam P. Huynh, David R. Jackson, Stuart A. Long, and Donald R. Wilton

Department of Electrical and Computer Engineering
University of Houston, Houston, TX 77204-4005

Dielectric resonator antennas (DRAs) are attractive in many microwave and millimeter-wave applications because they have low conductor loss and little or no surface-wave loss, together with a larger impedance bandwidth (typically about 10%) compared to microstrip antennas. However for applications that require even much wider bandwidths, such as broadband or ultra wideband (UWB) antennas, further bandwidth enhancement is desired.

In this work, two simple cylindrical DRA structures are examined: A probe-fed cylindrical DRA and one that is aperture-coupled by a slot in the ground plane and fed by a microstrip line underneath. Although these are perhaps the simplest possible DRA configurations, it appears that no comprehensive optimization study has yet been performed in which permittivity, aspect ratio, and relevant feed parameters are all varied in order to optimize the design. The advantage of optimizing these basic structures is that simplicity in design is maintained. The goal is to find an optimum combination of aspect ratio d/a (height to radius ratio) and permittivity that yields the largest impedance bandwidth while preserving the desired radiation characteristics of the dominant mode. For probe-fed DRAs, a pattern constraint that the cross-polarization level is below −10.0 dB is imposed. For aperture-coupled DRAs the cross-polarization level is not an issue, but nulls sometimes form in the pattern, and hence a pattern constraint is imposed that acceptable patterns must have all null levels greater than −10.0 dB.

Results show that for probe-fed DRAs the optimum combinations of aspect ratio and permittivity involve d/a from 2.5 to 4.0 and ε_r from 5.0 to 8.0, and the maximum bandwidth attainable is about 46%. Bandwidths that are greater than about 30% correspond to a double resonance in the impedance response. On the other hand, for aperture-coupled DRAs the optimum combinations of aspect ratio and permittivity involve d/a values from 0.4 to 1.5 and ε_r from 3.0 to 8.0, and the maximum bandwidth attainable is about 30%. In either case the effects of dielectric loss on the bandwidth are not noticeable until the loss tangent is greater than about 0.01.

An Optical Alignment Tool for Simultaneous Imaging and Precision Alignment of Two mmWave Antennas

Joshua Gordon, David Novotny

National Institute of Standards and Technology
Physical Measurement Laboratory
325 Broadway
Boulder, CO 80305
josh.gordon@nist.gov

In recent years, more and more systems are being developed in the mm-wave and terahertz frequency ranges. At these high frequencies (50-500 GHz), wavelengths approach sub-millimeter dimensions. With such wavelength scales, the mechanical alignment of waveguide and antenna components becomes increasingly difficult. Antenna characterization techniques such as those used in extrapolation measurements, near field measurements, and general spatial antenna characterization require the precise positioning of antenna components. At these frequencies, new techniques must be developed for achieving the same alignment tolerances that has traditionally been straightforward to achieve in the MHz and lower GHz regimes. We present an optical imaging tool, the Overlay Imaging Aligner (OIA) developed at NIST Boulder, CO, to aid in the mechanical alignment of antenna components in the mm-wave and low-THz frequency regimes (50-500 GHz) where the size of the wavelengths pose significant challenges for alignment. The OIA uses a polarization-selective, machine-vision approach to generate two simultaneous and overlaid, real-time digital images along a common axis. This allows for aligning two antenna components to within fractions of a wavelength in the mm-wave and THz frequency regimes. The combination of simultaneous imaging and laser alignment capabilities of the OIA allows alignment of two antennas as well as quasi-optical focusing and beam shaping optics along the same axis. The overall concept, optical design, function, performance characteristics and application examples are presented. Examples of the alignment of two horns to a common axis, as well as, the alignment of two-horns to two-beam shaping lenses to a common axis performed with the OIA are presented. Data at specific frequencies in the WR-2.2 band are presented that compare the alignment achieved with the OIA to an electrical alignment.

Multiple-Beam Control and Switching Using a Luneburg Lens Antenna

Rafael Sabory-García*, Min Liang, Wei-Ren Ng, M. E. Gehm and Hao Xin
Electrical and Computer Engineering Department, University of Arizona, Tucson, Arizona, 85721, USA

This paper presents the manner, behavior and response of controlling multiple RF transmission devices, VCOs in this case, for multiple simultaneous or independent transmission beams through a Luneburg lens antenna. The Luneburg lens used is designed to operate from 3 GHz to 13 GHz. Multiple-beam control and switching are demonstrated at 5 GHz.

Antennas and arrays that can generate multiple and electronically switchable beams are desired for many communication and sensing applications. Luneburg lens is a well-known device used for scanning radiation beam over wide spatial angles. A 3D Luneburg lens has the ability to focus a plane wave coming from any direction to the opposite point of the sphere. Or, vice versa, any point source placed on the surface of the lens produces a highly directive beam toward the opposite point of the sphere. Therefore, placing several microwave sources (e.g., VCOs with small dipole radiators) at the surface of the lens yields an antenna that is able to transmit power to multiple directions simultaneously.

In this work, a Luneburg lens antenna is designed, fabricated and tested. The fabrication of the lens was implemented using polymer jetting technique (Ziran Wu, J. Kinast, M. E. Gehm, and Hao Xin, "Rapid and inexpensive fabrication of terahertz EM bandgap structures," Opt. Express, vol. 16, pp. 16442-16451, Oct. 2008.), which enables quite convenient, fast and inexpensive fabrication of components of arbitrary shapes with resolution of THz wavelength scale. The Luneburg lens and VCO setup is shown in Fig. 1. In our experiment, four VCOs are placed on the equator of the spherical lens with equal spacing and biased to generate slightly different frequencies around 5 GHz to prevent interference among the sources. The measured radiation patterns with different combinations of the four transmitter elements being turned on are shown in Fig. 2. The results clearly show a good performance of multiple beams without overlapping. Potential applications of this Luneburg lens antenna include broadband direction finding, alternative for phased arrays, 3D radar, etc.

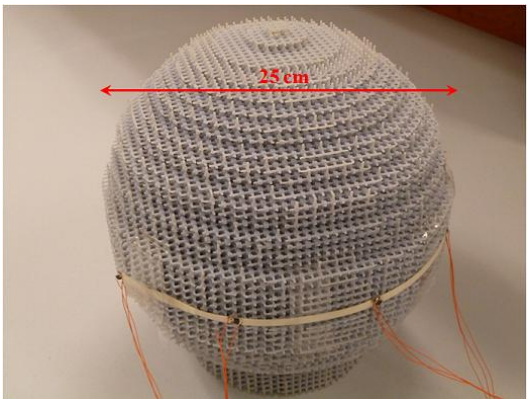

Fig.1 VCO and Luneburg lens setup.

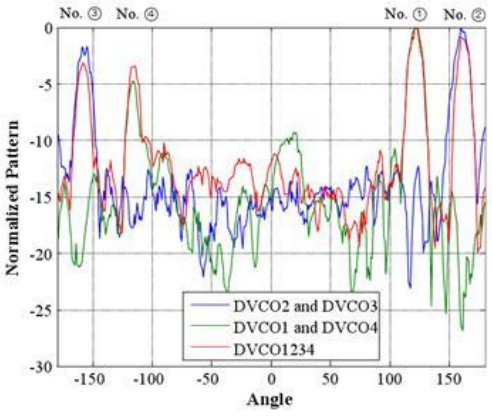

Fig.2 Measured radiation pattern with different VCO combinations.

Analysis and Design Process of a Stripline Archimedean Spiral Antenna

Teng-Kai Chen* and Gregory H. Huff
Electromagnetics and Microwave Laboratory
Department of Electrical and Computer Engineering
Texas A&M University, College Station, TX 77843-3128

The spiral antennas have long been a popular choice for broadband radiating systems. Over the years, a lot of research has been focused on examining the properties of Archimedean spiral antennas more than equiangular spiral antennas in various configurations; this includes spirals on a dielectric substrate backed by a conducting plane reflector and spirals backed by an electromagnetic band-gap (EBG) reflector. In these and other areas of spiral antenna research, most antenna designs are proposed and their properties are studied heuristically since there are very few guidelines on how to design these spiral antennas accurately. This often leads to the use of numerical methods and experimental design studies as a way to characterize the antenna properties. While this remains a viable way to study these designs, a closed-form analytical procedure may improve the design process.

This work provides a design process for a stripline Archimedean spiral antenna in which one arm has been transformed into stripline structure to provide a potentially simpler feed network than the conventional center-fed or gap-fed spiral antenna. An analysis of impedance properties and radiation mechanism for this antenna design is performed first. These illustrate that the stripline implementation of Dyson balun facilitates mode converter and power splitter in this configuration, where the impedance matching between two different transmission line structures (parallel elevated slot line and stripline) correlates directly to the power transmitted into the spiral's radiating mode. The radiation of the spiral antenna occurs when the two elevated slot line modes are in-phase, and the proposed design process in this work uses this concept of impedance matching. A conformal mapping analysis on the characteristic impedance of parallel elevated slot line mode is also derived for the purpose of designing the spiral antenna without numerical treatment. A compact (45 mm × 40 mm × 1.016 mm) bidirectional stripline Archimedean spiral antenna operating from 2 GHz to over 20 GHz is designed using this process with a full-wave simulation tool to optimize the geometry of spiral center. The measurement of the final design shows a good agreement with the simulated results.

Understanding the Cross-pol Generation in Patch Antennas: A Near-Field Approach

Shubhendu Bhardwaj* and Yahya Rahmat-Samii
Department of Electrical Engineering, University of California, Los Angeles
420 Westwood Plaza, Los Angeles, CA 90095-1594, USA

The microstrip patch antennas have gained their popularity in a variety of antenna applications. Even though this technology has evolved from simple rectangular patches to complex designs like slotted and stacked patches, the rectangular patch antenna in its basic form is still being widely used due to its simplicity of design. Also, rectangular patch antennas can be easily utilized in polarization diversity environment due to similarity in shape in two orthogonal planes. In spite of these advantages, due to asymmetrical excitation, the rectangular patch antennas do suffer from high cross-pol in H-plane. There have been various studies in past which have characterized H-plane cross-pol theoretically and experimentally. In this study, the H-plane cross-pol of rectangular patch antenna has been studied as an effect of change in near-field due to asymmetrical probe excitation along its non-radiating edges.

The far-field of patch antenna can be obtained from near-field by NF-FF transformation. It can be proven by vector potential approach that H-plane cross-pol in the far-field is a consequence of fringing near-fields near the non-radiating edges directed normal to it. Due to cosine distribution of fields within the patch, these near-fields are seen as anti-symmetric fields over each non-radiating edges. Ideally, these fields are exactly anti-symmetric and should yield a low H-plane cross-pol in far-field. But asymmetric probe excitation creates a deviation from exact anti-symmetry of these fields which is the cause of higher cross-pol in H-plane. In order to quantify the deviation, this lack in anti-symmetry can also be modeled as phase and amplitude errors.

It has been found that these phase and amplitude errors are directly related to far-field cross-polarization level in H-plane. With this relation, parametric study of variation of these errors by varying geometrical parameters –like width of the patch, thickness of the patch and position of probe and with frequency of operation has been conducted. It has been found that errors in phase and magnitude decrease, as the feeding point is moved near to the edge of the patch leading to decrease in H-plane cross-pol. With increasing width or thickness, these errors are found to be increasing, causing an increase in H-plane cross-pol. These errors are also found to be dependent on the frequency of operation for a given microstrip patch antenna structure.

The paper presents an intuitive understanding of the cross-pol generation in terms of antenna near-field. With this as background, there is a potential for development of novel patch antenna geometries with reduced cross-polarization level.

Electromagnetic Wave Tunneling Through Multiple Epsilon-Negative Metamaterial Layers: A Microwave Filter Theory Approach

Chien-Hao Liu [(1)], and Nader Behdad [(1)]
(1) Department of Electrical and Computer Engineering, University of Wisconsin-Madison, Madison, WI 53706, USA

Materials with negative permittivity or negative permeability values do not allow the propagation of electromagnetic waves. Plasmas are examples of naturally occurring ENG media and are opaque below their plasma frequency. However, under certain circumstances these materials can be made completely transparent and electromagnetic (EM) waves can tunnel through them. In this paper, we examine the problem of EM wave tunneling through an arbitrary number of epsilon-negative (ENG) metamaterial layers that are surrounded by very thin double-positive (DPS) dielectric substrates with high dielectric constant values. We demonstrate that the problem of EM wave tunneling through such a structure has an equivalent problem in the field of microwave filter theory. Using the analogies that exist between these two fields, we demonstrate that a multi-layer structure composed of N DPS layers that sandwich N-1 ENG layers can be made completely transparent in a frequency range where the ENG layers are normally opaque (N>1 is an integer number). We will also present an analytical method that can be used to synthesize such multi-layer structures from the characteristics of their desired responses (e.g. the bandwidth of the transmission window, characteristics of the transmission coefficient, etc.). We present two examples that demonstrate the validity of the proposed analytical synthesis method. These two examples are simulated both analytically (e.g. by using the wave transfer matrix technique) and numerically (e.g. by using full-wave EM simulations). Finally, using the duality principle, we expand these analytical results to the problem of EM wave tunneling through multiple mu-negative metamaterial layers.

Small Anti-Jam GPS Arrays Loaded With Metamaterial Isolators for Reduced Mutual Coupling

Ahmad A. Gheethan* (1), and Gokhan Mumcu(1)
(1) Center for Wireless and Microwave Information Systems, Department of Electrical Engineering, University of South Florida, 4202 E. Fowler Ave. Tampa, FL, 33620 USA

Integration of anti-jam GPS arrays with small platforms requires several miniaturized antennas to be tightly packed within a compact volume. In such configurations, high levels of mutual coupling can cause degradations in the impedance matching and pattern performance of the antenna elements. Previously, metamaterial isolators made up from stacks of spiral resonators (SRs) were employed to suppress mutual couplings in tightly packed 1D linearly polarized arrays (K. Buell, H. Mosallaei, and K. Sarabandi, "Metamaterial Insulator Enabled Superdirective Array," IEEE Transactions on Antennas and Propagation, Vol. 55, NO. 4, April 2007). More recently, we have demonstrated that such techniques can also be applied for reducing mutual coupling between circularly-polarized GPS antennas (A. Gheethan and G. Mumcu, "Coupling reduction of coupled double loop GPS antennas using split ring resonators," IEEE APS Symposium 2011, pp.2613-2616) if the resonators are placed strategically within the array. Specifically, such resonators must be positioned to only interact with the magnetic fields having linkage between an antenna element to another (i.e. coupling magnetic field). On the other hand, their interaction with the magnetic fields generated by single standalone elements must be minimized to prevent a negative impact on impedance matching. As compared to linearly polarized antennas, this constitutes a major design challenge as a standalone CP antenna generates strong magnetic fields that surround all of its volume. Consequently, the number of resonators and their position within the miniature GPS array must be carefully chosen.

Our previous study considered coupling suppression in a four element (2×2) 3.5″×3.5″ GPS array that was constructed from electrically small coupled double loop antennas. In this paper, we will first extend this coupling reduction technique to a five element circular GPS array having <5″ diameter. In addition, we will utilize the computed radiation pattern and scattering parameters of the arrays to investigate the effect of coupling suppression on their nulling performance.

Waveguide Power Divider Based on ENZ Material

Santosh Seran and J. Patrick Donohoe

Department of Electrical and Computer Engineering
Mississippi State University
Mississippi State, MS 39762, USA

Applications of epsilon-near-zero (ENZ) materials for designing novel devices have been a subject of significant interest for the past decade. ENZ materials have been utilized to implement novel electromagnetic behaviors such as super coupling through a narrow waveguide, image transport through a subwavelength hole [M. Silverinha and N. Engheta, 97,157403 (2006) and Phys. Rev. Lett., 102, 103902(2009)], and enhanced transmission through an ENZ slit [D. C. Adams et.al Phys. Rev. Lett.,107,133901 (2011)].

In this presentation, the applicability of ENZ materials for the design of an N:1 waveguide power divider is demonstrated. The design presented is simple and easy to implement in rectangular waveguides since a waveguide operated at its cutoff frequency behaves as an ENZ material [Brian Edwards et al. Phys. Rev. Lett., 100, 033903(2008)]. The exact expression for the reflection coefficient for a system of N+1 waveguides connected by an ENZ junction is first derived. From the reflection coefficient expression, one observes that the input waveguide is matched by choosing the height of the waveguide equal to the sum of the heights of the output waveguides and by choosing the effective area of the ENZ material to be very small. In addition, the ratio of the heights of each output waveguide to the input waveguide determines the power coupled to each output waveguide. Matching the different heights to the output waveguides to the dimensions of the input waveguide can be accomplished by using $\lambda/4$ impedance transformers. The theoretical model is simulated in CST Microwave Studio and demonstrations to illustrate the efficacy of the proposed design are presented. Also, different design strategies are discussed. The design wavelength is suitable for high power applications.

Supercoupling of Electromagnetic Energy from a Waveguide to Free Space Using ENZ Materials

Santosh Seran and J. Patrick Donohoe

Department of Electrical and Computer Engineering
Mississippi State University
Mississippi State, MS 39762, USA

Epsilon-near-zero (ENZ) materials have been shown to exhibit super coupling properties in applications such as super coupling through a narrow waveguide, transport of an image through a subwavelength hole [M. Silverinha and N. Engheta, 97,157403 (2006) and Phys. Rev. Lett., 102, 103902(2009)], enhanced and suppressed radiation [Y. Jin et al, Optics Express, Vol. 18, Issue 16, pp 16587], and increased transmission through a ENZ loaded slit [D. C. Adams et.al Phys. Rev. Lett.,107,133901 (2011)].

In this presentation, we consider the possibility of implementing super coupling from a waveguide to free space with an ENZ junction. An open-ended waveguide terminated to free space exhibits impedance mismatching due the capacitance present at the open end of the waveguide. It is presumed that by adding inductance, the waveguide can be matched. An ENZ material is basically an inductor, since it can only store magnetic energy. Thus, the addition of the ENZ material should improve matching and enhanced transmission. The exact closed form analytical expression for the reflection coefficient for a waveguide connected to free space with an ENZ junction is first derived. From the expression for the reflection coefficient, it is observed that the super coupling occurs for certain geometries of the waveguide and ENZ junction. In addition, the size of the ENZ junction required is small compared to wavelength and in practice would be limited by the minimum size of ENZ material required. The theory is further validated by simulating the model in CST Microwave Studio using a 2D wire medium for the ENZ material. The simulated model corresponds well with the theoretically predicted results. Also, extension of the model to both coaxial and rectangular waveguide geometries is discussed. The proposed concept holds promise for the design of small antennas.

Effect of Scatterer Size Variations on the Reflection and Transmission Properties of a Metafilm

Kendra L. Kumley* and Edward F. Kuester
University of Colorado, Boulder, CO, 80309 USA,
kumley@colorado.edu

In metamaterial and metasurface measurements, it is usually accepted that there will be a certain amount of uncertainty that is inherent in the measurement system. Anomalous ripples in the material response are often attributed to measurement or fabrication errors. Metamaterials and metasurfaces are typically constructed using arrays of periodically arranged scatterers or apertures in order to achieve some desired electromagnetic behavior such as negative refractive index, total reflection or transmission, etc. Most models of such media assume perfect periodicity of the structure, and have not examined the sensitivity of the effective electromagnetic properties to variations of structural parameters from this ideal. In the present work, we will examine this question, and the additional role that loss plays for the following two metafilms: 1) a two-dimensional square array of homogeneous dielectric spheres, and 2) a 2×4 array of homogeneous dielectric cubes; both arranged in free space.

Since we have previously considered the effect of random displacements of the metafilm scatterers from perfect periodicity (E. F. Kuester *et al.*, *Metamaterials 2010*, 13-16 September, 2010, Karlsruhe, Germany), we assume here perfect regularity of the periodic lattice and equal permittivity of each sphere/cube, and (pseudo-) randomly perturb the spheres radii. The electromagnetic behavior of the metafilms has been modeled by simulations using commercial finite-element-method (FEM) software. The metafilm of spheres is additionally modeled analytically, in an approximation based on the generalized sheet transition condition (GSTC) method introduced in (Kuester *et al.*, *IEEE Trans. Ant. Prop.*, **51**, 2641-2651, 2003) and further developed in (Holloway *et al.*, *IEEE Trans. Electromag. Compat.*, **47**, 853-865, 2005) and (Holloway *et al.*, *IET Micr. Ant. Prop.*, **4**, 1111-1122, 2010). Additionally, measurements of the metafilm of cubes placed inside a rectangular waveguide have been made with a Vector Network Analyzer.

When the spheres radii vary by even a small amount, FEM simulations predict the occurrence of extremely sharp resonances in the scattering parameters S_{11} and S_{21} of plane waves incident on the metafilm. The type of asymmetry in the predicted resonance curves is characteristic of what have been called Fano resonances. They appear in results of both the GSTC and FEM models, and also appear for the metafilm of cubes. Finally, we will consider the impact the loss of the material of the sphere/cube has on these resonances. We will show that there is an inverse relationship between the loss tangent of the sphere material and the magnitude of the resonances. Taking all these results into account, we will explore the anamolies found in the measurements, and discuss the implications of the resonances on practical applications of metafilms.

Generalized Retrieval Procedure to Determine Local Effective Parameters of Metamaterials Based on First-Principle Homogenization Theory

Xing-Xiang Liu, Andrea Alù
Department of Electrical and Computer Engineering,
The University of Texas at Austin, Austin, TX 78712, U.S.A.

In this work, we present a generalized retrieval procedure to define physically meaningful homogenized parameters for a wide class of periodic metamaterials, based on a rigorous first-principle homogenization approach. It is shown that an *ab-initio* homogenization approach, which properly defines macroscopic average fields and polarizations based on the microscopic field distributions in each unit cell, and that takes into account the full dynamic coupling within the array, may provide constitutive parameters that are inherently local and independent of the form of external excitation. By taking advantage of this formulation, we propose a new retrieval method to calculate the effective parameters of a generic metamaterial sample and we verify its accuracy by comparing it with conventional retrieval methods and full-wave simulations. We also provide insightful discussions on the relation between this rigorous description of metamaterials and the conventional non-local description in terms of retrieved permittivity and permeability. We first show that both descriptions may be obtained from the scattering parameters of a metamaterial sample, and we compare their frequency dispersion, highlighting their different physical meaning. We propose and compare three alternative numerical approaches, based on our homogenization theory, to derive the conventional permittivity and permeability of a metamaterial array from the calculated microscopic field distributions in the array, and we associate their inherent nonlocal properties to the specific distribution of induced polarization currents in each unit cell. We then show the reasons behind the restoration of the local material properties in our proposed description of the array in terms of first-principle constitutive parameters. Our approach may be generally applied to several realistic metamaterial geometries, even considering technological disorder and imperfections caused by the fabrication process.

Exact Representations of 3D Periodic Metamaterial Arrays by Generalized Electric and Magnetic Polarization Densities

Arthur D. Yaghjian
Research Consultant, Concord, MA 01742, USA

Unlike most natural materials, metamaterials are highly spatially dispersive as well as temporally (frequency) dispersive because the value of the electrical separation distances of their inclusions (artificial "molecules") is not extremely small compared to unity over their operational bandwidths. To characterize the effects of spatial dispersion in plasmas and crystals, Landau & Lifshitz (Electrodynamics of Continuous Media), Silin & Rukhadze (Electromagnetic Properties of Plasma and Plasma-Like Media), and Agranovich & Ginzburg (Crystal Optics with Spatial Dispersion, and Excitons) decompose the fields and sources into a spectrum of plane waves, each with $e^{i(\boldsymbol{\beta}\cdot\mathbf{r}-\omega t)}$ space-time dependence, such that at a given frequency ω, the three components of the propagation vector $\boldsymbol{\beta}$ can take on any real value. These authors proceed to combine all electric and magnetic polarization effects (including all multipoles) into a single electric-magnetic polarization density, $\mathbf{P}_L(\boldsymbol{\beta},\omega) = -\mathbf{J}(\boldsymbol{\beta},\omega)/(i\omega)$. They then assign a single susceptibility $\overline{\boldsymbol{\chi}}_L(\boldsymbol{\beta},\omega)$ to this polarization vector such that $\mathbf{P}_L(\boldsymbol{\beta},\omega) = \epsilon_0\overline{\boldsymbol{\chi}}_L(\boldsymbol{\beta},\omega)\cdot\mathbf{E}(\boldsymbol{\beta},\omega)$, where $\mathbf{E}(\boldsymbol{\beta},\omega)$ is the spectral electric field. More recently, Silveirinha (Metamaterials Handbook, Vol. I, Ch. 10, CRC Press, 2009) has extended and applied this single-polarization formulation to periodic metamaterials.

Although the single-polarization formulation is both exact and elegant, it has some serious drawbacks. For instance, practical solutions to the Maxwellian microscopic equations for metamaterial arrays usually require the separate determination of electric and magnetic polarizations, whether or not the two polarizations are eventually combined. Moreover, the $\overline{\boldsymbol{\chi}}_L$ susceptibility for the single polarization does not reduce to a scalar even if the medium is an isotropic dielectric and, thus, in reality requires no fewer unknowns than the conventional formulation that uses both electric an magnetic polarization densities. Furthermore, the single-polarization formulation is based upon electric current (for example, Amperian magnetic polarization with equivalent electric-current density $\nabla\times\boldsymbol{\mathcal{M}}(\mathbf{r},t)$), whereas it proves essential for determining the momentum-energy transfer in ordinary (nondiamagnetic) magnetic materials to represent magnetization by magnetic-charge separation (magnetic polarization with equivalent magnetic current density $-i\omega\mu_0\boldsymbol{\mathcal{M}}(\mathbf{r},t)$).

To alleviate the drawbacks of the single-polarization approach, Fietz & Shvets (Physica B, 405, 2930, 2010) and Alù (Physical Review B, 84, 075153, 2011) have developed bianisotropic homogenization methods for periodic metamaterials based upon approximate representations of electric and magnetic polarization densities.

In the present paper, two sets of exact Maxwellian representations for the primary Floquet modes of three-dimensional (3D) periodic metamaterial arrays are derived, one in terms of generalized electric charge-current polarization densities, and the other in terms of generalized magnetic charge-current polarization densities. The inclusions of the 3D metamaterial arrays can be composed of linear perfectly conducting, resistive, dielectric, and magnetic material, including diamagnetic material. Since the representations are exact, the constitutive parameters are perfectly causal. A numerical example of causal permittivity and diamagnetic permeability will be given for perfectly conducting spherical inclusions with the spatial-dispersion propagation vector $\boldsymbol{\beta}$ chosen to approach zero.

Traveling Waves on Three-Dimensional Simple-Tetragonal Periodic Arrays of Two Different Magnetodielectric Spheres

Nicola Bowler[(1)], and Yang Li[(2)]
(1) Materials Science and Engineering, Iowa State University, USA
(2) Electrical and Computer Engineering, Iowa State University, USA

A general theory has been developed to describe traveling waves on three-dimensional (3D) periodic arrays of two sets of magnetodielectric spheres arbitrarily arranged on a simple tetragonal lattice. In this way, the effect of arrangement of the spheres, on the double-negative (DNG) bandwidth, is thoroughly examined. The result is eventually expressed in the form of k-β (dispersion) equations. To improve the computational efficiency, rapidly converging expressions and their double summation form are derived for slowly converging summations in the k-β equations. The dispersion diagrams of seven different arrangements of the spheres, Figure 1, are analyzed for three combinations of sphere types: i) dielectric spheres with equal permittivity but different radius, ii) dielectric spheres with equal radius but different permittivity and iii) one set of spheres is purely dielectric while the other set is magnetic. Analysis of the three combinations of sphere types predicts narrow double-negative (DNG) bandwidths for spheres combinations i) and ii), and wider DNG bandwidths for spheres combination iii), which is a similar finding to that of results reported in previous literature for a subset of the arrangements examined here. The maximum bandwidths of the DNG region provided by different arrangements for spheres combinations i) to iii) are, respectively, 0.21% with arrangement (d), 0.069% with arrangement (c), and 7.403% with arrangement (b).

Although purely dielectric materials with relative permittivity much greater than one above 1 GHz are available, the potential impact of purely dielectric DNG metamaterials still depends on whether the narrow bandwidths achievable are acceptable for particular applications. Since purely magnetic materials with relative permeability much greater than one above 1 GHz are not currently available, the practicality of fabricating DNG meta-materials using arrays with spheres combination iii) is questionable at present, but should be pursued because it yields much wider DNG bandwidths than those of spheres combinations i) and ii).

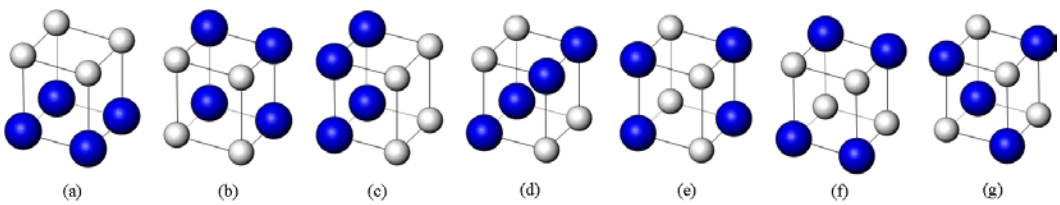

Fig. 1. Seven different periodic arrangements of two types of dielectric spheres on a simple-tetragonal lattice. The direction of wave propagation is vertical.

Complex Modes and Artificial Magnetism in Composite Materials Made of Spherical Particles Accounting for Coupled Electric and Magnetic Dipoles

Salvatore Campione*, and Filippo Capolino
Department of Electrical Engineering and Computer Science, University of California, Irvine, CA, 92697, USA, http://capolino.eng.uci.edu/

Artificial composite materials proved to be a feasible way to increase the degrees of freedom in the interaction of electromagnetic (EM) fields with matter. Based upon the metamaterial (MTM) point of view, composite materials add very interesting possibilities to control EM waves from microwaves to optical frequencies. The lack of strong magnetism in natural materials has motivated in recent years the use of MTMs to produce artificial magnetism from non-magnetic materials, especially at high frequencies where natural magnetism disappears.

A comprehensive way to understand and classify collective resonances in composite materials is by modal analyses of arrays periodic in 3D (three dimensions). In this work, coupled electric and magnetic dipoles are adopted to characterize the modes with complex wavenumber in composite materials made of particles with spherical shape. The approach described in the present paper allows for the tracking and especially for the characterization of the evolution of all modes, varying frequency.

The Ewald representation of the required dyadic periodic Green's functions to represent the field in 3D periodic arrays of spherical particles is derived, which can be analytically continued into the complex wavenumber space, accounting also for coupling between the electric and magnetic dipoles. The formulation presented in this work is general and could be adopted for different frequency ranges and/or constitutive non-magnetic material properties.

We then analyze two different metamaterial examples, one at millimeter the other at infrared waves, of spheres made of non-magnetic materials (e.g., polaritonic materials), observing the generation of artificial magnetism. Homogenized permeability and refractive index are obtained by adopting different retrieval methods and their agreement and disagreement is discussed. We have observed that accounting for the dipole coupling is needed to achieve more accurate results.

Multi-layer Tensor Impedance Surface Analysis

Amit M. Patel*, Anthony Grbic
Department of Electrical Engineering and Computer Science,
University of Michigan, Ann Arbor, MI, 48105,
Email: amitmp@umich.edu, agrbic@umich.edu

The propagation characteristics of electromagnetic waves on various isotropic (scalar) impedance surfaces have been studied for some time, in order to control surface waves and leaky-wave radiation. One and two dimensional periodic impedance surfaces as well as tensor impedance surfaces, have been explored for enhanced control of wave guidance. The desire to integrate antennas and other electromagnetic devices onto the surfaces of vehicles and other platforms has driven this interest in both scalar and tensor impedance surfaces. Planar leaky-wave antennas have been designed using tunable scalar impedance surfaces as well as sinusoidally modulated surface impedance profiles. Additionally, artificial impedance substrates have been explored as a method for antenna miniaturization and bandwidth enhancement. Further, great strides have been made in realizing practical printed devices such as holographic antennas and polarization controlling surfaces, by exploiting the anisotropic properties of tensor surfaces.

Tensor impedance surfaces have been implemented as multi-layer structures, consisting of planar metallic patterns printed over a grounded dielectric substrate. To date, it has been assumed that these multi-layer structures can be approximated as single surfaces. Using this approximation can simplify the design process but may inadequately model propagation and guidance characteristics. A more accurate method for analyzing and designing tensor impedance surfaces is described in this paper. The tensor impedance surface is modeled as a multi-layer structure consisting of a tensor sheet impedance over a grounded dielectric substrate.

In this work, a novel method for analytically predicting the full modal behavior of a multi-layer tensor impedance is presented. First, the dispersion equation of an arbitrary tensor sheet impedance over a grounded dielectric substrate (multi-layer structure) is derived. Next, a two-dimensional sheet impedance extraction method is presented. Specifically, the method can extract the tensor sheet impedance of a metallic pattern printed on a grounded dielectric substrate from two simple normal-incidence simulations using a full-wave solver. By combining the dispersion equation for the multi-layer structure and the sheet impedance extraction method, the full modal behavior of an example geometry is predicted analytically and verified through full-wave eigen-mode simulations.

A Wide Band Conformal Antenna inside Composite Material

Yun Seo Koo*[(1)], Richard Fink[(2)], Ahmad Hoorfar[(3)], Aly E. Fathy[(1)]
(1) University of Tennessee, Knoxville, TN, 37996, USA
(2) Applied Nanotech, Inc, Austin, 78758, TX, USA
(3) Villanova University, Villanova, 19085, PA, USA

Various types of vehicles such as tanks and HUMVEEs need to be covered with heavy ballistic panels for protection against improvised explosive devices. But, there is still a need to provide communications and jamming. Hence, antennas should be embedded within or mounted on such protective panels. Such antennas need to be light-weight, rugged, and cover wide frequency range.

The panels are generally designed based on mechanical constraints. They are characterized too for their electrical properties including dielectric constant and loss tangent. The fiber based panel demonstrated a dielectric constant of 4.5 and relatively low loss tangent of 0.02. Various antenna structures were investigated including slots (Y. Wang, A. E. Fathy, and M. R. Mahfouz, IEEE Antennas and Propagation International Symposium, pp. 2219-2122, 2011), patches, and bowties. The design goals were geared towards developing wide band antenna while having a compact size. Along these lines, a broad band conformal slot antenna design has been developed and integrated with a ballistic panel.

For ease of fabrication, the developed slot antenna was printed on FR4 substrate ($\varepsilon_r = 4.4$) with a thickness of 1.57 mm and $\tan\delta = 0.02$ and sandwiched between fiber slabs. This substrate has a dielectric constant very close to that of the ballistic panel and the slot antenna is fed using a Y-shape feeding line and tapered microstrip slot for wide band operation while having a compact size.

The developed slot antenna is sandwiched between two ballistic panels. At 1 GHz, the aperture size is λ/3 and the antenna height is λ/5. The antenna design is backed by a high impedance surface (D. Sievenpiper, L. Zhang, R. Broas, N. Alexopolous, and E. Yablonóvitch, IEEE Transactions on Microwave Theory and Techniques, Vol. 47, no.11, Nov. 1999), which consists of a lattice of square metal plates and a ferrite slab.

The dimension of the high impedance structure is determined using Reflection Phase Characterization Method (F. Yang, and Y. Rahmat-Samii, IEEE Transactions and Antennas and Propagation, Vol. 51, no.10, Oct. 2003). The fabricated antenna has demonstrated a broadband performance in the 1 to 4 GHz frequency range and has over 3 dB gain. The total dimension of the structure is 10cm × 10cm × 6cm.

Silicon Carbide (SiC) Antennas for High Temperature and High Power Applications

Tutku Karacolak*(1), Rooban Venkatesh K. G. Thirumalai(2), J. Neil Merrett(3), Yaroslav Koshka(2), and Erdem Topsakal(2)

[1]School of Engineering and Computer Science
Washington State University Vancouver
Vancouver, WA 98686, USA

[2]Department of Electrical and Computer Engineering
Mississippi State University
Mississippi State, MS 39762, USA

[3]Air Force Research Laboratory
Wright-Patterson Air Force Base, OH 45433, USA

Silicon carbide (SiC) materials have attracted great interest recently in high temperature and high power electronics applications due to its wide energy band-gap, high thermal conductivity, excellent physical stability, and maximum operating temperature. These advantages of SiC make it superior to other commonly used semiconductor materials such as silicon (Si) and gallium arsenide (GaAs) which have been used in the fabrication of modern electronic devices. One of the emerging applications of SiC is the design of microstrip patch antennas which are widely used in military and commercial wireless communications. Printed microstrip patch antennas are low profile, low weight, and can easily be integrated with other circuitry including SiC IC devices. Therefore, microstrip patch antennas utilizing semi-insulating SiC substrates are perfect candidates for high-performance aircraft, spacecraft, satellite, and missile applications. Moreover, the dielectric properties of SiC allows for antenna miniaturization and higher antenna efficiency due to its high dielectric constant ($\varepsilon_r \cong 10$) and low conductivity ($\sigma = 10^{-5}$ S/m) values.

In this study, the main objective is to combine highly doped and semi-insulating silicon carbide (SiC) materials to design and fabricate patch antennas for extreme environments. To do so, we start with sample patch antenna design operating at 10 GHz to investigate the feasibility of the proposed idea. Following the simulations, the designed antennas are fabricated that consist of a semi-insulating SiC dielectric medium and gold layers on the front and back of the SiC substrate. Reflection coefficient measurements are performed for validation and compared with the simulations. A good agreement is seen at the band of operation. Results regarding antenna parameters such as return loss and radiation pattern are presented. The fabrication process of the antennas is also explained in details.

C-shaped, E-shaped and U-slotted Patch Antennas: A Comprehensive Comparative Study

Shubhendu Bhardwaj* and Yahya Rahmat-Samii
Department of Electrical Engineering, University of California, Los Angeles
420 Westwood Plaza, Los Angeles, CA 90095-1594, USA

Microstrip patch antenna technology has seen an evolutionary development from simple rectangular patch antennas to various configurations of slotted patch antenna. Slotted antennas have particularly gained their importance because of their miniaturized size, high bandwidth and multi-band characteristics. Interestingly, position and orientation of slots in slotted patch antennas can significantly affect various features of antenna like bandwidth, resonant frequency, cross-pol etc. This study is aimed at understanding and comparing different characteristics of these slotted antennas.

In this paper four popular types of slotted antenna topologies- C-shaped, double C-shaped, U-slotted and E-shaped patch antennas have been comparatively analyzed for the wireless communication band of 1.9 GHz to 2.4 GHz. These antenna topologies have been compared in terms of their bandwidth, size, RF-mechanism, cross-pol and gain. The comparison has been done against a simple square patch antenna operating in the same frequency band. It has been shown by numerical simulations that C-shaped and double C-shaped antennas, even though show a 60% and 70% miniaturization, have a reduced bandwidth of around 0.8% and 1.27% respectively. U-slotted and E-shaped configurations, owning to dual mode wideband operation, have high bandwidth of 24% and 27% respectively, but do suffer from a minor penalty of size.

In order to understand the varying cross polarization levels in these antennas, the near-field plots of these antennas have been studied. The near-field of an antenna is dependent on its geometry and far-field of the antenna can be obtained by NF-FF transformation. Therefore, effect of slots on the far-field characteristics can be understood using these near-field plots. Using this analysis, it has been found that introduction of slots parallel to radiating edges introduces asymmetry of near-fields across E-plane of the antenna, increasing its cross-pol in E-plane. This is the cause of increased cross-pol in E-plane for C and double C-shaped patch antennas. By applying similar reasoning for U-slotted and E-shaped patch antennas, a higher level of cross-pol in H-plane can be explained for these antennas too.

The study presents a just comparison of these slotted antenna types, showing their pros and cons for a given frequency band. Such a study is important not only for understanding different mechanisms in slotted antennas but also for choosing an appropriate antenna topology for a given set of requirements.

Next Generation MEMS Reconfigurable E-Shaped Patch Antenna Design using Particle Swarm Optimization

Joshua Kovitz*, Harish Rajagopalan, and Yahya Rahmat-Samii
Department of Electrical Engineering, University of California, Los Angeles
420 Westwood Plaza, Los Angeles, CA 90095-1594, USA
jmkovitz@ucla.edu, harish@ee.ucla.edu, rahmat@ee.ucla.edu

The rapid progression of wireless communication systems has imposed significant demands on the antenna performance utilized in these systems. Generally, these requirements in terms of size, cost, gain, and overall performance are satisfied by varying existing antenna topologies. *Trial-and-error* methods can be cumbersome and time consuming in highly dimensional optimization problems (typical for these antennas), sometimes without ever achieving the performance desired. Therefore, there is a need to implement novel antenna solutions, especially to satisfy the ever increasing demands of wireless mobile systems. Here, we apply the utilization of optimization schemes with numerical solvers for reconfigurable antenna designs.

This research investigates the use of E-shaped patch antennas as reconfigurable antennas suitable for wireless communication systems, which can benefit from a reconfigurable antenna's flexibility. The E-shaped patch antenna is chosen due to its design complexity involving several parameters, and its geometry provides straightforward implementation and integration of MEMS switches (easy access to bias lines). Optimizing these designs represents a highly dimensional, multimodal, and nonlinear optimization problem. Gradient based methods suffer from the inability to compute the derivative exactly, and these methods perform poorly in the global optimization problem, where the initial guess might not be located within the neighborhood of the global extremum. Therefore, this problem requires a global optimizer which works well under these conditions, and Particle Swarm Optimization (PSO) has proven effective for these problems. PSO is also chosen here because of its inherent algorithmic simplicity and also its robustness.

While the optimization program can certainly find the best values for each of the design parameters, it does not automatically map the physical problem to the optimization problem. It is the antenna designer's responsibility to define the geometry with the smallest possible number of parameters to be optimized. Therefore, a discussion of the physical principles of the E-shaped patch antenna is given, along with possible configurations for reconfigurability. Frequency reconfigurable and polarization reconfigurable design concepts are introduced, and the computational models for determining the performance of the antennas are given. Next, PSO is applied to the geometries in order to find the peak performance design. The resulting designs from the optimization are then fabricated using MEMS switches and measured using UCLA's anechoic chambers. It is anticipated that these designs provide the desired reconfigurability that enables the future design of versatile communication systems.

Highly Flexible Textile Antennas on Organza and Polymer Substrates

Zheyu Wang*, Lanlin Zhang, Yakup Bayram, Dimitris Psychoudakis,
and John L. Volakis
ElectroScience Laboratory, Department of Electrical and Computer Engineering,
The Ohio State University, Columbus OH 43212, USA

We present a new class of highly flexible antennas based on embroidered conductive textiles (E-textiles) on polymer-ceramic composites. These flexible antennas are desired for conformal and light-weight installations of airborne antennas and for wearable electronic devices. The presented E-textile antennas and circuits offer attractive mechanical and Radio Frequency (RF) performance when compared to conventional flat and rigid printed circuit alternatives.

The proposed conductive textiles are composed of high strength and flexible fiber cores with conductive metallic coatings. In this study, Ag coated Zylon fibers (Amberstrand® fibers) were used, with a DC resistivity as low as 0.8 Ω/m. However, other conductive fibers are available. The textile circuit and antenna components are embroidered onto organza fabric using automatic embroidery process. Key to achieving high conductivity is the employed automated high density stitching. For our case, we achieved over 70 stitches per square centimeter.

The organza antenna and circuit can be placed on a flexible polymer susbtrate for mounting. Specifically, RF substrates were fabricated by tape-casting composites of polydimethylsiloxane (PDMS) and rare-earth titanate ceramics (RET). Mixing RET into PDMS allowed for variable dielectric constants, and even varying substrate across the lateral dimension of the layer. Fabricated composite substrates were found to be provide tunable dielectric constants from ε_r=3 to 13 with a low $\tan\delta < 10^{-2}$ up to several GHz.

For experimental evaluation, basic prototypes were fabricated. These included transmission lines (TL), patch antennas, antenna array, and multilayer RF components connected with vias. In all case these were fabricated by assembling textile antennas onto polymer substrates. Measurements of the prototypes were conducted, under both planar and curved configurations, and compared to their copper counterparts for validation. It was found that the measured RF characteristics of the prototype antennas were remarkably good at UHF frequency band, and very close to copper's performance. These results clearly demonstrated the promise of flexible textile RF components on polymer substrates.

Pixelated dielectric composite substrates for microwave frequency applications

Lanlin Zhang, Dimitris Psychoudakis and John L. Volakis
ElectroScience Laboratory, Department of Electrical and Computer Engineering
The Ohio State University, Columbus OH 43212, USA
E-mail: zhang.471@osu,edu, dpsycho@ece.osu.edu, volakis.1@osu.edu

We introduce an innovative class of dielectric polymer composites using a new fabrication process based on pixelated dielectric structures. These substrates/composites can promote electromagnetic device miniaturization, performance optimization by varying dielectric properties, and energy efficiency.

Traditional dielectric materials provide single values for the substrate over a band of frequencies. Often, this implies that low permittivity need be used to achieve good device efficiency. However, higher dielectric constants are needed for device miniaturization and variable substrate materials are required for impedance matching over large frequencies ranges. By having variable dielectric properties within the substrate, the new pixelated composite offers unprecedented design freedom and topology optimization. Fabrication of the proposed composites start with microscopically engineered dielectric polymer pastes. These are subsequently assembled to form pre-designed pixelated substrates. The pastes are composed of low-cost and low-loss polymers mixed with titanate ceramics or metallic silver nanostructures as the dispersed phases. The polymer matrix also offers low temperature fabrication and handling, and this highly attractive with industrial manufacturing processes. Upon assembly and arrangement, the composite pastes are then automatically casted and rapidly cured to realize desired pixelated substrates. This automatic fabrication method is accurate and reproducible, as well as time and energy efficient. This design concept will be demonstrated by fabricating and testing basic antenna structures. The process allows not only for increased antenna gain (enhanced electromagnetic performance) but also for a new direction in wideband RF component fabrication.

SPECIAL SESSION on Flexible Electronics organized by Tentzeris & Volakis

Inkjet-Printed Flexible "Smart-Skin" Wireless Sensors

V. Lakafosis*, R. Vyas, A. Traille, H. Lee, and M. M. Tentzeris
School of ECE, Georgia Tech, Atlanta, GA 30332-250

The ever-increasing need for ubiquitous cognition of our environment prompts the integration of unobtrusive, extremely low-cost and passively-powered wireless sensors in our surroundings. Smart skins, i.e. thin layers of modified materials on top of surfaces that surround our every-day lives, constitute ideal such sensor candidates and true enablers of the pervasive awareness vision. In this paper we are presenting various types of ultra-high-sensitive smart skin sensors for authentication and seal proof, metallic structural strain detection and ammonia (NH_3) sensing. These low-profile smart skin prototypes share not only all the aforementioned desired characteristics but also high levels of sensitivity and a flexible and rugged design.

An arbitrary constellation of small, thin pieces of metallic conductors and/or one or more discrete dielectric materials that are randomly dispersed and spatially fixed into a 2 cm x 2 cm x 1 mm, RF wave permeable dielectric fixative can behave as certificates of authenticity and seal proof. The idea is that these modified smart skins, which can be integrated into parts of object surfaces or product openings, yield a hard-to-predict, unique signature of S_{21} when brought within the reactive near-field area of a reader's antenna array. Not only is the cost of producing these random unique physical structures comparable to the price of typical RFID tags but also their uniqueness incurs prohibitively high expenses for an adversary to even nearly reproduce them. Fabricated copper- and plastic PET-based smart skin certificates are shown to produce a signature consisting of 72 S_{21} couplings that are extracted by the corresponding antenna element couplings of our custom fabricated 50 US dollars reader.

Fatigue-induced fractures and cracks are among the most common concerns for inspectors of large metallic constructions, such as highway bridges. The low-profile design that serves here as smart skin strain sensor is a quarter-wave rectangular folded patch antenna that adopts a specially chosen substrate material with low dielectric attenuation, as well as an inexpensive off the-shelf RFID chip for signal modulation. The basic concept is to exploit the strain-dependent behavior of the antenna radiation as the sensing mechanism. In particular, when a small piece of 2D antenna is under strain/deformation, its resonance frequency may change accordingly, which can be wirelessly interrogated by an RFID reader... The average transmitted power threshold levels for the RFID tag and the mapping of the resonance frequency to the corresponding strain level demonstrate strong linearity between the interrogated resonance frequency and the strain experienced by the antenna.

Carbon nanotubes (CNTs) alter their material properties, in particular the load permittivity, when in the presence of a given gas substance, such as ammonia (NH_3). By integrating CNTs on antenna structures we achieve shifts in the latter's resonant frequency. We optimize single-walled CNTs for a given compound by functionalizing them and, thus, enhance the above effect.

Considerations with numeric stability when optimizing MOMI for long range propagation computations

Daniel E. Davis*, Benjamin A. Westin, and Gary S. Brown
Virginia Polytechnic Institute and State University, Blacksburg, VA, 24060, USA

The magnetic field integral equation (MFIE) or combined field integral equations (CFIE) provide full wave solutions to electromagnetic scattering problems. The MFIE and CFIE are useful for propagation problems because they can accurately represent the scattering from a broad range of rough surfaces. However, because the MFIE and CFIE produce dense matrices, with sampling of the surface required at approximately 10 samples per electromagnetic wavelength, storing the matrix for a long propagation path can be impractical or impossible. The method of ordered multiple interactions (MOMI), an iterative technique, overcomes these storage limits as it does not require the interaction matrix to be stored, and elements of the matrix only need to be computed as they are needed. Furthermore, MOMI converges to a solution quickly, requiring few iterations for most problems. However, MOMI also has significant drawbacks, as computing the matrix is computationally expensive, and MOMI must recompute the matrix each time it is used if the matrix is too large to store. Also, MOMI requires sequential solution of the rows of the matrix, making it difficult to parallelize.

There are a number of techniques which can be used to improve the speed of the computations that MOMI performs, including methods of parallelization and vectorization, improvements to the algorithm to reduce the needed number of iterations, and improvements to the discretization process to reduce size of the propagator matrix. However, over long propagation paths, a variety of numeric factors can reduce the accuracy of results or prevent convergence. Thus, the tradeoff between techniques for optimizing the computation, and numeric factors affecting accuracy and convergence, is examined. The oscillatory nature of the kernel can cause numeric stability issues if the computations are not appropriately ordered. Thus, optimizations must be carefully applied to preserve the order of operations. Additionally, some optimizations, such as vectorization of the matrix element computations, provide a direct trade-off between the speed of computation and the accuracy of kernel elements. These must be balanced to retain a reasonable level of accuracy in the propagator matrix. Furthermore, applying some optimizations inconsistently, such as during the computation of the solution of the equivalent currents but not during the scattering of those currents, can result in additional numeric problems which may only become apparent when solving long range problems.

Drift-diffusion and transport models for the analysis of non-local plasmas and metamaterials

Ebrahim Forati[(1)] , George W. Hanson [(1)] , Tao Shen[2] and Thomas Wong[2]

(1) Dept. of Electrical Engineering and Computer Science, University of Wisconsin-Milwaukee, Milwaukee, WI 53211, USA, E-mail: george@uwm.edu
(2)Department of Electrical and Computer Engineering, Illinois Institute of Technology, Chicago, IL 60616, USA, E-mail: twong@ece.iit.edu

A general non-local relationship between current and field is

$$\boldsymbol{J}(\boldsymbol{r},\omega) = \int \bar{\boldsymbol{\sigma}}(\boldsymbol{r}-\boldsymbol{r}',\omega).\boldsymbol{E}(\boldsymbol{r}',\omega)\, d^3r',$$

and in the spatial transform domain we have

$$\boldsymbol{J}(\boldsymbol{q},\omega) = \bar{\boldsymbol{\sigma}}(\boldsymbol{q},\omega).\boldsymbol{E}(\boldsymbol{q},\omega).$$

Similar expressions relate **D** and **E** for dielectrics. For some problems one can work directly in the spatial transform domain (e.g., plane-wave scattering from planar structures), and in other cases it may be useful to form an integral equation for the response from a given excitation. In this work we show that it is possible (and in some cases more convenient) to form and solve an equivalent integrodifferential equation based on the drift diffusion model

$$\boldsymbol{J}(\boldsymbol{r},\omega) = \sigma(\omega).\boldsymbol{E}(\boldsymbol{r},\omega) - D(\omega)\nabla\rho(\boldsymbol{r},\omega)$$

rather than solve an integral equation based on non-locality of conductivity. We also present a similar form for metamaterials involving the flow of polarization. For typical spatially-dispersive conductivities and permittivities the drift diffusion model is equivalent to the convolution integral relationship, and can be used to express the nonlocal nature of the problem in many electromagnetic formulations (*IEEE Antennas and Propagation Magazine*, v. 52, pp. 198-207, Oct. 2010). This integrodifferential equation can be formed for the actual conduction current or for equivalent polarization current (e.g., using the volume equivalent principle). It is shown that this integrodifferential equation can be reduced to a differential equation with a simple analytical solution for one dimensional problems. As an example, a plasma layer sandwiched between two semi-infinite air layers is considered, and results are compared to a numerical solution of different formulations of the general transport equation (*2011 IEEE International Symposium on IEEE Antennas and Propagation*, pp. 1613-1616, 2011).

Rules for Adoption of Expansion and Integration Orders in Moment-Method Computation of Electromagnetic Scattering and Radiation

Nada J. Šekeljić*[(1)], Elene Chobanyan[(1)], Milan M. Ilić[(1),(2)], and Branislav M. Notaroš[(1)]
(1) Electrical & Computer Engineering Department, Colorado State University, Fort Collins, CO
(2) School of Electrical Engineering, University of Belgrade, Serbia
inadasek@engr.colostate.edu, sihaia@lamar.colostate.edu, milan.ilic@etf.rs,
notaros@colostate.edu

This paper presents results of our continued study of higher order parameters in computational electromagnetics (CEM), in which we investigate and evaluate the behavior of higher order hierarchical CEM numerical solutions to electromagnetic scattering and radiation problems by running an exhaustive series of simulations and systematically varying and studying the key higher order modeling parameters and their influence on the solutions. In particular, we focus here on the method of moments (MoM) to solve surface integral equations for arbitrary metallic and piecewise homogeneous dielectric structures and consider polynomial orders of basis functions (*N*) for expansions of surface electric and magnetic currents in the model and orders of Gauss-Legendre integration formulas – numbers of integration points (*NGL*) used for integrations of potential and field integrals in MoM generalized impedances (matrix elements).

In addition to simulations of several classes of *p*-, *h*-, and *hp*-refined canonical models of cubical and spherical metallic and dielectric scatterers, we present a very extensive numerical analysis and study of the NASA almond, which is an EMCC (Electromagnetic Code Consortium) benchmark target and one of the most popular benchmarking examples for both research and commercial CEM codes, in several frequency ranges. Also, we study higher order modeling parameters in antenna examples. In addition to models composed only from quadrilateral surface elements with isotropic expansion and integration orders and meshes that are refined isotropically in all directions, we present a discussion of situations when the parameters are changed anisotropically along the element edges. In addition to far-field computations, where the radar cross-section (RCS) error is evaluated, we investigate errors in calculations of the near field, current distribution, and antenna impedance. Based on the study, we present general guidelines and quantitative recipes for adoptions of optimal *N* and *NGL* and for various refinements – in a form of a table of parameters, which can readily be implemented in models and simulations. Possible variations of parameter values in far- vs. near-field and RCS vs. antenna-impedance computations are discussed.

The developed sets of rules for adopting the optimal *N* and *NGL* simulation parameters in a typical higher order MoM simulation should be of significant interest and value for MoM practitioners and application engineers using higher order MoM software, and may result in considerable reductions of the overall simulation (modeling plus computation) time. For instance, computations involving unreasonably high or low *N* and *NGL* orders could result in meaningless models and simulations (that often cannot be refined) and/or in an unnecessarily extensive utilization of computational resources (e.g., orders of magnitude longer computational times). The ultimate goal is to reduce the large gap between the rising academic interest in the higher order CEM and its actual usefulness and use in electromagnetics research and engineering applications.

Efficient Electromagnetic Analysis Using Electrically Large Curved *p*-Refined Hierarchical Anisotropic Inhomogeneous Finite Elements

Ana B. Manić*[(1)], Sanja B. Manić[(1)], Slobodan V. Savić[(2)], Milan M. Ilić[(1),(2)], and Branislav M. Notaroš[(1)]
(1) Electrical & Computer Engineering Department, Colorado State University, Fort Collins, CO
(2) School of Electrical Engineering, University of Belgrade, Serbia
anamanic@engr.colostate.edu, smanic@engr.colostate.edu, ssavic@etf.rs, milan.ilic@etf.rs, notaros@colostate.edu

The finite element method (FEM) in its various forms and implementations has been effectively used for solving both open-region (e.g., antenna/scattering) and closed-region (e.g., waveguide/cavity) electromagnetic problems. By its inherent features, the FEM is especially suitable for three-dimensional (3-D) frequency-domain modeling, analysis, and design of electromagnetic structures that contain geometrical and material complexities. Traditional FEM tools are low-order (small-domain or subdomain) techniques – the electromagnetic structure under consideration is modeled by volume geometrical elements that are electrically very small, on the order of $\lambda/10$ in each dimension, λ being the wavelength in the medium, and with planar sides, and the fields within the elements are approximated by low-order basis functions, which results in very large requirements in computational resources. An alternative is the higher order (large-domain or entire-domain) computational approach, which utilizes higher order basis functions defined on large (e.g., on the order of λ in each dimension) curvilinear geometrical elements. However, although higher order FEM modeling is becoming a mainstream activity in FEM research and practice, there seems to be a lack of investigations and reported results on the actual higher order and large-domain modeling of material complexities and a full exploitation of modeling and computational flexibility, versatility, and efficiency of large curved finite elements with *p*-refined high-order field approximations in applications involving arbitrary material anisotropy and inhomogeneity.

This paper presents accurate and efficient solutions in the frequency domain of 3-D open- and closed-region problems in the presence of general anisotropic inhomogeneous electromagnetic materials using higher order large-domain FEM modeling. The solutions implement Lagrange-type generalized curved parametric hexahedral finite elements of arbitrary geometrical-mapping orders for the approximation of geometry in conjunction with higher order curl-conforming hierarchical polynomial vector basis functions of arbitrary field-expansion orders for the approximation of fields within the elements. Elements are generally filled with anisotropic inhomogeneous materials with continuous spatial variations of complex relative permittivity and permeability tensors described by Lagrange interpolation polynomials of arbitrary material-representation orders.

Analysis of open-region scattering structures is performed truncating the FEM domain by a hybridization with a higher order method of moments. Analysis of closed-region microwave waveguide structures introduces a simple single-mode boundary condition across waveguide ports. Examples to be presented demonstrate efficient and accurate simulations of anisotropic continuously inhomogeneous scattering and waveguide structures using large (extending 2λ in each dimension) anisotropic inhomogeneous curved finite elements with *p*-refined field distributions of high (e.g., seventh) approximation orders.

Time-Domain Response of 3-D Waveguide and Scattering Structures Calculated by Higher Order Frequency-Domain FEM Technique and DFT

Sanja B. Manić*[(1)], Slobodan V. Savić[(2)], Milan M. Ilić[(1),(2)], and Branislav M. Notaroš[(1)]
(1) Electrical & Computer Engineering Department, Colorado State University, Fort Collins, CO
(2) School of Electrical Engineering, University of Belgrade, Serbia
smanic@engr.colostate.edu, ssavic@etf.rs, milan.ilic@etf.rs, notaros@colostate.edu

The finite element method (FEM) is one of the most powerful and versatile general numerical tools for full-wave computations based on discretizing partial differential equations in electromagnetics. It has been especially effectively used in simulations of three-dimensional (3-D) closed- and open-region electromagnetic structures in the frequency domain. However, time-domain analysis and characterization of such structures and evaluation of associated transient electromagnetic phenomena are also of great practical importance for a number of well-established and emerging areas of applied electromagnetics, including wideband communication, electromagnetic compatibility, packaging, signal integrity, material characterization, and other applications. For this purpose, time-domain FEM techniques have recently been developed that allow electromagnetic phenomena to be modeled directly in the time domain. When compared to frequency-domain FEM solutions, time-domain FEM formulations enable effective modeling of time-varying and nonlinear problems and fast broadband simulations, at the expense of the additional discretization, in the time domain, and the associated numerical complexities, and programming and implementation difficulties.

An alternative approach, an indirect time-domain analysis, that is, finding the transient response of an electromagnetic structure based on the frequency-domain FEM analysis coupled to the discrete Fourier transform (DFT) and its inverse (IDFT), has not been widely exploited. This is most likely because such an analysis would require FEM solutions with many unknowns at many discrete frequency points, which may be computationally prohibitively costly. However, with a highly efficient and appropriately designed frequency-domain FEM technique, it is possible to obtain very fast and accurate time-domain solutions performing computations in the frequency domain along with the DFT/IDFT (E. M. Klopf, S. B. Manic, M. M. Ilic, and B. M. Notaros, "Efficient Time-Domain Analysis of Waveguide Discontinuities Using Higher Order FEM in Frequency Domain," Progress In Electromagnetics Research, Vol. 120, 2011, pp. 215-234). Our solutions are based on a higher order large-domain 3-D FEM implementing Lagrange-type generalized curved parametric hexahedral finite elements, filled with anisotropic inhomogeneous materials with continuous spatial variations of complex relative permittivity and permeability tensors, and curl-conforming hierarchical polynomial vector basis functions for the approximation of the electric field intensity vector within the elements, in conjunction with standard DFT and IDFT algorithms. In this paper, we extend the time-from-frequency-domain FEM approach to additional examples of closed-region microwave waveguide structures, with a simple single-mode boundary condition introduced across the waveguide ports and a large buffer finite element at each port to ensure relaxation of higher modes. We also analyze open-region scattering structures, with a truncation of the FEM domain by a hybridization with a higher order method of moments. Numerical examples demonstrate excellent numerical properties of the time-from-frequency-domain FEM solver based on a small total number of unknowns in higher order solutions, modeling flexibility using large curved inhomogeneous finite elements, and fast FEM solutions at multiple frequencies needed for the IDFT.

Multiphysics Modeling of Opto-Electronic Nano-Structures Towards Optimization of different Solar Cells

Ahmadreza Ghahremani*, Aly E Fathy
EECS Department, University of Tennessee, Knoxville, TN 37996, USA,
aghahrem@utk.edu

Development of CAD tools for optical devices is under way to include multi-physics tools. Previously, tools like "RCWA" were used for the diffraction mode of periodic structure analysis, while FDTD was typically used as a general numerical method for analyzing field propagation in the time domain to investigate transmission, reflection, and absorption of electromagnetic energy for devices like optical ring resonators. Meanwhile, for sources it is essential to analyze the semiconductor physics, generation and recombination of electron/hole pairs and the photons generation efficiency linking current to light like in lasers, LEDs, photodiodes, and solar cells.

Today, emerging multi-physics CAD tools can combine various required analysis. Multiphysics tool is the best option to extract different optoelectronic results like total light absorption or transmission, electric field intensity, J-V curves and quantum efficiency in one platform. It can provide EM analysis, electrostatic, and carrier transport analysis. It can describe the physics behind the operation of optoelectronic devices. Such multi-physics tools include RSOFT and COMSOL. For example, COMSOL has different modules for electromagnetic analysis, chemical analysis, and thermal analysis as well that can be used in a static or a dynamic mode.

In this paper, we simulate different kinds of solar cells by using an optoelectronic simulator (RSOFT) and compare their characteristics. Such analysis can has been used to optimize the optical and electrical efficiency related to solar cells such as increasing effective path length, using nano structures as a grating or DBR reflectors, analyzing thin film surface Plasmon and the effect of nano particles. An example of a very thin solar cells made by organic materials will be given including methods to improve their quantum and electrical efficiency.

[1]. A Yakimov, et al, *Appl. Phys. Letters, 80 1667-1669 (2002)*
[2]. N. N. Feng, et all. "Design of highly efficient light-trapping structure for thin-film crystalline silicon solar cells," *IEEE Trans. on Electron Devices, 54 1926 (2007)*
[3]. B. Rand, et al*, J. Appl. Phys. 96 7519 (2004)*

A PASSIVE BISTATIC RADAR FOR DETECTION OF AIRCRAFT USING NON-COOPERATING SPACEBORNE TRANSMITTERS

William C. Barott* [(1)] and Brian Butka [(1)]
(1) Embry-Riddle Aeronautical University, Daytona Beach, FL 32114
Electrical, Computer, Software, and Systems Engineering Department

This talk reports on the construction of a demonstration platform for a passive ground-based primary radar station for monitoring aircraft. This system uses existing satellite transmitters as illuminators for the radar system, and a receive-only ground station. Existing passive radars use ground-based illuminators, and while many satellites are too-weak, several transmitters of suitable strength exist, including digital audio broadcast satellites. Success using satellites as illuminators is enabled by extensive signal processing and using integration times that are longer than current systems. Some of these algorithms are similar to those used in radio astronomy for weak signal detection.

We report specifically on observations utilizing the 2.3 GHz downlink from the geostationary XM-Radio as the radar illuminator for the S-band Array for Bistatic Electromagnetic Ranging Technology Demonstrator Array (SABER-TDA). This system is located at Embry-Riddle Aeronautical University, near the Daytona International Airport. Data taken with the SABER-TDA has shown echoes of aircraft proximate to the site, and supports expectations that the next phase of work will provide accurate position and velocity measurements of aircraft or small unmanned aircraft at ranges of tens to hundreds of nautical miles from the ground station.

Passive bistatic radar stations offer light-weight, low-cost, portable, and field-deployable options to supplement deficiencies in the National Airspace System (NAS) and homeland security surveillance networks. Potential applications include providing coverage in remote mountainous regions, low-altitude en-route primary radar coverage throughout the continental United States, and low-altitude interdiction efforts in coastal areas. As a field-deployable system, this could also be used to quickly restore primary radar coverage in the event that a disaster or terrorist event disables existing primary radars. Additionally, the portable and non-emitting nature of the radar permits use in a wide range of applications where emitting radars are unacceptable.

Time-Reversal based Change Detection Algorithm for Ground Penetrating Radar Applications

M. E. Yavuz[1], A. E. Fouda*[2], and F. L. Teixeira[2]

[1] Intel Corporation, Hillsboro, OR, 97124, yavuz.5@osu.edu
[2] ElectroScience Lab., Dept. of Electrical and Computer Engineering, The Ohio State University, Columbus, OH, 43212, fouda.1@osu.edu, teixeira@ece.osu.edu

Ground-penetrating radar (GPR) is a well-established geophysical remote sensing method utilized to obtain information about the subsurface. It has been widely employed in applications such as detection of buried objects (e.g. land mines, unexploded ordnances or utilities), shallow geophysical exploration, civil engineering and archeology. The success of GPR largely depends on the information that can be extracted from the collected GPR data. In many subsurface detection scenarios, the clutter may dominate the data and results in a degradation in the GPR performance. For example, in the case of shallow buried mines, the response recorded by the GPR mainly comes from the (rough) ground surface. Also, depending on the frequency of operation, temporal responses of the surface and the shallow mines can overlap each other thereby eliminating the option of time-gating for improved GPR responses. Additionally, in the case of plastic mines and lossy subsurface, the scattered energy from the targets might be very low. Such challenges are among the limiting factors for the improved performance of GPR surveys.

In this study, we present a time-reversal (TR) based algorithm for improved detection of shallow land mines. TR has been first introduced in acoustics and since then it has proved to be effective in positively exploiting the multiple scattering in the medium to achieve super-resolution focusing. Here, we apply the space-frequency TR imaging algorithm [M. E. Yavuz and F. L. Teixeira, *IEEE Trans. Geosci. Remote Sensing*, vol. 46, pp. 1115-1124, 2008] to the appropriately selected sets of radargrams obtained during a given GPR survey. A radargram is obtained by the collection of individual A-scans each of which corresponds to the recorded GPR response at a single location. Basically, when the GPR is away from the target of interest, the radargram carries the (rough) surface information and when the GPR is in the vicinity of the target of interest, its scattering information affects the radargram. When the space-frequency TR imaging algorithm is applied to the different sections of the radargrams, the singular values and corresponding vectors might possess information that can allow the detection of change in the subsurface. Test cases will include both homogeneous and rough surfaces as well as different GPR transmitter/receiver configurations. The basic setup for GPR setup will include a single transmitter and a receiver in a common-offset configuration. A further advanced setup will include a single transmitter but with dual receivers to obtain the differential response of the subsurface and then apply the TR based algorithms to the differential responses.

Integration of Si/SiGe Transmitter Towards Sub-Millimeter Accuracy for UWB System

Essam Elkhouly[(1)], Dayang Lin[(3)], Quanhua Liu[(1)], M. Mahfouz[(2)] , Aly Fathy[(1)], H. Schumacher[(3)]
(1) EECS Department, University of Tennessee, Knoxville, TN 37996, USA, elkhouly@utk.edu
(2) MABE Department, University of Tennessee, Knoxville, TN 37996, USA
(3) Institut für Elektronische Bauelemente und Schaltungen, Ulm University, 89069 Ulm, Germany

Indoor precise localization is an advantageous tool for many applications i.e. surgical navigation, wireless heart monitoring, tumor detection, and sensitive nuclear material inventory tracking. A number of competing technologies such as RFID, FMCW, and UWB. FMCW indoor operations suffer from multipath interference which can be easily overcome by the tiny temporal width of the UWB pulse.

At the University of Tennessee, we built a system that achieves a 3D dynamic accuracy of 5-6 mm. The developed system is comprised of a 300ps smooth pulse generator with a 3 GHz bandwidth, and a sub-sampler of a 100 GSPS equivalent true time sampling rate. The narrow signal detection is based on a leading edge algorithm implemented using FPGA board. Results were verified using an opto-tracker as explained in detail in (C. Zhang, M. Kuhn, B. Merkl, A. Fathy, M. Mahfouz, “Real-time non-coherent UWB positioning radar with millimeter range accuracy: theory and experiment,” in IEEE Trans. Microwave Theory Tech., 58(1), 2010, pp. 9-20).

The developed transmitter consists of a Step Recovery Diode arranged to produce a 300 ps pulse that is modulated by an 8 GHz carrier. Such system has some drawbacks i.e. high power consumption, complexity, limited pulse repetition rate and comprising of numerous stages. However, The SRD pulse generation is a random process and the whole system requires a separate Mixer and Oscillator which adds more to the jitter. Recently, the SRD pulse generator was replaced by a transmitter developed at Ulm University (D. Lin, A. Trasser and H. Schumacher, " Si/SiGe HBT differential impulse generator for high-speed UWB applications", in ELECTRONICS LETTERS,Vol. 46, No. 24). The new pulse generator is based on Schmitt trigger and the oscillation starts upon imbalance not noise and produces up-converted pulse that complies with FCC UWB mask regulations. The Si/SiGe HBT chip is a differential impulse generator with a pulse repetition rate of up to 1 GHz.

The newly integrated transmitter has been used and demonstrated a great power save and small driving signal requirement with sinusoidal input which makes the tag integration easier. The less random noise and pulse variation make the system more stable and significantly speed up computation convergence.

A Sub-wavelength RF Source Tracking Device for GPS-denied Environments

Fikadu T Dagefu* and Kamal Sarabandi
Department of Electrical Engineering and Computer Science, The University of Michigan, Ann Arbor, MI. 48109-2122

The ability to accurately detect the direction of arrival and track the location of a source in complex and GPS-denied environments is useful for a wide variety of applications such as fire and earthquake rescue missions, user position estimation in mobile communications and for security systems. Another application of interest pertains to real time positioning and tracking of robotic platforms that are used to enhance tactical situational awareness in complex environments including urban and indoor scenarios. A specific example of this is assisting the aforementioned platform in high-resolution navigation in these cluttered environments. For a narrowband signal being transmitted by the antenna mounted on a robotic platform, the signal at the receiver located somewhere within or outside the environment of interest consists of the direct and scattered components from the objects within the environment. The path lengths of multiply scattered fields can be quite different from other field components (direct). High level of multipath makes the task of tracking the source very challenging. The tradeoff is between the size of the antenna and the level of multipath. To minimize these effects, the use of miniaturized antennas operating in the HF range is proposed.

In this work, a Sub-wavelength source tracking system utilizing highly miniaturized antennas in the HF range for applications in GPS-denied environments such as indoor and urban scenarios is proposed. In order to track a source in such environments, a radio triangulation approach that combines directional finding and interferometry approaches is pursued. A low-profile and highly miniaturized antenna (with $\lambda/300$ height and $\lambda/100$ lateral dimensions) designed to efficiently generate omnidirectional and vertically polarized field is presented. At such low frequencies the phase difference between the signals at the Rx antennas (an important quantity of interest), is too small to be accurately measured. To address this issue, a biomimetic circuit that mimics the hearing mechanism of a fly (Ormia Ochracea) is designed and fabricated. With this circuit, very small phase differences are amplified to measurable values. Numerical models based on Geometrical Optics and full-wave solvers are used to investigate the proposed HF source tracking approach. The design and fabrication of various components along with the integration of system prototype and test results in various environments (with different levels of multipath) is described.

Parametric and Experimental Study on the Statistical Stability of Ultrawideband Time-Reversal Imaging in Random Media

A. E. Fouda*, V. Lopez-Castellanos, and F. L. Teixeira
ElectroScience Lab., Dept. of Electrical and Computer Engineering,
The Ohio State University, Columbus, OH 43212.

Time-reversal (TR) was introduced as a technique for (re)focusing waves in rich scattering environments [M. Fink, *J. Phys. D.*, vol. 26, pp. 1333-1350, 1993]. It is based on the invariance of the wave equation under time-reversal (assuming lossless, reciprocal media). Time-reversed waves can be backpropagated in the original physical medium (physical TR) or in a synthetic imaging medium (synthetic TR, or TR imaging). The former approach is used to focus waves on the source/scatterer location and finds applications in medical therapy, and in acoustic and/or wireless communications equalization and covertness. Synthetic TR, on the other hand, is typically used for imaging and characterization of targets.

Ultrawideband (UWB) TR exhibits the distinctive property of *statistical stability* [G. Papanicolaou, L. Ryzhik, and K. Solna, *SIAM J. Appl. Math.*, vol. 64, pp. 1133-1155, 2004]. This feature is of particular importance for imaging targets in media whose properties are not known deterministically (random media). In this case, sufficiently spaced frequency components constituting the image are "incoherent" in the sense of having decorrelated amplitude and phase among them. Under UWB operation, this frequency decorrelation leads to "self-averaging", and therefore "stable" images, i.e. that depend only on the statistical properties of the random medium and not on the particular realization.

In this work, we carry out a study on the statistical stability of UWB TR for imaging in random media under different combinations of random medium parameters and interrogating signal properties. We examine conditions under which frequency decorrelation in random media provides more effective self-averaging and therefore better statistical stability. We present simulation results for imaging of sources embedded in continuous random media using both limited-aspect (linear) and full-aspect (circular) sensor arrays. This study is also extended to the case of imaging sources under rough surfaces using linear sensor arrays. Finally, we present an experimental demonstration of the statistical stability of UWB TR imaging in random media composed of randomly deployed discrete dielectric scatterers. We conduct our measurements using a recently developed UWB time-domain radar that provides a useful bandwidth of 40 GHz. We study the effect of scatterers permittivity and fractional volume on the degree of frequency decorrelation.

Comparison of Multistatic Radar Ambiguity Functions

Tegan Webster,[1] Jerry Kim,[1] Ivan Bradaric,[2] and Margaret Cheney[3]
[1] Radar Division, Naval Research Laboratory, Washington, DC 20375, USA
[2] Capraro Technologies, Utica, NY 13501, USA
[3] Department of Mathematical Sciences, Rensselaer Polytechnic Institute, Troy, NY 12180, USA

The classical ambiguity function (CAF) has been widely used as a means to assess the performance of monostatic radar systems. In past years numerous approaches for extending the CAF to the multistatic case have been presented. Whereas the CAF is primarily determined by the choice of waveform, the multistatic ambiguity function (MAF) incorporates various aspects of the multistatic radar problem, including not only the choice of waveform for each transmitter, but also the geometry of the transmitters and receivers as well. In this paper two closely related but different MAFs are presented, one deterministically derived and the other statistically derived. Analytic expressions for the two MAFs are shown for the case of one transmitter and multiple receivers and for the case of multiple transmitters and receivers. A single target is assumed to be located within the scene of interest and this target may have zero or nonzero velocity.

The deterministically derived model incorporates the single-scattering assumption for the scattered field and applies to point-like, slowly moving targets that are small in comparison to the wavelength of the incident field. The resulting MAF is obtained by weighting the data at each antenna and adding the data coherently.

The statistically derived model, on the other hand, applies to a Swerling II target; the resulting received signal, after processing, is Rayleigh-distributed with zero-mean, Gaussian, equal-variance, real and imaginary components. The statistically derived model further includes the assumption that the noise component is Rayleigh-distributed with white, zero-mean, Gaussian, equal-variance, real and imaginary components with a constant power spectral density. The data at each antenna is noncoherently summed, with Neyman-Pearson-inspired weights, to produce the MAF.

The paper only presents numerical simulations of the two MAFs for a single transmitter and multiple receivers arranged in several geometries. Despite differences in the underlying assumptions of the two MAFs discussed here, the models are found to yield comparable simulation results.

Time-Reversal Techniques for MISO and MIMO Wireless Communication Systems

A. E. Fouda* and F. L. Teixeira
ElectroScience Lab., Dept. of Electrical and Computer Engineering,
The Ohio State University, Columbus, OH 43212.

We consider the application of different time-reversal (TR) signal processing and beamforming techniques to multiple-input single-output (MISO) and multiple-input multiple-output (MIMO) communication systems. Conventional TR beamforming provides spatial focusing at the intended receiver; however it does not yield perfect channel equalization. Time-reversed pilot can be normalized to provide perfect equalization on the expense of power level. This equalization is particularly important for high data rates; where the bit error rate performance is dominated by internal noise due to intersymbol interference. To increase physical layer covertness, TR beamforming is combined with multiple-signal-classification (MUSIC) technique to produce null fields at eavesdroppers. This technique is also applied to MIMO setups to eliminate interuser interference and hence increase the system capacity. Differential TR is used to obtain and update pilot signals for passive moving receivers, i.e. those that cannot (or do not) transmit pilot signals. The time-reversed differential backscattering obtained from radar acquisitions achieves satisfactory spatial and temporal focusing at the moving receiver.

USE OF EVOLUTIONARY ALGORITHMS FOR MULTIUSER MIMO-OFDM SYSTEMS

Mina Labib*[(1)], Amir I. Zaghloul[(1,2)]
[(1)] Bradley Department of Electrical and Computer Engineering
Virginia Tech, VA 24061
E-mail: mlabib@vt.edu
[(2)] US Army Research Laboratory, Adelphi, MD 20783

Deployment of MIMO systems is one of the most promising techniques that were proposed to improve the performance of the wireless channel and increase the capacity. Using MIMO Systems combined with OFDM technique is a popular method that can be used to deliver the fast growing demand for high data rate in wireless communication systems.

Multiuser MIMO was proposed to support multiple users within the same cell using the same frequency-time resource by exploiting the multi-user diversity in the spatial domain. So MU-MIMO provides a significant gain over the single user MIMO in terms of capacity and spectral efficiency. However, the associated detection techniques for MU-MIMO are more complicated and more computationally intensive compared to the detection techniques for SU-MIMO. The major problem in most of the multiuser detection algorithms currently in the open literature is the performance in the rank-deficient scenario, when the number of users exceeds the number of antenna elements at the base station.

On the other hand, the Evolutionary Algorithms are stochastic search techniques that imitate the metaphor of natural biological evolution. Recently, several types of Evolutionary algorithms, such as the Genetic Algorithm (GA) and the Particle Swarm Optimization (PSO) algorithm, have been proposed to be used for MIMO systems.

In this paper, we investigate using different techniques of the Evolutionary Algorithms, such as GA and PSO in the multiuser detection for MU-MIMO and compare their performance with the computationally simple Minimum Mean Square Error (MMSE) Multiuser Detector, as well as the computationally intensive Maximum Likelihood (ML) Multiuser Detector.

Reconfigurable Antennas, Preemptive Switching and Virtual Channel Management

Jean-Francois Chamberland, Gregory H. Huff, and Srinivas Shakkottai
Texas A&M University, ECE Dept., TX 77843-3128, USA

Emerging wireless communication systems must be designed to accommodate the various applications that compose an evolving digital landscape. Throughput and delay are two prime determinants of service quality and their relative importance varies depending on current activities. Advances in reconfigurable antennas collectively offer a valuable means to enhance the statistical profile of fading channels and, thereby, improve perceived link conditions. High-performance reconfigurable antenna technologies are especially beneficial in the context of delay-sensitive communication, where correlation over time can lead to severe degradation. Antennas designed to intentionally and reversibly alter the character of their performance-governing electromagnetic fields can be used to create multiple virtual channels between a source and its destination. By changing the directional and polarization properties of radiation patterns, a reconfiguration event can alter the gain of a fading channel. However, the transition process consumes resources in terms of time and energy. It is therefore important to derive a sound methodology to efficiently tradeoff cost and potential rewards. This project introduces a mathematical framework to model the concurrent evolution of multiple virtual channels. Based on Markov chains, the proposed framework is rich enough to account for dependencies over time and across virtual channels. The theory of Markov decision processes is subsequently applied to assess the potential benefits of reconfigurable systems, compared to current static implementations. Estimation techniques are outlined as a means of acquiring channel state information, which ultimately dictates when to trigger a reconfiguration event. Application to Wi-Fi access points and mobile devices are discussed using a testbed on the Android platform.

CRYSTALLOGRAPHIC-BASED ANTENNA CONFIGURATIONS FOR DIRECTION-OF-ARRIVAL ESTIMATION

[1,2]Zhenchun Xia, [1]Gregory H. Huff, [1]Jean-Francois Chamberland,
[1]Henry Pfister, and [2]Raktim Bhattacharya
[1]Department of Electrical and Computer Engineering
[2]Department of Aerospace Engineering
Texas A&M University, College Station, TX 77843-3128 USA

A wide variety of direction-of-arrival (DOA) techniques can be implemented for the detection of incident electromagnetic waves. These can be split into two overarching categories based on the antenna system and signal processing techniques. The first of these encompass antenna-centric methods such as the classical sum-difference beamforming methods which use phased arrays and/or separate transmit and receive arrays. The second and more signal-processing intensive methods are often subspace-based to exploit the eigenvalue nature of the incoming signals, of which the multiple signal classification (MUSIC) algorithm remains quite popular and very robust. The latter of these can encompass a wide variety of implementations that range from compact vector-based sampling at a point in space up to the use of spatially large arrays to gather the sensor information. In all, the antenna parameters and spatial configuration or orientation of antenna elements plays a large role in the performance of the system.

This study examines the impact of volumetric antenna configurations based on the topological arrangement elements in crystallographic lattice configurations (crystal systems). The MUSIC algorithm will be used to examine several performance metrics related these configurations, which will also include several aperiodic and dual-band configurations of antenna elements to evaluate crystal systems based on binary compounds. These will be compared to planar and other common periodic element configurations to evaluate aliasing, accuracy, and sampling rates in clean and noisy environments. The number of elements and their spacing will also be used to characterize the accuracy and overall system complexity resulting from the use of these volumetric element configurations.

Improving Efficiency of a Linear Amplifier by Injection of Second Harmonic Power at the Output

Asmita Dani*, Michael Roberg, and Zoya Popovic
Department of Electrical, Computer and Energy Engineering
University of Colorado, Boulder, USA

High efficiency RF power amplifiers are usually highly compressed and driven, leading to nonlinear behavior. In harmonically-terminated classes of operation, e.g. classes F and F^{-1}, the nonlinearity of the input capacitance produces harmonic content at the output of the device which is then shaped to obtain high efficiency. An alternative method to harmonic shaping of the voltage and current waveforms at the output of the transistor is to inject harmonic content with appropriate amplitude and relative phase. This can be done while operating the PA in a more linear regime, such as class A/AB.

Here we present experimental and theoretical results for a 2^{nd} harmonic injected PA at 2.45 GHz obtained with a Cree GaN 6-W packaged HEMT (CGH40006P). A 0.5-6GHz class-AB PA with this device gives less than 60% drain efficiency. The demonstrated improvement in efficiency for the harmonically-injected PA is above 75%, including the power of the 2^{nd} harmonic. The efficiency can be traded for output power, and a drain efficiency as high as 82% is obtained at reduced power. The injection is accomplished with a low-loss three-port network designed to have high isolation for the fundamental at the injection port and the harmonic at the through port. The power at the second harmonic that needs to be injected for optimal efficiency improvement is found to be very sensitive to the relative phase. For overall high efficiency, the efficiency of the injection circuit is also important (A. AlMuhaisen *et al*., IEEE MTT-S, 664-667, 2010). In the demonstrated PA, the efficiency of the harmonic injecting circuit was around 55%. The $P_{out}(P_{in})$ saturation curve for the harmonically-injected PA shows a higher compression point than the class-AB PA alone, indicating increased linearity at higher power levels.

Channel-Based Wireless Encryption Using Reconfigurable Antennas

D. L. Rolando, Hung D. Ly, Tie Liu, G. H. Huff, J. P. Erskine, J. B. Yang, and J. A. Joachim
Department of Electrical and Computer Engineering
Texas A&M University, College Station, TX 77843-3128 USA

Encrypted wireless communication has a multitude of different applications, ranging from private communication using cell phones to business transactions and military intelligence. There are two general types of encryption systems possible: public key and private key. In a public key system, anyone can have the encryption key, but only the designated recipient has the decryption key. This scheme makes public key systems inherently more secure (since the key can be safeguarded by the recipient), but they are typically computationally expensive. In private key systems, both the encryption and decryption keys are kept exclusively among the users. However, since the keys must be transferred between users, security with a private key is always an issue.

This work introduces a new secure encryption technique for private key systems. Instead of having a fixed preexisting key, this technique uses a non-fixed key that is continuously generated at regular intervals using the ever-changing characteristics of a wireless channel. Specifically, a key is generated using the complex signal phase and magnitude seen by the receiver. The signal phase will be unique for different channels, and the channel itself will be constantly changing (in real-world scenarios), making eavesdropping exceptionally difficult and the key virtually impossible to crack. As an extra layer of security, the proposed system also employs polarization-reconfigurable antennas for both the transmitter and receiver. Each reconfiguration state of the system will have its own unique phase signature, allowing the generated key to be changed even if the channel and spatial orientations of the transmitter and receiver remain the same. The proposed technique was demonstrated experimentally using two polarization-reconfigurable cross dipole antennas operating in the 2.4 GHz ISM band. Phase measurements were taken using a network analyzer and used to generate simple private keys. The antenna design, key generation algorithm, and experimental setup and procedure will be presented, and considerations for implementation in real world environments will be discussed.

Device and System Challenges for Video-Rate THz Radar Imaging

Ken B. Cooper
Jet Propulsion Laboratory, California Institute of Technology, Pasadena, CA 91109

The technique of THz radar imaging has been developed by the Jet Propulsion Laboratory (JPL) as a means of remotely screening people for concealed objects such as weapons, bombs, or illicit substances. JPL's radar operates near 670 GHz, where atmospheric absorption is negligible over the relevant standoff distances, and where cm-scale resolution at 25 m range is possible with an aperture diameter of 1 m. Beam penetration through clothing is also good at this frequency. To overcome the image speckle and clutter interference that can plague both active and passive submillimeter-wave imagers, the JPL radar operates in an ultra-wideband radar mode to discriminate between layers of clothing, concealed objects, and human skin with cm-scale resolution. By scanning a THz beam over a target, the accumulated time-of-flight (i.e. range) measurements can be used to reconstruct three-dimensional target profiles and reveal concealed objects of arbitrary material, incidence angle, and temperature with excellent resolution.

However, for real-life applications where persons subject to scanning are in motion or where large fields of view are desirable, an order-of-magnitude improvement in the currently achievable ~1 Hz imaging speed is needed to attain the necessary near-video frame rates. Some major engineering challenges for reaching this goal include accelerating the RF waveform generation, opto-mechanical beam scanning, and signal processing chain. But the hurdle with the biggest payoff is likely to be the development of a THz transceiver focal plane array, which can reduce the imaging time in proportion to the number of radar beams simultaneously scanned over a target. This talk will describe our efforts to attain video-rate THz radar imaging, with an emphasis on the development of a THz transceiver array. With a design that integrates F-band power amplifier MMICS, GaAs Schottky diode multiplier and mixer devices, and high-isolation waveguide duplexers into a monolithic stack of micromachined silicon wafers, we envision the development of a module with the potential for wide use in science and engineering beyond personnel screening applications.

DEVELOPMENT OF A CALIBRATED FREQUENCY-DOMAIN SCATTEROMETER IN THE mmWave TO SUB-TERAHERTZ RANGE

David Novotny, Joshua Gordon, Edwin Heilweil, Shu-Zee A. Lo,
Erich Grossman, Brian Stillwell, Jeff Guerrieri

National Institute of Standards and Technology
Physical Measurement Laboratory
325 Broadway
Boulder, CO 80305
http://www.nist.gov/pml/electromagnetics/rf_fields/antenna.cfm

NIST has developed a broadband, 200-500 GHz, scatterometer system to accurately characterize the scattering of materials and small objects. The output from the system is dense spectrum, bidirectional reflectance distribution function (BDRF) data that can be propagated into detection models and used to develop standard materials to compare performance of various detection and imaging systems. The scatterometer is built upon a commercial frequency-domain network analyzer with stabilization techniques used to minimize drift due to movement and temperature changes. The high degree of stabilization leads to minimally movement-independent calibrations that allow for high-resolution, time-domain transforms that provide the ability to suppress spurious signals. Reflectance from a variety of standard targets and sample materials highlight stability, repeatability, and dynamic range of the system. Analysis is being performed to extend the frequency range of the system from 110 to 750 GHz.

Another NIST project team has developed a time-domain THz pulsed system capable of performing BRDF scattering measurements with a fast rise-time, pulse width spectrum from approximately 100 GHz to 2 THz. Correlations between these systems on a variety of simple targets will be shown. The dual, independent methods for determining BRDF of standard samples highlights the confidence of the data.

The overarching goal of the project is to develop standard metrics for BRDF measurements and high-confidence baseline input for higher order modeling that can be used to more accurately determine detection thresholds. The consistent analysis of conical slab targets, simple gratings and more complex targets show the usefulness of the system beyond a general research tool and more of a metrology grade instrument.

Modulated Multimode Mixing Illumination for the Elimination of Speckle and Target Orientation Requirements in Active Imaging

Mark A. Patrick[(1)], Colin D. Joye[(2)], and Frank C. De Lucia* [(1)]
(1) Physics Department, Ohio State University, Columbus, OH 43210, USA
(2) U.S. Naval Research Laboratory, Washington DC, 20375

We have previously proposed that the speckle and other deleterious interference phenomena associated with active imaging could be overcome by modulated multimode mixing illumination. The motivation for this is the desire to make images comparable to those of passive images (e. g. no speckle and no requirements for specular reflections from strategically oriented targets), but with orders of magnitude greater sensitivity. In principle, this could be accomplished by modulating the intensity of the many modes in the 'blackbody' on a time scale short in comparison to the pixel dwell time so that the speckle pattern from a particular combination of modes would be random relative to the other mode combinations, thus allowing the speckle to be averaged away.

A key enabler of the strategy is the fact that small amounts of power in a single microwave mode are very 'hot' (1 mW in a 1 MHz bandwidth corresponds to 10^{14} K). As a result, even in large volumes (e. g. arenas or 'urban canyons') it is possible to fill the many modes associated with this volume with radiation that corresponds to a relatively high temperature.

We made a preliminary demonstration at 640 GHz based on a simple object (a toy gun) in a controlled small enclosure (a 4 ft x 4 ft x 8 ft aluminum foil box). By use of a 5 W 220 GHz EIK klystron amplifier, we have now been able to demonstrate modulated multimode mixing illumination in the large enclosed volume (150 ft long by 70 ft high) of the atrium of the OSU Physics Building.

We will present results that show:

1. Even with a simple illumination scheme and mode modulator, the speckle reduction is very high.
2. The images still show some specular reflections as particularly hot spots. This is not dissimilar to pictures taken outside in bright sun light for which there are glints that come from specular reflections from the sun. Complete mode mixing would correspond to the optical case of a cloudy day.
3. In general there will be more specular reflections at 220 GHz than in the optical because the world is more specular at long wavelength.
4. The ¼" cables that suspend light reflectors in the atrium of the OSU Physics Department are more visible in the mm image than in an optical image.

Even with our simple initial illumination strategy the images are far from system noise limited and it should be possible to extend this approach to substantially longer ranges. We will discuss the illumination and modulation strategies that will play an important role in this extension as well as in the extension of this approach to other scenarios.

APPLICATION OF PHOTONIC PROCESSING TO INTERFEROMETRIC PASSIVE MILLIMETER-WAVE IMAGING

Christopher A. Schuetz[*1], Richard D. Martin[1], Thomas E. Dillon[1],*
Julien Macario[2], Peng Yao[2], Dennis W. Prather[2]

[1]*Phase Sensitive Innovations, Inc., Newark, DE*
[2]*Electrical and Computer Engineering, University of Delaware, Newark, DE*

Abstract

Passive millimeter-wave and terahertz imagers have numerous potential applications from security screening to flight aids in atmospheric obscurants. However, practical limitations in the sensitivity and resolution achievable by such imagers have largely prevented their widespread usage. At terrestrial temperatures, sensitivity on the order of picowatts is required to generate meaningful passive imagery. At these relatively long wavelengths, large apertures are required to generate images with sufficient resolution for most applications, which precludes traditional focal plane array technologies for many applications. To overcome these limitations, an interferometric imager based on photonic upconversion and processing is presented. In this sensor configuration, the millimeter-wave signal received by a distributed antenna array is converted at each element into sidebands on an optical carrier, routed to a central processor using optical fiber, and reimaged after filtering in the optical domain. In this manner, a real-time passive millimeter-wave image is generated directly on an optical camera, without the need for complex correlation algorithms to analyze data from the distributed antenna array. Herein, we present a functional prototype of this imaging system working at 35 GHz as well as progress towards a functional 77 GHz array optimized for use as a helicopter landing aid in degraded visual environments. A key aspect of the ability to move to higher functional frequencies has been the ability to fabricate faster optical modulators, which serve to convert the received millimeter-wave signal into the optical domain. To this end, we will present development efforts for these modulators, which have extended the usable frequencies of lithium-niobate travelling-wave modulators to beyond 200 GHz and the implications that such modulators will have on future array designs.

Terahertz Characterization of Biological Tissues

Woon-Gi Yeo, Niru K. Nahar, Robert Lee, John L. Volakis, and Charles L. Hitchcock
ElectroScience Laboratory, Electrical and Computer Engineering Dept.
The Ohio State University, 1330 Kinnear Rd., Columbus, OH 43212

Sensing in the terahertz spectrum provides an alternative modality to traditional approaches in the microwave and optical regimes for a wide range of applications from material characterization to medical imaging. This modality offers many advantages such as large available bandwidth, unique spectroscopic data of materials, and it is non-ionizing. In particular, terahertz spectroscopic data based on the inter-molecular vibration can be utilized for chemical recognition and differentiation of cancerous tissue. Here, we present preliminary experimental data for material characterization of biological tissues using terahertz pulsed imaging system (TPI) and terahertz pulsed spectrometer (TPS), both manufactured by Teraview.

As an initial study, several measurements were conducted to show high resolution images and to characterize material properties of biological items. The examples to be presented include: (a) fresh green tree leaves, (b) formalin treated human lung tissues with metastatic disease, (c) wild and farm raised salmon tissues. The terahertz image of a fresh leaf shows a detailed map of water distribution, and the image of human lung tissue shows good contrast between cancerous and non-cancerous area. In addition, raw data of tissues were processed with reference and baseline measurements to allow for the extraction of effective refractive indices and absorption coefficients of organic surfaces/layers. In all cases, it is demonstrated that discriminatory information can be obtained from terahertz spectroscopic data for detection of small surface or tissue details. Thus, terahertz can be used for fine resolution images and characterization of biological tissues to identify small changes in tissue or fluid content within the imaged surface/layer.

in vivo THz Medical Imaging

Zachary Taylor*[1], Jun Sung[1], Rahul Singh[1], Martin Culjat[1], Jean Pierre Hubschman[2], Neha Bajwa[1], Priyamvada Tewari[1], Elliott Brown[3], Warren Grundfest[1]
[1]Bioengineering, UCLA, Los Angeles
[2]Jules Stein Eye Institute, UCLA, Los Angeles
[3]Physics, Wright State University, Dayton

Medical imaging has been the subject of much interest in the THz community recently due to promising results obtained in *ex vivo* and *in vivo* tissues. The dielectric properties of water and other tissue constituents at THz frequencies are quite unique and significant contrast can be generated with THz illumination that is unavailable to currently accepted medical imaging modalities. This abstract presents a pulsed, reflective THz imaging system operating at ~525 GHz center frequency with ~ 125 GHz of bandwidth and developed specifically for *in vivo* medical imaging applications. Illumination center frequency and bandwidth are motivated by resolution and hydration sensitivity and the details of these tradeoffs are discussed. Following system phenomenology discussions two promising THz medical imaging applications are presented; burns wound assessment and corneal hydration sensing. For burns, THz images are presented of 2nd degree, partial thickness burns obtained in rat models *in vivo* over a 72 hour period. These results clearly show the evolution of wound edema and may eventually provide burn surgeons with tools for early severity assessment. For cornea, images are presented of corneal hydration obtained *in vivo* from 78% - 81 % hydration by volume. The data indicates a hydration sensitivity of less than 0.2% by volume and may offer ophthalmologists a diagnostic for the early detection of corneal graft rejection, Fuchs' dystrophy, and other diseases/pathologies associated with corneal health.

Heterostructure Backward Diode Detectors for Millimeter-wave through THz Detection and Imaging

Patrick Fay*[(1)], Ze Zhang[(1)], Yi Xie[(1)], and M. I. Shams[(1)]
(1) Dept. of Electrical Engineering, Univ. of Notre Dame,
http://www.nd.edu/~hscdlab

High performance direct detectors are important components for a range of millimeter-wave and THz systems. Applications such as radiometers for remote sensing as well as active and passive imaging systems for security, medical, and defense-related applications can potentially benefit from improvements in detector performance through reduction in pre-amplification requirements and attendant improvements in system size, power consumption, and complexity. Millimeter-wave direct detectors have been demonstrated based on Schottky and planar-doped barrier diodes, and Schottky diodes have been demonstrated to operate to THz frequencies. However, the physical principles underlying these devices' operation impose fundamental limits on their sensitivity. Zero-bias heterostructure backward diodes offer a promising alternative to these established technologies; since these devices rely on interband tunneling instead of thermionic emission for producing their nonlinear current-voltage characteristics, curvature coefficients above the thermionic limit of $\gamma=q/kT$ can be obtained, leading to the demonstration of higher detection sensitivities than competing approaches and low noise equivalent power (e.g., Zhang et al., IEEE Microwave and Wireless Components Lett., 21, 267-269, 2011).

A recently-developed physics-based model that allows accurate projection of the current-voltage and capacitance characteristics of heterostructure backward diodes has provided new insights into device design and optimization. At the same time, advances in fabrication processing have both improved discrete device performance as well as allowed the demonstration of 5,000-pixel monolithically-integrated planar antenna-coupled focal plane arrays using these devices (e.g., D. Burdette et al., SPIE Defense, Security and Sensing Conf., paper 8023-14, 2011). The combination of these parallel advances in fundamental device-level understanding and practical implementation promise significant gains in detector performance and open up alternative circuit and system configurations. The performance of detectors based on these design and process improvements—including demonstration of intrinsic cutoff frequencies (as projected from measurement-based equivalent circuit models) of 8 THz and experimental characterization of detectors at G-band and above—will be discussed, and the prospects for future performance and functional integration will be addressed.

MEMS-based Uncooled THz Detectors for Staring Imagers

J. A. Cox, R.Higashi, F. Nusseibeh, C. Zins
Honeywell Sensors & Wireless Laboratory
Plymouth, MN, USA

Abstract

We review our previous work to develop an uncooled THz detector capable of achieving an NEΔT ~0.5K at 30Hz frame rate. Both predicted and measured results of performance metrics (responsivity, NEP, response time, spectral bandwidth) are presented with the usual reservations regarding lack of a traceable radiometric source. The measured performance agrees reasonably well with predictions and is consistent with attaining our NEΔT goal. Thus far, 1x4 detector arrays have fabricated, and 1x8 focal plane arrays have been developed and tested. We briefly discuss our vision to achieve a128x128 detector array needed for a practical staring THz imager and describe the technology challenges needed to realize it.

Characterization of THz Power Detectors at 119μm and 394μm Wavelengths

Nina P. Basta*[(1)(2)], John Lehman[(2)], Erich Grossman[(2)]
and Marla Dowell[(2)]
(1) McGill University, Montréal, Canada
(2) NIST, Boulder CO, USA

New power detectors in the THz frequency range at wavelengths below 400μm are being developed and need to be characterized. This paper presents measurements of absolute responsivity for a variety of detectors at 119μm and 394μm wavelengths of the terahertz range of the spectrum. The responsivity of ten different detectors (thermopiles, pyroelectrics and chrome black organic coatings), manufactured by several different commercial companies or fabricated at NIST, was compared to that of a commercial absolute power meter reading.

The measurements were performed using a THz CO_2 laser at 119μm and 394μm with methanol and formic acid in the cavity, respectively. The output power of the laser exceeded 10mW at both wavelengths. The laser beam is coupled to the detector through a series of mirrors and apertures and the nominal incident power at the reference plane is measured with a commercial absolute power meter and normalized to the reading of a monitor at the laser output, as shown in the block diagram in the figure below. The purpose of the monitor wa to remove laser power drifts. Ten detectors types were characterized at 119μm, and seven at 394μm. Each power detector reading was normalized by switching between the commercial absolute power meter and the detector under test, resulting in a relative efficiency expressed in W/W. The responsivity was calculated by averaging the readings in two different ways to help determine measurement uncertainties. Measurement results showing the absolute responsivities and associated uncertainties will be presented.

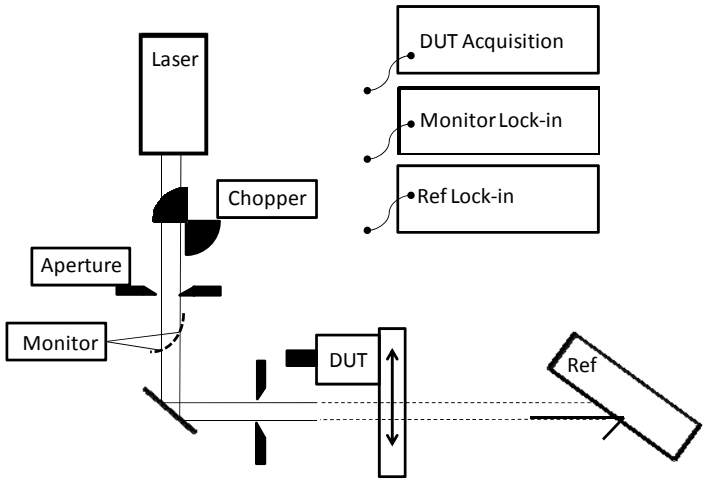

Waveguide Flange Misalignment and Calibration at Submillimeter Wavelengths

R.M. Weikle, II, H. Li, A. Arsenovic, J.L. Hesler[†], and A.R. Kerr[††]

Charles L. Brown Department of Electrical and Computer Engineering
University of Virginia, Charlottesville, VA 22904

[†] Virginia Diodes, Inc., 979 Second Street, S.E. Suite 309
Charlottesville, VA 22902

[††] National Radio Astronomy Observatory
1180 Boxwood Estate Rd., Charlottesville, VA 22903

Rectangular waveguide is the primary transmission medium for submillimeter-wave systems operating from 300 GHz to 1 THz and the UG-387 flange remains the most common interface for mating waveguide components over this frequency range. Alignment of UG-387 flanges is accomplished with pins and alignment holes that are placed near the flange perimeter and, under the standard MIL SPEC tolerances, misalignments of up to 0.006 inches (150 μm) are possible. With the advent of vector network analyzers operating to 1 THz, misalignment of waveguides at flange interfaces resulting from practical machining tolerances can be a significant source of measurement error and is now recognized as a fundamental problem limiting calibration and measurement precision at frequencies greater than 300 GHz [1]. In response, a number of new waveguide flange concepts have been investigated to address flange misalignment and the P1785 working group of the IEEE is currently undertaking a study to recommend standards for waveguide interfaces for frequencies above 110 GHz. Among the new flange concepts being considered is a modified UG-387 that utilizes tighter machining tolerances [2] and the ring-centered flange where alignment is accomplished using a precision coupling ring that fits over raised bosses centered on each waveguide [3].

This paper discusses the waveguide interface concepts currently being investigated to address flange misalignment and presents measurement data comparing the connection repeatability of the standard UG-387 flange with competing designs, including the modified UG-387 and ring-centered flange. Comparisons of flange performance and repeatability are made using two methods: (1) a load-separation technique that compares the relative changes in the flange return loss over repeated connection-disconnection cycles and (2) calibrated measurements that utilize a set of standards that is insensitive to flange misalignment. These standards include a flush waveguide short, a pair of offset shorts with different (but unspecified) delays and a waveguide radiating open [4].

[1] D.F. Williams, "500 GHz – 750 GHz rectangular-waveguide vector-network-analyzer calibrations," to appear in the *IEEE Trans. on Terahertz Science. and Tech*., 2011.

[2] J.L. Hesler, A.R. Kerr, W. Grammer, and E. Wollack, "Recommendations for Waveguide Interfaces to 1 THz," *Proc. 18th International Symposium on Space Terahertz Technology*, Pasadena, 21-23 March 2007, pp.100-103.

[3] H. Li, A.R. Kerr, J.L. Hesler, H. Xu, and R.M Weikle, II, "A ring-centered waveguide flange for millimeter wave and submillimeter wave applications," *IEEE MTT-S International Microwave Symposium Digest*, Anaheim, CA, pp. 604–607, May 2010.

[4] Z. Liu and R.M. Weikle, II, "A reflectometer calibration method resistant to waveguide flange misalignment," *IEEE Trans. Microwave Theory Tech*., vol. 54, no.6, pp. 2447–2454, 2006.

Point and Remote Chemical Sensors in the Millimeter and Submillimeter Spectral Region

Frank C. De Lucia
Physics Department, Ohio State University, Columbus, OH 43210, USA

Point and remote sensing of chemicals in the terahertz have become important and popular topics. The physical bases of the various techniques that have been considered are the strong and complex signatures associated with the rotational degrees of freedom of molecules.

While there are commonalities between point and remote sensors in this spectral region, there are also significant differences. Chief among these are the large pressure broadened linewidths associated with atmospheric pressure. These large linewidths significantly reduce specificity and make separation of signatures from background and clutter difficult.

With the growth of technologies for the spectral region between the microwave and the infrared (variously referred to as the millimeter, nearmillimeter, submillimeter, terahertz, and far infrared), many different implementations of chemical sensors have been proposed and demonstrated.

Here we will consider both results obtained in our own work, as well as those from systems described in the literature. We will pay particular attention to the wide variations of spectra among molecules and the role of this variation in the selection of 'demonstration' spectra. We will also consider the impact of this variation on the generally of the several implementations. While most of our focus will be on these rotational sensors, comparisons with the more widely known vibrational sensors in the infrared will also be made. We will show explicitly the many orders of magnitude differences in important figures of merit, such as sensitivity and specificity, which occur among different approaches.

We will also consider paths forward, with particular emphasis on practical implementations that have the potential of being attractive to wide audiences.

CW THz Photomixer Beam Characterization

Richard A. Chamberlin*[1] and Erich N. Grossman[2]

[1] The University of Colorado, Boulder, CO, USA

[2] National Institute of Standards and Technology, Boulder, USA

We measured photomixer beam cross section, beam spread as a function of distance, spectral response, and other characteristics of two nominally identical, commercial photomixer chips (ErAs:GaAs). THz photomixing current from the 9x9 um active area on the chip drove a broad bandwidth square spiral antenna which radiated power into a silicon hyper-hemispherical lens, which in turn coupled the THz radiation into free space. The silicon lens was not anti-reflection coated. The chips were operated with a 20volt DC bias and about 20mW of total CW laser power. The laser power was provided by combining beams from two commercially acquired DFB diode lasers operating near 780 nm. The lasers were tuned by temperature control and could provide difference frequencies ranging from zero to 1.4 GHz. THz radiation from the chip/lens assemblies was detected and characterized using an antenna coupled room temperature microbolometer designed and fabricated at NIST (NEP 100 pW/$\sqrt{Hz}$) (Dietlein et al. Proc SPIE v6549, 65490-M, 2007). We were able to detect radiation from the THz photomixers under test from about 100 GHz to 1.4 THz. The radiated power peaked at about 200 GHz with an estimated peak power of about 0.1 uW based on measurements with a Thomas Keating power meter. The beams radiated from the chip/lens assemblies had multimodal cross sections from 100 to 600 GHz. Above about 600 GHz our system had insufficient s/n to make reliable characterizations of the beam cross sections. Multimodal beam cross sections were unexpected, and may be due to the bow-tie optical resonance modes recently described by Boriskin and Sauleau (J. Opt. Soc. Am. A/Vol. 27, No. 11/November 2010).

Micro-fabricated W-band and G-band Frequency Scanned Antenna Arrays

Leonardo Ranzani*(1), Evan Cullens(1), Kenneth Vanhille(2), Zoya Popovic(1)
(1) University of Colorado, Boulder, CO
(2) Nuvotronics, LLC, Roanoke, VA

Beam steering antenna arrays have been extensively studied in the past as they are a key element in object tracking and planetary landing systems. Such antennas emit a narrow beam with a scan angle that can be controlled by changing the relative phase shift between the array elements. In standard phased arrays, tunable phase shifters are used to control the position and shape of the beam. Such a solution however is costly and can be impractical above V-band, because of cost and losses in tunable phase shifters. A suitable alternative is using frequency-scanned arrays. In this case the antenna elements are fed serially so that the relative delay between the antenna elements is constant, but the phase shift is controlled by tuning the signal frequency.

In this talk, a new type of frequency scanned slot array operating in W-band from 85 to 110GHz based on micro-coaxial technology will be described. The proposed device is characterized by lower weight and size, compared to its V- or K-band alternatives and is capable of achieving more than 30 degree scanning and a steering angle per unit frequency of 1 deg/GHz. The slot array is fed by a micro-coaxial line. The feed was realized using the PolyStrata(R) process. In such a technology, single mode micro-coaxial lines can be realized at W-band having loss as low as 0.1dB/cm and low dispersion. Various approaches to increase the operating bandwidth and the slot array scanning angle were employed in the design. In particular the coaxial inner conductor was meandered to increase the delay between subsequent slots and, therefore, the scanning range. At the same time good matching, with better than 10dB return loss was obtained in the 85 to 110GHz range by using double-slot radiators and by suitably changing the center conductor width in the proximity of the slots. Extensions to G-band waveguide-based arrays (shown in the figure) will also be discussed for the 130-180GHz range, in which case the natural or purposely increased dispersion of the waveguide is used for scanning. The final device has potential applications to space exploration and planetary landing systems.

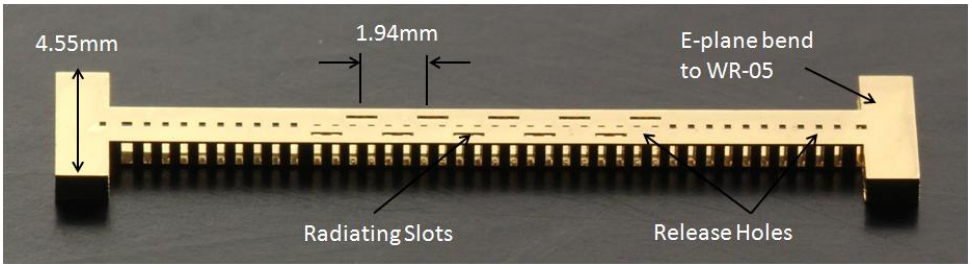

Contactless THz Probes for Device Characterization

Georgios Trichopoulos*, Kagan Topalli, and Kubilay Sertel
ElectroScience Laboratory, Dept. of ECE
The Ohio State University, Columbus, OH USA

Recent advances in novel THz devices that exploit ultrafast quantum mechanical transitions in semiconductor systems (such as tunneling, plasma waves, etc.) are enabling new sensors for the THz band. New devices, such as heterostructure backward diodes (HBDs), 2D electron gas (2DEG) field effect transistors (FETs), high electron mobility transistors (HEMTs), metal-insulator-insulator-metal (MIIM) junctions and quantum cascade structures can now be produced with cutoff frequencies well beyond 1 THz. However, device characterization at such high frequencies is not straightforward due to the limitations of existing measurement tools. High speed devices are typically characterized by contact probes in the mmW regime. For the sub-millimeter and THz band such probes are not readily available.

Here, we propose a *contactless* probe for characterizing ultrafast semiconductor devices in the sub-millimeter and THz regime. These new probes can be used in conjunction with available THz VNA extension modules. The device under test is integrated with receiving/transmitting planar THz antennas in coplanar waveguide environment. The network analyzer ports are connected to two standard horn antennas that face a hemispherical lens forming a contactless quasi-optical link to the coplanar-waveguide environment between the receiving and transmitting THz antennas. Similar to contact probe calibration, standard loads (short/open/through/match) are needed to de-embed the propagation path between the analyzer ports and the THz device.

The proposed setup allows for high frequency characterization (0.1 – 2 THz), exceeding the limits of current characterization tools. During the conference initial measurements will be presented that validate the accuracy and capability of the method.

A Standard for Characterizing Antenna Performance in the Time Domain

Everett G. Farr*
Farr Fields, LC, Albuquerque, NM, 87123, http://www.Farr-Research.com

There are already standards for characterizing antenna performance in the frequency domain, but no such standard exists in the time domain. This becomes a problem if, for example, one wishes to buy or sell an antenna with a specified performance in the time domain. In the frequency domain, one normally uses antenna gain, but this offers little information about the antenna's time domain performance.

A number of earlier papers have addressed this issue (e.g., C. E. Baum, "General Properties of Antennas," Sensor and Simulation Note 330, July 1991). However, the fact that no standard yet exists suggests that previous methods may have been too complicated. We show here that with proper normalization, the equations simplify to a very concise and useful form.

To characterize an antenna in the time domain, a function should have five characteristics. It should fully describe antenna performance with equations that are as simple as possible. It should describe antenna performance in both transmission and reception. It should describe antenna performance in both the frequency and time domains. It should be simply related to frequency domain standards, such as gain, realized gain, and antenna factor. Finally, it should be simply related to quantities that are measurable in the laboratory, typically with an oscilloscope.

In this spirit, we propose a function that satisfies all five criteria. It is hoped that this function will become a standard of comparison for all antennas in the time domain.

We begin by introducing the function of interest, along with the relevant antenna equations. It is convenient to manipulate antenna equations that have been specialized to radiation on boresight with dominant polarization. We prove the antenna equations, using an argument of reciprocity. We generalize the results to all angles and polarizations. We show the relationship between our function and other commonly used antenna terms, such as gain and realized gain. Finally, we discuss candidate names for the proposed function.

The Effect of a Local Ground Plane on the Radiation Characteristics of the Impulse Radiating Antenna (IRA)

D. V. Giri*[(1)] and F. M. Tesche [(2)]
[1]Pro-Tech, 11 C Orchard Court, Alamo, CA 94507-1541
[2]F. M. Tesche, EM Consultant, Saluda, NC

Abstract

This paper discusses a modification of the free-space radiated field from an impulse radiating antenna to take into account the effects of a lossy ground plane (earth) in the vicinity of the antenna. Such effects, which become important at certain distances from the antenna, cause the observed fields to differ significantly from those predicted from the isolated antenna. The development of the impulse radiating antenna (IRA) has provided a useful tool, both for testing facilities and systems for their responses to high-power electromagnetic (HPEM) fields. Starting from the original paper describing the concept behind this antenna, there have been a series of papers tracing the development of this antenna and documenting its operating characteristics. Generally, this antenna produces a fast-rising impulse-like pulse, preceded by a "pre-pulse" contribution to the field.

An interesting observation from test programs involving the IRA is that when the antenna is near the ground to illuminate ground-based targets, the IRA field changes its wave shape as the distance from the antenna to the observation location increases. The radiated wave shape is well known in theory and practice, but as the distance increases, the waveform becomes more like a doublet – having a positive and negative peak of comparable magnitudes due to the presence of the ground. As an example of this effect, Figure 1 plots the measured waveform from a 1.8 m diameter IRA with a 2.8 kV pulser source, at a distance of 40 m, with the ground present. A calculated waveform that accounts for the presence of the lossy ground is also shown in the figure. The waveform change is clearly due to the nearly simultaneous arrival of an earth-reflected waveform component to the observation point.

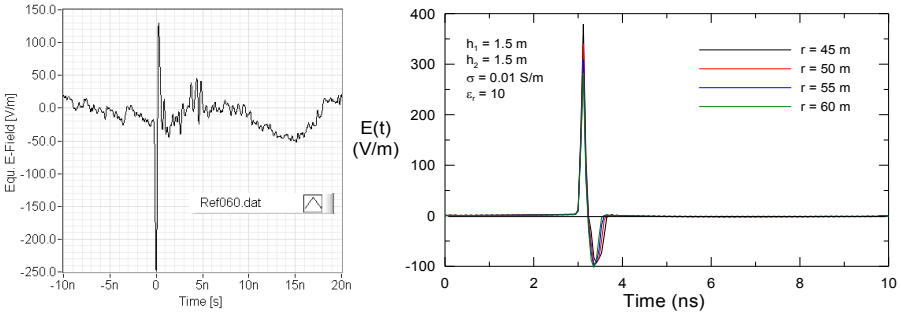

Figure 1. **Plots of measured IRA E-field at a range of 40 m from the antenna (left) and a calculated waveform at various distances (right)**

In this paper, we will describe and illustrate the behavior of the IRA near the lossy ground.

Photoionization Processes in Lightning Return-Stroke Initiation Conditions

Robert L Gardner*, Consultant
6152 Manchester Park Circle
Alexandria, VA 22310
Robert.L.Gardner@verizon.net

Longmire, et al, [*Phys. Fl., 27*, p. 2694, 1984] proposed a propagation mechanism for streamer propagation in neutral plasma appropriate to a nuclear lightning environment. The model assumed a conducting streamer that formed when the enhanced fields around the streamer tip reached the air avalanche field. A three species air chemistry model was used along with thermal reservoirs for molecular heating along with neutral and ionized atoms representing oxygen and nitrogen. The model suggested a propagation velocity of 10^5 m/s, consistent with photographs of nuclear lightning, but substantially below that of natural lightning, so work began to understand the initial conditions for a similar model for the natural lightning environment. Radiative transport is key to predicting the propagation speed near c that is observed and predicted by Baum [Lightning Phenomenology Note 5, EMP Note Series, www.ece.unm.edu/summa/notes]

Natural lightning leader processes can lower several coulombs of charge into a column that eventually becomes the return-stroke channel. That charge has to wait while the full channel forms and the charges attach to air molecules under those low field conditions forming species like 0^2-. These heavy species are not very mobile and move at velocities much lower than the electron drift velocity of about 10^5 m/s. The like charges repel each other and spread the charge out first as free electrons then as charged molecules as the electric fields get lower than the air avalanche value. Analytic and numerical models were developed to show the charged-species channel expansion. This model showed a column of charge that expanded to about a meter in diameter and consisted of relatively evenly spaced charged species [Proceedings, International Conference on Electromagnetics in Advanced Applications, Sydney, September, 2010]. The hot gas at the tip also emits photons that travel forward in the low-density channel left from the leader processes. These photons scatter electrons and allow a substantial increase the propagation velocity. The velocity of the peak current slows because of the plasma channel losses confining the high frequency emission to the first few meters of the return stroke channel.

X-rays Produced by First and Subsequent Strokes in Natural Lightning

S. Mallick* [(1)], V. A. Rakov[(1)], J. R. Dwyer[(2)], and J. A. Cramer[(3)]
(1) Department of ECE, University of Florida, Gainesville, FL, USA
(2) Department of PSS, Florida Institute of Technology, Melbourne, FL, USA
(3) Vaisala Inc., Tucson, AZ, USA

An x-ray detector, consisting of a NaI scintillator and a photomultiplier tube, was used at the Lightning Observatory in Gainesville (LOG), Florida, to record x-ray emissions produced by natural lightning. Corresponding electric field and electric field derivative waveforms were also recorded. A total of 12 negative flashes with at least one stroke within a distance of 2 km from LOG were analyzed. The total number of strokes within 2 km of LOG was 23 (8 first and 15 subsequent), all recorded on July 31, 2011. We searched for x-rays produced by leaders during 2 ms prior to the beginning of the return stroke. Out of the 23 strokes, 3 produced single x-ray pulses, 11 produced x-ray bursts (sequences of two or more pulses), and 9 did not produce detectable x-ray emissions. The occurrence of x-rays is 88% and 47% for first and subsequent strokes, respectively. Examples of x-rays produced by three strokes within the same flash are shown on a 200-μs time scale in Fig. 1.

The occurrence of x-rays showed a tendency to increase with increasing NLDN-reported peak current and with decreasing distance. All four strokes with the highest peak currents, in the 40 to 60 kA range, were accompanied by x-ray bursts. Although the sample size is small, there appears to be a trend for the x-ray energy (for the largest pulse in the case of burst) to increase with increasing peak current.

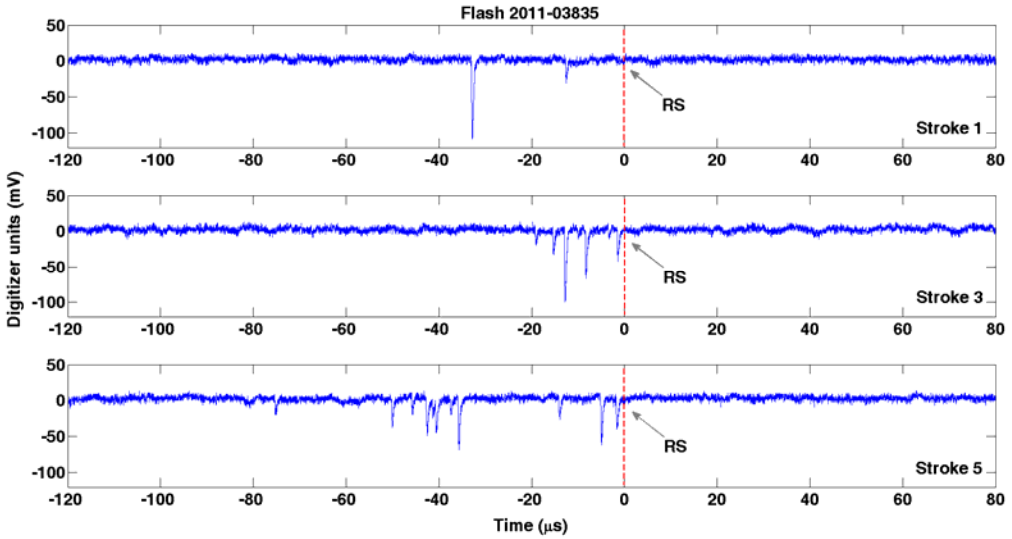

Fig. 1. X-rays produced by stroke 1 (top), stroke 3 (middle), and stroke 5 (bottom) of 11-stroke flash 2011-03835. Strokes 2 and 4 did not produce detectable x-rays. Strokes 6 to 11 were not recorded at LOG. NLDN-reported distances for strokes 1 to 5 were 0.9 to 1.4 km. Vertical broken lines labeled RS indicates the approximate position of the return stroke.

Time domain fractal lightning modeling study of field change array data

Can Liang[1], Brant E Carlson[1, 2], Phillip M Bitzer[3], Hugh J Christian[3], Nikolai G Lehtinen[1], Umran S Inan[1,4]

1. Electrical Engineering, Stanford University, Stanford, CA, United States.
2. University of Bergen, Bergen, Norway.
3. University of Alabama, Huntsville, AL, United States.
4. Electrical Engineering Department, Koç University, Rumelifeneri Yolu, 34450 Sariyer Istanbul, Turkey

Even though lightning flashes and the associated phenomena have been well documented under many different environmental conditions, with various types of instruments, our understanding of the physical processes involved remains incomplete. This is partly due to the fact that the intrinsic complexity of lightning often makes it difficult to make detailed and quantitative connection between experimental data and theories about certain fundamental physical processes.

In this paper, through the study of Time Domain Fractal Lightning Modeling (TDFL) together with data from the Huntsville Alabama Marx Meter Array (HAMMA), we show that TDFL provides effective means for interpreting observational data in terms of theories of fundamental physical processes.

TDFL is capable of modeling lightning flashes starting with the initial breakdown and continuing until the flashes cease to be active. The flashes can be intra-cloud discharges or cloud-to-ground discharges. On its own, TDFL extends lightning channels using a stochastic model depending on various physical parameters. In other cases, as in the study to be presented, TDFL can accept constrains on the discharge geometry derived from data. In comparison with previous Fractal Lightning models, TDFL offers many advantages. For example, it works in the time domain and does not assume quasi-static lightning channel at any iteration by using the Method of Moments (MoM) to solve the Electrical Field Integral Equation (EFIE) with effectively unconstrained channel geometry. As a result, it provides information on the time evolution of both current and charge distribution along the channel and predicts the resulting electrostatic and electromagnetic signals for comparison to data. It also can be used to study other physical effects such as the corona sheath, space leader development, and time-evolving channel impedance.

HAMMA is a network of electric field change meters (Marx meters) with high time resolution capable of reconstructing the geometry and time development of the charge motions in a lightning discharge. The network provides lightning mapping capability and electric field records.

In this study, HAMMA network data are used to constrain the initial conditions and development of TDFL simulations, and the TDFL results are used to interpret the field change data from the network. The role of the evolution of the lightning channel electrical properties, the channel corona sheath, and the geometric development of the channel are examined, and the physical implications of the HAMMA data are studied.

Automated and Adaptive RF Effects Testing

Everett G. Farr* [(1)], Leland H. Bowen[(1)], W. Scott Bigelow[(1)],
Robert L. Gardner[(2)], and Peter Finlay[(3)]
(1) Farr Fields, LC, Albuquerque, NM, 87123, http://www.Farr-Research.com
(2) Consultant, Alexandria, VA
(3) Air Force Research Laboratory, Directed Energy Directorate,
Kirtland AFB, NM

The vulnerability of electronics to radio frequency (RF) fields has been well documented. This has led to a major effort to test electronics to find the minimum field or power at which an effect is observed. However, such testing is time-consuming, due to the large number of source variables of interest. One typically searches for the minimum electric field that causes upset, as a function of center frequency, pulse width, pulse repetition frequency, number of pulses, and bandwidth. It is impossible to test all combinations of all the variables, so one must intelligently select the source parameters most likely to expose the greatest vulnerability.

To select source parameters, we propose using standard techniques from minimization theory. Within a space of two or more variables, we search for the combination that upsets the system at the lowest power or field level. We begin by measuring the vulnerability levels on a coarse grid; and then fit a surface to the measured data. We then find the minimum of the surface, and measure the vulnerability at the minimum. With the new data, the process repeats iteratively until it converges.

Ideally, the entire process can be automated. The source variables can all be controlled electronically. In addition, one can determine automatically whether the test object has been upset, and send a reset command if necessary. This leads to a completely automated system that intelligently selects the test parameters, monitors the status of the device, and converges on a minimum upset threshold. During this first implementation, some manual operations were required; however, these can be automated at a later date.

In this project, we investigated the vulnerability of media converters (MCs) to pulsed RF fields. MCs are network devices that convert signal on Cat 5 Ethernet cable to optical fiber, and are known to be vulnerable. We tested these devices by pinging a remote computer, and observing the field levels at which the pings failed to return. We searched a space of source variables, and converged on a minimum upset threshold in the middle of a test space. Most of the operations were carried out automatically.

Random Non-Directed and Directed Graph Models for Mobile Resilient Sensor and Information Systems

Ira Kohlberg
Kohlberg Associates Inc.
11308 South Shore Road
Reston, VA 20190
ira.kohlberg@gmail.com

Abstract

High-power natural and Intentional Electromagnetic Interference (IEMI) pulses on sensor and information systems nodes can cause combinations of short-term upset, long-term upset, and permanent damage to equipment. Any of these effects will degrade the performance of these systems. Mostly, these effects cause bit and message errors, but, on some occasions, physical damage also occurs. In this paper, we provide new theoretical principles based on random graph theory and percolation theory to evaluate the resilience of large, random, geometric, ad-hoc networks formed with non-directed and directed graphs. By combining these graphical representations in a common theoretical framework, we provide a basis for expanding the theory to inhomogeneous networks that are more closely connected to those found in nature and in the military. The proposed metric for survivability is the network's ability to remain radio-frequency connected with a suitable surviving fraction of nodes. The networks of interest are assumed to have large number of nodes, which makes them robust against node failure under normal conditions. Of particular interest are Mobil Ad-Hoc Networks (MANETs) that are comprised of mobile and typically random nodes that have enough power to originate, receive, and relay packets by multi-hop transport. The nodes are randomly positioned, and their statistical properties (e.g., average concentration) are space dependent. It is necessary to demonstrate their resilience against enemy attack by showing that connectedness is maintained at a sufficient throughput. In this exploratory study, we examine the issue of connectedness for three circumstances from an analytical viewpoint: (1) networks comprised of both non-directed and directed graphs, (2) spatially inhomogeneous random geometric networks, and (3) network throughput and resilience based on the renormalization group. The aforementioned methods allow one to make estimates of system performance without getting bogged-down in unnecessary and often incorrect extra detail that obscures the salient physical features of the network under attack.

Characterization of Autoemission Reflection for Precise Radiometer Calibration

Albin J. Gasiewski*[(1)], David Kraft[(1)] and Vladimir Leuski[(1)]
(1) Center for Environmental Technology,
Dept. of Electrical Computer and Energy Engineering,
University of Colorado at Boulder, Boulder, CO 80309-0425, USA

Calibration of spaceborne microwave radiometers to precisions required for assessing climate trends requires biases less than ~0.05 K to be identified. The use of warm pyramidal blackbody targets closely coupled to the radiometer antenna to establish thermal reference points has become standard for this purpose, although the effects of small standing waves generated by the radiometer itself can be considerable. We illustrate these effects using a 55-GHz radiometer and precision scanned pyramidal target, along with coherent processing of the detected power. Of particular interest is the reflection of microwave radiation produced by the radiometer itself ("autoemission"). For a typical close-coupled warm target this radiation reflects directly back into the radiometer feedhorn and can contribute substantially to the detected power. Ideally, reflected radiation causes a constant additive bias, but if the geometric distance between the target and feedhorn changes by even a small fraction (typically as small as ~λ/16) the standing wave produced by this radiation will affect the amplitude of the reflected noise at the receiver, and thus introduce a time-varying signal in the detected power. For bands that are essential to temperature and water vapor sounding of the atmosphere (50-57 and ~183 GHz) the critical perturbation distances are as small as 0.3 and 0.1 mm, respectively. Future THz receivers for ice cloud measurements will result in even smaller critical distances. Given that it is difficult to control feedhorn-warm target geometry over the lifetime of a sensor to such levels it is important to understand the degree to which variations in the autoemission standing wave ratio (SW) affect the detected power in radiometer systems

BEAM-EFFICIENCY EXTRACTION METHOD FOR BRIGHTNESS-TEMPERATURE MEASUREMENT

Dazhen Gu*[(1)], Derek Houtz[(1,2)], James Randa[(1,3)], and David K. Walker[(1)]
(1) National Institute of Standards and Technology, Boulder, CO 80305 USA
(2) Department of Aerospace Engineering Sciences, University of Colorado, Boulder, CO 80309 USA
(3) Department of Physics, University of Colorado, Boulder, CO 80309 USA

The development of a standard radiometer for brightness-temperature standards at microwave frequencies would allow the precise calibration of the blackbody targets in ground-based facilities. We report a measurement technique to extract the antenna beam efficiency with solely passive radiometric measurements for characterizing the brightness temperature of the blackbody radiator. The determination of the beam efficiency traditionally requires the knowledge of the antenna pattern, which is measured in an antenna range. There are different complications associated with the indoor and outdoor antenna ranges. Environment noise is uncontrollable in the outside ranges, while indoor ranges have space limitation in particular when the far-field condition is required.

The method we propose allows us to skip the complexities that are often encountered during the measurement and calculation of the antenna pattern. Taking advantage of the variable heating capability available on most blackbody targets, we varied the temperature of a heated blackbody target and ran a series of radiometric measurements. The study was conducted in an anechoic chamber that provides relatively stable background radiation. We were able to extract the beam-efficiency of a pyramidal horn antenna that is separated from the target in a number of distances in the WR-42 (18 to 26.5 GHz) frequency band. The uncertainty analysis showed that the error of the beam efficiency was about 1% in the close range (50 cm separation) and about 7% in the far range (450 cm separation), indicating a very good measurement accuracy.

We further measured and calculated the brightness temperature of the blackbody target at the distances where we already knew the extracted beam efficiency. The extracted brightness temperature was slightly lower than the physical temperature and showed about 1 K uncertainty when the target was located no more than 1 m away from the antenna. The result satisfies the accuracy criteria of some parameters for climate change investigation.

Wideband Electromagnetic Analysis of Pyramidal Radiometer Calibration Targets using FDTD

Srikumar Sandeep[(1)] and Albin J. Gasiewski [(1)]
(1) University of Colorado, Boulder, CO , 80302-0425, USA

Precise absolute calibration of radiometers for Earth remote sensing applications, specifically, long-term climate measurement, requires knowledge of the brightness temperature when viewing calibration references to an absolute accuracy of ~50 mK or better. Accurate electromagnetic and thermal analysis is essential for designing wideband radiometer calibration targets as well as for understanding the electromagnetic wave interaction with these structures. Typical external calibration references are periodic arrays of wedges or pyramids constructed of a thermally-conductive substrate (typically aluminum or magnesium) coated with a thin layer of microwave absorbing material (e.g., Emerson-Cummings MF-112™ or equivalent).

To study calibration target emission a general three dimensional Finite Difference Time Domain (FDTD) engine was developed for full wave simulation of doubly periodic lossy structures. The primary advantage of FDTD is that being a time domain method it facilitates the estimation of the broad frequency response of the system with a single transient pulse excitation. The formulation is based on modeling of dispersive media using piecewise linear recursive convolution (PLRC), use of a uniaxial perfectly matched layer (UPML) absorbing boundary condition, and symmetric/periodic boundary conditions appropriate for a quarter unit cell of the pyramidal array geometry. The numerical accuracy of the code is ascertained by estimating the transmission coefficient of an infinite magneto-dielectric dispersive slab and comparing simulated results with known analytical results, along with energy conservation for a perfectly reflecting pyramidal surface. FDTD modeling of dispersive radar absorbing material is performed by fitting the measured complex permittivity and permeability data to a series of Debye terms using a genetic algorithm (GA). Prony's extrapolation is employed to obtain the field values at time instants after the FDTD simulation period.

The validated code was used to study the wideband (6-200 GHz) emissivity performance of several calibration target configurations with varying coating thickness, base width, and base to height ratio. Results relevant for radiometer calibration using external references will be presented.

Optimal Calibration of Passive Microwave Radiometers for the 2008 Arctic Mechanisms of Interactions Between the Surface and Atmosphere (AMISA) Mission

Michael Zucker[(1)] and Albin J. Gasiewski [(1)]
(1) University of Colorado, Boulder, CO , 80302-0425, USA

Microwave radiometry is a useful means for estimating various geophysical parameters such as sea coverage and snow overburden, atmospheric water vapor, and cloud liquid and ice content. Accurate passive microwave radiometer calibration is a critical step in extracting such parameters from airborne and satellite measurements. Brightness temperatures used for geophysical parameter estimation are generally required to absolute accuracies of ~1K to as low as ~0.1K or better for climatologically studies. Sensitive radiometer systems (amplifiers, mixers, etc.) typically exhibit both slowly drifting and abruptly changing gains and offsets. The optimal estimation of these system processes as well leakage and channel crosstalk parameters is crucial in analyzing microwave observations with minimal error.

Optimal calibration is achieved through periodic observation of stable references such as thermal blackbody targets, noise diodes, cold-FET amplifiers, or plasma sources. A combination of methods using both infrequent external thermal blackbody views and brief frequent internal noise sources has proven practical for airborne systems such as the Polarmetric Scanning Radiometer (PSR) and is proposed for spaceborne systems such as GeoMAS. External targets such as warm blackbodies and cold space are highly stable sources whose emissions are well characterizable (e.g., using thermistors or ephemeris data). However, gain and offset fluctuations in radiometer systems such as PSR and GeoMAS occur on much shorter time scales (typically seconds to tens of seconds) than practical for external calibration. A solution to this problem is to use fast switched internal noise references feeding the receiver by, for example, use of a Dicke switch or noise injection. These reference measurements do not require physical movement the radiometer, but rather a simple electronic means (e.g., PIN diodes, ferrite switches, MEMS switches, plasma-discharge switches, or heated thin films) to rapidly alternate temperature weightings between the scene and noise sources. Using infrequent absolute gain and offset estimates calculated from external measurements the noise temperature for the internal sources can be estimated each time the system performs an external calibration. The system gain and offset can then be tracked continually during scene measurements provided that the internal sources are stable.

This described method was implemented for calibration of the PSR during the AMISA 2008 arctic science flight campaign. The results along with error calculations will be presented.

Improved Jacobian Formulation for A Scattering-Based Discrete Ordinate Radiative Transfer Model

Miao Tian and Albin J. Gasiewski

Center for Environmental Technology
Department of Electrical and Computer Engineering
University of Colorado at Boulder

ABSTRACT

A unified microwave radiative transfer (UMRT) model has being developed for rapid calculation of the thermal radiation emitted from any set of planar layered geophysical media. The layers can be comprised of either dense or tenuous Mie spherical scatterers. Rapid calculation of the tangent linear relationship (Jacobian) between the brightness temperatures with respect to any radiative parameter of interest, such as scattering and absorption coefficients, medium temperature and lapse rate, mean particle size, stickiness parameter, and others is incorporated. UMRT employs a multi-stream discrete-ordinate layer-adding algorithm by incorporating the analytical diagonalization and factorization technique of symmetric and positive definite matrices from the discrete ordinate tangent linear radiative transfer (DOTLRT) model devised by Voronovich et al.

In extending DOTLRT UMRT includes both Mie theory and dense media radiative transfer theory developed by Tsang, employs refractive correction at layer boundaries, and models coupling of the vertically- and horizontally-polarized radiation intensities within each layer. The model also permits the thermal radiation of a layer to be linear in height. Refractive compensation is performed by applying Snell's law and a cubic spline interpolation matrix along with correction for multiple incoherent reflections. The model computes the associated Jacobians under the complete UMRT framework.

This paper focuses on validation of the UMRT development code by imposing energy conservation and comparing results with those of DOTLRT under same input conditions. Details of the UMRT formulation with the associated Jacobian procedure are presented. Numerical examples using both nominal and real environmental conditions will also be presented and discussed.

An Overland Wet Path Delay Retrieval Algorithm for Nadir-Viewing Microwave Radiometers

Kyle L. Gilliam[1*], Xavier Bosch-Lluis[1], Steven C. Reising[1], Alan B. Tanner[2]

1. Microwave Systems Laboratory, Department of Electrical and Computer Eng., Colorado State University, Fort Collins, CO 80523.
2. Jet Propulsion Laboratory, California Institute of Technology, Pasadena, CA 91109

Currently, only geographically sparse data are available for over-land wet-tropospheric path delay, since it is limited to radiosonde launches and ground-based radiometer and radar measurements. In the past, wet path delay measurements have been limited to oceanic cases because the emissivity of the ocean is generally well understood. Overland wet-tropospheric path delay measurements have the additional complication of highly variable surface emissivities on both spatial and temporal scales. Additionally, the emissivity of such surfaces is difficult to categorize since they contain many different features, including vegetation, snow, soil moisture, and soil composition. It is only recently that global measurements of soil emissivity have been derived from global brightness temperature measurements, including those from the Special Sensor Microwave/Imager (SSM/I) on Defense Meteorological Satellite Program (DMSP) satellites.

Knowledge of the wet-tropospheric path delay would provide several benefits to the scientific community. One target area of this information concerns the hydrology of inland lakes and rivers, one of the two key science objectives of the Surface Water and Ocean Topography (SWOT) mission, an NRC Earth Science Decadal Survey mission planned for launch in 2020. Additionally, information concerning the water vapor content over land could be used for initialization of numerical weather prediction models.

We have developed a new algorithm to retrieve wet path delay from nadir-viewing millimeter-wave radiometers operating in the window regions between the oxygen absorption complex centered at 60 GHz and the oxygen and water vapor absorption lines at 118 GHz and 183 GHz, respectively. This algorithm uses the ratio of differences in brightness temperatures of two nearby scenes to resolve the wet atmospheric absorption coefficient, assuming a known dry absorption coefficient obtained from the Rosenkranz atmospheric absorption model. Minimization of a cost function derived from a radiative transfer model is performed using two degrees of freedom. Results of the retrieval error are presented for realistic estimates of radiometric noise. Simulation results using emissivity models for fresh and sea water, as well as various soil compositions (e.g. silt, clay and sand), are presented to provide an overview of the performance of the retrieval algorithm from measured brightness temperatures in the presence of noise.

Remote Sensing of Tropospheric Humidity using a Ground-Based Network of Scanning Compact Microwave Radiometers

Swaroop Sahoo[1]*, Xavier Bosch-Lluis[1], Steven C. Reising[1], J. Vivekanandan[2]
1. Microwave Systems Laboratory, Department of Electrical and Computer Eng., Colorado State University, Fort Collins, CO 80523.
2. Earth Observing Laboratory, National Center for Atmospheric Research, Boulder, CO 80301.

Thermodynamic properties of the troposphere, particularly water vapor content and temperature, change in response to physical mechanisms, including frictional drag, evaporation, transpiration, heat transfer, pollutant emission and flow modification due to terrain. The planetary boundary layer (PBL) is characterized by a greater rate of change in the thermodynamic state of the atmosphere than at higher altitudes in the troposphere. Typically, such changes in the PBL occur on time scales of less than one hour; whereas changes in the upper troposphere occur on much longer time scales. Observation of these changes, such as large horizontal gradients in vertical wind speed, is important for improved weather prediction. Additionally, high spatial resolution, temporal resolution and accuracy of measured thermodynamic profiles, especially water vapor and temperature, are also important for initialization of numerical weather prediction models. Sensitivity studies for severe storm prediction indicate that a lack of accurate observations of water vapor densities throughout the lower troposphere limits the forecasting of severe storms. Water vapor measurements from network of radiometers may be useful for improved accuracy of severe weather prediction.

The HUMidity EXperiment 2011 (HUMEX11) was conducted to validate remote sensing of tropospheric humidity using a ground-based network of scanning, compact microwave radiometers. Scientific objectives included the measurement of water vapor profiles in the lower troposphere with high vertical and temporal resolution and the measurement of the planetary boundary layer (PBL) height. A network of microwave radiometers was deployed to measure an atmospheric volume using various scanning patterns near the U.S. Department of Energy (DOE)'s Atmospheric Radiation Measurement (ARM) Southern Great Plains (SGP) Climate Research Facility. Since the same volume of the atmosphere was viewed from multiple perspectives, algebraic reconstruction tomography will be used to derive the 2-D and 3-D distribution of water vapor using tomographic inversion. The principal reason for conducting the campaign at the SGP Climate Research Facility was the ability to compare the water vapor profile results with other measurements, including the Atmospheric Emitted Radiance Interferometer (AERI) infrared profiler, ARM microwave radiometers, Raman lidar and four daily radiosondes. Algebraic reconstruction tomography will be used for retrieving the 2-D water vapor density field from the measured brightness temperature. Observation system simulation experiments (OSSE) will be performed to validate the 2-D humidity field using radiosonde data. The preliminary results and statistical analysis of the field experiment will be presented and discussed.

An Anisotropic Ocean Surface Emissivity Model Based on WindSat Polarimetric Brightness Observations

Dean F. Smith*[(1)], Albin J. Gasiewski[(1)], Srikumar Sandeep[(1)], and Bob L. Weber[(2)]
(1) Dept of ECEE, University of Colorado, Boulder, CO 80309 USA
(2) DeTect, Inc, Longmont, CO, 80501, USA

The goal of this research has been to develop a standardized fast full-Stokes ocean surface emissivity model with Jacobian for a wind-driven ocean surface applicable at arbitrary microwave frequencies, polarizations, and incidence angles. The model is based on the Ohio State University (OSU) two-scale code for surface emission developed by Johnson (2006, IEEE TGRS, 44, 560) but modified as follows: (1) the Meissner-Wentz dielectric permittivity (2012, IEEE TGRS, submitted) replaces the original permittivity, (2) the Elfouhaily sea surface spectrum (1997, JGR, 102, C7,15781) replaces the Durden-Vesecky spectrum (1985, IEEE TGRS, OE-10, 445), but the Durden-Vesecky angular spreading function is retained, (3) the high-frequency portion of the Elfouhaily spectrum is multiplied by the Pierson-Moskowitz shape spectrum to correct an error in the original paper, (4) the generalized Phillips-Kitaigorodskii equilibrium range parameter for short waves is modeled as a continuous function of the friction velocity at the water surface to eliminate a discontinuous jump in the original paper. A total of five physical tuning parameters were identified, including the spectral strength and the hydrodynamic modulation factor. The short wave part of the spectrum is also allowed to have an arbitrary ratio relative to the long wave part. The foam fraction is multiplied by a variable correction factor, and also modulated to allow an anisotropic foam fraction with more foam on the leeward side of a wave. The model is being tuned against multi-year sequences of WindSat and Special Sensor Microwave/Imager (SSMI) data as analyzed by Meissner and Wentz (2012, IEEE TGRS, submitted) for up to four Stokes brightnesses and in all angular harmonics up to two in twenty five wind bins from 0.5-25.5 m/s and of 1 m/s width. As a result there are 40 brightnesses per wind bin, for a total of 1000 brightnesses used to constrain the modified model. A chi-squared tuning criterion based on error standard deviations provided by Meissner (2011, private communication), along with an initial manual tuning followed by automated conjugate gradient search based on the modified Powell's Method (1992, Press, Teukolsky, Vetterling, and Flannery, *Numerical Recipes in Fortran Second Edition*) are being used to optimize the parameter set. The results of this minimization and its implications for wideband ocean emissivity modeling will be presented.

Nanosatellites for Earth Environmental Monitoring: The MicroMAS Project[1]

William J. Blackwell, G. Allen, M. Bury, R. Efromson, C. Galbraith, T. Hancock, R. Leslie, I. Osaretin, L. Retherford, M. Scarito, M. Shields, D. Toher, K. Wight
Lincoln Laboratory, Massachusetts Institute of Technology
244 Wood St., Lexington, MA 02420-9185 U.S.A.
wjb@LL.MIT.EDU, 781-981-7973

David W. Miller
Space Systems Laboratory, Massachusetts Institute of Technology
77 Massachusetts Ave., Cambridge, MA 02139

Abstract

The Micro-sized Microwave Atmospheric Satellite (MicroMAS) is a 3U cubesat (30x10x10 cm, ~4kg) hosting a passive microwave spectrometer operating near the 118.75-GHz oxygen absorption line. The focus of the first MicroMAS mission (hereafter, MicroMAS-1) is to observe convective thunderstorms, tropical cyclones, and hurricanes from a near-equatorial orbit at approximately 500-km altitude. A MicroMAS flight unit is currently being developed in anticipation of a 2014 launch. A parabolic reflector is mechanically rotated as the spacecraft orbits the earth, thus directing a cross-track scanned beam with FWHM beamwidth of 2.2-degrees, yielding an approximately 25-km diameter footprint from a nominal altitude of 500 km. Radiometric calibration is carried out using observations of cold space, the earth's limb, and an internal noise diode that is weakly coupled through the RF front-end electronics. A key technology feature is the development of an ultra-compact intermediate frequency processor module for channelization, detection, and A-to-D conversion. The antenna system and RF front-end electronics are highly integrated and miniaturized. A MicroMAS-2 mission is currently being planned using a multi-band spectrometer operating near 118 and 183 GHz in a sun-synchronous orbit of approximately 800-km altitude. A HyMAS-1 (Hyperspectral Microwave Atmospheric Satellite) mission with approximately 50 channels near 118 and 183 GHz is also being planned. In this talk, the mission concept of operations will be discussed, the radiometer payload will be described, and the spacecraft subsystems (avionics, power, communications, attitude determination and control, and mechanical structures) will be summarized. Test data from the recently completed MicroMAS Engineering Development Model (EDM) will also be presented.

[1]This work was sponsored by the National Aeronautics and Space Administration under Air Force contract FA8721-05-C-0002. Opinions, interpretations, conclusions, and recommendations are those of the authors and not necessarily endorsed by the United States Government.

Abstract/Paper Title

AIRBORNE AND FUTURE GEOSTATIONARY ATMOSPHERIC SOUNDING APPLYING THE LATEST LNA MMIC TECHNOLOGY

List of Authors

Kangaslahti, P., Jet Propulsion Laboratory, California Institute of Technology; Lim, B., Jet Propulsion Laboratory, California Institute of Technology; Gaier, T., Jet Propulsion Laboratory, California Institute of Technology; (Presenting); Tanner, A., Jet Propulsion Laboratory, California Institute of Technology; Varonen, M., Jet Propulsion Laboratory, California Institute of Technology; Samoska, L., Jet Propulsion Laboratory, California Institute of Technology; Brown, S., Jet Propulsion Laboratory, California Institute of Technology; Lambrigtsen, B., Jet Propulsion Laboratory, California Institute of Technology; Reising, S., Colorado State University, California Institute of Technology; Tanabe, J., Jet Propulsion Laboratory, California Institute of Technology; Montes, O., Jet Propulsion Laboratory, California Institute of Technology; Dawson, D., Jet Propulsion Laboratory, California Institute of Technology

Abstract Text

The sensitivity of millimeter receivers improved significantly by the introduction of low noise 35nm gate length InP MMIC amplifiers. We currently achieve 3 dB noise figure at 180 GHz and 2 dB noise figure at 90 GHz with our low noise amplifiers in room temperature. These amplifiers and the receivers we have built using them have made it possible to conduct airborne measurement campaigns from the Global Hawk unmanned aerial vehicle, develop millimeter wave internally calibrated radiometers for altimeter radar path delay correction, and build prototypes of large arrays of millimeter receivers for a geostationary interferometric sounder. We use the developed millimeter wave receivers to measure temperature and humidity profiles in the atmosphere and in hurricanes as well as to characterize the path delay error in ocean topography altimetry.

Application of Wideband Single Sideband THz Receivers to Spaceborne Measurement of Cloud Ice

Albin J. Gasiewski*[(1)], William Deal[(2)], Michael McGrath[(3)], K. Franklin Evans[(4)], Aaron Swanson[(2)], David Walker[(5)], Stefan Buehler[(6)], Ginger Drake[(3)], and Neil White[(3)]

(1) Dept. of ECEE, University of Colorado at Boulder, Boulder, CO 80309, USA
(2) Northrop Grumman Corporation, Redondo Beach, CA, 90278, USA
(3) Laboratory for Space Physics, University of Colorado at Boulder, USA
(4) Dept. of ATOC, University of Colorado at Boulder, USA
(5) National Institute of Standards and Technology, Boulder, CO, 80305
(6) Lulea Institute of Technology, Kiruna, Sweden

The NRC 2007 Decadal Survey identified the need for an aerosol and cloud profile mission as a tier-2 activity with potential implementation as an Earth Venture class mission. The proposed International Space Station Atmospheric Sounder Instrument (ISSASI) addresses the need for spatially-resolved measurements of cloud ice water path (IWP) and cloud ice particle size (D_{me}) within the midlatitudes to tropics (55^{o}S to 55^{o}N latitude) for use in constraining global climate models (GCMs). Cloud IWP is one of the most underconstrained and poorly measured of climatologically-relevant variables, exhibiting a huge range of over ~20x in globally averaged IWP among the twenty IPCC AR4 models. Ice clouds have a strong influence on both the shortwave and longwave radiation budget and play an important role in precipitation processes.

ISSASI uses a set of passive millimeter- and submillimeter-wave imaging channels at the 118, 183, 325, 424, and 670 GHz bands in a cross-track scanning instrument. Channels are selected to provide high sensitivity to IWP and mean ice particle size along with mid-to-upper tropospheric water vapor and temperature profiles. Each band uses a single sideband monolithic microwave integrated circuit (MMIC) receiver with up to ~30 GHz bandwidth to implement a set of channels with particularly low noise, high sensitivity to cloud IWP and D_{me}, and sounding and differential spectrum ice sensing capabilities. The overall channel set permits discrimination of IWP from background water vapor and temperature fields while simultaneously providing information on humidity-ice-temperature dynamics in the upper troposphere. A spatial resolution of ~10 km permits study of cloud ice processes on a scale relevant for most convective and stratiform cloud processes.

THE GEOSTAR ASIC DIGITAL CORRELATOR

Christopher S. Ruf*[(1)], Bruce Block[(1)], Michael Flynn[(2)], Phil Knag[(2)], Aaron Rocca[(2)], Zhengya Zhang[(2)], Todd Gaier[(3)], Bjorn Lambrigtsen[(3)], Alan Tanner [(3)]
(1) Space Physics Research Laboratory,
University of Michigan, Ann Arbor, MI USA
(2) Electrical Engineering and Computer Science,
University of Michigan, Ann Arbor, MI USA
(3) Jet Propulsion Laboratory,
California Institute of Technology, Pasadena, CA USA

GeoSTAR is a 50-60 and 165-183 GHz synthetic thinned aperture radiometer (STAR) imager/sounder in development for eventual deployment in Geosynchronous Earth Orbit (GEO). The instrument is designed to provide continuous all weather precipitation monitoring and temperature and humidity sounding. Technology development efforts are currently underway to enable the GeoSTAR mission. These include the development of modular RF front end calibration and downconversion stages, IF signal conditioning and distribution stages, digital back end correlators, and overall system architecture and calibration studies. This talk will present an overview of the system level design, followed by more detailed descriptions of the work underway to develop the digital correlator.

The correlator consists of banks of low bit, high speed digitizers (one for each signal from the antenna array) followed by a large matrix of cross-correlators (one correlator cell for each pair of signals from the antenna array). Because the number of correlator cells required grows as N^2 (where N is the number of antenna array elements) and because N will be of order ~100 for the spaceflight system, considerable emphasis has been placed on reducing the power required per correlator cell. Application Specific Integrated Circuit (ASIC) chips are being designed and fabricated for this purpose. In addition, because of the considerable power required to support chip-to-chip interfaces between high speed digitizer outputs and correlator inputs, the digitizers are also being developed with the same ASIC process, so the two stages of processing can be integrated onto a single chip.

Chip clock speed, radiation tolerance, and other requirements will be presented, together with design and layout considerations and test and characterization plans.

Design and Analysis of a Hyperspectral Microwave Receiver Subsystem[1]

William J. Blackwell, C. Galbraith, T. Hancock, R. Leslie, I. Osaretin, M. Shields
Lincoln Laboratory, Massachusetts Institute of Technology
244 Wood St., Lexington, MA 02420-9185 U.S.A.
wjb@LL.MIT.EDU, 781-981-7973

Paul E. Racette and L. M. Hilliard
NASA Goddard Space Flight Center
8800 Greenbelt Rd., Greenbelt, MD, 20771

Abstract

Recent technology advances have significantly and profoundly changed the landscape of modern radiometry by enabling miniaturized, low-power, and low-noise radio-frequency receivers operating at frequencies up to 200 GHz. These advances enable the practical use of receiver arrays to multiplex multiple broad frequency bands into many spectral channels. We use the term "hyperspectral microwave" to refer generically to microwave sounding systems with approximately 50 spectral channels or more. In this paper, we report on the design and analysis of the receiver subsystem (lensed antenna, RF front-end electronics, and IF processor module) for the Hyperspectral Microwave Atmospheric Sounder (HyMAS) comprising multiple receivers near the oxygen absorption line at 118.75 GHz and the water vapor absorption line at 183.31 GHz. The hyperspectral microwave receiver system will be integrated into a scanhead compatible with the NASA GSFC Conical Scanning Microwave Imaging Radiometer (CoSMIR) airborne system to facilitate demonstration and performance characterization.

Four identical radiometers will be used to cover 108-119 GHz. Subharmonic mixers will be pumped by phase-locked oscillators, and single-sideband operation will be achieved by waveguide filtering of the lower sideband. A relatively high IF frequency is chosen to facilitate miniaturization of the IF processor module. Corrugated feed antennas with lenses are used to achieve a FWHM beamwidth of approximately 3.5 degrees. Two polarizations are measured by each feed to increase overall channel count, and multiple options will be considered during the design phase for the polarization diplexing approach. Broadband operation over a relatively high intermediate frequency range (18-29 GHz) is a technical challenge of the front-end receiver systems, and a receiver temperature of approximately 2000-3000K is expected over the receiver bandwidth. This performance, together with ~100-msec integration times typical of airborne operation, yields channel NEDTs of approximately 0.35K, which is adequate to demonstrate the hyperspectral microwave concept by comparing profile retrievals with high-fidelity ground-truth available either by coincident overpasses of hyperspectral infrared sounders and/or in situ radiosonde/dropsonde measurements.

[1] This work was sponsored by the National Aeronautics and Space Administration under Air Force contract FA8721-05-C-0002. Opinions, interpretations, conclusions, and recommendations are those of the authors and not necessarily endorsed by the United States Government.

RFI-mitigating Multichannel Dual Polarization Airborne L-band Radiometer

Fredrick Solheim, Radiometrics Corporation

With the launch of ESA's SMOS and planned 2014 launch of NASA's SMAP satellite radiometers, there is a need for development and improvement of algorithms and models to interpret the L-band radiometer observations, and for calibration and validation of the satellite radiometers. RFI from spurious and harmonic transmissions as well as other sources is often present in the commonly utilized 1400-1427 MHz reserved astronomy band, contaminating the thermal spectrum. It is found that this reserved band can be nearly as active as the bands adjacent in some environments. The radiometer system below was therefore designed to receive over an expanded band to increase sensitivity and utility.

An advanced dual polarization L-band airborne radiometer system is described. This system spans 1400 to 1550 MHz in 386 channels, measured every 10 microseconds by sampling the high side downconverted IF power with a fast A2D sampler and then Fourier processed in real time into the frequency domain through an FPGA. Subbands 25 MHz wide can also be selected. RFI is then easily identified and can be removed with a number of automated processing methods applied to the frequency domain and to the time series of the spectrum. The RF section is held to a constant physical temperature within +/-0.03C. The system has a dynamic range of about 70 dB. A blanking prefiltering circuit eliminates large spikes.

This L-band system is part of a complement of dual polarization radiometers, including at 6.9, 19, 37, and 89 GHz, being flown on the Meteorological Services Canada Twin Otter. The antenna is a 19 element muffin-tin array, minimizing the depth of the antenna for the aircraft mount.

A portable dual temperature (heated/ambient) blackbody calibration target was designed to closely couple to the antenna while on the aircraft and is described.

Simultaneous Retrieval of Ocean Surface Salinity and Wind Using Aquarius' Combined Active-Passive L-band Data

SIMON YUEH, WENQING TANG, AND ALEXANDER FORE
JET PROPULSION LABORATORY, CALIFORNIA INSTITUTE OF TECHNOLGOY

Aquarius is a combined passive/active L-band microwave instrument developed to map the salinity field at the surface of the ocean from space. The data will support studies of the coupling between ocean circulation, the global water cycle, and climate. The primary science objective of this mission is to monitor the seasonal and interannual variation of the large scale features of the surface salinity field in the open ocean with a spatial resolution of 150 km and a retrieval accuracy of 0.2 psu globally on a monthly basis. The measurement principle is based on the response of the L-band (1.413 GHz) sea surface brightness temperatures to sea surface salinity. To achieve the required 0.2 psu accuracy, the impact of sea surface roughness (e.g. wind-generated ripples and waves), along with several additional factors impacting the observed brightness temperature, must be corrected to better than a few tenths of a degree Kelvin. To this end, Aquarius includes a scatterometer to help correct for this surface roughness effect.

The Aquarius/SACD was launched successfully on June 10, 2011, and the instrument was turned on in late August. The data acquired since then showed that the instrument has been performing very well. The radiometer calibration appeared to have a slow drift of less than a few tenths of Kelvin in 2-3 weeks. The scatterometer calibration was also very stable with the drift of less than 0.1 dB in one week. The baseline algorithm for Aquarius uses the scatterometer data in conjunction with the NCEP wind direction to derive the ocean surface wind speed and then a radiometer roughness correction. Using the data acquired in the first few weeks, we were able to derive a preliminary geophysical model function (GMF) for Aquarius. The retrieved wind speed using the scatterometer backscatter data showed good consistency with the NCEP matchups and collocated SSMI F17 winds with the root mean square difference between 2 to 3 meters per second.

In addition, the preliminary GMF has very good agreement with the PALSAR radar GMF and the JPL aircraft Passive/Active L-band Sensor (PALS) data acquired during the High Ocean Wind (HOW) Campaign in 2009. Using the synergistic characteristics of the active and passive data, we are able to derive the surface salinity and wind simultaneously using the Combined Active-Passive (CAP) data from Aquarius. The CAP algorithm has significant advantage over the baseline algorithm because it does not require the use of ancillary wind direction information for retrieval. This paper will describe the Aquarius calibration, the CAP algorithm and its use for salinity and wind retrieval.

The Global Precipitation Measurement (GPM) Mission and Falling Snow Algorithm Development

Gail Skofronick Jackson and Arthur Y. Hou

NASA Goddard Space Flight Center, Code 613.1, Greenbelt, MD, 20771, USA,
301-614-5720, Gail.S.Jackson@nasa.gov

High spatial and temporal resolution global precipitation estimates are important for an improved understanding of the Earth's atmospheric, hydrological, and energy cycles. Such observations can be used in societal applications such as in agriculture prediction fields, hurricane tracking, flood and landslide prediction, and climate change modeling. Thus, the upcoming NASA/JAXA Global Precipitation Measurement (GPM) mission seeks to estimate precipitation (falling snow as well as liquid rain) globally using physically-based retrieval approaches. The GPM concept centers on deploying a Core spacecraft carrying a dual-frequency Ku and Ka-band precipitation radar and a microwave radiometric imager with channels from 10 to 183 GHz to serve as a precipitation physics observatory and a calibration reference to unify a constellation of dedicated and operational passive microwave sensors. A summary of the GPM mission, scientific objectives, sensor characteristics, and expected precipitation products will be provided.

Progress and challenges associated with algorithm development work for GPM snowfall detection and estimation will also be presented. The challenges for falling snow retrievals include a typically weak signal-to-noise ratio and non-linear, under-constrained relationships between the falling snow and the remotely sensed satellite observations. In order to guide retrieval algorithm development for current and future active and passive precipitation missions, sensitivity analyses were performed to better ascertain the relationships between multi-frequency microwave and millimeter-wave sensor observations and the falling snow/underlying field of view. In addition, thresholds of detection for various sensor channel configurations, snow event system characteristics, snowflake particle assumptions, and surface types were studied. Results will be presented for active radar at Ku, Ka, and W-band and for passive radiometer channels from 10 to 183 GHz.

Development and Demonstration of 92, 130, and 166 GHz Radiometers for Improved Coastal Wet-Tropospheric Correction on SWOT

Darrin Albers*[(1)], Alexander Lee[(1)], Steven C. Reising[(1)], Shannon T. Brown [(2)], Pekka Kangaslahti[(2)], Douglas E. Dawson[(2)], Todd C. Gaier[(2)], Oliver Montes[(2)], Daniel J. Hoppe [(2)] and Behrouz Khayatian[(2)]

(1) Microwave Systems Laboratory, Colorado State University, Fort Collins, CO 80523 USA
(2) Jet Propulsion Laboratory, California Institute of Technology, Pasadena, CA 91109 USA

Current satellite ocean altimeters include nadir-viewing, co-located 18-37 GHz multi-channel microwave radiometers to measure wet-tropospheric path delay. Due to the area of the surface instantaneous fields of view (IFOV) at these frequencies, the accuracy of wet path retrievals begins to degrade at approximately 40 km from the coasts. In addition, they do not provide wet path delay estimates over land. A viable approach to meet these needs is the addition of millimeter-wave window channels at 90-170 GHz, with inherently finer spatial resolution for a given antenna size. The addition of these millimeter-wave channels to current Jason-class radiometers is expected to improve retrievals of wet-tropospheric delay in coastal areas and to increase the potential for over-land retrievals.

The principal objective of this research is to assess the ability of higher-frequency radiometers to meet the needs of the Surface Water and Ocean Topography (SWOT) mission recommended by the U.S. National Research Council's Earth Science Decadal Survey and planned for launch in 2020. The primary objectives of SWOT are to characterize ocean sub-mesoscale processes on 10-km and larger scales in the global oceans, and to measure the global water storage in inland surface water bodies, including rivers, lakes, reservoirs, and wetlands.

Millimeter-wave window channels centered at 92, 130, and 166 GHz can improve wet-path delay retrievals in coastal regions. MMIC-based radiometers have been developed at these three center frequencies to demonstrate new component technology, including PIN-diode switches and noise diodes for internal calibration and a tri-frequency horn with triplexer. These direct-detection radiometers have low mass, small volume and low power consumption. We will present measured receiver noise temperatures and radiometric resolution, $NE\Delta T$, for the 92, 130, and 166 GHz radiometers. Measured results of PIN-diode switches and noise diodes, as well as internal calibration stability, will be presented for each of the three radiometers. Results from the design, fabrication, and testing of 92, 130 and 166 GHz radiometers will be used define radiometer requirements for future satellite altimetry missions with improved coastal wet-path delay retrievals.

Stability of Millimeter-Wave Radiometers Using Internal Calibration Sources

Chaitali R. Parashare*[1], Pekka P. Kangaslahti[1], Shannon T. Brown[1], Douglas E. Dawson[1], Todd C. Gaier[1], Sharmila Padmanabhan[1], Steven C. Reising[2], Oliver Montes[1], James. S. Shell[1], Dennis Harding[1], Daniel Higley[1], and Stephen Pomes[1]

[1]Jet Propulsion Laboratory, California Institute of Technology, Pasadena, CA
[2]Electrical and Computer Engineering, Colorado State University, Fort Collins, CO

Conventional satellite ocean altimeters include a nadir-viewing, co-located 18-37 GHz microwave radiometer to measure wet tropospheric path delay. Due to the area of the surface instantaneous fields of view (IFOV) at these frequencies, the accuracy of wet path retrievals begins to degrade at approximately 50 km from the coasts. Additional higher-frequency microwave channels (90-170 GHz) are being added to the Jason-class radiometers in order to improve retrievals of wet tropospheric delay in coastal areas and to increase the potential for over-land retrievals. The low-power, low-mass and small-volume direct-detection millimeter-wave radiometers will be centered at the 92, 130, and 166 GHz atmospheric window frequencies, which are optimum for wet path delay retrievals in coastal regions.

The radiometers include several LNAs, a band definition filter and a diode detector. The goal is to achieve calibration stability of 0.1 K over 120 s with a system noise temperature of 1300 K or better. Since the system parameters such as gain and noise temperature fluctuate with time, frequent and accurate calibration is essential. We plan to implement internal calibration using noise diodes and Dicke-switched matched loads to facilitate a fixed radiometer field of view and avoid any moving parts. A radiometer test bed has been developed to evaluate the system performance and characterize the stability of the internal calibration approach at these frequencies. The brightness temperature of the noise diode, the receiver gain, and the system noise temperature are being characterized over temperature to assess stability and evaluate accuracy on the calibrated antenna brightness temperature (T_A). We will present the results of the stability analysis for the 130 GHz and 166 GHz radiometers.

A Bayes algorithm to separate precipitation from ground clutter using scan-to-scan correlation technique

Yinguang Li[1,3], Guifu Zhang[2,3], Richard J. Doviak[4] , and Darcy S. Saxion[5]

1: School of Electrical and Computer Engineering, the University of Oklahoma, Norman, OK, USA

2: School of Meteorology, the University of Oklahoma, Norman, OK, USA

3: Atmospheric Radar Research Center, the University of Oklahoma, Norman, OK, USA

4: National Severe Storm Laboratory, Norman, OK, USA

5: NEXRAD Radar Operation Center, Norman, OK, USA

Ground clutter (GC) is received when the mainlobe or sidelobes of the antenna illuminate objects on the ground. Weather radar data measured at low elevations can be highly contaminated by ground clutter. It is desirable to identify precipitation in clutter-contaminated weather radar data. A method of scan-to-scan correlation is proposed and studied. Weather signals are correlated from pulse to pulse but not from scan to scan because the common correlation time of weather signals is around 10 ms while the time for NEXRAD to complete an azimuthal scan at a low elevation is around 32 s. However, ground clutter signals from the same location but observed on two adjacent scans can be highly correlated. Thus, the correlation time of GC and weather are significantly different. Furthermore, the dual-scan data is available from NEXRAD radars for observations at the lowest elevation angles. For example, in the VCP 21 mode, the radar scans twice at elevation angles at 0.5° and 1.5° with different PRTs (Pulse Repetition Time). Cross-correlation coefficient between these dual-scan time-series data collected at the same elevation is calculated and used to distinguish clutter from weather signals. Two discriminants are combined to distinguish ground clutter from weather signals, which are the magnitude of the cross-correlation coefficient between adjacent scans at zero lag $|\rho_{12}(0)|$ and the phase fluctuations of the cross-correlation coefficient between adjacent scans around the zero lag (i.e., CCCPF, Cross-Correlation Coefficient Phase Fluctuations). The statistical properties of the two discriminants are described, and a *simple Bayes* classifier is introduced and implemented. The method is demonstrated with data collected by KOUN radar – a prototype for NEXRAD with dual-polarization capability.

Two-year Evaluation of the Quantitative Precipitation Estimation in the CASA IP5 Weather Radar Network Test bed

V. Chandrasekar and Haonan Chen
Colorado State University, Fort Collins, Colorado, USA

The X-band weather radar network developed under NSF-ERC Collaborative Adaptive Sensing of the Atmosphere (CASA) project has greatly enhanced the remote sensing of weather in the lower atmosphere (0-3 km AGL) by deploying a network of shorter-range, low-cost X-band radars. An important advantage of such a network is that it enables quantitative precipitation estimation (QPE) measurements at a higher spatio-temporal resolution, which has the potential to improve the prediction of high-risk floods in an urban scenario. QPE plays an important role in the forecast of floods by measuring rainfall intensity and accumulation. The dual-pol CASA radars employ the measurement of specific differential phase (Kdp) for QPE process. Unlike the rainfall estimation based on the power products such as Z and Zdr, Kdp-based QPE is less sensitive to the drop size distribution (DSD). Another advantage of relying on a dual-pol product like Kdp to estimate rainfall is that it is relatively less prone to the calibration errors. Being the range derivative of the differential phase shift, Kdp is less susceptible to the path attenuation. The R-Kdp estimator is also immune to the partial beam blockage and hail contamination. This paper deals with the evaluation of the quantitative rainfall measurement system in the CASA IP5 network during the years 2010 and 2011. The QPE products obtained during the spring period during these two years are used to demonstrate the performance of the Kdp-based rainfall estimation method. Further, a cross-validation of these results is carried out with the data obtained from several rain gauges located within the IP5 test bed with coverage overlapping with the individual radar nodes.

Drop size distribution retrieval using dual frequency and dual polarization ground radar

Minda, Le[(1)], V. Chandrasekar [(1)]
(1) Colorado State University, fort Collins, CO, USA

Space-borne weather radar mounted on satellite provides a practical means to obtain useful regional as well as global precipitation measurements. The Global Precipitation Measurement (GPM) mission is planned to be the next satellite mission to obtain global precipitation measurements. The core satellite will be equipped with a dual frequency (Ku/Ka band) precipitation radar (DPR). Ground validation is an integral part of all satellite precipitation missions. Ground validation helps to characterize errors, quantify measurement uncertainty, and, most importantly, provides insight into the physical basis of the retrieval algorithms. The GPM validation falls in the general class of validation and integration of information from a variety of space-borne observing platforms with ground-based measurements. Dual polarization ground radar is a powerful tool that can be used to address a number of important questions that arise in the validation process, especially those associated with precipitation microphysics and algorithm development. The estimation of the drop size distribution (DSD) parameters of precipitation particles helps to achieve more accurate estimation of precipitation rate. A dual frequency and dual polarization ground radar operating at Ku and Ka band has been built to perform cross validation with GPM-DPR.

In Le and Chandrasekar (2011), a drop size distribution retrieval algorithm was developed for this dual frequency and dual polarization ground radar combining attributes from dual-frequency ratio DFR and dual polarization parameters. However, estimation was focused on rain region. In this paper, the evaluation of the retrieval algorithm will be extended to melting and ice region. The dataset is from simulation in order to have knowledge of true DSDs. Different error sources such as snow density, raindrop shape variability, measurement errors, will be considered in analysis.

A Winter Storm Transition Revealed With Polarimetric Radar and 2DVD Observations

Petar Bukovcic*[1,3,4], Dusan Zrnic [2], and Guifu Zhang[3]
(1) Cooperative Institute for Mesoscale Meteorological Studies, University of Oklahoma, and NOAA/OAR National Severe Storms Laboratory, Norman, Oklahoma
(2) National Severe Storms Laboratory, NOAA, Norman, Oklahoma
(3) School of Meteorology, University of Oklahoma, Norman, Oklahoma
(4) Atmospheric Radar Research Center, University of Oklahoma, Norman, Oklahoma

A better understanding of rain microphysical properties is needed for accurate rain estimation and model parameterization. Polarimetric radars measure reflectivity at horizontal and vertical polarization $Z_{H,V}$, differential reflectivity Z_{DR}, differential propagation phase Φ_{DP}, and co-polar correlation coefficient ρ_{hv} that depend on cloud/precipitation physics. Polarimetric radar measurements provide information about hydrometeor size, shape, orientation, and phase and allow retrieval of drop size distributions (DSDs). The two dimensional video disdrometer (2DVD) directly measures the shape, size, and falling velocity of precipitation particles, which is essential for interpreting polarization radar data. A joint radar-disdrometer study allows to further understand precipitation microphysics and to reveal the cause of discrepancies.

Observations and analysis of a mixed-phase precipitation event data, collected with S-band polarimetric KOUN radar and 2DVD in Oklahoma during the winter season of 2007, is presented. Radar measurements and retrieved raindrop size distributions are compared with the disdrometer observations. In the initial period of the storm huge discrepancies between radar and 2DVD measurements occurred due to ice/mixed phase of precipitation. Microphysical parameters such as rainfall rate R and median volume diameter D_0 of radar retrieved DSDs, as well as radar measured Z_H, Z_{DR}, and ρ_{hv} generally agree with 2DVD observations, except for the initial stage of the storm when the ice phase occurred. During this period, a decline of several dB in reflectivity values was diagnosed because of change in dielectric constant. Coincidentally, a reduction in ρ_{hv} occurred, mainly due to low signal to noise ratio (SNR). Single frequency radar is not sufficient to fully characterize the ice-phase precipitation microphysics for the period, thus other observed information may be needed.

Index Terms— winter transition, polarimetry, 2DVD, remote sensing

Vertical profiles statistics of polarimetric radar measurements in the Mediterranean region

R. Bechini[(1)], V. Chandrasekar* [(2)], and L. Baldini[(2)]
(1) Arpa Piemonte, Torino, Italy, Wash., DC, 20031, http://www.arpa.piemonte.it
(2) Colorado State University, Fort Collins, USA
(3) Institute of Atmospheric Sciences and Climate-CNR, Roma, Italy

One year of data collected by an operational C-band radar in Italy are processed in order to derive meaningful statistics on the vertical profiles of polarimetric radar parameters: reflectivity, differential reflectivity, specific differential phase and correlation coefficident. The polarimetric C-band radar of Torino (Italy), on the top of a 740 m height hill, provides continuous monitoring over the North-West Italy subalpine region, through 5-minutes volume scans. The analysed data were collected between 2009 and 2011. Only events where at least one rain-gauge in the area of interest recorded at least 5 mm of cumulated rainfall were considered, leading to a selection of 64 significant precipitation events.
The derived vertical profiles from the selected events allow a microphysical characterization of the vertical structure of the atmosphere under different precipitating conditions, allowing to identify specific habits and growth/decay processes of precipitation particles .
Of special interest are the high value of K_{dp} repeatedly observed in the ice region of stratiform precipitation system. The regions of enhanced K_{dp} are observed near the -15°C isotherm and are likely related to the growth of plate-like crystals. The observed values of specific differential phase shift are only few tenths of deg/km at S-band but due to the scaling with frequency are accordingly higher at C-band. These values are attributed to the presence of denditric crystals, whose growth is especially favoured in the supersaturated environment around -15°C. Electromagnetic scattering simulations using the T-matrix method are also performed in order to verify the hypothesis about the microphysical origin of these specific polarimetric signatures.

A 449-MHZ WIND PROFILER RADAR WITH LOW-COST 2.5-KW TRANSMITTER

Brad Lindseth* [1,2], William O.J. Brown[1], Jim Jordan[3], Daniel Law[3], Terry Hock[1], Stephen A. Cohn[1], and Zoya Popovic[2]
(1) National Center for Atmospheric Research, Boulder, CO, 80301, http://www.eol.ucar.edu
(2) University of Colorado at Boulder, Boulder, CO
(3) National Oceanic and Atmospheric Administration, Boulder, CO

The National Center for Atmospheric Research's (NCAR) Earth Observing Laboratory deploys sophisticated instruments and networks to support atmospheric research by university investigators. Among these are wind profiler radars and sounding systems, primarily for boundary layer and precipitation studies. In addition to our existing 915-MHz wind profilers, we have recently developed a prototype 449-MHz spaced antenna wind profiler radar. This wind profiler has a modular 54-element hexagonal antenna array that can be expanded to a larger array size and is designed to allow detection of winds at higher altitudes and with better time resolution than the 915-MHz systems. The spaced antenna technique that is used allows computation of horizontal winds from cross-correlation between receivers instead of Doppler shift of steered beams. Low-cost LDMOS 1-kW push-pull pulse amplifier modules are combined to form a 2.5-kW transmitter, with P3dB of 2640W, 63% average drain efficiency at 10% duty cycle, and gain of 15 dB. Coherent and spectral averaging provide detection of radar returns from clear-air Bragg scatter at signal levels of -150 dBm.

The profiler is designed for 2-3 month deployments. A three hexagon/receiver version of the system was initially operated in Boulder and then deployed to the Persistent Cold-Air Pool Study (PCAPS) project in Salt Lake City, Utah during winter 2010-2011. Performance of the 449-MHz wind profiler was compared to radiosondes and a 915-MHz wind profiler at the same location. A seven hexagon/receiver system is currently being built and should be operational in late 2012. The higher transmit power and larger aperture will allow wind profiling through the boundary layer and up to 7 km. These systems will be available for deployment for land or ship-based projects.

Cross-Polarization Reduction of the Phased Array Radar for Precipitation Measurements

Shaya Karimkashi*, Guifu Zhang
Atmospheric Radar Research Center, University of Oklahoma, Norman, Oklahoma, USA

Currently, the National Weather Service uses mechanically steering reflector antenna radars for weather surveillance and hazard detection&warning. However, the data update interval of this system is more than five minutes, which is a significant limitation for severe weather detection and warning. A much faster data update can be achieved using a phased array antenna which uses electronic control of signal producing constructive interference in the desired beam-pointing direction. Although a very fast data update can be obtained using phased array antennas, the cross polarization level is usually higher than that of reflector antennas. Although the cross polarization level can be substantially decreased using the imaged feed configurations [K. Woelders and J. Granholm, IEEE Trans. AP, 45, 1727-1740, 1997], this technique is not effective when the beam is scanned off broadside. The simulation results show that the cross polarization level is substantially increased when the beam is scanned off broadside.

Here, a recently introduced technique is used to reduce the cross polarization level of dual polarization microstrip array antennas [G. Zhang; R. J. Doviak, D. S. Zrnic, J. Crain, D. Staiman, Y. Al-Rashid, Trans. Geoscience and Remote Sensing, 47, 3679-3689, 2009]. Using this method, the co-polar radiation pattern of the H-polarization is used to cancel out the cross-polar pattern of the V-polarization. In order to show the concept, a 4by4 microstrip patch array antenna is designed and modeled at the frequency of 2.71GHz. The simulation results show a very high cross polarization level when the beam is pointed to $\theta = 60°$ and $\varphi = 30°$ (Fig. 1). In order to reduce the cross-polar level, the excitation coefficients of the second polarization (H) are calculated in a way to cancel out the cross-polar pattern of the first polarization (V). Simulation results show that using this technique the cross-polar level has been substantially decreased (Fig. 2).

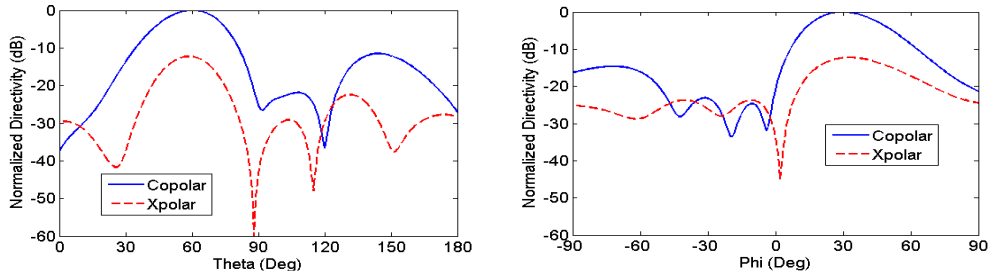

(a) (b)

Fig. 1: The co-polar and cross-polar pattern of the 4by4 array antenna at (a) phi = 30° and (b) theta = 60° planes before correction.

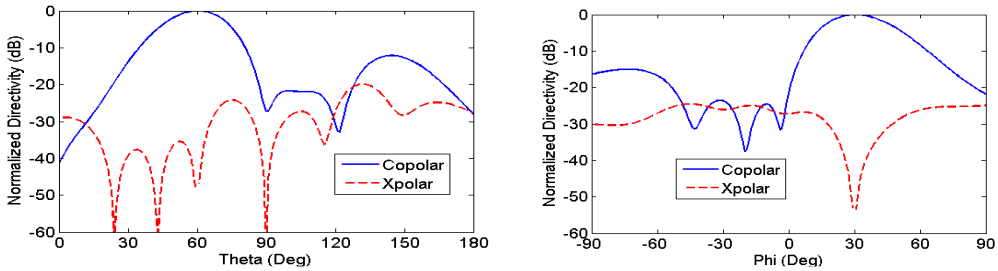

(a) (b)

Fig. 2: The co-polar and cross-polar pattern of the 4by4 array antenna at (a) phi = 30° and (b) theta = 60° planes after correction.

Short Pulse Focused Beam and Power Transfer Through Turbulence and Discrete Scatterers

Akira Ishimaru, Matthew Stoneback, and Yasuo Kuga

Department of Electrical Engineering
University of Washington, Seattle, WA 98195

As a beam wave propagates through a random medium, the beam shape at a short distance may be substantially the same as in free space. However, the beam spot wanders due to random motion of the turbulence. At a short time which is shorter than the wandering time, the beam radius is close to that in free space and is called the short-term beam spread. The wanders of the beam center can be observed when averaged over a longer time. These phenomenons have been intensively studied.

This paper discusses two related topics. One is the propagation of a short pulse focused beam and MCF (Muted Coherence Function). In order to study short pulse propagation, it is necessary to consider two-frequency MCF. For a short exposure, it is also necessary to consider the fourth-order moment and the scintillation index. Secondly, we consider the power incident on the object and the absorbed power. This absorbed power then causes the temperature rise of the object. Two-frequency MCF is used with the complex Gaussian assumption to obtain approximate fourth-order moment. For a short term pulse, the fourth-order moment needs to be used to obtain the peak field inside the target. The second-moment is the average power over a long time. Here we used a short term fourth-order moment, which contains high spatial frequencies and it is assumed that the short term peak intensity is close to the fourth-order moment.

The short term field inside the target is used to calculate the energy absorbed per unit volume during a short time . This absorbed power is used to calculate the temperature rise of the object together with the density and specific heat of the material.

If the object is metal and the incident beam is a high power laser, we can calculate a dielectric constant of the metal by using a Drude model. Calculation is made for copper target, and the temperature rise is calculated for different turbulence strength, aperture size, propagation distance, wavelength and transmitted power.

Polarimetric techniques for identification of biological and chemical materials: Comparison of methods based on Mueller matrices, lateral and surface waves.

Ezekiel Bahar
Electrical Engineering Department University of Nebraska-Lincoln, Lincoln, Nebraska 68588-0511
Phone: 402-472-1966 Fax: 402-472-4732 email: ebahar@unl.edu

Abstract

Optical polarimetric techniques have been used to identify and characterize biological and chemical materials based on their optical activity. They have broad applications in biophysics, biophotonics, biochemistry, biomedicine, and pharmacology. Explicit analytical expressions, in terms of the chiral measure, are presented for the reflection and transmission matrices for waves incident upon an optically active slab surrounded by free space. These expressions are derived for arbitrary angles of incidence in free space and account for multiple reflections within the slab. For optically active materials with small chiral measures, $f = k_1\beta_1$, (k_1 is the wave number of the host medium and β_1 is the chiral parameter) the cross polarized coefficients are proportional to the chiral measure and the like polarized coefficients are not impacted by chirality, up to the first order terms in the chiral parameter f. The analysis was carried out for chiral media characterized by the Drude-Born-Federov constitutive relations and the invariant constitutive relations for gyrotropic media. Explicit expressions for the Mueller matrix elements are also presented. These matrix elements contain the footprints of the optical activity.

The most commonly used technique to extract the parameters related to the optical activity (optical rotation and circular dichroism) and the index of depolarization is polar decomposition, whereby the Mueller matrix is expressed as a product of three matrices, the depolarization, the retardation and the diattenuation matrices due to birefringence of the characteristic waves in optically active media. The principal parameters, optical rotation, diattenuation and the depolarizing coefficient are defined in terms of the elements of the polarization matrix, the retardation matrix and the diattenuation matrix. To perform the polar decomposition it is necessary to accurately measure all sixteen elements of the Mueller matrix. These principal parameters are also expressed in terms of measurements of specific elements of the Mueller matrix that can be measured with a relatively high degree of accuracy at optimal angles of incidence. These elements are proportional to the cross polarized reflection coefficients (to first order in the chiral measure f) that are located in the off diagonal quadrants of the Mueller matrix. Precise physical interpretations of the analytical expressions have been presented. Numerical simulations of these results are in agreement with independent experimental results. Thus only a limited number of measurements of Mueller matrix elements need to be conducted. Built in redundancies of the measurements of specific pairs of Mueller matrix elements can be introduced to reduce the occurrence of false alarms. These measurements critically depend on the angles of incidence.

Explicit expressions have been derived for the like and cross polarized components of the lateral waves and guided surface waves (plasmons). Embedded in the expressions for the cross polarized coefficients are the footprints of the optical activity of the material.

Concept of coherence in adaptive systems and its applications

Valerian I. Tatarskii[1] and Viatcheslav V. Tatarskii[2]

[1] Radio-Hydro-Physics LLC, Fairmont, WV, 26554

[2] Georgia Institute of Technology, School of Earth and Atmospheric Sciences Atlanta, Georgia, 30332-0340

Adaptive optical systems (AOS) are intended for compensation of atmospheric distortions. In the papers Tatarskii, V. I. (1981). "Adaptive systems and coherence. I." Radiophysics and Quantum Electronics 24(7): 590-597 (part 1) and 598-607 (part 2), a new general approach for describing AOS was presented. It was shown that for AOS the common concept of coherence must be modified for conditional coherence. A new statistical characteristic of wave field in adaptive systems, the conditional coherence function

$$\Gamma\left(\mathbf{r}_1, \mathbf{r}_2 | \xi_1, ..., \xi_n\right) = \left\langle u\left(\mathbf{r}_1\right) u^*\left(\mathbf{r}_2\right) | \xi_1, ..., \xi_n \right\rangle,$$

was introduced. Here, $\xi_1[u], ..., \xi_n[u]$ are some measured characteristics of the instant field. For example, they can be measured tilts of wave-front in several points of telescope aperture. The angle brackets $\langle ...|... \rangle$ denote the conditional averaging under condition that the values ξ_i are fixed. It was shown that in the absence of measuring noises this function determines both the optimal structure and the possible advantage of adaptive system. For the case of presence of measuring additive noises an integral equation for the optimal phase correction function was obtained for given set of measured parameters of wave fields at the aperture. An example of random wave field having Gaussian phase fluctuations is considered, for which the problem of determining an optimal phase correction function can be completely solved in explicit form. For this solution, each measured parameter is associated with the specific contribution to phase correcting function. For any signal/noise ratio this function is unambiguously determined by the conventional coherence function.

One of the practical results obtained in this paper is as follows: for any given measured parameters ξ_i of an optical field at the aperture there exist set of optimal phase correction functions $\Lambda_k(\vec{\rho})$, and contribution to the phase correction in a point $\vec{\rho}$ is equal to $\Sigma \xi_k \Lambda_k(\vec{\rho})$. The equation for Λ_k was obtained and its solution for some simple optical systems was determined with account of additive measuring noise. In the papers Tatarskii, V. I. (1982). "Quantum noise in adaptive optical systems. I." Radiophysics and Quantum Electronics 25(8): 632-639, Tatarskii, V. I. (1982). "Quantum noise in adaptive optical systems. II." Radiophysics and Quantum Electronics 25(9): 731-742 the similar consideration was performed for the case of quantum noise (photons counting).

Important advantage of this method is the possibility to perform all necessary calculations of $\Lambda_k(\vec{\rho})$ prior to real measurements. During operation of the adaptive system it will be necessary only to measure phase differences in several pairs of points at the aperture and perform very simple and fast calculations of sum $\Sigma \xi_k \Lambda_k(\vec{\rho})$. This method also can be used in combination with the model-independent AOS for accelerating of calculations by the optimal choice of initial shape of phase correctors. Several examples considered.

Imaging through obscuring media by suppression of diffusion in the mutual coherence function

E. Bleszynski*, M. Bleszynski, and T. Jaroszewicz
Monopole Research, Thousand Oaks, CA 91360, USA

We discuss a method of range measurement in the context of imaging through obscuring random media characterized by scattering-induced attenuation. The proposed technique is applicable to measurements utilizing chirped signals and consists of detecting and appropriate processing the two-frequency mutual coherence function (MCF). In addition to conventional signal compression (by means of a matched filter), the processing involves filtering out small relative-frequency contributions to the MCF. The latter procedure, which we describe as "interference gating", extracts the "image-bearing" component of the *incoherent* contribution to the MCF by counteracting the signal spreading in time, caused by the wave diffusion in the medium. As a result, it allows achieving range resolution inversely proportional to the signal bandwidth.

Our interference gating technique is motivated by properties of the MCF evolution with the propagation distance. That evolution can be described as a sequence of interactions of the propagating field and its conjugate with the medium inhomogeneities; in-between the interactions the field and its conjugate acquire phases proportional to their frequencies. Therefore, if the frequencies of the field and its conjugate are nearly equal, the phases also nearly cancel, and the propagation resembles a random-walk or diffusion. Conversely, by suppressing contributions of small relative frequencies, we can inhibit the diffusive processes; in the remaining contributions, interference of the phase factors corresponding to different frequencies gives rise to aligned wave-type propagation, similar to that of the (coherent) mean field.

The present developments can be viewed as an extension of the previous investigations of the reduced attenuation of wide-band pulses in dispersive media (including random particulate media). The former research concentrated on the propagation of the mean field, i.e., the coherent contribution to the field energy. Here we exploit the fact that part of the energy disappearing from the coherent field is not lost to dissipation, but only scattered, and thus still present in the incoherent component of the MCF (and field intensity). The proposed approach, by utilizing not only the coherent but also image-bearing incoherent contributions to the field energy, allows further increase of the available energy and thus an improvement of the signal-to-noise ratio of the image.

Some Insight into Large Amplitude Small Period (LASP) Surface Scattering

Gary S. Brown, Electromagnetic Interactions Lab., Bradley Dept. of Electrical & Computer Engineering, Virginia Tech, Blacksburg, VA 24061

The problem of scattering of a beam of radiation by a sinusoidally, rough, extended, perfectly conducting, two-dimensional surface is not one that can be dealt with analytically. It becomes particularly interesting when the period or wavelength of the roughness is less than one-half the electromagnetic (EM) wavelength and the amplitude exceeds one-tenth the EM wavelength. This has been called LASP (Large Amplitude Small Period) scattering and it is characterized by unusual electromagnetic behavior. For TE polarization, the current is found to be concentrated on the crests of the sinusoidal surface, the scattered field is an almost exact replica of the field reflected from a flat surface, and the point of scattering on the surface seems to be the crests. For TM polarization, the current is zero on the crests of the surface and appears to concentrate in the trough regions of the surface giving rise to a similar replica of the reflected field that seems to come from the troughs of the surface. It is also found that once the surface wavelength becomes less than one-half the EM wavelength, the nature of the currents for both polarizations do not change, i.e., they may increase in amplitude and shrink in support but they do not change their fundamental shape. This current scaling results in the scattered field appearing even closer to a flat surface reflected field.

In this presentation an explanation will be presented as to why the currents for the two polarizations are significantly different with the edge condition responsible for the TE behavior and standing waves in the trough region of the surface responsible for the TM behavior. These currents have very limited spatial support and effectively lead to a point sampling of the free space Green function at the crests (TE) and troughs (TM) every one-half wavelength or $2k_o$. This sequence of sampled Green functions is exactly as Huygens postulated the manner in which a wavefront travels in homogeneous space. Since the incident field's highest frequency content is k_o, a sampling frequency of $2k_o$ is, according to Nyquist, sufficient to perfectly reconstruct the crest (TE) or trough (TM) fields which, in turn, carry the information about the incident field. Thus, the combined point-like sampling of the incident field by the crests and troughs of the surface combined with the greater than $2k_o$ sampling rate lead to a near perfect replica of the flat surface reflected field.

Boundary Conditions for Radiative Transfer Equations for Layered Random Media

Saba Mudaliar
Air Force Research Laboratory, Sensors Directorate, 2241 Avionic Circle,
Wright-Patterson AFB, OH 45433, USA

Radiative transfer theory has been extensively used in remote sensing applications involving the model of layered random media. In this approach the problem is formulated as a system of radiative transfer (RT) equations together with appropriate boundary conditions. The RT equations very well describe the multiple scattering processes due to volumetric fluctuations. The boundary conditions are imposed separately and independently using the Kirchhoff approximation. To examine the validity of this scheme we follow a statistical wave approach to this problem. The geometry of the problem that we have taken for illustration consists of a random medium layer with rough boundaries. The volumetric and surface fluctuations are assumed to be independent of each other. Using the well known Green's function of the unperturbed problem we represent the electric fields for our problem as a system of integral equation where the volumetric and surface fluctuations are treated in a unified manner. Based on this system of integral equations we proceed to carry out a multiple scattering analysis. First we derive the mean Green's functions by solving the Dyson equation on employing a first order approximation to the mass operator. We next derive an integral equation (Bethe-Salpeter equation) for the coherence function and employ the ladder approximation to the intensity operator. Using the Wigner transforms to link the coherence functions with radiant intensities, we arrive at a system of coupled transport equations for the radiant intensities. On differentiation we obtain the conventional radiative transfer equations in integro-differential form. However, the boundary conditions that we get are quite different from those of the conventional RT system. One reason for this is multiple scattering and coupling of volumetric scattering with surface scattering. In the case of planar interfaces this coupling vanishes and we do obtain the boundary conditions identical to the conventional RT system. However, for the case of rough interfaces the boundary conditions that we obtain are in the form of coupled integral equations. Only on imposing further approximations we can obtain the conventional boundary conditions. We hence see that the boundary conditions associated with the classical RT approach to our problem involve more approximations than believed to be sufficient.

A Study of the Fourth-Order Small Perturbation Method for Scattering from Two-Layer Rough Surfaces

Metin A. Demir[(1)], Joel T. Johnson* [(2)], and Tom J. Zajdel[(2)]
(1) Aselsan, Inc. Yenimahalle, Ankara, Turkey
(2) Department ofElectrical and Computer Engineering and
ElectroScience Laboratory, The Ohio State University, Columbus, OH.

The problem of scattering from two rough surfaces in a layered geometry is of interest due to its applications in the remote sensing of soil moisture, sea ice, and other geophysical effects as well as applications in optics. A variety of methods for predicting scattering have been explored, including both approximate and numerically exact approaches. The small perturbation method (SPM) is an approximate method of particular interest, because it is most applicable at low electromagnetic frequencies where penetration into the sub-surface medium is more likely. The SPM produces a series expansion of observed fields in terms of surface heights. Several recent works have explored scattering in this problem using only the first order term for observed fields. However this approach does not allow the prediction of cross-polarized backscatter, and also neglects any "coupling" effects between roughness on the two interfaces if the two interfaces are assumed to have uncorrelated roughness.

A recent extension of the SPM solution for scattered fields up to third order in surface height will be reported in this presentation. This solution enables the normalized radar cross section (NRCS) for the two-layer problem to be determined up to fourth order in surface height. It will be shown that the fourth order NRCS includes distinct contributions from upper and lower interface roughness, as well as an "interaction" term that couples the upper and lower interface roughness. A comparison with NRCS values computed using the "numerically exact" method of moments in the full bistatic scattering pattern will be shown for verification, and NRCS values at second order and fourth order will also be compared in order to assess convergence of the SPM series. Although the number of parameters inherent in the two-layer rough surface scattering problem makes an exhaustive study of scattering effects difficult, several illustrative examples will be presented to capture a range of scattering behaviors. The results emphasize the importance of interactions between the rough surfaces in producing cross-polarized backscattering, and also indicate an increased significance of fourth-order contributions in the two-layer geometry as compared to the single-layer case.

Bistatic Scattering Effects of a Finite-support Surface Roughness Spectrum

Benjamin A. Westin*, Daniel E. Davis, Gary S. Brown
ElectroMagnetic Interactions Laboratory
Virginia Polytechnic Institute and State University, Blacksburg, VA, 24060

The method of ordered multiple interactions (MOMI) is applied to solving the electromagnetic scattering from randomly rough dielectric surfaces. These surfaces are constructed according to a rough surface power spectral density. Frequently, it happens that the power spectral density of the surface is not well known. For example, the roughness spectrum may be artificially truncated at the low- or high-frequency ends, or the mean-squared height and slope might be erroneous. When the surface roughness is such that Bragg resonance is expected to contribute significantly, placing finite limits on the surface-generating roughness spectrum can have a pronounced impact on the scattering patterns.

This paper discusses the effects that appear in the bistatic scattering when a finitely supported surface roughness spectrum is introduced. For the case of a power-law spectrum, these effects are examined using the incoherent normalized radar cross-section (NRCS) as the extent of the roughness spectrum varies. A steep reduction in the bistatic NRCS is observed in both the forward and backward directions, for angular directions beyond the maximum Bragg-resonant angles of the limited spectrum.

The absence of Bragg scattering is used to demonstrate the increasing importance of a quasi-specular physical optics-type phenomenon as the scattering angle approaches that of specular reflection. This single-bounce scattering reaches its peak value at the nominal specular angle, where it smoothly picks up as the dominant mechanism when Bragg resonance is no longer supported for angles beyond specular. The two physical processes are made apparent by viewing the NRCS for two surface roughness spectra having different low-frequency limits.

The Bragg cutoff is discussed relative to the Fourier transform of the illuminating field, as this contains a spectrum of incident waves, some of which support Bragg resonance and some of which do not. The falloff in the NRCS is less dramatic when a narrowly-tapered incident field creates a broad incident spectrum. Effects of the surface roughness, material properties, and polarization are also considered, as these parameters impact the dominant scattering mechanisms and can lessen the consequence of the roughness spectrum limits. The scattering cutoff is also demonstrated as a means to determine the upper and lower bounds of the roughness spectrum.

3D Scattering from Layered Subsurfaces with Buried Root-Like Discrete Random Media

Xueyang Duan* and Mahta Moghaddam
Department of Electrical and Computer Engineering, the University of Michigan, Ann Arbor, MI 48109 USA.
E-mail: xduan@umich.edu, mmoghadd@umich.edu

Subsurface and root-zone soil moisture is one of the key geophysical quantities in the study of global water and carbon cycles, knowing the global distribution of which will enhance our understanding of the Earth ecosystem, and therefore enable our prediction of long-term climate change in future. In order to measure the soil moisture distribution in a global scale, active microwave remote sensing or radar technology is of great interest for its temporal and spacial efficiency of measurements, and low-frequency (e.g., P-band) radar systems are commonly used for sensing the subsurface and root-zone soil moisture. In order to quantitatively interpret data obtained from these radar measurements, we need accurate and efficient algorithms solving 3D electromagnetic scattering from the subsurface and root-zone structures. Recent researches have been focusing on scattering from either layered rough surfaces or discrete random media, however, no work has been presented to solve scattering from the combining structure of layered surfaces with buried random media, which is a more accurate description of the natural existing vegetated ground. This is the focus of this paper.

In this work, we solve electromagnetic scattering from ground structure of more than three layers (two rough surfaces). Root-like random media with a homogeneous lossy background present in the layer beneath the top ground surface. This random media layer simulates the distribution of vegetation roots, which usually expand within the top 30 cm to 50 cm soil. The bottom layer of the structure is a homogeneous medium modeling the stratum of clay or bedrock, where usually appear no roots and little variation of soil moisture. More layers may exist in between the random media layer and the bottom layer for changing soil composition or dielectric property.

To obtain the total scattering of above structure, scattering matrices (S matrix) of surfaces and layers are cascaded to include all interactions among them. For the random rough surfaces on top and among layers, we solve scattering matrix of each using stabilized extended boundary condition method (SEBCM) that we developed previously. This method has advantages of large validity regime of surface roughnesses over the analytical solutions (e.g., small perturbation method (SPM) and small slope approximation (SSA)), and higher computational efficiency over the full numerical methods (e.g., method of moments (MoM)). The scattering matrix of the root-like random media is obtained by considering it as clusters of cylinders. To find its scattering matrix, we view the cylindrical cluster as cascaded short cylinders, whose transition matrix (T matrix) is solved firstly using extended boundary condition method (EBCM). Then with the generalized iterative EBCM we developed, the T matrix of the cluster can be found, from which, the S matrix is computed through a non-trivial plane wave expansion of spherical harmonics and multipole expansion of plane waves. Besides the rough surfaces and random media layers, homogeneous layer scattering matrices are degraded and used as propagation matrices. Validation has been done for above solutions of rough surface scattering and root-like cylindrical cluster scattering. Results of the combining structure will be presented in this work.

The solution of 3D electromagnetic scattering from layered rough surfaces with buried root-like discrete random medium we present here has more accurate description of the ground exiting in nature. This will help us better understand wave interactions in the subsurface and root-zone soil moisture remote sensing. Further development of this solution includes combination with scattering from the vegetation layer above the ground, and implementing of dielectric profile within the root layer.

Fast Computation of the Second-Order Successive Scattering By Two Scatterers in the Fresnel Region Of Each Other

Ronald J. Hooker* and Roger H. Lang
Department of Electrical and Computer Engineering, The George Washington University, Washington, DC 20052, http://www.gwu.edu

Abstract

In this paper, we investigate successive scattering from tree branches by introducing an efficient approach to determine the scattered field from one branch to another when the branches are near to each other. This sort of higher-order scattering mechanism within a vegetative canopy is of increasing interest to the Earth science remote sensing community. The purpose of the present work is to verify the accuracy and computational efficiency of an analytic scattering model suitable for use in creating higher fidelity canopy simulations. Such applications require these types of calculations for a large number of scatterers, making solutions by numerical methods unacceptably slow. Our approach offers faster results relative to traditional moment methods.

We consider a physical arrangement where the branches may be arbitrarily oriented and in proximity to each other to account for near-field interaction for microwave frequencies of interest (L- through X-Band). First, a successive scattering methodology is used to derive the second-order scattered field for the case of two generic scatterers in proximity to each other. Such a two-body system represents the simplest arrangement to address near-field volume scattering. Next, we apply the general formula to find the second-order bistatic scattering amplitude for a pair of tree branches modeled as finite length thin cylinders. To improve computational efficiency, the solution is then specialized to the Fresnel region. The second-order bistatic scattering amplitude results by the Fresnel model compare favorably with an exact solution over the Fresnel range of interaction distances. Further, it is demonstrated that using the far field approximation for two scatterers in the Fresnel region of one another can yield significant deviations from the exact results.

A methodology to derive fine resolution rain attenuation fields starting from NWP data

L. Luini[(1)], C. Capsoni[(1)]
(1) Politecnico di Milano, Piazza L. da Vinci 32, Milano (Italy), luini@elet.polimi.it

Modern satellite telecommunication (TLC) systems are increasingly being employed for the provision not only of enriched broadcast contents (e.g. High Definition TV with multiple audio tracks), but also of advanced interactive services (e.g. Internet connectivity). For this reason the operational frequency is nowadays gradually shifting from the Ku band to higher bands (Ka and Q/V), which, however, unfortunately implies a much higher sensitivity to the atmospheric constituents, i.e. precipitation, clouds and gases. As a consequence, advanced techniques are necessary to counteract the strong detrimental effects of the atmosphere and thus, to achieve the desired service availability and quality. Among these techniques, commonly referred to as Propagation Impairments Mitigation Techniques (PIMTs), the propagation-based ones take advantage of the non uniform distribution in space of the atmospheric constituents, especially of rain, which has the prevalent impact on radio waves at any frequency. This is the case of site diversity schemes, that rely on the use of properly spaced multiple receiving stations to increase the availability of the system, or of smart reconfigurable techniques which redistribute the common resources available onboard so as to irradiate more power towards the regions severely affected by atmospheric impairments. In this scenario, the design of PIMTs and the assessment of their effectiveness require a detailed knowledge of the meteorological environment (more specifically, of the rainfall spatial distribution) where the system is expected to operate. Unfortunately, high quality rainfall data with the fine temporal (1 minute) and spatial (1 km × 1 km) resolutions required to properly sample the precipitation process are not widely available worldwide. On the other hand, the always increasing availability and accuracy of rainfall products derived from Numerical Weather Prediction (NWP) models or from meteorological re-analysis projects represent a key resource to obtain information on the rain field on a global basis, provided that adequate techniques are applied to somehow remove or mitigate the effects of the long integration time and the large integration area typically characterizing these kind of products.

This contribution shows how rainfall data included by the European Center for Medium-range Weather Forecast (ECMWF) in the ERA40 database can be employed to derive detailed information on the rain field over large areas (country or continental scale). Specifically, the total rain amount, M_t, and convective rain amount, M_c, accumulated in 6-hours on a 1.125°×1.125° latitude/longitude grid, are firstly used to derive an estimate of the rain rate spatial distribution, in terms of complementary cumulative distribution function (hereinafter indicated as $P_S(R)$), for each pixel in the area of interest and relative to the accumulation interval. As a further step, the MultiEXCELL model, modified so as to receive as input the estimated $P_S(R)$, is employed to generate radar-like synthetic rain fields with fine spatial resolution (1 km × 1 km) which can be employed, for example, to design and operate an onboard reconfigurable antenna system, to evaluate the effects of precipitation on radio links between an Earth station and an Earth Observation (EO) satellite or, again, to dimension the space-segment resources of an advanced system using ACM (Adaptive Coding and Modulation). The methodology described in this contribution represents the main step towards the development of a comprehensive NWP-driven tool aimed at assessing the impact of all atmospheric constituents, i.e. also of clouds and gases, on advanced satellite TLC systems.

WORLDWIDE DUCTING PROBABILITIES FROM RADIOSONDE DATA: A COMPARISON OF HISTORICAL AND MODERN DATA

T.R. Hanley* [(1)], J.Z. Gehman[(1)]
(1) The Johns Hopkins University Applied Physics Laboratory, Laurel, MD

Radio frequency (RF) ducting phenomena can give rise to anomalous propagation for low-elevation-angle paths in the troposphere that can severely impact the performance of communications and radar systems. RF ducting is induced by strong vertical gradients in temperature and (especially) water vapor. Meteorologically, these gradients are usually associated with boundary layer inversions. The statistical nature of these phenomena is often budgeted in system design and link margins. The probabilities of ducting occurrences can be estimated for locations around the world based on historical radiosonde data.

Radiosondes, which are commonly referred to as weather balloons, measure temperature, relative humidity, barometric pressure, and winds as a function of altitude. They are normally launched twice daily at hundreds of stations around the world and have been for well over half a century. These radiosonde data, sampled at so-called "mandatory" and "significant" altitudes, are shared worldwide and cataloged by various agencies. Several analyses of ducting occurrence have utilized these data. Prominent examples include Bean, et al.'s 1966 "World Atlas of Atmospheric Radio Refractivity," SPAWAR Systems Center Pacific's Ducting Climatology Summary (DCS) (based on a 1977 GTE Sylvania report), as well as ITU-R Recommendation P.453 (last updated in 2003 using radiosonde data from 1977-1996). These references are still in widespread use today for RF systems design and analysis efforts.

Numerous improvements in radiosonde technology and reporting practices have been made since these studies were performed. Temperature and humidity sensors now have greater accuracy and faster response times, making them better at measuring the steep gradients that give rise to ducting. Automated detection of significant levels and an emphasis on more reporting levels has led to greater vertical resolution over time. And recently, several stations in the US have started cataloging their data at full vertical resolution (typically 5 meters in altitude) as a part of the National Weather Service's Radiosonde Replacement System (RRS).

Statistics from various radiosonde launch sites will be presented to show that these sensor and reporting changes have a significant impact on duct-occurrence statistics. Further analyses between high-resolution (5 meter) data and the mandatory/significant level data will be presented showing the impact of vertical sampling and ground station bias on ducting statistics.

WRF-model assimilation of angle-of-arrival excess measurements from an antenna of GPS receivers

Francois Vandenberghe*(1), Bonnie Valant-Spaight [(2)] and Martin Hall[(3),]

(1) National Center for Atmospheric Research, Boulder, CO, USA
(2) Propagation Research Associates Inc., Marietta, GA, USA

The concept of the assimilation of the bending angle caused by atmospheric refraction of the electromagnetic signal emitted by one of the GPS satellites and received by a low earth orbit satellite has been demonstrated in 1995 during the first GPS Met experiment. With the launch of the COSMIC constellation in 2006, bending angle assimilation in global models is now becoming a routine operation in most meteorological operational centers. The concept has been extended for GPS ground receivers and regional models. By tracking a GPS satellite with an antenna of receivers, it is possible to estimate the difference between the satellite elevation angle and the actual arrival angle of the transmitted signal in the line of sight of the antenna. The concept was demonstrated during a field campaign at Vandenberg AFB during the month of August 2009. 60 hours of transmission were recorded, resulting in more than 200,000 angle-of-arrival excess (AOAE) measurements were collected. Those measurements were assimilated through the use of a fast raytracing observation operator and its adjoint into a high-resolution (Δx=3.3km) version of the Weather Research and Forecast model. The results of the AOAE data assimilation, in terms of 6-hr forecasts, were compared to similar runs without observations and with assimilation of conventional observations (sounding, surface reports, aircraft, etc). Preliminary verification statistics against independent data show significant improvements in model forecast skills for wind speed and direction and a slightly negative impact on temperature and moisture. AOAE observations and the method for their assimilation in numerical weather prediction models will be presented; the potential of the technique for supporting electronic wave propagation will be discussed.

A Comparison of Measured and Modeled Meteorology for a Unique Data Set

Victor R. Wiss*[(1)], Isha M. Renta [(1)], and Katherine L. Horgan[(2)]
(1) Naval Surface Warfare Center Dahlgren Division, Dahlgren, VA USA

In September of 2010, a unique opportunity was taken to make multiple, simultaneous balloon sounding measurements of the marine atmospheric boundary layer in the area of Wallops Island, VA USA, along a radial from the shore line to a distance of approximately 30 nmi from shore. Previously, the only way to obtain several atmospheric profiles along a bearing was to fly a sawtooth pattern using a properly-instrumented helicopter, providing profiles offset in time. The method used at Wallops Island, VA provided vertical profiles coincident in time but fewer profiles than the helicopter technique. During this event, the Coupled Ocean / Atmosphere Mesoscale Prediction System (COAMPS®) provided numerical weather prediction analysis and forecasts during the timeframe of the sounding measurements. Also measured were the bulk meteorological parameters necessary for evaluating evaporation ducting at the locations of and simultaneous to the balloon soundings.

This paper will describe the weather conditions present during the test event, and show a comparison of measured meteorological data to the COAMPS® modeled data for the over-water radial of interest for both balloon soundings and surface measurements. The analysis will include modified refractivity profiles along the bearing of interest calculated from both measurements and COAMPS® model output. These results will include evaporation ducting calculated by the Naval Surface Warfare Center Dahlgren Division (NSWCDD) Surface Layer Blending Technique (SLBT) for both the COAMPS® model data and balloon sounding measurements. The impact of radio frequency propagation on a notional radar will be shown for both the measured and modeled refractivity environments.

Horizontal Resolution Comparison in the Coupled Ocean / Atmosphere Mesoscale Prediction System (COAMPS®) and its Effect on Refractivity During a Sea Breeze Event

Katherine L. Horgan*[(1)], Robert E. Marshall [(1)], and Tracy Haack[(2)]
(1) Naval Surface Warfare Center Dahlgren Division, Dahlgren, VA USA
(2) Naval Research Laboratory, Monterey, CA USA

Sea breeze circulations are created by the differential heating of land versus water in coastal regions. This temperature difference results in a circulation that advects moist air off the sea over the land. The resulting vertical moisture gradient has been shown to be of significant strength to create surface-based ducting in the littoral regions. Sea breezes are most common in the summer when temperature differences between land and water are maximized.

A strong sea breeze circulation was observed off the Baja peninsula during the daytime hours of 27 – 29 June 2005. Twelve radiosonde measurements were taken from a ship that moved around the peninsula over the course of the three sea breeze days, measuring effects in the Bay of California and at two different places along the oceanside of the Baja peninsula. Surface-based ducting was measured in all twelve radiosondes. The Coupled Ocean / Atmosphere Mesoscale Prediction System (COAMPS®) was run over the region to study the effect of horizontal resolution on refractivity predictions. The COAMPS® domain included grids at 81, 27, 9, 3, and 1 km horizontal resolution with 70 vertical levels, spaced throughout the vertical domain. Earlier studies that have compared horizontal resolution in NWP models over Wallops Island, VA USA indicated a point of diminishing returns when horizontal resolution is decreased past 3 or 4 km. This discrepancy may be due timing of synoptic scale features that cause ducting events.

This study will focus on the results from the 9, 3, and 1 km horizontal resolution grids. Initial results show an improvement in the refractivity forecast from 9 km to 3 km horizontal resolution when comparing the mean normalized bias and root mean square error. Performance statistics for duct height, M-deficit, and critical angle will be presented along with comparisons of multi-wavelength notional radar performance at the three resolutions.

The Role of Planetary Boundary Layer Physics in Mesoscale NWP Model-EM Propagation Predictions

Tracy Haack
Naval Research Laboratory-Monterey, Marine Meteorology Division

URSI/NRS Meeting
Boulder, CO
4-7 January 2012

Studies of atmosphere-ocean heterogeneity in littoral settings have amplified the importance of several key aspects of high-resolution numerical weather prediction (NWP) modeling systems that are now routinely used to gauge environmental effects on radars and sensor performance. These studies have previously revealed the larger role of lateral boundary conditions on establishing the broad-scale "weather" scene and air-mass transitions, while illuminating the more subtle effects of increased spatial resolution in the model, both horizontal and vertical, as well as in the sea surface temperature (SST), on variability and accuracy in predictions of the littoral environment. Diurnal changes in near-shore SST of 2-3º were shown to affect both the onset and duration of coastal ducting events off Wallops Island, VA despite large synoptic forcing often present there in the springtime, indicating the necessity of fully-coupled air-sea modeling. In this study we examine another crucial component of the Navy's high-resolution prediction system COAMPS®[1] influencing atmospheric ducting and electromagnetic (EM) propagation, the role of planetary boundary layer (PBL) physics. All NWP models contain a PBL parameterization used to represent vertical mixing and turbulent processes between and within model layers. These physics describe how heat, moisture and momentum are fluxed through the atmosphere and are primarily responsible for its vertical gradient structure that determines the strength, height and thickness of trapping layers.

The current PBL in COAMPS is a turbulent-kinetic-energy (TKE) based, local mixing scheme which allows for strong mesoscale circulations and high spatial variability. However, statistical analysis of important parameters within the PBL against vertical profile measurements off Wallops Island suggests a cool, moist bias exists above the surface layer. In the present study, we investigate whether the over-prediction of moisture is a result of TKE vertical transport by comparing results of two other commonly used PBL schemes available from the Weather Research and Forecasting Model (WRF) physics package. Both are 'non-local' mixing schemes within a PBL determined by the bulk Richardson number -- the ratio of mechanical to thermal energy. Although the two WRF schemes are similar otherwise, one (YSU) outperforms the other as it has been modified to increase mixing over the stable ocean and in the entrainment layer at the PBL top. The YSU also showed improvement over COAMPS TKE by reducing mean temperature and moisture biases for the 7-day observation period in April/May 2000 off Wallops Island.

[1] COAMPS is a registered trademark of the Naval Research Laboratory.

Analysis of Southern California Climatology for Modeling and Simulation Applications

Ian Will
Naval Research Lab, 4555 Overlook Ave. SW, Wash., DC, 20375

The region of Southern California is a frequent location for various operations of the US Navy. Many of these are supported by modeling and simulation efforts that require representations of the natural environment for proper assessment of system performance. In order to support one such modeling and simulation effort, a typical week is being recreated in high resolution for use in a variety of models of different types. However, what defines "typical?" How can "representative" be quantified? Which week in the past decade is the most typical of the Southern California climate? Can these qualitative adjectives be quantified relative to a particular region's climate and the needs of the modeling and simulation community?

To begin addressing this one must first define the needs of the modeling and simulation community. These will be discussed in terms of classes of models with each having primary and secondary environmental factors. Primary factors are the factors which impact model performance most significantly, secondary factors are those which impact model performance to a lesser extent, or from which other primary factors are derived.

Once the factors which impact a model's performance are understood, one must consider how those factors are expressed in a particular region over an annual cycle. To understand those, historical measurements of those factors must be accessed and characterized. Potential sources include archives of measurements, such as those collected by data buoys or radiosondes. Another source are global re-analyses, such as the Climate Forecast System Reanalysis undertaken by the National Oceanic and Atmospheric Administration's National Center for Environmental Prediction in 2009. These re-forecast data sets have many advantages, but also some potential pitfalls for certain factors. The relative merits of these sources will be discussed and those used in my analysis will be highlighted.

After the typical annual expression of pertinent environmental factors is understood, one must consider comparative analysis of specific measurements against others. When there are many factors involved, this can be challenging to optimize. One approach is to use a mean square error against a hypothetical mean instance as a common measurement. The report will discuss the details of my implementation and present the results.

Uncertainty Projection Between Refractivity From Clutter and Numerical Weather Prediction

Caglar Yardim*[(1)], Ali Karimian [(1)], Peter Gerstoft [(1)], and Ted Rogers[(2)]
(1) Marine Physical Lab, UCSD, La Jolla CA, USA
(2) SSC Pacific, San Diego CA, USA

Numerical weather prediction (NWP) methods such as the Coupled Ocean Atmospheric Mesoscale Prediction System (COAMPS) have been used successfully to predict the lower atmospheric refractivity profile. The meteorological parameters can be converted into range-dependent M-profile and/or evaporation duct height information.

Refractivity from clutter (RFC) refers to techniques that estimate the atmospheric refractivity profile from radar clutter returns. This is done using a split-step fast Fourier transform based parabolic equation approximation to the wave equation which can compute the clutter return in complex environments with varying index of refraction. It can give more detailed duct height information both spatially and temporally but it only works within the radar range and it has some inherent limitations such as inability to detect elevated ducts.

It is possible to improve both methods and get more reliable ducting information buy using them together. In such a scenario, NWP is first used to predict the ducting condition and then RFC starts the inversion from data obtained from NWP. Hence the RFC will perform data fusion using NWP, radar clutter, and climatology statistics. The resulting refractivity and uncertainty can be projected into meteorological parameter domain and enable NWP to update its estimate, again fusing the data from these two sources. Work presented here is the results of a preliminary study about how the RFC output (in terms of evaporation duct height and along with its uncertainty) will affect atmospheric properties such as temperature, wind speed, humidity, etc. These can be merged with the parameter uncertainties obtained by ensemble methods to get better NWP results. The analysis is performed using the Navy Atmospheric Vertical Surface Layer Model (NAVSLaM).

Numerical Weather Prediction Supporting Advanced Radar Technology Integrated System Testbed Integration and Trials Test Effort

Dr. Lonnie E. Carpenter*[(1)], Katherine L. Horgan [(1)], Isha M. Renta[(1)],
and Victor R. Wiss[(1)]
(1) Naval Surface Warfare Center Dahlgren Division, Dahlgren, VA USA

The Advanced Radar Technology Integrated System Testbed (ARTIST) Program was a joint program between the United Kingdom and the United States. Each country developed their own system testbed (radar) and then integrated technologies into those testbeds. The program culminated with both the UK ARTIST Radar and the US ARTIST Radar being installed at Wallops Island, VA with the technologies being demonstrated side by side in this maritime environment. The site installation, system testing and integration and trials occurred from February 2010 to November 2010.

From early March to the end of trials in November numerical weather prediction was performed in support of this testing. This paper will focus on the classic ways that numerical weather prediction supported RF propagation prediction but will also touch on the other impacts to radar testing that were supported by numerical weather prediction. Those familiar with propagation analysis are aware of the large data set from Wallops Island testing of 2000. That data set contains a large variety of propagation conditions. As a result of this history, mesoscale weather models were run with a 3 km by 3 km grid over Wallops Island, VA generating environmental prediction in 4 hour increments. Four to Five of these environmental files were generated to support the 16 to 20 hours of daily on site testing. These files were then input into Advanced Refractive Effects Prediction System (AREPS) with a common generic radar model with sufficient fidelity to predict impacts to each of the radar systems.

The results of performing these predictions impacted both phases of testing. These results prevented valuable integration and system test time being wasted on phenomenology that was environmentally based. It also showed success predicting the azimuthal and time varying characteristics of the propagation. The trials portion was impacted by giving insight into the amount of time necessary to assess the propagation dependent clutter environment. These propagation forecasts were used by the US and UK teams in evaluating their radar set ups and the need for clutter collection in advance of the days trials to tune set ups. Finally, the time variant characteristics were used to decide if these clutter collection and tunings needed to be performed during breaks in the trials. Finally, the numerical weather prediction model was use to make go/no go decisions with respect to trials. Some trials were dependent on sea conditions for safety of personnel, on these days outputs from the model fed the decision process along with meteorological buoy data. Another important characteristic for radar testing over water is sea clutter, surface wind prediction combined with the meteorological buoy data were important in prediction when variations in this clutter environment would occur over different days.

Characterizing Near-Surface Refractivity Conditions when Using Numerical Weather Prediction Model Data for Electromagnetic System Performance Predictions

Paul Frederickson
Department of Meteorology, Naval Postgraduate School, Monterey, CA

The U.S. Navy is becoming increasingly reliant on the use of numerical weather prediction (NWP) model data to predict electromagnetic (EM) system performance for operational planning purposes. A major challenge when using NWP model data for such purposes is properly characterizing the horizontally and time-varying surface-layer refractivity conditions, especially the evaporation duct. The evaporation duct is a ubiquitous and persistent refractivity feature that forms just above the ocean surface that has a very strong impact on near-horizon propagation. Since NWP models have insufficient vertical resolution to characterize the evaporation duct and often must use simplified surface-layer parameterization schemes, a 'bulk' surface-layer refractivity model must be used with NWP-based EM prediction systems. The surface-layer model uses the NWP data fields as input to produce near-surface vertical refractivity profiles at each grid point that can properly resolve and characterize the evaporation duct.

Surface-layer refractivity models rely upon empirical Monin-Obukhov similarity theory dimensionless profile functions to produce an estimate of the near-surface modified refractivity profile. Many different functions can be found in the literature and the choice of functions used in different stability conditions has a strong impact on the resulting behavior of the evaporation duct model. In this presentation we will examine the impact of using different profile functions on EM propagation predictions. In addition, the bulk model refractivity profiles must be smoothly blended onto the bottom of the NWP model refractivity profiles in such a way that prevents erroneous refractivity features from being introduced into the resulting profile and that also preserves the shape of the surface-layer model refractivity profile in most instances. In this presentation we examine and compare the use of different refractivity profile blending schemes in different stability conditions and model situations and present comparisons with actual combined meteorological and propagation measurements from field campaigns.

Radio Science at the 2012 World Radiocommunication Conference

Andrew W. Clegg
National Science Foundation
Arlington VA 22230

The International Telecommunication Union (ITU) holds a World Radiocommunication Conference (WRC) approximately every three to four years. At the WRC, delegates from virtually all radio-using countries around the world meet for several weeks to discuss and resolve technical and regulatory issues related to well-defined agenda items that were established at, and studied since, the previous WRC. The end results of a WRC include agreements for modifications to the ITU's Radio Regulations, which in turn are usually adopted by individual administrations for incorporation in their own domestic rules and regulations governing the use of the radio spectrum. The next WRC (WRC-12) begins on January 23rd, 2012, and will be held at the ITU headquarters in Geneva, Switzerland.

The WRC-12 agenda includes several items of interest to the radio science community. These topics include: the use of frequencies between 275 - 3,000 GHz by passive services including radio astronomy and remote sensing; the allocation of spectrum to the space research service (Earth-to-space) in the band 22.55 - 23.15 GHz; allocations to HF and VHF oceanographic radars in the range 3 - 50 MHz; consideration of the needs of passive lightning detection systems in frequency bands below 20 kHz; and the consideration of a new allocation to the amateur radio service in parts of the band 415 - 526.5 kHz.

This talk will summarize the status of the studies related to these agenda items going into WRC-12, and, to the extent practicable, present the most likely outcomes and their impact to the radio science community.

Radar Power Amplifier Spectrum Optimization for Chirp Waveforms Using ACPR Load-Pull Measurements

Josh Martin[(1)], Matthew Moldovan[(1)], Charles Baylis[(1)] and Robert J. Marks II[(1)]
(1) Wireless and Microwave Circuits and Systems Program, Department of Electrical and Computer Engineering, Baylor University, Waco, TX 76798-7356

Radar transmitters must operate with high power efficiency while abiding within increasingly strict spectral requirements. Spectral masks govern the out-of-band leakage that can be produced; this leakage is a byproduct of both the waveform and the load impedance terminating the amplifier. Spectral leakage can be minimized to meet spectral mask requirements by increasing the linearity of amplifier operation. A recent conference paper submission details a test-bed concept that has now been constructed at Baylor University to enable the joint optimization of the waveform and load impedance for linearity and efficiency (Baylis *et al.*, IEEE Waveform Diversity Conference, Submitted June 2011). Maximizing the power transmitted and the associated power efficiency are critical to preserving the detection capabilities of radar systems. Achieving power efficiency often comes at the cost of linearity, creating a tradeoff between linearity and efficiency in power amplifier design that has been well documented. Load-pull is a type of microwave measurement that can be used to vary load impedance (and hence reflection coefficient) to try to optimize the power-added efficiency and the linearity. The linearity is often measured in the load-pull using the adjacent-channel power ratio (ACPR), which is the ratio of the power over a specified bandwidth in the neighboring channel to the power over a specified bandwidth within the assigned channel for the signal. ACPR load-pull hence measures the spectral leakage directly for different load impedances and provides a metric for which the load impedance can be optimized. Load-pull has been successfully demonstrated for digital signals in several works, including ACPR load-pull for digital signals; however, most of this work has a communication focus. Our work applies load-pull to radar transmitter optimization.

This paper focuses on performing load-pull measurements to assess the tradeoff of linearity and efficiency for different chirp waveforms. MATLAB has been used to create and upload two radar-specific waveforms into a signal generator: a linear up-chirp and linear down-chirp. As these chirps were passed through an amplifier driven into its nonlinear region, spectral spreading was observed in the amplifier output spectra for the two waveforms. ACPR load-pull was used to find the load impedance that minimizes this unwanted spectral spreading.

We demonstrate load-pull results for a 2-dB compression input power of a packaged amplifier for the up-chirp and down-chirp waveforms. The minimum "high-channel" ACPR was found to be -31.44 dBc for the up-chirp waveform and -33.50 dBc for the down-chirp at very similar reflection coefficients. This indicates that lower spectral leakage seems to be obtained for the down-chirp waveform. The maximum output power results for the up-chirp (18.86 dBm) and down-chirp (18.93 dBm) are very similar. The conclusion from the data is therefore that the down-chirp seems to produce slightly better linearity, while the output power for both waveforms is similar. The paper details an experimental approach to apply this new test bed for optimization of load impedance over different chirp waveforms. This sets the stage for developing a computationally intelligent search that will allow testing of multiple chirp waveforms with impedance variation.

Revising ITU-R Recommendation P.528 to Support Satellite Frequency Sharing Studies

Teresa L. Rusyn
U.S. Department of Commerce, NTIA/ITS, Boulder, Colorado, 80305, USA,
http://its.bldrdoc.gov

Sharing frequency bands is now necessary in aeronautical and satellite services as well as terrestrial wireless services. However, the propagation models used for frequency sharing studies for terrestrial systems does not accurately predict interference levels for the aeronautical and satellite based systems. ITU-R recommendation P.528 is based on curves calculated by the IF77 propagation model. It is the appropriate recommendation to use in such cases. Unfortunately, the curves and limited development in the recommendation are barely useful in today's world of satellite interference issues.

An international correspondence group within Study Group 3 of the ITU-R is revising P.528. The plan for the revision effort is using a two-stage approach. The first stage will reformat and expand the current set of curves and will include an interpolation method for the five parameters required by the recommendation. The second stage, which will be starting in 2012, would move away from the curve based method and develop a computational method.

Presently, recommendation P.528 contains only a limited set of curves, but, perhaps the biggest limitation in the recommendation is that there is no guidance for interpolation between the curves. The first revision adds two frequencies, three antenna heights (to h1 only), and two time percentages. The revision, also, includes an interpolation method for antenna heights h1 and h2, distance, frequency and time percentage.

The second revision effort will develop a computational method based on the IF77 propagation model. This work will be a multi-year effort and will start after the first revision is presented to the Study Group 3 meetings in October 2011.
Revising ITU-R recommendation P.528 is essential to support the present situation of frequency sharing. There is a multi-year, multi-stage effort working on revising the recommendation. The first revision of P.528 is a short term solution to increase the recommendation's usability while the second revision is being completed.

2011 Spectrum Survey Occupancy Measurements in Denver, CO

Chriss Hammerschmidt, Heather Ottke, Randy Hoffman
NTIA, Institute for Telecommunication Sciences
Boulder, CO

The Institute for Telecommunications (ITS), the research laboratory for the National Telecommunications and Information Administration (NTIA), has recently completed the first of several spectrum occupancy measurement campaigns. The measurements spanned a frequency range from 108 MHz to 10 GHz. Specialized techniques were used to capture the characteristics of different types of emitted signals. A brief discussion of measurement techniques will be followed by results from our most recent measurement campaign.

The president released a memorandum tasking NTIA, in collaboration with the Federal Communications Commission (FCC), "to make available a total of 500 MHz of Federal and nonfederal spectrum over the next 10 years suitable, for both mobile and fixed wireless broadband use." We believe one of the ways to find this new spectrum is to measure the occupancy of the existing spectrum. ITS uses its state-of-the art mobile spectrum measurement laboratory called the Radio Spectrum Measurement Sciences (RSMS) truck which provides 60 dB of shielding from outside radio sources. The measurement system uses a combination of antennas, preselector/preamplifiers, spectrum analyzers, and computers. Our goal is to measure the radio spectrum at locations either chosen by us or those associated with NTIA's report, "An Assessment of the Near-Term Viability of Accommodating Wireless Broadband Systems in the 1675-1710 MHz, 1755-1780 MHz, 3500-3650 MHz, and 4200-4220 MHz, 4380-4400 MHz Bands."

We have developed several measurement methods customized for specific signal emission types. These are spectrum-swept, spectrum-stepped, time-domain with FFT processing, azimuthal-scanning, and stepped-amplitude probability distribution (APD) algorithms. Spectrum-swept measurements are the most general type of measurement method and are applied to the most types of signals. Spectrum-stepped measurements were specifically designed to measure radar emissions. Time-domain measurements with FFT processing were designed to minimize the influence of impulsive noise in Land Mobile Radio (LMR) emission bands. Azimuthal-scanning techniques are designed to measure emissions in the point-to-point microwave bands and stepped-APD measurements are designed to measure and insert attenuation in bands where both low- and high-level signals coexist.

Spectrum Challenges in Radar Design

Lawrence Cohen*(1), Eric L. Mokole (1)
(1) Naval Research Laboratory, Wash., DC 20375, USA

The spectrum environment worldwide has changed drastically in the last 5 years. With the explosion of wireless systems in the traditional frequency bands where radar reigned as primary for decades, radar designers are challenged by how to coexist with these wireless systems. Given the thirst for high-speed broadband and the revenue that it brings to companies and governments, the desire for traditional radar spectrum will continue to grow. The band from 3000-4000 MHz is in contention because wireless and radar systems have very good RF propagation characteristics at these frequencies. This presentation explores current and future radar frequency bands that may be jeopardized by the infiltration of WiMAX and Long Term Evolution (LTE). Not only are the transmitter topologies and waveforms for radars addressed, but their possible effects on the operation of wireless systems like WiMAX and LTE are also discussed. As a means of mitigating interference between the radar and wireless communities, potential designs of radar transmitters for achieving more spectrally efficient radars are presented. Furthermore, possible undesired impacts of wireless type signals, particularly OFDM, on radar receivers and design steps that lessen these negative effects are discussed. Finally, the concept of coexistence through cognitive radar/radio is explored. In particular, cognitive radar/radio is defined, and the required components and technological hurdles that need to be overcome for successful radar operation in contested radar spectrum are addressed.

Third-Order Intermodulation Products, What They Mean and How They are Measured

Eric L. Mokole*(1), Lawrence Cohen(1), and Tegan Webster(1)
(1) Naval Research Laboratory, Wash., DC 20375, USA

Intermodulation is defined as the modulation of the components of a complex wave by each other, producing new waves whose frequencies are equal to the sums and differences of integral multiples of the component frequencies of the original complex wave (N. Sclater and J. Markus, McGraw-Hill Electronics Dictionary 6th Ed., 234, 1997). Many receivers, in radars and communications systems, use low noise amplifiers (LNA) and mixers as part of their analog processing chain. LNAs are operated in the linear portion of their characteristic curve to avoid the generation or mixing of the components of the complex signal to be amplified. Mixers, on the other hand, take advantage of the modulation process to down convert a signal, usually from a higher frequency to a lower frequency for ease in further amplification and processing. Unfortunately, desirable and undesirable signal components can cause an LNA to become non-linear, which can result in the generation of in-band spectral products. Likewise, a mixer can also process these components, resulting in unwanted in-band components. Generally, the voltage transfer function of any non-linear device, saturated LNA, or mixer can be expressed as a Taylor series in terms of the input voltage. The cubic term in the Taylor series results in the generation of third-order intermodulation products. Third-order intermodulation products are particularly troublesome because they generally cannot be filtered and consequently fall within the desired passband.

This presentation reviews the theory behind the generation of intermodulation products and in particular the third-order products. Several scenarios are modeled and discussed. Finally, the quantification of third-order intermodulation products through the application of a two-tone test is described, with sample results shown for a given receiver LNA-mixer configuration.

Radio Frequency Interference Analysis of L-band Microwave Radiometry Missions

Mustafa Aksoy*, Joel T. Johnson
Dept. of Electrical and Computer Engineering and ElectroScience Lab,
The Ohio State University, Columbus, OH, USA

There are three missions either currently operating or planning to operate L-band microwave radiometers in orbit for observations of soil moisture and ocean salinity. ESA's Soil Moisture and Ocean Salinity (SMOS) mission has been providing brightness temperature measurements since Nov 2009 and NASA's Aquarius mission began observations in August 2011. NASA's Soil Moisture Active/Passive (SMAP) mission, scheduled for launch in 2014, will continue these measurements into the future.

SMOS provides multi-angular fully polarimetric observations through the use of an interferometric radiometer. SMOS data has a 1.2 second time resolution in a single frequency channel. Aquarius also uses a single frequency channel in a real-aperture, three antenna footprint measurement, but provides a finer time resolution of 10 msec to improve the detection and mitigation of pulsed interference. Aquarius also provides measurements of the 3rd (but not 4th) Stokes parameter of the observed scene. SMAP will use a single footprint real-aperture system and will provide all four Stokes parameters, but will also include a digital backend to enable both time and frequency resolution, as well as computation of kurtosis properties of observed fields.

Despite operating in the protected 1400-1427 MHz portion of the microwave spectrum, both SMOS and Aquarius show significant RFI corruption; numerous studies are in progress to detect and mitigate RFI for these missions, especially the difficult-to-detect "low-level" interference case.

In this presentation, characteristics of the SMOS, Aquarius, and SMAP observations will first be reviewed and compared for their expected ability to detect and mitigate RFI. RFI analyses of SMOS data will then be discussed. Artifacts detected in initial SMOS data and an example artifact clearance algorithm will be presented. Sample spatial, temporal and statistical RFI properties of SMOS observations will also be reported. Initial RFI analysis results for Aquarius data will also be provided, as well as comparisons of SMOS and Aquarius RFI properties. Attempts to develop algorithms for "low level" RFI by correlating SMOS and Aquarius observations and utilizing their polarimetric, multi angular (SMOS) and temporal (Aquarius) properties will also be presented. Finally, implications of these studies for the design and development of RFI detection and mitigation approaches for NASA's SMAP system will be discussed.

RFI analysis and algorithm development using direct-sampled data measured during the CARVE flight mission

Sidharth Misra*, Sharmila Padmanabhan, Ian O'Dwyer, Steve Dinardo and Todd Gaier
Jet Propulsion Laboratory, California Institute of Technology, Pasadena, CA

In recent years passive microwave measurements made by space-borne and air-borne missions have been corrupted by man-made Radio Frequency Interference (RFI) sources. Measurements from satellite missions such as SMOS show that even the protected 21cm hydrogen line is affected by RFI (Balling et al., TGRS 2010). The following talk will focus on RFI observed by flights made under the CARVE ventures program. Passive microwave data at L-band was obtained from flights over Grand Junction and Alaska during Fall 2010. Measurements were made using the Passive/Active L/S Band (PALS) radiometer, with a direct sampling digital backend.

The direct-sampling digital backend developed under a JPL R&TD demonstrator program is the key technology that allows for advanced RFI analysis and new algorithm development. The backend measures raw radiometer pre-detection voltages at a high sampling rate and full observed bandwidth. This data set allows the implementation of any RFI detection algorithm in post-processing at variable radiometer integration period.

The flexibility of the digital backend allows analysis of the performance of the various RFI detection algorithms currently in use. The pre-detected samples measured at a fine temporal resolution allows the formation of an RFI "ground-truth" based on which other detection algorithms can be compared. The CARVE backend data is used to analyze, compare and contrast the temporal based "glitch-detector" algorithm implemented by the Aquarius mission (Johnson et al., TGRS 2004; Misra and Ruf, TGRS 2008), the spectral based Cross-Frequency RFI detector developed by (Guner et al., TGRS 2010) and the statistical based kurtosis detection algorithm (Ruf et al., TGRS 2006) implemented by the SMAP mission. As noted in (Misra et al., 2009; Misra et al., TGRS 2010), these individual RFI detection strategies perform poorly based on certain types of RFI observed. An optimal combination of these RFI detection strategies would remove such deficiencies and enhance RFI detectability. The following talk will also discuss the development of such an optimal detection algorithm.

A brief description of the CARVE flight campaign and hardware will be presented. Results from the RFI analysis will be discussed comparing the performance of different detection and mitigation algorithms. Initial results for the development of an optimal RFI detection algorithm will be presented. Further work resulting in the development of new RFI detection algorithms will also be discussed.

MITIGATING WIND TURBINE INTERFERENCE TO RADAR BY ADAPTIVE PROCESSING BASED ON TELEMETRY

Fanxing Kong[1,2], Yan Zhang[1,2] , Robert Palmer[1,3], Ying Bai[1,2]
1 Atmospheric Radar Research Center, University of Oklahoma, Norman, Oklahoma, USA
2 School of Electrical and Computer Engineering, University of Oklahoma, Norman, Oklahoma USA
3 School of Meteorology, University of Oklahoma, Norman, Oklahoma, USA

As the wind industry grows rapidly in the past decade, many wind turbines have been installed across the country. These extremely large structures have raised concerns in the radar community about their ElectroMagnetic Interference (EMI) to current radar networks. It has been reported that the large RCS of wind turbines could bias radar reflectivity estimate. Because the wind turbines are non-stationary, the Doppler spectra are also contaminated, thus classic ground clutter filters have failed to remove these interference.

Each modern wind turbine is equipped with highly precise sensors, collecting information such as rotation speed, blade position, yaw angle, pitch angle, etc. If such information can be telemetered to radar operators in real time, it is possible to predict the wind turbine radar signatures and mitigate it from contaminated data. To demonstrate this, the Radar Wind Turbine Testbed (RWT2) has been developed at the Atmospheric Radar Research Center of the University of Oklahoma. It includes a scaled wind turbine model and a time-domain scatterometer. The model is a 1:100 replica of a full-size wind turbine. Two motors are installed to emulate the blade rotation and the yaw. The scatterometer is a polarimetric pulse Doppler radar, designed for characterizing the wind turbine radar signatures of the model. The range resolution is better than 1.2 m for laboratory measurements. The scaled measurements are implemented in the anechoic chamber to avoid interference.

In the hardware-based demonstration, the yaw angle and rotation speed are assumed known. The contaminated data and pre-stored data are correlated and the segment with the highest cross-correlation coefficient in the pre-stored data is processed adaptively using a Wiener filter to compensate possible linear distortions. The demonstration shows that if certain telemetry information is available, it is by all means possible to mitigate the wind turbine interference to radar in real time.

Interference Suppression Studies with the Phased Array Antenna at the National Weather Radar Testbed

Mark Yeary*[1,2], Jerry Crain[1,2], and Chris Curtis[3]
(1) University of Oklahoma, School of ECE, Norman, OK, 73019 USA
(2) Atmospheric Radar Research Center, Norman, OK, 72072 USA
(3) National Severe Storms Lab, Norman, OK, 73072 USA

The phased array antenna at the National Weather Radar Testbed (NWRT) provides a unique opportunity to test the effectiveness of using its sidelobe cancelling channels to detect and subsequently mitigate interfering signals. The NWRT, located in Norman, Oklahoma, employs an S-band SPY-1A antenna from the Office of Naval Research.

About the radar: the phased array at NWRT operates at 3.2 GHz with peak power of 750 kW. The SPY-1A is a passive phased-array with 4352 elements. Its beam width is 1.5 degrees at broadside and 2.1 degrees at +/- 45 degrees off broadside. The antenna is tilted 10 degrees in elevation and is located 12m above the ground.

Sidelobe cancelling channels are receive-only auxiliary channels that are separate from the main array. Six of these channels are located around the periphery of the array. These channels have been designed to have low gain and wide beamwidth to detect unwanted signals, e.g., clutter, interference, and non-friendly jammers. In other applications, these types of channels have already been used on: jammer suppression on various radars; wind profiling radars to mitigate ground clutter, and some of the same techniques can be applied to weather surveillance radars. With the recent deployment of an eight-channel multi-channel receiver on the NWRT, the sum channel and sidelobe channel data can be recorded and processed to research different techniques for addressing the interference contamination problem.

As the density of electromagnetic environments continues to increase, this paper will shed new light, as innovative antenna concepts may be employed to provide solutions by filtering in the spatial domain, as opposed to the temporal domain. For example, nulls may be steered in the direction of unwanted contamination. This paper will examine some of the existing algorithms for employing sidelobe cancellers, in the context of existing radars and the NWRT in particular. Preliminary results from our simulations and outdoor experiments will be presented.

Wave Shadowing and Modulation of Microwave Backscatter from the Ocean

William J. Plant and Gordon Farquharson
Applied Physics Laboratory
University of Washington

September 20, 2011

Abstract: Shadowing and modulation of microwave backscatter by ocean waves are studied using coherent X-band radars. Two types of shadowing are investigated: geometric shadowing (complete blockage of incident rays) and partial shadowing (diffraction combined with weak scatterers). We show that, at a particular range (grazing angle), received power levels less than or equal to the noise level of the radar occur primarily where the incident power is low. Furthermore, in most cases, the fraction of samples of received power near the noise level depends on polarization. Since geometric shadowing should not depend on either the incident power level or the polarization, we conclude that it plays little role in microwave backscatter from the ocean, even at low grazing angles. Comparison with Milder's (2003) prediction of the fraction of a rough surface that is illuminated under geometric shadowing assumptions confirms this conclusion. We also study the modulation of microwave backscatter by ocean waves using these data. Phase differences between received power and scatterer velocity are found to depend on polarization and antenna look direction. Modulation patterns at VV polarization appear to be rather well explained by composite surface theory, having phases between power and velocity that are positive looking upwave and negative looking downwave. For HH polarization, however, other effects, probably due to breaking, come into play and overshadow composite surface effects of free waves. These breaking wave effects cause the modulation phase difference to be near zero for upwave looks and near 180^o for downwind looks. A simple linear model that involves both breaking and freely-propagating waves but does not include any shadowing effects is shown to account for observed phases differences at both polarizations to within about 15^o. Both the shadowing and modulation results are very relevant to ongoing attempts to measure phase-resolved ocean waves using shipboard radars. They imply that at VV polarization, cross section modulation is closely related to wave slope and height but at HH polarization, both the cross section and the scatterer velocity modulation are more closely related to breaking waves.

Radar Division Backscattering from the Sea Surface under the Small-Slope Approximation

Jimmy Alatishe*[(1)] and Wasyl Wasylkiwskyj[(2)]
(1) Naval Research Laboratory, Washington, DC 20375,
jimmy.alatishe@nrl.navy.mil
(2) The George Washington University, Washington, DC 20052, USA

Generally, the measured radar cross-section per unit area of a rough surface depends not only on the physical and statistical properties of the surface itself but also on the properties of the receiving antenna (radiation pattern and polarization). As was first derived by the second author (W. Wasylkiwskyj, "A new formulation for coherent backscattering from distributed targets," 2007 IEEE Antennas and Propagation International Symposium, June 14, 2007) and further investigated by both authors (W. Wasylkiwskyj and J. Alatishe, "Coherent scattering from distributed targets," IEEE MRRS-2008 Symposium Proceedings, pp. 36-41), EM backscattering by an irregular dielectric-air interface can depend to a significant extent on the relative dimensions of the antenna beam footprint and the spatial correlation length of the surface irregularities. These dependencies were corroborated by the numerical results for the small-amplitude approximation that were presented at the 2010 URSI-USNC meeting (W. Wasylkiwskyj and J. Alatishe, "Comparison of alternative models for EM backscattering from the sea surface under the small amplitude approximation," URSI-USNC National Radio Science Meeting, January 6-9, 2010) Presently we apply our coherent backscattering model to scattering from the ocean surface. We employ the small-slope approximation together with the simplified boundary matching technique introduced by Voronovich and obtain numerical results for backscattering from a fully developed sea using the Pierson-Moskowitz, the Pierson-Neumann, and the Elfouhaily models for the spatial ocean spectrum. The computed average backscattering cross is parameterized with respect to wind speed, wind direction, antenna radiation pattern and antenna orientation. The results show good agreement with published measured data for the average radar cross section σ_0 at X-Band.

Multiple Grazing Angle Sea Clutter Modeling

Ali Karimian[1], Caglar Yardim[1], Peter Gerstoft[1], William S. Hodgkiss[1], and Amalia E. Barrios[2]

[1] Marine Physical Laboratory, Scripps Inst. of Oceanography, University of California San Diego, USA.

[2] Atmospheric Propagation Branch, Space and Naval Warfare Systems Center, San Diego, California, USA.

Radar clutter in a non-standard atmosphere usually is modeled based on a single grazing angle at each range. Instead, the angular distribution of incident energy can be used to obtain a more accurate model of the clutter. Angular spectral estimation provides the grazing angle distribution of propagating energy. However, a large gradient in the refractivity profile, e.g. an evaporation duct, distorts plane wave spectral estimation. Ray tracing is used in these situations, but has its own limitations. These limitations require a cumbersome and ad hoc switching rule between ray tracing and the parabolic equation propagation model. Curved wave spectral estimation (CWS) is introduced that gives reliable results for any refractivity profile, in contrast to plane wave spectral estimation. CWS is used to derive multiple grazing angle clutter, a model for ocean surface clutter in the microwave region that depends on all incident angles at each range and their corresponding power.

Experiments for RF Tomography

Vittorio Picco*[(1)], Tadahiro Negishi[(1)], Marcus Stephens[(1)], Shingo Nishikata[(2)], and Danilo Erricolo[(1)]

(1) University of Illinois at Chicago,
Department of Electrical and Computer Engineering (MC 154)
851 South Morgan Street, Chicago, IL 60607-7053, USA
(2) Mitsubishi Heavy Industries, LTD., Nagoya Guidance & Propulsion Systems Works
1200, Higashi Tanaka, Komaki, Aichi prefecture, 485-8561, Japan

vpicco2@uic.edu, tnegis2@uic.edu, msteph5@uic.edu, snishi2@uic.edu,
derric1@uic.edu

RF tomography was first introduced by Wicks (M. C. Wicks, "RF tomography with application to ground penetrating radars," *Proc. IEEE 41st ACSSC*, Nov. 4–7, 2007, pp. 2017–2022.) and it is more precisely described in some recent publications (L. Lo Monte, D. Erricolo, F. Soldovieri, M.C. Wicks, "Radio Frequency Tomography for Tunnel Detection", *IEEE Trans. Geoscience and Remote Sensing*, Vol. 48, No. 3, March 2010, pp. 1128-1137; L. Lo Monte, D. Erricolo, F. Soldovieri, M.C. Wicks, "RF Tomography for Below-Ground Imaging of Extended Areas and Close-in Sensing", *IEEE Geoscience and Remote Sensing Lett.*, Vol. 7, No. 3, July 2010, pp. 496-500).

A system using RF tomography employs a set of low-cost, configurable electromagnetic transmitters and receivers placed around the region of interest. This system conceptually operates in three stages. The first stage is dedicated to the configuration of the system. During this stage, sensors accurately identify their position, orientation and time reference. During the second stage, transmitters radiate known waveforms. Spatially distributed receivers collect samples of the total electric field. In addition, waveform diversity in various dimensions including space, time, frequency, and polarization is used. During the third stage, receivers relay the collected data to a control center for processing and imaging.

The purpose of these experiments is to verify the quality of images of underground cavities obtained using RF Tomography methods. While various numerical simulation have supported claims of advantages of RF tomography, no experimental verifications have been made so far. Unfortunately, field experiments are very time consuming and costly. Therefore, this work describes anechoic room measurements on scaled models in free space that simulate some of the challenges one expects to face in the real world.

A Semi-empirical model for Predicting Signal Strength at VHF and UHF band using Surface Refractivity Measurement at Nsukka, South-Eastern Nigeria

B.G. Ayantunji*., Y. Najib*, O. Anthony[1] I.A. Obi* and P.N. Okeke*

***Centre for Basic Space Science, UNN**

[1]Dept. of Physics and Astronomy, UNN

Corresponding Author: ayantunji@cbssonline.com

The signal strength from three terrestrial TV stations, namely, Nigeria Television Authority (NTA), Enugu, Enugu State Broadcasting Service (ESBS), Enugu and African Independent Television (AIT), Enugu, were monitored at University of Nigeria, Nsukka (UNN) about 50Km on line of sight (LOS) from the stations over a Period of six months. The three stations are broadcasting at 194.85 – 196.20MHz (NTA), 531.75MHz (AIT) and 702.25-703.20MHZ respectively. Surface refractivity measurement was also carried out at Nsukka over the same period of time using meteorological data of temperature, humidity and pressure collected with the aid of a Vantage Pro II automatic weather station. The ITU-R model for calculation of refractivity was employed for calculation of refractivity. The data sets was divided using the average monthly relative humidity into rainy and dry months. Whenever the average relative humidity is less than 10% the month is considered dry else rainy month. The diurnal variation of both sets of data was determine using statistical averaging of corresponding measurement for each hour. The result obtained showed a strong correlation between signal strength and surface refractivity. A regression curve was plotted and a semi-empirical model was obtained from the regression curve. The model obtained from the regression curve was used to predict signal strength for a known refractivity value and the result was compare with the measured value under the same atmospheric condition.

A Coupled FDTD/SAMI3 Model for Electromagnetic Wave Propagation in the Earth-Ionosphere System

Jiajun Niu* and Jamesina J. Simpson
ECE Department, University of New Mexico, Albuquerque, NM

There are many technologies relying heavily on our knowledge of the Earth's ionosphere, such as long-distance communications, navigation using Global Position Systems (GPS) and over the horizon radar. Inaccurate knowledge of the electromagnetic (EM) characteristics of the ionosphere and the state of transmission path between transmitters and receivers can largely deteriorate the performance of these technologies.

Among the existing methods for calculating EM wave propagation in the ionosphere, ray theory, mode theory, and the finite-difference time-domain (FDTD) method are the three main techniques adopted by industry and academia. Ray-like methods require the least computational resources, but they only provide an approximation of the characteristics along dominant propagation path and their solutions are at discrete frequencies. Furthermore, neither ray theory nor mode theory is capable of handling both arbitrarily complex vertical and horizontal inhomogeneities in the ionosphere.

In this presentation, we present a coupled FDTD/SAMI3 model for simulating the VLF-HF EM wave propagation within the Earth-ionosphere system. This model is based on the three-dimensional (3D) FDTD global electrodynamics model (J.J. Simpson, *Surveys Geophys.*, 30, 105-130, 2009), the 3D FDTD magnetized ionospheric plasma algorithm (Y. Yu and J.J. Simpson, *IEEE Trans. Antennas Propag.*, 58, 469-478, 2010), and the Naval Research Lab's SAMI3 (Sami3 is Also a Model of the Ionosphere) (J.D. Huba, G. Joyce and J.A. Fedder, *J. Geophys. Res.*, 105, 23035-23053, 2000). This comprehensive model takes into account the details of the Earth's topography/bathymetry, 3D lithosphere composition data, the composition of the Earth's ionosphere, and the geomagnetic field. Specifically, SAMI3 solves for the structure of the ionosphere and the FDTD models solve for the EM wave propagation through that structured ionosphere. Thus, the coupled FDTD/SAMI3 model is capable of simulating the physics of EM wave propagation through the ionosphere as well as the complicated scattering of the EM waves at and along the Earth's surface and other obstacles.

Evaluating Rayleigh Distribution Assumptions in Fading Channel Models

Timothy Riley* & Christopher Behm
U.S. Department of Commerce, NTIA/ITS, Boulder, Colorado, 80305, USA

Wireless communication systems must contend with time variations in received signal level that are characteristic of the propagation channel. Propagation channel fading at VHF and above is predominantly caused by the complex scattering environment through which the radio waves travel. The techniques used in receiver design to mitigate the effects of fading are well established, but the constraints of limited spectral resources and the detrimental characteristics of the propagation environment demand increasingly complex modulation techniques to accomplish this mitigation. To maintain system reliability and usability, receivers must be built to increasingly higher tolerances to cope with propagation-induced errors.

As a result of its involvement in the effort to standardize the various public-safety communication systems, the Institute for Telecommunication Sciences (ITS) has re-examined the fading channel. Specifically, we reassessed the assumptions implicit in the understanding of fading channels. This effort involved the measurement, analysis, and assessment of propagation fading and describes the limitations of classical fading theories when applied to ever more sophisticated modulation techniques. The ultimate purpose is to investigate the statistical fading behavior of the radio channel within time frames significant to the reception of digitally-modulated signals. Measurements of mobile radio channels were conducted in multiple environments and the fast fading characteristics of these channels were analyzed. The measured data was analyzed without bias toward conventional fading assumptions to provide an independent theoretical understanding of RF fading propagation. The efficacy of classical fading theory in the testing of existing and proposed public-safety VHF and UHF transceivers was assessed by comparing the measured data to the requirements for Rayleigh simulators as set forth in industry-standardized test procedures.

Free-Field Measurements of the Electrical Properties of Soil Using the Surface Wave Propagation between Two Monopole Antennas

Nicholas DeMinco, Robert T. Johnk, Paul McKenna, Chriss Hammerschmidt, and Wayde Allen
U.S. Department of Commerce, Institute for Telecommunication Sciences
Boulder, Colorado

This paper describes a radio-frequency (RF) near-Earth measurement and analysis program that was performed at the Institute for Telecommunication Sciences (ITS) at the Table Mountain Field Site (TMFS). The objective of the program was to provide estimates of the electrical properties of the ground (conductivity and permittivity) at TMFS, and also to develop improved radio-wave propagation prediction tools and models for close-in distances and very low antenna heights. The measurement system uses transmission measurements of the surface wave between two monopoles placed close to the ground at a fixed separation distance. The electrical properties of the ground (soil) are extracted by comparing measured data with known analytical models and optimizing the results. These ground constants can have a significant effect on the RF propagation near the ground and need to be accurately characterized. The measurement system provides two-port transmission measurements between two resonant ground-plane mounted monopole antennas placed a at fixed separation distance and close to ground. The core of this measurement system is a vector network analyzer that performs a two-port stepped-frequency measurement of S-Parameter S_{21}, over wide frequency ranges (300 kHz to 6 GHz) between the two monopole antennas. Data was extracted from this data over a frequency range of 30 MHz to 915 MHz. Antenna efficiencies and gains were factored into the measurement results at tuned as well as off-tuned frequencies of the monopoles to facilitate the computation of propagation loss between the antennas and the determination of the effective conductivity and dielectric constant (permittivity) of the ground. The monopoles are typically placed 8.9 cm above ground for maximum sensitivity and practical considerations of feeding the monopole antenna from below the ground plane. For the frequencies under consideration (30 to 915 MHz), this is essentially equivalent to a zero height antenna, because the wavelengths are between 0.328 and 10 meters. The propagation between the antennas is predominantly via the Norton Surface Wave, because the antennas are very close to Earth. At this height the direct and reflected waves cancel each other resulting in only the surface-wave component of the ground wave as the mechanism for radio-wave propagation. The skin depth of the propagating wave into the ground is quite large, so the use of the surface wave results in an aggregate measure of the ground constants of the soil.

IMPACT OF METEOROLOGICAL PARAMETERS ON THE VLF-LF PROPAGATION AT MIDLATITUDES

A.A.Egoshin, V.M.Ermak, Yu.I.Zetzer, S.I.Kozlov, V.P.Kudryavtsev, A.N.Lyakhov, Yu.V.Poklad, E.N.Yakimenko

Institute of Geospheres Dynamics

119334, Moscow, Leninskij pr. 38,korp.1, Russia, alyakhov@idg.chph.ras.ru

Further analysis of the data of the European VLF-LF stations signals measured at "Mikhnevo" geophysical observatory (54.94N, 37.73W) is presented. The comparison between the measurements and EOS-Aura satellite data has shown that significant variations of the neutral atmosphere temperature profile cause the transit from unimodal probability distribution for the amplitude of VLF signal to the bimodal one. The same splitting in LF range is observed under the appearance of additional maxima of water content at 40-60 km. Such a transition can be interpreted as dynamical bifurcation process.

The same effects are observed in A118 SID station data with some new effects. Namely, the bimodality is observed only on eastward and westward paths, not on the northward.

These results confirm the results of SAVNET group and supplement them with the need to integrate water vapor into consideration. The numerical simulation using D-layer plasmachemical model confirms that the observed middle atmosphere variations can lead to the amplitude deviation close to those measured at Mikhnevo.

Spectral analysis of long-term measurements at Mikhnevo and at the A118 France SID station has shown that the time periods of disrupted diurnal dynamics of the signal amplitude correspond to the detection of planetary wave periods in the spectra. Statistically significant periods are 1.5-3, 4-7, 15 and 20 days, thus some of them are close to Rossby waves periods.

Low Earth Orbit Spectrum Analyzer for Ionospheric Disturbances

Mario I. Ortega*[(1)], Anthony J. Bentley[(1)], Nicholas R. Clegg[(1)], Bryan M. Hare[(1)], Rosemary R. Williams[(1)], and Scott C. Wilson[(1)]
(1) Electrical and Computer Engineering, University of New Mexico, Albuquerque, NM 87106

The National Science Foundation (NSF), through the Research Experience for Undergraduates Grant (REU), has provided the Configurable Space Microsystems Innovations and Applications Center (COSMIAC) at the University of New Mexico (UNM) with funds to design, prototype, and launch a satellite based spectrum analyzer capable of measuring total electron content (TEC). This system, called LEISA (Low Earth-Orbit Ionospheric Spectrum Analyzer), will consist of various space borne sensors and will be coupled with corresponding ground stations for appropriate data transference. Its purpose is to measure the distortion of radio waves produced by intracloud lightning in order to map the ionosphere's TEC. Using an onboard analog-to-digital converter (ADC) and Field Programmable Gate Array (FPGA), LEISA will digitize, record, and timestamp RF signals that it receives from lightning events. When this data from the satellite constellation is coupled with various ground stations the lightning event's location can be determined with a time of flight calculation. This process will provide real time ionospheric data to clientele using a platform that is easy to develop and implement while remaining relatively inexpensive. Such a platform will allow for the real time analysis of the ionosphere that is necessary for scientific modeling and GPS corrections in many academic, commercial, and government activities.

LEISA is being developed by students of various disciplines including engineering and science backgrounds from New Mexico State University, University of Idaho, and the University of New Mexico. Students have become familiar with lightning propagation and ionospheric behavior and have used various models to understand lightning behavior. This project is intended to expand upon and improve previous ionospheric research missions such as the Fast On-orbit Recording of Transient Effects (FORTE) and Cibola Flight Experiment (CFE) satellite missions launched by Los Alamos National Laboratories (LANL) in the past two decades.

The Vary-Chap topside electron density profile for IRI and GIRO

Bodo W. Reinisch[1,2], Patrick Nsumei[1], Xueqin Huang[1], and Dieter Bilitza[3]

[1] Center for Atmospheric Research, University of Massachusetts, 600 Suffolk Street 3rd floor, Lowell, MA 01854 USA, Tel: +1 978-934-4900, Fax: +1 978-459-791, Bodo.Reinisch@digisonde.com, Patrick_Nsumei@uml.edu, Xueqin_Huang@uml.edu

[2] Lowell Digisonde International, LLC, 175 Cabot St, Suite 200, Lowell, MA 01854 Tel: +1 978-735-4752, Fax: +1 978-735-4754, Bodo.Reinisch@digisonde.com

[3] Space Weather Laboratory, George Mason University, Fairfax, VA 22030

Tel: +1 703-993-3807, Fax: +1 703-993-9300, dbilitza@gmu.edu

Using ISIS-2 topside sounding data, a new representative model of the topside electron density distribution in form of "Vary-Chap" functions is being developed for use in IRI [Bilitza et al., 2011], and for the profile extension above hmF2 of bottomside profiles measured by the Digisonde Global Ionospheric Radio Observatory (GIRO). A major challenge for topside *N(h)* modeling is finding a suitable mathematical representation of the topside vertical profiles. Many representations have been proposed including exponential functions, Epstein functions , sech-squared functions, and Chapman functions with one or two constant scale heights. The Vary-Chap function is a generalized α-Chapman profile, based on the work by Rishbeth and Garriott [1969], that uses a continuously varying shape function S(h):

$$\frac{N(h)}{N_m} = [S(h)]^{-1/2} \exp\left[\frac{1}{2}[1 - Y(h) - \exp(-Y(h))]\right], \qquad Y(h) = \frac{1}{h_m}\int_{h_m}^{h} \frac{dx}{S(x)} \tag{1}$$

Here N_m and h_m are the density and height of the F2 peak, i.e., NmF2 and hmF2. According to Huang and Reinisch [2001] Equation (1) can be solved for S(h) as function of N(h):

$$S(h) = \left(\frac{N(h)}{N_m}\right)^{-2}\left\{1 + \int_1^z \left(\frac{N(z)}{N_m}\right)^2 dz\right\}\left[1 - \ln\left\{1 + \int_1^z \left(\frac{N(z)}{N_m}\right)^2 dz\right\}\right], \qquad z = \frac{h}{h_m} \tag{2}$$

Shape functions S(h) were calculated for ~ 80,000 ISIS-2 topside profiles, and a parameterized function S*(h) was fitted to each shape function where

$$S^* = \frac{1}{S_1(h)} + \frac{1}{S_2(h)} \tag{3}$$

with $S_1(h) = c_1\left[\sec h^2\left(\frac{z-1}{\beta}\right)\right]^{-1}$ and $S_2(h) = c_2\frac{\left[1+z^2\right]^{\alpha}}{z}$, $\alpha > 1$, $z = h/h_m$.

The coefficients c_1 and c_2 are functions of the parameters α, β, and h_T where h_T is considered the transition height where S_1=S_2, α defines the steepness of S*(h) for heights above h_T, and β defines the topside layer thickness.

This functional representation characterizes the shape of the topside profile without directly depending on the F2 peak density. The function S*(h) in (3) allows to solve the integral in (1) analytically, assuring time-efficient processing of the profile data. The three parameters in S* are binned according to local time, latitude, season, and peak height to establish a model of the topside profile for specified values of foF2 and hmF2.

Assimilation of GIRO data in the Real-Time IRI

Ivan A. Galkin*[(1)], Bodo W. Reinisch[(1,2)], Xueqin Huang[(1)] and Dieter Bilitza[(3)]
(1)University of Massachusetts, Lowell, MA 01851, http://ulcar.uml.edu
(2) Lowell Digisonde International, LLC, Lowell, MA USA

Conventional wisdom has long held that an empirical model that represents an average essence of the measurement data will have limited success in describing the variety of short-term events. The ionospheric forecasting community therefore, has been focusing on the development of comprehensive theoretical models that assimilate real-time sensor data. Meanwhile, the computational ease of empirical models made them readily available to the wide audience of space physics and radiowave propagation communities. The IRI model, an empirical model of monthly median ionospheric characteristics, has been shown to consistently out-perform other empirical and theoretical models. The next challenge for IRI is therefore to employ data-assimilative capabilities so as to further its proven competitive performance to the ionospheric conditions far from an average quiet-time behavior. We show the roadmap of building an Assimilative Real-Time extension of the IRI model, IRI^{ART}.

The IRI climatological specification will benefit most from assimilating the F2 peak data, hmF2 (height) and NmF2 (density). Among multiple sources of the F2 peak data, the vertical HF sounding technique (ionosonde) continues to be the workhorse of ionospheric diagnostics providing a long record of reliable NmF2 and hmF2 measurements and low-latency real-time capability. The continually growing Global Ionospheric Radio Observatory (GIRO), with 42 locations reporting data in real-time, is one of the prime F2 peak data supplier.

New concepts are discussed that attribute data-assimilative properties to a data-based empirical model. Such task has been previously approached with limited success, and the challenges of assimilating sparse, unevenly spaced, and noisy NmF2/hmF2 data were rendered unbridgeable. We propose a new "morphing" assimilation technique that introduces corrections to diurnal and spatial harmonics of the IRI representation rather than adjust its output values. The IRI^{ART} will morph the global diurnal IRI specification into matching a sliding 24 hour window of GIRO data. To produce new spatial expansion coefficients, a physics-guided interpolation of missing data is used, driven by a recursive feed-back neural network optimizer.

The "community" feel of IRI, free from large computational demands and waiting time, will be preserved by building a Rapid Assimilation Platform for Ionospheric Density (RAPID) with a historic database and a dissemination platform of 15-minute cadency coefficients that transform IRI to IRI^{ART}. Once implemented, RAPID will establish a valuable data resource for retrospective, nowcasting, and forecasting research to the ionospheric community.

INITIAL ASSESSMENT OF THE NEW-GENERATION METEOR RADARS TO MEASURE GRAVITY WAVES MOMENTUM FLUXES

D. Janches[1], D.C. Fritts[2] and W.K. Hocking[3]

1. Space Weather Lab, GSFC/NASA, Greenbelt MD, USA
2. CoRA/NWRA, Boulder CO, USA
3. Department of Physics and Astronomy, University of Western Ontario, London ON, Canada

A "hotspot" of small-scale gravity wave activity extending from the troposphere into the mesosphere and lower thermosphere (MLT) is centered over the Drake Passage. This region is also characterized by a maximum of the semidiurnal tide at these latitudes, and the lack of other MLT wind measurements in this latitude band. Two new-generation meteor radars were installed at both ends of the 'hot-spot'. The Southern Argentina Agile Meteor Radar (SAAMER) was installed on Tierra del Fuego (53.8°S) in May 2008 and the Drake Antarctic Agile Meteor Radar (DrAAMER) at the Brazilian Antarctic Comandante Ferraz Base (62.1° S) in March 2010. These radars were specifically designed to measure gravity waves (GW) momentum fluxes (MF) in the MLT region. This paper describes the motivations for the radars location as well as its measurement capabilities. We present tests of the SAAMER, DrAAMER and classical designs of meteor radars to evaluate their ability to perform these measurements. Test results for specified mean, tidal, and GW fields, including tidal amplitudes and GW momentum fluxes varying strongly with altitude and/or time, suggest that the distribution of meteors throughout the diurnal cycle and averaged over a month allows characterization of both monthly mean profiles and diurnal variations of the GW momentum fluxes for the new-generation radar design. Applications of the same methods for real data suggest confidence in the monthly mean profiles and the composite day diurnal variations of GW momentum fluxes at altitudes where meteor counts are sufficient to yield good statistical fits to the data.

Electric field and Conductivity variations near Substorm onset times

Krishna Prasad Gudivada[*1, 2] and B.J.Watkins[1]
[1]Geophysical Institute
[2]Department of Electrical Engineering
University of Alaska Fairbanks,
Fairbanks, Alaska 99775, USA

The Poker Flat, Alaska (65.12^{o} N, 147.8^{o} W) incoherent-scatter radar has been used to study the variations of the auroral zone electric field and ionospheric conductivity for times near the onset of auroral substorm. During the period of observation, the radar was operated with thirteen antenna positions with successive pulses transmitted in different directions. F-region plasma drift data were thus determined for each antenna position with time integration of three minutes. The Electric field components in the north-south and east-west directions were computed for F-region ion vector velocity from radar long pulse data. The E-region conductivities were derived from short pulse alternating code data.

The north-south and east-west component of the large scale convection electric fields show variations at the beginning of the substorm growth phase (about one hour before substorm onset).The east-west electric field component goes to near zero values corresponding to a transition from westward plasma drift to near zero values. There is a corresponding enhancement to about 20mv/m of the westward electric field (Southward Plasma motion) during the substorm growth phase.

Near the Substorm onset time (determined from magnetometer), there is change to eastward plasma flow (Southward E-field Component of about 10mv/m) and a persistent southward plasma flow (Westward E-field Component).

The Conductivity variations have also been examined near substorm onset time using the electron density data from the radar, E-region Hall and Pedersen Conductivities are enhanced at the substorm onset time. With the time resolution (3 Minutes) of the data, we observed that the enhanced southward E-field Component and enhanced conductivities occur simultaneously.

Incoherent Scatter Radar Analysis in a Flexible Software Radar Framework

Philip J. Erickson*, William C. Rideout, and Frank D. Lind
Atmospheric Sciences Group, MIT Haystack Observatory, Westford, MA 01886

For more than six decades, the incoherent scatter radar technique has provided the most powerful ground based remote sensing tool for directly probing variations in a large number of ionospheric physical parameters, including electron density, electron and ion temperature, ion composition, velocity, and ion-neutral collision frequency. The nature of the incoherent scattering process requires that the radar receiving system be able to capture a RF bandwidth which scales in a manner dictated by the transmitter frequency and plasma parameters. For traditional 'ion line' scattering, this value is approximately 10 to 200 kHz at UHF frequencies for typical tropical and mid-latitude ionospheres. Due to rapid advances in both analog to digital conversion capture bandwidth and processing power, it has been possible since the 1990s to use general purpose computing combined with flexible sampling cards to construct a software radar system which can handle these bandwidths and perform all necessary instrumental corrections, correlations, and inverse analysis using standard incoherent scatter theories. At Millstone Hill, the MIDAS series of platforms has since 2001 been a production level software radar implementation in both monostatic and bistatic architectures.

Successful incoherent scatter software radars must perform a number of tasks which are invariant to the particular large aperture system on which they are implemented. For instance, every production software radar implementation requires a calibration system which can directly examine baseband complex voltages and other higher order products in order to verify linearity and spectral shape and to construct accurate system impulse responses. For beam geometries which have magnetic aspect angles greater than 1-2 degrees from perpendicularity, the inverse analysis process yielding plasma parameters has many features which are independent of the transmitter frequency and plasma conditions, especially in the case of traditional height-integrated (gated) spectra or autocorrelation functions. The flexible nature of software radar systems allows a degree of generality in these important tasks in a manner which was previously very difficult with embedded hardware solutions, and the general computing implementation of these codes maximizes reusability.

We present architectures for incoherent scatter radar analysis which emphasize reconfigurability and generic processing in a production software framework. We highlight in particular the system calibration and inverse plasma parameter fitting process as examples, identifying algorithms and implementations which minimize the need to rewrite analysis code. Specific processing examples will be given in which baseband complex receiver voltages from multiple incoherent scatter radar systems are analyzed using the same software radar signal analysis chain.

Digital Array Radar for a Global Geospace Array

Frank D. Lind[(1)], Philip J. Erickson[(1)], James R. Marchese[(1)]

(1) MIT Haystack Observatory, Route 40, Westford, MA 01886 USA

The Geospace Environment encompasses the Earth's Ionosphere, Plasmasphere, and Magnetosphere and their coupling to both the Heliosphere (above) and the lower atmosphere (below). Understanding the dynamics of Geospace phenomena requires global measurement capabilities which encompass the full range of important physical processes, provide wide coverage of critical regions, and allows for detailed investigations into the underlying physics. These measurements must be of fundamental physical parameters, available on an ongoing basis, and made in a sustained and sustainable manner.

Radio and radar instrumentation have historically played a key role in the observation of the Geospace environment. Ground based radio instrumentation has, in particular, provided a sustained record of observation and scientific discovery. However, the modern instrumentation network which has been constructed by the ground based radio science community has many issues. It is greatly limited by the ad-hoc and incremental nature of its creation, the differing technologies used for its implementation, and the cost and complexity associated with its maintenance and operations. For example, the existing incoherent scatter radar facilities provide coverage of significant portions of the globe but are not uniformly capable, operate intermittently, have high operational costs, and often must make operational choices which limit the applicability of the observations which are made. It is difficult to break free of these limitations due to the embedded costs, required resources, and the perceived risk of major changes. To address these issues requires a paradigm change.

Digital Array Radar is a key technology which will enable wide scale observation of the Geospace Environment using both active and passive techniques. Ultimately the most successful application of this technology depends on low costs for both its deployment and operations. There are several concepts critical to the development and application of digital array radars for Geospace science applications. These concepts include the consistent use of architectures which lower the complexity the radar aperture while maximizing science capability. The use of software radar technology and a well defined coherence boundary to shift functionality to software running on high performance computing systems. As well as a focus on technologies which enable a high level of integration, large scale component reuse, and significant system simplification. The ultimate goal is to capture the majority of instrument function in slowly evolving software while greatly lowering the cost per element compared to existing systems. We will discuss technical approaches to achieve these requirements, discuss ongoing efforts as a motivation, and describe an incremental approach to developing the needed technologies. As part of this we will discuss the EISCAT 3D radar system, currently under development, as a major step towards the development of such digital radar array capabilities.

The Search for Ionospheric Effects at 150 MHz with PAPER

Nicole Gugliucci*[1,2], Richard Bradley[2], and PAPER Collaboration[??]

[1] University of Virginia, Dept. of Astronomy
[2] National Radio Astronomy Observatory

PAPER (the Precision Array to Probe the Epoch of Reionization) is a telescope designed to detect the redshifted hydrogen signal from the early universe. The hydrogen is at a redshift $\sim 6 - 14$, bringing the spin-flip transition of neutral hydrogen from 1.4 GHz to a regime between 100 and 230 GHz. PAPER has a test site with 32 antennas in the Radio Quiet Zone of Green Bank, West Virginia, and a 64-antenna array at the Square Kilometer Array candidate site in the Karoo, South Africa.

Astronomical observations at such low frequencies are made more challenging by the refractive properties of the ionosphere. We present the angular shifts in bright source positions (Cyg A, Cas A, Vir A, and Tau A) as probes of the variations in the total electron content (TEC) along the lines of sight between the sources and the 32-element array in Green Bank. With an integration time of 10 seconds, we can probe for the small fluctuations, using the visibilities, that may be the most difficult to calibrate in upcoming experiments and observations. More sensitive probes of longer timescales are also done by imaging the sky with both the 32 and 64-element arrays. Here again, the bright source position stability is used as an indicator of the TEC stability. The wideband nature of the PAPER instrument enables it to probe the effects of a varying TEC over a nearly 100 MHz bandwidth. We compare these measurements to more traditional methods of probing the ionosphere, such as GPS satellites, and we discuss the implications that these measurements will have on experiments aimed at detecting the epoch of reionization.

Total Electron Content Anomaly Over Mid-North America

Alexander P. Davidson*[(1)], Anthea J. Coster[(2)], Shunrong Zhang[(2)]
Evan Thomas[(2)]

(1) Phillips Academy, Andover
(2) MIT Haystack Observatoy, Westford, USA
(3) Virginia Tech, Blacksburg, USA

For many years, the world-wide network of GPS receivers has been used to produce global TEC maps. Having a large number of GPS receivers available aids the receiver bias estimation procedure; a parameter needed to derive the TEC information from GPS signal delay differences. GPS coverage is particularly good over the continental US, thereby strengthening the TEC estimation over the US. Recently, Zhang et al. [2011] have reported on a pronounced east-west difference in the TEC observed over the continental US. They attribute this difference in the TEC to the changing direction of the geomagnetic declination over the US. The zero magnetic declination over the US occurs at approximately 92-95 degrees W. longitude.

We report here on a different, but perhaps related, phenomenon: an anomaly in the total electron content that appears in GPS TEC maps at approximately the same location over several years. This anomaly can be observed between 35 and 45 degrees N latitude and between 100 and 105 degrees W longitude, although this position shifts as a function of time of day. At approximately 8 or 9 am local time, this anomaly can be seen at its furthest west position at approximately 105 degrees W longitude, and at 100 W longitude at approximately 19:00 local time. The anomaly is seen primarily in March and, in 2008, the anomaly was as large as 5 TEC higher than the surrounding TEC values. Multiple GPS processing techniques observe this phenomenon. We report here on the observed hourly, day-to-day, and seasonal characteristics of this anomaly and discuss possible mechanisms for its production. We suspect that the orientation of the Earth's magnetic field, combined with thermal winds, are accountable for the TEC anomaly that is observed.

A routine validation of near-real time GAIM assimilation of ground and space-borne GPS TEC data using independent data sources

Komjathy, A., P. Stephens, M. Butala, B. D. Wilson, O. Verkhoglyadova, A. J. Mannucci
Jet Propulsion Laboratory, California Institute of Technology

Data assimilation techniques for ionospheric space weather are increasingly successful due to the growing abundance of data from ground and space-based GPS receivers and new UV remote sensing satellites. The six-satellite COSMIC/FORMOSAT-3 constellation, launched in April 2006, now provides unprecedented global coverage from 1500-2000 radio occultation measurements daily. The Global Assimilative Ionosphere Model (GAIM) developed at NASA's Jet Propulsion Laboratory (JPL) has been adapted to process COSMIC data simultaneously with ground-based TEC data in near real-time (NRT). Calibrated measurements of ionospheric total electron content (TEC) from COSMIC suitable for input into GAIM are currently made available with latencies between 30 and 120 minutes. Ground GPS receiver networks continue to provide near real-time TEC data from two worldwide networks consisting of ~75 sites capable of 5-minute latency, and ~125 additional hourly sites, operated by JPL and others. GAIM combines ground TEC data with vertically resolved occultation data from COSMIC to produce three-dimensional, global electron density distributions that reproduce the hour-to-hour ionospheric “weather” much more accurately than has been possible before the COSMIC era.

We will describe the status of a new processing system for ground and space data that produces ionospheric “nowcasts” in near real-time (latency measured in minutes). We will introduce our routine validation of near real-time GAIM results using independent processing schemes including operational daily GAIM runs, Jason-derived vertical TEC and ionosonde measurements.

Modeling MSTID Propagation with the SAMI3 framework

Timothy M. Duly[(1)], Jonathan J. Makela [(1)], Joe Huba[(2)], and Jonathan Krall[(2)]
(1)University of Illinois at Urbana–Champaign, Urbana, IL, USA
(2) Naval Research Laboratory, Washington D.C.,USA

Recent optical observations (Miller et al., 2009; Makela et al., 2010) have suggested that electrified, nighttime medium-scale traveling ionospheric disturbances (MSTIDs) can propagate to low latitudes, where they can potentially act as a seed mechanism for the development of equatorial plasma bubbles. Using the SAMI3 model, Krall et al (2011) demonstrated that this was, indeed, a plausible seeding mechanism. However, this initial modeling study used an imposed electric field that was consistent with previous MSTID observations. Here, the SAMI3 framework is used to self consistently model the development of MSTIDs. Specifically, the effect of neutral winds on the propagation of MSTIDs is studied. The simulations provide a more complete picture of MSTID formulation, propagation toward the equator, and finally seeding of Equatorial Spread F.

Global Observations of Sub-Auroral Polarization Stream (SAPS) Events from Mid-Latitude SuperDARN Radars

Joseph B. H. Baker[(1)], Lasse B. N. Clausen [(2)], Bharat S. R. Kunduri[(1)], J. Michael Ruohoniemi[(1)], Evan G. Thomas[(1)]

(1) Center for Space Science and Engineering Research, Virginia Tech, Blacksburg, VA, 24061
(2) Institute for Geophysics and Extraterrestrial Physics, Technical University of Braunschweig, Braunschweig, Germany

The spatial coverage of the Super Dual Auroral Radar Network (SuperDARN) has expanded considerably in recent years with the construction of several new radars at middle latitudes in both hemispheres. Mid-latitude SuperDARN radars provide enhanced capabilities to investigate the electrodynamics of the subauroral ionosphere with unprecedented temporal resolution and spatial coverage. During periods of quiet geomagnetic activity mid-latitude SuperDARN radars tend to see long-lived bands of subauroral ionospheric irregularities co-rotating or drifting slowly westward across the night side. During geomagnetic storms the radars are able to monitor the development of strong westward flows in Sub-Auroral Polarization Stream (SAPS) channels, which appear equatorward of the auroral oval when the boundaries of ion and electron precipitation become separated from each other to form a poleward electric field. SuperDARN radars are able to continuously monitor the electrodynamics of SAPS features over extended spatial scales for several hours. In this presentation, we examine a number of case study examples of SAPS events that have been observed by SuperDARN radars over the past two years. We examine instantaneous variations in the direction and magnitude of the SAPS flows seen by different radars at different local times; an exponential dependence is identified, consistent with recent modeling. We also examine the magnetic conjugacy of SAPS features observed simultaneously by the mid-latitude Wallops and Blackstone radars in the northern hemisphere and the Falkland Islands radar in the southern hemisphere. We use empirical magnetic field models to map the radar measurements between the hemispheres to rigorously examine the north-south consistency between the SAPS flows. The interhemispheric observations identify significant north-south differences in both the magnitude of the SAPS flows and the width of the SAPS channels but there is also broad consistency in the cross-channel potential differences.

Comparisons of the NRL SAMI3 Physics-Based Ionospheric Model with Global Ionosonde, GPS, and COSMIC Electron Density Measurements

Carl L. Siefring[1], Paul A. Bernhardt[1], Anish Tondwalkar[2], Joseph D. Huba[1], Jonathan F. Krall[1], Sarah E. McDonald[3], John T. Emmert[3], Douglas P. Drob[3], Judith L. Lean[3], Glenn Joyce[4]

[1]Plasma Physics Division, Naval Research Laboratory, Washington, DC 20375, USA
[2]ASEE Science and Engineering Apprentice Program, Naval Research Laboratory, Washington DC 20375, USA
[3]Space Science Division, Naval Research Laboratory, Washington, DC 20375, USA
[4]Icarus Research, Inc., P.O. Box 30780, Bethesda, MD 20824, USA

The Naval Research Laboratory is conducting an interdisciplinary physics-based space weather model development and validation program called the Integrated Sun-Earth System for the Operational Environment (ISES-OE). As part of this program, for validation, numerous runs of the physics-based SAMI3 model have been made and compared to global measurements of electron density. The data sets includes: 1) Ionosonde foF2 and hmF2 measurements, 2) GPS Total Electron Content (TEC) measurements, and 3) COSMIC GPS occultation measurements. The comparisons presented will primarily center on Feb. 19 - April 19, 2008 which contains the most recent Whole Heliospheric Interval (WHI). This time period, during solar minimum, has only very modest solar activity and is a good test to validate the SAMI3 simulations of the base-state ionosphere. The results indicate that the SAMI3 has too much plasma in the topside ionosphere and too little in the bottomside ionosphere.

We are investigating the possible causes this discrepancy. One possibility is that the atmosphere is more contracted than would be expected for the historically quite solar minimum conditions during the 2008 WHI. The NRLMSISE atmospheric model used in SAMI3 is an empirical model based on measurements, but there are no data for the F10.7 levels seen during this interval. We will report on the effects that exospheric temperature, electron production and loss rates, and neutral winds have on the ability of SAMI3 to correctly match the global electron density data sets.

This work supported by the Naval Research Laboratory Base Program.

Simultaneous observations of mid-latitude ionospheric density structures by SuperDARN radars and the global GPS receiver network

Evan. G. Thomas[(1)], Joseph. B. H. Baker[(1)], J Michael Ruohoniemi[(1)], Lasse B. N. Clausen[(2)], Anthea J. Coster[(3)]

(1) Bradley Dept. of Electrical and Computer Engineering, Virginia Tech, Blacksburg, VA, USA

(2) Institute for Geophysics and Extraterrestrial Physics, TU Braunschweig, Braunschweig, Lower Saxony, Germany

(3) Atmospheric Sciences Group, MIT Haystack Observatory, Westford, MA, USA

Total electron content (TEC) data measured from ground-based GPS receivers is compared to HF backscatter from ionospheric irregularities obtained by SuperDARN radars. A focus is placed on mid-latitudes over North America where recent expansion of the SuperDARN network allows for unprecedented coverage over areas where the density of GPS receivers is greatest. Of interest is the relationship between large-scale plasma structures seen in globally gridded TEC measurements processed at MIT Haystack Observatory and small-scale ionospheric plasma irregularities seen by the SuperDARN radars. Specifically, we examine the extent to which the small-scale irregularities form in regions of high electron density gradients located at the edges of large-scale TEC features. We present a detailed analysis of several sub-auroral polarization stream (SAPS) events observed by the new mid-latitude chain of radars during 2010-2011. In particular, we demonstrate that the ionospheric radar backscatter tends to form at the poleward edge of the mid-latitude low density TEC trough during times of enhanced geomagnetic activity. A need for future collaborative experiments with incoherent scatter radars to obtain ionospheric density profiles of the trough region during these events is also exhibited.

The effects of 3D error covariance and background model bias for an ionospheric data assimilation model

C. Y. Lin* [1,2,3], T. Matsuo [1,2], E. A. Araujo-Pradere [1,2], and J. Y. Liu [3]
(1) Cooperative Institute for Research in Environmental Sciences, University of Colorado, Boulder, Colorado, USA
(2) Space Weather Prediction Center, National Oceanic and Atmospheric Administration, Boulder, Colorado, USA
(3) Institute of Space Science, National Central University, Jhongli, TAIWAN

NOAA/SWPC data assimilation model for the ionosphere is based on the Gauss-Markov Kalman filter with the International Reference Ionosphere (IRI) as the background model, with the electron density profiles described in terms of a handful of Empirical Orthogonal Functions (EOF). To obtain assimilative analyses over the Northern America, EOF coefficients at a given longitude-latitude grid location are inferred from ground-based GPS total electron content (TEC) data by using a Kalman filter. The model has been proved to have an accuracy of about 2 TECu (10^{16} #/cm^2) on average over CONUS, when used for ground-based GPS data.

However, we have found that the model is not suited to assimilate FORMOSAT-3/COSMIC (F-3/C) GPS occultation TEC data. Due to the fact that occultation observation paths pass through large longitude latitude areas at different altitudes, the original EOF-based method with 2D background error covariance cannot be applied to occultation data. To overcome the limitation of the EOF-based method, we used the 3D background error covariance to assimilate both space-based F-3/C occultation data and ground-based GPS observation data.

Moreover, we have found that IRI shows regional biases with respect to F-3/C occultation TEC and ground-based GPS observation TEC. The bias correction is also an important issue to increase the accuracy of the assimilation result. We characterize regional IRI background model biases, by comparing simulated synthetic TEC to the two sets of GPS data: F-3/C occultation and ground-based GPS data. Finally, the effects of different 3D covariance assumptions on assimilation analyses will also be discussed.

Data assimilation of FORMOSAT-3/COSMIC electron densities using the NCAR TIE-GCM

I T. Lee(1,2), T. Matsuo(3), A. Richmond(1), J. Y. Liu(2), W. Wang(1), C. H. Lin(4), M. Q. Chen(2)

(1) High Altitude Observatory, National Center for Atmospheric Research, Boulder, CO, USA

(2) Institute of Space Science, National Central University, Chung-Li, Taiwan

(3) University of Colorado at Boulder, Boulder, CO, USA

(4) Department of Earth Science, National Cheng Kung University, Tainan, Taiwan

This paper presents our research effort to develop an assimilation model for the FORMOSAT-3/COSMIC (F3/C) GPS Occultation Experiment (GOX) observations by means of ensemble Kalman filtering using the NCAR Thermosphere Ionosphere Electrodynamics General Circulation Model (TIE-GCM) as a forecast model. More than 2000 electron density profiles are retrieved daily from the F3/C GOX, uniformly distributed around the globe. They provide an excellent opportunity to monitor the global ionospheric electron density structure, especially over oceans, deserts, and the polar regions. The NCAR TIE-GCM is a three-dimensional, time-dependent model of the Earth's neutral upper atmosphere and ionosphere which provides self-consistent solutions for the coupled nonlinear equations of hydrodynamics, thermodynamics, and continuity of the neutral gas and plasma. The Data Assimilation Research Testbed (DART), an open-source community facility for ensemble Kalman filtering (EnKF), is also used in our research.

The F3/C GOX observations are combined with the TIE-GCM simulations by EnKF algorithms implemented in DART to compute the expected value of electron density, which is 'the best' estimate of the current model state. A number of filtering experiments are conducted with real F3/C electron density profiles and the results are compared with independent ground-base observations. This paper shows the improvement of the critical ionospheric modeled parameters such as NmF2 and hmF2, and furthermore discusses the limitations of the model and the impact of ensemble member creation on the assimilation results.

The Taiwan Ionospheric Model (TWIM) and its Applications on HF Propagation and GPS Ionospheric Correction

L.-C. Tsai*[1, 2], E. P. Macalalad[2], G. H. Chen[3], and M. H. Tian[4]
(1) Center for Space and Remote Sensing Research, National Central University (NCU), Chung-Li, Taiwan
(2) Institute of Space Science, NCU, Chung-Li, Taiwan
(3) Multimedia and Game Science Department, Taipei College of Maritime Technology (TCMT), Taipei, Taiwan
(4) Department of Marine Leisure and Tourism, TCMT, Taipei, Taiwan

A three-dimensional ionospheric electron density (*Ne*) model (L.-C. Tsai, C. H. Liu, T. Y. Hsiao, and J. Y. Huang, Radio Sci., 44, doi:10.1029/2009RS004154, 2009) has been named the TaiWan Ionospheric Model (TWIM) and constructed from global distributed ionosonde *foF2* and *foE* data and vertical *Ne* profiles retrieved from FormoSat3/COSMIC GPS radio occultation measurements. The TWIM exhibits vertically-fitted α-Chapman-type layers, with distinct F2, F1, E, and D layers, and surface spherical harmonics approaches for the fitted layer parameters including peak density, peak density height, and scale height. These results are useful in investigation of near-Earth space and large-scale *Ne* distribution. This way the continuity of *Ne* and its derivatives is also maintained for practical schemes for providing reliable radio propagation predictions. We have presented a numerical and step by step ray-tracing method (L.-C. Tsai, C. H. Liu, and J. Y. Huang, Radio Sci., 45, doi:10.1029/2010RS004359, 2010) on the TWIM and including an Earth-centered magnetic dipole and horizontal *Ne* gradient effects. The methodology has been evaluated by comparing synthetic vertical ionograms generated by the method with experimental ionosonde observations and also applied to find practical high-frequency radio transmitters with determined angles of arrival and oblique incidence ray tracing. Furthermore, the ray-tracing methodology also has potential applicability to ionospheric correction as applied to GPS positioning. In this paper, ionospheric corrections for single-frequency GPS pseudoranges using the TWIM are presented. Its performance with respect with the ionospheric correction using other ionospheric models is also presented.

LaTeX Template and Sample for 2008 USNC/URSI National Radio Science Meeting, URSI Format

Thomas L. Gaussiran II*, Roy S. Calfas, and David Rainwater
Applied Research Laboratories, The University of Texas at Austin,
Austin, TX

Data assimilation tools for ionosphere specification are entering a second generation of sophistication. We report on two of the tools developed at ARL:UT. The first is a new background specification ensemble model that combines USU GAIM, RIB-G and IRI in a weighted fashion depending on variance estimates. The weighting procedure combines both electron densities and their associated uncertainties. The second tool, the Texas Reconfigurable Ionosphere Plasmasphere Logarithmic Data Assimilator (TRIPL-DA), is based on 3DVAR techniques. It ingests ionospheric data to modify a background specification (like those listed above, or an ensemble of them) at a user-specified resolution, which may be higher than that of the background model. TRIPL-DA's focus is on efficient and modular implementation of a variety of data types, given the reasonable assumption that much more abundant data will be available in the future; first-principles physics modeling is left to the background models, which are an excellent starting point but are only a fallback to real data. TRIPL-DA can assimilate numerous data types, including absolute or relative TEC (GPS, DORIS, etc.), and point measurements (in–situ electron density, ionosonde soundings). User-specified grids may be global or regional, regular or irregular; resolution is limited only by available computing power, including vertically to arbitrary altitudes. TRIPL-DA includes error and correlation estimates, including from the background model; and instrumentation & representativeness errors, among others. A unique feature is that it operates in log space, which guarantees positive-definite electron density specifications. We will present an overview of the ensemble model and data assimilation tool, and show several examples of ionosphere specifications generated from various data source types. Finally, we present new results characterizing the intrinsic uncertainties of various ray data types and the origins of the various errors.

Frequency Response and Polarization of ELF/VLF Signals Generated at the HAARP Facility

Jason Carpenter, Ryan Jacobs, Mark Golkowski

Department of Electrical Engineering, University of Colorado Denver

The HAARP facility, near Gakona, Alaska, makes use of 3.6MW of power in the high frequency range (3-10MHz) to heat the D-region of the ionosphere and transmit ELF/VLF (500Hz-10kHz) radiation through amplitude modulation of the HF beam. At long distances (>700 km), the effective radiation pattern of HAARP generated ELF signals is known to resemble that of a linear dipole that is dominated by modulation of the ionospheric Hall conductivity. However, closer to the HAARP array (<100 km) the relative role of Hall vs. Pedersen conductivity modulations has not been fully quantified. There is some disagreement among researchers as to whether the signals observed in the Earth Ionosphere wave guide are due more to horizontal currents directly modulated by the HAARP facility or if the vertical 'loop back' currents also play a role. Also, HAARP generated ELF signals are known to exhibit an amplitude dependence on modulation frequency. Numerous papers cite a maximum in ELF radiation around 2 kHz. There are several explanations for this observed maximum including the resonance at these frequencies as waves reflect in the Earth ionosphere cavity, ionospheric physics where the heating and cooling rates are such that modulation at this frequency is favored. and the cutoff frequency for the qTE1 and qTM1 modes of the Earth-ionosphere waveguide. We present results of an experiment where a series of ELF/VLF tones were transmitted with HAARP and observed at multiple locations of various distance from the HAARP facility. The amplitude dependence as a function of frequency and the ratio of Hall and Pedersen conductivities are determined at each site.

The Future of Rocket Exhaust Interactions in the Ionosphere after the Space Shuttle

Paul A. Bernhardt
Plasma Physics Division, Naval Research Laboratory, Washington, DC 20375

Wayne Scales, Haiyang Fu, Alireza Mahmoudian, Maitrayee BordikarBradley
Department of Electrical and Computer Engineering and Center for Space and Engineering Research, Virginia Tech, Blacksburg, VA

Since the launch of Vanguard in 1959, the space research community has been aware that rocket exhaust produces a disturbance in ionosphere. Launches of large rockets from many countries have produced engine burns in the ionosphere that create large area reductions in electron density. These reductions have been mainly observed using radio beacon observations of total electron content from geostationary satellites (ATS-6) and mid-earth-orbit (MEO) GPS satellites. During the era of the Space Shuttle, dedicated burns of the OMS engines in the F-layer were detected with enhanced optical intensities, the excitation of low frequency plasma turbulence, and the launch of a variety of plasma low frequency waves such as fast and slow MHD, ion acoustic, lower hybrid, and whistler modes. Each OMS engine on the Space Shuttle injected 10 kg/s of exhaust in the form of hydrocarbon products of gas phase combustion. These burns were scheduled over ground radars or for detection by the Air Force C/NOFS satellite. Future rocket experiments are being planned to make measurements rocket exhaust effects from both serendipitous and dedicated engine burns in the ionosphere. The SPACE-X Falcon Heavy and NASA's new Space Launch System (SLS) launch vehicles will provide not only enhanced payload capability but they can produce measureable perturbations in the plasma of the E- and F-layer ionospheres. The Falcon 9 rocket produces 1667 kg/s of rocket exhaust during the first 170 seconds of burn. After the second stage ignites, 129 kg/s exhaust is produced for 345 seconds. The rocket exhaust is composed of CO, H_2O, H_2, CO_2, and OH. These molecules charge exchange with atomic oxygen in the ionosphere to produce molecular ions moving faster than the sound speed. These pick-up ions drive plasma wave turbulence before they recombine with ambient electrons. Solid rocket motors are also fired in the upper atmosphere to produce both molecular ions and high speed particulates of aluminum oxide. For example, the second Charged Aerosol Release Experiment (CARE II) will use a solid rocket motor to inject molecules and particulates into the upper atmosphere. The CARE II payload will consist of both in situ and radio beacon instruments to detect electric fields, plasma waves, ion and neutral composition, and particulates. CARE II is planned for launch from Andoya Norway in the late summer of 2013 or 2014. Ground measurements will be made of radar scatter from the engine exhaust interactions and optical emissions from both sunlight scatted from exhaust particulates and luminous emissions excited by electron-ion recombination. Computer simulations with both fluid and particle-in-cell models are used to predict the changes produced during CARE II. The physical mechanisms for production of plasma turbulence during CARE II include dust streaming instability and strong electric field shears at the interface between the exhaust cloud and the ambient ionosphere.

The imminent completion of the major tasks in the construction of the New Arecibo HF facility means that we must verify that the components are working as intended. In particular, the antenna system and the transmitters must be separately commissioned before they can be connected together so that we an be sure it will provide 83 dbW at 8.175 MHz, and 80 dbW at 5.1 MHz. The transmitters have untuned outputs with five different sections covering the range of 5 MHz to 26 MHz. Thus, it is very important that the load presented to each transmitter be as close as possible to the ideal 50 ohms. In particular, it is desirable to eliminate the reactive part of the load since this can reduce the efficiency of the transmitter and reduce the available output power.

The antenna system will be ready for initial testing in October. It
Illuminates the 305 meter dish using dipoles near the surface of the dish transmitting upward to a wire mesh sub-reflector. There are three crossed dipoles for each of the two frequencies.

The dipoles will be supported on towers mounted on concrete pads underneath the dish. Each dipole element will be connected to a transmitter through a three inch coax line. The tower foundations are nearly complete, and the towers will be erected in early October, and we expect to have at least one crossed dipole in place for initial testing by the end of the month.

We will need to make some measurements on the antenna system to ensure that it meets our requirements. This consists of matching the antenna impedance to the transmission line and the transmitter closely enough to meet the transmitter specifications. We have additional requirements; for example, it is necessary for efficient use of the facility that the polarization be close to circular. In most experiments, we want O mode excitation. If we were to transmit linear only half the power would reach the reflection height. The symmetry of the system assures that most of the conditions for achieving accurate circular polarization are met, but one condition is not: that exciting the transmitters driving the orthogonal elements at 90 degrees assures 90 degree separation in the corresponding antenna currents. The reason for this is the unusual relative orientations of the the three sets of crossed dipoles used for each of the two frequencies.

One of the dipoles of each pair points toward the center of the array. If we think of the three crossed dipoles as consisting of a reference and two that are excited relative to it, one is excited 120 degrees ahead, and the other 120 degrees behind. The two elements in each crossed pair must have currents shifted by 90 degrees. In most systems all the elements excited 90 degrees apart are also spatially orthogonal. That is not the case in this array; modeling results showed that matching is easier in this configuration. This is apparently due to a higher degree of symmetry in the mutual impedances. Recent analysis shows that we expect that it will be necessary to excite the transmitters at 90 degrees plus or minus some offset in order to achieve 90 degrees in the antenna currents. We must make measurements of the mutual impedances i order to determine the size of this offset. There is one adjustment on the balun for each antenna element, and this will be adjusted for the best match. We also have the possibility to make a second adjustment. Each transmission line is used for one of the two frequencies, not both. Therefore, it can be cut to the length that gives the best load at the transmitter. Of course, one cannot improve the antenna-line match by this method, but it is possible to rotate the impedance at the line input towards real, thus reducing the dissipation in the transmitters.

The commissioning tasks that we complete in the next few months will affect the scientific usefulness of the facility, especially in the first campaign. It is important that we bring up the system in an efficient and orderly fashion.

SATURATION EFFECTS IN THE VLF SCATTERING OFF HF HEATED IONOSPHERE

Nikolai G. Lehtinen*[1], Timothy F. Bell[1], Umran S. Inan[1,2]

[1]Stanford University, Stanford, CA
[2]Koç University, Istanbul

Abstract

The HAARP ionospheric HF heating facility modifies the electron-neutral collision frequency in the *D*-region ionosphere, which creates a disturbance in the conductivity of this region. The VLF waves from Navy transmitters scatter off this disturbance, which results in a perturbation of the VLF amplitude and phase of the narrow-band signal of the VLF transmitter. This perturbation may be detected both by ground-based receivers and satellites with VLF instruments. For small disturbances of conductivity, the Born approximation may be used, which neglects the scattered field inside the disturbance compared to the incident VLF field. This method was previously used in combination with the Stanford Full-Wave Method (Stanford FWM), e.g., for calculations of scattering off lightning-created *D*-region disturbances [*Lehtinen et al.*, 2010, doi:10.1029/2009JA014776], and may be used in the case when HF power of the heater is small and the resulting change of the conductivity in *D*-region is also small. However, when for high HF power heating, the disturbance in the conductivity may be strong and therefore strongly affect the propagation of the VLF wave, so that the scattered field inside the disturbance region may be of the same order as the incident wave, which renders the use of the Born approximation invalid. In order to tackle with this problem, we introduce a novel computational technique which combines the Stanford FWM with the method of moments (MoM). This novel technique may be used for general problems of calculation of scattering on spatially localized strong perturbations in stratified media. In MoM, one solves the discretized version of an integral equation which represents the scattered field is as a convolution of the Green's function with the electric current source. The current in this case is due to the change in the conductivity of the *D*-region acting on the total electric field consisting of both incident and scattered fields. The Green's functions in the present case are to be calculated for the Earth-atmosphere-ionosphere system which is represented as a stratified medium, which is solved by application of the Stanford FWM. On the contrary to the use of the Born approximation, the MoM allows us to calculate the effects of the total field and thus may be applied to situations with any level of perturbation. We show how the field measured on the ground and at a satellite deviates from that calculated previously in the Born approximation, which in most cases overestimates the scattering by strong disturbances. In this way, we demonstrate the saturation effects in the VLF perturbations for strong HF heating.

High Frequency Resolution and High Spatial Resolution TOA Analysis for ELF/VLF Wave Generation Experiments at HAARP

Shuji Fujimaru* and Robert C. Moore
Department of Electrical and Computer Engineering, University of Florida, Gainesville, Florida, USA.

Modulated HF heating of the ionosphere in the presence of natural ionospheric current sources has been used as a method to generate electromagnetic ELF/VLF waves since the 1970's. In the ∼1-5 kHz band, the amplitude and phase of the received ELF/VLF signal depends on the amplitude and phase of the conductivity modulation generated throughout the HF-heated ionospheric body (constituting a distributed current source region), as well as on the signal propagation parameters (i.e., the attenuation and phase constants) between each of the current sources and the receiver. ELF/VLF wave generation experiments have often used linear frequency-time modulation ramps to quickly provide a measure of the generated ELF/VLF amplitude as a function of modulation frequency. In this work, time-of-arrival (TOA) analysis is applied to differentiate between line-of-sight and ionospherically-reflected signal paths, determining the amplitude and phase of each component observed at the receiver. The method has been improved to provide higher frequency resolution than past work. The new analysis technique is applied to experimental observations of ELF/VLF signals generated by modulated heating at HAARP. Additional experimental results are presented for ELF/VLF waves generated using a variable-pulse-length beam painting technique. The technique, when combined with TOA analysis, provides the ability to determine the source region characteristics with relatively high spatial resolution. Observations were performed during the 2011 HAARP Summer Student Research Campaign (SSRC). We present measurements of the amplitude *and* phase of the received ELF/VLF signal as a function of frequency using this technique, which accounts for the observed frequency-dependent signal group delay, and compare the results with those of other analysis techniques.

Approximating *D*-region electron densities using ELF/VLF wave generation experiments at HAARP

Divya Agrawal* and Robert C. Moore
Department of Electrical and Computer Engineering, University of Florida, Gainesville, Florida, USA.

Dual-beam ionospheric HF heating experiments performed at the High-frequency Active Auroral Research Program (HAARP) are used to approximate electron densities within the *D*-region ionosphere. ELF/VLF waves are generated using an amplitude-modulated HF beam, while a second HF beam simultaneously broadcasts a CW wave using a variety of HF power levels, modifying the efficiency of ELF/VLF conductivity modulation and thereby ELF/VLF wave generation. Experimental observations and theoretical predictions are used to demonstrate that the magnitude of the first ELF/VLF harmonic observed at a ground-based receiver sensitively depends on the effective radiated power (ERP) and the frequency of the CW beam. A newly-developed dual-beam HF heating model is employed together with a variety of realistic electron density and temperature profiles to predict the expected dependence of the ELF/VLF signal magnitude on the CW power level. The results demonstrate that the dependence of ELF/VLF magnitude on the CW power level is more sensitive to the electron density profile than to the electron temperature profile, particularly at low CW beam power levels. The wide distribution predicted for ELF/VLF magnitudes as a function of electron density profile indicates that similar HF power dependent experiments may eventually be used to identify a best-fit electron density profile above HAARP. Similar experiments performed in 2011 varied the modulation waveform. We present the initial experimental results analyzing the higher-order harmonics generated using the different modulation waveforms. The dependence on CW power level varies among the different modulation formats. We will compare these observations with the output of the ionospheric HF heating model.

Investigation of Dusty Space Plasmas in the Near-Earth Space Environment Using the Active Modification of Polar Mesospheric Summer Echoes

Alireza Mahmoudian, Wayne Scales
Bradley Department of Electrical and Computer Engineering Department,
Virginia Tech

Dusty plasmas are rather common in space, being found in planetary rings, interstellar clouds, cometary plasma tails, and the ionosphere of the Earth and other planets. Over 40 metric tons of meteoric dust enters the earth's atmosphere every day. This dust settles and creates natural dust layers in the altitude range between 80 and 100 kilometers which spans the earth's upper mesosphere to lower thermosphere. Since these dust layers are immersed in the earth's upper atmosphere, they become charged due to collection of electrons and ions from the earth's ionospheric plasma. Noctilucent Clouds NLCs are a fascinating visual manifestation of these dust layers. So-called Polar Mesospheric Summer Echoes PMSEs are radar echoes that are a direct consequence of the sub-visible charged dust that exists at altitudes above NLC regions. Polar Mesospheric Summer Echoes (PMSE) are strong echoes that have been typically observed in the frequency range from 50MHz to 1.3GHz and in the altitude about 85km. PMSEs are produced by scattering from electron irregularities due to electron charging on the irregular sub-visible mesospheric dust layer. The radar echoes occur at half the radar wavelength therefore the wavelength of the irregularities are roughly in the range of 10cm to 10m. The cause of dust density structures and their persistence over relatively long intervals (10s to 100s of milliseconds) had been an open scientific question and longtime controversial topic. In recent years there has been an extensive effort to investigate the polar mesospheric cloud parameters using the temporal evolution of radar echoes associated with the PMSE active modification experiments.

The first objective of this presentation is to consider the temporal behavior of electron irregularity amplitude after turn-on and turn-off of radio wave heating. The variation of plasma parameters and their effect on electron irregularity amplitude is studied. The results described in this presentation obtained using mesospheric parameters measured in recent in-situ experiments and are based on the radar facilities frequencies which are available at EISCAT and HAARP for actual experimental predictions. The computational results will be compared with the data from recent active modification of PMSE experiments at 56MHz, 224MHz and 930MHz. In particular, the effect of positive dust particles on the electron irregularity amplitude has been investigated. The measured positive and negative dust particles in recent in-situ experiments are considered to study the anti-correlation and correlation of the irregularities in the electron and ion densities which shows good agreement with the experimental data. In the second part of the presentation, an analytical model developed to validate the computational model will be introduced and possible diagnostic information regarding the charged dust layer and plasma parameters is investigated.

High power HF radio waves exciting the ionosphere provide aeronomers with a unique space-based laboratory capability. The High-Frequency Active Auroral Research Program (HAARP) in Gakona, Alaksa is the world's largest heating facility, providing effective radiated powers in the gigawatt range. Experiments performed at HAARP have allowed researchers to study many non-linear effects of wave-plasma interactions. Stimulated Electromagnetic Emission (SEE) is of interest to the ionospheric community for its diagnostic purposes. Typical SEE experiments at HAARP have focused on characterizing the parametric decay of the electromagnetic pump wave into several different wave modes such as upper and lower hybrid, ion acoustic, ion-Bernstein and electron-Bernstein. These production modes have been extensively studied at HAARP using traditional beam heating patterns and SEE detection.

New results are present from HAARP experiments using a "twisted beam" excitation mode. Unlike traditional heating beams used at HAARP or other heating facilities, the twisted beam attempts to impart orbital angular momentum (OHM) into the heating region. Analysis of twisted beam heating shows that the SEE results obtained are nearly identical to the modes without OHM. One difference in the twisted beam mode is the heating region produced is in the shape of a ring as opposed to the more traditional "solid spot" region. The ring heating pattern may be more conducive to the creation of artificial airglow layers. The results of these runs include artificial layer creation and evolution as pertaining to the twisted beam pattern. The SEE measurements aid the interpretation of the twisted beam interactions in the ionosphere.

Wave Disturbances in the Ionosphere Accompanying the Plasma Modification by SURA Facility Radiation

Leonid. F. Chernogor[1,2], Igor F. Domnin[2], Sergii V. Panasenko*[2], and Valery P. Uryadov[3]
(1) Dept. of Space Radio Physics, Kharkiv V. N. Karazin National University, Kharkiv, Ukraine
(2) Institute of Ionosphere, Kharkiv, Ukraine
(3) Radiophysical Research Institute, N. Novgorod, Russia

The results of wave disturbances observation in the ionosphere which accompanied periodic near-Earth plasma heating by high-power HF SURA facility radiation with solar terminator moving through the observation site and magnetically conjugate region were presented. The experiments to modify the ionosphere were conducted on August 31 – September 2, 2009 and September 20 – 23, 2010 between 12:50 and 17:40 UT. The temporal and height variations of electron density obtained by Kharkiv incoherent scatter radar were analyzed. The main feature of the present study was that the diagnostic instrument was located 1000 km away from the SURA facility.

The ionospheric modifications were detected to significantly change the spectral content of wave disturbances in the electron density. The wave disturbance with a period of near 30 min that correspond to facility cyclic heating and with relative amplitude of 0.08 – 0.10 was at the heights of 200 – 300 km with time delay of 60 – 90 min between the first heating start and wave observation. The apparent wave velocity of this wave disturbance was in the range of 200 – 600 m/s, assuming that it was generated by plasma heating. The internal gravity waves and the traveling ionospheric disturbances are known to have such horizontal velocities.

The disturbances with periods of 60, 90, 120 and 150 – 180 min were also. Their relative amplitude was about 0.02 – 0.10 and reached to 0.15 – 0.20 after the moving of solar terminator. The spectral components with periods of 4 –5 min which correspond to infrasound waves occurred during SURA operation at all height regions of observation in 2009.

Thus, the effect observed over Kharkiv may be explained by the generation and/or amplification of traveling ionospheric disturbances. This inferred wave pattern was in good agreement with theoretical estimates. The interaction of subsystems in the Earth – the atmosphere – the ionosphere – the magnetosphere system may possibly contribute to this observable effect. In addition, the wave disturbances with the period of about 30 min may also be generated by solar terminator moving. Long-term, regular measurements are needed to more accurately separate the effects of ionosphere heating from those of terminator moving.

Investigating the Threshold and Strength of Emission Lines Generated by Magnetized Stimulated Brillouin Scatter (MSBS) using HAARP facilities

A. Mahmoudian[1], W. A. Scales[1], P. A. Bernhardt[2], S. Briczinski[2]

[1]Electrical and Computer Engineering Department, Virginia Tech
[2]Plasma Physics Division, Naval Research Laboratory, Washington, D.C. 20375, USA

The High-Frequency Active Auroral Research Program (HAARP) in Gakona, Alaska provides effective radiated powers in the megawatt range that have allowed researchers to study many non-linear effects of wave-plasma interactions. Stimulated Electromagnetic Emission (SEE) is of interest to the ionospheric community for its diagnostic purposes. In recent HAARP heating experiments, it has been shown that during the Magnetized Stimulated Brillouin Scattering MSBS instability, the pumped electromagnetic wave may decay into an electromagnetic wave and a low frequency electrostatic wave (either ion acoustic IA wave or electrostatic ion cyclotron EIC wave).
According to the matching conditions, the O-mode electromagnetic wave can excite either an ion-acoustic wave with a frequency less than the ion cyclotron frequency that propagates along the magnetic field or an electrostatic ion cyclotron (EIC) wave with frequency just above the ion cyclotron frequency that propagates at an angle with respect to the magnetic field.

Using Stimulated Electromagnetic Emission (SEE) spectral features, side bands which extend above and below the pump frequency can yield significant diagnostics for the modified ionosphere. It has been shown that the IA wave frequency offsets can be used to measure electron temperature in the heated ionosphere and EIC wave offsets can be used as a sensitive method to determine the ion species by measuring ion mass using the ion gyro-frequency offset.
In this presentation the results of SEE experiment at 2010 PARS summer school and 2011 SSRC will be discussed. The experiment was performed at the 3rd electron gyro harmonic with frequency sweeping, power stepping and beam angle variation. Three diagnostics were implemented to study the SEE. There were 1) A 4 channel spectrum analyzer SEE receiver, 2) the University of Alaska SuperDARN radar facility and, 3) the MUIR incoherent scatter radar.

The experimental results aimed to show the threshold for transmitter power to excite IA wave propagating along the magnetic field line as well as for EIC wave while transmitter antenna beam pointed at an angle with respect to magnetic field.
A full wave solution has been used to estimate the amplitude of the electric field at interaction altitude. This electric field amplitude will be used to estimate the growth rate of IA and EIC waves using the solution of the nonlinear dispersion relation. The estimated growth rate using the theoretical model will be used to make quantitative comparisons with the threshold of SBS lines in the experiment.

On Demand Space Plasma Generation: The Metal Oxide Space Cloud Experiment

Ronald G. Caton[(1)], Todd R. Pedersen [(1),] Keith M. Groves[(2)], Theodore L. Beach[(3)] and Paul A. Bernhardt[(4)]

(1) Air Force Research Laboratory, Space Vehicles Directorate, Kirtland AFB, NM
(2) Boston College, Institute for Scientific Research, Chestnut Hill, MA
(3) Creare Inc., Hanover, NH
(4) Naval Research Laboratory, Plasma Physics Division, Washington DC

The Air Force Research Laboratory will conduct an experiment on the artificial generation of ionization clouds with heavy metal vapor releases in the ionosphere from sounding rockets. The Metal Oxide Space Cloud experiment (MOSC) consists of multiple rocket launches from the Kwajalein Atoll with releases of samarium vapor near 200 km and 130 km. The exothermic reaction of vaporized samarium metal with background oxygen atoms will create a long-lived and localized plasma cloud: $Sm + O \rightarrow SmO^{+} + e^{-}$. In at least two previous experiments, samarium gas releases in the ionosphere have shown evidence of significant ionization; however, no direct measurements of the densities were made. The primary objective of MOSC is to fully characterize the physical, spectral and plasma density composition of the artificial plasma as a function of release altitude and time. In addition to samarium canisters, the rocket payload will include a Coherent Electromagnetic Radio Tomography (CERTO) beacon with ground observing sites arranged for best reception of the signal through the cloud. Incoherent scatter probing of the ionization cloud with the ALTAIR radar facility will provide electron densities. GPS scintillation and TEC receivers will be collocated with All-Sky Imagers and HF receive equipment designed to monitor signals from a digisonde on the island of Roi-Namur. An optical spectrograph will provide details on the spectral characteristics of the plasma cloud. Results will be used to improve existing models and tailor future experiments targeted at demonstrating the ability to temporarily control the RF propagation environment through an on-demand modification of the ionosphere. Among the many questions this experiment is designed to investigate is whether an artificially generated local enhancement to the E-region conductivity will result in a regional suppression of scintillation?

The Use of Simulations for Interpreting Beacon Satellite

C. L. Rino[1], C. S. Carrano[2]

[1]Rino Consulting, Menlo Park, CA, United States
[2]Institute for Scientific Research, Boston College, Chesnut, Hill, MA, United States

Scintillation data from low earth-orbiting (LEO) satellites have been collected since Sputnik was launched in 1957. However, analysis tools have advanced to the point where geometrical dependencies, high-fidelity models, and advanced data processing techniques can be fully exploited. Three-dimensional numerical simulations are limited more by the size of the parameter space than the computation required for individual realizations. Moreover, in-situ measurements have shown that the ionospheric electron density structure can be characterized by a muiti-component power-law spectral density function. These developments provide a framework for generating high-fidelity realizations of representative local structure. The results provide a test bed for data analysis procedures that can identify statistically homogeneous segments and extract measures that characterize spatially varying structure.

In general, reconciling model predictions with data involves three critical operations, namely **signal processing** to extract the propagation-induced modulation of the received signal, **data processing** to identify homogeneous segments and extract statistical measures of structure characteristics, and **model-based data interpretation** to validate scientific hypotheses that explain the structure creation and evolution. Signal processing is often taken for granted, but strong scatter degrades data acquisition for interpretative analysis just as it degrades the performance of a communication or surveillance system. Similarly, varying geometry and large-scale structure distributions limit the extent of data segments that can be exploited for structure characterization. Any underlying structure model must support sensitivity to parameter changes that can be measured under expected operational conditions.

This paper will demonstrate the use of high-fidelity three-dimensional simulations to evaluate the requirements for model-based data interpretation. New data analysis procedures are introduced that perform time-to-space conversion, wavelet-based segmentation, and scale spectra used in conjunction with conventional spectral analysis for structure characterization. Identification of data segments that admit homogeneous structure over large enough intervals to support statistical structure characterization is a critical concern. Although correlation scales impact system performance most directly, the turbulent strength and power-law index of the dominant power-law segment establishes all the critical signal structure characteristics. Measurements are limited by competing resolution and signal-to-noise requirements. Simulations have the unique advantage of known inputs.

TURBULENCE DETECTION USING GNSS OCCULTATIONS

L. Cornman

Research Applications Laboratory, National Center for Atmospheric Research, Boulder, CO, United States

Abstract

The increased availability of Global Navigation Satellite Systems (GNSS) radio occultation (RO) data offers the ability to detect and study turbulence in the Earth's atmosphere. An analysis of how RO data can be used to determine the strength and location of turbulent regions is presented. This includes a discussion of a model for the power spectrum of the log-amplitude and phase fluctuations measured at the receiver due to a fluctuating permittivity field. This model is based on well-known weak scattering theory, but also accounts for the motion of the transmitter, receiver, and the permittivity field itself. A brief description of the assumptions that go into the model - as well as the real-world aspects of the problem that were left out - is presented. An in-depth analysis on the estimation of the model parameters is then presented. Parameter estimators based on maximum likelihood techniques are introduced and some of their statistical properties are studied. These estimators are then applied to simulated log-amplitude RO signals. This includes the analysis of statistics derived from a large number of realizations, as well as case studies that illustrate specific aspects of the problem. In using the maximum likelihood methods for this application, it is assumed that the power spectral values are exponentially distributed. However, it will be shown that some standard probabilistic methods (e.g., Pearson chi-square test) for determining goodness of fit to the distribution do not have sufficient skill to be used as an indicator of outliers in the parameter estimation. Improvements to the basic estimation methods are discussed, and their beneficial properties are illustrated.

The estimation techniques are then applied to real GNSS occultation data. The purpose of this analysis is to show how the power spectral model portrays many of the essential features in the real data, rather than an in-depth study. One aspect that is seen in the real data, but not addressed in our model, is layered - but not turbulent - structures. A brief discussion of the theoretical problems inherent in including these effects is given. This is followed by a simulated example of a layered structure embedded in isotropic turbulence.

Deducing Ionospheric Turbulence Parameters from Beacon Satellite Scintillation Measurements

Charles S. Carrano[(1)], Charles L. Rino[(2)], Ronald G. Caton[(3)], Keith M. Groves[(1)]
(1) Boston College, Chestnut Hill, MA, 02467
(2) Rino Consulting, Menlo Park, CA
(3) Kirtland AFB, Albuquerque, NM

We present an iterative approach for deducing ionospheric turbulence parameters from beacon satellite scintillation measurements which is applicable in both weak and strong scattering environments. We use Rino's model for the autocorrelation of phase (Rino, *Radio Sci*, 14, 1135-1145, 1979) with the numerical approach of Booker and MajidiAhi (*J. Atmos. Terr. Phys*, 43, 11, 1199-1214, 1981) to calculate the temporal spectrum of intensity fluctuations due to passage through a phase-changing screen. The screen parameters are determined by minimizing the difference between the measured and calculated intensity spectra in a least-squares sense using the downhill simplex method. Using a combination of theory, numerical simulations, and measurements of VHF and GPS scintillations at Ascension Island (7.96ºS, 14.41ºW), we demonstrate that the turbulent intensity and phase spectral index can be accurately retrieved even when the scintillations are saturated (S_4~1). For the case of non-evolving irregularities, the zonal drift velocity can also be retrieved (e.g. Figure 1). Finally, if the drift is known, the anisotropy ratio of the irregularities can be retrieved, but with limited accuracy because the intensity spectrum becomes insensitive to this ratio once it exceeds about 20.

When the scattering is weak, our estimates of the turbulent intensity and phase spectral index agree with those implied by Rino's analytic weak scatter theory (Rino, *Radio Sci*, 14, 1135-1145, 1979). When the scattering is strong, no analytic theory is available. In this case, the spectral index cannot be estimated from the spectrum of measured phase because it has been altered by diffraction. The spectral index cannot be estimated directly from the intensity spectrum either, as it departs from power-law form, broadening about the Fresnel frequency, except at asymptotically high frequencies where the spectrum is often obscured by receiver noise. The turbulent intensity cannot be estimated from the scintillation index (S_4) once it saturates to unity because it no longer depends on the scintillation strength. Our technique overcomes these difficulties and works equally well in strong and weak scatter environments. Previous authors (Franke and Liu, *Radio Sci*., 20, 3, 403-415, 1985) have shown that the decorrelation time (τ) can be used to infer the turbulent strength when S_4 is saturated. We argue that it is more effective to use the entire spectrum of intensity fluctuations, not just S_4 and τ, to infer the turbulence parameters.

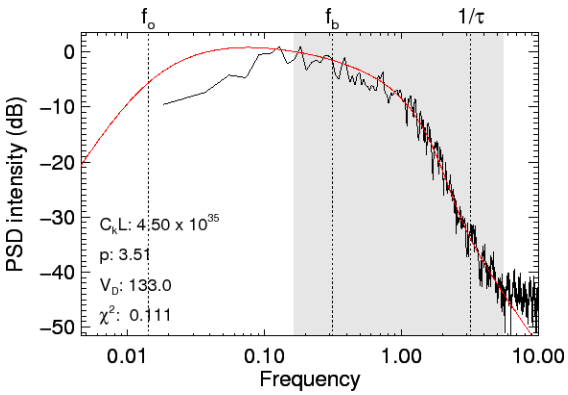

Figure 1. Spectrum of calculated (red) and measured (black) intensity fluctuations for GPS PRN 04 at Ascension Island (7 Mar 2002, 22:05 UT), along with the deduced turbulence parameters and χ^2 of the fit. Vertical lines indicate frequencies corresponding to the outer scale, Fresnel break scale, and decorrelation time. An independent measure of the zonal drift, using the spaced receiver technique, is V_D=140m/s.

Remote Sensing of Ionospheric Irregularities: CITRIS Measurements of TEC and Radio Scintillation

Carl L. Siefring and Paul A. Bernhardt
Naval Research Laboratory, Plasma Physics Division, Washington, DC 20375

Unique data on ionospheric plasma irregularities and radio scintillations from the Naval Research Laboratory CITRIS (Scintillation and TEC Receiver in Space) instrument will be presented. CITRIS is a multi-band receiver that recorded TEC (Total Electron Content) and scintillations from Low-Earth Orbit (LEO) on STPSat1. The 555+/5 km altitude 35° inclination orbit covers low and mid-latitudes, large portions of the Earth (including the Pacific, African and South American sectors), during unusually quite solar activity from April 2007 to March 2009. The measurements require propagation from a transmitter to a receiver through the F-region plasma. CITRIS used both 1) satellite beacons in LEO, such as the NRL CERTO (Coherent Electromagnetic Radio TOmography) three-frequency beacons transmitting at 150/400/1067 MHz and 2) the French global network of ground-based DORIS (Doppler Orbitography and Radiopositioning Integrated by Satellite) beacons transmitting at 401.25 and 2036.25 MHz.

This talk will concentrate on the analysis of satellite-to-satellite (CERTO-to-CITRIS) measurements. The data indicate the usefulness of monitoring such propagation paths. A summary of favorable configurations for LEO-to-LEO satellites is provided. The combination of TEC and scintillation measurements yield information on a range of scale-sizes from >1 km to about 100 m. In the case of Spread-F, ionospheric irregularities start with large scale size density gradients (100s of km) and cascade through complex processes to short scale sizes (10s of meters). It is typically the 100 m-1 km scale features that harm communication and navigation systems through scintillations.

This work supported by the Naval Research Laboratory Base Program.

Tandem Instrumented CubeSats in Low Earth Orbit for Continuous Occultation Observations of the Ionosphere

P.A. Bernhardt[1], Carl L. Siefring[1], Joe D. Huba[1], John Abrams[2], Scott Miller[2], Nestor Voronka[3]
[1]Plasma Physics Division, Naval Research Laboratory, Washington, DC 20375
[2]ARES Corporation, Torrance, CA 90502,
[3]Tethers Unlimited Inc., Bothell, WA 98011-8804

Ionospheric occultation involves a radio beacon transmitter on a satellite propagating a near line-of-sight signal to a receiver on another satellite with a ray path passing trough the ionosphere. Satellites in low-earth-orbit perform GPS occultations by sporadically recording the phase and amplitudes of L-Band signals from GPS satellites at a much higher altitude. The advantage of the GPS occultation technique is that there are a large number of GPS satellites available for the LEO satellite to observe the ionosphere and provide electron density profiles. These profiles represent a profile averaged over about 500 km in horizontal range along the occultation propagation path. The disadvantages of the GPS occultation technique are (1) the measurements are not continuous because they only use GPS satellites near the plane of the LEO satellite orbit near the horizon, (2) only L-Band observations are made limiting the radio frequency range of the scintillation information, and (3) the location of a disturbance along the propagation path is not known to better than ~200 km accuracy.

A new concept, called the Tandem Instrumented CubeSats Experiment (TICE), has been developed using a pair of CubeSats orbiting in tandem in a common orbit plane. With a ~4000 km range between the satellites, the propagation path will have constant tangent height around 80 km altitude well below the E- and F-layer ionospheres. The radio link between the transmitter CubeSat and receiver CubeSat will be continuous so that there will be no data gaps in the ionospheric measurements. Irregularities found in the orbit plane in the ionosphere are observed in two regions on either side of the path tangent point. The ionospheric irregularities will be triangulated from the tandem satellite observations to provide both location and scintillation strength. The space-based observations of the ionosphere will (1) determine the locations of plasma regions where radio propagation is affected and (2) collect data that supports physics and empirical models of the ionosphere. TICE will use UHF and L-Band transmissions to provide high accuracy total electron content (TEC) as well as radio scintillation data in each frequency band. Along with a radio beacon receiver or transmitter, each CubeSat will have a plasma probe to provide in situ measurements the electron density and density irregularities. The operations of the TICE satellite system has been simulated using plasma densities provided by the NRL SAMI3 model. The data from TICE can be directly assimilated into global ionospheric models.

The construction of the ground-based GPS TEC map over US using the non-stationary wavelet-based error covariance

Yang-Yi Sun*[(1),(2),(3)], Tomoko Matsuo[(1),(2)], Eduardo A. Araujo-Pradere[(1),(2)], and Jann-Yenq Liu[(3)]

(1) Cooperative Institute for Research in Environmental Sciences, University of Colorado, Boulder, Colorado, USA.

(2) Space Environmental Center, NOAA, Boulder, Colorado, USA.

(3) Institute of Space Science, National Central University, Jhongli, Taiwan.

In this study, we used the non-stationary wavelet-based and the stationary Gaussian background error covariances with the Kalman filter update formulas to construct the total electron content (TEC) map over US from ground-based GPS data, and further examined the impacts of the stationary and non-stationary covariances on TEC maps for different spatial scale under the geomagnetic disturbed and quiet conditions on March 31, 2001 and March 11, 2001, respectively. Our results show that large spatial scale (>300km) structures in the TEC map, such as the storm enhanced density (SED) for the intense storm on March 31, 2001, can be well constructed by using both wavelet–based and Gaussian background error covariances; while the wavelet-based background error covariance can help better describe the finer TEC structures (<300km) in both disturbed and quiet geomagnetic condition.

Recent Results from GNSS-Reflections Remote Sensing

Stephen T. Lowe
Jet Propulsion Laboratory / California Institute of Technology

This talk will discuss the science goals of GNSS-Reflections remote sensing and review the current state of its development, with emphasis on global, space-based applications. A review of the basic principles and signal processing steps needed to extract observables will be outlined. Proposed mission scenarios will be reviewed and compared for their science objectives, system design and hardware constraints. Recent results from the GNSS-R 2010 Workshop will also be summarized. A new, proposed signal-processing scheme presented there will be discussed and compared to other competing techniques, and related to mission system design. Finally, a discussion of how OSSEs will likely be required to create the science case for GNSS-R missions.

Polarimetric Bistatic Scattering Patterns of Circularly Polarized Waves from Ocean-Like Surfaces

Jeffrey D. Ouellette* [(1)], Joel T. Johnson[(1)]
(1) The Ohio State University, Columbus, OH, USA

The use of GNSS receivers for earth remote sensing is becoming an increasingly attractive approach for complementing satellite-borne remote sensing systems. GNSS-R provides a relatively inexpensive, passive method for observing ocean properties such as altimetry, wind speed, and salinity. GNSS reflections are primarily assumed to be of interest in near specular regions, although some bistatic systems have been proposed that could potentially observe reflections in other bistatic configurations, including those outside the plane of incidence. It would therefore be beneficial to examine and attempt to model the full polarimetric bistatic scattering pattern produced by a circularly-polarized wave impinging upon an ocean surface. Polarimetric correlations are also of particular interest for understanding the physical properties of polarization signatures of ocean-like media.

Existing analytical models for rough-surface scattering can be extended to predict out-of-plane bistatic scattering. This presentation will focus on the results of one such analytical model: the Small Slope Approximation (SSA). The SSA model provides a truncated series of field terms which reduces to the Small Perturbation Method (SPM) and to the Kirchoff Approximation (KA) in the low and high frequency limits respectively. Computations from this theory will be illustrated using two terms from the field series solution so that three terms are obtained in the series for normalized radar cross section. The ocean-like surface considered in this study will be assumed to be a Gaussian random process with an isotropic, composite surface spectrum.

NRCS predictions for the complete bistatic scattering pattern will be presented in RR, LL, RL, and LR polarizations. Polarimetric correlations will also be presented along with a discussion of the properties observed. The influence of varied incidence angles will also be illustrated. The implications of the results for current and future remote sensing systems will be discussed.

THE CYCLONE GLOBAL NAVIGATION SATELLITE SYSTEM (CYGNSS) MISSION

Christopher S. Ruf*[1], Scott Gleason[2], Zorana Jelenak[3], Stephen Katzberg[4], Aaron Ridley[1], Randall Rose[5], John Scherrer[5] and Valery Zavorotny[6]
(1) University of Michigan, Ann Arbor, MI USA
(2) Concordia University, Montreal, QC, Canada
(3) NOAA/NESDIS/StAR-UCAR, Silver Spring, MD USA
(4) South Carolina State University, Orangeburg, SC USA
(5) Southwest Research Institute, San Antonio, TX USA
(6) NOAA Earth System Research Laboratory, Boulder, CO USA

The Cyclone Global Navigation Satellite System (CYGNSS) is a spaceborne mission concept focused on tropical cyclone (TC) inner core process studies. CYGNSS attempts to resolve the principle deficiencies with current TC intensity forecasts, which lies in inadequate observations and modeling of the inner core. The inadequacy in observations results from two causes: 1) Much of the inner core ocean surface is obscured from conventional remote sensing instruments by intense precipitation in the eye wall and inner rain bands. 2) The rapidly evolving (genesis and intensification) stages of the TC life cycle are poorly sampled in time by conventional polar-orbiting, wide-swath surface wind imagers. CYGNSS is specifically designed to address these two limitations by combining the all-weather performance of GNSS bistatic ocean surface scatterometry with the sampling properties of a constellation of satellites. The use of a dense constellation of nanosatellite results in spatial and temporal sampling properties that are markedly different from conventional imagers. Detailed simulation studies will be presented which examine the sampling as functions of various orbit parameters of the constellation. Detailed historical records of actual TC storm tracks are overlaid onto a simulated time series of the surface wind sampling enabled by the constellation. For comparison purposes, a similar analysis is conducted using the sampling properties of several past and present conventional spaceborne ocean wind scatterometers. Differences in the ability of the sensors to resolve the evolution of the TC inner core are examined. A candidate low-cost spacecraft and GNSS receiver design are considered which could practically be used in an affordable constellation mission. Compromises in some aspects of the design are necessary (e.g. limiting the downward looking antenna gain) in order to keep the system small and affordable. The signal-to-noise ratio of the measured scattered signal, and the resulting uncertainty in retrieved surface wind speed, are also examined.

GNSS and Radio Beacons Reflected Waveforms Modeled with Small Slope Approximation

Alexander G. Voronovich[(1)], Valery U. Zavorotny[(1)]
(1) Earth System Research Laboratory, NOAA, Boulder Colorado

Currently, theoretical predictions for the performance of GNSS remote sensing applications such as altimetry and scatterometry are mostly based on the geometric optics (GO) limit of the Kirchhoff (physical optics) model. For weak GNSS signals received by low-gain antennas the most of the reflected power arrives from the quasi-specularly scattering zone. For this bistatic forward-scattering regime and for a predominant, left-hand circularly polarized (LHCP) scattered component the GO model works quite satisfactory. However, the GO cannot correctly predict a right-hand circularly polarized (RHCP) scattered component, or it can be insufficient for scattering angles when quasi-specular reflections are affected or dominated by diffraction or Bragg scattering.

Recently a successful use of powerful radio beacon signals such as signals of XM Radio satellites for ocean scatterometry was demonstrated. These experiments make relevant considering bistatic scattering regimes other than forward scattering, e.g., out-of-plane bistatic scattering. Same is true for GNSS scattered signals received with high-gain antennas. More advanced approach to address this problem would be a so-called small-slope approximation (SSA) that accounts for both quasi-specular and diffraction mechanisms.

The use of the first-order SSA for calculating of the LHCP scattered component of the GNSS signal was already demonstrated, however, it cannot correctly predict the RHCP scattered component and effects of out-of-plane bistatic scattering. The second-order SSA is needed to overcome these difficulties. Here we present results of numerical simulations of LHCP and RHCP normalized bistatic cross sections for the case of ocean surface elevations described by Gaussian statistics and the empirical wave spectrum. Based on obtained cross sections reflected waveforms are produced for the case of GNSS and XM Radio signals.

Ocean Surface Wind Speed Measurements from High-Altitude Aircraft Using GPS Delay-Doppler Maps

Valery U. Zavorotny[(1)], Nereida Rodriguez-Alvarez[(1,2)], Dennis M. Akos[(3)]
(1) Earth System Research Laboratory, NOAA, Boulder Colorado
(2) Universitat Politècnica de Catalunya and IEEC CRAE/UPC, Barcelona, Spain
(3) Department of Aerospace Engineering Sciences, University of Colorado at Boulder

Traditionally, GPS ocean surface wind speed measurements rely on sensitivity of the correlation waveform of GPS reflected signals to L-band filtered surface roughness, namely, to slope variance of such a surface. The correlation waveform emerges as a result of de-spreading of the in-phase (I) and in-quadrature (Q) components of the GPS reflected signal received by the relatively low-amplitude and slow flying platform. A Doppler frequency dimension can be added to the de-spread signal if the receiver platform flies fast and at high altitudes. In this case, various areas of the rough surface introduce various Doppler shifts into the scattered signal allowing so called delay-Doppler mapping (DDM). Typically, this situation is associated with satellite-based GPS bistatic radars. Actually, the DDM regime can be achieved using a high-altitude jet aircraft for a receiver platform.

A CU software bistatic radar system was installed on the NOAA Gulfstream-IV jet aircraft and operated during four flights in January, 2010 at altitudes, ~13,000 m across the Northern Pacific Ocean. Wind speed and direction were available from dropsondes deployed from the same aircraft. Here we present the analysis of delay-Doppler maps (DDM) obtained as a result of processing of the collected I and Q data. Thereafter, the DDMs were used to retrieve surface wind speed employing several different algorithms. In contrast to previous works where surface winds have been retrieved by fitting the theoretically modeled curves into measured correlation waveforms, here we do not use any theoretical model. Instead, the DDMs characteristics are calibrated against the surface winds obtained in simultaneous dropsonde measurements.

Snow monitoring at Niwot Ridge using GPS interferometric reflectometry

Felipe G. Nievinski* (1), Kristine M. Larson (1)
(1) University of Colorado, Boulder, CO, 80309

GPS interferometric reflectometry (GPS-IR) is a method that exploits multipath for ground-based remote sensing in the surroundings of a GPS antenna. It operates on L-band, leveraging hundreds of conventional GPS sites existing in the U.S., with a typical footprint of 30-meter radius. As line-of-sight and coherently reflected signals go in and out of phase, the power recorded by a GPS receiver goes through peaks and troughs that can be related to land surface characteristics, such as soil moisture and snow depth.

Here we examine the capability of GPS-IR to retrieve snow depth. A forward/inverse model originally developed for snow depth was recently extended to account for layering to study both synthetic and real observations. GPS snow depth retrievals are compared with a terrestrial scanning laser, an airborne LIDAR campaign, manual stake surveys, and ultrasonic depth sensors. Additionally, we explore the possibility of retrieving snow density. This will determine the feasibility and limitations of GPS-IR for monitoring of snow water equivalent (SWE), the amount of water stored in the snowpack.

All data were collected between 2009-2011 at Niwot Ridge LTER in Colorado, at a 3,500-m altitude alpine tundra site. Niwot receives around 1,000 mm of precipitation per year and has a mean annual air temperature of -3.8ºC. Snow density and temperature is measured in 10-cm vertical increments at snowpits dug approximately every week. The GPS system allows for measurement of the snowpack several times a day at multiple azimuths as satellites rise and set. The peak snow depth was 1.7m in 2009/2010 and 2.5 m in 2010/2011. Snow density ranged from 200 to 600 kg/m³.

GNSS-R advances at the Remote Sensing Lab – UPC

A. Camps[1], N. Rodriguez-Alvarez[1], E. Valencia[1], H. Park[1], J. F. Marchan-Hernandez[2], A. Aguasca[1], M. Vall-llossera[1], I. Ramos-Perez[1], G. Forte[1], X. Bosch-Lluis[3*]

(1) Universitat Politecnica de Catalunya and IEEC/CRAE-UPC, Campus Nord UPC, Building D3, 08034 Barcelona, Spain
(2) Institut Cartografic de Catalunya, Parc de Montjuic - 08038 Barcelona, Spain
(3) Microwave Systems Lab, Department of Electrical and Computer Eng., Colorado State University, Fort Collins, CO 80523, USA.

The *Passive Advanced Unit (PAU) for ocean monitoring* is a new instrument concept originally proposed in 2003 to the European Science Foundation (ESF) within the frame of the EURYI program to test the feasibility of using GNSS signals of opportunity Reflected (GNSS-R) over the sea surface to make sea state measurements and perform the sea roughness correction of the L-band brightness temperature and improve the quality of the sea surface salinity (SSS) retrievals. During the last 6 years the Remote Sensing Lab. has been working on it and other instrument configurations have been devised and implemented. It was found that the GNSS-R could also be applied to soil moisture and vegetation mapping, water level and snow height monitoring. Directly related to PAU, two prototypes have been developed, both working at GPS L1 band: PAU-RA a real aperture version of the instrument with a 4x4 element array with digital beamforming (2 simultaneous beams) and polarization synthesis, making use of the innovative radiometer topology to avoid the input switch, and PAU-SA a synthetic aperture version of the instrument, which is also used to test potential new technology developments and algorithms for future aperture synthesis interferometric radiometers and SMOS follow-on missions.

In parallel to these two instruments and in order to advance faster in scientific studies regarding to GNSS-R techniques, other instruments have been developed testing concepts and giving good results: PAU-OR with just one receiver for ground tests, and griPAU its second version of a real-time 64x64 points Delay Dopler Map (DDM) instrument, and PAU-ORA, a lighter version of PAU-OR for aircraft operations from a remote controlled plane.

As a result of these developments and studies, a space-borne version of griPAU is currently under development by the company ADTelecom S.A. to be boarded in the Instituto Nacional de Tecnicas Aerospaciales (INTA) MicroSat-1 mission. Also, a new type of GNSS-R instrument (SMIGOL) that measures the interference pattern (IP) between the direct and reflected GNSS signals was developed for soil moisture, vegetation, and topography monitoring, and after, used for snow and water level in reservoirs monitoring.

Outstanding Issues in Understanding the Role of VLF Waves in the Inner Magnetosphere

Michael J. Starks*[(1)], Jonah J. Colman[(1)], Jay M. Albert[(1)], Richard S. Selesnick[(1)], Christopher E. Sillence[(1)]and Richard A. Quinn[(2)]

(1) Air Force Research Laboratory, Space Vehicles Directorate, Kirtland AFB, NM, USA

(2) AER, Inc., Lexington, MA, USA

The importance of very low frequency radio waves to the dynamics and structure of trapped electrons in the inner magnetosphere has long been appreciated by the radiation belt community. An unbroken thread of cause-and-effect hypotheses extends from the early observations of terrestrial transmitters, lightning and precipitating particles to the modern day. To a real extent, the processes operating below L = 2 have been considered well-understood, and focus within the community has largely shifted to the much more dynamic, data-starved (and therefore challenging) outer zone. However, recent modeling and validation efforts using more sophisticated simulations and improved satellite data sets have cast doubt on current assessments of the balance of power in the inner magnetosphere, and in particular for L < 2. Long believed to be critical to explaining observed particle lifetimes in this region, terrestrial VLF transmitters appear not to play a dominant role except in specific, limited circumstances, which in itself is a challenging feature to explain. By contrast, the importance of lightning-generated VLF seems underappreciated and responsible for substantial variability in the near-Earth VLF flux. Finally, previous modeling efforts that restrict wave-particle interaction calculations to the magnetic equatorial plane may significantly underestimate the effects of these combined wave sources, as off-equatorial resonance contributions are often non-negligible for certain particles. In this presentation, we review the current models and recent evidence of discrepancies. The results of new wave-particle simulations, lightning climatology efforts, VLF propagation models, and data analyses will be presented in an effort to construct a road-map toward bringing the models into agreement with reality.

SAID/SAPS-related VLF waves and the outer radiation belt boundary

Evgeny Mishin[(1)], Jay Albert[(1)], Ondrej Santolik[(2)]
(1) Space Vehicles Directorate, Air Force Research Laboratory, Kirtland AFB, NM 87117, USA
(2) Department of Space Physics, Institute of Atmospheric Physics, Praha, Czech Republic

We explore Cluster and CRRES observations of plasmaspheric broadband hiss-like VLF emissions related with subauroral ion drifts/polarization streams (SAID/SAPS) to numerically simulate losses of energetic outer zone electrons due to wave-particle interactions. These emissions represent a distinctive subset of substorm/storm-related VLF activity in the region co-located with substorm injected energetic ions. Significant values of pitch-angle diffusion coefficients suggest that SAID/SAPS-related VLF waves could be responsible for the alteration of the outer radiation belt boundary during (sub)storms..

High-Power Radio Wave Heating of the D-Region Ionosphere Above HAARP

Robert C. Moore*
Department of Electrical and Computer Engineering, University of Florida, Gainesville, Florida, USA.

This paper summarizes D-region modification experiments performed at the High-frequency Active Auroral Research Program (HAARP) observatory in 2011. Observations focus on ELF/VLF wave generation experiments, HF cross-modulation experiments, and dual-beam heating experiments. The new ELF/VLF modulation formats used in 2011 provide a means to demonstrate significant improvements in ELF/VLF wave generation efficiency. A variety of HF beam patterns were implemented and compared, and the results indicate that relatively narrow HF beam patterns may be used to estimate the efficiencies of ELF/VLF wave generation for presently unrealizable HF beam patterns. New beam-painting techniques were implemented in order to determine the distribution of ELF/VLF source currents with relatively high spatial resolution. Results indicate that partial beam-painting sweeps generate larger ELF/VLF amplitudes, require less transmitter power, and thus have a higher HF-to-ELF/VLF conversion efficiency. New techniques for extracting the frequency-dependence of ELF/VLF wave propagation are also demonstrated. HF cross-modulation experiments are used to assess the modulated rate of absorption in the D-region ionosphere as a function of altitude. The HAARP digisonde was used to assess the aggregate rate of ambient and HAARP-modified absorption between 1 and 7 MHz. Dual-beam HF heating experiments demonstrate the ELF/VLF wave generation dependence on the powers of the beams. First harmonic observations at low power are tied closely to the electron density profile of the D-region ionosphere. Higher harmonic observations exhibit different dependencies on HF power than the first harmonic, and are possibly tied to the electron temperature profile. Each of these experimental observations is compared with the predictions of an ionospheric HF heating model.

Alfvén Waves, Current Sheets and the Evolution of Auroral Forms

Christopher C. Chaston* (1)
(1) Space Sciences Laboratory, University of California, Berkeley, CA, 94720

Using observations and numerical techniques we examine the evolution of auroral forms. It is shown how current sheets and Alfven waves become unstable to a variety of plasma instabilities which lead to vortex formation and a broad spectrum of Alfvénic fluctuations. It is shown how this process drives the evolution of auroral forms observed in camera observations both from space and from the ground. From statistical field and plasma observations we demonstrate how the energy transport across scales initiated through this process is sufficient to power the particle acceleration observed. From imaging observations evidence for the action of an Alfven wave cascade is demonstrated from a consideration of the spectral variation of auroral motions and intensity to reveal both the Alfvénic nature of these motions and of auroral arc structuring.

Depending on the nature and distribution of plasma along the geomagnetic field this evolution is initiated by well known plasma instabilities. Simulations suggest that in the case of significant cold plasma densities extending along the field-line the process is initiated through reconnection across current sheets above the auroral arc associated with a tearing instability (C. E. Seyler, J. Geophys. Res., 95, 17199). With more tenuous and hotter plasmas flow shears become sufficient to drive the Kelvin-Helmholtz instability. We show that these processes provide flows and current sheet distortions very similar to those observed under each of these conditions. On smaller scales secondary processes become important and lead to robust scaling laws of spectral energy density with wavenumber. These scaling laws are well represented in fields and optical observations.

ULF Waves Generated by the Ionospheric Feedback Instability near Discrete Aurora

Anatoly V. Streltsov*[(1)], Nan Jia[(2)], Eric D. Donovan[(3)],
Harald U. Frey[(4)], Todd R. Pedersen[(5)]
(1) Department of Physical Sciences, Embry-Riddle Aeronautical University, Daytona Beach, FL, USA.
(2) Thayer School of Engineering, Dartmouth College, Hanover, NH, USA.
(3) Physics Department, University of Calgary, Calgary, Canada.
(4) Space Sciences Laboratory, University of California, Berkeley, CA, USA.
(5) Space Vehicles Directorate, AFRL, Kirtland AFB, Albuquerque, NM, USA.

Ground-based magnetometers frequently detect localized packages of intense electromagnetic waves with frequencies of several mHz in a close vicinity to discrete auroral arcs. One of the main questions which remains unanswered for a number of years is how and where these waves are generated. Some studies suggest that they are generated in the magnetosphere by mode coupling/conversion between compressible and shear MHD modes, and their frequencies are primarily determined by the frequencies of magnetospheric drivers (e.g., irregularities in the solar wind or periodicities associated with the KH instability). Other studies suggest that these waves can be generated by electromagnetic coupling between the ionosphere and the magnetosphere, and parameters of the ionosphere play important role in determining their frequencies and other spatiotemporal characteristics.

We present results from a numerical study of generation of ULF waves in the ionospheric region adjacent to the bright discrete arc. There the ionospheric density can be depleted by the downward/return magnetic field-aligned-current (FAC) carrying electrons from the ionosphere. The closure of the magnetospheric FACs through the low-conducting ionosphere causes electric field, which may serve as an energy source for the development of the ionospheric feedback instability (IFI). This instability has been studied extensively during several decades assuming that the background plasma and the perpendicular electric field are homogeneous in the direction perpendicular to the ambient magnetic field. We extend these studies to the case of a density cavity in the ionosphere and magnetosphere and the inhomogeneous electric field. These density cavities are expected to occur in the vicinity of discrete auroral arcs associating with intense FACs which can substantially modify density and the electric field in the ionosphere. Our study demonstrates that the cavity 1) localizes the development of the instability in the direction across the ambient magnetic field; 2) saturate the amplitude of the feedback-unstable ULF waves and corresponding density perturbations and 3) broaden the spectrum of the generated waves. We discuss relations between our numerical results and observations.

Effect of Hall Conductivity on Feedback-Unstable ULF Waves at High Latitudes

Nan Jia and Anatoly V. Streltsov
Thayer School of Engineering, Dartmouth College, Hanover, NH 03755, USA.

Small-scale, intense ultra-low-frequency electromagnetic waves and magnetic field-aligned currents (FACs) are frequently detected by low-orbiting satellites above the auroral ionosphere. Observations show that these waves frequently coincide with precipitation of energetic electrons into the ionosphere, ion outflow, ion heating, and density cavities at low altitudes, which suggests that small-scale ULF waves play a significant role in the re-distribution of plasma content between the ionosphere and the magnetosphere and other important aspects of magnetosphere-ionosphere interactions at high latitudes. This suggestion motivates our interest to study geophysical processes responsible for the generation and controlling spatiotemporal properties of small-scale FACs. One of these mechanisms is the ionospheric feedback instability (IFI), which occurs when ionospheric conductivity is low and the large-scale electric field exists in the ionosphere. The instability has been explored and described in many papers which were mostly focused on wave generation and spatiotemporal dynamics of Pedersen conductivity, caused by precipitation of energetic electrons into the ionosphere. The effect of Hall conductivity has been neglected in most of these studies, particularly in numerical ones, because taking into account of this effect requires development of a 3D numerical model for the magnetosphere with 2D ionospheric boundary conditions. We present results from numerical simulations of such new model, which uses reduced, two-fluid MHD equations to model ULF waves in the magnetosphere. The model also includes effect of variation of Hall and Pedersen conductivities in the ionosphere caused by FACs, and active feedback of these variations on the dynamics of FAC in the magnetosphere. In this talk we present results from a simulations showing development of the ionospheric feedback instability with and without effects of the Hall conductivity. In particular, we consider the situation when the background plasma density and the electric field in the ionosphere are inhomogeneous in the direction across the ambient magnetic field. Such situation frequently arises in the vicinity of bright discrete auroral arcs, produced by a system of FACs interacting with the ionosphere. The results from our numerical modeling are compared with selected observations.

SPACECRAFT CHARGING IN A DUST-RICH ENVIRONMENT

H.-W. Hsu*[1], M. Horanyi[1], S. Kempf[1], and E. Grün[2]

[1] LASP, University of Colorado at Boulder, USA
[2] MPI für Kernphysik, Heidelberg, Germany

One of the most remarkable discoveries of the Cassini-Huegens mission at Saturn is the detection of a plume of gas and icy dust emanating from the south polar region of Enceladus. The water vapor plume is found to be the major source of the Enceladus neutral torus and the magnetospheric plasma, while icy dust grains emitted as collimated jets replenish the diffuse E ring that extends from Enceladus to the orbit of Titan. Since the discovery of Enceladus' plume, several close flybys are planed to understand the plume properties as well as the dust-moon-magnetosphere interactions. In addition to the Cosmic Dust Analyser (CDA), under certain conditions Cassini plasma / radio wave instruments (e.g., RPWS, CAPS, and INMS) are capable of detecting charged dust particles. The in-situ plasma/dust measurements collectively provide important informations of this dust-rich plasma environment.

A significant electron deficiency in the vicinity of Enceladus has been reported based on the Cassini Langmuir probe measurements and has been interpreted as an indication of the "dusty plasma" condition. Furthermore, the modeled spacecraft potential is significantly more negative than indicated by the Cassini Langmuir probe measurements. In this work we consider the dust influence to the spacecraft charging by taking two dust–related charging currents into account: (a) the convective dust current; and (b) the impact plasma dust current. The convective dust current is the ram current carried by the charged dust to the spacecraft. The impact plasma dust current is the collection of impact-generated plasma from the dust-spacecraft impacts. Our results show that these dust currents are important at high spacecraft speed or in regions with a low plasma-to-dust ratio, and can lead to reduced spacecraft charging.

Observation of Whistler Wave Resonances in Laboratory Plasma

Bill Amatucci* [(1)], Dave Blackwell[(1)], Erik Tejero[(1)], Chris Cothran[(2)], Leonid Rudakov[(3)], Guru Ganguli[(1)], and Dave Walker[(2)]
(1) Plasma Physics Div., Naval Research Laboratory, Washington, DC
(2) Global Strategies North America, Inc, Crofton, MD
(3) Icarus Research, Bethesda, MD

Whistler waves are pervasive in ionospheric and magnetospheric plasmas. The whistler mode propagates along the magnetic field as a right-hand elliptically polarized wave with frequency well above the ion cyclotron frequency, but below the electron cyclotron frequency. Broadband bursts of electromagnetic noise released during lightning discharges provide a steady terrestrial source of whistlers in space, while within the magnetosphere itself, locally generated whistler modes such as chorus and VLF hiss are abundant. Naturally occurring electromagnetic whistler mode signals frequently propagate down to the surface of the Earth, where they can be detected in the Very Low Frequency (VLF) range.

Numerous advances in understanding the basic whistler wave propagation physics have been made since the earliest observations. The waves have been extensively studied *in situ* using sounding rockets and satellites, via ground-based transmitters and receivers, through theoretical investigations, and they have also been studied in laboratory experiments. Numerous laboratory and space experiments have investigated many aspects of whistler waves, from the basic propagation characteristics to interesting nonlinear effects. In particular, Stenzel and co-workers and Boswell and co-workers have investigated many aspects of whistler wave propagation in laboratory plasmas. Observations of whistlers in the ionosphere and magnetosphere are abundant. Yet, despite the wealth of space and laboratory observations, many important issues regarding the nonlinear behavior of these waves, such as self-ducting of large amplitude whistlers, amplification and secondary whistler emission in the presence of energetic electrons, and whistler-plasma interactions are not yet fully understood.

In order to investigate the effects of large amplitude whistler waves, standing whistler wave patterns have been created in the NRL Space Physics Simulation Chamber. Partial reflection of antenna-launched whistler waves from the chamber end boundaries creates a combination of standing and traveling waves. By controlling the axial magnetic field profile, cyclotron absorption of whistlers can occur before reflection, leaving only the forward propagating waves. By comparing standing wave amplitudes to the forward propagating, cavity Q's in excess of 30 have been observed. Under uniform axial magnetic field conditions, the addition of planar conducting grids near the ends of the plasma column improves reflection and increases the value of Q. This work was supported by the Naval Research Laboratory Base Program.

Laboratory Studies of Electromagnetic Velocity Shear-Driven Instabilities

Erik M. Tejero*[(1)], William E. Amatucci [(1)], Christopher Crabtree [(1)], Guru Ganguli [(1)], and Christopher D. Cothran[(2)]
(1) Naval Research Laboratory, Washington, DC, 20375
(2) Sotera Defense Solutions, Crofton, MD

Observations of low frequency, electromagnetic ion cyclotron waves have been made in many regions of the space environment. Many theoretical mechanisms have been presented to account for these waves and the resulting transversely accelerated ions. Sheared flows produced by localized electric fields coupled with a perpendicular magnetic field are a potentially important energy source that can create waves of this type. *In situ* observations of sheared plasma flows collocated with electromagnetic wave activity have led to a laboratory effort to investigate the impact of electromagnetic, velocity shear-driven instabilities on the near-Earth space plasma dynamics. Under scaled ionospheric conditions in the NRL Space Physics Simulation Chamber, the transition from electrostatic to electromagnetic ion cyclotron wave propagation is being investigated.

Previous experiments at NRL demonstrated that transverse sheared plasma flows can independently drive electrostatic ion cyclotron waves. It was also observed that these waves were capable of heating the ions in the direction transverse to the magnetic field. The ongoing experiments at NRL are characterizing the electromagnetic ion cyclotron waves driven by the sheared flows. The growth rate, parallel and perpendicular wavelengths, ratio of wave electric to magnetic field fluctuations, and critical velocity are measured as the plasma beta is increased. A recent extension to the theory for this instability that accounts for rotational effects provides a more natural comparison to the experiment. Experimental observations and a comparison to this theory will be presented. This work is supported by the Naval Research Laboratory Base Program and NASA.

Using laser-produced energetic electrons to model ionospheric phenomena in the laboratory

Stephen Vincena
UCLA Department of Physics and Astronomy
Basic Plasma Science Facility
1000 Veteran Avenue, Room 15-70
Los Angeles, CA, 90095-1696, USA
vincena@physics.ucla.edu

Bursts of energetic electrons are commonly observed throughout the earth's auroral zone and are associated with a host of physical phenomena including Very Low Frequency (VLF) saucers, Alfvén waves, and (possibly) electron phase-space holes. In this laboratory experiment, a burst of field-aligned electrons is produced by the expansion of a dense, laser-produced plasma (lpp) into a uniform, lower density background plasma. The experiment is conducted in the upgraded **La**rge **P**lasma **D**evice (**LaPD**) at UCLA's Basic Plasma Science Facility.

The background plasma is He, Ne, or Ar, with plasma parameters: ω_{ce}/ω_{pe}=0.1—0.3, $T_e/T_i \approx 6$, plasma radius=66 r_{ci}, length=17m. Various solid targets are struck with a NdYAG laser (1J, 7ns pulse) focused to a spot size of less than one millimeter. The ions in the lpp (with energies of several keV) are initially unmagnetized. The electrons, however, remain magnetized and a fraction of them jet away from the point source of the laser impact in a field-aligned burst, perhaps forming a beam-like distribution similar to auroral electrons. The current systems from the lpp evolve in an entirely self-consistent manner, without the need for artificially imposed bias potentials.

We present data on the generation of broadband lower hybrid waves by the energetic electrons; the observation of a relatively large amplitude bipolar electric field pulse with a temporal width equal to the lower hybrid period; we also present measurements on the trapping of the lower hybrid waves as they propagate across the background magnetic field and encounter a pre-generated, cylindrical depletion in plasma density with both cross-fields size and density gradient scale length equal to several electron inertial lengths—as are also present in the earth's auroral ionosphere. Wave frequency spectra vs. distance perpendicular to the background field are presented in direct analogy to the frequency vs. time spectrograms of VLF saucers.

Work supported by DOE and NSF.

We will present results from ongoing experimental investigations of the possibilty of nonlinear mode conversion between lower hybrid and whistler waves that can occur at high incident whistler wave amplitude. Recent theoretical results suggest that under certain conditions the direction of the wave vector can be greatly changed with only a small change in the frequency spectrum due to wave scattering from density perturbations created by the ponderomotive force of the initial wave. The experiments are performed in the NRL Space Physics Simulation Chamber facility. The waves are excited with coaxial-ring and dipole antennas which operate from a few kHz to 1 GHz in the power range of 1 milliwatt to 10's of watts. The transmitted wave signals are received by smaller electrostatic and electromagnetic antennas which can be moved in the radial and axial directions. The phase and amplitude data is Fourier analyzed over 2-D space to give perpendicular and parallel wavelengths. A controllable magnetic field profile is used run the experiment as either an infinite plasma or resonant cavity.

This work supported by the Naval Research Laboratory Base Program.

The high beta solar wind plasma turbulence is dominated by the kinetic Alfven waves (KAW) [1]. Though the measured high-energy tail on the electron distribution function can be a signature of the presence of whistler waves (WW) as well [2]. In Maxwellian plasma both KAW and WW are Landau damped at high beta, and only for the specific case of WW with $k_\perp = 0$ is there no Landau damping. Due to the inhomogeneous solar wind plasma these parallel propagating WW should quickly develop large perpendicular wavenumbers $\langle k_\perp \rangle > \langle k_\parallel \rangle$. However, as we have shown recently using measured KAW spectra, Landau damping establishes a plateau in the parallel electron distribution function and damping is strongly diminished [3]. The theory of WW in high beta inhomogeneous plasma will be presented and the impact of the electron cyclotron resonance with WW on the evolution of the electrons high energy tail will be discussed.

[1] O. Alexandrova *et. al.*, PRL (2009) ; F. Sahraoui *et. al.*, PRL (2010).
[2] T. Nieves-Chinchilla and A. F. Vin˜as, JGR (2008).
[3] L. Rudakov *et. al.*, Phys. Plasma, **18**, 012307 (2011).

* This work supported by Naval Research Laboratory Base Program

Methodology for investigation of ionosphere plasma-wave processes in the near surface region of super-large space objects.

S.I.Klimov, V.A.Grushin, D.I.Novikov
Space Research Institute (IKI) of RAS

Measurement of environmental parameters (concentration, temperature of charged components, electric and magnetic fields) on board of the spacecraft (SC) moving in space is not an easy task, because the SC itself changes these parameters. The measurement of environmental electrodynamics parameters is complicated by the fact, that under the influence of electric and magnetic fields, charged particle fluxes and optical radiation, existing in the space plasma, the outer surface of the spacecraft acquires an electric charge (potential).

The floating potential is an integral parameter characterizing the interaction of the spacecraft with the surrounding plasma, which is expressed by the zero value of the total SC current. Actually the floating potential is a continuously changing (dynamic) parameter, which small-scale measure of its dynamic are the leak-in current fluctuations, that for example on the MIR were in the range from 10^{-5} to $2.2 \cdot 10^{-4}$ A/cm^2 (sometimes even more).

On the ISS orbits, because of its supersonic movement in the plasma ionosphere, the basic external factor stabilizing the potential, is the presence of thermal plasma which provides the final plasma resistance and the run off of the non-equilibrium charge from the SC for a short enough time. The MIR is, above all, a probe with a very large area and complex surface configuration. The maximal length, taken by one of the construction axes of the MIR, is 30 m. Evaluation of the total surface area of the the MIR with an accuracy of about 20% gives a value of 1700 m^2. Of great importance for the interaction of the spacecraft with the space plasma is the ratio of the surface areas made of conductive and nonconductive materials. For the MIR, the estimation shows that the total surface area includes about 70% of non-conductive surface (it is - mostly screen-vacuum thermal insulation, non-conductive surface of the solar panels and other design elements) and about 30% conducting surfaces (metal). In some studies it is noted, that there exists a proportional relationship between the potential value and the geometric dimensions.

The plasma-wave complex is a set of scientific devices with both self -dependent and inter-dependent functional use, and also a set of devices used for control functioning modes of scientific devices, acquisition, processing and data storage the measurements, providing the communication between onboard systems of the ISS, keep- up of thermal mode. The complex of physical parameters planned for measuring in the process of implementation of international «OBSTANOVKA 1-st stage» experiment (Bulgaria, Hungary, Poland, Russia, Ukraine, UK http://www.cosmos.ru/obstanovka/eng/index.htm) will allow to investigate many physical phenomena in ionosphere and in the zone which is very near to the surface of the ISS.

Arbitrary Amplitude Ion-Acoustic Solitons in Dusty Plasmas

T.V. Losseva* (1), S.I. Popel (1), A.P. Golub' (1)
(1) Institute of Geospheres Dynamics of the Russian Academy of Sciences,
119334, Leninsky pr., 38, korp.1, Moscow, Russia, losseva@idg.chph.ras.ru

Description of arbitrary amplitude ion-acoustic solitons in dusty plasmas for a broad range of external conditions is given. The cases of the absence and the presence of electromagnetic radiation are investigated. Intensive electromagnetic radiation results in positive dust particle charges due to the photoelectric effect, while in the absence of electromagnetic radiation dust particles acquire negative electric charges. The ranges of the existence of conservative solitons are determined in terms of plasma parameters and Mach numbers. It is shown that in the case of negative dust particle charges both compressive and rarefactive solitons can exist, while in the case of positive dust particle charges only compressive solitons can propagate in plasmas. Dissipative processes occurring during the propagation of dust ion-acoustic perturbations (charging of dust grains, absorption of ions by grains, transfer of ion momentum to the grains, as well as ion-neutral collisions) are taken into account. Temporal evolutions of the compressive and rarefactive soliton-like perturbation as well as the interaction of two soliton-like perturbations are studied numerically. It is shown that the amplitude of the evolving perturbation at any moment is given by the amplitude of the conservative soliton for the corresponding Mach number (so far as the conservative soliton exists). It should be noted that in dusty plasmas with positively charged dust the solitons are damped much slower and propagate to longer distances than in the case of plasmas with negatively dust charges. The soliton-like perturbations are shown to possess the main properties of the solitons, in particular, the interacting perturbations conserve their form. This work was supported by the Russian Foundation for Basic Research.

Design and Multipacting Simulation of Double-Gap Buncher Cavity

Ki R. Shin*(1), Yoon W. Kang(2), and Aly E. Fathy(1)
(1) University of Tennessee, Knoxville, TN, 37996, USA
(2) ORNL, Oak Ridge, TN, 37831, USA

Spallation Neutron Source (SNS) at Oak Ridge National Laboratory (ORNL) utilizes four single-gap buncher cavities in the medium energy beam transport (MEBT) system (J. Staples, D. Oshatz, and T.Saleh, Linac, 2000). The current utilized design of elliptical cavity design with reentrant nose cones (Jim Potter, SNS Front-End Systems Technical Note FE-EE-019, 2000) is a good choice to achieve high quality factor (Q) with strong fields. This design however, may have high gap voltage which constraints system operability due to voltage breakdown and non-ionizing radiation for low beta ion beam application since the gap lengths are required to be small. A new double-gap buncher cavity design has been investigated to improve such deficiency. The new design aims at reducing the gap peak voltage by insertion of a drift tube which makes a double-gap for interaction with the particles. Preliminary computer simulations indicate that the total gap voltage of the double-gap cavity is almost identical to that of a single-gap cavity even with its reduced peak voltage of each gap. A two dimensional particle dynamics simulation was carried out to validate this new design.

Designs of particle accelerators deal with RF/beam energy transfer. In real situation especially for low velocity particles, the efficiency of the energy transfer is limited by the induced electron currents by the surface electron emission. The secondary electron emission that is responsible for the Multipacting phenomenon is a critical issue for operability and RF power loss since it creates more electrons with each RF period (A. Hatch, Nuclear Instruments and Methods, 41, 261-271, 1966). Therefore, Multipacting characteristic of the new double-gap buncher cavity design has been studied to assess the performance of the cavity. The new structure is not axisymmetric and three dimensional simulations are required. For this study, Furman probabilistic model (M. Furman and M. Pivi, SLAC-PUB-9912, 2003) in CST Particle Studio is used to simulate the Multipacting effects. An optimization process of the cavity design to minimize Multipacting will be also presented and discussed.

SIMULATIONS OF RADIATION BELT ELECTRON DYNAMICS IN HIGH-SPEED-STREAM STORMS

Anthony A. Chan[(1)], Yen-fei Chen [(1)], and Scot R. Elkington[(2)]
(1) Rice University, Houston, TX, USA
(2) University of Colorado, Boulder, Colorado, USA

Magnetospheric MHD waves in the mHz frequency range can strongly affect radiation belt electrons through radial transport, energization, and loss, and the power spectral density (PSD) of the MHD waves plays an important role in computing radial diffusion coefficients. In this paper, power spectral densities are calculated for a high-speed-stream storm in October 2002 using LFM global MHD simulations. Comparisons are made with measurements of MHD waves using GOES-8 and CRRES satellites. The PSD is also used to estimate radial diffusion coefficients, which are compared with previous diffusion coefficients. Radial diffusion simulation codes are run to compare calculated phase-space densities with observational data at GPS locations, for selected high-speed-stream storms. The radial diffusion coefficients show good consistency between LFM runs (simulation) and satellites (observation) when $L<7$. Based on these results, we seek to understand how to combine electric and magnetic radial diffusion coefficients to provide a more precise description of radial transport in the radiation belts.

WHISTLER MODE SIGNALS AT L=1.9 CONJUGATE TO A RUSSIAN ALPHA TRANSMITTER: STATISTICS AND MODELING

Morris B Cohen*[1], Mark Golkowski[2], Nikolai G. Lehtinen[1], Umran S. Inan[1,3], and Michel Parrot[4]

[1]Stanford University STAR Laboratory, Stanford, CA
[2]University of Colorado Denver, Denver, CO
[3]Koc University, Sariyer Istanbul, Turkey
[4]LPC2E/CNRS, Orleans, France

The Russian 'Alpha' transmitters broadcast alternating pulses between 11-15 kHz, nominally used for navigation. A fraction of the VLF energy escapes into the magnetosphere, is guided by ducts, amplified by interaction with radiation belt particles, and observed at the geomagnetic conjugate point. We analyze VLF data from Adelaide, Australia, conjugate to the Komsomolsk transmitter. An automated detection scheme separates the subionospheric and magnetospheric signals, after removing the dominant noise source from lightning-generated radio atmospherics. We track availability of ducts at L=1.9 and find them present often. We connect the ground signal to the signal observed by the DEMETER spacecraft, which also observe triggered emissions and spectral broadening. We correlate to geomagnetic conditions to assess the role of wave growth and triggering from wave-particle interactions. The result is essentially a mid-latitude pulsed VLF magnetospheric injection experiment. We also find a strong diurnal variation in the magnetospheric signal, and apply a full-wave model of transionospheric propagation to include the effects of ionospheric absorption on both ends. We discuss statistics on the growth rates, saturation amplitudes, and propagation delays, as a proxy for magnetospheric conditions. We report on the conditions that lead to triggering and to what extent they may be observed at these latitudes.

New Proxy for the Analysis of Non-linear Wave Growth in Chorus Waves and Triggered Emissions

Mark Golkowski* [(1)], Andrew R. Gibby [(2)]
(1)Department of Electrical Engineering, University of Colorado Denver, Denver, CO, USA
(2) Arion Systems Inc., Chantilly, VA, USA

Magnetospheric chorus and VLF triggered emissions have been well documented in a number of studies spanning several decades. These nonlinear phenomena are both characterized by the generation of narrowband, high-intensity, changing frequency plasma emissions in the whistler mode. Additionally, the emissions are "free running." That is, once the emissions have developed, the frequency-time characteristics of the emitted wave energy are independent of the frequency-time behavior of any triggering source, if present. Chorus is characterized by the spontaneous generation of these free running emissions, while triggered emissions are characterized by the presence of an externally imposed "triggering"' wave.

The nonlinear whistler mode instability associated with magnetospheric chorus and VLF triggered emissions has historically confounded analytical treatment. However, following up on recent studies we present an analytical approach based on a new proxy, namely the derivative of nonlinear current with respect to wave amplitude. Using this proxy we compare linear Vlasov theory with a nonlinear treatment based on the formation of a phase-space hole. We find the conditions on the energetic electron distribution under which the nonlinear instability can initiate. We find that initiation of the nonlinear instability at the equator requires a non-zero frequency sweep rate. The expression for our sweep rate is different from that recently published by other authors. Furthermore, the requirement on distribution function anisotropy for initiation of the nonlinear instability off the equator is more severe than the requirement specified by linear theory. Applying the theory to emissions triggered by a constant frequency input wave, we find that the initiation of the instability by a constant frequency triggering wave must occur at a location upstream of the geomagnetic equator.

KEY PARAMETERS CONTROLLING THE NONLINEAR CYCLOTRON INSTABILITY FOR WHISTLER MODE WAVES IN THE MAGNETOSPHERE

V. Harid[1], M. Golkowski[2], M. Cohen[1], T. F. Bell[1], U. S. Inan[1]

[1]Electrical Engineering, Stanford University, Stanford, CA, United States
[2]Electrical Engineering, University of Colorado, Denver, Denver, CO, United States

Nonlinear amplification of whistler mode waves in the Earth's magnetosphere, due to gyroresonance with energetic electrons, has been investigated extensively with theory, experimental observations and computer simulations. It is generally accepted that non-linear effects are dominated by resonant and near-resonant electrons that are phase-trapped in the wave potential well. Numerous authors have investigated particle phase trapping in the non-linear growth process; however, the role of de-trapping has been comparatively ignored. We consider the effects of particle trapping and de-trapping on non-linear wave growth. The formation of the phase-space hole is considered by numerous authors to be the primary result of particle trapping. In addition, the phase-space hole is thought to be the chief parameter that controls non-linear amplification and the triggering of free running plasma emissions. To isolate the effects of particle trapping, we evaluate the phase-space hole model [Omura et al., JGR, 113, 2008] as the primary source of the resonant currents. We show the capability and validity of this model to produce non-linear wave growth and frequency change. To demonstrate the importance of particle de-trapping, we use an established hybrid code for VLF triggered emissions [Gibby et al., JGR, 113, 2008] to determine the physical location along the field line at which the transition from linear to nonlinear growth occurs. In particular, we show that temporal growth initiates off the equator, after particles escape from the wave potential well. That is, the detrapping of resonant and near-resonant electrons is a crucial process for the initiation of the non-linear instability.

OFF EQUATORIAL CHORUS WAVES OBSERVED BY THE POLAR PLASMA WAVE INSTRUMENT AND IMPLICATIONS FOR THE RADIATION BELTS

Nicholas L. Bunch[1], Maria Spasojevic[1], Yuri Y. Shprits[2], and Daniel I. Golden[1]

[1] STAR Lab, Dept. of Electrical Engineering, Stanford University, Stanford, CA USA

[2] IGPP and Dept. of Atmospheric Sciences, UCLA, Los Angeles, CA USA

Magnetospheric chorus waves play an astonishing role in Earths radiation belts by contributing to both electron acceleration and loss. Despite the controlling effect of off-equatorial chorus on the most energetic radiation belt (>MeV) electrons, characterization of chorus to date has focused on the equatorial region. However, by employing wave observations from the Plasma Wave Instrument (PWI) onboard the Polar spacecraft has helped to extend our characterization of chorus away from the equator such that we can better understand chorus in this region, and more completely model the impact of chorus on radiation belt dynamics. Statistical analysis of chorus waves using Polar shows distributions of amplitude and occurrence that vary substantially for different types of driving conditions. Although waves of significant amplitude occur at latitudes >45° in all magnetic local time sectors, occurrence rates are highest in the midnight, dawn, and noon time sectors where significant time-averaged amplitudes are confined below ∼15° at midnight, and ∼50° at noon. Chorus observed near the equator exhibits similar proportions of upper and lower band, however in the off-equatorial region chorus appears to be dominantly lower band with varying frequency extent for different regions. Analysis of wave activity for various types of driving conditions reveals varying distributions for occurrence rate, typical amplitude, and mean amplitude as a function of radial distance, local time, and latitude. Preliminary analysis suggests that typical wave amplitudes may increase with latitude in the dawn sector under most conditions, and in the noon sector during moderate activity, whereas waves at noon appear consistently intense across a range of latitudes for increased activity levels. Finally, working toward a global parameterization for inclusion in radiation belt models, trends exhibited by chorus amplitude time series are characterized using an autoregressive moving average technique, and a Gaussian mixture model is employed in study of spectral extent to account for banded structure. These observations from the Polar PWI will allow for significant improvements in definition of global radiation belt wave models, and extend our understanding of the role of chorus in the magnetosphere.

Weak Turbulence in the Magnetosphere: Formation of Whistler Wave Cavity by Nonlinear Scattering[a]

C. Crabtree[1], L. Rudakov[2], G. Ganguli[1], M. Mithaiwala[1], V. Galinsky[3], and V. Shevchenko[3]

[1] Plasma Physics Division, Naval Research Laboratory, Washington, DC 20375-5346, USA

[2] Icarus Research Inc., P.O. Box 30870, Bethesda, MD 20824-0780, USA

[3] University of California–San Diego, San Diego, CA, USA

[a]This work is supported by the Naval Research Laboratory Base Program.

We consider the weak turbulence of whistler waves in the in low-β inner magnetosphere of the Earth. Whistler waves with frequencies, originating in the ionosphere, propagate radially outward and can trigger nonlinear induced scattering by thermal electrons provided the wave energy density is large enough. Nonlinear scattering can substantially change the direction of the wave vector of whistler waves and hence the direction of energy flux with only a small change in the frequency. A portion of whistler waves return to the ionosphere with a smaller perpendicular wave vector resulting in diminished linear damping and enhanced ability to pitch-angle scatter trapped electrons. In addition, a portion of the scattered wave packets can be reflected near the ionosphere back into the magnetosphere. Through multiple nonlinear scatterings and ionospheric reflections a long-lived wave cavity containing turbulent whistler waves can be formed with the appropriate properties to more efficiently pitch-angle scatter trapped electrons. The primary consequence on the Earths radiation belts is to reduce the lifetime of the trapped electron population.

Modeling Quasi-linear and Nonlinear Wave-Particle Interactions in the Radiation Belts

Jay M. Albert*
Air Force Research Laboratory, Kirtland AFB, NM, 87117

Properly treating wave-particle interactions is crucial to understanding, modeling, and predicting the behavior of radiation belt electrons. In recent years, coherent, very large amplitude whistler mode waves have been observed in the near-Earth magnetosphere, and the usual quasi-linear treatment alone cannot capture the nonlinear interactions such waves are known to cause. Cyclotron-resonant interactions can drive rapid changes in both particle energy and pitch angle, which can result in precipitation into the atmosphere. In limiting cases, analytical estimates of nonlinear particle behavior have been developed, and recently refined. For small amplitude waves, quasi-linear diffusion is recovered as an average over interactions with individual waves, but phase bunching and phase trapping, caused by larger amplitude waves, can also be treated. These tend to result in a directed, not random, walk in velocity space. The applicability of the nonlinear mechanisms is determined by a dimensionless parameter (the "inhomogeneity ratio") that depends on the ratio of the amplitude of the wave magnetic field to the variation of the background geomagnetic field along the field line, as well as the energy and pitch angle of the particle. The analytical results can be used to formulate a combined diffusion-advection description of the evolution of phase space density, which is suitable for large scale, long term modeling of the radiation belts using relatively simple and efficient numerical techniques. This description will be reviewed, sample evaluations using current empirical models of whistler waves will be presented, and the implications for global radiation belt electron behavior will be discussed.

ENHANCED SCATTERING AT SELECTED ELECTRON ENERGIES BY DISPERSING LIGHTNING WHISTLERS

David S. Lauben[1]*, Timothy F. Bell[1], Nikolai G. Lehtinen[1], Umran S. Inan[1,2]

[1]Stanford University STAR Laboratory, Stanford, CA
[2]Koc University, Rumeli Feneri Yolu, Istanbul,Turkey,

The usual frequency-time dispersion of lightning-generated whistlers propagating through the magnetosphere between conjugate hemispheres leads to an evolving distribution of wave frequency over magnetic latitude which in turn presents a systematic variation in the resonance condition presented to particles traversing the wave field. For certain conditions identified herein, this variation in frequency along the field-line counter-balances the change in gyrofrequency, leading to extended interaction lengths and enhanced scattering at selected resonant parallel velocities and corresponding energy/pitch-angle combinations. Calculations using proven formulations for first-order wave/particle gyroresonant scattering indicate that peak pitch-angle deflections caused by otherwise nominal ~10pT whistler wave intensities can approach ~1° for certain cuts in electron phase-space density. Furthermore, this degree of scattering appears possible over a broad range of L-shells and for non-ducted and ducted whistlers alike, leading to the implication that perhaps the most readily observable loss-cone precipitation flux detected by satellites and most prominent D-region disturbances inferred via subionospheric vlf remote sensing may in fact be associated with a relatively small fraction of precipitating electrons carved from a limited slice in electron phase-space density. In addition, since these extended interaction lengths are seen to cause significant gyrophase bunching at the point of electron exit the wave field, the possibility for wave growth and further enhanced scattering from regions beyond the critical wave/particle encounter latitude is explored. Finally, implications for electron lifetimes and the possible formation of electron phase-space holes are discussed.

PhOCAL 2011: FIRST RESULTS

Walter A. Lyons*[(1)], Steven Cummer[(2)], Steve Rutledge [(3)], Timothy Lang[(3)], Tiffany Meyer[(3)], Tom Warner[(4)]

(1) FMA Research, Ft. Collins, CO, 80524, http://www.FMA-Research.com
(2) Duke University, Durham, NC, USA
(3) Colorado State University, Ft. Collins, CO, USA
(4) SD School of Mines & Technology, Rapid City, SD, USA

A multi-institution, multi-year effort, "Physical Origins of Coupling to the Upper Atmosphere from Lightning [PhOCAL]," was designed to document the exceptional tropospheric electrical discharges that induce Transient Luminous Events (TLEs). Central to the effort is obtaining comprehensive observations of TLE-parent lightning discharges, as well as the storm morphologies which produce them, in order to enable the formulation and evaluation of theoretical models of TLEs. This paper documents the efforts of several team members during the 2011 season. An automated TLE camera network has been established to monitor above 3-D Lightning Mapping Arrays (LMAs) in Oklahoma, Texas, New Mexico, Alabama, Florida and Washington, DC. In addition, the first intensive field program deployed a mobile vehicle within storms traversing LMAs in order to capture high-speed lightning video of the TLE-parent CG concurrent with high-speed intensified images of the resultant TLE obtained by cameras ~400 km distant. Additional data characterizing the parent discharge include the NLDN, the National Charge Moment Change Network (CMCN) and ULF/ELF/LF receivers. We also describe the fruitful cooperative efforts with numerous external investigators and "citizen scientists" who established TLE monitoring cameras and share their results with the scientific community. Initial results include numerous sprites (including a negative event), several gigantic jets above LMAs, CGs which induced both sprites and "lightning triggered lightning" (upward discharges from tall towers), color imagery of a gigantic jets above tropical convective systems, and a gigantic jet occurring within a complex discharge also creating sprites. A pattern is beginning to emerge which characterizes the classes of deep convective storms that produce lightning discharges than result in blue jets and gigantic jets. A climatology of impulse charge moment changes over CONUS also is beginning to yield clues as to regions of high productivity for different classes of TLEs.

A WAVEGUIDE MODEL OF THE RETURN STROKE CHANNEL WITH A METAMATERIAL CORONA

Nikolai G. Lehtinen*

Stanford University, Stanford, CA

Abstract

We model the return stroke channel as a three layer cylindrical waveguide, consisting of (1) highly conducting thin core channel; (2) "metamaterial" corona, i.e., corona with an effective bulk anisotropic dielectric permittivity tensor which is due to the fine structure of leaders branching away from the main channel; and (3) the surrounding non-conducting air. The lowest axially symmetric mode (TM mode) in this waveguide represents the return stroke current wave. We find time- and space- domain solutions for the current wave in a channel connected to the ground driven by an axial current of Bruce-Golde model temporal shape concentrated at the point of the channel connection to the ground. The front of the current wave is found to be dispersed, and the speed of the front is significantly (by a factor of 5-10 for some parameters) slower than the speed of light. The calculated radial electric field is found to be consistent with experimental measurements. When the second layer of the waveguide is filled with an isotropic material (isotropic corona), the slowdown of the wave front is found to be smaller. The time- and space- domain calculations are also supported by the numerical solution of a dispersion equation, which shows that the phase velocity may be significantly less than the speed of light. The transmission-line (TL) representation of such a waveguide is also discussed. Beside the attempt to find an explanation for the low speed of the return stroke, this study is also motivated by the results of the recently developed [e.g., Carlson et al, 2011, XXX URSI GASS, Lutfi Kirdar Convention and Exhibition Centre, Istanbul, Turkey] time-domain fractal lightning model (TDFL), which show short leaders branching away from the main channel of the return stroke.

Theoretical Analysis of Elves Generated by Rocket-Triggered Lightning

Christopher J. Biagi* and Robert C. Moore
Department of Electrical and Computer Engineering, University of Florida, Gainesville, Florida, USA.

Intense lightning discharges have been identified as the driving sources for a number of energetic ionospheric effects, including the production of transient luminous events and perturbations to the amplitude and phase of subionospherically-propagating VLF signals, for instance. In particular, the electromagnetic pulse (EMP) launched by a lightning return stroke disturbs the lower ionosphere in the form of high-altitude luminous emissions known as elves. Elves are luminous rings that occur at ∼90 km altitude, and they expand rapidly (in less than ∼1 ms) to great radial distances (100s of km).

Lightning research presently being conducted at International Center for Lightning Research and Testing (ICLRT), located at Camp Blanding, Florida, focuses on rocket-and-wire triggered lightning, or rocket-triggered lightning. Focusing on rocket-triggered lightning allows for the optimal placement of scientific instrumentation, for example, because the location and timing of the lightning flash are known. One of the most important measurements at the ICLRT is the channel-base current measurement. For each successful rocket-triggered flash, the lightning current is directly measured at the channel base across a resistive shunt. Rocket-triggered lightning is typically weaker than natural lightning, with average HF peak currents of ∼15 kA. Elves produced by natural lightning are typically associated with HF field derived peak currents of >45 kA. Based on a comparison of these quantities, it seems unlikely that rocket-triggered lightning can produce elves. The production of elves is driven by lower-than-HF frequency fields, however, and, as can be demonstrated with channel-base current observations, the singular HF peak current value does not properly represent the return stroke energy at lower frequencies.

The theoretical modeling tools for elves have been well-developed. In this work, we present elves modeling results using a new model that incorporates the lightning channel-base current directly measured at the ICLRT. Results for current waveforms with different spectral content are presented and compared with the results of a typical analysis of elves produced by natural lightning.

Understanding sprite morphology

Jianqi Qin, Sebastien Celestin, and Victor P. Pasko
CSSL, Penn State University, University Park, Pennsylvania, USA

Sprites [Sentman et al., GRL, 22, 1205, 1995] are transient luminous events that are usually produced by positive cloud-to-ground lightning discharges (+CGs). Extensive observations using high-speed telescopic imagers show that these optical phenomena exhibit different morphologies, such as columniform sprites with no upward streamers that follow +CGs with currents ranging from about 23 to 100 kA [e.g., Wescott et al., JASTP, 60, 733, 1998], or carrot sprites with both downward and upward streamers [e.g., Stenbaek-Nielsen and McHarg, JPD, 41, 234009, 2008]. Numerical simulations using a quasi-static electric model in [Qin et al., JGR, 116, A06305, 2011] indicate that sprite initiation is mostly determined by the charge moment change produced by the lightning discharges and the ambient electron density profile. However, the understanding of specific characteristics related to sprite morphology is still in preliminary stages, the related examples include the formation of the upper diffuse region of sprites [Pasko and Stenbaek-Nielsen, GRL, 29, 1440, 2002], and the initiation mechanism related to some sprite events in which the upward streamers start from a lower altitude compared to the earlier downward streamers [Stenbaek-Nielsen and McHarg, JPD, 2008; Li and Cummer, JGR, 116, A01301, 2011]. Recently, observations have revealed interesting differences between columniform sprite events and carrot sprite events that require further theoretical understanding [Stenbaek-Nielsen et al., JGR, 115, A00E12, 2010]. In the present work, we use a quasi-static electric model described in [Qin et al., 2011] to simulate the electrodynamics in the upper atmosphere in order to investigate the conditions under which the establishment of high electric field by +CGs leads to the production of columniform sprites or carrot sprites.

Investigation of luminosity and propagation characteristics of sprite streamers initiated from small ionospheric disturbances in lightning electric field below breakdown threshold field

Burcu Kosar, Ningyu Liu, and Hamid K. Rassoul
Department of Physics and Space Sciences,
Florida Institute of Technology, Melbourne, FL 32901, USA

Sprite discharges are large scale natural plasma phenomena occurring due to penetration of quasi-electrostatic lightning field to mesospheric/lower ionospheric altitudes [*Pasko*, JGR, 115, 2010]. They consist of filamentary plasma channels known as streamers that are highly non-linear and self-organized ionization waves. It has been generally believed that sprites occur when the lightning field exceeds the conventional breakdown threshold field, E_k, in the lower ionosphere. However, recent analysis of high-speed video observations of sprites and electromagnetic measurements of lightning field found that sprite streamers often appear in the lightning field below the breakdown field with a magnitude as low as $0.2E_k$ [*Hu et al.*, JGR, 112, D13115, 2007; *Li et al.*, JGR, 113, D20206, 2008].

Liu et al. [PRL, submitted] studied a possible mechanism for sprite streamer initiation from small ionospheric disturbances in lightning electric field of $0.5E_k$. In this talk, we report a follow up study on this work. We report streamer simulation results for more field cases with the lowest field of $0.3E_k$. We observe successful formation of streamers for all cases. In addition, our simulation results indicate that the initial ionization patch may become very bright following the streamer formation and its brightness persists as the streamer continues its propagation. The overall luminous structure of the streamer and the ionization patch is very similar to the appearance of initiation of single sprite streamer in high speed images [*McHarg et al.*, GRL, 34, L06804, 2007; *Stenbaek-Nielsen et al.*, GRL, 34, L11105, 2007; *Stenbaek-Nielsen and McHarg*, J. Phys D: Appl. Phys., 41, 2008]. We further examine the effect of the variation of ionization density on the brightening of the patch and formulate a simple analytical approach to explain the brightening of the ionization patch as well as the luminous streamer trail. Finally, comparisons between the streamers from the ionization patch and those forming in the vicinity of a conducting sphere in an electric field below E_k show that the exponential growth rates associated with streamer characteristics are very similar.

LIGHTNING INDUCED SFERICS CORRELATED WITH WHISTLER PROPAGATION

Andrew Compston[1]*, Ryan Said[1], Ivan Linscott[1], Morris Cohen[1], Umran Inan[1,2], Nikolai Lehtinen[1], Michel Parrot[3]

[1]Electrical Engineering, Stanford University, Stanford, CA
[2]Koc University, Rumeli Feneri Yolu, Istanbul,Turkey,
[3]LPC2E, CNRS, Orleans, France

Lightning discharges generate broadband electromagnetic pulses, known as sferics, that efficiently propagate through the Earth-ionosphere waveguide over long distances. Some sferic energy can escape the Earth-ionosphere waveguide and propagate in a whistler mode, enabled by Earth's magnetic field, through the ionosphere. Because a sferic is an impulse, the whistler it generates can be viewed as the impulse response of the ionosphere. In this presentation, we correlate lightning discharge location, time, and peak current data from the National Lightning Detection Network (NLDN) in the United States with burst mode electric field measurements from the DEMETER spacecraft in Low Earth Orbit to quantify and model whistler propagation through the ionosphere. By pairing each whistler with its parent lightning strike, we can tease out and compare the effects on the signal due to propagation through a known distance in the Earth-ionosphere waveguide and the effects due to propagation through the ionosphere itself. Because the ionosphere has different properties depending on whether or not it is illuminated by the sun, we look at both daytime and nighttime conditions. Using the International Reference Ionosphere (IRI) model for ionosphere electron density and the International Geomagnetic Reference Field (IGRF) model for magnetic field, we also compare the measured propagated signal with the Full Wave Method (FWM) finite element numerical code developed by N. G. Lehtinen and U. S. Inan. While a few studies have analyzed whistler propagation through the ionosphere using spacecraft measurements, spacecraft data have yet to be compared with the FWM as we have done here.

Ionospheric effects of whistler waves launched by rocket-triggered lightning

Christopher J. Biagi*[1], Robert C. Moore[1], and Mark Golkowski[2]

[1] Department of Electrical and Computer Engineering, University of Florida, Gainesville, Florida, USA.

[2] Department of Electrical Engineering, University of Colorado Denver, Denver, Colorado, USA.

Lightning-induced electron precipitation (LEP) is one of the primary mechanisms for energetic electron loss from Earth's radiation belts. The spatial and temporal structure of LEP are affected by parameters such as the lightning return stroke peak current and spectral distribution as well as the location of the lightning flash. While previous works have emphasized lightning location and the return stroke peak current in quantifying lightning's role in radiation belt electron loss, the spectrum of the lightning return stroke has received far less attention. Rocket-triggered lightning experiments performed at the International Center for Lightning Research and Testing (ICLRT) at Camp Blanding, Florida, provide a means to directly measure the spectral content of individual lightning return strokes. Using an integrated set of numerical models we use the observed rocket-triggered lightning channel-base currents to calculate the latitudinal dependence of the precipitation signature. The model results indicate that rocket-triggered lightning may produce detectable LEP events and that return strokes with higher ELF (3 Hz−3 kHz) content cause proportionally more ionospheric ionization and precipitate more electrons at higher latitudes than return strokes with higher VLF (3 kHz−30 kHz) content. Furthermore, we can demonstrate that the predicted spatio-temporal signature of the induced electron precipitation is highly dependent upon the return stroke spectral content. As a result, we postulate that the ability to directly measure the channel-base current of the rocket-triggered lightning return stroke enables us to estimate the spectral profile of energetic electrons precipitated from the Earth's radiation belts and to predict the geographic location and magnitude of electron precipitation.

The method of study in the ionosphere of the physical processes, occur in high-altitude atmospheric thunderstorm

S.I.Klimov[1], G.K.Garipov[2], V.M.Gotlib[1], A.V.Gurevich[3], J-L.Pincon[4] S.I.Svertilov[2], L.M.Zelenyi[1],
[1)] Space Research Institute (IKI) of RAS, Profsoyuznaya 84/32, 117997 GSP-7 Moscow, Russia; [2)] Institute of Nuclear Physics (SINP), Moscow Sate University, Moscow, Russia; [3)] P.N.Lebedev Physical Institute (FIAN) of RAS, Moscow Russia; [4)] *Centre d'Etude Spatiale des Rayonnements, CNRS, Toulouse, France*

A number of the physical phenomena in the atmosphere, which fundamentally changed our idea about the lightning discharges, are discovered in recent years. IKI with participation of SINP (Russia), FIAN (Russia), LC SRI NANU-NKAU (Lviv, Ukraine) and Etvos University (Budapest, Hungary) is developed of complexes of scientific instruments (12.5 kg):

- X-ray - gamma detector (range of X-ray and gamma emission - 50-500 keV),
- UV detector (range emission - 180-400 nm, 650-800 nm),
- radiofrequency analyzer (26 - 48 MHz).
- camera of optical range (spatial resolution 300 m).
- plasma-wave complex (0.1-40 kHz).

Micro-satellite "Chibis-M" now designed in IKI. Total mass "Chibis-M" with support systems, construction and scientific instruments - 40 kg.

The study of physical processes with the atmospheric lightning discharges on the base of microsatellite "Chibis-M" (IKI RAS) and TARANIS (CNES) is oriented to detailed studies of the dynamic characteristics of the pulses of radio-, ultraviolet- and gamma-radiation, generated in the process of high-altitude atmospheric discharge. Analysis showed the need for the simultaneous measurement of radio- and gamma- emissions in the sub-microsecond temporary range. Also the project seeks support for the coordination of three missions: Chibis-M (Russia), TARANIS (France), ASIM (Denmark) and ensuring their ground-based observational support. These missions are dedicated to studies of fascinating physical effects which already had changed fundamentally our notions about the lightning discharges in the atmosphere.

This work partially supported by RFBR Grant (France-Russia) № 10-05-93107. Discussion of the methodical questions of atmospheric lightning discharges study was carried out within the framework ISSI Team: CARNES (Coupling of Atmosphere Regions with Near-Earth Space)

Lightning morphology and impulse charge moment changes of high peak current negative strokes

Abstract. We have analyzed very high-frequency lightning mapping observations and remote magnetic field measurements of negative cloud-to-ground (CG) strokes with high estimated peak currents to identify connections between lightning morphology and impulse charge transfer in such strokes. Four lightning morphologies are identified for a total of 2126 strokes within optimum range of the North Alabama Lightning Mapping Array, and statistical distributions of impulse charge moment changes are given for each of these types. Almost all (>95%) of the largest impulse charge moments (greater than –200 C·km in this dataset) are not produced by strokes in ordinary negative CG flashes. Instead, negative strokes with the largest charge moments are almost exclusively associated with two unusual types of flash that both initially develop as positive (normal) intracloud lightning. In the first type the negative stroke with high charge moments results from a negative leader that descends from the mid-level negative charge region after the upper-level negative lightning channel has stopped propagating. In the second type, the upper level negative leader of the intracloud lightning progresses towards ground as a so-called 'bolt-from-the-blue' to generate the negative stroke. Measurements of four strokes associated with negative polarity sprites suggest that all four were likely produced by the first unusual type of lightning. Our results highlight that estimated peak current and impulse charge transfer are not always well correlated, and that in-cloud lightning structure strongly influences charge transfer on short timescales in negative strokes.

Numerical Modeling of Initiation of Lightning Leaders from Tall Structures by Sprite-producing Lightning Discharges

Victor P. Pasko
CSSL, Penn State University, University Park, Pennsylvania, USA

It is well established by now that large charge transfers between cloud and ground in positive cloud-to-ground lightning discharges (+CGs) can lead to transient electric field enhancements at mesospheric and lower ionospheric altitudes. In these events the electric field can exceed the conventional breakdown field and lead to formation of transient luminous events referred to as sprites and sprite halos [e.g., Qin et al., JGR, 116, A06305, 2011, and references therein]. Stanley and Heavner [Proc. 12th International Conference on Atmospheric Electricity, Versailles, France, 2003] reported that the large and rapid charge transfer of +CGs producing sprites can also initiate upward positive leaders from tall structures. These authors also presented data analysis indicating that structures with >400 m height have a significantly enhanced probability of launching upward positive leaders that may culminate in a -CG return stroke to the structure. The effect can be understood by considering the field intensification at the top of the tall structure combined with fast application of the field preventing formation and shielding effects of ion corona [Brook et al., JGR, 66, 3967, 1961]. In the present work we utilize the most recent modeling approaches developed at Penn State [e.g., Riousset et al., JGR, 115, A00E10, 2010] to quantify the conditions leading to initiation of positive leaders from tall structures following sprite-producing +CGs. Experiments show that the streamer zone transforms into leader when voltage drop along the streamer zone exceeds 400 kV [e.g., Aleksandrov et al., J. Phys. D: Appl. Phys., 38, 1225, 2005]. For a formed leader half of the voltage drops in the streamer zone, and another half in free space ahead of the streamer zone [Bazelyan and Raizer, Lightning physics and lightning protection, p. 62, 2000]. In our analysis therefore we assume that minimum voltage at the tip of the tower should exceed 800 kV for sustainment of upward propagating leader. The results indicate, in particular, that a charge moment change of 390 C km in a +CG can lead to leader initiation from a 457 m tower approximately 15 km from the +CG, in good agreement with observations reported in [Stanley and Heavner, 2003]. We report detailed relationships, including analytical estimates and numerical modeling results, providing information on the charge moment charges versus tower height and radial position with respect to +CG required for initiation of upward leaders.

REMOTE SENSING OF ELECTRIC FIELDS ABOVE THUNDERSTORMS VIA THE KERR EFFECT: INSTRUMENT STATUS

David S. Lauben[1]*, Morris B Cohen[1]*, Brant E. Carlson[2], Robert A. Marshall, Umran S. Inan[1,3]

[1]Stanford University STAR Laboratory, Stanford, CA
[2]University of Bergen, Norway
[3]Koc University, Rumeli Feneri Yolu, Istanbul,Turkey,

Measurement of quasi-electrostatic electric fields above thunderstorms remains an important but difficult challenge regarding fundamental lightning physics. Specially instrumented aircraft have taken some data in the past but are expensive to operate and subject to potentially hazardous charging/discharging conditions. High-altitude balloons have also proven useful but are generally limited to brief uncontrolled ascents through the thunderstorm region, and are often terminated early by direct mid-cloud lightning strikes. Recently, a ground-based instrument for measuring perturbations in the Kerr-effect birefringence of linearly polarized background skylight has been proposed as a means for measuring the transient fluctuations in the electric field above thunderstorms throughout the lightning electrification and discharge cycle. While the Kerr-effect goes as $|E|^2$, estimates for the induced perturbations caused by anticipated ~100 kV/m electric fields extending over typical ~km scale thundercloud regions nonetheless shows a need for several cm^2-sr entrance geometric factor and part-per-million sensitivity in the effective differential polarimeter detector output. This paper reviews (a) estimates of background skylight intensity and polarization, (b) calculations of Kerr-effect polarization perturbations associated with a range of assumed transient electric field fluctuations, (c) simulations of intervening atmospheric scattering effects and attenuation between the affected above-cloud region and ground-based remote sensing site, and (d) progress to date on instrument optical and electronic design and development, including laboratory-based performance measurements, with a view to establish viable operational conditions and constraints for field use.

High Energy Observations of Terrestrial Gamma-Ray Flashes by AGILE

M. Tavani* [(1)], M. Marisaldi [(2)], F. Fuschino [(2)], C. Labanti [(2)], A. Argan [(3)], on behalf of the AGILE Team.
(1) INAF-IASF Roma and University of Tor Vergata, Rome, Italy
(2) INAF-IASF Bologna, Bologna, Italy
(3) INAF Headquarters, Rome, Italy

The AGILE satellite, operating since mid 2007 and primarily devoted to high-energy astrophysics, is one of the only three currently operating space instruments capable of detecting Terrestrial Gamma-Ray Flashes (TGFs), together with RHESSI and Fermi-GBM. Thanks to the AGILE Mini-Calorimeter instrument energy range extended up to 100MeV, its flexible trigger logic on sub-millisecond time scales and its Low Equatorial Orbit with only 2.5 degree inclination, AGILE is detecting more than 10 TGFs/month, adding a wealth of observations with an unprecedented exposure density above the equator, where both lightning activity and TGF detection peak.

Since the 2009-2010 discovery of a power-law spectral component surprisingly detected up to 100 MeV, AGILE has been collecting additional TGF data with a substantial improvement of the statistics. AGILE discoveries in TGF science reported up to now concern the high energy extension of the TGF spectrum up to 100 MeV, which is difficult to reconcile with current theoretical models, and the TGF localization in gamma-rays from space by the AGILE gamma-ray imaging detector.

In this presentation we will review the characteristics of the 2.5-years AGILE TGF sample, consisting of about 300 events, focusing on the TGF high-energy spectral characteristics above 40 MeV. We will discuss the comparison between AGILE TGFs and global lightning activity, based on LIS/OTD observations, in the frame of a climatological study of TGFs. Theoretical implications of HE-TGFs on particle acceleration in thunderstorms will be discussed as well as the possible important impacts of HE-TGFs in the atmospheric environment. The atmosphere during severe thunderstorms becomes a most efficient particle accelerator on Earth, challenging current models of TGF production.

Spectral and temporal characteristics of terrestrial gamma-ray flashes produced by energetic electrons during the stepping of lightning leaders

Sebastien Celestin and Victor P. Pasko
Communications and Space Sciences Laboratory, Pennsylvania State University, University Park, Pennsylvania, USA

Terrestrial gamma-ray flashes (TGFs) are bursts of high-energy photons originating from the Earth's atmosphere in association with thunderstorm activity. TGFs were serendipitously discovered by BATSE detector aboard the Compton Gamma-Ray Observatory originally launched to perform observations of celestial gamma-ray sources [Fishman et al., Science, 264, 1313, 1994]. These events have also been detected by the Reuven Ramaty High Energy Solar Spectroscopic Imager (RHESSI) satellite [Smith et al., Science, 307, 1085, 2005], the Astrorivelatore Gamma a Immagini Leggero (AGILE) satellite [Marisaldi et al., JGR, 115, A00E13, 2010], and the Fermi Gamma-ray Space Telescope [Briggs et al., JGR, 115, A07323, 2010]. Moreover, measurements have correlated TGFs with initial development stages of normal polarity intracloud lightning that transports negative charge upward (+IC) [e.g., Lu et al., JGR, 116, A03316, 2011]. Photon spectra corresponding to well-established model of relativistic runaway electron avalanches (RREAs) over large distance in thunderstorms usually provide a very good agreement with satellite observations [Dwyer and Smith, GRL, 32, L22804, 2005]. However, it has been suggested that long unbranched +IC lightning leaders could produce a sufficient number of energetic electrons to explain TGFs without invoking further amplification in RREAs [Celestin and Pasko, JGR, 116, A03315, 2011]. In this work, we use Monte Carlo models to study the spectral and temporal characteristics of photons detected at low-orbit satellite altitudes associated with energetic electrons produced during the negative corona flashes of stepping negative leaders in +IC discharges. We will show that the obtained spectra agree with current satellite measurements, which further suggests that TGFs can be produced directly by lightning discharges. Additionally, we will compare our results on the temporal characteristics of TGFs at satellite altitudes to recent observations by the Fermi Gamma-Ray Space Telescope [Fishman et al., JGR, 116, A07304, 2011].

The CHAMPS (Charge and Mass of Meteoritic Smoke Particles) Rocket Campaign

Shannon Dickson[(1)], Mihaly Horanyi[(1)], Scott Knappmiller[(1)], Devin Konecny[(1)], Scott Robertson[(1)], Zoltan Sternovsky[(1)], Biff Williams[(2)], Diego Janches[(3)], Martin Friedrich[(4)], Michael Gausa[(5)], Jorg Gumbel[(6)]

(1) University of Colorado, Boulder, CO USA 80304
(2) Northwest Research Associates, Boulder, CO USA 80301
(3) Goddard Space Flight Center, Greenbelt MD, USA 20771
(4) Graz University of Technology, 8010 Graz, Austria
(5) Andoya Rocket Range, Andenes, Norway
(6) Stockholm University, 10691 Stockholm, Sweden

The CHAMPS (charge and mass of meteoritic smoke particles) rocket campaign is a pair of sounding rockets to be launched from the Andoya Rocket Range, Norway, in October 2011 that will investigate the charge and mass distribution of meteoritic smoke particles (MSPs) at 70 – 100 km altitude. MSPs are the likely condensation nuclei for the icy particles responsible for polar mesospheric summer echoes (PMSE) and noctilucent clouds (NLC) that occur in the polar summer mesosphere. Launches will occur after the NLC season to avoid detection of ice. The CHAMPS payload is based upon the successful MASS (Mesospheric Aerosol Sampling Spectrometer) payload that returned data on the size distribution of charged NLC particles above Andoya in August, 2007. The payload will carry the Mesospheric Aerosol Sampling Spectrometer (MASS) for charged aerosol particles that will simultaneously record the number density of both positive and negative aerosol particles in five ranges of mass. The payloads will also carry Langmuir probes, a positive ion probe, Faraday rotation antennas, Lyman alpha detectors, and dust impact detectors. Daytime and nighttime launches will help to find the roles of photoemission and photodetachment in determining the charge state of MSPs. Simultaneous measurements of electron and ion density will help verify models for charge balance. If MSPs are charged, the critical radius at which they become condensation nuclei is decreased. Previous rocket campaigns have found both positive and negative charges in layers in the mesosphere, which may be explained by photo-charging of a fraction of the MSPs. A first look at the data will be presented.

MODELING PLASMA FORMATION FROM HYPERVELOCITY METEOROID IMPACTS

Alex Fletcher*, Sigrid Close

Department of Aeronautics & Astronautics, Stanford University, Stanford, CA

We present results from a model that describes the interaction of a hypervelocity meteoroid impact with a spacecraft, which can result in electrical damage. A meteoroid impact of sufficient velocity will vaporize and ionize both the projectile and part of the spacecraft, forming plasma that expands into the surrounding vacuum. The impact induces a strong shock wave in the target. We construct a solution to the flow behind this shock using symmetry methods in powers of the inverse shock Mach number squared. The solution is coupled to finite ionization and recombination rates, which are calculated using collisional cross sections. The plasma generated by a hypervelocity impact has densities greater than that of the solid state target, and thus the rates of ionization and recombination are significantly modified by this super dense environment. From the impact energy and material properties, we calculate the total charge generated, ion charge states, plasma density profile, and temperature profile. We compare the analytic model to a computational simulation of the impact. The simulation uses a two dimensional axisymmetric fluid model with the same finite rates of ionization and recombination, as well as a general equation of state. We find the vaporization and ionization process takes between 1 and 10 nanoseconds, after which the plasma is free to expand into vacuum. We calculate peak plasma densities on the order of 10^28 m^-3 and temperatures on the order of 30 eV. Ion charge states of +2, +3, and sometimes higher are easily reached, at least temporarily. This is partially due to the effects of the super dense plasma environment. The total charge generated is overestimated when compared to experimental measurements. The model is most appropriate for high velocity impacts (>50 km/s) since the projectile is not considered.

First Detection of Meteoric Smoke using the Poker Flat Incoherent Scatter Radar (PFISR)

V. Hsu[1], J. T. Fentzke[2], C.M.G. Brum[3]

[1]University of Illinios, Dept. of Electrical and Computer Engineering, Urbana, IL.
[2]Johns Hopkins University Applied Physics Laboratory, Laurel, MD.
[3]Arecibo Observatory, SAS Department, Arecibo, PR.

In this work we present the first results of meteor smoke particles (MSPs) detected in the D-region plasma above the 449 MHz Poker Flat Incoherent Scatter Radar (PFISR) in Alaska (67°N, 149°W). MSPs are believed to be the major source of condensation nuclei for the formation of ice particles, the precursor for Polar Mesospheric Clouds (PMCs) and Polar Mesospheric Summer Echoes (PMSE). In addition, they are thought to contribute to D-region chemistry by providing a surface on which heterogeneous chemistry occurs (Summers and Siskand, 1999). Our results are obtained by utilizing a similar fitting method derived for use at other High Power Large Aperture Radar (HPLA) sites that treats the measured radar signal as the sum of two Lorentzian functions [Strelnikova et al., 2007]. This method allows us to determine particle size distributions and smoke densities (when calibrated electron density data is available) in the range of approximately 70 to 90 km altitude depending on background atmospheric composition. We present results from a period of strong D-Region ionization when the detected signal-to-noise (SNR) from the D-region is strongest (12 - 19 UT). Observed particle sizes were found to range from ~0.2 nm to ~4.5 nm. The altitudinal variation of particles sizes was more pronounced in the region 70-80 km than at altitudes above 80 km, while the temporal variation was seen to be minimal, which is in agreement with previous MSP studies (Fentzke et al., 2009). We also introduce an alternate technique in quantifying MSP sizes, which involves increasing the degrees of freedom in the previous fitting method. This fitting procedure eliminates the dependence on the MSIS-00 model temperature, and could potentially become a new method for deriving atmospheric temperature in this altitude range. We compare the two fitting techniques, and discuss the validity of the calculated neutral temperatures. Our results provide insight into the presence and distribution of charged meteoric dust in the polar mesopause region resulting from the condensation of ablated material of meteoric origin. Furthermore, we compare our results to other HPLA radar sites at high latitude (EISCAT) as well as low latitude (Arecibo) to verify our results and investigate any latitudinal variation that may exist.

Electric potential distributions above a surface in a magnetic dipole field

X. Wang[1,3], S. Robertson[2,3], and M. Horanyi[1,2,3]
[1] Laboratory for Atmospheric and Space Physics, University of Colorado, Boulder, Colorado 80309
[2] Department of Physics, University of Colorado, Boulder, Colorado 80309
[3] NASA Lunar Science Institute: Colorado Center for Lunar Dust and Atmospheric Studies, Boulder, Colorado, 80309

The Moon does not have a global magnetic field, unlike the Earth, rather it has strong crustal magnetic anomalies. Data from Lunar Prospector (LP) and SELENE (Kaguya) observed strong interactions between the solar wind and these localized magnetic fields. In our laboratory experiment we use a horseshoe permanent magnet as an analogue to create a magnetic dipole field above an insulating surface in plasma. We observed a complex potential distribution above the surface. In these experiments, electrons are magnetized with gyro-radii r smaller than the distances from the surface d ($r < d$), while the ions remain un-magnetized with $r > d$. A non-monotonic sheath forms above the surface in the center of the magnetic dipole. Unlike negative charging on surfaces by electrons with higher mobility, the potential on the surface in the central dipole is found slightly more positive than the bulk plasma potential, signaling that the surface charging is dominated by the cold unmagnetized ions while the electrons are excluded due to magnetic shielding. A potential minimum is found in the shielding region between the surface and the bulk plasma, most likely caused by the electrons that access the region due to the collision and are mirror-trapped between the two magnetic cusps. The value of the potential minimum with respect to the bulk plasma potential decreases with increasing the plasma density and neutral pressure due to collisional spreading their spatial density distribution in the sheath. The potential on the surface fluctuates in the radial direction along the central dipole field line. While these conditions differ from the lunar surface, the underlying physical processes can be identified in these experiments, and help our understanding of the role magnetic anomalies might play in the formation of lunar swirls, for example.

Modeling Dust Clouds on the Moon

Jamey Szalay*[1,2] and Mihály Horányi[1,2]

[1] Laboratory for Atmospheric and Space Physics, University of Colorado at Boulder, Boulder, Colorado, USA

[2] Department of Physics, University of Colorado at Boulder, Boulder, Colorado, USA

The lunar environment is a complex and dynamic system. Without an appreciable atmosphere or large-scale magnetic field, with the exception of regions with strong magnetic anomalies, the solar wind freely reaches the lunar surfaces. Combined with photoemission from the lunar surface due to direct exposure to solar UV radiation, this can lead to surface charging, near-surface electric fields, and the mobilization and transport of the lunar soil. Images taken by Surveyors 5, 6, & 7 have indicated the presence of lofted dust clouds along with estimates for their spatial extent and density. A 1D hybrid code, treating electrons and ions as fluids and the dust grain as particles, has been developed to constrain the properties of these clouds. This presentation will discuss the preliminary results of this model and compare its prediction to existing observations.

The Electrostatic Lunar Dust Analyzer (ELDA): Data Analysis

Jianfeng Xie,[1,2] Zoltan Sternovsky,[1,3] Eberhard Grün,[1] Siegfried Auer,[4] Mihaly Horanyi,[1,2] Huy Le,[1] Keith Drake[1]

[1] *Laboratory for Atmospheric and Space Physics, University of Colorado, Boulder, CO*

[2] *Physics Department, University of Colorado, Boulder, CO*

[3] *Aerospace Engineering Sciences, University of Colorado, Boulder, CO*

[4] *A&M Associates, P. O. Box 421, Basye, VA*

Jianfeng.Xie@colorado.edu

Abstract*:* Continual micrometeoroid bombardment and electrostatic charging of the lunar surface are natural mechanisms that can mobilize micron and sub-micron sized dust particles on the lunar surface. The characteristics of these dust populations are of scientific interest and engineering importance for the design of future equipment to operate on the lunar surface. The mobilized grains are expected to have a low velocity, which makes their detection difficult by traditional methods based on momentum transfer or impact energy. The Electrostatic Lunar Dust Analyzer (ELDA) is a recently developed instrument concept, where the charge on the moving dust is detected. ELDA consists of two Dust Trajectory Sensor (DTS) units combined with an electrostatic-deflection field region (DFR). The DFR uses a high electrostatic field to bend the electrically charged grain's natural trajectory. The two DTS units measure the charge and velocity of a dust grain before and after its deflection, respectively. We use this deflection measurement in conjunction with charge information to determine the grain's mass. The first basic prototype of the ELDA instrument has been constructed, tested and characterized in the laboratory. The analysis of DTS data from a dust particle moving a straight line without accelerator has shown that it is possible to achieve very high accuracy of the dust velocity (<1%) and dust direction (< 1 degree). The analysis is based on matching the data to numerical simulations and the best fit yields the particle characteristics. However, the particles in ELDA do not move on straight-line trajectories due to gravitational acceleration. The data analysis algorithm has been extended for applicability to the ELDA instrument. The particle's mass is calculated from the trajectories trough the instrument and amount of deflection with the DFR.

Understanding spacecraft failures by characterizing hypervelocity impact plasmas

Nicolas Lee*[(1)] and Sigrid Close[(1)]
(1) Stanford University, Stanford CA, USA

We present the first end-to-end study analyzing the effect on spacecraft charge conditions of electrical failures caused by meteoroid and orbital debris impacts. Specifically, we discuss results from a ground-based experiment studying the plasma expansion from hypervelocity impacts on representative spacecraft surfaces and a corresponding plasma expansion model to interpret the data.

The experiment was conducted at the Max Planck Institute for Nuclear Physics in Heidelberg, Germany, where a Van de Graaff dust accelerator was used to shoot iron dust particles between 10^{-16} g and 10^{-11} g at speeds of up to 60 km/s into a variety of targets including bare metal targets and samples of representative spacecraft surfaces. The goal of this experiment was to characterize the plasma expansion and associated RF emission from impacts on these targets under a range of surface charging conditions.

Results are analyzed from sensor observations of plasma generated by impacts on an electrically-biased tungsten target. The voltage biases applied to the target ranged from -1000 V to +1000 V. We find that the detected ion species are consistent with literature and that the initial plasma speed distribution corresponds to a 10~eV Gaussian. Plasma generated from impacts on targets with different biases are seen to behave very differently: on positive targets, different ion species can be separated macroscopically; on negatively-charged targets, multiple electrostatic discharge events can occur from a single impact; and on grounded targets, electron oscillation in a quasineutral plasma is a viable mechanism for producing an electromagnetic pulse.

These results can inform the design and operation of satellites in order to prevent impact-related electrical anomalies. Since spacecraft charging effects are strongly dependent on orientation and surface material, deleterious electrical effects of hypervelocity impacts can be mitigated through consideration of the spacecraft geometry and its interaction with the space environment.

Detection of Radio Frequency Emissions from Hypervelocity Impacts

David Strauss[1], Ivan Linscott[1], Theresa Johnson[2], Nicolas Lee[2], Ashish Goel[2], and Sigrid Close[2]

[1] Stanford University, Electrical Engineering, Stanford, CA, 94305
[2] Stanford University, Aeronautics and Astronomics, Stanford, CA, 94305

Experiments were conducted at the Max Planck Institute for Nuclear Physics Dust Accelerator Facility to characterize the production and expansion of impact generated plasmas. These tests were conducted to investigate theory about micrometeoroid impacts on orbiting spacecraft [CCC+10]. A set of six radio frequency (RF) sensors, three at 916MHz and three at 315MHz, observed impact related emissions under certain target and biasing conditions. Here we present the characteristic radio frequency emissions observed in the chamber associated with dust particle impacts together with methods for separating these emissions from the noisy, multi-path environment where the experiments were conducted.

We observed more than 6,000 impacts of iron dust particles between 1 femtogram and 10 picograms, accelerated to velocities between 4 and 50 km/s. Targets of tungsten, copper, aluminum, and solar panel segments were used. Three narrowband patch antennas, resonant at 916MHz with 28dB gain and three narrowband patch antennas resonant at 315MHz with 38dB gain were placed between 4 and 10 cm from the target. Two retarding potential analyzers (RPAs), a photomultiplier tube, and electric field stub antennas were also located in the test chamber. Measurements were made with multiple spatial arrangements of targets and sensors.

The vacuum chamber in which the experiments were conducted is a complicated RF environment. Irregular scatterers and an abundance of strong noise sources make it difficult to detect weak RF emissions. Using adaptive beamforming and noise subspace projection methods, data from multiple, spatially distributed sensors were fused to improve detection and mitigate the noise and scattering in the measurement environment.

Under certain target and biasing conditions, RF emissions associated with impact were observed. Using beamforming and noise subspace projection these impact signatures can be differentiated from the known noise processes in the chamber.

References

[CCC+10] S. Close, P. Colestock, L. Cox, M. Kelley, and N. Lee. Electromagnetic pulses generated by meteoroid impacts on spacecraft. *Journal of Geophysical Research*, 115(A12):1–7, December 2010.

Electric Field Characteristics from Hypervelocity Particle Impact Plasma

Theresa Johnson[*], David Strauss[†], Ivan Linscott[‡], Sigrid Close[§], Richard Adamo[**]

Experiments dedicated to detecting radiofrequency emissions in hypervelocity particle impacts have been conducted by Bianchi (1983) and Takano (2002). Bianchi detected 100kHz-200kHz emission from the acceleration of ~1g aluminum particles 10 km/s into hard materials in a vacuum chamber. Takano detected emission at 22GHz using a heterodyne receiver and acceleration of iron particles into a vacuum chamber at 2, 4 and 6.7 km/s. Our experiment represents the first ground-based campaign dedicated to detection of RF emission due to hypervelocity dust particle impact at impact speeds attained during meteor showers. Ground based tests are performed at the Max-Planck-Institute für Kernphysik Van de Graaff accelerator in Heidelberg, Germany to explore methods for radiofrequency emission associated with hypervelocity particle impact.

The motivations for studying hypervelocity impact-generated plasma emission properties include satellite electrical anomalies at the height of meteor showers. Meteoroids and dust traveling between 11 and 72.8 km/s are constantly bombarding spacecraft while on orbit. These hypervelocity particles may cause electrical anomalies in satellites through electromagnetic pulse (EMP) or electrostatic discharge (ESD) (Close, et al. 2010). Ground tests are conducted by firing iron femtogram particles at speeds in excess of 11 km/s at target materials situated in a 1m diameter vacuum chamber. A set of narrow-band patch antennas and a point electric field sensor are used to detect RF emission. Retarding potential analyzers are used to detect plasma energy and a photomultiplier tube is used to detect ultraviolet emission. Preliminary analysis of the electric field sensor provides evidence of the broadband emission due to electrostatic discharge.

The E-field sensors were developed by researchers at SRI, and consist of a capacitive coupled electric field stub that can be attached to a 1 cm diameter target. The target has the ability to be charged at up to +/- 1kV, or held at ground, to mimic a variety of on-orbit satellite conditions. One E-field sensor, used as the target, was aligned in the MPI dust accelerator close to the center of the beam line and hypervelocity dust impacts. The dust particles are charged in the process of acceleration and that charge may be deposited on the E-field sensor's target during impact. Additional charge is liberated upon both approach to a charged target, and upon impact and formation of the plasma cloud. E-field sensors are also placed in the vicinity of the impact region in order to capture radiated emissions and electric field strength in the vicinity of the target. Using a combination of a preamp in the sensor, and an additional LNA with 13-39 dB of gain outside the impact chamber, high SNR voltage pulses were recorded using a 5 GS/s sampling scope.

The E-field sensors' signals are classified according to impact parameters such as mass, velocity and particle charge and analyzed in conjunction with corresponding signals in the plasma, ultraviolet and patch antenna suite. The aim is toward the development of a dynamical model describing the plasma formation and evolution and corresponding methods for RF emission.

References

Bianchi, R., Capaccioni, F., Cerroni, P., et al. Radiofrequency emission observed during macroscopic hypervelocity impact experiments. Nature 308 (26), 830–832, 1984.

Close, S., P. Colestock, L. Cox, M. Kelley, and N. Lee. "Electromagnetic Pulses generated by meteoroid impacts on spacecraft." *J. Geophys. Res.*, 2010: 115.

Takano, T., Y. Murotani, K. Maki, T. Toda, A. Fujiwara, S. Hasegawa, A. Yamori, and H. Yano, Microwave emission due to hypervelocity impacts and its correlation with mechanical destruction, *J. Appl. Phys.*, vol. 92, no. 9, pp. 5550–5554, 2002.

---

[*] Ph.D. Candidate, Department of Aeronautics and Astronautics, Stanford University
[†] Ph.D. Candidate, Department of Electrical Engineering, Stanford University
[‡] Research Scientist, Department of Electrical Engineering, Stanford University
[§] Assistant Professor, Department of Aeronautics and Astronautics, Stanford University
[**] Deputy Director, Space Technology and Integration Program, SRI International, Menlo Park, CA

DISCRIMINATING ESD VS EMP EFFECTS IN HYPERVELOCITY IMPACT EXPERIMENTS

David S. Lauben[1]*, Sigrid Close[1], Theresa L. Johnson[1], Nicolas Lee[1], Ivan R. Linscott[1], David A. Strauss[1]

[1]Stanford University STAR Laboratory, Stanford, CA

Recently, a resurgence of theoretical and ground-based experimental activity has occurred to investigate potentially hazardous electromagnetic effects associated with the impulsive creation and explosive expansion of plasma plumes produced by hypervelocity ($v > 10$ km/s) micrometeoroid impacts to spacecraft.

Historically, electrical anomalies aboard spacecraft have been associated with classic and reasonably well understood mechanisms, including surface dielectric charging (absolute and differential) by differential ion flux and photoionization, deep dielectric and floating internal metallic structure charging from penetrating charged particles, and electronic circuit upsets or damage from such particles.

Then, when considering hypervelocity micrometeoroid impacts, the usual first concern is ballistic mechanical damage, for which the Whipple shield is devised to disrupt and disperse incoming particle momentum. So, perhaps less obvious is the fact that for sufficiently high velocities, the mechanical impact can lead to an electrical effect from the small but relatively energetic fraction of ejecta which is ionized by the impact. Since the ionized charge grows at power-law rate once the impact velocity exceeds the shock-wave speed in the participating materials, the effects can grow dramatically for high-end interstellar velocities (to ~450 km/s), whence ever-increasing kinetic energy is delivered to ever-decreasing volume.

The net effects of interest--those which can lead to spacecraft anomalies—can take one or more of several basic forms: (1) the ionized ejecta can suddenly form a conducting bridge between two or more satellite elements having dissimilar potentials (differentially charged dielectrics, high-voltage solar-array wiring, etc.), triggering an electrostatic discharge (ESD), (2) the free electrons in the plume can oscillate coherently about the leading-edge of the expanding (predominantly) positive ion cloud, generating a brief, pure electromagnetic pulse (EMP), which may overload a radio front-end, (3) the ionized, vaporized gaseous plume, upon stagnating at some adjacent satellite surface (or aperture), can vaporize that surface (or internals) as well as additional surfaces within radiative view.

Discriminating between these (and possibly other) mechanisms in ground and space-based experiments is difficult at best. Ejecta-initiated ESD generates secondary EMP, radio detectors for measuring EMP might also respond to impinging charge, and bolometers for measuring thermal flash may also respond to low-frequency EMP. In addition, ground-based hypervelocity experiments utilizing electrostatic accelerators must account for the charge carried by the incoming particle, and also for possible radio emissions which may emanate from the target as the particle charge is dispersed over the target face.

This paper reviews these concepts and past experiments, and suggests means and techniques by which such combined effects might be disentangled.

Colorado Software Defined Radar: Hardware, Results, Reconfigurabity and Deployment

Cody Vaudrin* and Scott Palo
Department of Aerospace Engineering Sciences, University of Colorado at Boulder

An overview and hardware update of the Colorado Software Defined Radar (CoSRad). A brief hardware examination focused on the frequency planning and echo detection aspects of CoSRad is followed by a description and demonstration of the coherent echo detection software and newly developed visualization tools using data recently acquired at Platteville, Colorado and at the Jicamarca Radio Observatory. The frequency dependence of meteor trail detection rates is discussed followed by observational comparisons between systems. An educational slide provides an overview of the topics of noise, oversampling and gain in direct-convert systems. Finally, we present of a number of interesting echoes extracted from various data sets. These echoes exhibit various unusual characteristics including long duration (over 10 seconds), range spreading, large power vacillations and periodicities.

CoSRad's reconfigurability is showcased through a description of current and past experiments with a variety of existing radar systems including those located at Jicamarca, Platteville, Argentina and the South Pole. We also discuss a NOAA Linear Frequency Modulation Continuous Wave (LFMCW) Tropospheric Boundary Layer Radar based on the CoSRad architecture. Basic theory of LFMCW radar and our approach to data acquisition using CoSRad is outlined. Geographically distributed synchronization of multiple receivers is mentioned and the basic characteristics of GPS-derived timing signals are presented and connected to the CoSRad measurement technique. Our talk concludes with various logistical elements and anecdotes including cost and the challenges involved with deploying hardware in hostile remote environments.

Characterizing Meteoroid Bulk Densities

S. Close[(1)], A. Macdonell[(2)], S. Pifko[(1)], R. Volz[(1)], M. Oppenheim[(2)]
[(1)] Stanford University, Stanford, CA
[(2)] Boston University, Boston, MA

We present a new technique for calculating bulk densities of low-mass (< 1 g) meteoroids using a scattering model applied to the high-density plasma formed around the meteoroid as it enters Earth's atmosphere. These plasmas, referred to as head echoes, travel at or near the speed of the meteoroid, thereby allowing the determination of the ballistic coefficient (mass divided by physical cross-section), which depends upon speed and deceleration. Concurrently, we apply a scattering model to the returned signal strength of the head echo in order to correlate radar-cross-section (RCS) to plasma density and meteoroid mass. In this way, we can uniquely solve for the meteoroid mass, radius and bulk density independently. We have applied this new technique to head echo data collected in 2007 and 2008 simultaneously at VHF (160 MHz) and UHF (422 MHz) at ALTAIR, which is a high-power large-aperture (HPLA) radar located on the Kwajalein Atoll. These data include approximately 20,000 detections with dual-frequency, dual-polarization, and monopulse (i.e. angle) returns. Our results show a clear dependence between meteoroid bulk density and altitude of head echo formation, as well as dependence between meteoroid bulk density and 3D speed. The highest bulk densities are detected at the lowest altitudes and lowest speeds. We also present results from an orbital analysis that correlates density to inclination and eccentricity. Additionally, we stipulate that the approximations in deriving the ballistic parameter, in addition to neglecting fragmentation, suggests that the traditional ballistic parameter must be used with caution when determining meteoroid parameters.

Preliminary Radar Observations from the Penn Sate Meteor Radar

J. V. Urbina[1], L. P. Dyrud[2], J. Fentzke[2], R. Seal[1], and R. Sorbello[1]

(1) Communications and Space, Sciences Laboratory, Pennsylvania State University, University Park, PA, USA
(2) Applied Physics Laboratory, John Hopkins University, Columbia, MD, USA

Specular meteor radars transmit only a few kilowatts of peak power, and are often operated in an all-sky mode, resulting in low detection sensitivity. In the past ten years, high power and large aperture (HPLA) radars, which transmit megawatts of power, have been applied to the detection of meteors as well. Because of this difference in transmitted power density, existing classical meteor radars only observe strong reflections from specular trails. HPLA radars also observe specular trails, but more frequently observe meteors via head-echoes and non specular trails (when the radar **k** vector is oriented perpendicular to the Earth's magnetic field). We show that the Penn State Meteor Radar, installed near the main university campus, at Rock Springs, Pennsylvania (76°W, 34°N), and transmitting less than 30 kW peak power, with a large collection area, can easily observe the specular meteor trail reflections, and also have sufficient power to detect frequently non-specular trail observations. The radar comprises two radar subsystems that make the system operable in classical all-sky meteor configuration with low peak power of about 5kW; and in narrow beam mode with peak power of about 25 kW, and oriented perpendicular to the Earth's magnetic field at meteor heights. We analyze the general characteristics of the meteor reflections detected with these radar systems during different time periods and compare them with meteor events obtained with radars of similar sensitivities at Camp Santiago, Puerto Rico and Fort Macon, North Carolina. We show that the measured diurnal variation in meteor rates are not the same from radar to radar or even between different reflection mechanisms detected by the same instrument.
. The results confirm those from other HPLA radars and show some additional interesting features.

Waveform Effects on HPLA Radar Meteor Measurements

Ryan Volz* and Sigrid Close
Stanford University, Aeronautics and Astronautics, Stanford, CA

Meteor studies using high-power large-aperture (HPLA) radars depend on a wide number of parameters including time, location, beam direction, baseband frequency, antenna (gain and beamshape), polarization (transmit and receive), pulse (length and encoding), and more. Some of these parameters are fixed for a particular radar system, while others, notably (for our purposes) polarization and pulse, can be varied. Comparing and combining meteor results from the many HPLA radars in use is challenging because of this proliferation of parameters and the difficulty in determining how they individually affect the results.

To help resolve some of these effects, we collected approximately 48 hours of meteor data using the Jicamarca 50 MHz radar transmitting a repeating sequence of five different waveforms, one per pulse. The pulses were transmitted in a single circular polarization and received in dual circular polarization. The five pulse waveforms included the three most popular for HPLA meteor studies: uncoded, Barker-13, and linear frequency modulation (LFM) chirp. The remaining two pulse waveforms, a minimum peak sidelobe binary code and a pseudorandom binary code, were included to facilitate development of new decoding techniques. By alternating the encoding with each pulse, our goal is to examine the same meteor under different illuminations in order to directly compare the effects of the waveform. Receiving with two orthogonal polarizations allows us to determine how the meteor backscatter affects polarization of the transmitted wave.

Our results confirm the known strengths and weaknesses of each waveform but more importantly illustrate how different waveforms can give apparently different answers in cases of distributed or multiple scatterers (such as head and trail interference). We discuss examples of these instances and suggest plasma configurations that could explain them. The apparent contradictions give some clues as to what is really happening, but more work is needed to bridge the gap in understanding.

Meteor “head echo” intensities are typically recorded by high-power large-aperture (HPLA) radar systems. These meteor observations have been analyzed extensively to measure parameters such as Doppler velocities, composition and mass estimates. The majority of observations conducted with these radar instruments utilize the maximum available transmitter power in an attempt to obtain the highest observable meteor flux rate. However, direct power law studies on the relationship between transmitter power and radar backscatter cross-section remain very rare. We present observations from two HPLAs investigating meteoroid cross-section dependence on illuminating power. Our meteor observations were conducted during two separate campaigns using HPLA systems at Arecibo Observatory (AO; center frequency 430 MHz), and Millstone Hill (MH; center frequency 440 MHz). The meteor observations at AO were conducted over the course of three different years on the same calendar dates. The MH observations were conducted on a single day by alternating at 30 minute intervals between full and half transmitter power. AO and MH were chosen due to their close proximity in transmitter frequency as well as the ability to set up nearly identical transmit and receive modes. For each facility, the same post-experiment searching algorithm was used on the collected data of varying power to ensure maximum meteor detections. We present our observed parameters from both facilities. We discuss how varying transmitter power at the HLPAs directly influences the total meteor counts detected as well as the possibility of a power law correlating signal to noise ratio with meteor detection flux rates. These results are significant in understanding systematic effects involved in estimating the Earth’s total meteor flux.

On the Effect of Turbulence on Specular Meteor Echoes

F. R. Galindo[1], J. V. Urbina[1], L. P. Dyrud[2] and J. Fentzke[2]

(1) Communications and Space, Sciences Laboratory, Pennsylvania State University,
University Park, PA, USA
(2) Applied Physics Laboratory, John Hopkins University, Columbia, MD, USA

We present preliminary results of a numerical model developed to study the effect of turbulences on underdense specular meteor echoes. Understanding meteor trail plasma turbulence is important because turbulent meteor trails are visible as non-specular trails to coherent radars, and turbulence influences the evolution of specular meteor radar trails, particularly regarding the inference of mesospheric temperatures from trail diffusion rates, and their usage for meteor scatter communication systems. The architecture of the numerical model traces meteor trail evolution from ablation and ionization processes through the creation of the actual specular meteor echo. Thus, this meteor model represents a valuable tool for the analysis of specular meteor physics. We compare our simulation results with the general characteristics of meteor echoes detected with two different data radar systems. The first radar operated at 50 MHz with moderate peak power of about 30 kW and was oriented perpendicular to the Earth's magnetic field while the second radar also operated at 50 MHz but with relative low peak power of about 5 kW. The latter radar was configured in classical all-sky mode observation. By comparing data from the different meteor systems, our preliminary studies illustrate the significant effect that neutral atmospheric winds and density, and ionospheric plasma density have on the variability of meteor trail evolution and the observation of non- specular meteor trails, and demonstrate that trails are far less likely to become and remain turbulent in daylight, explaining several observational trends using non-specular and specular meteor trails.

Non-Specular Modeling with Discrete Power Intervals

Heather Jiles[1]*, Lars Dyrud[1], Jonathan T. Fentzke[1], Freddie Galindo[2], Julio Urbina[2]

[1]Johns Hopkins University Applied Physics Laboratory
[2]The Pennsylvania State University, Department of Electrical Engineering
*Student

We present a new modeling effort for the Radar Cross Section of non-specular echoes, defined as enduring radar scatter from irregularities induced by plasma turbulence that are spread in range. We model these non-specular trails by computing the return power from discrete intervals using the diffusing electron line density profile generated by the governing physics of an ablating meteor. In addition, we use a simplified model for the non-specular trail at each altitude by assuming the plasma diffuses radially and is confined to discrete altitude bins. The trail RCS is determined by summing the contribution of the scattered E field from the sub-sampled altitude bins as the trail evolves in time and space under the influence of the background ionospheric and atmospheric parameters. The goal of this effort is to present the predicted return power and RCS from non-specular trails with this new model and compare these results to radar observations. We find that the new model explains the relatively flat signal to noise ratio (SNR) of non-specular trails as a function of time, which is in stark contrast to the exponential decay curves of specular trails. The results demonstrate an improved ability to characterize non-specular trails and a promising new capability for meteor modeling and applications, and represent a major improvement to the previous model assumption that non-specular trails remained reflective while plasma turbulent.

On August 7, 8, and 9, 2010 meteor data were collected between 1:00 AM and 9:00 AM local time using both the 430 MHz and 46.8 MHz radars. Both radars used the same modulation waveform, consisting of a digitally generated chirp that was converted to analog I and Q baseband signals using digital to analog converters. The chirp range was -0.5 to 0.5 MHz. A complex modulator generated the 430 MHz transmitter intermediate frequency centered at 30 MHz. The use of additional mixers allowed shifting to 46.8 MHz. The purpose of the experiment was to increase both range resolution and sensitivity over previous observations, and to collect dual polarization data with the 46.8 MHz radar. This paper does not discuss the dual polarization data.

The AO radar interface, a complex baseband system, recorded the 430 MHz data and the primary channel of the 46.8 MHz data. A digital receiver, primarily used for plasma line data, recorded both channels of the 46.8 MHz data. A method was developed for analyzing the data to search for detections of micrometeors. Signals of particular interest were those that show a “beating” pattern in the signal to noise ratio plots. This type of signal indicates a multi-piece meteor detection, when it was previously assumed that micrometeors enter that atmosphere as singles. These signals are extracted from the main data set and broken down into I and Q components, and additional analysis is used to show that the signal is a superimposed sine waves (from multiple pieces) as opposed to an amplitude modulation. Approximately 1,700 meteor echoes were detected in the data, with 90 signals showing a beating pattern. The purpose of this paper is to discuss the method of analysis, the detected signals, and the implications for meteor echo research.

Influence of ionospheric electrojets on meteor trail evolution

Lars Dyrud[1], Jonathan T. Fentzke[1], Julio Urbina[2]

[1]Johns Hopkins University Applied Physics Laboratory
[2] Penn State University

We present the first global simulations on the occurrence of meteor trail plasma irregularities to incorporate the electrodynamics of the auroral zone and the equatorial electro-jet. The electojet regions of the earth are peculiar locations for meteor trail evolution because strong electric fields dominate the meteor trail evolution by generating mini-electrojets with even stronger polarization fields. As the results show, electrojet meteors are far more likely to be turbulent than other geographic locations where neutral winds dominate polarization fields. Understanding meteor trail plasma turbulence is important in part because turbulent meteor trails are visible as non-specular trails to coherent radars. Turbulence also influences the evolution of specular radar meteor trails; this fact is important for the inference of mesospheric temperatures from the trail diffusion rates, and their usage for meteor burst communication. We provide evidence of the significant effect that neutral atmospheric winds and ionospheric plasma density, and ionospheric electric fields have on the variability of meteor trail evolution and on the observation of non-specular meteor trails.

A PROBABILISTIC APPROACH TO ESTIMATING METEOROID PRESENCE IN EARTH ORBIT FROM GROUND-BASED RADAR OBSERVATIONS

Steven Pifko* [(1)], Diego Janches [(2)], and Sigrid Close[(1)]
(1) Space Environment & Satellite Systems Lab, Department of Aeronautics and Astronautics, Stanford University, Stanford, CA 94305, USA
(2) Space Weather Lab, GSFC/NASA, Greenbelt, MD 20771, USA

The risk of meteoroid impact is a serious threat to spacecraft, and several satellite failures and anomalies have occurred due to collisions with these highly energetic particles. Most spacecraft anomalies attributed to meteoroid impacts appear to correlate with times of meteor showers. However, the continuous presence of sporadic meteoroids provides a much greater flux of particles and, due to their less predictable nature, a much greater threat of impact than meteoroids from showers. In addition, many anomalies from meteoroid impacts may go undiagnosed because it is difficult to detect that an impact occurred, especially one from smaller meteoroids, which make up the bulk of the incoming material, since they will not cause any significant mechanical damage or momentum change to the spacecraft. However, they may result in electrical upsets.

In order to properly assess and mitigate the risk of these events, the distribution of meteoroids over the range of altitudes in which satellites operate must be modeled and continually monitored. Ground-based observation of meteors is an inexpensive and widespread means of achieving this, provided that the distribution at higher altitudes can be determined from these measurements conducted over an altitude range of 70-130 km. In this presentation, a method for modelling the distribution over the range of orbital altitudes is described. This method uses orbital dynamics to characterize the probability that a meteoroid in an orbit about the Earth will reach a given altitude. This allows for the estimation of meteoroid flux at any altitude using meteor observations from ground-based systems, such as radar. The presented method is applied to space-based measurements from the Long Duration Exposure Facility (LDEF) and is compared to data collected by three radar systems: the ARPA Long-Range Tracking and Instrumentation Radar (ALTAIR), the MU radar, and the Southern Argentine Agile Meteor Radar (SAAMER).

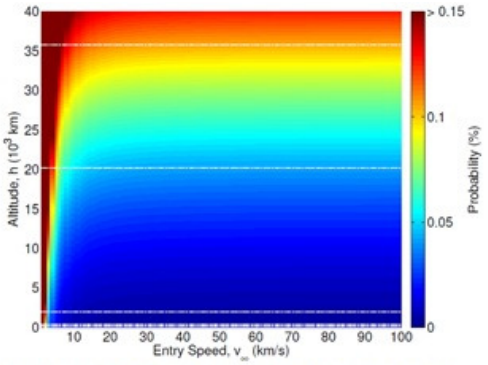

Figure 1. $P(h_p \leq h)$. The probability a meteoroid with speed, v_∞, entering Earth's gravitational Sphere of Influence (SOI) will reach an altitude, h.

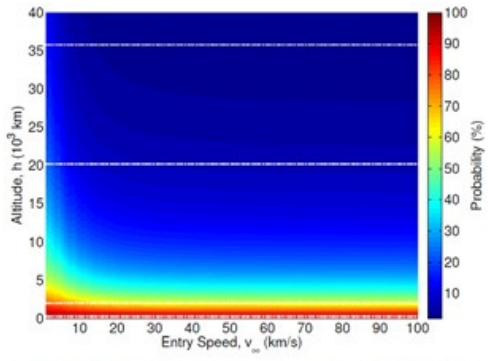

Figure 2. $P(h_p \leq 100\ km \mid h_p \leq h)$. The probability a meteoroid with entry speed, v_∞, will reach observation altitude (100 km) given that it reaches altitude, h.

THE UC BERKELEY UNDERGRADUATE RADIO ASTRONOMY LABORATORY

Geoffrey C. Bower, Carl Heiles, Aaron Parsons, and Andrew Siemion
Astronomy Department & Radio Astronomy Laboratory, UC Berkeley,
Berkeley, CA

The Undergraduate Radio Astronomy Laboratory at UC Berkeley emphasizes the development of deep capabilities in data gathering, analysis, and presentation. Students achieve expertise in these areas because the labs include the complete range of activities normally encountered in observational or experimental research. Students use laboratory equipment to measure the fundamental parameters of devices and systems, make astronomical observations with those systems, write software in Linux and IDL to control equipment and analyze the results, and write formal lab reports in LaTeX. We avoid "black box" equipment or "cookbook" procedures. The students leave the course having gained experience and knowledge, and a "feel" for how to proceed when faced with sometimes recalcitrant equipment and imperfect data. A by-product of the training has been an increase in student involvement in undergraduate research projects. These innovations have led to a major that has doubled in size and become more gender-balanced.

The Radio Astronomy Lab is structured around teaching the fundamentals of how cosmic radio waves are detected and propagate through the apparatus and electronics of radio telescopes, and how those signals are converted into images and spectra that demonstrate astrophysical principles. Students use bench experiments, operate telescopes, program general purpose computers for analysis, give informal oral reports to their classmates, and produce formal written reports as part of the lab. Connections to techniques used in consumer electronics are frequently made throughout the course to give external relevance.

Individual labs include activities around digital sampling and Fourier transforms, an X-band interferometer for measuring the position and diameter of the Sun and Moon, a horn antenna for detection of the 21-cm transition, and mapping of the 21-cm line using a 3.5-m dish antenna. In recent years, we have introduced a new segment that includes programming of field programmable gate arrays (FPGAs). A new ROACH-based spectrometer will permit pulsar detection and polarimetric OH spectroscopy with the 3.5-m dish. Graduate and undergraduate students have been involved in the design and implementation of new experiments.

An Inexpensive, Table-Top Interferometer and Undergraduate Labs To Teach the Basics of Aperture Synthesist

Jonathan M. Marr*[1], Alan E. E. Rogers[2], Vincent L. Fish[2], and Martina B. Arndt[3]

[1] Union College, Schenectady, NY, USA <marrj@union.edu>
[2] MIT Haystack Observatory, Westford, MA, USA
[3] Bridgewater State College, Bridgewater, MA, USA

The radio astronomical technique of aperture synthesis has been a significant instrument in the advancement of humanity's understanding of the universe. Yet, because of the complexity of the math involved, this important technique is almost always excluded from an undergraduate curriculum in physics and astronomy, leaving the interested students mystified about how instruments like the Very Large Array actually work.

We have developed an inexpensive ($500), easy-to-assemble, table-top interferometer lab set-up and a set of undergraduate labs that provide students with hands-on experience in the fundamentals of aperture synthesis. The interferometer, which was originally developed at the MIT Haystack Observatory as a Very Small Radio Telescope (VSRT) to observe the Sun, uses satellite TV electronics and compact fluorescent lamps are used as strong table-top microwave signal sources.

The labs are easily performed and convey an intuitive sense of how combining the signals from an array of antennas reveals information about the structure of a radio source. Students obtain measures of the interferometer response as a function of antenna separation distance and discover that a double source produces an oscillating function and that a resolved source produces a decreasing function. Although a thorough mathematical explanation of the process is helpful for advanced students, these labs can be completed without the mathematical lectures and still impart a general conceptual understanding to the lower level students.

Information about purchasing and assembling the VRST interferometer can be found at http://www.haystack.mit.edu/edu/undergrad/VSRT/index.html. The lab instructions, along with an explanation of how the VSRT interferometer works, and a free-downloadable package of java programs, called "VSRTI_Plotter", which we developed to facilitate the data processing and analysis of these labs, are available at https://www1.union.edu/marrj/radioastro/labfiles.html.

We are grateful for the contributions by Preethi Pratap, Madeleine Needles, Adam Pere, Karel Durkota, and Francis Wilkin.

Measuring CMB temperature with an inexpensive, student-built lab experiment

Meredith A. MacGregor* [(1)], John M. Kovac[(1)], Robert Wilson[(2)], Robert Kimberk[(2)], and Students of Harvard Astro. 191[(1)]
(1) Harvard University, Department of Astronomy, Cambridge, MA
(2) Smithsonian Astrophysical Observatory, Cambridge, MA

The Cosmic Microwave Background (CMB) was first detected in 1965 using the 20-foot horn-reflector at Bell Labs. Since that time, a number of measurements made with advanced instruments have not only confirmed the existence of the CMB, but also succeeded in precisely measuring its temperature and placing limits on its isotropy. For this student project, we aimed to build a telescope out of commercially available materials that was capable of repeating these measurements and making an independent detection of the CMB. While this is not the first undergraduate teaching lab to succeed in detecting the CMB, it is unique in being carried out using an entirely student-built instrument. Furthermore, all elements of the telescope were constructed from inexpensive parts using methodology that could be easily replicated. The two elements that proved to be most critical to the success of the project were a compact optical design with an unobstructed aperture and minimal sidelobes, as well as careful calibration using well-designed external temperature loads. With sufficient attention paid to these two components, a commercially available Low-Noise Mixing Block (LNB) proved to be an adequate front end for the radiometer. After its completion, the telescope was placed on the roof of the Harvard-Smithsonian Center for Astrophysics in Cambridge, MA. With one day of observations in April 2011, students were able to successfully measure the temperature of the CMB at both 11.2 and 12.2 GHz, using both vertical and horizontal polarizations. The average temperature measured at 11.2 GHz was 3.09 ± 0.47 K, while the average temperature measured at 12.2 GHz was 3.826 ± 0.85 K, with the quoted errors reflecting student estimates of statistical and various systematic uncertainties. The lab is being repeated in Fall 2011 with further refinements.

The Arecibo Remote Command Center (ARCC) on the campus of the University of Texas at Brownsville is a fully operational command and control room which allows students to control, in real time, major radio astronomy facilities such as the Arecibo and Green Bank radio telescopes. Students from the high school, undergraduate, and graduate level are performing observations and analyzing the resulting data from these facilities. The ARCC students have discovered over 16 radio pulsars as well as evidence for faster-than-light pulse propagation in the interstellar medium. Given the number of student involved, the ARCC program itself will be one of the nation's top producers of Hispanic physicists. This talk will give an overview of the ARCC program and how it uses radio astronomy to attract and retain students into scientific and engineering careers.

GASE INTERFEROMETRY AND COSMOLOGY ON THE ROOF

Recent theoretical developments concerning the plasma physics near the GRB blast wave have renewed interest in the properties of impulsive low frequency radio emission from GRBs. Prompt coherent low frequency radio emission would provide a unique probe of the plasma conditions near the blast wave during the period of peak particle acceleration and gamma ray emission. In this talk we re-introduce the GRB All-sky Spectrometer Experiment (GASE, pronounced ‘gaze’). This experiment will make use of advances in digital technology to record 4 MHz of bandwidth in eight 30 MHz dipole antennas for two hours after a Swift trigger is received. Due to the long dispersion delay at low frequencies, this allows contemporaneous measurements of the gamma ray and radio emission. The high spectral resolution of GASE will allow the predicted prompt 30 MHz signal from GRBs to be fully de-dispersed and identified. The combination of high spectral resolution and full horizon-to-horizon imaging will provide stringent rejection of radio interference.

The GASE array has recently been reassembled on the roof of the electrical engineering department at the University of Washington in Seattle. Both at Haystack (former location) and Seattle, GASE has been constructed and operated almost entirely by undergraduates. All parts, from repairing baluns, to writing the DAQ firmware, to the software correlator and fully custom analysis stack have been performed by students. This small interferometer has been an excellent teaching tool, and might serve as a useful prototype for teaching interferometers at other universities.

The Long Wavelength Array: A Dynamic Observatory for Radio Astronomy Education

Jacob M. Hartman[1], Gregory B. Taylor[2], Steven W. Ellingson[3], and the LWA Collaboration[4]

[1] Jet Propulsion Laboratory, Pasadena, CA
[2] University of New Mexico, Albuquerque, NM
[3] Virginia Polytechnic Institute and State University, Blacksburg, VA
[4] http://lwa.unm.edu

The Long Wavelength Array (LWA) is a powerful educational instrument for University students ranging from beginning undergraduates to the most advanced graduate students. For introductory courses, the first LWA station (LWA1) provides live, real-time imaging of the full sky, which offers students a new way to appreciate the dynamic nature of familiar sky objects. For somewhat more advanced students, LWA dipoles can be readily constructed and instrumented to observe our Milky Way galaxy, the Sun, Jupiter, and a few other bright sources. Such projects are already being done at the National Autonomous University of Mexico, the University of New Mexico, and the University of Texas at Brownsville. For graduate students, the LWA1 will offer a Student Observing Program, in which a few hours of observations are granted on the LWA1 to explore the cosmos in class projects. One unique aspect of the LWA1 is that it is one of the first large-N ($N > 100$) interferometers. Software to handle the 33,153 baselines produced is currently under development at UNM and Virginia Tech. Students can also explore beamforming techniques with LWA1, which will be of great interest to future large-N instruments.

SETI OPEN SOURCE DATA AND ANALYSIS TOOLS

Jon Richards, G. R. Harp
The SETI institute, Mountain View, CA http://setiquest.org

The SETI Institute operates the cm-wave Allen Telescope Array (ATA) radio telescope located in Northern California. The ATA is the primary instrument the SETI Institute uses to search the heavens for signals that may represent intelligent life outside our solar system.

The ATA officially began SETI observations in 2007, and 2 years ago it opened its doors to *citizen scientists* around the world through setiQuest. SetiQuest (http://setiQuest.org) is a SETI Institute initiative that makes data, signal search software, and system documentation from the ATA available to the public. Citizens are invited to participate in a widening variety of programs tied to the ATA, including: visual analysis of SETI waterfalls to identify signals with unusual signatures, or to observe in bands where RFI is present; analysis of real-time captures of data from the telescope using MatLab and a suite of C-based command line programs or with processing of their own invention.

We shall discuss the recent release of several tera-bytes of telescope data available for download, which we call setiQuest Data. We will describe how this data has been collected by the ATA antennas starting January of 2010 at regular intervals and made public on the internet. To aid any citizen scientist who wishes to explore this data, we will discuss our command-line toolkit (setiKit) which offers a gateway to data analysis, and setiExplorer, a prototype waterfall-based signal detector used for visual analysis of setiQuest Data. Armed with these tools citizen scientists can become involved in the search for extraterrestrial intelligence.

LaTeX SOFTWARE DEFINED RADIO: A LOW COST INTRODUCTION TO RADIO ASTRONOMY FOR MEXICAN UNIVERSITIES AND HIGH SCHOOLS

Stan E. Kurtz[1], David E. Fields[2], and Marcus D. Leech[3]

[1] Morelia, MichoacAn MExico
[2] Harriman, TN, USA
[3] Ottawa, Ontario, Canada

Radio astronomy is typically an expensive proposition, using large parabolic antennas, cryogenic receivers, and high-tech correlators. The economic challenge is often too daunting for many smaller institutions to undertake significant instrumental programs. The incorporation of digital signal processing techniques into radio astronomy is cutting edge technology. It is being implemented in the backends of existing radio telescopes such as the 100-meter Green Bank Telescope. Moreover, it forms the basis of new radio telescopes, including SKA pathfinders such as the Long Wavelength Array, the Allen Array, and the Murchison Wide Field Array. Many of the tasks originally done by analog RF electronics, including frequency conversion and filtering, are now being passed to the digital domain. General purpose platforms are being developed by CASPER and other groups. These platforms (ROACH and RHINO), although economical by professional radio astronomy standards, are relatively high performance (and hence relatively high cost) alternatives. Software Defined Radio modules, coupled with GNU Radio software, provide an economical means for smaller institutions to participate in this revolution in radio astronomy instrumentation. In this paper we present a summary of activities being developed in Mexican universities, technology institutes, and high schools with the goal of introducing students to radio astronomy based on radio telescopes built with Software Defined Radio techniques. We describe projects ranging in frequency from 20 MHz to 12.2 GHz, using both special purpose and off-the-shelf satellite television front ends. Some of these projects will use a novel low-cost Software Defined Radio module under development by the Society of Amateur Radio Astronomers; we will provide an overview of and update on this development effort.

The Atacama Large Millimeter/submillimeter Array: An Update

Jeff Mangum*(1)
(1) National Radio Astronomy Observatory, Charlottesville, VA

The Atacama Large Millimeter/submillimeter Array (ALMA) is rapidly proceeding through its commissioning stages at its Andean Mountain site in northern Chile. Tests at the atmospherically superb 5050 meter altitude Array Operations Site and readiness reviews held during the 2010-11 period resulted in a successful call for proposals on 30 June 2011. The Cycle 0 call garnered 919 distinct proposals. Early Science Cycle 0 begins on 30 September 2011.

16 antennas of the final 66 stand ready to produce the deepest integrations ever achieved of the cool thermal Universe. The array is equipped with four of its eventual complement of ten receivers: Band 3 (84 to 116 GHz), Band 6 (211 to 275 GHz), Band 7 (275 to 373 GHz), and Band 9 (602 to 720 GHz). When fully complemented with ten receivers ALMA will operate over a decade of bandwidth from 10 mm to 0.35 mm. Currenly ALMA's sensitivity reaches roughly 0.5 mJy in one minute of integration at Band 3. Cycle 0 will utilize two array configurations; a compact configuration with minimum/maximum baselines of 18/25 m, and an extended configuration with minimum/maximum baselines of 36/400 m. The extended configuration will offer spatial resolution as small as 0.2 arcseconds. Early Science Cycle 0 holds the promise of producing some of the most sensitive and detailed measurements of the universe as viewed from the southern hemisphere.

The Early Science Cycle 1 observing period begins 1 August 2012 and is expected to provide 32 antennas. During Cycle 1 the array will reach a sensitivity of 0.2 mJy in a minute and may extend to baselines of nearly a kilometer.

The Improved C-Band System on the VLBA

Robert Hayward[1] and Steven Durand[1]

[1]National Radio Astronomy Observatory
1003 Lopezville Road, Socorro New Mexico USA 87801, 575.835.7000
rhayward@nrao.edu and sdurand@nrao.edu

Abstract

The Very Long Baseline Array (VLBA), consisting of ten 25 meter antennas, is one of the world's premier astronomical radio telescopes. A project to expand the bandwidth of its C-Band receiver system was launched in 2011. The project required a new wideband 4-8 GHz receiver, a new down-converter and a new digital recording system. The designs are now complete and are being implemented incrementally on the array with a completion date planned for late 2012.

The new C-band system is a wideband instrument in contrast to the current narrow 4.5-5.2 GHz capability. The astronomical signals are captured by a low-noise, circular polarized receiver with an octave bandwidth which provides access to sky frequencies across the full 4-8 GHz frequency range. The down-converters parse and convert the receiver signals into two 512 MHz bandpass signals per polarization. Each of the four IF signals are digitized at a rate of 1024 MHz by an 8-bit sampler for a total RF bandwidth of 1024 MHz per polarization.

The VLBA is engaged in a long-term program to map the structure and dynamics of the spiral arms within our Milky Way Galaxy. The new system will allow the VLBA to access the strong methanol maser transition at 6.7 GHz, currently not observable, and will enable distance measurements accurate to 10% out to distances of 10 kiloparsecs.

Astrometric observations of parallax and proper motion with the VLBA can be hindered by phase variations arising in the troposphere and ionosphere. The widely spaced frequencies that will now be possible with the new C-Band system will enable direct measurements of these dispersive effects and allow them to largely be removed from the observations. For continuum observations, using multi-frequency synthesis algorithms for combining the baselines from the 2:1 range in frequency will not only improve the signal-to-noise ratio but provide better imaging fidelity because of the increased *uv*-coverage in the aperture plane.

This paper will discuss wideband techniques used to receive, down-convert, sample, and record the astronomical data. Performance data from the feeds, receivers, frequency converters, and the digital back-end recording system will be presented. The VLBA C-band project is a success in many ways. The new hardware meets or exceeds the original scientific requirements and the wideband techniques used throughout the instrument are applicable to the next generation of radio telescopes.

ALMA SYSTEM VERIFICATION

Richard A. Sramek* (1)
(1) National Radio Astronomy Observatory, Longmont, CO

ALMA, the Atacama Large Millimeter/submillimeter Array, is an international astronomy facility and synthesis radio telescope currently under construction in northern Chile's Atacama desert at an altitude of 5,000 meters above sea level. The first of the 66 antennas of the array was moved to the high site in September 2009 and by the end of 2011 there will likely be more than 20 operational antennas; early science observations were underway in October 2011.

As the array has grown and science commissioning has progressed, a program of System Verification (SV) has been developed and is being executed. The purpose of SV is to measure the performance of the instrument that is being delivered compared to the System Technical Requirements. These tests are being carried out by the ALMA science and engineering staffs. Results will be presented in this paper on topics such as antenna surface and pointing accuracy, array phase and amplitude stability with time and angle, bandpass stability, spurious signal levels, the suppression of spurs using LO off-setting and 180d Walsh switching, return to phase after frequency change, cross-polarization levels, cross-polarization stability with time, angle and frequency, and other test results.

As SV tests are being performed, unexpected problems and instabilities are sometimes discovered; System Verification then becomes System Diagnostics as the testing is redirected to characterize and understand the origin of performance defects, and to develop mitigation plans. This is a multidisciplinary effort by scientists, engineers and control software developers. Examples that will be discussed here include the loss of coherence when Walsh switching is turned on, a 7.8 MHz comb of spurs in baseband, phase errors with a sinusoidal variation in time, plus others.

Commissioning, Operations, and Early Results for the Long Wavelength Array

Joe Craig[1] On Behalf of the LWA Collaboration
(1) University of New Mexico, 1009 Bradbury, Albuquerque, NM 87131

We are living in an era of resurgent interest in astronomy at long wavelengths, as witnessed by the development of new low frequency telescopes around the world, including LOFAR, MWA, PAPER, and the LWA. The LWA is designed for both long-wavelength astrophysics and ionospheric science. Science to be addressed with the LWA includes first stars and dark ages, the acceleration of relativistic particles, physics of the interstellar and intergalactic media, transient science, solar science and space weather, and "discovery science"; that is, the search for previously unknown sources and phenomena. The first station of the LWA, consisting of 256 antennas (LWA-1) has recently been completed and commissioning is under-way. We will discuss the engineering challenges and design implementations which have brought LWA-1 to fruition. We will also present early science results obtained through the commissioning phase.

RESULTS FROM LWA1 COMMISSIONING: SENSITIVITY, BEAM CHARACTERISTICS, AND CALIBRATION

Steve Ellingson[1] and the LWA Collaboration[2]

[1] Bradley Department of Electrical & Computer Engineering,
Virginia Tech, Blacksburg, VA 24061
[2] http://lwa.unm.edu

The first station of the Long Wavelength Array, called "LWA1", is a new radio telescope operating in the frequency range 24–87 MHz (Galactic noise-dominated), located near the center of the EVLA. LWA1 consists of 258 pairs of dipole-type antennas whose outputs can be formed into beams, or recorded separately using one the instrument's transient buffer modes. This talk presents some results from commissioning of LWA1 using the "transient buffer – narrowband" (TBN) mode. TBN allows up to 10 hours of continuous streaming of 67 kHz bandwidth from all 516 dipoles + 4 additional test signals, at any center frequency in the tuning range. Since TBN captures the signal from every dipole independently, it is possible to perform experiments in calibration, beamforming, and correlation entirely in software, after the observation. Using TBN, we demonstrate the calibration of the array using only astronomical sources, and subsequently generate beams which can be accurately pointed and are capable of hours of precise sidereal tracking without recalibration. The observations are then used to calculate beam sensitivity (specifically, system equivalent flux density) as function of pointing in zenith angle (which determines beam shape) and celestial coordinates (which determines system temperature). We demonstrate the use of separate dipoles on long baselines – "outriggers" – combined with observations of strong astronomical sources to measure the beamwidth and sidelobe characteristics of the beam. We also demonstrate the use of an outrigger antenna to make precise measurements of patterns of the individual dipoles in the array, which is of interest due to effect of mutual coupling in perturbing these patterns. Finally, we demonstrate the efficacy of spatial nulling, which has applications in mitigation of radio frequency interference, and reducing the effect of strong sources outside the beam in certain types of observations. Collaborators in the development of LWA1 include NASA Jet Propulsion Laboratory, Los Alamos National Laboratory, National Radio Astronomy Observatory, U.S. Naval Research Laboratory, University of New Mexico, and Virginia Tech.

Current Optics Design for the U.S. SKA Technology Development Project

William A. Imbriale (1), Lynn Baker (2), and German Cortes-Medellin (2)

(1) Jet propulsion Laboratory, California Institute of Technology, Pasadena, California

(2) Cornell University, Ithaca, New York

The U.S. design concept for the Square Kilometer Array (SKA) program is based on utilizing a large number of 15 meter dish antennas. The Technology Development Project (TDP) is planning to design and build the first of these antennas to provide a demonstration of the technology and a solid base on which to estimate costs. This paper discusses the latest design tradeoffs for selecting both the optics and feed design.

The optics design will utilize dual, shaped offset reflectors for the SKA / TDP antennas. The offset optics provides a clear optical path and aperture which does not scatter any radiation out of the focused region. Combined with low illumination at the edges of the two reflectors, this can lead to very low sidelobes away from the main beam and its first few sidelobes. The very small wide angle sidelobes from a good offset design reduce the received levels of strong sources out of the field of view, enhancing high dynamic range, a key scientific requirement. They also provide enhanced rejection of RFI, especially from satellites. Dual reflector shaping is also used to provide high aperture efficiency with low edge illuminations thus minimizing the noise temperature contribution.

Whereas one or two wideband feeds can cover the entire SKA mid-frequency band, it takes at least 5 octave band corrugated horns to accomplish the same task. However, it is well known that there is a significant penalty in efficiency, return loss, noise temperature and cross-polarization for using a wideband feed versus a corrugated horn. Thus the baseline plan is to use a series of octave band corrugated horns to cover the required frequency. In this way, the optimum character of the optics design can be demonstrated.

There is also the need for very wide bandwidth feeds. Among the feeds currently under consideration are the QSC feed developed by Cornell, the Log periodic dipole antenna developed for the ATA project, a Quad-ridged Flared Horn developed by Cal Tech and the Eleven feed developed by Chalmers University.

The real issue is to quantify the loss in performance for the wideband feed in order to select the optimum design in terms of total system cost.

Wideband 3-mm Receiver Development For CARMA

James W. Lamb[(1)]
(1) California Institute of Technology, Big Pine., CA, 93513, USA

CARMA, the Combined Array for Millimeter-wave Astronomy, a university based facility has, six 10.4 m diameter antennas, nine 6.1 m diameter antennas, and eight 3.5 m diameter antennas. All have receivers operating in the 3-mm band. The two larger types also observe at 1-mm, while the small antennas have 1-cm receivers.

All 23 antennas may currently be cross-correlated in a single interferometric array in the common frequency band from about 85 GHz to 116 GHz. The 10.4-m and 6.1-m antenna receivers use double-sideband SIS mixers with noise temperatures of ~30-50 K DSB. The 3.5-m antennas have millimeter integrated circuit (MMIC) receivers with noise temperatures of ~40-70 K. For all receivers the IF band is 1–9 GHz in a single linear polarization. There is a tradeoff of sky frequency coverage of the DSB receivers against the improved sensitivity of the SSB receivers. When the two types of receiver are operated in the same array, rather than in separate subarrays, the tradeoff is worse since only one sideband is common to all receivers. Currently, the spectral line correlator can process a maximum of 2 GHz of bandwidth per antenna, which may be augmented by the wideband correlator, adding 8 GHz to eight of the antennas (but overlapping with the spectral line coverage).

We propose to significantly increase the throughput of the instrument by increasing bandwidth of the 3-mm receivers, as well as adding the second polarization. The new receivers will have polarizing orthomode transducers to accept two circular polarizations that are then fed to MMIC amplifiers. The amplifiers will be obtained through a collaboration with Caltech's Cahill Radio Astronomy Lab and JPL which have development funding from the Keck Institute for Space Studies. These are expected to exhibit noise temperatures <40 K across the 85–116 GHz band, based on preliminary measurements. Two MMICs will be used to obtain sufficient gain to drive solid state mixers. Balanced Schottky mixers will be configured as a sideband separating downconverter. Waveguide quadrature and in-phase splitters will divide the LO and signal to the two mixers, followed by stripline quadrature hybrids to extract the two sidebands. IF amplifiers covering the band 1–18 GHz will boost the signal for transmission on an analog optical fiber link. This will deliver two sidebands of 17 GHz for each of two polarizations, a total instantaneous bandwidth bandwidth of 68 GHz.

This design is compatible with the existing receiver scheme which is a subset of the coverage. It will therefore be possible to stage a gradual upgrade without sacrificing significant observing time. Further details will be given in the presentation.

W-band Heterodyne Module Development for Large Arrays

R. Gawande[1], K. Cleary[1], T. Readhead[1], R. Reeves[1], T. Gaier[2], P. Kangaslahti[2], L. Samoska[2], S. Church[3], M. Sieth[3], P. Voll[3], A. Harris[4],

Development of ultra low noise, large focal plane arrays will greatly enhance our ability to survey large areas of the sky and enable future discoveries in radio astronomy.

We present the design and measurement results of the W-band heterodyne MMIC (Monolithic Millimeter Integrated Circuit) modules developed as part of the MAS (Millimeter Array Spectrograph) project. The MMIC modules house a chain of W-band low-noise amplifiers (LNAs), a band-defining filter and sub-harmonic mixers. A WR-10 waveguide serves as the input to the module. A waveguide probe couples the signals into the input LNA. The amplified RF signal is divided using a Wilkinson splitter and fed into two mixers. The LO at half the RF frequency is split using a Wilkinson splitter and fed in phase quadrature to the two mixers to produce the "I" and "Q" outputs at the IF ports of the two mixers.

The W-band MMIC LNAs used in this work are from the Northrop Grumman Aerospace System (NGAS) InP High Electron Mobility Transistor (HEMT) fabrication process having 35 nm gate lengths. The input MMIC was carefully chosen based on the cryogenically-probed S-parameter and noise data in order to minimize the overall module noise. The combination of the LNAs is selected such that a large effective bandwidth can be achieved, based on an ADS simulation of the cryogenically-probed S-parameters. The gain of the cascade should be large enough to overcome the mixer conversion loss and backend noise but small enough to ensure linear operation. Special care is taken during the assembly to avoid any stability issues due to cavity feedback.

The module is characterized using Y-factor method. For measurements at the ambient temperature, room temperature absorber is used as the hot load and liquid Nitrogen as the cold load. For cryogenic measurements, the noise and gain of the module are measured using a variable temperature load (VTL) at the input.

We will present the results of the two W-band heterodyne modules developed using two different combinations of MMIC amplifiers. A noise temperature between 30 to 60 K is achieved over a frequency range of 75 to 115 GHz.

"A cryogenic probe station for W-band MMIC Low Noise Amplifiers"

There is a clear trend towards focal-plane arrays in order to increase array sensitivity and mapping speed for applications such as CMB B-mode detection, molecular spectroscopy and others. W-band is an attractive frequency band for such applications. Recent advances in microwave miniaturization techniques and in the performance of front-end LNAs are enabling the development of such arrays. The very largest arrays will require high levels of component integration in order to be cost effective. Therefore, since significant gains in array sensitivity can be made by improving the performance of the individual front-end amplifiers in each array element, cryogenic screening of front-end amplifiers for noise temperature will be necessary.

Furthermore, the data from such cryogenic screening would benefit the MMIC foundries, as it would contribute directly to the understanding of their fabrication processes.

The CRAL (Cahill Radio Astronomy Lab) at Caltech, has designed and tested a cryogenic probe station for W-band MMIC amplifiers that can measure both noise temperature and S-parameters of large chip quantities in a single cool-down. The station was designed to accommodate up to 4-inch diameter wafers (cooled to ~18K). The S-parameter measurement configuration uses a vector network analyzer (VNA) with W-band frequency converters which connect via waveguide with co-planar waveguide (CPW) probes. In the noise temperature measurement configuration, the input probe is connected to a variable-temperature load and the output probe is connected to a power sensor via a heterodyne receiver.

In this talk, we describe our cryogenic probe station, discuss the challenges encountered in its development and show the latest results from cryogenic probing of 35nm InP W-band MMIC LNAs.

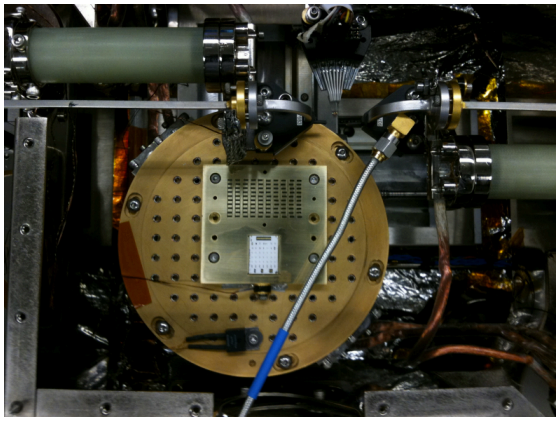

Efficient Snapshot Calibration for Polarimetric Phased Array Radiometers

T. D. Webb*, K. F. Warnick
Department of Electrical and Computer Engineering
Brigham Young University
Provo, Utah, USA

March 16, 2011

Abstract

Several research institutes worldwide are developing phased array feeds (PAFs) for wide-field L-band radio astronomical observations. PAFs offer faster survey speeds and larger fields of view than standard single-pixel feeds, which allows rapid sky surveys and significantly increased scientific capability. For many deep space sources, polarization state information plays an important role in understanding cosmological processes, so accurate polarimetric calibration techniques for PAFs are required. Existing polarimetric calibration methods require as many as four polarized calibrator sources, are based on assumptions about the form of the system Mueller matrix that limit the generality of the method, or require long observations of a polarized source which is time-consuming for multiple PAF beams. This paper introduces a more efficient method of calibration that uses only three snapshot observations of bright astronomical calibrator sources, one unpolarized and two partially polarized. The method makes no assumptions about the orientation of the feed elements and is robust with respect to mechanical degradations such as imperfect alignment of the phased array antenna elements.

We also demonstrate remarkable stability in the polarimetric accuracy of the calibrator over the field of view. This enables us to attempt calibration with only a measurement at bore sight. Avoiding polarimetric measurements at every beam could save hours of calibration time.

Technical Tutorial: Delay/Delay-Rate Filters for Low-Frequency Interferometers

Aaron R. Parsons
Univ. of California, Berkeley. 601 Campbell Hall, Berkeley, CA 94720
USA; aparsons@berkeley.edu

Low-frequency, wide-field radio interferometers suffer generally from an overabundance of information. Large fields-of-view complicate array calibration by decreasing the extent to which any single source dominates the correlated flux between antennas. Without isolation of sources, self-calibration must rely on prior models of the sky and primary beam response pattern to divide out the baseline-dependent interference pattern.

Delay/Delay-Rate filtering is a technique operating independently on each baseline for leveraging wide-bandwidth (and particularly, wide fractional bandwidth) observations to isolate sources for more robust self-calibration without requiring detailed sky models. These filters geometrically isolate a region of sky in the Fourier domains complimentary to spectral frequency and time, but maintain convolving kernels that can be used to reconstruct passband and primary beam information, even in situations where RFI-excision has introduced sharp discontinuities that give such kernels broad sidelobes.

This technique has proven to be especially valuable for low-frequency observations of the epoch of reionization. One of the major complications of using an interferometer to probe the power spectrum of reionization is the frequency-dependence of the spatial wavemode sampled by a pair of antennas. This frequency-dependent response causes foregrounds, which are differentiated from the target signal by their spectral smoothness, to appear unsmooth. For this application, the principles of delay/delay-rate filtering prove to be particularly enlightening for understanding how current and future arrays targeting reionization may differentiate foregrounds from the high-redshift 21cm emission that they seek to measure.

Enabling Next Generation Dark Energy and Epoch of Reionization Radio Observatories with the MOFF Correlator

Proposed 21 cm cosmology observatories for studying the epoch of reionization (z 6–15) and dark energy ($z 0–6) envision compact arrays with tens of thousands of antenna elements. Fully correlating this many elements is computationally expensive using traditional XF or FX correlators, and has led some groups to reconsider direct imaging/FFT correlators. In this paper we develop a variation of the direct imaging correlator we call the MOFF correlator. The MOFF correlator shares the computational advantages of a direct imaging correlator, while avoiding a number of its shortcomings. In particular the MOFF correlator makes no constraints on the antenna arrangement or type, provides a fully calibrated output image including widefield polarimetry and non-coplanar baseline effects, and can be orders-of-magnitude more efficient than XF or FX correlators for compact radio cosmology arrays.

The HI cosmology and second generation Epoch of Reionization instruments are similar in their instrumental characteristics, featuring compact arrangements of many thousands of antennas. The many short baselines and wide field of view maximizes the sensitivity of power spectrum measurements over all scales, however, it also puts enormous processing demands on the correlator system. A radio correlator measures the cross-power correlation between all antenna pairs in many narrow frequency channels, and for a modern FX correlator the computation scales as the square of the number of antennas. The correlator under construction for the MWA requires 15.5 trillion complex multiplies and accumulations per second (Tcmacs) for 512 antennas and 31 MHz of bandwidth. For many of the proposed radio cosmology instruments this quickly scales into the peta-flop regime, making the correlator a dominant cost for these arrays. This has driven some concepts such as the Omniscope and cylinder telescopes to use direct imaging correlators, despite their significant shortcomings.

In this paper we introduce the MOFF (Modular Optimal Frequency Fourier) correlator concept. The MOFF correlator incorporates the gridding and calibration usually associated with post-correlation image processing into the correlation process. This work expands on direct imaging correlator concepts by Daishido (Proc. SPIE) and Rogers (ATA Memo Series, 102), with particular emphases on data calibration and modular design. For the compact antenna layouts of proposed radio cosmology telescopes, the MOFF correlator is very efficient, makes no constraints on the antenna placement, and produces a provably optimal data product.

The MMIC Frontier for Radio Astronomy

Matthew A. Morgan
National Radio Astronomy Observatory, Charlottesville, VA. 22936

The advent of Monolithic Microwave/Millimeter-Wave Integrated Circuit (MMIC) technology revolutionized the commercial wireless industry by directly addressing the consumer's demand for more compact, lower-cost, versatile electronics. Its adoption in radio astronomy has been somewhat slower due to more stringent high-performance requirements, especially in a few niche areas like cryogenic noise temperature and wide instantaneous bandwidth. Nevertheless, MMIC technology is poised to bring about the next generation of astrophysical instrumentation, leveraging the huge growth in commercial product lines, wafer processes, and packaging techniques. Once exclusively an in-house capability for custom design solutions, a wide range of MMIC processes are now available for contract use, and MMIC die of every variety are available for purchase from multiple vendors at low cost in small to large quantities.

To make optimal use of this technology in the demanding field of radio astronomy instrumentation, however, one must be mindful of both its advantages and its limitations. Current receiver architecture is dominated by convention – design decisions made long ago to address the particular qualities of the then available components. The most successful MMIC-based receivers today will not be those that simply replace connectorized components with MMIC die in a traditional block diagram, but instead those in which the entire receiver architecture is re-optimized around the strengths and weaknesses of the current technology.

This tutorial will cover the key principles of state-of-the-art MMIC-based and highly-integrated receiver design by a series of recent real-world examples. These will include the development of custom MMIC layouts, multi-chip modules, fabrication, assembly, and testing, both on-wafer and in-package. It will review some of the top challenges facing the radio astronomy MMIC community today, current areas of active research, and future directions with the potential for great advances to be made.

GPUs in Radio Astronomy

Paul Demorest*
National Radio Astronomy Observatory, Charlottesville, VA

Over the past several years there has been an explosion of interest in the use of graphics processing units (GPUs) for general-purpose computation. Modern GPUs contain a set of highly parallel multiprocessor units capable of efficiently executing a single operation on many data values simultaneously. For algorithms that map well onto this parallel architecture, order-of-magnitude improvements in computational performance per cost are possible when compared with "conventional" approaches. In combination with the high-speed internal data bus and networking capability of current computer systems, GPU processing now presents an attractive choice for real-time digital signal processing in radio astronomy applications.

The programming tools available for GPU computing have also seen rapid growth over this time period, and it is now possible for anyone skilled in standard C programming to quickly begin producing useful GPU code. However getting the most out of GPUs still requires a good understanding of the GPU architecture, especially with regard to memory layout and access patterns. In some cases, familiar algorithms developed over many years experience with single-processor systems need to be entirely rearranged to be efficient on the GPU.

Here I will discuss the current state of GPU usage in radio astronomy, as well as a short tutorial on the basics of GPU programming. GPU-based systems for coherent dedispersion of pulsar signals, high-resolution radio spectroscopy, real-time transient searches, and interferometric correlators are either in development or already deployed at radio observatories around the world. Drawing from these projects, I will present real-world examples of GPU-based instruments and the relevant design choices. I will also present some more detailed examples from my own work on pulsar signal processing on GPUs.

The 36-ft millimeter-wave radio telescope of the NRAO was a daring concept when it was proposed. This talk will review its evolution into perhaps the most popular public-observatory telescope in the United States. In spite of many technical problems initially, the telescope revolutionized our understanding of how stars form and of chemical activity within the "dark" material of spiral galaxies. It's ultimate child will be the ALMA mm-wave array now under construction at a 16,500-m site in the Andes in Chile, a 50-antenna synthesis array supported by European countries, North American countries, Japan, and Chile. The 36-ft telescope's success is due in great part to the vision of two giants in US astronomy---Frank Drake and the late Frank Low---and to the flexibility of the US National Science Foundation in the 1960s.

Recent Advances with EDGES and the Status of Global 21 cm Experiments

Alan E. E. Rogers
MIT Haystack Observatory
and
Judd D. Bowman
Arizona State University

ABSTRACT:

Experiments to detect of the global 21 cm signature in the sky noise spectrum between 40 - 200 MHz have become an active area of development in the last year. Many of these experiments share a common approach of using a single broadband antenna combined with a carefully calibrated receiver to measure the all-sky radio spectrum and search for tiny spectral distortions from neutral hydrogen at high redshift that should imprinted on the bright Galactic synchrotron spectrum that dominates the sky noise power.

The Experiment to Detect the Global Eor Signature (EDGES) was able to set a lower limit of $\Delta z>0.06$ for the duration of the reionization epoch, assuming it occurred between redshifts $13>z>6$, by maintaining smooth enough frequency response so that the signature of highly redshifted 21-cm line emission of only about 20 milliK over the strong (>100 K) foreground of Galactic and extragalactic noise would have been detected. In order to detect or set limits on the 21-cm line from the early universe with the much more gradual signature expected from theoretical models an accurate calibration method is being developed to significantly reduce the level of systematics that currently limit EDGES.

This calibration involves using the EDGES 3-position switched spectrometer to calibrate the internal noise source by measuring the spectrum of a heated resistor, calibrate the low noise amplifier (LNA) noise waves from the spectrum of an open low loss cable and make ancillary measurements of the impedance of the LNA, antenna and open low loss cable with a vector network analyzer (VNA). The details of the calibration method, using standard 50 ohm VNA measurements, based on a noise wave model are given.

Simulations of the accuracy needed to reduce the systematics to the level needed to extend the global measurements to more gradual signals from the 21-cm line are also shown along with initial results of the calibration method.

We will also provide a brief overview of other Global 21 cm experiments.

A concept for a new space-based cosmology mission called the Dark Ages Radio Explorer (DARE) will be presented in this talk. DARE's science objectives include (1) When did the first stars form? (2) When did the first accreting black holes form? (3) When did Reionization begin? (4) What surprises does the end of the Dark Ages hold (e.g., Dark Matter decay)? DARE will use the highly-redshifted hyperfine 21-cm transition from neutral hydrogen to track the formation of the first luminous objects by their impact on the intergalactic medium during the end of the Dark Ages and during Cosmic Dawn (redshifts z=11–35). It will measure the sky-averaged spin temperature of neutral hydrogen at the unexplored epoch 80-420 million years after the Big Bang, providing the first evidence of the earliest stars and galaxies to illuminate the cosmos and testing our models of galaxy formation. DARE's approach is to measure the expected spectral features in the sky-averaged, redshifted 21-cm signal over a radio bandpass of 40-120 MHz. DARE orbits the Moon for a mission lifetime of 3 years and takes data above the lunar farside, the only location in the inner solar system proven to be free of human-generated radio frequency interference and any significant ionosphere. The science instrument is composed of a low frequency radiometer, including electrically-short, tapered, bi-conical dipole antennas, a receiver, and a digital spectrometer. The smooth frequency response of the antennas and the differential spectral calibration approach using a Markov Chain Monte Carlo technique will be applied to detect the weak cosmic 21-cm signal in the presence of the intense solar system and Galactic foreground emissions.

We have recently identified four fundamental foreground contaminations for Epoch of Reionization and Dark Energy power spectrum observations. This insight will enable us to identify the sources of contamination at below the imaging threshold, and naturally leads to a quantitative method for comparing HERA instruments.

These foreground contaminants are the basis of the 'mode-mixing' contamination which has been the dominant concern of the EoR power spectrum community in the past few years. Three of the four contaminants leave a wedge-shaped 'EoR' window in which the 21 cm cosmology signal can be observed with negligible interference from the foregrounds. The fourth however contaminates this window, and emphasizes the importance of calibration for 21 cm cosmology measurements. This window has been seen in simulation, but a qualitative and quantitative description of its origin is just now emerging. T

These effects are fundamentally related to loss of information during the measurement process, and is not due to assumptions in the analysis process. Thus these foregrounds cannot be mitigated with simple corrections. Additionally, the mathematics behind this work leads to a method for quantitatively comparing different 21 cm instruments, calibration schemes, and analyses approaches. Being able to directly compare different HERA approaches will be important in defining future 21 cm cosmology arrays.

In this talk I will present these recent advances in understanding the EoR foregrounds and present data from the MWA prototype showing that the observed foregrounds are matching simulations. I will also show results leading towards the generation of the first robust determinations of EoR upper limits where the systematic contributions can be estimated.

PAPER-64: Minimum- and Maximum-Redundancy Observations

Aaron R. Parsons
Univ. of California, Berkeley. 601 Campbell Hall, Berkeley, CA 94720
USA; aparsons@berkeley.edu

In July, 2011, the deployment of the Precision Array to Probe the Epoch of Reionization (PAPER) at the South African Radio Quiet Zone in the Karoo was upgraded from 32 to 64 crossed-dipole antennas. Observations with this array in a minimum-redundancy, imaging configuration commenced shortly thereafter. This observation campaign aims to characterize the foreground emission that must be removed or otherwise suppressed in observations seeking to measure 21cm emission from the Epoch of Reionization (EoR).

PAPER has also begun an observation campaign with antennas in a maximum-redundancy configuration optimized for sensitivity in power-spectrum measurements. These on-going observations aim to achieve the sensitivity required to detect the power spectrum of 21cm EoR emission, and will leverage recent progress with foreground characterization and delay-spectrum foreground isolation techniques to obtain a measurement that is convincingly free of foregrounds.

In this paper, we report broadly on the recent progress of the PAPER experiment, and discuss in detail our strategy detecting the EoR signal. In particular, we report on the measured foreground characteristics that will most influence our ability to remove foregrounds from our observations, and examine how our on-going maximum-redundancy observations are integrating versus time and baseline.

Updates on the GMRT-EoR Project

Tzu-Ching Chang
ASIAA

The GMRT-EoR project is an on-going effort aiming to measure the 21-cm power spectrum at the Epoch of reionization (EoR), revealing unique details of the reionization process. The Giant Metrewave Radio Telescope (GMRT) in India is a low-frequency radio interferometer, consists of 30 dishes each of 45-meter in diameter. The central 13 elements distributed within 1-km radius are suitable for the large-scale 21-cm power spectrum measurements and provide superb sensitivity. The forecast indicates that with 100 hours of observation, a detection of the 21-cm fluctuation power spectrum at redshifts between 8 and 9 is feasible. Our team has been working on the EoR project since 2006; we helped build the GMRT software correlator which is now fully functional and enables high time and frequency resoltuions, useful for minimizing the impact of systematics and for optimal calibration. We have made steady progress in Radio Frequency Interference (RFI) mitigation and developed precision calibration technique which makes use of pulsars for phase calibration. We have published limits on the polarized foreground measurements, and an upper limit on the amplitude of the 21-cm power spectrum at a mean redshift of 8.6. We have been improving the analysis algorithm, incorporating the CBIgridr code (Myers et al. 2003), originally for the Cosmic Microwave Background (CMB) analysis, and extending it to the three-dimensional power spectrum measurement for 21-cm. I will present updates on the analysis and the preliminary results.

Deep LOFAR observations of potential EoR fields

M.A. Brentjens
ASTRON, Dwingeloo, The Netherlands, http://www.astron.nl

One of the six key science goals of the Dutch-led low frequency array, LOFAR, is the statistical detection of H-I brightness fluctuations at the epoch of cosmic reionization.

Early 2011, we commenced a weekly observing program of two fields: the north celestial pole, and 3C 196. The program aimed to find out just how far LOFAR's sensitivity could be pushed, and what ultimately prevented us from reaching the thermal noise. We were not disappointed. Despite malfunctioning antenna hardware and many issues with unfinished software and firmware, our group presented the deepest images yet at 150 MHz at the EoR conference in Zadar, Croatia. Both maps reached 300 μJy bean^{-1} noise levels at a resolution of 8 arc seconds. The dynamic range of the 3C 196 map is greater than 200 000:1.

Since then, the hardware issues with the antennae have been solved, and the imaging and calibration software has seen major improvements with the application of the SAGECAL algorithm and use of acceptable deconvolution in the presence of time-variable station beams.

The core array of 48 30 m wide stations was finalized in September 2011, allowing us to re-observe the pilot survey with a much improved instrument. The observed system noise is now within 5% of the expected system noise.

We will present our current deepest wide-field images of LOFAR EoR target fields, and discuss their limitations and foreground characteristics. We will also discuss the observing strategy and data reduction procedures that were developed based on our experience from the pilot survey. The LOFAR EoR group is ready for prime time.

Observing Cosmic Dawn with the Long Wavelength Array

Jacob M. Hartman[1] and the LWA Collaboration[2]

[1] Jet Propulsion Laboratory, Pasadena, CA
[2] http://lwa.unm.edu

The formation of the first stars, galaxies, and black holes—Cosmic Dawn—is the next frontier in observational cosmology. Neutral hydrogen gas dominates the universe during this epoch, and its redshifted 21 cm line encodes unique information about the first luminous objects. The first station of the Long Wavelength Array (LWA), which has recently commenced initial science observation, provides an unprecedented opportunity to detect or meaningfully constrain the sky-averaged 21 cm spectral signature at 20–84 MHz. The station's 256 tied-dipole antennas are well-matched to the frequency range of the strongest predicted feature, an absorption trough at $z \sim 20$. The wide bandwidth of the LWA covers multiple inflection points in the expected 21 cm signature, which is critical for its identification and interpretation. Finally, the station's digital backend is capable of phasing the antennas to form multiple beams on the sky. By simultaneous forming a science beam that targets a relatively cold region of sky where the Galactic synchrotron foreground is greatly reduced, and a calibrator beam trained on a bright source with a smooth spectrum, the LWA enables a new approach to calibration that exploits the calibrator source as a spectral reference for the science field, potentially allowing the bandpass to be corrected to high precision. This approach requires precise calibration and novel beamforming techniques to prevent frequency-dependent sidelobes from coupling angular Galactic structure into the spectral measurement. We are now quantifying the electromagnetic properties of the first LWA station and exploring the use beam defocusing, null steering, sidelobe "shimmering," and other techniques to reduce foreground coupling.

When did the first stars form? Did supermassive black holes form at the same time, earlier, or later? One of the great challenges of cosmology today is the study of these first generation objects. The Large Aperture Experiment to Detect the Dark Ages (LEDA) project seeks to detect, in total-power, hyperfine emission from neutral Hydrogen (21 cm rest wavelength) in the intergalactic medium about 100 million years after the Big Bang (redshifts 16-40). Detection would deliver the first observational constraints on models of structure formation and the first pockets of star and black holes formation in the Universe.

LEDA will develop and integrate signal processing instrumentation into the new first station of the Long Wavelength Array (LWA). This comprises a large-N correlator serving all 512 dipole antennas of the LWA-1, leveraging a packetized CASPER architecture and combining FPGAs and GPUs for the F and X stages. Iterative calibration and imaging will rely on warped snapshot imaging and be drawn from a GPU-enabled library (cuWARP) that is designed specifically to support wide-field full polarization imaging with fixed dipole arrays. Calibration techniques will include peeling, correction for ionospheric refraction, direction dependent dipole gains, deconvolution via forward modeling, and exploration of pulsar data analysis to improve performance. Accurate calibration and imaging will be crucial requirements for LEDA, necessary to subtract the bright foreground sky and detect the faint neutral Hydrogen signal. From the computational standpoint, LEDA is a O(100) TeraFlop per second challenge that enables a scalable architecture looking toward development of radio arrays requiring power efficient 10 PetaFlop per second performance. Stage two of the Hydrogen Epoch of Reionization Array (HERA2) is one example.

A Constraint on the 21-cm Signal at z=20 from VLA Observations

Katie M. Chynoweth[1], Joseph Lazio[2], and Joseph Helmboldt[3]

[1] NRC Fellow, Naval Research Laboratory, Washington, DC 20375
[2] Jet Propulsion Laboratory/California Institute of Technology, Pasadena, CA 91106
and NASA Lunar Science Institute, NASA/Ames Research Center, Moffett Field, CA 94089
[3] Naval Research Laboratory, Washington, DC 20375

The neutral hydrogen (HI) in the intergalactic medium (IGM) at high redshift should produce its characteristic 21-cm, hyperfine transition. Because of the high redshift, this HI signal will appear at much longer wavelengths (lower frequencies). The temperature evolution of the IGM should be below that of the cosmic microwave background (CMB), so that this highly redshifted HI signal should appear in absorption relative to the CMB. However, the magnitude of the maximum absorption and the redshift (frequency) at which it occurs is sensitive to a number of factors, including the mass function of the first stars, their formation rate, and when the first strong heating sources (likely to have been accreting black holes) formed.

We present Very Large Array observations at a frequency of 74 MHz ($z \sim 18$) that provide the first constraints on this highly redshifted HI signal. We obtain only upper limits, but we illustrate the methods by which future ground-, space-, and lunar-based observations could improve these upper limits and ultimately detect the signal. The predicted 21-cm absorption signal at z=20 ranges from 10 to 10^3 mK, depending on the source of heating and/or ionization. We find an upper limit to the signal of order 10^{6-8} mK, or 10^{12-14} mK^2 in the angular power spectrum. This constraint, while many orders of magnitude above the expected signal, is comparable to the constraint placed by the PAPER project at z=10 (Parsons et al., Astronomical Journal, 139, 4, 1468-1480).

A PAPER SOUTHERN SKY CATALOG

Daniel C. Jacobs[1], James E. Aguirre[1], Aaron R. Parsons[2], Jonathan C. Pober[2], Richard F. Bradley[4], Chris L. Carilli[6], Nicole E. Gugliucci[5], Jason R. Manley[7], Carel van der Merwe[7], David F. Moore[1], and Chaitali R. Parashare[3]

[1] Dept of Physics and Astron. U. of Pennsylvania, Philadelphia, PA
[2] Astron. Dept., U. California, Berkeley, CA
[3] Dept. of Electrical and Computer Eng., U. Virginia,Charlottesville, VA
[4] Natl. Radio Astron. Obs., Charlottesville, VA
[5] Astronomy Dept., U. Virginia, Charlottesville, VA
[6] Natl. Radio Astron. Obs., Socorro, NM
[7] Karoo Array Telescope, Capetown, South Africa

Over the last 20 years we have learned that the contents of the universe are spit into 76% Dark Energy and 24% Matter, 17% of which is ordinary matter. Of the ordinary matter the bulk is hydrogen which forms the raw material for building stars. The universe began 14 Billion years ago with an expanding space-time and quickly began After about 300,000 years this all cooled enough for the plasma to recombine into neutral hydrogen gas and release photons which we eventually observe redshifted into the radio; the Cosmic Microwave Background (CMB). Nearly half a billion years passed before the slow process of gravitational collapse would lead to the formation of the first galaxies and the (re) ionization of the ubiquitous hydrogen. This Epoch of Reionization (EoR) is the next major unexplored cosmological milestone. At the current time the space between galaxies is almost completely ionized, therefor we know that the universe must have undergone a global phase transition. The nature of the ionizing sources, whether young galaxies or accreting massive black holes is unknown. Neither do we know when this reionization occured or how long it took.

Models suggest that we can detect fluctuations in the 21cm hydrogen emission line as ionization proceeds and high contrast ionized holes are carved in the neutral hydrogen. Detecting these fluctuations is one of the few direct probes of the reionization process but is a difficult task requiring a new generation of low frequency radio telescopes. Motivated by the breadth of unknowns, the Precision Array for Probing the Epoch of Reionization (PAPER) has been slowly building in complexity while folding the results of observations back into improving the design and operation of the telescope. As part of this process, this thesis analyzes early observations to explore three major areas of concern in detecting EoR: contamination by foreground sources, calibration stability and limiting sensitivity. Catalogs produced from this early data show good agreement with previous measurements. We conclude that the calibration is stable and sensitivity floors are close to the expected theoretical levels.

A New Technique for Primary Beam Calibration of Drift-Scanning, Wide-Field Antenna Elements

Jonathan C. Pober and Aaron R. Parsons
Univ. of California, Berkeley. B-20 Hearst Field Annex, Berkeley, CA 94720 USA; jpober@berkeley.edu

We present a new technique for calibrating the primary beam of a wide-field, drift-scanning antenna element. Drift-scanning prevents the use of standard beam calibration routines, as one can no longer point at and dither across a calibrator source. Instead, sources pass through only a small portion of the beam as they track overhead, necessitating the use of many calibrator sources to model the beam. The situation is further complicated by difficult-to-parametrize beam shapes and the sparsity of good catalog data at the low frequency where these elements are often used.

In order to overcome these challenges, we use measurements of "perceived source fluxes as they pass through our beam. However, in these measurements, there is a degeneracy between the inherent flux of a source and the primary beam response in a given direction. We break this degeneracy by building up a network of "crossing points, points where the perceived flux of multiple sources have been measured. Such crossing points do not naturally occur, as sources at 2 different declinations will never pass through the same part of the beam. By assuming 180° rotational symmetry in our beam – the only assumption about beam shape necessary for this method – we create many points where sources cross the mirror image tracks of other sources. We then use a least-squares inversion to solve for the beam response and sources flux simultaneously, all referenced to one absolute flux calibrator.

We illustrate the method with both real and simulated observations from the Precision Array for Probing the Epoch of Reionization (PAPER). We also comment on the applicability of the technique for other arrays and the potential for more accurate degrees of calibrations.

Modeling of Radar Scatter from Icy and Young Rough Lunar Craters

Thomas W. Thompson*(1), Eugene A. Ustinov(1)
Paul D. Spudis(2), and Brian W. Fessler(2)
(1) Caltech/JPL, Pasadena, CA 91109
(2) Lunar and Planetary Institute, Houston, TX 77058

For lunar orbital synthetic aperture radars, such as the Chandrayaan Mini-RF operating at S-band (13-cm) wavelength and the Lunar Reconnaissance Orbiter Mini-RF operating at S-band and X-band (3-cm) wavelengths, it is important to understand the radar backscattering differences between icy and young, rough craters. Assuming a mixing model consisting of diffuse and quasi-specular scattering components, we have modeled the opposite-sense circular (OC) and same-sense circular (SC) backscattering characteristics of these craters. The specular component, consisting of only OC echoes, represents the echoes from the surface and subsurface layers that are flat and oriented perpendicular to the radar's line-of-sight. The diffuse component, consisting of both SC and OC echoes, represents echoes associated with either rocks or ice. Also, diffuse echoes are assumed to have backscatter that is proportional to the cosine of the incidence angle. We have modeled how these two (specular and diffuse) radar scattering components could be modulated by factors such as surface roughness associated with young craters. Also, we have modeled how ice radar scattering components could be modulated by a thin regolith covering, and/or by the situation where ice occupies small patches within a larger radar pixel.

This modeling was examined for 4 nonpolar craters and 12 polar craters using LRO Mini-RF 13-cm wavelength data. Results indicate that icy craters and young rough craters can be distinguished from each other based upon their SC enhancements (α) and OC enhancements (γ). In addition, we examined the craters that have unusual circular polarization ratios (CPRs) that likely result from a double bounce mode of scattering. Our results show that blocky fresh craters, icy craters, and craters exhibiting double bounce scattering can be separated from each other based on the values of α, γ, the ratio of α to γ and the weighted sum of α and γ.

Part of this research was carried out at the Jet Propulsion Laboratory, California Institute of Technology, under a contract with the National Aeronautics and Space Administration.

KA-BAND SOLAR FLUX STUDY FOR G/T MEASUREMENTS

Art Densmore* [1, 2], Gerry Seck[1], and Yahya Rahmat-Samii[2]
[1] L-3 Communications, Datron Advanced Technologies Division
200 W Los Angeles Avenue, Simi Valley, California 93065
Art.Densmore@L-3com.com, Gerry.Seck@L-3com.com
[2] Electrical Engineering Department, University of California Los Angeles
420 Westwood Plaza, Los Angeles, California 90095
adensmore@ucla.edu, rahmat@ee.ucla.edu

The quality of an antenna system's receive performance is represented by the ratio, G/T, of the antenna receive-gain to system-noise temperature, which can be directly measured at the system level, using a strong source of noise, of a known power level and located far enough away that at radio frequencies it appears effectively as a *point*-source (small enough to sample the peak level of the antenna pattern). The Sun is a strong source of noise and is very distant, but it's huge – one-half deg apparent optical diameter – and the level of noise that it emits above 15 GHz is not usually published.

The Sun's apparent radio diameter is somewhat larger than its optical diameter and small enough that medium-gain antenna systems can use the Sun for G/T measurements, as long as the Sun's noise-power level, in the frequency band of interest, is known well enough to support the required accuracy for the G/T measurements. The National Oceanic and Atmospheric Administration (NOAA) measures and publishes the Sun's radio noise emission levels daily, for frequencies from 2-15 GHz. Publications that characterize the Sun's radio noise levels above 15 GHz are hard to come by though. Frequency extrapolations of the NOAA data can be considered for approximate measurements above 15 GHz, but we have found such extrapolations to lack the accuracy required for our antenna system tests at Ka-band.

Thus we undertook a study of the Sun's noise-power level at Ka-band, and in this presentation we summarize the results. Our study involved a detailed literature search as well as our own measurements of the Sun, calibrating the Sun with respect to the Moon, and using a clever method to minimize the affects of atmospheric attenuation, which can significantly affect such radiometry measurements at Ka-band. We have surveyed an archive of NOAA solar flux data dating back to 1991 and identified particularly pertinent publications by Kennewell (Australian Space Academy), Slobin and Pham (NASA JPL), Daywitt (National Bureau of Standards), Linsky (Univ. Colorado, Boulder), and Zheleznyakov (Radio Emission of the Sun and Planets), addressing Ka solar flux, and compare all these data/models to the blackbody model of the Sun's radiation for perspective. We conducted our measurements in 2010 around 27 GHz, found good agreement with one particular of the above referenced solar flux model publications, which appears the most modest of the above estimates of solar flux, and we've corresponded with that author to discussed validation of our results.

Next Generation Polarimeter Modules for the QUIET Experiment

Kieran Cleary[(1)], Rodrigo Reeves[(1)], Rohit Gawande[(1)], Anthony Readhead[(1)], Todd Gaier[(2)], Pekka Kangaslahti[(2)], Lorene Samoska[(2)], Mikko Varonen[(2)], Hogan Nguyen[(3)], Fritz DeJong[(3)], Donna Kubik[(3)], Osamu Tajima[(4)], Masaya Hasegawa[(4)], Makoto Ngai[(4)], Koji Ishidoshiro[(4)], Sarah Church[(5)], Patricia Voll[(5)], Mark McCulloch[(6)], Lucio Piccirillo[(6)]

(1) California Institute of Technology, Pasadena, CA 91125

(2) Jet Propulsion Laboratory, Pasadena, CA 91106

(3) Fermi National Accelerator Laboratory, Batavia, IL 60510-5011

(4) High Energy Accelerator Research Organization (KEK), Tsukuba, Ibaraki Prefecture, Japan

(5) Stanford University and Kavli Institute for Particle Astrophysics & Cosmology, Stanford, CA 94305

(6) University of Manchester, Manchester, M13 9PL, UK

The Q/U Imaging ExperimenT (QUIET) is designed to measure the B-mode of the cosmic microwave background (CMB) polarization. In Phase I of this experiment, focal-plane arrays with central frequencies at 43 GHz (Q-band) and 95 GHz (W-band) were deployed at the Chajnantor plateau in northern Chile. These arrays consisted of 17 and 84 individual polarimeter modules, respectively.

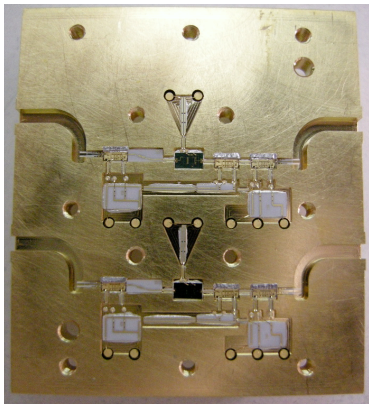

Interior of amplifier section of next-generation QUIET polarimeter

Each polarimeter is a complete pseudo-correlation receiver capable of measuring Stokes *Q* and *U* directly and simultaneously. These polarimeters use InP HEMT MMIC amplifiers with 100 nm gate lengths. The input amplifiers used in the W-band polarimeters had noise temperatures of around 50-80 K when packaged individually in WR-10 blocks. However, in the field, the noise temperature was measured to be around 120 K.

The next phase of QUIET involves scaling the array size in order to achieve the sensitivity necessary to constrain the B-mode to a scalar-to-tensor ratio, $r < 0.01$. An increased number of polarimeters with better noise temperatures compared to Phase I is essential to improve the sensitivity of the experiment in a cost-effective manner. Therefore, we began a program to i) understand the source of the sensitivity degradation in the Phase I W-band polarimeters and ii) demonstrate a noise temperature limited only by that of the input HEMT amplifiers. Our goal is the development of a next-generation polarimeter which has an average 35K noise temperature, then to prepare for mass-production of 500 such polarimeters.

In parallel with this development work, we have also been working with the Jet Propulsion Laboratory (JPL) and Northrop Grumman Aerospace Systems (NGAS) on a program to improve the fundamental performance of the HEMT amplifiers at cryogenic temperatures, using a new 35 nm gate-length process at NGAS.

In this talk, we present our progress towards the next generation of QUIET polarimeters.

Ultra-Wideband Sampler (10 to 20 GSps) Analysis and Test Results

D. W. Hawkins*[1], D. P. Woody[1], and K. P. Rauch[2]

[1]Caltech/CARMA, Big Pine, CA 93513
[2]U. Maryland/CARMA, College Park, MD 20742,
http://www.mmarray.org

Ultra-wideband samplers with sampling rates of 10 Gsps to 20 Gsps (giga-samples per second) coupled with new generation Field Programmable Gate Arrays (FPGAs) can now process the multi-gigahertz bandwidths available from current-generation radio astronomy receivers. FPGAs from Altera and Xilinx now have transceiver input/output rates in excess of 10Gbps, allowing direct capture of digital data from the wideband samplers, and transmission of processed data in standard 10 or 40 GbE (gigabit ethernet) data format. The FPGA density allows for the generation of narrower bandwidth signals using digital demodulation and filtering, or spectral analysis via polyphase filtering.

Wideband samplers enable full utilization of the wide bandwidth available from current and future generations of front-end amplifiers and heterodyne mixers and can dramatically increase the sensitivity and capability of most radio telescopes. Ultrawideband samplers are an effective alternative to the development (and expense) of analog components, directly converting the wideband astronomical signals into the digital domain where the relentless advance of Moore's law can be exploited.

The initial application of wideband samplers is to improve the sensitivity and capability of the 23 element CARMA[1] interferometer. The technology will however, be immediately applicable to many other interferometer arrays and single dish telescopes. The added processed bandwidth will directly improve the sensitivity for continuum observations and give increased spectral bandwidth for line searches and multi-line observations. The reduced amount of RF and analog electronics will make it practical to implement full bandwidth capability on dual-polarization and multipixel systems. The range of radio astronomy science that can benefit from this development ranges from cosmology investigations using the SZ effect to planetary line observations and everything in between.

Because the initial application of the ultra-wideband samplers is for the CARMA system which utilizes double sideband heterodyne as well as HEMT and MMIC amplifier front ends, we will address the delay and phase switching issues associated with interferometers. This automatically encompasses essentially all issues or techniques that are important for single sideband interferometers or single dish spectrometers.

We will present analysis and test results for ultra-wideband samplers from Hittite, Adsantec, and Micram, interfaced to Altera Stratix IV FPGAs.

[1]Combined Array for Research in Millimeter-Wave Astronomy

GPU Accelerated Processing For VLBI Digital Backends

Mark McCurry*[1], Christopher Beaudoin[2], and Geoffrey B. Crew[2]

[1] ECE Department, Clarkson University, Potsdam, NY
[2] MIT Haystack, Westford, MA

This paper presents an evaluation of the use of a graphics processor for realtime radio astronomy Digital Signal Processing (DSP) as applied to Very Long Baseline Interferometry (VLBI). Current MIT Haystack VLBI DSP uses the Reconfigurable Open Architecture Computing Hardware (ROACH) platform, due in part to its high data throughputs. With increases in GPU hardware performance and lowering prices, GPUs have become a significant rising technology, which this paper investigates.

To evaluate this new platform, a prototype GPU application was designed and constructed to perform frequency channelization using Nvidia's Compute Unified Device Architecture (CUDA), and calculations were then performed on Nvidia GPU cards. An external 1 GHz networked Analog Digital Converter (ADC) in the ROACH platform provided Radio Frequency (RF) time samples, which were processed in realtime with the tested cards. A Polyphase Filter Bank (PFB) implemented on the graphics processor was used to perform the channelization. The PFB was used due to its prominence in the VLBI field for good channel separation and low performance overhead. The PFB processor was tested with a 32 channel, 256 tap prototype filter, 8 bit input samples, and 2 bit output samples.

Benchmark results incorporating a Nvidia Tesla C2050 show a maximum data rate of 890 Mega-samples per second for realtime operations. On a considerably cheaper Nvidia 470 GTX 640 Mega-samples per second was achievable. Instruction throughput and library constraints are the current limitations, which could be solved by more recent processors and custom DSP routines, respectively. This makes GPUs an interesting candidate for a cost effective upgrade as both software and hardware systems progress.

Instrumentation for real-time cyclic spectroscopy of pulsar signals

Glenn Jones*[1] and Paul B. Demorest[2]

[1] NRAO Postdoc resident at Caltech, Pasadena, CA 91125
[2] NRAO, Charlottesville, VA

Precision pulsar timing observations are subject to many effects from the interstellar medium (ISM) which corrupt the signal and reduce the resulting time resolution. The largest effect, dispersion, is now routinely corrected for using the technique of coherent dedispersion, where a digital filter is used to invert the linear transfer function of the interstellar medium. Inhomogeneities in the ISM give rise to more subtle corruption in the form of scattering and scintillation. Much research has been done to study and characterize these effects with the hope of mitigating them. These effects span a wide range of time and frequency scales. The trade off between time and frequency resolution inherent in traditional spectral analysis reduces the amount of information about the perturbations which can be obtained using this method.

Cyclic spectroscopy has recently been shown to be very effective at studying the effects of the interstellar medium on pulsar signals. This technique takes advantage of the periodic nature of pulsar signals to improve the time-frequency resolution of perturbative features in the ISM. It also preserves phase information about the transfer function of the scattering medium which is lost in intensity spectra. To form the complete cyclic spectrum, baseband signals from overlapping filterbank channels are required, which increases the computational demand over a traditional coherent pulsar spectrometer. We are implementing an FPGA-based digital filterbank front-end which will be combined with a GPU based signal processor to compute the cyclic spectrum in real time. We will discuss the cyclic spectroscopy technique, details of the implementation, and initial results from this instrument.

The detection of fast (< 1 s) radio transients requires that digital data be analyzed with high time resolution and sufficient spectral resolution to allow dispersion searching. The resulting data rates are likely to be far higher than can be stored for later analysis, so this is a classic "big data" problem. JPL is developing several technologies to address big data challenges in an end-to-end manner. The current development is focused on three areas: 1) lower-power architectures for digital signal processing to keep the generation of high data rates affordable, 2) machine learning algorithms to provide "data triage" in real time to keep the volume of data to be stored viable, and 3) data archive designs that are scalable and flexible to allow efficient data access and mining. There has been significant progress in all three of these areas, including a careful study of ASIC architectures for cross-correlation that provides an order-of-magnitude reduction in power consumption compared with traditional design approaches. Data adaptive transient detection algorithms have been deployed on the VLBA (the V-FASTR program) and are being adapted for use at other observatories. This software selects the most valuable (small) fraction of incoming data for long-term storage, prior to the usual averaging over time and frequency. It is also useful for RFI identification and the detection of transient anomalies in high-rate monitor and control data. Finally, a scalable data archive system first developed by JPL for Earth science missions (PCS/OODT) is being adapted for use by radio observatories and other (non-astronomy) facilities. This open-source system leverages large previous investments. Each of these technologies is likely to be applicable to a wide range of high-data-rate facilities and instruments. This research has been carried out at the Jet Propulsion Laboratory, California Institute of Technology, under contract with the US National Aeronautics and Space Administration.

Signal extraction for sky-averaged 21-cm experiments

Geraint J. A. Harker*[1], Jonathan R. Pritchard[2], Jack O. Burns[1], and Judd D. Bowman[3]

[1] Center for Astrophysics and Space Astronomy, Department of Astrophysics and Planetary Sciences, University of Colorado Boulder, CO 80309, USA

[2] Harvard-Smithsonian Center for Astrophysics, 60 Garden Street, Cambridge, MA 02138, USA

[3] Arizona State University, School of Earth and Space Exploration, Tempe, AZ 85287, USA

Experiments to detect the highly redshifted 21-cm line of atomic hydrogen promise to be able to probe the intergalactic medium during the epoch of reionization (EoR), the cosmic dawn (when the first stars and accreting black holes began to flood the Universe with radiation) and even the preceding dark ages. These require features of between a few millikelvin and tens of millikelvin to be measured from spectra averaged over a large fraction of the sky, at frequencies of around 100–200 MHz for the EoR, around 40–120 MHz for the cosmic dawn, and even lower frequencies for the dark ages.

Other astrophysical sources radiate strongly at these frequencies and on these spatial scales, with brightness temperatures of hundreds or even thousands of kelvin. To extract the high redshift signal, we must therefore be able to remove these 'foregrounds' to an accuracy of roughly one part in 10^6, making use of the fact that they are spectrally smooth and vary over the sky, while the redshifted 21-cm signal has spectral features and is constant over the sky (on sufficiently large angular scales). This in turn places stringent requirements on the accuracy with which the response of the instrument must be known. Moreover, it is likely that this response must be inferred from the science data themselves since we will be unable to measure it to the required accuracy in the laboratory.

The *Dark Ages Radio Explorer* (*DARE*) is a proposed satellite which would measure the redshifted 21-cm spectrum at 40–120 MHz from lunar orbit, taking data only over the far side of the Moon where RFI from the Earth is blocked out. We describe a technique, based on a Markov Chain Monte Carlo algorithm, for simultaneously fitting the foregrounds, extracting the signal and finding the instrument response for *DARE* (G.J.A. Harker et al., Mon. Not. R. Astron. Soc., in press). All the components are described by parametrized models, giving a parameter space with dozens of dimensions. Our method allows us to infer the best-fitting values of these parameters and derive rigorous confidence regions on them. We show how the algorithm performs when applied to a synthetic data set from *DARE*, incorporating realistic models for the 21-cm signal, galactic, extragalactic and solar system foregrounds, and the instrument response. The results demonstrate the feasibility of the experiment. Similar techniques may be applicable to ground-based experiments such as EDGES.

A Radio Search for Extraterrestrial Intelligence in the Kepler Field

A.P.V. Siemion[1], P. Demorest[2], A. Gautam[1], E. Korpela[1], R. Maddalena[2], D. Werthimer[1], J. Cobb[1], J. Ford[2], A. Howard[1], G. Langston[2], M. Lebofsky[1], G. Marcy[1], and J. Tarter[3]

[1] University of California, Berkeley, Berkeley, California, United States
[2] National Radio Astronomy Observatory, Green Bank, West Virginia, United States
[3] SETI Institute, Mountain View, California, United States

In February 2011, The Kepler Transiting Planet Survey announced the identification of 54 planet candidates located in or near the so-called 'habitable zone,' the region around a host star where liquid water could exist on a planet's surface. Many of these planet candidates are just marginally larger than the Earth. In March of 2011, we searched this population for radio sources indicative of an engineered origin. Our search included both targeted observations of known Kepler Objects of Interest (KOIs) and a raster scan of the entire 105 sq. deg. Kepler Field. The search was conducted using the 100 meter Green Bank Telescope, the most sensitive single dish radio telescope on the planet capable of viewing this field. Time domain voltages at 2 bits/sample were recorded over an 800 MHz dual-polarization band centered at 1.5 GHz using the Green Bank Ultimate Pulsar Processor (GUPPI). The total aggregate data rate for this experiment was 800 MBps and the complete data set is approximately 50 TB. These data are being searched for both temporally narrow (broad band pulsed) and spectrally narrow (sinusoidal continuous-wave) emission, using both in-house computing resources and the distributed computing projects SETI@Home II and Astropulse. Here we will discuss the search methodology, observations, sensitivity and early results.

Measuring the small-scale CMB polarization with ACTPol

Michael D. Niemack[(1)] for the ACTPol Collaboration
(1) National Institute of Standards and Technology and University of Colorado, Boulder, Colorado, USA

ACTPol is the first polarization sensitive receiver for the six-meter Atacama Cosmology Telescope (ACT) in Chile. The receiver is nearing completion and will be deployed to observe the cosmic microwave background (CMB) polarization at 150 GHz on arcminute scales in 2012. Then, it will be upgraded for simultaneous 90 GHz and 150 GHz observations starting in 2013. These observations will enable us to probe inflation and early dark energy, to characterize the gravitational lensing of the CMB, and to constrain the sum of the neutrino masses. Our observing fields will overlap with the SDSS BOSS survey as well as the XMM-LSS field, enabling a variety of cross-correlation science, including growth of structure from Sunyaev Zel'dovich galaxy clusters and independent constraints on the sum of the neutrino masses. We describe the ACTPol science objectives as well as the design and status of the instrument.

Porcine Models in Telemetry: Hydration Effects and Tissue Storage Protocol

Robbin Bertucci (1), Jun Liao (1), and Erdem Topsakal (2),

Department of Agricultural and Biological Engineering (1)
Department of Electrical and Computer Engineering (2)
Mississippi State University
Mississippi State, MS 39762, USA

The dielectric properties of biological tissues are of important use to various biomedical applications involving electromagnetic fields such as hyperthermia treatments, ablation, and implantable devices. These electrical properties can lead to better treatment of various conditions and diseases. For years the conductivities and permittivities of tissues and organs have been studied. Of the published data on dielectric properties, many of the results vary from source to source with limited frequency ranges, varying measurements, and lack of tissue and organ storage and excision methodology. These discrepancies could be due to the variation in tissue type, anisotropy, and hydration. The need for a standard set of dielectric properties is crucial. To obtain these measurements, the issues dealing with a tissue storage protocol and standard animal model need to be addressed.

In this study, we present the effect of hydration of tissues on the dielectric properties obtained. A porcine model is chosen based on the similarities to human tissue found in other biomedical applications. Porcine lower extremities were obtained from a local abattoir (Sansing, Maben, MS). Skin, muscle, and fat tissue samples were tested using a coaxial cable and network analyzer to obtain the dielectric properties. To examine the effects of hydration and storage techniques two main methods were performed. First the tissues were excised immediately and tested every hour for four hours. Then the same samples were dehydrated using a lyophilizer (Labconco), and the properties were measured again. Last the tissues were rehydrated over 48 hours in phosphate buffer saline (PBS) solution and re-measured. To compare these results with properly stored tissue, new samples were excised immediately and measured. These samples were stored in PBS at 4°C for four hours, and then the dielectric properties were re-measured. Results were compiled comparing not only the hydration effects but also human versus porcine tissue. In conclusion, the dielectric values showed vast dependence on hydration and storage techniques, and the porcine model proved to be a good substitute for human tissue in electrical property studies.

Specific Absorption Ratio (SAR) reduction in Wireless Power Transfer System using Multi-Coil Approach

Anil Kumar RamRakhyani and Gianluca Lazzi
Department of Electrical and Computer Engineering, University of Utah
Salt Lake City, UT, 84112, USA

Implantable devices are popular in health and medical applications due to their ability to locally stimulate internal organs and/or monitor and communicate the internal vital signs to the outer world. Their power requirement depends on their specific applications and operating conditions. Some implants use (rechargeable) batteries; however, wireless power transfer schemes are often used in implantable devices to avoid trans-cutaneous wiring and recharge or replace the device battery. Inductive coupling is a popular technique for wireless power transfer, particularly in biomedical implants. In typical designs, an external coil is used to generate time varying magnetic field in close proximity of implant coil. The current in each coil depend on the coupling between external and implant coils and electrical properties (inductance and resistance) of the individual component in the system. In situation requiring relatively large power transfers, such as that encountered in high-data rate neurostimulators with high-electrode count, induced Specific Absortion Rates (SARs) or fields need to be considered among the design parameters and minimized.

Multi-coil based power delivery (A. K. RamRakhyani et al., IEEE TBCAS'11) is an novel wireless power transfer technique that uses three or four coils for wireless power transfer, instead of the traditional two. In the multi-coil approach, the adverse effect of low coupling coefficient between primary and secondary coils is compensated with high quality (Q) factor coils, resulting in improved system efficiency. Using high–Q passive resonating coils, multi-coil systems require lower current in the external coils to generate adequate power in the implant device.

In this work, a traditional two coil wireless power system is taken as a design example and compared to the equivalent four-coil system. The primary coil of the two-coil system is divided into two concentric coils (driver and transmitter coils) such that sum of the number of turns of the new coils are the same of the original primary coil. Similarly, a receiver and a load coil are utilized on the secondary side. Simulation and experiments are performed for new four-coil based system and results compared with those for the two-coil system. Results show that, compared to the traditional two-coil system, the four-coil system can lead to a significant reduction in the required current in the external coil necessary to generate unity current in the implanted electronics, leading to reduced fields and SAR induced in the human tissue.

Miniaturized, Parylene-based, Wireless Intraocular Pressure Sensor System Using Harmonic Detection Technique

Tse-Yu Lin* [(1)], Byungguk Kim[(1)], Dohyuk Ha [(1)], Wilhelmine N. de Vries[(2)], Robin W. Irazoqui[(3)], Simon W. M. John[(2)], Pedro P. Irazoqui[(1)], and William J. Chappell[(1)]
(1) Purdue University, West Lafayette, IN 47907, USA
(2) The Jackson Laboratory, Bar Harbor, ME, 04609, USA
(3) Universitat de Girona, 17017 Girona, Cataluña, Spain

Wireless sensor systems facilitate and broaden the capability in experiments for biomedical research. Moreover, mice are widely use in animal study since it provides a cost effective, short life-cycle platform to investigate various genetic diseases. Such a wireless system is particularly beneficial for the glaucoma study for mice in realizing large data acquisition. The elevated intraocular pressure (IOP) is highly related to the glaucoma (O.V. Savinova, *et al*, *BMC Genetics*, 2:12, 2001). To decipher the connection between the high IOP and glaucoma, the tracking of IOP change around the clock is necessary. The current accurate approach of IOP measurement is using the micro-cannulation method which injects a micro-needle to the mouse eye and obtains the IOP data (S.W.M. John, *et al*, *Invest. Ophthalmol. Vis. Sci.*, 38, 249-257, 1997). However, this measurement can only be performed once a week for healing purposes and this approach requires intensive labor work in chronic study. Therefore, a wireless implantable-pressure-sensor system enabling more frequent measurement of several reading within an hour is highly required. The implant site is the anterior chamber of a mouse eye with the depth of 300 μm and the diameter less than 3 mm. Due to the small size of the mouse eye and surgical limitations, the final packaged device should be a biocompatible, flexible, compressible, self-expandable, and thin enough for implantation. Also, a measurement technique which is less sensitive to the effect of the high multi-path environment is highly demanded for the IOP detection with high resolution.

This paper demonstrates a passive pressure detection scheme using ultra-thin Parylene substrate of 10 μm on which a self-expandable Nitinol antenna (T. Lin, *et al*, *IEEE MTT-S Int. Microwave Symp.*, June 2011) and a capacitive MEMS pressure sensor are integrated. The antenna dimension is 2.2 mm in loop diameter and 25 μm as the wire diameter. The base capacitance of the pressure sensor is approximately 1 pF at 2 GHz and the capacitance of the Schottky diode is 0.14 pF. Those three components form a LC resonator. The resonance frequency changes with respect to the capacitance in the MEMS pressure sensor. At atmospheric pressure, the resonance occurs at 2.2 GHz range where the 2.2 mm loop antenna is electrically small and inefficient. Moreover, receiving the reflection from the electrically small antenna to determine the resonance suffers from the multi-path from the environment. Thus, detecting the harmonics from the diode is more efficient since no transmitting source operates at the harmonic frequency (J. R. Riley, *et al*, 279, 29-30, 1996). Furthermore, the band of isolation between the fundamental tone and the harmonics can be easily accomplished by applying low-pass filter and high-pass filter, respectively. To prove the concept of detecting the harmonic frequency shift according to the resonance as well as the capacitance, a varactor circuit with base capacitance of 0.6 pF at 2.3 GHz is used to mimic the MEMS sensor. By varying the biasing voltage of the varactor, the capacitance changes accordingly. A 30 dBm continuous-wave RF signal ranges from 2.3 to 3.1 GHz as fundamental signal is transmitted through a broadband horn antenna for frequency sweep with 2 MHz step. The corresponding 3rd harmonic signal generated by the tag is received by another external receiver. It takes 10 minutes to finish one sweep which contains 400 points. The experimental results show sensitivity of 4MHz resonant frequency shift corresponds to 4 fF change in capacitance. It shows the feasibility of the detection of IOP using the harmonic detection scheme. To achieve a real-time measurement, a fast sweep-speed transceiver will be used to reduce the sweeping time into 10 seconds for a sweep with 400 points. Furthermore, *In-Vivo* test using the implantable harmonic tag including the MEMS sensor instead of the varactor, will be conducted in the future.

Determining the Relative Permittivity of Human Body Masses

Safa Salman*, Dimitris Psychoudakis and John L. Volakis
ElectroScience Laboratory, Dept. of Electrical and Computer Engineering
The Ohio State University, Columbus OH 43212, USA

Continuous real-time monitoring of the dielectric properties of embedded tissues and organs is critical for early detection of common medical conditions. More specifically, swelling, change in water content and tumor composition can be detected using equipment that can sense dielectric constant variations without a need for surgery. The permittivity serves as a suitable identifier in detecting changes in internal organs.

The goal of this study is to develop a microwave sensing antenna system capable of inferring the dielectric constant of an inner (embedded) layer in a multilayer dielectric body by positioning electrodes/antennas across the surface of the body. Emphasis is given on detection the dielectric constant of the inner layer deep into the human torso. In this case, it is desirable that the methodology be resistant to changes in the outer layers (skin, fat, muscle etc.). This is required to avoid calibration of the system for each individual user, lowering the cost and increasing ease of use.

Specifically, we propose to use several electrodes, placed on the human skin, operating at 50 MHz to propagate signals through several human tissue layers. In this design, the first or one electrode is excited while the others receive the signal propagated through the tissues. The premise is that the electrode furthest away from the excited one will more sensitive to the lower layers whereas the closest electrode is mostly affected by the skin layer(s). In this manner, the transmission coefficients (S-parameters) can be isolated from effects caused by inner and outer layers. To monitor changes in the deeper masses of the body, the signals between the nearby electrodes are used to calibrate out effects due to the skin, expected to be more constant.

A Miniaturized Implantable Antenna for Continuous Glucose Monitoring

Kristin Sharp and Erdem Topsakal

Department of Electrical and Computer Engineering
Mississippi State University
Mississippi State, MS 39762, USA

Implantable antennas allow for remote communication and constant monitoring. These antennas are a crucial part of medical telemetry. One of the major issues in designing implantable antennas is the size of the antenna. The antenna needs to be small in size and yet efficient enough to transmit to a nearby receiver (20m-30m away). In the past, our group designed and in vivo tested a small size implantable antenna for continuous glucose monitoring. Although the size of that antenna was around 2cm x 2cm and provided the intended communication link up to 30m, our studies showed that the same performance can be achieved with a smaller antenna size (~1cmx1cm).

In this study, we will present a 1cmx1cm dual band antenna which operates in Industrial, Scientific, and Medical (ISM) band (2.4 GHz – 2.48 GHz) and Medical Implant Communications Service (MICS) band (402 MHz – 405 MHz). The fabricated antenna is tested using in vitro skin and muscle mimicking gels. In order to test the communication performance of the antenna we used a commercially available transceiver by Zarlink. We have obtained satisfactory results.

Integration of Cell Phone Imaging with Microchip ELISA to Detect Ovarian Cancer HE4 Biomarker in Urine at the Point-of-Care

ShuQi Wang [1], Xiaohu Zhao [1], Imran Khimji [1], Ragip Akbas [2], Weiliang Qiu [3], Dale Edwards [4], Daniel W. Cramer [4], Bin Ye 4, *, Utkan Demirci [1,5,] *

[1] Demirci Bio-Acoustic-MEMS in Medicine (BAMM) Laboratory, Department of Medicine, Brigham and Women's Hospital, Harvard Medical School, Cambridge, MA 02139, USA.

[2] Autodesk, Inc. 100 Commercial St. Manchester, NH 03101, USA.

[3] Channing Laboratory, Brigham and Women's Hospital, Harvard Medical School, Boston, MA 02115, USA.

[4] Department of Obstetrics and Gynecology and Reproductive Biology, Brigham and Women's Hospital, Harvard Medical School, Boston, MA 02115, USA.

[5] Harvard-MIT Health Sciences and Technology, Cambridge, MA 02139, USA.

* udemirci@rics.bwh.harvard.edu or binyedavid@gmail.com

With fast advances in mobile technology, smart phones have been utilized to facilitate rapid diagnosis for point-of-care. Here, we report a cell phone based detection module that was integrated with a mobile application for immediate data processing of microchip ELISA results without referring to peripheral equipment for read-out and analysis. Ovarian cancer is asymptomatic at early stages and most patients present with advanced levels of disease. Lack of cost-effective methods that can achieve frequent, simple and non-invasive testing hinders early detection and causes high mortality in ovarian cancer patients. As such, we developed a simple and inexpensive microchip ELISA to quantify an ovarian cancer biomarker, HE4, in urine, which was integrated with the cell phone based detection module or charge-coupled device (CCD). The HE4 level detected by a cell phone or a lensless CCD system was significantly elevated in urine samples from cancer patients ($n = 19$) than healthy controls ($n = 20$) ($p < 0.001$). Receiver operating characteristic (ROC) analyses showed that the microchip ELISA coupled with a cell phone running an automated analysis mobile application had a sensitivity of 89.5% at a specificity of 90%. Under the same specificity, the microchip ELISA coupled with a CCD had a sensitivity of 84.2%. In conclusion, integration of microchip ELISA with cell phone/CCD-based colorimetric measurement technology can be used to detect HE4 biomarker at the point-of-care (POC), paving the way to create bedside technologies for diagnostics and treatment monitoring. With the integrated mobile application, this module can be employed in both resource-rich and resource-limited settings because of increasingly available mobile networks, whereby the appropriate clinical information can be instantly and remotely transferred between patients and physicians.

Robust and Efficient Reconfigurable RF Front End for Implantable Biomedical Devices

Anatoly A. Yakovlev, Ada S. Y. Poon
Stanford, CA

In recent years, much research has been done in the field of biomedical devices with goals to improve in-vivo detection and treatment of various diseases, and to monitor the physiological signals of patients, all while making these devices more accessible and affordable. This requires reducing the size, complexity, power consumption, and cost of these devices without sacrificing robustness and integrity. Remote sensing and wireless powering play key roles in minimally invasive and portable devices. While wireless powering and sensing is not a new concept, much improvement is needed to meet the set goals. Future applications will also require improved quality of service with corresponding higher data rate requirements. Environmentally robust data link to/from the device, however, often occupies a significant portion of the power budget. These constraints impose strict power consumption and efficiency requirements on the entire system.

Many existing biomedical implantable devices operate in the low-MHz frequency range, such as the widely accepted 13.56 MHz ISM band. Adhering to this frequency band imposes additional difficulties in designing efficient high data rate transceivers. Recent work by O'Driscoll, Poon, and Meng (ISSCC Technical Digest, February 2009) demonstrated that mm-sized antennas in biological tissue achieve optimal power transfer efficiency in the low-GHz range [1]. Taking advantage of this relaxes the constraints on data link and the quality factor of the antenna and matching network, and allows for optimization of power harvesting and telemetry circuitry, at the price of reduced separation distance over which the link is functional. Reduced operating range does not pose a big problem as these devices are typically implanted a few millimeters below skin surface with total separation distance on the order of several centimeters. As an added advantage, link gain is less sensitive to antenna alignment at higher frequencies.

One of the key limiting factors in battery-less devices is low available power due to inefficiencies of energy harvesting and wireless power link. Low available power at the device also demands the use of low power on-chip circuitry, including receiver, transmitter, controllers, and auxiliary circuitry. Therefore, this research focuses on both improving wireless link via system and circuit level techniques, such as improving link gain, and efficiencies of rectifiers and regulators. Additionally, emphasis is put on design of robust, energy efficient, high data rate transceivers that are reconfigurable to be adapted to a wide variety of biomedical applications, such as Autonomous Locomotive Implant, implantable pH sensors, and intracardiac probe.

One recent example is a chip fabricated in TSMC 65nm standard CMOS process that achieves high-Q on-chip matching network, high efficiency rectifier and regulator, and very robust and highly reconfigurable asynchronous demodulator that features clock and data recovery that achieves very competitive 0.5 pJ/bit energy efficiency and operates at very low modulation depth with up to 25 Mbps data rate, significantly outperforming many of the recently published data demodulators for biomedical implants.

The first part of the talk will cover several low power sensing mechanisms that are commonly used, describe known challenges and propose some techniques to overcome these challenges. The second part of the talk will focus on a specific application of wireless data and power delivery to a millimeter-size autonomous locomotive implant that was taped out in TSMC 65nm process. The implant harvests energy to power on-chip circuits and receives commands to propel and navigate itself in a liquid medium. The talk will briefly describe the idea behind electromagnetic propulsion, challenges involved in the design of the system and provide both system and circuit level solutions that were employed to overcome these challenges.

A Non-invasive Technique for Blood Glucose Monitoring

Mina Tahai and Erdem Topsakal

Department of Electrical and Computer Engineering
Mississippi State University, Mississippi State, MS 39762, USA

Monitoring a patient's plasma blood glucose level is important for various health conditions such as diabetes. Since an individual's blood glucose concentration can vary almost hourly depending on his/her level of physical activity, the medications ingested, stress levels, and food consumption, just to name a few parameters, it is difficult to know what a patient's blood glucose concentration is at any given time without testing it right then. With such factors altering glucose levels and the lack of continuous monitoring, it is difficult for individual's with such health conditions to maintain normal glucose concentrations.

In this study, we present a non-invasive blood glucose monitor that provides constant input of plasma blood glucose concentration from the ulnar vein. The device is placed on the plantar plane of the human wrist and an electromagnetic signal is transmitted from an antenna through the superficial layers of the skin. The transmission of the reflected signal is then analyzed and graphically compared to the control data set at 0 mg/dL. The shift between the base of the control graph and the input data indicates the individual's current blood glucose level. It has been proven that blood plasma glucose levels are most sensitive to detection at high frequencies of electromagnetic radiation. In order to evaluate the accuracy of the results the signal transmission was tested at 24 GHz, and 60 GHz. For testing, a computer model was created and the results are presented and discussed in regards to the efficacy of the device.

Compact Nested Dipole Probe for Near-Field Radiometric Temperature Measurement of the Body

R. Scheeler*, X. Palomer, and Z. Popović
Dept. of Electrical, Computer, and Energy Engineering, Univ. of Colorado at Boulder, Boulder, CO, USA

A compact nested dipole probe has been designed for application in near-field microwave radiometry. The probe was designed specifically for the application of determining the temperature of the human heart. The probe would be used in conjunction with a radiometer to measure deep-seated temperature profiles inside the human body in the area of the heart.

The nested dipole probe in Figure 1 is comprised of two dipoles that are folded in a spiral fashion to reduce the size of the entire probe. Two separate feeds cover the 406.1 to 410 MHz and 1.4 to 1.427 GHz bands allocated for radio-astronomy. The design was first simulated with a model for the human sternum comprised of complex permittivity layers to simulate human tissues (S. Gabriel, R. W. Lau, and C. Gabriel, Phys. Med. Biol., 41, 11, 2251, 1996.). The simulation assumes an infinite transverse extent for the layers of tissues. The metal footprint is 24 mm X 24 mm and is printed on Rogers 3010 25 mil thickness substrate (ε_r=10.2).

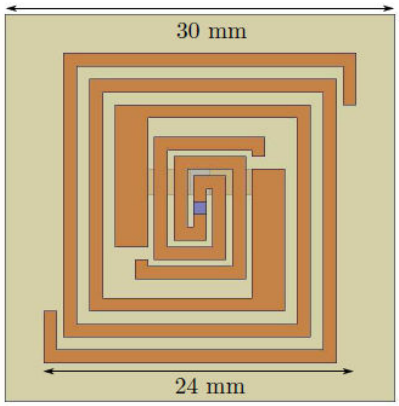

Figure 1: Nested dipole probe covering the frequency bands of 406.1-410 MHz and 1.4 to 1.427 GHz.

The input match of the two probes was measured on the human sternum just above the heart using a network analyzer. The measure results were compared with simulated results as shown in Figure 2. A return loss greater than 20 dB for the frequencies from 406.1 to 410 MHz and 1.4 to 1.427 GHz was achieved and is in good agreement with simulation.

The far-field pattern of the probe was measured at 1.4 GHz a non-shielded environment. Two measurements were made to characterize the operation of the probe: human test subject, and 4 cm thick skin muscle phantom. The maximum far-field gain for the human and phantom was -19.55 dBi and -19.36 dBi respectively.

Towards a Minimally-Invasive Applicator For Cancer Ablation

Kyle Loizos*[(1)], Carlos J. Cela[(1)], Erik S. Gamez[(1)], Darin Y. Furgeson[(1)], Gianluca Lazzi[(1)]
[(1)]The University of Utah, Salt Lake City, UT, USA.

Hyperthermia applicators allow for treatment of cancer by targeting malignant cells through a lethal focal locoregional temperature increase. Hyperthermic ablation can be used to treat a wide variety of tumors using a variety of systems including ultrasound, radiofrequency, and microwaves. This treatment is minimally invasive and can be applied in cases where surgery is contraindicated; it also has multiple benefits over conventional surgical intervention, including low incidence of bleeding, low incidence of infection, and faster healing. Following thermal ablation, the tumor becomes scar tissue and is ultimately reabsorbed by the body. In addition, in most cases a cancerous tumor can be treated in a few applications, with minimal risk to the patient, and the patient can return home in a day or two.

The design process for this kind of applicator is different from that of conventional antenna. Fist, while the antenna is designed to operate in the far field region, because of the wavelengths involved and the strong attenuation as a function of distance, it is desirable for a cancer ablation applicator to operate in the near field region. Secondly, while achieving optimal matching and consequently optimal power transfer is important in a conventional antenna, efficiency is less important than the power deposition pattern in the near field region for an ablation applicator. An ideal applicator will transfer power to a specific area in a way that the surrounding tissue is not affected.

In this presentation a 3 GHz minimally-invasive cancer ablation applicator will be introduced and its performance and applications discussed.

Computational Study of External Fixation Devices Surface Heating in 1.5T and 3T MRI Systems

Yan Liu* [(1)], Jianxiang Shen [(1)], Ji Chen[(1)], and Wolfgang Kainz[(2)]
(1) University of Houston, Houston, TX, 77204, USA
(2) U.S. Food and Drug Administration, Rockville, MD, 20852, USA

In magnetic resonance imaging (MRI) systems, strong electromagnetic fields at 64MHz and 128MHz are generated by RF coil. These electromagnetic signals can penetrate into human subjects and interact significantly with implantable medical devices. Such interactions often lead to high temperature rises in the vicinity of implantable devices. To evaluate the potential heating effect, both numerical simulations and experimental studies were conducted to access/evaluate the temperature rise (*Muranaka, et al. Jpn. J. Radiol. Technol. 2010*, and *Longman, et al. JMRI, 2011*). The temperature rises near these devices are related the device difference dimension, shape as well as the placement of the device inside the human body. Recently, there has been a growing interest in understanding the MRI safety issue for external fixation device (*Luechinger et al. J Biomed Mater Res, 2007*) which is partially implanted inside the human body and partially exposed outside the human body. Since the electric field strength in free space inside the RF coil can be much higher than that inside human body, the potential heating for external fixation devices could possibly increase to a higher level.

In this work, we investigate the critical parameters related to the heating of external fixation devices. The ASTM phantom is placed in the MRI environment to investigate the change of insertion depth and pin spacing that would affect heating level. Simulation results demonstrate that the heating effect is mainly due to the surface current on clamps and connecting bars. Metal, dielectric and carbon fiber materials are also used for connecting bars and the effects on temperature rise will be discussed.

Magnetic Nanoparticle and Magnetic Field Based Assembly for Microscale Hydrogels

Feng Xu, Dylan Finley, Yuree Sung, Banu Sridharan, Umut A. Gurkan, Utkan Demirci*

Harvard Medical School, Harvard-MIT Health Sciences & Technology, Cambridge

* udemirci@rics.bwh.harvard.edu

Microscale hydrogels (microgels) enable engineering of tissues with control over microarchitecture, which has potential widespread applications in regenerative medicine and pharmaceutical research. These applications require manipulation of microgels with spatial control, such as patterning arrays of cell-laden gel constructs for high throughput screening applications. This paper presents a novel magnetic nanoparticle (MNP) and magnetic field based assembly method of microgels, where MNPs were encapsulated in microgels to form a new biomaterial (M-gels).

The micromold method was used for fabricating MNP-encapsulating hydrogels. The array formation was developed by magnetically manipulating the M-gels suspended in PBS into separate groups in a chamber made of poly(methyl methacrylate) (PMMA). Permanent magnets (50.8 mm x 12.7 mm x 1.59 mm; K&J Magnetics) were arranged face-to-face with dielectric spacers, and placed under the chamber bottom to manipulate the scattered M-gels to a row formation. The magnets were removed from the chamber, rotated by 90 degrees, and reapplied to the chamber to re-manipulate the M-gels from the row formation into an array formation leading to assembled 3D M-gel aggregates in each array element location. The assembly process took only 5 seconds to collect a 10 mm diameter single-layer spheroid and less than 1 second to assemble rows. These time scales indicate a potential for high throughput when assembling multi-layered spheroids and arrays. Magnetic directed assembly has shown the ability to quickly assemble 3D multi-layer spheroids, linear geometries and array geometries. Also, magnetic manipulation provides spatial control over groups of microgels in order to form the array geometry. This magnetic assembly method could be an enabling tool for different areas including tissue engineering, regenerative medicine and high throughput screening applications.

We demonstrated that M-gels can be manipulated using magnetic fields and assembled into three-dimensional (3D) complex constructs. We also formed three-dimensional (3D) hydrogel arrays by organizing and assembling M-gels using spatially controlled magnetic fields. Therefore, the presented system can be used as an enabling tool to rapidly engineer 3D tissue-like structures for tissue engineering, regenerative medicine and pharmaceutical research. Overall, the MNP based assembly method of microgels will become an enabling biotechnological tool, holds great potentials for tissue engineering and regenerative medicine.

Microwave-induced thermoacoustic imaging hybrid FDTD modeling and experimental study

Ryan Jacobs*, Yiming Deng and Mark Golkowski

Departments of Electrical Engineering and Bioengineering, University of Colorado Denver, Denver, CO 80217

Ultrasonography is widely used in medical practice as a low-cost alternative and supplement to magnetic resonance imaging (MRI). Although ultrasonography has relatively high image resolution (depending on the ultrasonic wavelength at diagnostic frequencies), it suffers from low image contrast of soft tissues. Microwave-induced thermoacoustic imaging (MI-TAI) is a noninvasive modality, which can improve tissue contrast using thermoelastic wave generation induced by microwave absorption. In MI-TAI tissue is irradiated with sub-microsecond electromagnetic pulses yielding the generation of acoustic waves in the tissue that can be received with an ultrasound receiver. The advantage of this technique lies in combining the high contrast of microwave absorption coefficients for different biological tissues and the superior spatial resolution of ultrasonic waves. Such technology is important in providing a low-cost alternative to MRI

Preliminary research on MI-TAI has been conducted over the past several years; most recently a hybrid finite-difference-time-domain (FDTD) model was developed and validated. In this paper we present an experimental setup that combines both microwave induced ultrasonic wave generation with ultrasonography. We utilize a microwave power supply with 2 kW peak power and 1 microsecond pulse length that radiates at 2.4 GHz. The pulse repetition rate is up to 20 kHz. The sample is contained in an RF shielded safflower oil tank. Acoustic signals are observed using an Olympus 5800PR pulse receiver system. The experimental setup is used on samples ranging from tissue phantoms to concrete samples. The concrete samples are used to assess thermoacoustic imaging capabilities for nondestructive testing of structures and/or materials characterization, while the biological phantoms assess the technique for medical applications.

*Corresponding author: Ryan Jacobs ryan.jacobs@ucdenver.edu

Sensor Development For In Vivo Dielectric Property Measurement

Camerin Hahn[(1)] and Sima Noghanian[(1)]
The University of North Dakota, Grand Forks, ND

As studies regarding the dielectric properties of biological tissues are reviewed, only a few have adequately addressed the possible changes in the dielectric properties of in vivo tissues. Studies have shown that a dramatic change in dielectric properties occurs within the first few minutes of surgery and during the excision process. This phenomenon has been attributed to several factors: reduction in blood flow, temperature, or pressure reduction. To properly study the dielectric properties of in vivo tissue a sensor must be designed to measure dielectric properties while contained inside of the body. Currently, dielectric properties measurements are mostly performed based on transmission line technique, which requires a source and a receiver (usually bulky), to be attached to the probe that is in contact with the tissue. In this paper we investigate a technique for measuring dielectric properties of a medium without the need for a wired link. In addition, we propose implanting the sensor in tissue, therefore, the device must be small and have minimum power consumption. This implantable sensor that we propose can transmit information to a receiver outside the body and this information is used to monitor the changes in the dielectric properties continuously.

Thermal Acoustic Signals with Different Microwave Pulses and Detection Targets

Xiong Wang[1,*], Daniel Bauer[2], Russell Witte[2] and Hao Xin[1]

[1]Department of Electrical and Computer Engineering
[2]Department of Radiology
The University of Arizona, Tucson, AZ, USA

Microwave-induced thermal acoustic imaging (TAI), combining high contrast of microwave imaging and high resolution of ultrasound imaging, is a promising imaging modality for breast cancer detection (R. A. Kruger *et al*, Radiology, vol. 216, 279-283, 2000). In TAI, electromagnetically lossy breast tissues absorb energy irradiated by a pulsed microwave signal and acoustic waves are produced as a consequence of the thermoelastic expansion effect, Fig. 1. An image of the spatial distribution of microwave energy absorption is possible to be reconstructed by processing the measured acoustic signal. A breast image generated by TAI is shown Fig. 2.

To efficiently detect a breast tumor by TAI, understanding the characteristics of the acoustic signal emanated by a tumor source is important. In this work, the governing equations of the acoustic wave generation are first solved analytically based on the absorbed microwave energy, described by specific absorption rate (SAR). A general formula is then deduced to express the time-domain acoustic pressure due to an arbitrary microwave pulse and an arbitrary SAR source representing the tumor. Thermoacoustic signals generated by tumor targets with different sizes, geometries and spatial SAR distributions using microwave pulses with different widths and envelope shapes are theoretically investigated. Assumption is applied that the whole structure is acoustically homogeneous. Detailed analyses are provided to interpret the underlying physics of the obtained pressures. Frequency-domain pressures are also achieved to establish the dependence of the acoustic spectrum on the microwave pulse and tumor. Information in the acoustic spectrum is significant in optimizing the microwave pulse, determining the acoustic transducer to be used and evaluating the spatial resolution of the imaging.

Although accurate pressure due to a tumor target should be calculated by rigorous numerical techniques (for example, finite-difference time-domain (FDTD)) since the acoustic property of a human breast is actually inhomogeneous, such analytical results can provide a useful estimation of the acoustic signal profile. In addition, the analytical method is much more advantageous in terms of computation time and resource requirement compared to the full-wave numerical method.

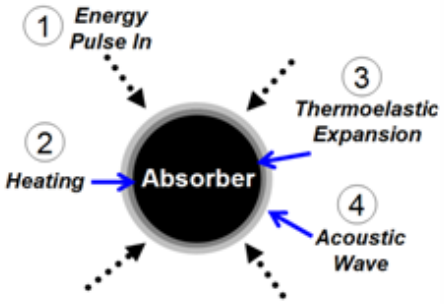

Fig. 1. Four-step physical process known as the thermal acoustic effect.

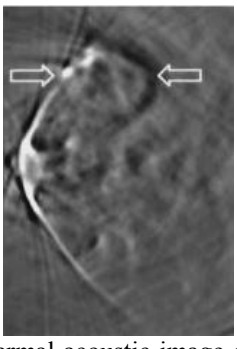

Fig. 2. Thermal acoustic image of a human breast (by R. A. Kruger).

Beamforming-Enhanced Inverse Scattering for Microwave Breast Imaging

Matthew J. Burfeindt*, Susan C. Hagness, and Barry D. Van Veen
Department of Electrical and Computer Engineering
University of Wisconsin–Madison, Madison, WI 53706

Microwave imaging has emerged as a possible alternative or complement to X-ray mammography for breast density evaluation, screening and diagnosis of cancer, and monitoring of treatment. Quantitative images are attainable through the use of inverse scattering algorithms that estimate the dielectric properties profile of the breast. However, inverse scattering techniques require solving an ill-posed system that is by nature very sensitive to noise and interference.

We present a transmit-receive beamforming-enhanced version of the Distorted Born Iterative Method (DBIM) for solving the inverse scattering problem. Incorporating transmit-receive beamforming into the imaging system offers the potential to mitigate the effects of noise on the dielectric reconstructions. We leverage the flexibility of a numerical testbed to evaluate the potential of this new approach. Here, the measurement of scattered signals is simulated using FDTD. We use the beamforming-enhanced algorithm to create reconstructions of two-dimensional dielectric profiles taken from anatomically realistic numerical breast phantoms. The reconstructions are created for signal-to-noise ratios (SNR) ranging from 40 dB to 10 dB. They are compared to reconstructions created using the standard DBIM algorithm. For high SNR (approaching 40 dB) the beamforming-enhanced and standard algorithms create reconstructions that are of similar fidelity relative to the true dielectric profiles. For SNR below 20 dB, the beamforming-enhanced algorithm creates reconstructions that are significantly more faithful to the true profiles. Thus, the beamforming-enhanced algorithm is much less sensitive to noise. These promising results show that the technique warrants further investigation and development.

Evaluation of a Full-Cavity Numerical Characterization Approach for an Experimental Microwave Breast Imaging System

Mark Haynes*, John Stang, and Mahta Moghaddam
University of Michigan, 1301 Beal Ave, Ann Arbor, MI, 48109
mshaynes@umich.edu, jonhstan@umich.edu, mmoghadd@umich.edu

The number of experimental prototype systems for microwave breast imaging is rapidly increasing. These systems are designed test time-domain beam focusing and full-wave inverse scattering imaging algorithms to image dielectric contrasts between healthy and malignant tissue. Unlike free-space imaging systems, the characterization of breast imaging systems is complicated by several factors: compact arrangements of many antennas creates a cavity-like structure, the antenna incident fields include all background multiple scattering, and the breast and the antennas are in each other's near-field. To model these effects, investigators have turned to full numeric simulation of the imaging structure, but methods of formally including the results of simulations in the algorithms and further relating the algorithms to experimental data have lagged behind.

In previous work, we derived a new scattered field integral operator which allows us to formally relate the fields in the imaging domain to scattered field S-parameter measurements given by a Vector Network Analyzer (VNA). We showed that only knowledge of the background incident fields is required, and that this formalism applies to cavity scattering situations. We have integrated this methodology into our inverse scattering algorithm, which is based on the Born Iterative Method.

We have constructed a prototype breast imaging system. The cavity is made up 12 concentric, vertical panels of microwave substrate on which three antenna are etched on each. The antennas are connected through a solid-state switching matrix to a VNA. The cavity is filled with an oil/water coupling medium with a relative permittivity and conductivity of 21 and 0.475 Siemens/per, respectively. The antennas are printed bow-ties which operate at 2.75 GHz in the fluid.

We use Ansoft HFSS to model the entire cavity and use it to estimate the incident fields throughout the cavity. We show how we make the numerical characterization, imaging algorithm, and experimental system consistent. We give imaging results of permittivity and conductivity for both synthetic and measured data of simple targets. Ongoing work also includes imaging more realistic breast phantoms in experiment.

Virtual Electrodes: Increasing Spatial Resolution of Neural Interfaces Beyond the Actual Electrode Count

Carlos J. Cela*(1), Kyle Loizos(1), Gianluca Lazzi(1)
(1) The University of Utah, Salt Lake City, UT, USA

Implanted neural interfaces allow for communication between electronics and the human nervous system, often using an implanted electrode array to excite neural tissue, record signals, or both. Depending on their intended function, the implanted electrode array may have many individually controlled electrodes, each fed by a wire. On certain applications like the artificial retina, the electrode array is dense, with desirable electrode count in the hundreds or even thousands of elements.

With neural interfaces becoming increasingly sophisticated, current fabrication technology using bio-compatible materials challenged in its ability to feed excitation signals to each electrode in the implanted array. This is particularly true when the application requires the use of a flexible dielectric substrate as support for the electrodes, as it is the case of epiretinal implants. A related challenge is to route hundreds or perhaps thousands of individual wires from the electrodes to the electronics of the device.

A virtual electrode is conceptually a device that is able to establish areas of relatively high current density magnitude not directly under a physical electrode. By using this property, several desirable effects can be achieved: first, the effective electrode count of an array can be increased beyond the actual number of physical electrodes; second, virtual electrodes allow for finer control of charge injection in proximity of the electrode array. These effects help overcoming some of the fabrication challenges, and provide the additional benefit of a finer control of the shape of the charge injection into the tissue.

In this presentation, current designs for virtual electrodes with be shown, as well as possible applications and data describing performance for different configurations.

A Transcutaneous Microwave Thermal Therapy System Prototype For Breast Cancer Treatment Using Image Based Time-Reversal Focusing

John P. Stang*, Mark Haynes, and Mahta Moghaddam
University of Michigan, Ann Arbor, MI, 48109

In the current standard-of-care treatments for breast cancer (surgery, chemotherapy, hormonal therapy, and radiation therapy), there remains a need for the reduction of local recurrence, harmful side-effects, and cosmetic harm. Toward that end, a transcutaneous microwave thermal therapy system is being developed for the targeted treatment of breast cancer cells using focused microwaves as an adjuvant to radiation, chemotherapy, and high intensity focused ultrasound (HIFU).

In the microwave therapy system currently under development, a cylindrical array of antennas operating at 915 MHz is used to focus continuous-wave microwave energy transcutaneously into the pendent breast suspended in a coupling medium. Prior imaging studies are used to ascertain the material properties of the breast tissue, and this data is incorporated into a multiphysics model. Time-reversal techniques are employed to find a solution (relative amplitudes and phase) for focusing at a given location, and to precondition a weighted inverse solver that can optimize treatment planning for ablation at the tumor location while minimizing thermal dose elsewhere in the breast.

In earlier numerical and experimental studies of our time-reversal methods applied to 2D focusing, we have demonstrated that therapeutic levels of heat deposition with good targeting accuracy can be achieved at the target location using a twelve element array and an appropriately matched coupling medium. A more careful study of the thermal distribution throughout the volume of the therapeutic chamber has been undertaken using an array of switched thermocouples to generate 3D maps of the temperature profile. Experimental results of focused heating tests in various tissue mimicking phantoms that examine the effects of tissue permittivity, conductivity, and heterogeneity on focused heating will be shown. Finally, initial synthetic results of 3D focusing using a hemispherical array will be presented.

Upon completion, the focused microwave thermal therapy system will have the potential to reduce tumor size prior to surgery (along with preoperative chemotherapy if needed), to completely ablate the tumor without surgery, or as an adjuvant to postoperative radiation therapy and chemotherapy.

Optimization Approach for Microstrip Spiral Antennas Used in Deep Tissue Radiometry

Sara Salahi*(1), Paolo F. Maccarini(2), Alina Boico(2), and Paul R. Stauffer(2)
(1) Biomedical Engineering, Duke University, Durham, NC
(2) Radiation Oncology, Duke University, Durham, NC

Vesicoureteral reflux (VUR) is a dysfunction of the urinary system often seen in young children. It is characterized by retrograde flow of urine from the bladder thru the ureters to the kidneys. The current method for diagnosing VUR involves injection of a contrast agent into the bladder via invasive Foley catheter followed by x-ray imaging of the kidneys. As a non-invasive, non-ionizing radiation diagnostic alternative, we are developing an approach for detecting VUR by gently warming urine in the bladder while monitoring kidney temperature with a microwave radiometer. In order to monitor kidney temperature effectively, the radiometric antenna must be optimized to maximally collect radiated energy from a 60cc kidney that is located approximately 2-4cm deep in the abdomen. This effort describes a novel 3D simulation-based approach for radiometric antenna optimization and quantitative results of the benefits of using this approach for improving antenna design.

Statistically Accurate Patient Model. Skin and fat thickness as well as depth and volume of the kidney vary significantly. To maximize the total power the antenna receives from the kidney in the greatest number of children, an average patient model was constructed based on measurements from CT scans and ultrasound images of 40 children. The resulting "average child" has skin thickness of 1mm, fat thickness of 3mm, kidney isocenter depth of 3.5cm and kidney volume of 60cc. A 3D simulation model was created using VSG Avizo® by segmenting the CT data set of the constructed "average child" anatomy. This model was then imported into Ansys HFSS™ and each tissue was assigned dielectric properties (Gabriel, 1996) for antenna optimization.

Antenna Optimization. The efficiency of a logarithmic spiral antenna was maximized over a 1-2GHz band by performing a parametric optimization in HFSS™ to determine the ideal number of turns, radius of spiral trace, and the dielectric constants and thicknesses of coverlay and substrate layers. Antenna efficiency (η) was defined as $\eta = \int_{kidney} PD_i \,/\, \int_{all\ tissues} PD_i$ where PD is power density. To account for continuous variation in antenna pattern and radiometer gain (G) across the measurement band, the total power received from the kidney was defined as $P_{total} = \eta_i * (1 - |S_{11}|^2)_i * G_i$ where η, S_{11} and G are evaluated at the same frequency (i) and integrated across the band with 100MHz resolution.

This optimization scheme produced an antenna that was able to collect up to 14% of its received power from a 60cc kidney 3.5cm deep in the abdomen. The results were validated in multilayer phantom studies with a 1.35GHz radiometer.

Microwave Radiometry For Non-Invasive Detection of Vesicoureteral Reflux

Paul Stauffer*[1], Paolo Maccarini[1], Sara Salahi[1], Kavitha Arunachalam[2] and Brent Snow[3]
[1]Radiation Oncology Dept., Duke University, Durham NC
[2]Dept. of Engineering Design, Indian Institute of Technology Madras, Chennai India
[3]Primary Childrens Medical Center, University of Utah, Salt Lake City, UT

Vesicoureteral reflux (VUR) is a serious health problem in young children (ages 0-5), often leading to permanent renal damage. The most common methods of diagnosing VUR involve traumatic X-ray or radionuclide imaging of contrast agent injected into the bladder through an invasive Foley catheter. We present an alternative non-invasive approach to detect VUR by gently warming urine in the bladder with external microwave antennas and simultaneously monitoring for any rise in kidney temperature with microwave radiometry.

To investigate this new diagnostic approach, we designed and tested a high-sensitivity total power radiometer with EMI-shielded log spiral microstrip receive antenna having high gain on-axis to sense changes in volume average tissue temperature up to 4 cm deep. To induce a kidney temperature rise in patients with VUR, we developed a system to gently warm urine inside the bladder using a conformal array of two 915 MHz square slot microstrip antennas. A power modulation approach was investigated to reduce heating of perfused superficial tissue relative to the non-perfused urine inside the bladder. To demonstrate our ability to warm bladder without trauma to surrounding tissue and to detect a small temperature rise at depth, measurements were performed in multilayer phantoms and in vitro and in vivo porcine experiments with a circulating saline catheter-mounted 10-30 mL balloon "kidney" model implanted 3-4 cm deep.

In temperature-controlled muscle phantom experiments, we demonstrated local heating of 60-180 ml urine reservoirs located 1-3 cm deep and radiometric detection of 5-10°C temperature rise in circulating saline "kidneys" implanted 2-4 cm deep. In vitro and in vivo porcine experiments demonstrated effective heating of bladder to 40-44°C while maintaining overlying tissues <38°C using two power-modulated 3cm square microstrip antennas coupled to tissue with a thin room temperature waterbolus. Pathologic evaluation of the in vivo pig experiments confirmed lack of tissue damage in tissues surrounding the bladder for up to three 20 minute bladder exposures separated by 15 min for cooldown to normothermic conditions. A 1.35 GHz radiometer with 500 MHz integration band clearly detected 6°C transient and 2°C steady-state rise in temperature of 30 ml Foley balloon "kidneys" buried adjacent to the kidney inside 34°C pig abdomen.

This work demonstrates that a lightweight and low profile 915 MHz power modulated two antenna array can gently warm bladder urine while a total power radiometer with log spiral antenna detects a temperature rise as small as 2°C in 30 ml of "urine" at 2-4 cm depth in phantom models and porcine tissues, demonstrating more than sufficient sensitivity to detect the reflux of warm urine from bladder to kidney. This deep tissue radiometric monitoring approach appears suitable for non-invasive detection of VUR.

Microwave Probe Array for Dielectric Surgical Margin Testing

Paul M. Meaney, Tian Zhou, Neil Epstein, Keith D. Paulsen
Thayer School of Engineering, Dartmouth College, Hanover, NH USA
Kuang-Chi Institute of Advanced Technology, Guangdong, China

Abstract: The principle goal in breast conservation surgery is to minimize the removal of healthy tissue while completely excising the malignancy. If the tumor is not completely removed there is a high possibility of local recurrence. The current standard of care is to perform an additional operation and re-excise the offending tissue if there is evidence of tumor presence within the first 1-2 mm on any sample surface. There is a significant need to be able to test the excised tissue in the OR and quickly determine whether additional tissue should be removed to minimize additional surgical procedures. Several technologies are currently being developed to meet this need including optical and fluorescence-based approaches, terahertz techniques and even microwave dielectric approaches, which each exploit property contrast between normal and malignant tissue. In each method, the investigators utilize a single point probe and raster scan it across the tissue surface in a mechanized sequence to cover the full extent of the tissue. The first two are somewhat limited in depth sensitivity with the former having the additional challenge of the light not being able to penetrate through the surface identifying inking that is standard procedure in the clinic. The microwave is unique in that it is well known that dielectric measurements can readily penetrate several mm of a tissue sample and recover a weighted average of the properties within that zone.

We are currently developing a microwave probe array for assessing tumor surgical margins real-time in the operating room. For this device we have printed several probes on a rigid circuit board with quasi-coaxial interfaces on the underneath surface of the board. Early experiments have validated that these printed probes perform equivalently to standard coaxial probes for frequencies up to roughly 4 GHz. As we develop this concept and further miniaturize the array, operation should easily extend to higher frequencies. By being able to translate the notion of a probe to a printed circuit, we have opened up the dielectric measurement concept to a wide range of technological advances. Circuit designers routinely create RF connections through multi-layer boards up to high microwave frequencies. In this realm, we are developing the concept of a switchable array with elements on the exposed bottom surface in a relatively tightly packed arrangement. For surgical margin testing, this device will provide the necessary depth penetration while also allowing for testing over a useful footprint providing a more operator-friendly interface than the developing raster scanning approaches.

Angora: An Open-Source Finite-Difference Time-Domain Software Package

Ilker R. Capoglu*[(1)], Allen Taflove[(2)], and Vadim Backman[(1)]
(1) Biomedical Engineering Department, Northwestern University, Evanston, IL
(2) Electrical Engineering and Computer Science Department, Northwestern University, Evanston, IL

In this talk, we will introduce an open-source software package that provides numerical solutions to an extremely wide range of electromagnetic problems using the finite-difference time-domain (FDTD) method. The software, named *Angora*, has been developed partly due to funding from the National Institutes of Health (NIH.) It is available for download under the GNU Public License (GPL,) which protects the rights of the user to use, modify and redistribute the software as long as the resulting code is also open source. We will give a detailed account of the features of the software, explain its use and present some example results. Angora has features that are useful for antenna problems in the RF frequency range, as well as capabilities that allow the modeling of optical problems in the nanometer scale. Major features of Angora are as follows: automatic build system for GNU/Linux, 3D parallelization using the MPI standard, user-friendly configuration, full support for multilayered media, extensive shape and material support, plane-wave and more complex (coherent and partially-coherent) incident beams, near-field-to-far-field transforms (time-domain and frequency domain,) field value recording and movie creation, random-medium generation and numerical optical imaging of the structure under analysis.

Optimization of Silicon Photonic Biosensors

Michael Gould[(1)], Elijah Christensen[(2)], Daniel M. Ratner[(2)] and Michael Hochberg[(1)]
(1) Department of Electrical Engineering, University of Washington, Seattle, WA 98195
(2) Department of Bioengineering, University of Washington, Seattle, WA 98195

Silicon photonics has traditionally been explored for applications in telecommunications and high speed signal processing. However, there has recently been a significant amount of research looking into the sensing capabilities of silicon photonic systems, and in fact there is at least one commercial silicon photonic biosensing system currently on the market.

This product is based on optical ring resonators built on a silicon-on-insulator (SOI) ridge waveguides. We demonstrate a significant improvement in device sensitivity to both bulk refractive index changes and surface binding through optimization of waveguide geometry, using both narrower ridges and slot waveguides, compared to the published performance of the only silicon photonics-based commercial tool. The narrow ridge waveguide devices show a factor of 2 improvement in sensitivity to bulk refractive index changes over the commercial device, while the slot waveguides show a factor of 3. This is in close agreement to theoretical predictions, and suggests that considerably more sensitive devices are possible, particularly through the use of slot waveguides.

We show the behaviour of the devices due to surface changes as well. Once again slot waveguide based devices showed significantly higher sensitivity than ridges. In detecting the deposition of proteins RNase B and BSA, the slots showed twice the sensitivity of our narrow ridges and 4 times the sensitivity of the commercial devices.

Near-infrared narrow-band imaging of tumors using plasmonic gold nanoparticles

Priyaveena Puvanakrishnan[1], Parmeswaran Diagaradjane[2], Jon A. Schwartz[3], Sunil Krishnan[2], James W. Tunnell[1]

[1]Department of Biomedical Engineering, University of Texas at Austin, Texas
[2] The University of Texas M.D Anderson Cancer Center, Houston, Texas,
[3]Nanospectra Biosciences Inc., Houston, Texas

A significant challenge in the surgical resection of tumors is accurate identification of tumor margins. Current methods for margin detection are time-intensive and often result in incomplete tumor excision and recurrence of disease. Gold nanoparticles (GNPs) have recently gained significant traction as nanovectors for combined imaging and photothermal therapy of tumors. Delivered systemically, GNP's preferentially accumulate at the tumor site via the enhanced permeability and retention effect, and when irradiated with sufficient NIR light, produce sufficient heat to treat tumor tissue. The objective of this study was to determine the potential of GNP for real-time tumor margin detection using near-infrared narrowband imaging (NIRNBI). NIRNBI images narrow wavelength bands to enhance contrast from plasmonic particles in a widefield, portable and non-contact device that is clinically compatible for real-time tumor margin demarcation. The NIRNBI system consists of 1) two LED's: green (530 nm) and NIR (780 nm) LED for illuminating the blood vessels and GNP, respectively, 2) a filter wheel for wavelength selection, and 3) a CCD to collect reflected light from the sample. The NIRNBI system acquires and processes images at a rate of at least 5 frames per second. We have developed custom control software with a graphical user interface that handles both image acquisition and processing/display in real-time. We used Swiss *nu/nu* mice with a subcutaneous tumor xenograft model that received intravenous administration of gold nanoshells and gold nanorods. We determined the GNP's distribution and accumulation pattern within tumors using NIRNBI. *Ex vivo* NIRNBI of tumor xenografts demonstrated a highly heterogeneous distribution of GNP within the tumor with higher accumulation at the cortex. GNPs were observed in unique patterns surrounding the perivascular region. The GNPs clearly defined the tumor while surrounding normal tissue did not indicate the presence of particles. These results demonstrate the feasibility of NIRNBI in demarcating tumor margins during surgical resection and potentially guiding photo-thermal ablation of tumors.

Spatial light interference microscopy (SLIM)

Gabriel Popescu
Quantitative Light Imaging Laboratory, Department of Electrical and Computer Engineering, Beckman Institute for Advanced Science & Technology, University of Illinois at Urbana-Champaign, Urbana, IL 61801.

Most living cells do not absorb or scatter light significantly, i.e. they are essentially transparent, or phase objects. Phase contrast microscopy proposed by Zernike represented a major advance in intrinsic contrast imaging, as it revealed inner details of transparent structures without staining or tagging. While phase contrast is sensitive to minute optical path-length changes in the cell, down to the nanoscale, the information retrieved is only qualitative. Quantifying cell-induced shifts in the optical path-lengths permits nanometer scale measurements of structures and motions in a non-contact, non-invasive manner. Thus, quantitative phase imaging (QPI) has recently become an active field of study and various experimental approaches have been proposed.

Despite these significant technological advances, the range of QPI applications in biology has been largely limited to red blood cell imaging or assessment of global cell parameters such as dry mass, average refractive index, and statistical parameters of tissue slices. This limitation is due to two main reasons, as follows. First, because of speckle generated by the high temporal coherence of the light used (typically lasers), the contrast in QPI images has never matched that exhibited in white light techniques such as phase contrast and Nomarski. Second, the experimental setups tend to be rather complex, of high maintenance, which limits their in-depth biological applicability.

We present SLIM as a novel, highly sensitive QPI method, which promises to enable unprecedented structure and dynamics studies in biology and beyond. SLIM combines Zernike's phase contrast method by revealing the intrinsic contrast of transparent samples, with Gabor's holography by rendering quantitative phase maps across the sample. Because of the extremely short coherence length of this illumination light, approximately 1.2 μm, SLIM provides speckle-free imaging with sub-nanometer spatial background noise. Further, the SLIM image is intrinsically registered with the other channels of the microscope, including fluorescence, which enables powerful multimodal investigations.

Multi-Channel Diffuse Optical Spectroscopic Imaging

Hosain Haghany, Albert Cerussi, Keun-Sik No, Jing Liu, Bruce J. Tromberg
Laser Microbeam and Medical Program (LAMMP), Beckman Laser Institute and Medical Clinic,
Department of Physics and Astronomy, University of California, Irvine 92617

Diffuse optical spectroscopic imaging (DOSI) is a non-invasive, low-spatial resolution functional imaging technique that utilizes non-ionizing near-infrared (NIR) light (650 to 1000nm). Within this spectral region, light propagation in tissue is dominated by multiple scattering and penetration is relatively high (i.e. several centimeters) because of low absorption. Tissue measurements employing time- or frequency-domain photon migration (FDPM) techniques combined with photon diffusion models are used to separate light absorption from scattering. These optical parameters (i.e. absorption and reduced scattering coefficients), can be related to tissue functional and structural properties, respectively.

We typically perform DOSI measurements using a home-built device that integrates multi-frequency, FDPM data with time-independent broadband spectroscopy. These features are built into handheld probe with a single source-detector pair. This “single view” instrument is capable of generating quantitative, high resolution (~1000 wavelength) absorption and reduced scattering spectra over a broad spectral band (~650-1000 nm). However, this approach is susceptible to partial volume effects that can diminish sensitivity to buried tumors and tissue heterogeneities.

In order to overcome this limitation, we have recently developed a multi-channel instrument that integrates several miniaturized DOSI components (mDOSI) into a network. Each mini system features full NIR broadband spectra by combining multi-frequency FDPM with steady state broadband spectroscopy. Therefore the multi-channel DOSI device significantly expands spatial information content and can provide a 3D map of tissue volume when combined with image reconstruction techniques. This talk presents the theory, instrumentation, and preliminary testing of a multi channel, handheld tomographic DOSI breast scanner. Results from tissue simulating phantom measurements and breast cancer patients will be shown highlighting spatial and spectral sensitivity to deeply-buried subsurface heterogeneities and tumors. The relationship between single- and multi-view methods and the impact of increasing channels on resolution and contrast will be discussed.

Jones Matrix Monte Carlo Simulation of Coherent Backscattering in Biological Media

Andrew J Radosevich* [(1)], Jeremy D Rogers [(1)], Allen Taflove[(2)], and Vadim Backman[(1)]
(1) Biomedical Engineering, Northwestern University, Evanston, Illinois 60208
(2) Electrical Engineering and Computer Science, Northwestern University, Evanston, Illinois 60208.

Coherent backscattering (CBS, also known as enhanced backscattering) is an interference phenomenon in which rays traveling time-reversed paths constructively interfere resulting in an angular intensity peak centered in the exact backscattering direction. Within a scattering medium, the shape of this angular peak is related to the spatial backscattering impulse-response through a Fourier transform relationship. As a result, measurements of EBS are extremely sensitive to the optical scattering and absorption properties. These properties include the reduced scattering coefficient (μ_s^*), absorption coefficient (μ_a), the anisotropy factor ($g = \langle\cos(\theta)\rangle$) as well as a parameter which describes the shape of the refractive index correlation function (m). Recently CBS has shown promise for the early detection of cancers originating in the colon, pancreas, and lung by detecting subtle changes in the structural organization and composition of diseased tissue. In order to accurately understand the origin of this signal, we have developed a polarized light Monte Carlo code for the simulation of multiply scattered light in a media such as biological tissue which are composed of a continuous distribution of randomly fluctuating refractive index.

In typical Monte Carlo simulations of the propagation of polarized light, the polarization state is monitored using the Stokes vectors which only contain information about the intensity of light. As a result, coherent phenomena such as CBS are not rigorously treated. We therefore have developed a code which tracks the amplitude and phase of the electric field using the Jones calculus formalism. Additionally, we employ the 'partial photon' technique for simulating backscattered light which significantly reduces computation time. In this work, we first discuss the implementation of this code and subsequently analyze the effects of the various optical properties on the shape of the CBS peak.

Numerical and In Vitro Phantoms for Hyperthermic Monitoring of Breast Cancer

Erin Colebeck[1], Toi Spates[1], Lynn Dyess[2], and Erdem Topsakal[1]

[1]Department of Electrical and Computer Engineering
Mississippi State University
Mississippi State, MS 39762, USA

[2]Department of Surgery and Physiology
University of South Alabama
Mobile, AL 36688, USA

There are several conventional techniques to screen for breast cancer today, but they each have limitations such as producing false positive results, causing pain and discomfort to the patients, and using ionizing radiation. These bottlenecks suggest that there is a need for the development of alternative techniques and approaches for detecting and monitoring breast cancer. Therefore, our technical goal is to develop an alternative technique based on cellular hyperthermia for early detection of breast cancer and monitoring. We hypothesize that the temperature within the breast will rise as the malignant cells divide and multiply, and these temperature changes can be used for early detection and monitoring.

To aid in the design of such technology, we have developed both numerical and in vitro phantoms. CT images were collected from 5 patients at University of South Alabama Cancer Center. Commercial software, ScanIP, is used to construct the 3D models specifying the different tissues along with the cancerous mass. Several in vitro heterogeneous phantoms were developed using these 3D models. Both numerical and *in vitro* phantoms are intended to be used in the development stages of the hyperthermia-based sensing and monitoring system.

Possible Application of Photonic Nanojets to Ultra Early-Stage Cancer Detection

Hamide Seidfaraji*[1], Cesar Mendez-Ruiz[2], and Jamesina J. Simpson[1]
(1) ECE Department, University of New Mexico, Albuquerque, NM, 87131, USA
(2) Intel Corporation, Guadalajara, Mexico

It is currently believed that internal refractive index fluctuations within biological cells increase and become more disordered during the initial stages of ultra early-stage cancer development. For example, a more aggressive human colorectal cancer cell line (HT-29) has been hypothesized to have 600×600×100 nm correlation lengths, while a less aggressive HT-29 colon cancer cell line is hypothesized to have a correlation length of 60×60×60 nm.

In this presentation, HT-29 cells are analyzed in a new way for determining cancer aggressiveness. Specifically, the backscattered cepstrum is obtained for photonic nanojet-illuminated HT-29 cells. This technique of employing the cepstrum as well as a photonic nanojet offers new advantages through unique capabilities for determining the internal structure and composition of cells at sub-diffraction scales. This work may thus have application to ultra-early stage cancer detection.

The cepstrum is defined here as taking the discrete Fourier transform (DFT) of the magnitude of the backscattered spectrum. The domain of the cepstrum is termed "quefrency" and integer multiples of the fundamental quefrency are termed "rahmonics." As for the coining of the word "cepstra," these terms are formed by altering the order of the initial letters of their corresponding terms in the frequency domain.

A photonic nanojet is defined as a narrow, high-intensity beam of light that emerges from the shadow side of a plane-wave-illuminated dielectric sphere or cylinder of diameter larger than the wavelength, λ. Photonic nanojets have previously been shown to provide sufficiently one-dimensional (1-D) illumination of three-dimensional (3-D) targets, yielding the ability to detect at distances of multiple wavelengths in the backscatter direction ultra-subwavelength inhomogeneities embedded within the dielectric targets.

Our FDTD-calculated results and analysis of the backscattered cepstrum of the photonic nanojet-illuminated HT-29 cells will be shown to demonstrate that (1) details of the internal composition of cells are more easily extracted from the backscatter of nanojet-illuminated cells than flat slabs; this could aid ultra early-stage cancer detection; (2) a clear means exists to distinguish between less and more aggressive cancer cell lines before these changes are histologically detectable.

Observing Geospace with GPS

Anthea J. Coster
MIT Haystack Observatory, Westford, MA 01886

Most of us know the Global Positioning System (GPS) as a means to track locations and times of events on Earth, and for such applications, ionospheric and magnetospheric effects are error sources that must be eliminated. However, for space physicists, the situation is reversed: the very effects that disrupt ground-based applications of GPS have enabled dramatic new ways to observe geospace, the region of space between the Earth's upper atmosphere and the outermost reaches of the Earth's magnetic field. GPS was originally designed with two frequencies specifically to enable the removal of the ionospheric error term for high precision uses. Ionospheric scientists were quick to recognize that GPS dual-frequency measurements could be used to measure the ionospheric total electron content (TEC) at multiple locations. As soon as the first experimental GPS satellites were launched (between 1978 and 1985), scientists began using GPS signals to monitor the ionosphere. Starting in the 1990's, the USNC-URSI scientific community was one of the first to include regular sessions on GPS observations of the ionosphere in their yearly meetings.

During the last decade, TEC maps derived from the global set of GPS data have provided a paradigm shift in the way that Earth's geospace environment is observed. Prior to GPS, most scientific measurements of the magnetosphere-ionosphere were from individual observing sites or systems providing information about one region or a single point. With GPS, by combining individual measurements from multiple receivers, high-resolution temporal and spatial information is available on a global scale. This enables "system" views of the global ionosphere in ways never before possible. As a result, a new understanding of the processes and linkages between atmospheric regions has been enabled.

After a review of GPS fundamentals, including an explanation of how GPS is used to measure properties of the atmosphere, this talk will highlight several science discoveries that have been made with GPS data. Among these include the global monitoring of large-scale geomagnetic storms using TEC maps derived from GPS data; correlation of ionospheric storm features with large-scale drainage plumes of the plasmasphere; observations of the effects of sudden stratospheric warmings on the ionosphere; and the teasing out of features of the TEC related to magnetic declination. In the future, virtual observatories will allow easy access to GPS data and enable their combination with other radar, magnetometer, and optical data to provide the big picture view of the geospace environment.

Evolution of the Global Navigation Satellite System (GNSS)

Christopher J. Hegarty
The MITRE Corporation, Bedford, MA 01730, http://www.mitre.org

The International Civil Aviation Organization (ICAO) originally defined the "Global Navigation Satellite System" (GNSS) as a singular noun meaning "a worldwide position and time determination system that includes one or more satellite constellations". Today "GNSS" is oftentimes used interchangeably with "satellite navigation system". Using the original ICAO definition, this plenary presentation provides an overview of the current status and future plans for the components of GNSS. The presentation addresses the following global or regional satellite navigation systems: the U.S. Global Positioning System (GPS), Russian Globalnaya Navigatsionnaya Sputnikovaya Sistema (GLONASS), European Galileo, Chinese Compass, Japanese Quasi Zenith Satellite System (QZSS), and Indian Regional Satellite Navigation System (IRNSS). For each system, the constellation, ground network, signals and services are described.